Available online at www.sciencedirect.com
ScienceDirect
Coordination Chemistry Reviews 251 (2007) 1311–1492
COORDINATION CHEMISTRY REVIEWS
www.elsevier.com/locate/ccr

Review

The development of compartmental macrocyclic Schiff bases and related polyamine derivatives

P.A. Vigato, S. Tamburini *, L. Bertolo

Istituto di Chimica Inorganica e delle Superfici, CNR, Area della Ricerca, Corso Stati Uniti 4, 35127 Padova, Italy

Received 24 July 2006; accepted 27 November 2006
Available online 30 November 2006

Contents

* Corresponding author. Tel.: +39 0498295963; fax: +39 0498702911.
E-mail address: tamburini@icis.cnr.it (S. Tamburini).

0010-8545/$ – see front matter
doi:10.1016/j.ccr.2006.11.016

Abstract

The design and synthesis of [1 + 1], [2 + 2], [3 + 3] or [3 + 2] macrocyclic or macrobicyclic Schiff bases, the multiple self-condensation procedure between appropriate polyformyl- and polyamine-precursors or the templating capability of different metal ions in directing the synthetic pathway toward specific compounds are reported together with the use of transmetalation reactions of particular complexes with a different metal salt in order to obtain not otherwise accessible complexes.

The reduction of the cyclic Schiff base or the reductive demetalation of the related complexes to the polyamine homologues is also considered.

These systems can form mononuclear, homo- and heterodinuclear (or polynuclear) complexes, when reacted with appropriate metal salts. Attention is especially devoted to the physico-chemical and structural aspects of the resulting systems, especially the magneto-structural relationships arising from the interaction of paramagnetic ions, coordinated inside a unique moiety.

The role of compartmental ligands, i.e. their ability to bind two or more metal ions in close proximity into two identical or different compartments, the presence of bridging groups inside these coordination moieties and their relevance in modulating the type and the extent of mutual interaction between the metal ions inside the adjacent chambers is also reviewed.

The insertion of asymmetry into these ligands provides important diversification of the coordinating sites and allows for different and well defined recognition processes involving specific cations and/or anions at the adjacent sites.

Keywords: Compartmental ligands; Macrocycles; Schiff bases; Macrobicycles; Macrocyclic polyamines; Dinuclear Complexes; Polynuclear complexes

1. Introduction

1.1. Macrocyclic Schiff bases and related polyamine derivatives

Schiff bases have been extensively employed in the understanding of molecular processes occurring in biochemistry, material science, catalysis, encapsulation, activation, transport and separation phenomena, hydrometallurgy, etc. [1,2].

A large variety of [1 + 1] and [2 + 2] macrocyclic ligands have been synthesized to ascertain correctly the role of the different donor atoms, their relative position, the number and size of the chelating rings formed, the flexibility and the shape of the coordinating moiety on the selective binding of charged or neutral species and on the properties arising from these aggregations [3,4].

The evolution of these Schiff bases has produced macrobicyclic ligands obtained in one-step multiple condensation reactions [4,5]; the cyclic [3 + 2] Schiff base condensation represents the extension of the [2 + 2] macrocyclic coordination systems into the third dimension.

The introduction of specific functionalities at the periphery of the coordinating moiety gives rise to quite sophisticated systems capable of contemporary multi-recognition processes, specific separation and transport processes across membranes or activation and catalysis in ecocompatible solvents.

For macrocyclic receptors the hole size represents an additional parameter which may influence greatly the ability to discriminate among the different charged or neutral species to be recognized. The progressive enlargement of the coordinating moiety allowed studies aimed at a deep understanding of physico-chemical properties arising from the simultaneous presence of two or more metal ions in close proximity within the same coordinating moiety.

Using compartmental ligands, binuclear complexes have been synthesized, where the two metal centers, if paramagnetic, interact with each other through the bridging donor atoms of the ligands in a ferromagnetic or antiferromagnetic way. By changing the type of the ligand, the distance between the two chambers and/or the paramagnetic centers, it is possible to vary considerably the magnetic interaction and, with particular complexes ferromagnetic interactions have been observed. Thus, these complexes may be good building blocks for the preparation of molecular magnets.

Complexes in which a single ligand organizes more than two metal centers into some predetermined arrangement, giving rise to unique behaviour, have been also designed, synthesized and fully characterized. They can be obtained by simple self-condensation of suitable formyl- or keto- and primary amine-precursors. Multiple self-condensation processes give rise to planar or tridimensional compounds in one step. Alternatively, they can be obtained by template procedure: this synthetic pathway directly gives the designed complexes. Moreover, these complexes can undergo transmetalation reactions when reacted with a different metal salt, allowing the formation of not otherwise accessible complexes. Template and transmetalation reactions quite often give rise to the designed complexes in high yield and in a satisfactory purity grade.

The macrocyclic systems can be functionalized by inserting appropriate groups in the aliphatic and/or aromatic chains of the formyl- or keto- and amine-precursors.

Furthermore, the Schiff bases can be reduced to the related polyamine derivatives, containing the same cyclic complexity, by reaction with an appropriate reducing agent. Similarly the related complexes can give rise to reductive decomplexation reactions when treated with appropriate reductants with the consequent formation of the corresponding polyamine derivatives. These polyamine compounds are less sensitive to hydrolysis and more flexible. Furthermore, they contain NH groups which may be further functionalized by appropriate synthetic procedures.

Depending on the shape of the formyl- and amine precursors and/or the metal ion template used, differing ring sizes can be formed during the cyclization reaction. If one dicarbonyl

moiety reacts with one diamine moiety a [1 + 1] macrocycle results; when two dicarbonyl precursors react with two diamines then a [2 + 2] macrocycle results while if three dicarbonyl precursors react with two tripodal triamines a [3 + 2] macrobicycle is formed, and so on. This synthetic procedure may form [3 + 3] or [4 + 4] superior macrocyclic homologues or [1 + 1] polymeric species. Similarly one tricarbonyl precursor reacts with a tripodal triamine to form a [1 + 1] macrobicyclic compound while three dicarbonyl precursors react with a tripodal amine to form [3 + 2] macrobicyclic compounds (Scheme 1).

The success of these cyclization reactions is usually identified by analysis of the infrared spectrum of the product: this should contain no absorptions due to the primary amine or carbonyl groups but should have a new band due to the presence of the imine bonds. NMR and mass spectrometry measurements offer further useful indication about the cyclic product obtained. When suitable crystals are available, X-

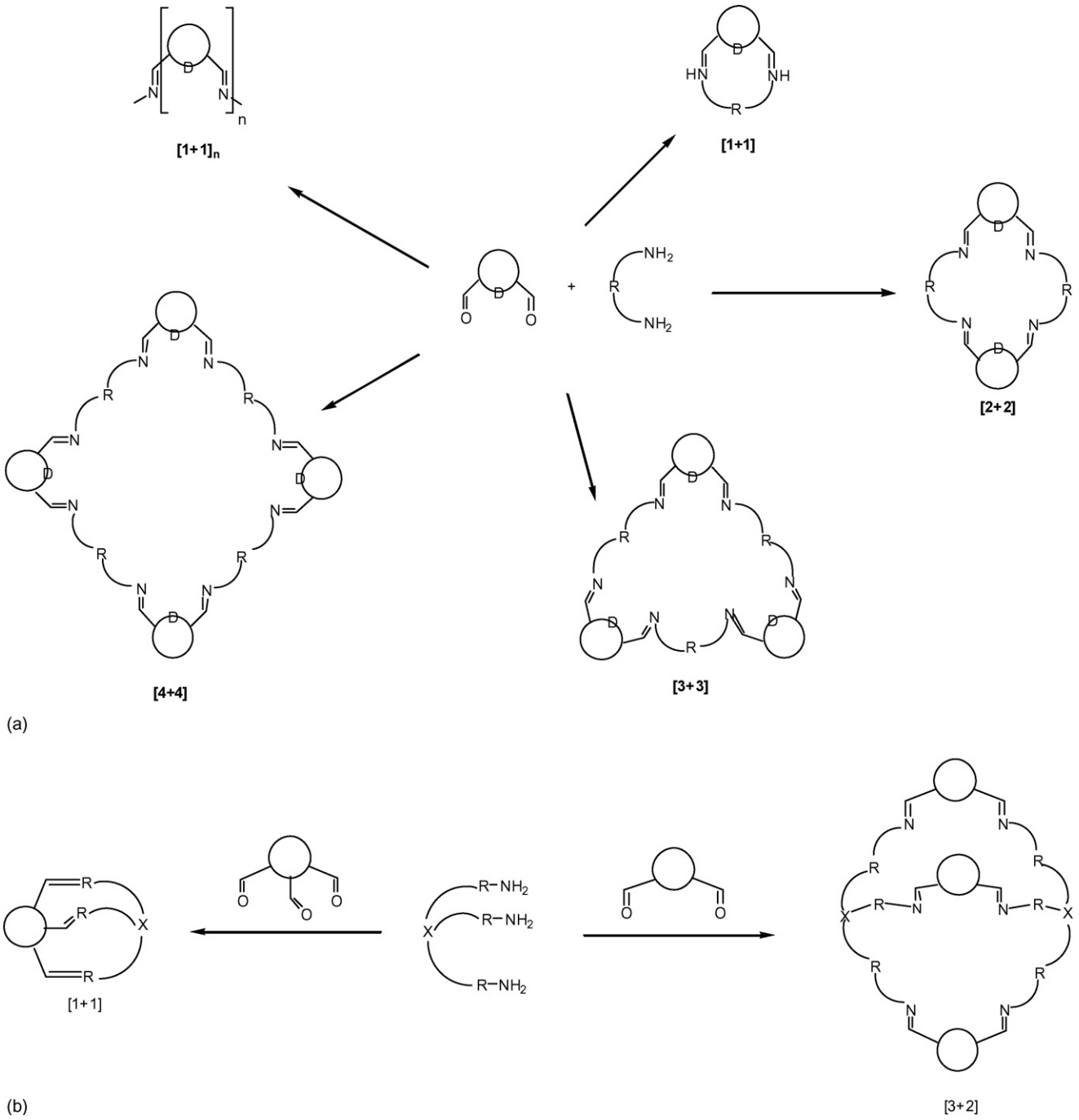

Scheme 1. Synthetic pathways of [1 + 1], [2 + 2], [3 + 3] or [4 + 4] macrocyclic and [1 + 1] polymeric (a) and macrobicyclic Schiff base derivatives (b) and their schematic representation (c).

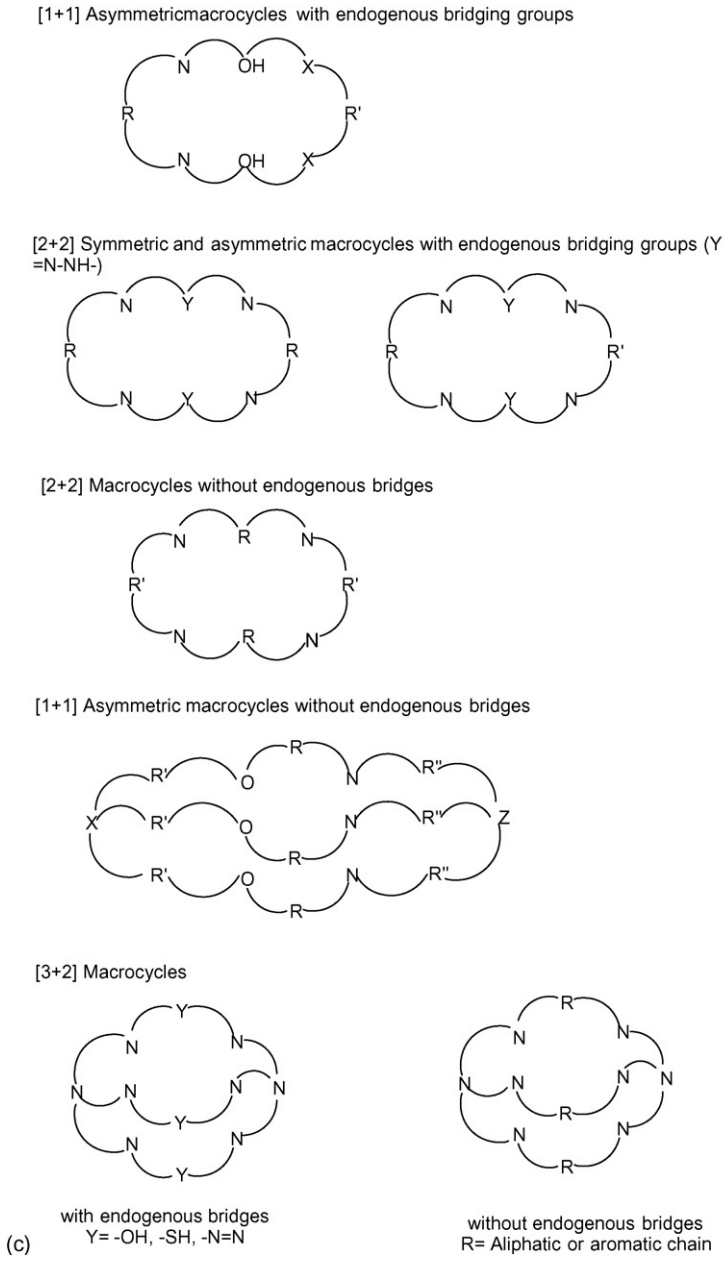

Scheme 1. (*Continued*).

ray diffractometric investigations give the final proof of the macrocyclic nature and the molecular complexity of these systems.

1.2. Aim of the review

This comprehensive list in addressed to review the most recent results obtained with compartmental macrocyclic or macropolycyclic Schiff bases and related reduced polyamines together with the homo- and/or heterodinuclear complexes mainly arising from their reaction with d- and/or f-metal ions and published between 2002 and 2005. The previous results on the same topics were covered by recent reviews [3,5]. Scheme 2 contains the diformyl-, diketo- or tripodal triformyl-precursors and the linear or tripodal polyamine derivatives especially used in the Schiff base condensation reactions, reported in the literature reviewed in the present article.

The preparation and properties of other, more sophisticated precursors and related macrocycles are reported in the appropriate sections together with their complexes.

The formyl-precursors can be derived into two classes: (i) those containing a bridging group between the formyl moieties; (ii) those containing a spacer group between the formyl moieties without bridging groups.

The employed amine precursors can bear additional donor groups in the lateral chains.

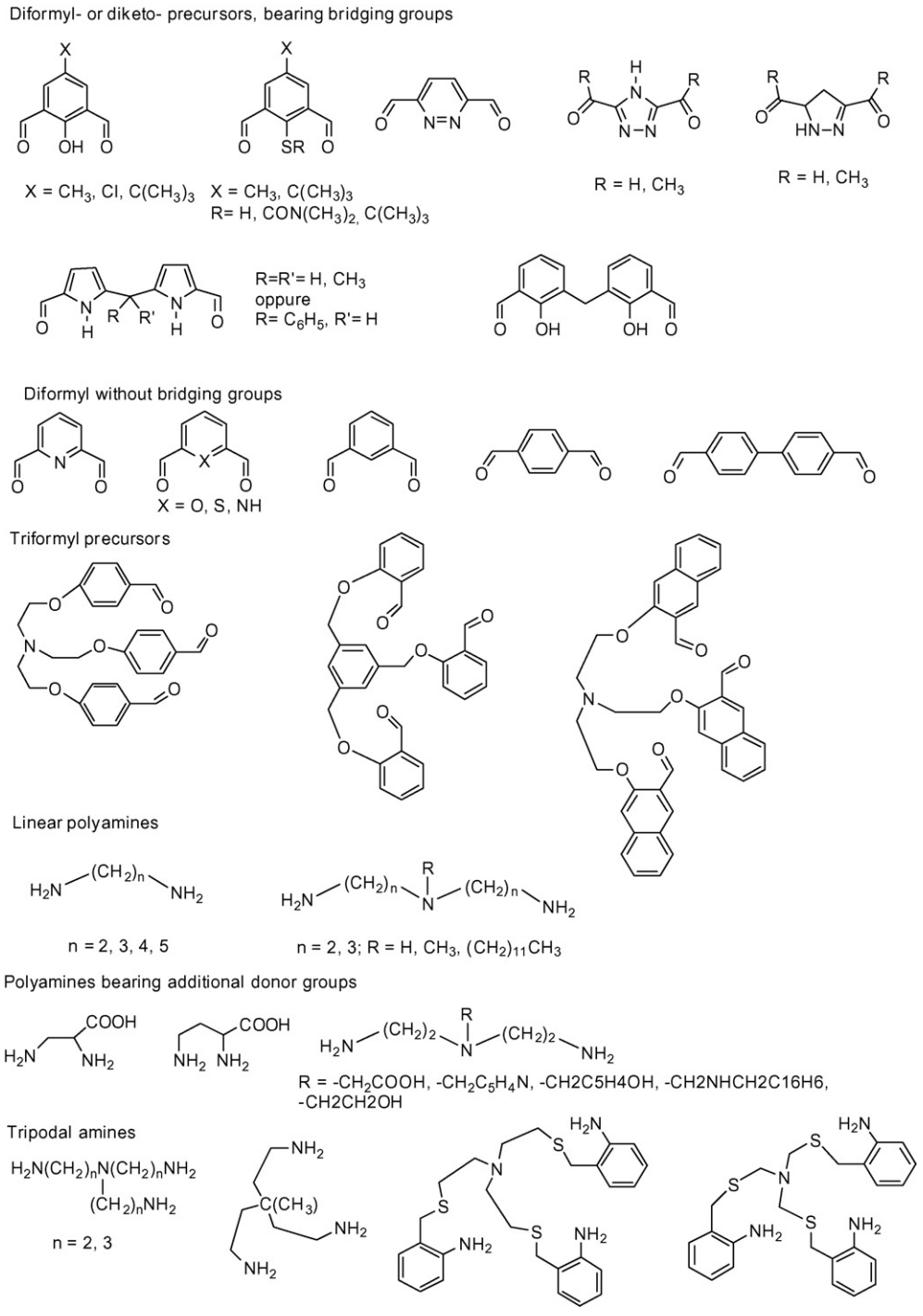

Scheme 2. Formyl- or keto- and amine precursors.

2. Macrocyclic Schiff base complexes and their reduced polyamine analogues

2.1. [1 + 1] macrocyclic ligands and related complexes

2.1.1. Phenolate-based systems

Variously diformyl precursors have been prepared respectively by the oxidation of 2,6-dimethanol-4-substitued phenol with MnO_2 in $CHCl_3$, (H-**1a**···H-**1c**) the reaction of 2,3-dihydroxy-benzaldehyde with the appropriate ditosilate derivative in the presence of NaH and in anhydrous dimethylsulphoxide (H_2-**3a**···H_2-**3c**), by the Mannich reaction of 5-substituted salicylaldehyde with the appropriate diamine and formaldehyde in alcoholic solution (H_2-**4**···H_2-**7**) or by reaction of the appropriate dioxadiazamacrocycle with 3-chloromethylsalicylaldehyde (H_2-**8**···H_2-**13**).

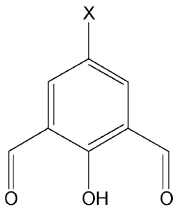

	x
H-**1a**	CH_3
H-**1b**	Cl
H-**1c**	$C(CH_3)_3$

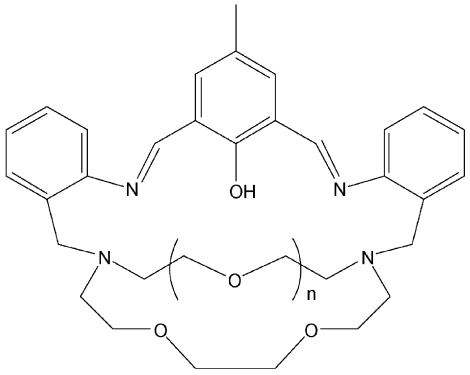

	n
H-**2a**	1
H-**2b**	2

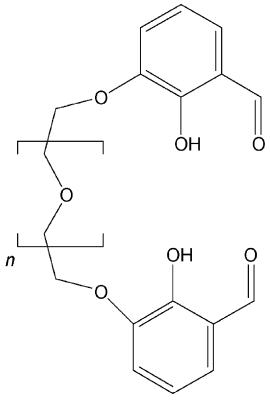

	n
H_2-**3a**	1
H_2-**3b**	2

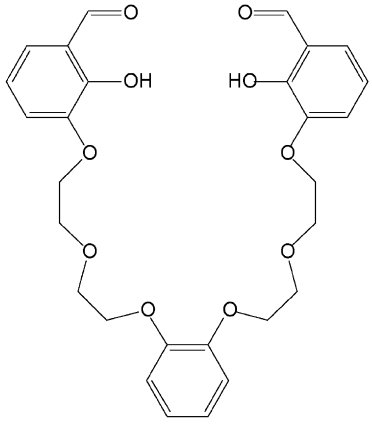

H_2-**3c**

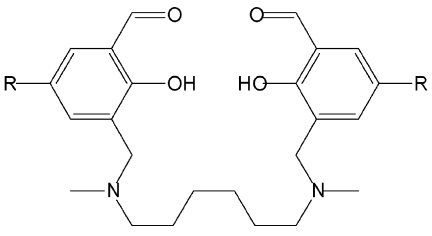

	R
H_2-**4a**	CH_3
H_2-**4b**	C_9H_{13}

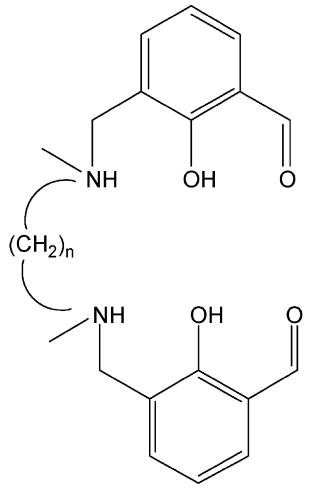

	n
H_2-**5**	2
H_2-**6**	3

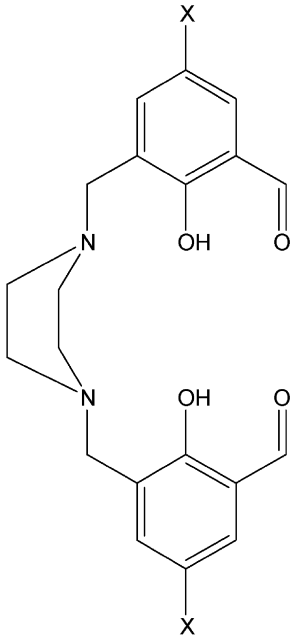

	X
H_2-**7a**	CH_3
H_2-**7b**	Br

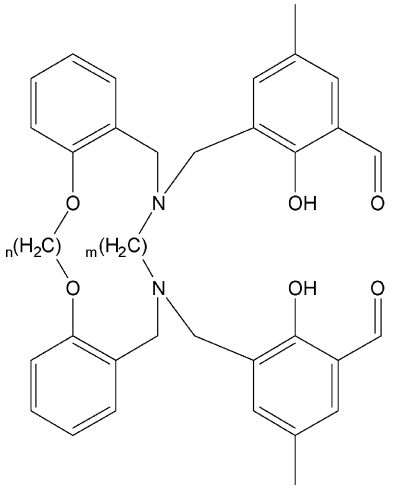

	n	m
H_2-**8**	2	2
H_2-**9**	2	3
H_2-**10**	2	4
H_2-**11**	3	2
H_2-**12**	3	3
H_2-**13**	3	4

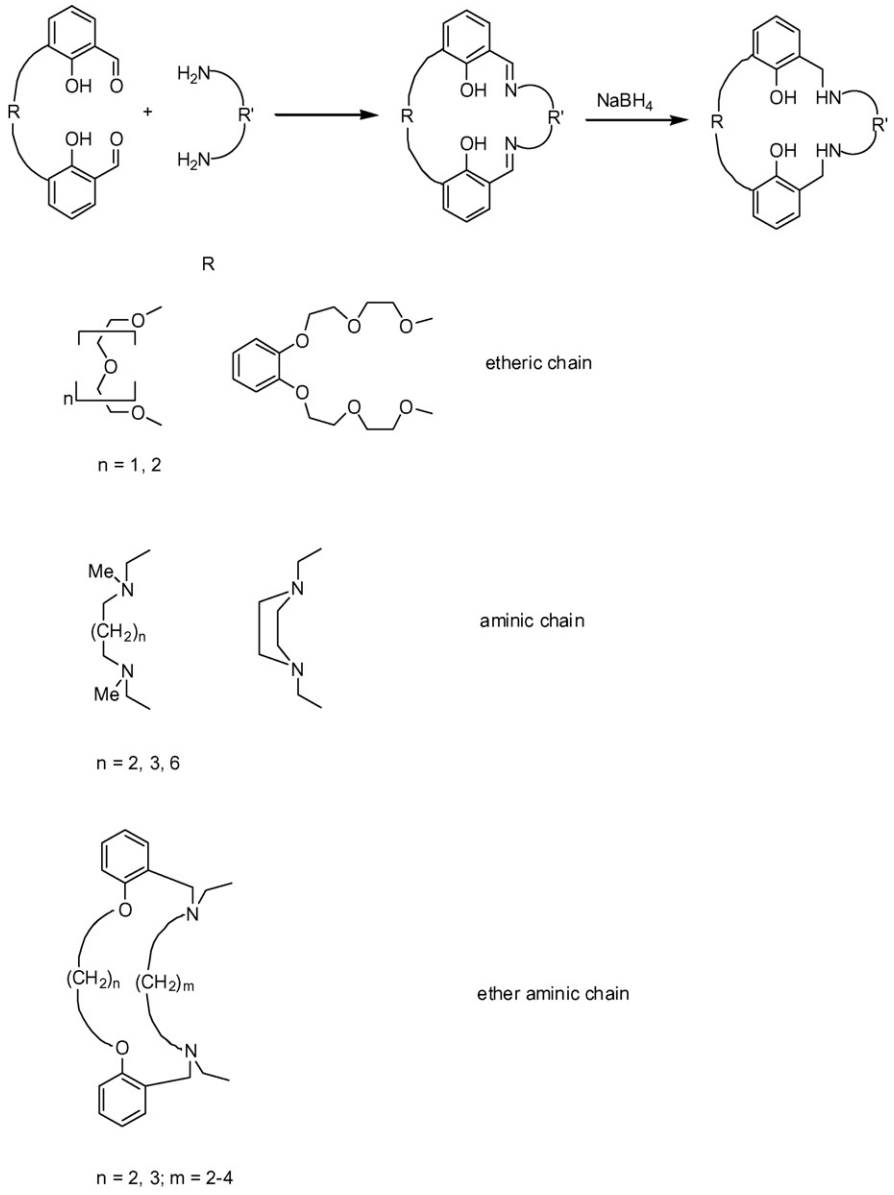

Scheme 3. Synthesis of the [1 + 1] compartmental macrocyclic Schiff base and their reduced polyamine derivatives.

According to the employed formyl- and/or amine precursors, differently shaped compartmental [1 + 1] macrocyclic Schiff bases and/or related complexes have been synthesized (Scheme 3). The formation of mononuclear complexes is of paramount relevance, because they represent the starting materials for further cation and/or anion selective recognition, transport and separation. They can be easily prepared when asymmetric compartmental ligands are employed because of the two different adjacent compartments which allow different and selective recognition processes.

It is well known that the diformyl derivatives **1a**–**1c** give rise to [2 + 2] Robson type symmetric compartmental macrocycles by self-condensation with primary diamines as H_2N-R-NH_2 (R = aliphatic or aromatic chain) or by template procedure in the presence of suitable metal ions [5]. The most recent examples of this class of compounds will be discussed in the appropriate section.

The same formyl derivatives, however, can form [1 + 1] macrocycles, when primary diamine containing appropriate chains are used. Thus, the bibracchial lariat ethers *N*,*N*′-bis(2-aminobenzyl)-1,10-diaza-15-crown-5 or *N*,*N*′-bis-(2-aminobenzyl)-4, 13-diaza-18-crown-6 form the related [1 + 1] macrocycles H-**2a** and H-**2b** by condensation with 2,6-diformyl-4-methylphenol in the presence of barium(II) and lead(II) salts as templating agents [6].

The effectiveness of barium(II) perchlorate to template the macrobicycles H-**2a** and H-**2b** and its ability to arrange the pendant arms of the diamine precursor *N*,*N*′-bis(2-aminobenzyl)-1,10-diaza-15-crown-5 or *N*,*N*′-bis(2-aminobenzyl)-4,13-diaza-18-crown-6 in a *syn* conformation was proved [5,6]. The corresponding template synthesis in the presence of barium thiocyanate under the same experimental conditions used with barium perchlorate was also tested. Whereas barium thiocyanate can template the formation of the largest macrobicycles H-**2b**

under the same experimental conditions used to prepare the barium perchlorate derivatives (i.e. 2–3 h of reaction in ethanol after complete addition of the precursors), it was not able to do it with the smaller H-**2a** [5,6]. Longer reaction times are necessary to get the expected macrobicycles H-**2a**, when barium thiocyanate is used as template of the reaction of the diamine precursor *N*,*N*′-bis(2-aminobenzyl)-1,10-diaza-15-crown-5 and 2,6-diformyl-4-methylphenol (a minimum of 2 days of refluxing and stirring).

Also, in the presence of thiocyanate, the barium(II) ion remains trapped in the formed macrobicyclic cavity and the corresponding macrocycle H-**2a** was isolated as the corresponding barium complex Ba(H-**2a**)$(SCN)_2{\cdot}2H_2O$. The compound behaves as 1:1 electrolyte in acetonitrile which confirms the presence of one thiocyanate group in the coordination sphere of barium(II) in this solution as it does in the solid state The X-ray structure confirms that the barium(II) ion is asymmetrically situated inside the macrocyclic cavity of H-**2a**, due to the proton transfer from the phenol group to the nitrogen atom of one of the imine groups. The barium ion is nine coordinate, bound to eight heteroatoms of the macrobicycle H-**2a** and to the nitrogen atom of a thiocyanate group.

A similar coordination was observed in the structure of $[Ba(H_2\text{-}\mathbf{2a})(ClO_4)(CH_3CN)](ClO_4){\cdot}0.5CH_3OH$. In the cation $[Ba(H\text{-}\mathbf{2a})(ClO_4)(CH_3CN)]^+$ the barium(II) ion is bound to seven of the eight heteroatom of H-**2a**, to the nitrogen atom of an acetonitrile molecule and to two oxygen atoms of one perchlorate group. The imine and phenol donors are involved in an intramolecular hydrogen-bonding interaction. Again a proton transfer from the phenol group to one imine atom has occurred. As a result, the protonated nitrogen does not belong to the coordination sphere of the barium(II) ion, which consequently is situated asymmetrically in the macrobicyclic cavity (Fig. 1a) [6].

The reaction of equimolar amounts of 2,6-diformyl-4-methylphenol and *N*,*N*′-bis(2-aminobenzyl)-4,13-diaza-18-crown-6 in the presence of lead(II) perchlorate in absolute ethanol gave $[Pb(H\text{-}\mathbf{2b})](ClO_4)_2{\cdot}2{\cdot}5H_2O$. IR and FAB-mass spectra confirmed that [1 + 1] cyclization condensation had occurred and the lead(II) complex was formed [6]. $[Pb(H\text{-}\mathbf{2b})](ClO_4)_2{\cdot}2{\cdot}5H_2O$ was also prepared by a transmetalation reaction using the corresponding barium complex, $[Ba(H\text{-}\mathbf{2b})](ClO_4)_2{\cdot}2H_2O$, and lead(II) perchlorate. The absence of peaks corresponding to species containing the {Ba(H-**2b**)} fragment in the FAB-mass spectrum coupled with the presence of peaks due to $[Pb(H\text{-}\mathbf{2b})(ClO_4)]^+$, $[Pb(H\text{-}\mathbf{2b})]^+$, and $[(H\text{-}\mathbf{2b}) + H]^+$ confirmed that the transmetalation reaction occurred and H-**2b** remained intact in the lead(II) complex [6].

In $[Pb(H\text{-}\mathbf{2b})](ClO_4)_2{\cdot}2{\cdot}5H_2O$ the lead(II) ion is asymmetrically placed at one end of the macrobicyclic cavity coordinated to one imine nitrogen atom, one pivotal nitrogen atom, the phenolate oxygen atom, and three oxygen atoms of the crown moiety. The other two heteroatoms of the macrobicyclic receptor, the imine and pivotal nitrogen atoms do not form a part of the lead(II) coordination environment The X-ray data suggest that proton transfer from phenol to imine nitrogen has occurred (Fig. 1b) [6].

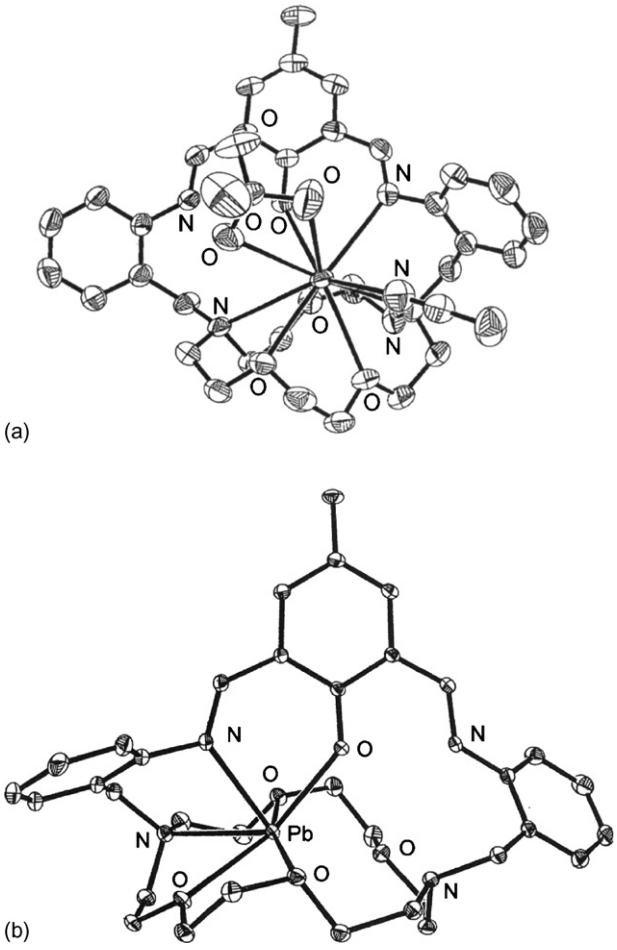

Fig. 1. Structure of $[Ba(H\text{-}\mathbf{2a})(ClO_4)(CH_3CN)]^+$ (a) and $[Pb(H\text{-}\mathbf{2a})]^{2+}$ (b).

The ^1H and ^{13}C NMR spectra of $[Pb(H\text{-}\mathbf{2b})](ClO_4)_2{\cdot}2{\cdot}5H_2O$ in CD_3CN indicate that this asymmetric structure is also maintained in solution [6].

The [1 + 1] macrocyclic Schiff bases derived from the diformyl-precursors $H_2\text{-}\mathbf{3}\cdots H_2\text{-}\mathbf{13}$, are asymmetric in nature and hence can give rise to mononuclear, homo- and heterodinuclear complexes, without positional isomers according to the experimental conditions employed.

The [1 + 1] cyclic Schiff bases $H_2\text{-}\mathbf{14}\cdots H_2\text{-}\mathbf{22}$, containing one N_2O_2 or N_3O_2 Schiff base site and one adjacent O_2O_3 or O_2O_4 crown-ether like site, have been prepared as yellow or yellow-orange air stable solids by self-condensation in methanol, under diluted conditions, of equimolecular amounts of the diformyl precursors $H_2\text{-}\mathbf{3a}$ or $H_2\text{-}\mathbf{3b}$ and the appropriate polyamine. They can be obtained also by demetalation with guanidinium sulphate of the appropriate macrocyclic barium diperchlorate complex, followed by extraction of the metal free macrocycle with $CHCl_3$. The [1 + 1] cyclic nature of these systems was inferred by FAB- and/or ESI-mass spectra, where the formation of the parent peak $[M + H]^+$ and/or $[M + Na]^+$ at the appropriate *m*/*z* values were detected [7].

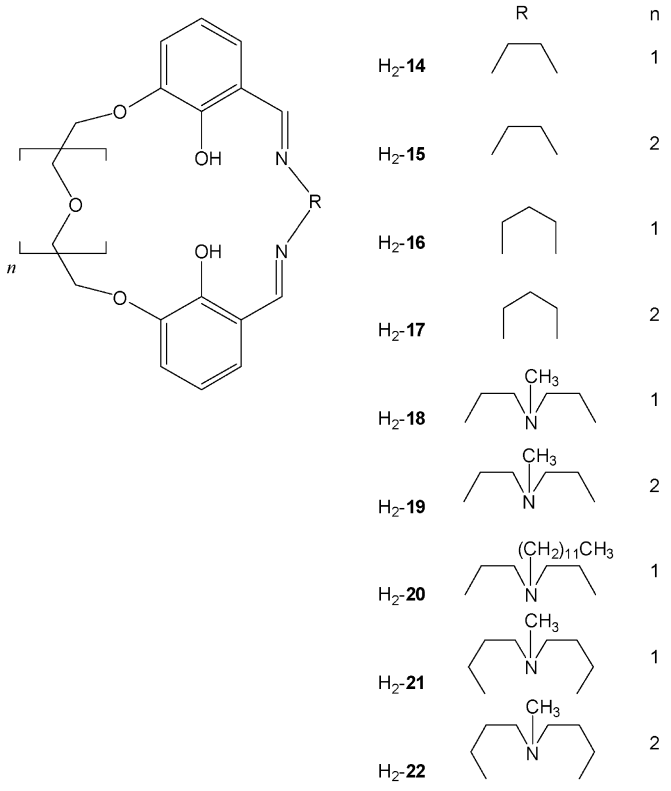

The similar series of macrocyclic compounds $[Na_2(L)]\cdot nH_2O$, containing a sodium(I) ion also into the crown-ether chamber, have been prepared using [Na_2(**3a**)] instead of H_2-**3a** as formyl precursor. It must be noted that [Na_2(**3a**)] was obtained as a yellow intermediate product during the above mentioned synthesis of the diformyl precursor H_2-**3a**, by reaction in anhydrous dimethylsulphoxide of diethyleneglicol ditosylate with 2,3-dihydroxybenzaldehyde in the presence of NaH [7].

In solution and/or in consequence of crystallization efforts, $[Na_2(L)]\cdot nH_2O$ can evolve into the mononuclear one $Na(H–L)\cdot nH_2O$, where the sodium(I) ion resides into the crown-ether chamber [7].

The condensation of 2,3-diaminopropionic acid monochlorohydrate or 2,4-diaminobutirric acid dichlorohydrate with 3,3′-(3-oxapentane-1,5-diyldioxy)bis(2-hydroxybenzaldehyde) in the presence of NaOH affords the [1 + 1] cyclic complexes Na(H_2-**23**)·H_2O and Na(H_2-**24**)·H_2O [7].

The cyclic Schiff bases H_2-**14**···H_2-**22** (or their sodium derivatives) have been reduced to the corresponding polyamines H_2-**25**···H_2-**31** by reaction with an excess of $NaBH_4$. The compounds are soluble in chlorinated solvents and insoluble in H_2O and hence can be purified by extracting the residue of the reaction with $CHCl_3$. The reduced polyamine derivatives maintain the [1 + 1] cyclic nature of the related Schiff bases as indicated by IR, NMR and mass spectrometry and confirmed by the single-crystal X-ray structure of [Na(H-**29**)]H_2O (Fig. 2) [6]. In this 'the five oxygen atoms of the macrocycle coordinate the sodium ion which occupies the vertex of a pentagonal pyramid. This constraints the whole molecule to assume a butterfly like shape with the wings constituted by the two benzene rings. Surprisingly, the sodium ion does not form other bonds or contacts, so it appears empty on the opposite side with respect to the ligand. The oxygen atoms form a plane, from which the sodium ion displaces of 0.79 Å [7].

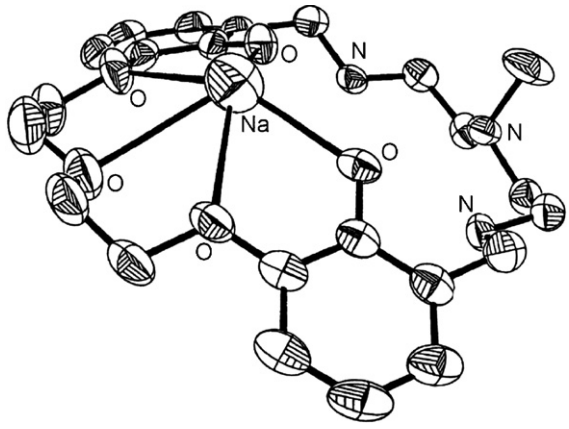

Fig. 2. Structure of [Na(H-**29**)].

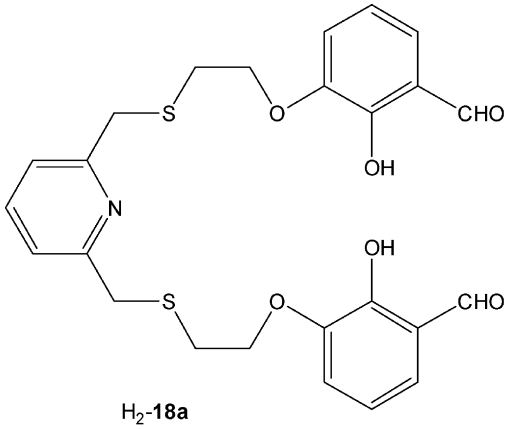

H_2-**18a**

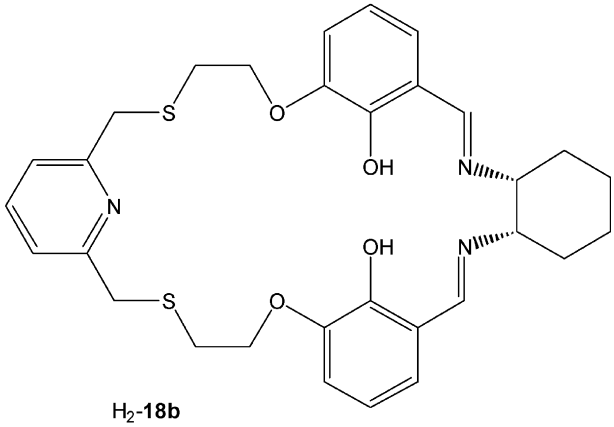

H_2-**18b**

The presence of a Schiff base site or of its reduced analogue respectively in H_2-**14**···H_2-**24** and H_2-**25**···H_2-**31** makes the preparation of transition metal complexes highly feasible. They have been synthesized by template condensation of the formyl- and amine precursors in the presence the appropriate metal salt

or by reaction of the preformed ligand with the desired metal salt. Thus, the Schiff bases H_2-**14**, H_2-**15**, H_2-**18** and H_2-**19** react with equimolecular amounts of $M(CH_3COO)_2{\cdot}nH_2O$ ($M = Cu^{II}$, Ni^{II}, Co^{II}) or $Mn(CH_3COO)_2{\cdot}2H_2O$ in refluxing alcoholic solution to form respectively $M(L){\cdot}nH_2O$ and $Mn(L)(CH_3COO){\cdot}nH_2O$. The same copper(II) and nickel(II) complexes have been obtained also by template procedure [7].

ESI-mass spectra exhibit the parent peak $[M(\mathbf{L})]^+$ at the appropriate *m/z* value. In particular when copper(II) salts were used, the complexes $[Cu(\mathbf{L})]{\cdot}H_2O$ were obtained while with the other metal ions M(**L**), M(H-**L**)(X) or $M(H_2\text{-}\mathbf{L})(X)_2$ ($X = Cl^-$, CH_3COO^-) are obtained, depending on the experimental conditions used. In strong basic media the complexes $M(\mathbf{L}){\cdot}nH_2O$ are obtained. These data are in line with a parallel potentiometric study which shows that the different complexes $[M(H_2\text{-}\mathbf{L})]^{2+}$, $[M(H\text{-}\mathbf{L})]^+$ and $[M(\mathbf{L})]$ are the predominant species in particular pH ranges [8]. These investigations also prove that the coordination of a metal ion (i.e. Cu^{II}) strongly stabilizes the Schiff bases in a large range of pH (3–11) and prevents their easy hydrolysis. This result opens new possibilities in the use of these systems in water solution usually forbidden to the Schiff bases.

The similar reaction of the preformed ligand H_2-**20** with copper(II) or nickel(II) acetate hydrate or the condensation of equimolar amount H_2-**3a** with 1,5-diamino-3-aza(dodecyl)pentane in the presence of the same metal salt gives rise to the complexes $[M(H_2\text{-}\mathbf{20})(CH_3COO)_2]{\cdot}nH_2O$. In the nickel(II) complex the metal ion has probably an octahedral environment with the acetate groups acting as monodentate ligands [7].

The reduced macrocycle H_2-**26** forms, when reacted with $Cu(CH_3COO)_2{\cdot}H_2O$ or $Mn(CH_3COO)_2{\cdot}2H_2O$ in a $CHCl_3$/CH_3OH and in a 1:1 molar ratio, respectively, $[Cu(\mathbf{26})]{\cdot}H_2O$ and $[Mn(\mathbf{26})(CH_3COO)]{\cdot}2H_2O$. Using the same experimental conditions, $Ni(CH_3COO)_2{\cdot}4H_2O$ and $Co(CH_3COO)_2{\cdot}4H_2O$ give rise respectively to $[Ni(H_2\text{-}\mathbf{26})(CH_3COO)_2]$ and $[Co(H_2\text{-}\mathbf{26})(CH_3COO)_2]$. Magnetic and UV–vis measurements indicate an octahedral configuration about the nickel(II) and cobalt(II) ion. For $[Mn(\mathbf{26})(CH_3COO)]{\cdot}2H_2O$ possibly a pentacoordination occurs while for $[Cu(\mathbf{26})(H_2O)]{\cdot}H_2O$ a square pyramidal pentacoordination about the metal ion was suggested [7].

These mononuclear complexes contain a free crown-ether like coordination chamber; hence they can be conveniently used as ligands for further complexation reactions. In particular, taking into consideration that sodium ion prefers the crown-ether site as ascertained by the X-ray structure of [Na(H-**29**)]·H_2O, they can be proposed as suitable receptors for the recognition of the sodium(I) ion. Similarly, the sodium(I) complexes can be used as receptors for transition metal ions. The final products are in both cases the same d,s-heterodinuclear complexes, where the transition metal ion occupies the Schiff base site and the sodium ion the crown-ether moiety, independently from the shape of the coordination chambers. Thus, by reaction of equimolar amount of the cyclic Schiff base (also prepared in situ) with the appropriate transition metal acetate in the presence of two equivalents of NaOH, the heterodinuclear complexes $MNa(L)(CH_3COO){\cdot}nH_2O$ ($M = Cu^{II}$, Ni^{II}, Co^{II}) and $MnNa(L)(CH_3COO)_2{\cdot}nH_2O$ ($H_2\text{-}L = H_2$-**14**, H_2-**15**, H_2-**18**, H_2-**19**, H_2-**22**) have been obtained. The same complexes have been prepared by the template condensation of the appropriate precursors in the presence of $M(CH_3COO)_2{\cdot}nH_2O$ and NaOH [7].

The magnetic moments and the UV–vis spectra of the complexes with H_2-**15** show that the square planar N_2O_2 coordination about the transition metal ion is maintained upon sodium(I) complexation.

These reactions give rise to the designed heterodinuclear complexes in high yield and in one pot owing to the above mentioned high selectivity of the two sites of the ligands respectively for the d transition metal ion and the sodium ion and hence to the impossibility to give rise to scrambling or migration reactions. The same complexes have been obtained when the preformed mononuclear transition metal complexes are reacted with sodium acetate or when the reaction of the acyclic sodium complex, $[Na_2(\mathbf{3a})]{\cdot}nH_2O$ or $[Na_2(\mathbf{3b})]{\cdot}nH_2O$ with the appropriate polyamine in the presence of the desired transition metal salt was carried out.

The [1 + 1] cyclic functionalized sodium Schiff bases $Na(H_2\text{-}\mathbf{23})\cdot H_2O$ and $Na(H_2\text{-}\mathbf{24})\cdot H_2O$, obtained by condensation of the H_2-**3a** with the appropriate amine precursor in the presence of NaOH, form $NiNa(\mathbf{23})\cdot H_2O$ or $NiNa(\mathbf{24})\cdot H_2O$ when reacted with nickel(II) acetate in a 1:1 molar ratio. A template procedure affords the same complexes. IR data suggest that the carboxylate group is also involved in the coordination to the transition metal ion which shows an octahedral coordination [7].

Analogously, the heterodinuclear complexes $MNa(R)(CH_3COO){\cdot}nH_2O$ or $MnNa(R)(CH_3COO)_2{\cdot}nH_2O$ ($H_2\text{-}R = H_2$-**25**$\cdots H_2$-**31**) have been obtained by reaction of the reduced macrocycles H_2-R with the appropriate metal acetate hydrate in the presence of NaOH in a molar ratio 1:1:2 [7].

Quantitative ^2H NMR analysis at the natural abundance represents a well recognized and efficient method for the identification of the origin of ethanol from different sources. An intrinsic limitation of the protocol used is the long time required, about 8 h, because of the long T_1 values of the ^2H resonances. $[Gd(H_2\text{-}\mathbf{18})(H_2O)_3(C_2H_5OH)](Cl)_3{\cdot}C_2H_5OH$, highly stable and soluble in alcoholic solution, was used as paramagnetic relaxation agent that significantly catalyzes the relaxation times and reduces the total time of quantitative ^2H NMR analysis at the natural abundance for the identification of the origin of ethanol from different sources. A characterization of the paramagnetic complex has been achieved by measuring the magnetic field dependence of the ^1H longitudinal nuclear magnetic relaxation time of a 1 mM solution in CH_3OD with a field-cycling relaxometer. The gadolinium(III) ion accommodates up to four methanol molecules in its inner coordination sphere, whose rapid exchange with the bulk provides an efficient relaxation mechanism. The addition of about 37 mg of the complex to a solution of ethanol (3.0 g) and tetramethylurea (1.5 g) results in the reduction of the experimental time of more than 50% with a S/N ratio compatible with that required for this application. The results show that a significant reduction in the time required for the use of the Martin method could be pursued by the addition of a suitable paramagnetic agent to the alcoholic specimen whose H/D partition has to be determined. The main drawback associated with this procedure is a significant broadening of the ethanolic resonances. One

may envisage the possibility of limiting this paramagnetically induced line broadening by improving the design of the metal complex without decreasing too much its relaxation efficiency. Moreover, a better understanding of the coordination properties of ethanol in this class of ternary complexes may provide novel insights for the development of specific shift reagents for ethanol for which one may foresee interesting applications [9].

Although the preformed Schiff bases H_2-**14**$\cdots H_2$-**17** can give rise to the mononuclear complexes [M(**L**)] (M = Cu^{II}, Ni^{II}, Zn^{II}) or [Ln(H_2-**L**)(H_2O)$_4$](Cl)$_3$ when reacted with the appropriate metal salt, the template procedure has to be preferred owing to the tedious and time consuming procedure for obtaining the [1 + 1] macrocycle in an acceptable degree of purity and yield [10].

Three different synthetic pathways afford the same d,f-heterodinuclear complexes although at times with a different solvent content: (i) reaction of M(**L**)·$n$$H_2O$ with $LnCl_3$·$n$$H_2O$; (ii) reaction of [Ln($H_2$-**L**)($H_2O$)$_4$]($Cl$)$_3$ with metal(II) chloride; and (iii) one pot reaction. However, it was verified that the complexes [Ln(H_2-**L**)(H_2O)$_4$](Cl)$_3$ are the most convenient ligand precursors and thus all the complexes were prepared by using the second procedure. The other two procedures were successfully tested in order to verify the feasibility [10].

The one-pot reaction, in particular, clearly shows that these ligands have the correct coordination moiety for a contemporary selective recognition of a d- and a 4f-metal ion. Thus, the heterodinuclear complexes [MLn(**L**)(Cl)$_3$(CH_3OH)] have been conveniently synthesized by treating the desired mononuclear lanthanide(III) complex [Ln(H_2-**L**)(H_2O)$_4$](Cl)$_3$ in hot methanol with MCl_2 (M = Cu^{II}, Ni^{II}, Zn^{II}) in the presence of N(Et)$_3$. However, the stability especially in solution of these heterodinuclear complexes varies considerably when changing the coordination shape of the two chambers. Because the complexes [MLn(**14**)(Cl)$_3$(CH_3OH)], though formed, are not stable enough in solution and attempts of crystallization failed, progressive enlargement the two bites was tested [7]. Again, the heterodinuclear $M^{II}Ln^{III}$ complexes of the macrocycles H_2-**15** and H_2-**16** are not stable in solution and tend to eliminate partially one of the two metal ions. When the correct coordination shape is used, i.e. with the ligand H_2-**17** where an enlargement of the aliphatic chain from CH_2CH_2 to $CH_2CH_2CH_2$ at the N_2O_2 chamber and a changing of the crown-ether chain from O_2O_3 to O_2O_4 with the addition of a –CH_2CH_2O– group occur, the resulting $M^{II}Ln^{III}$ complexes are very stable in solution and readily crystallized [10].

In the isostructural complexes [MLn(**17**)(Cl)$_3$(CH_3OH)] (MLn = $Cu^{II}La^{III}$, $Zn^{II}La^{III}$, $Cu^{II}Tb^{III}$) each lanthanide(III) ion is located in the O_2O_4 site and reaches the coordination number of nine by bonding the six oxygen atoms of the ligand, two chloride ions and the oxygen atom of one methanol molecule. The transition metal(II) ion occupies the N_2O_2 chamber, the phenolate oxygens working as bridges between the coordinated metal ions. The geometry around the lanthanide ions has been described as an hexagonal bipyramid, where the base is formed by the six oxygen atoms of the macrocycle. One vertex is a chloride ion, the other is the mid-point between the second chloride ion, and the oxygen of the coordinated methanol molecule. The polyhedron around the transition metal ion is a square pyramid, where the base is formed by the two phenolic bridging oxygens and the two iminic nitrogen atoms of the macrocycle, and the apex is occupied by the third chloride ion (Fig. 3a).

X-ray powder diffractograms of the dinuclear complexes [CuCe(**17**)(Cl)$_3$(CH_3OH)], [CuGd(**17**)(Cl)$_3$(CH_3OH)], [ZnCe(**17**)(Cl)$_3$(CH_3OH)], [ZnGd(**17**)(Cl)$_3$]·3H_2O and [ZnTb(**17**)(Cl)$_3$($EtOH$)] compared with that obtained by calculation from single crystal diffraction data of the $Cu^{II}La^{III}$ complex, demonstrate that the $Cu^{II}Ce^{III}$, $Zn^{II}Ce^{III}$, $Cu^{II}Gd^{III}$ and $Cu^{II}La^{III}$ complexes are all isostructural. Conversely, the diffractograms of the $Zn^{II}Tb^{III}$ and $Zn^{II}Gd^{III}$ complexes are different from each other and from the $Cu^{II}La^{III}$ one. In any case, the results obtained through the other physico-chemical characterization techniques strongly suggest that the coordination environment of the metal ion is closely related to that observed in the $Cu^{II}La^{III}$ and the isostructural compounds [10].

In the $Cu^{II}Gd^{III}$ complex a ferromagnetic coupling between Cu^{II} and Gd^{III} occurs (J = 2.49 cm^{-1}). The same magnetic behaviour was found in the $Cu^{II}Tb^{III}$ complex while in the $Cu^{II}Ce^{III}$ complex an antiferromagnetic interaction between the two metal ion seems to be operating [10].

[LnNa(**18**)(Cl)$_2$(CH_3OH)(H_2O)](Cl) (Ln = Tb^{III}, Dy^{III}, Tm^{III}, Yb^{III}) were prepared via transmetalation route of [LnNa(**18**)(Cl)$_2$(CH_3OH)] with an equimolar quantity of $CaCl_2$ in methanol, followed by crystallization of the resulting powder to eliminate the sodium chloride formed [11]. Similarly [LnLi(**18**)(Cl)$_2$(CH_3OH)] and [LnK(**18**)(Cl)$_2$(CH_3OH)] have been prepared [11].

The ^{1}H NMR spectra of the paramagnetic $Ln^{III}Ca^{III}$ complexes closely resemble those of the corresponding LnNa complexes. The strict similarity, in terms of chemical shift and bandwidth, between the set of proton resonances for [LnCa(**18**)(Cl)$_2$(CH_3OH)](Cl) and [LnCa(**18**)(Cl)$_2$(CH_3OH)] strongly suggests that in both cases the lanthanide ion is coordinated in the N_3O_2 Schiff base site. IR data agree with this suggestion.

In [YbCa(**18**)(Cl)$_2$(C_2H_5OH)(H_2O)](Cl)·2H_2O the macrocyclic ligand coordinates the ytterbium ion in the O_2N_3 chamber and the calcium ion in the O_2O_3 site. The heptacoordination around the lanthanide ion is completed by two chlorine ions in *trans* to each other and the resulting coordination geometry has been depicted as a pentagonal bipyramid with the two chloride ions in the apical positions. Another chloride ion and two water molecules are not coordinated. The calcium ion is heptacoordinated, being bonded to the two phenolic oxygen atoms, that act as a bridge to the ytterbium ion, to the three etheric oxygen atoms of the ligand and to one ethanol and one water molecules. A significant contact is also present between the calcium ion and the chloride ion, and this increases the coordination number of calcium ion to eight. Consequently, the coordination polyhedron has also been described as a square antiprism (Fig. 3b) [11].

The comparison between [YbCa(**18**)(Cl)$_2$(C_2H_5OH)(H_2O)]-(Cl)·2H_2O and [YbNa(**18**)(Cl)$_2$(CH_3OH)] [12] indicates remarkable differences in spite of the very similar ionic radii of the two metal ions (0.97 and 0.99 Å for Na^I and Ca^{II}, respec-

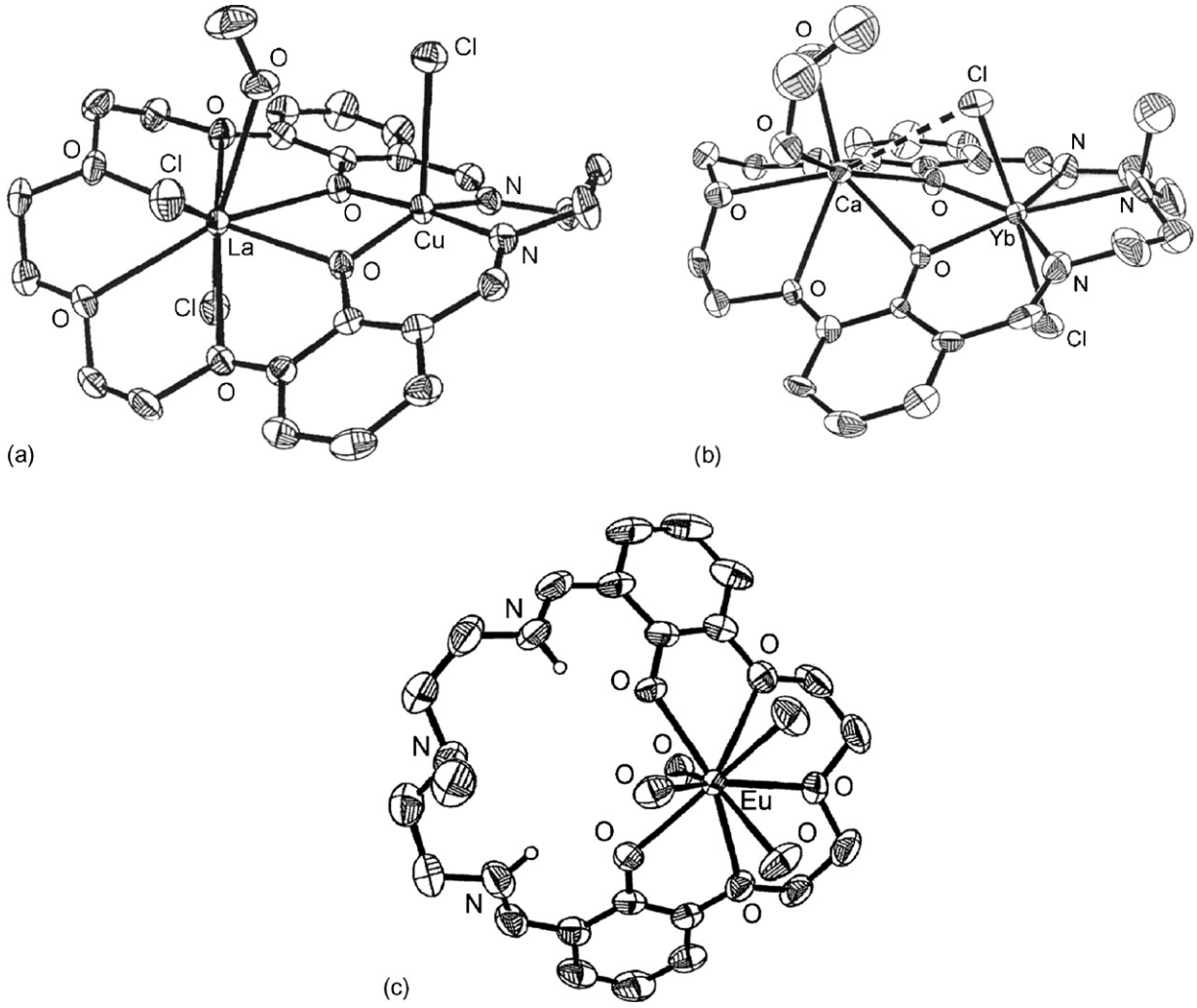

Fig. 3. Structure of [CuLa(**17**)$(Cl)_3(CH_3OH)$] (a) $[YbCa(\mathbf{18})(Cl)_2(C_2H_5OH)(H_2O)]^+$ (b) and $[Eu(H_2\text{-}\mathbf{18})(H_2O)_4]^{3+}$ (c).

tively). The most important structural difference is related to the coordination polyhedron around the sodium(I) and the calcium(II) ions: pentagonal pyramid for the former and square antiprism for the latter.

The selectivity of the etheric site toward alkali and alkaline earth metal ions has been quantitatively assessed by evaluating with ^{23}Na NMR the transmetalation reaction involving the coordinated sodium(I) ion in the complexes [LnNa(**18**)$(Cl)_2(CH_3OH)$] (Ln = Tb^{III}, Dy^{III}, Tm^{III}, Yb^{III}) and lithium(I), potassium(I) or calcium(II) ions. The affinity constants follow the general order $K_{Ca^{II}} \gg K_{Li^{I}} \geq K_{K^{I}}$ Quantitative kinetic analyses, performed on the complex [TmNa(**18**)$(Cl)_2(CH_3OH)$] with the use of ^{23}Na NMR spectroscopy at variable temperature in CD_3OD, prove that the exchange rate Na_{bound}/Na_{free} is independent from the presence of increasing amounts of water in the methanolic solution [11].

H_2-**18**, H_2-**19** and H_2-**21**, containing one Schiff base site with a N_3O_2 donor set connected by $–CH_2CH_2–$ or $–CH_2CH_2CH_2–$ aliphatic chains and one crown-ether like site with a O_2O_3 or O_2O_4 donor set, offer the possibility to verify the site occupancy preference of the lanthanide(III) ions in the solid state and in methanol or dimethylsulphoxide solutions, particularly the role of the different adjacent cavities on the formation of positional pure mononuclear complexes and consequently of pure heterodinuclear positional complexes on varying the cavity radius and the number of donor atoms [13].

In the mononuclear lanthanide(III) complexes Ln(H_2-L)$Cl_3 \cdot n H_2O$ (Ln = La^{III}, Ce^{III}, Pr^{III}, Nd^{III}, Sm^{III}, Eu^{III}, Gd^{III}, Tb^{III}, Dy^{III}, Ho^{III}, Er^{III}, Tm^{III}, Yb^{III}, Lu^{III}, Y^{III} for H_2-**18**; Ln = Lu^{III}, Eu^{III}, Tb^{III} for H_2-**17**, Ln = La^{III}, Eu^{III}, Tb^{III}, Ce^{III} for H_2-**21**) the lanthanide(III) ion resides into the crown-ether chamber in the solid state as verified by the X-ray structural determination of $[Ln(H_2\text{-}\mathbf{18})(H_2O)_4](Cl)_3$ (Ln = Ce^{III}, Gd^{III}, Dy^{III}, Lu^{III}) and more recently of $[Eu(H_2\text{-}\mathbf{18})(H_2O)_4](Cl)_3$, where the metal ion invariantly occupies the O_2O_3 crown-ether chamber in a nine coordinate environment, the remaining coordination positions being filled by the oxygen atoms of four water molecules. Remarkably, the two protons are bound to the imine nitrogen atoms and not to the phenolic oxygen atoms [13–15] (Fig. 3c).

When the mononuclear complexes $[Ln(H_2\text{-}\mathbf{L})(H_2O)_4](Cl)_3$ are dissolved in methanol, the lanthanide(III) ion prefers to lie in the crown ether site, possibly because of the protonation of the iminic nitrogens of the Schiff base as ascertained by the X-ray crystal structure of the europium(III) derivative with H_2-**18**. In dimethylsulphoxide a partial demetalation process, favoured by the solvent, occurs. This process can be followed by a site migration depending on the shape of the chambers: with H_2-**18** the metal ion prefers, although not exclusively, the N_3O_2 site and the final event is a mixture of the two isomers together with the free ligand; with H_2-**21** the [17]-membered N_3O_2 site is too large and does not accommodate any lanthanide ion and the final event is here a complete demetalation of the ligand; with H_2-**19** the [15]-membered N_3O_2 site fits well for the lanthanide ions while the [16]-membered O_4O_2 site does not. Furthermore, the enlargement of the whole coordination moiety, makes the N_3O_2 site more suitable for the lanthanide(III) ion; here the final event is an almost complete coordination of the lanthanide(III) ion into the Schiff base.

In order to verify the possibility to coordinate two lanthanide(III) ions inside the two adjacent coordination chambers of the ligands H_2-**18**, H_2-**19** and H_2-**21**, the formation of homodinuclear complexes was carried out first. Although the homodinuclear complexes $Ln_2(\mathbf{L})(Cl)_4{\cdot}4H_2O$ can be prepared through a step by step procedure by the reaction of the mononuclear complexes $[Ln(H_2\text{-}\mathbf{L})(H_2O)_4]Cl_3$ with $LnCl_3{\cdot}nH_2O$ and $[N(Et)_4](OH)$ in alcoholic solution and in a 1:1:2 molar ratio, the most convenient synthetic procedure is the one pot condensation in methanol of the appropriate diformyl- and amine-precursors in the presence of $LnCl_3{\cdot}nH_2O$ and $[N(Et)_4](OH)$ in a 1:1:2:2 molar ratio. The use of $[N(Et)_4](OH)$ instead of NaOH in the syntheses of lanthanide(III) complex with H_2-**18** was necessary for obtaining the homodinuclear complexes instead of heterodinuclear LnNa ones. For H_2-**19** and H_2-**21** the use of $[N(Et)_4](OH)$ was crucial to avoid the coprecipitation of NaCl with the complex. The elemental analyses, the homogeneity and the Ln:Cl = 1:2 ratio, determined by SEM-EDS, indicate that the homodinuclear complexes really occur. These complexes are no longer stable in solution and easily turn into the mononuclear ones with the metal ion in the crown ether site. Thus, attempts to recrystallize the homodinuclear complex $Eu_2(\mathbf{18})(Cl)_4{\cdot}4H_2O$ give rise to the mononuclear compound $[Eu(H_2\text{-}\mathbf{18})(H_2O)_4](Cl)_3$, as proved by the X-ray structural determination above reported, where the lanthanide(III) ion remains into the O_2O_3 site. The formation of homodinuclear complexes, which confirms that two lanthanide(III) ions can fill both the adjacent chambers of the prepared macrocyclic ligands, together with the availability of the O_2O_n pure positional mononuclear complexes, indicates that the synthesis of positionally pure heterodinuclear isomers could be feasible, at least in methanol, where the mononuclear complexes appear to be stable, with no or negligible lanthanide(III) site migration from the crown ether to the Schiff base site. Thus, the reaction of equimolar amounts of the appropriate mononuclear complex $[Ln(H_2\text{-}\mathbf{L})(H_2O)_4]Cl_3$ and the desired lanthanide(III) chloride, $Ln'Cl_3{\cdot}nH_2O$, in the presence of two equivalents of $[N(Et)_4](OH)$ would form the heterodinuclear complex $LnLn'(\mathbf{L})(Cl)_4{\cdot}nH_2O$ with the original lanthanide(III) ion (Ln) in the O_2O_n site and the incoming different lanthanide(III) ion (Ln′) in the N_3O_2 Schiff base site (not always true as demonstrated in solution studies). The preparation of a series positional isomeric heterodinuclear complexes was attempted following this synthetic pathway For instance, the reaction of $[Lu(H_2\text{-}\mathbf{21})(H_2O)_4](Cl)_3$ with $EuCl_3{\cdot}nH_2O$ would afford $LuEu(\mathbf{21})(Cl)_4{\cdot}nH_2O$ while the reaction of $[Eu(H_2\text{-}\mathbf{21})(H_2O)](Cl)_3$ with $LuCl_3{\cdot}nH_2O$ would give rise to the positional isomer $EuLu(\mathbf{21})(Cl)_4{\cdot}nH_2O$. Indeed, heterodinuclear complexes with the correct stoichiometry have been obtained as yellow orange precipitates from the alcoholic solution on partial evaporation of the solvent or by addition of small amount of diethyl ether. The presence in these complexes of two different lanthanide ions has been confirmed by SEM-EDS measurements which indicate a correct Ln:Ln′:Cl = 1:1:4 ratio [13].

ESI-mass spectra in methanol of homo- and heterodinuclear lanthanide(III) complexes show only the parent peak of the mononuclear complex indicating, as above reported, that the complexes are not stable in this solution [13].

Both homo- and heterodinuclear complexes have low solubility in methanol. An increased solubility is generally correlated to demetalation processes with the consequent formation of the more soluble mononuclear analogues. A satisfactorily description of the chemical behaviour of these complexes in methanol is highly facilitated by the identification of the NMR pattern of the related mononuclear complexes (especially the paramagnetic ones). According to the NMR data, the following chemical reactions occur: (i) simple demetalation (i.e. loss of one lanthanide(III) ion with the consequent formation of the mononuclear complexes), ascertained by a comparison of the resulting spectra with those of the related genuine mononuclear complexes with the metal ion residing in the Schiff base or crown-ether chamber; (ii) demetalation and migration with the consequent formation of the mononuclear complex with the metal ion residing in the opposite site with respect to that occupied in the starting complex; (iii) transmetalation and migration (only for heterodinuclear complexes) with the formation of a single heterodinuclear isomer ones independently from the starting heterodinuclear isomer; (iv) scrambling reaction with the simple dissolution of the heterodinuclear complexes.

The solubility of the complexes in dimethylsulphoxide is higher than in methanol. Analogously to that observed in CD_3OD, the identification of the chemical processes involving the homo- or heterodinuclear complexes derives from a comparison of their ^1H NMR spectra of these species with those of the related mononuclear ones.

Both homo- and heterodinuclear complexes with $[\mathbf{18}]^{2-}$, when dissolved in $(CD_3)_2SO$, give rise the corresponding mononuclear complex with the lanthanide(III) ion in the Schiff base site; in the case of the heterodinuclear complexes, the resulting species is the mononuclear complex with the smaller lanthanide(III) ion. Quite often, in addition to the NMR signals typical of these mononuclear species, those due to the mononuclear complex with the larger lanthanide(III) ion in the Schiff

base are also observed. The heterodinuclear complexes with $[\mathbf{21}]^{2-}$ show a solution behaviour similar to that of the related mononuclear complexes: generally the spectrum of the free ligand is recorded as observed for the EuTb and TbEu isomers, in consequence of complete demetalation processes. In the spectrum of the LuEu complex, in addition to the peaks of the free ligand, traces of the presence of the mononuclear europium(III) complex, with the metal ion in the Schiff base moiety, have been detected. In the EuLu isomer no traces of paramagnetic complex are found and the resulting NMR spectrum is more complex than that of the free ligand. The solution behaviour of homo- and heterodinuclear complexes with $[\mathbf{19}]^{2-}$ is quite clear. In agreement with the behaviour of the same complexes with $[\mathbf{18}]^{2-}$, the only species present in solution is the mononuclear complex with the metal ion, the smaller one in the case of the heterodinuclear complex, in the Schiff base site. For instance, the EuLu and EuLa complexes show the ^{1}H NMR spectrum respectively of the mononuclear N_3O_2 lutetium(III) complex (with an iminic peak up field 0.3 ppm with respect to the free ligand) and of the mononuclear N_3O_2 europium(III) complex. No evidences of the presence of homo- or heterodinuclear complexes have been detected.

Thus, the two adjacent coordination chambers of these ligands are both suitable for the encapsulation of a lanthanide(III) ion with the consequent formation of homo- or heterodinuclear complexes. The preparation of these complexes was successfully achieved respectively in a one pot or a step by step reaction; however, they are no longer stable in methanol or in dimethylsulphoxide solutions, their stability depending on the coordination moiety of the macrocycle and the solvent used. For the heterodinuclear complexes a further heavy problem is represented by transmetalation and/or migration reactions, which substantially modify the synthetic pathway quite often verifying the obtainment of the designed complexes. Thus, pure positional heterodinuclear complexes $LnLn'(\mathbf{L})(Cl)_4{\cdot}nH_2O$ $Ln'Ln(\mathbf{L})(Cl_4){\cdot}nH_2O$, although prepared and characterized thanks to the availability of the appropriate O_2O_n mononuclear complexes $[Ln(H_2\text{-}\mathbf{L})(H_2O)_4]Cl_3$ and $[Ln'(H_2\text{-}\mathbf{L})(H_2O)_4]Cl_3$, easily evolve in methanol or dimethylsulphoxide into a series of species which include mononuclear and the heterodinuclear complexes with a site occupancy of the metal ion different from that of the starting complexes (scrambling reactions). This means that the two chambers, owing to their different bite and donor atom set, can select the lanthanide ion to coordinate preferentially. Thus, there is the possibility to tune these molecular movements by changing the shape of the two coordination chambers, the solvent and the lanthanide(III) ions [13].

The synthesis of the diformyl precursor H_2-**18a** involves the coupling of the disodium salt of 2,6-bis(mercaptomethyl)pyridine with 3-(2-bromoethoxy)-2-(2-propenyloxy)benzaldehyde in tetrahydrofuran to give the allyl protected diformyl precursor; the allyl groups are then removed by palladium catalysis, to form the designed precursor H_2-**18a** [16]. This diformyl precursor reacts with *cis*-1,2-diaminocyclohexane in THF/CH_3OH and in the presence of $Ba(CF_3SO_3)_2$ as template, followed by transmetalation in situ with the desired metal acetate $M(CH_3COO)_2{\cdot}nH_2O$ ($M = Ni^{2+}$, UO_2^{2+}) to form the mononuclear complexes [Ni(**18b**)] and $[UO_2(\mathbf{18b})(H_2O)]$ [16]. Also in the absence of barium(II) salt the reaction takes place with a similar yield [16].

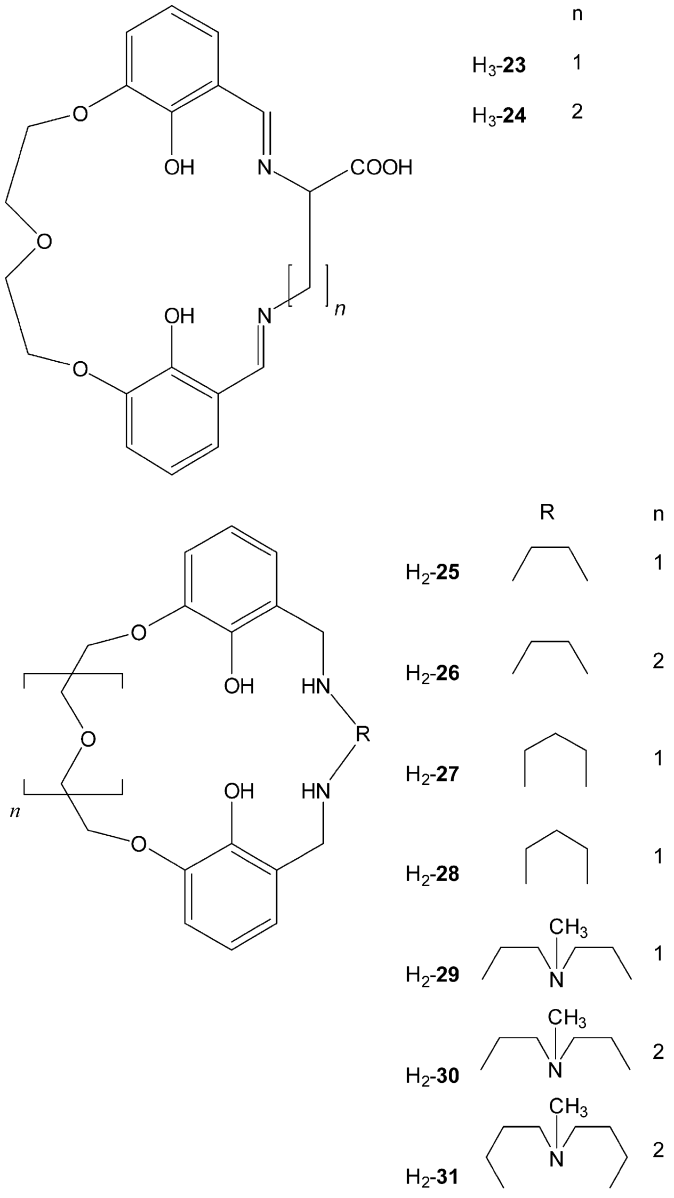

The nickel ion in the N_2O_2 ligand set shows a slightly deformed square planar conformation. The complex as a whole lies approximately on a plane, with the exception of the cyclohexane and pyridine rings, which are almost orthogonal to the mean plane of the macrocycle and in a relative transoid fashion (Fig. 4a) [16].

The uranyl moiety in $[UO_2(\mathbf{18b})(H_2O)]$ exhibits a pentagonal bipyramidal coordination. Two imine nitrogen atoms, two phenoxy oxygen atoms and one oxygen from a water molecule form the pentagonal base, which is almost planar, while the two uranyl oxygen atoms occupy the apex positions. The aromatic rings are planar and the cyclohexane ring adopts the typical chair

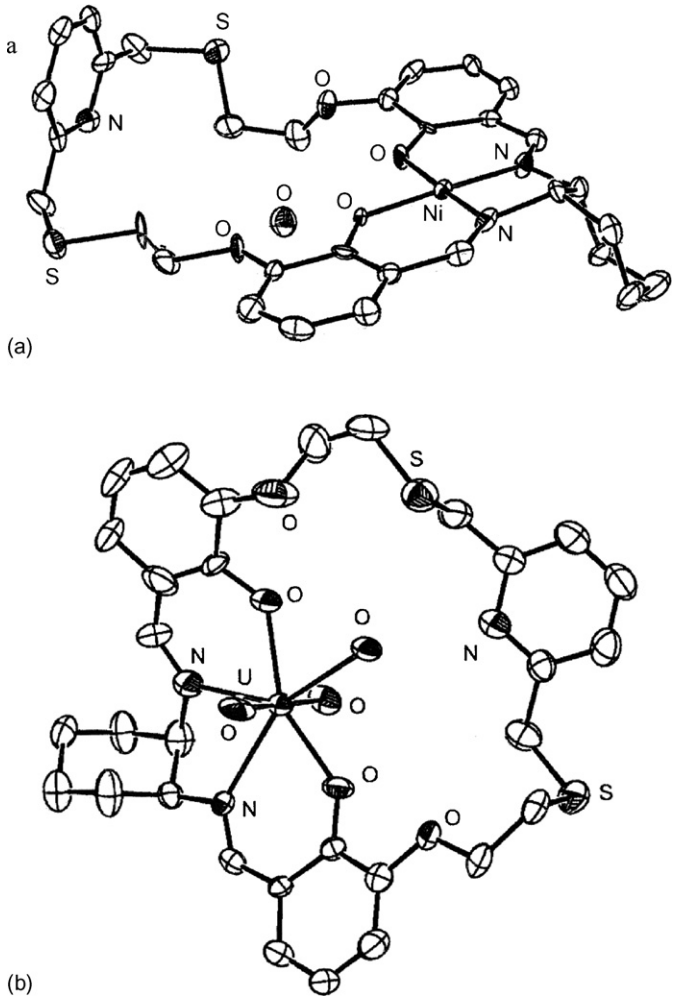

Fig. 4. Structure of [Ni(**18b**)] (a) and [UO_2(**18b**)(H_2O)] (b).

conformation. The uncomplexed bis(thiomethyl)pyridine group of the uranyl complex has one exocyclic and one endocyclic sulphur atom (Fig. 4b) [16].

The mononuclear complexes [Ni(**18b**)] and [UO_2(**18b**)(H_2O)] react at room temperature in methanol with [$Rh(CO)_2(Cl)]_2$ in the presence of [NH_4](PF_6) to afford [NiRh(**18b**)(CO)](PF_6) or [UO_2Rh(**18b**)(CO)](PF_6) [16]. Two conformers of [NiRh(**18b**)(CO)](PF_6) are observed in solution by IR and NMR spectroscopy, in a 5:1 ratio in CD_2Cl_2 which exhibit a fluxional behaviour and are shown to interconvert above room temperature in CD_3CN. The carbonyl rhodium group in the [NiRh(**18b**)(CO)](PF_6) reacts further with methyl iodide in CH_3CN to form oxidative addition products, the final complex being [NiRh(1**8b**)($COCH_3$)(I)](PF_6) [16].

The macrocycles H_3-**32**, H_2-**33** and H_3-**34**, bearing respectively a $–CH_2COOH$, $–CH_2C_5H_4N$ and $–CH_2C_6H_4OH$ pendant arm bonded to the aminic nitrogen atom, contain a O_2O_3 crown-ether-like chamber and a N_3XO_2 (X = O, N) Schiff base chamber. They were prepared by self-condensation and/or by template procedure [17].

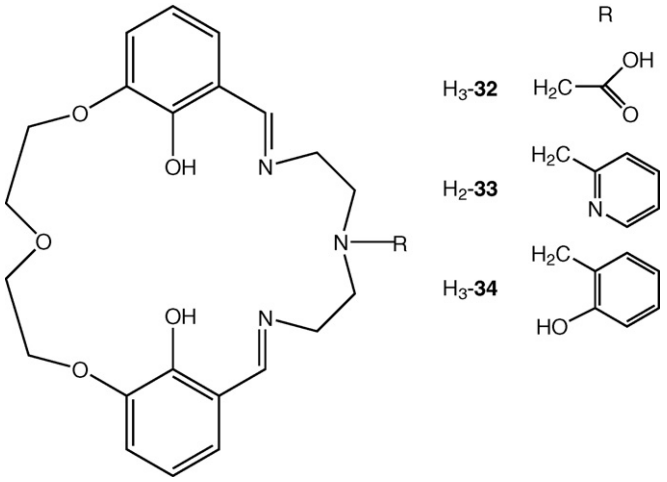

While H_3-**32** was not obtained in an acceptable amount by the condensation of the appropriate diformyl and polyamine precursors, the related trisodium derivative [Na_3(**32**)] has been synthesized in a considerable amount by reaction of the disodium diformyl precursor [Na_2(**3a**)] with the functionalized polyamine $H_2N(CH_2)_2N(CH_2COOH)(CH_2)_2NH_2{\cdot}3HCl$ [18] in the presence of NaOH, as confirmed by the ESI-mass spectrum in CH_3OH, which shows peaks due to [H_4-**32**]$^+$, [Na(H_2-**32**)], [Na_2(H-**32**)] and [Na_3(**32**)], respectively.

H_3-**34** was obtained as the sodium derivatives [Na_2(H-**34**)] or [Na(H_2-**34**)] by reaction of the appropriate precursors in the presence of NaOH in two different synthetic ways: [Na_2(H-**34**)] was prepared by condensation of [Na_2(**3a**)] and $H_2N(CH_2)_2N(CH_2C_6H_4OH)(CH_2)_2NH_2{\cdot}3H_2O$ [18] in methanol, whereas the condensation in diethyl ether of H_2-**3a**, $H_2N(CH_2)_2N(CH_2C_6H_4OH)(CH_2)_2NH_2{\cdot}3H_2O$ and NaOH, dissolved in a minimum amount of methanol, afforded [Na(H_2-**34**)]. IR spectra indicate that in [Na(H-**34**)] the sodium(I) ion is not bound to the iminic nitrogen and quite probably resides in the crown-ether site. Furthermore, the ESI-mass spectrum of [Na(H_2-**34**)] in CH_3OH shows the parent peak at *m*/*z* 542 due to [Na(H_3-**34**)]$^+$.

[Na_3(**32**)] reacts with the appropriate $LnCl_3{\cdot}nH_2O$ in methanol in a 1:1 molar ratio to yield, after a reflux of 2 h, $[LnNa_2(\mathbf{32})(Cl)_2]{\cdot}nH_2O{\cdot}x$NaCl (Ln = Y^{III}, Lu^{III}, Yb^{III}) and, after a reflux of 12 h, $[Ln_2(\mathbf{32})(Cl)_3]{\cdot}nH_2O{\cdot}x$NaCl (Ln = Y^{III}, Lu^{III}, Yb^{III}, Nd^{III}).

In $[LnNa_2(\mathbf{32})(Cl)_2]{\cdot}nH_2O$, quite probably one sodium ion resides into the crown-ether chamber and the other is linked to the carboxylate group. The IR spectra support a complexation of the lanthanide(III) ion inside the Schiff base site. NMR 2D data in methanol-d_4 of the diamagnetic and paramagnetic complexes add useful indications about the site occupancy of the metal ions. In particular they indicate that the europium ion is coordinated in the Schiff base site and the etheric region of the macrocycle is rigidly coordinated to the sodium ion. Furthermore, the acetate group is probably involved in the coordination of the paramagnetic ion. Moreover, the NMR features of the diamagnetic lutetium and lanthanum complexes suggest that the coordination proposed for the europium ion could be unrealistic for other LnNa complexes. The parent peaks at 644 and 666 *m*/*z* in the

ESI-mass spectra of europium and lutetium complexes respectively confirm the occurrence of the heterodinuclear species $\{LnNa(\mathbf{32})\}^+$ [17].

Surprisingly, the ^{23}Na NMR spectra in methanol of the paramagnetic complexes $[LnNa_2(Na_x\text{-}\mathbf{32})(Cl)_{1+x}]$ (Ln = Yb, Tm, Tb; $x = 0$, 1) do not show any ^{23}Na shift, thus proving that no interaction between the metal ions occurs. The reason for this failure, not easily explainable, is certainly due to a wrong Ln···Na alignment. Possibly, the coordination observed in the NMR data of the europium complex is not maintained in other complexes and the acetate group is competitive with the O_3O_2 site in coordinating the sodium ion, thus determining an incorrect stereochemistry for obtaining a relevant ^{23}Na shift. Alternatively, even if the lanthanide(III) ion were in the Schiff base site, its displacement from the equatorial plane toward the carboxylate group would give rise to an incorrect alignment [17].

It was suggested that in the formation of the homodinuclear species, the first event is the formation of the heterodinuclear LnNa complex with the lanthanide ion probably lying in the mean equatorial plane of the N_3O_2 donor set of the Schiff base, as already found for other similar lanthanide complexes. This is followed, in consequence of the prolonged reflux and subsequent release of the sodium(I) ion, by the coordination of a second lanthanide in the free O_3O_2 site which is the favourite site of the lanthanide(III) ion, as already ascertained [12–16]. The macrocycle does not have the correct coordination shape to encapsulate firmly into the mean equatorial plane both metal ions; consequently, the lanthanide ion coordinated to the Schiff base site, owing to the steric hindrance caused by the incoming second lanthanide ion, is pushed away from the N_3O_2 mean plane toward the acetate group. This causes a coordination lowering of the iminic nitrogen to the central metal ion with the consequent shift of the $\upsilon_{C=N}$ toward higher wavelengths. The NMR spectra of $[Lu_2(\mathbf{32})(Cl)_3]\cdot 0.3PrOH$ in CD_3OD show that the compound is not stable in solution. The complexity of the aromatic and iminic region testifies the presence of several species deriving from a demetalation reaction and the formation of positional isomeric mononuclear complexes. Another proof of this instability comes from the ESI-mass spectra of these complexes where no peak attributable to the homodinuclear specie was found [17].

As H_2-**33** or $[Na_2(\mathbf{33})]$ are not available, the pyridine-containing macrocycle was prepared by a template synthesis in presence of the desired lanthanide(III) chloride hydrate in methanol. It was found that when H_2-**3a** and $H_2N(CH_2)N(CH_2C_5N_4N)(CH_2)_2NH_2\cdot 3HCl$ [18] are condensed in presence of NaOH and $LnCl_3\cdot nH_2O$ in methanol in the molar ratio 1:1:3:1 and the reaction mixture is allowed to reflux for 1–2 h, the mononuclear complexes $[Ln(H\text{-}\mathbf{33})(Cl)_2]\cdot n NaCl\cdot mH_2O$ are obtained (Ln = Y^{III}, Yb^{III}, Lu^{III}, Tm^{III}, Tb^{III}, La^{III}, Ce^{III}); on the contrary, when the reflux is continued for 12 h, the homodinuclear complexes $[Ln_2(\mathbf{33})Cl_4]\cdot n NaCl\cdot mH_2O$ are collected (Ln = Y^{III}, La^{III}, Tb^{III}, Lu^{III}) [17].

The NMR spectra clearly show that the mononuclear lanthanum(III), ytterbium(III), and lutetium(III) complexes are contamined by small amounts of the related homodinuclear analogues. The NMR spectra of these dinuclear species, in fact, match perfectly with those of the by-products present in the mononuclear complexes. The main differences in these spectra are localized in the Schiff base protons: this confirms the above assumption that the Schiff base site is only partially involved in coordination. The solution instability of the dinuclear species represents a severe limitation to an exhaustive description of the behaviour of these complexes in solution.

In the mononuclear complexes, no evidence of sodium(I) coordination into the crown-ether moiety was found, probably because it may be more easily released than in the complexes derived from $[Na_3(\mathbf{32})]$, facilitating the formation of mononuclear lanthanide complexes. The liability of the sodium(I) ion in the crown-ether moiety, verified also by ^{23}Na NMR spectroscopy, is quite important in the determination of interesting LIS properties as reported ahead.

A study of the ^1H, $^{13}C\{^1H\}$ and 2D COSY, NOESY, HMQC NMR spectra in methanol-d_4 allows a complete assignment and interpretation of the peaks occurring in the mononuclear $[Ln(H\text{-}\mathbf{33})(Cl_2)]$ and dinuclear diamagnetic and paramagnetic $[Ln_2(\mathbf{33})(Cl)_4]$. Thus, for the paramagnetic complex $[Ce(H\text{-}\mathbf{33})(Cl)_2]\cdot 7H_2O$ the lanthanide ion was supposed to be coordinated in Schiff base site, with the pendant arm also involved in coordination.

ESI-mass spectra of these samples show the presence of signals related to the sodium or lanthanide mononuclear complexes, this proving the real occurrence of the mononuclear lanthanide(III) complexes. In a few cases moreover, the mononuclear lanthanide complexes encapsulate a methanol or chloride and/or water molecule. Again no evidence of homodinuclear species was found [17].

Although heterodinuclear LnNa complexes were not obtained with $[\mathbf{33}]^{2-}$, SEM-EDS measurements clearly prove the presence of NaCl in $[Yb(H\text{-}\mathbf{33})(Cl)_2]\cdot 7NaCl\cdot 0.1H_2O\cdot 1.6C_2H_5OH$ and $[Tm(H\text{-}\mathbf{33})(Cl)_2]\cdot 7.6NaCl\cdot C_2H_5OH$. 2D NMR measurements of these paramagnetic complexes indicate that the lanthanide(III) ion, probably owing to the presence of a pyridinic pendant arm, prefers the Schiff base site rather than the etheric one. Consequently, in methanolic solution, the sodium ion related to NaCl is partially coordinated to the lanthanide(III) complex and this coordination causes an high isotropic ^{23}Na shift (330 ppm for the thulium(III) complex at −20 °C). Furthermore, as expected, the ^{23}Na chemical shift linearly decreases with the increasing temperature. This behaviour parallels that observed in the complexes $[LnNa(\mathbf{18})(Cl)_2(CH_3OH)]$ [12,14] where X-ray structural determinations show that the lanthanide(III) ion resides in the N_3O_2 Schiff base chamber and the sodium(I) ion is in the crown-ether-like chamber. Thus, it was suggested that heterodinuclear complexes are formed and a site occupancy similar to that ascertained for $[LnNa(\mathbf{18})(Cl)_2(CH_3OH)]$ occurs, taking into account that the similar positional isomeric complexes with H_2-**18**, where the lanthanide(III) ion resides in the O_3O_2 chamber and the sodium(I) ion in the crown-ether site, show a negligible ^{23}Na chemical shift.

The formation of a LnNa heterodinuclear coordination is also proved by the ESI-mass spectra in methanol of the complexes.

The presence of peaks at 331.4 and 349.8 m/z ($z = 2$) of the lanthanum(III) and ytterbium(III) complexes respectively is a convincing evidence of the formation of $\{LnNa(\mathbf{33})\}^{2+}$ species.

The above mentioned liability of the sodium(I) ion is an interesting and useful feature in order to obtain powerful molecular shift devices as they need a quick complexation–decomplexation process of the species to be determined [17].

The mononuclear complexes [Ln(H$_3$-**34**)(Cl)$_3$] (Ln = Y^{III}, La^{III}, Eu^{III}, Tb^{III}, Lu^{III}) were synthesized by [1 + 1] condensation of the triamine precursor $H_2N(CH_2)_2N(CH_2C_6H_4OH)(CH_2)_2NH_2{\cdot}3HCl$ neutralized with LiOH, with the diformyl precursor H$_2$-**3a** in presence of $LnCl_3{\cdot}nH_2O$. The key of these synthesis is the use of LiOH as a neutralizing agent of the aminic precursor instead of NaOH; the lithium(I) ion is not a suitable competitor of the lanthanide(III) ion for the hard site and hence it allows the coordination of the lanthanide ion to the crown ether site. On the contrary, the sodium(I) ion strongly competes with the lanthanide(III) ion and makes the coordination of the 4f-ion very problematic or impossible [17].

Long refluxing times do not produce homodinuclear species. The complexes recovered after a 12 h reflux always reproduce the mononuclear or the hetero dinuclear LnNa complexes, respectively, when LiOH or NaOH are used. Quite interestingly, when a higher LiOH/H$_2$-**3a** ratio is used, the coordination site of the lanthanide ion can be chosen. More precisely, under basic conditions (LiOH:amine:H$_2$-**3a**:LnCl$_3$ = 6:1:1:1) complexes have been invariantly obtained with NMR and IR spectra clearly indicating that the lanthanide ion resides in the Schiff base site. Less basic conditions (LiOH:amine:H$_2$-**3a**:LnCl$_3$ = 3:1:1:1) always produce pure mononuclear complexes with the O_3O_2 crown ether site occupied by the lanthanide(III) ion [17].

The heterodinuclear complexes [LnNa(**34**)(Cl)]·xNaCl (Ln = Y^{III}, La^{III}, Ce^{III}, Eu^{III}, Tb^{III}, Dy^{III}, Er^{III}, Tm^{III}, Yb^{III}, Lu^{III}) were synthesized by condensation of methanolic solutions of $H_2N(CH_2)_2$-$N(CH_2C_6H_4OH)(CH_2)_2NH_2{\cdot}3HCl$ and H$_2$-**3a** in presence of NaOH and the appropriate $LnCl_3{\cdot}nH_2O$. in a 1:1:5:1 ratio [17].

The ESI-mass spectra in CH_3OH for each complex clearly show the parent peak due to the appropriate $\{LnNa\text{-}\mathbf{34}\}^+$ species, pointing out that additional NaCl or solvent molecules present in the sample are not directly involved in the coordination. In agreement with the related systems with H$_3$-**32** or H$_2$-**18** and with literature data [5], the presence of the sodium(I) ion, which preferentially fills the O_2O_3 site, forces the lanthanide(III) ion into the Schiff base moiety; this coordination is strengthened by the further coordination of the phenolic group, as confirmed in the solid state by X-ray diffractometry structural studies and in solution by NMR spectroscopy.

The complexes are very soluble in methanol and sparingly soluble in water. Consequently NMR spectra were carried out in CD_3OD. Moreover, the complexes are soluble and stable for a long period of time in a CD_3OD:D_2O = 1:1; the results in this solution completely parallel those obtained in CD_3OD.

NMR spectra of the paramagnetic europium(III) complexes is a powerful tool for a satisfactory understanding of the site occupancy of the lanthanide(III) ions. Differently from [Eu(H$_3$-**34**)(Cl)$_3$], where it was demonstrated that the europium(III) ion occupies the O_3O_2 site, in [EuNa(**34**)(Cl)] the europium ion lies in the N_3O_3 site. Furthermore, the pendant arm is clearly coordinated to the europium(III) ion. The complex is very rigid in solution, indicating that both coordination sites are firmly occupied by a metal ion.

^{23}Na NMR spectra of [LnNa(**34**)(Cl)] (where Ln = Yb^{III}, Tm^{III}, Tb^{III}, Dy^{III}) show these complexes have the same behaviour as those with [**33**]$^{2-}$. The presence of a broad resonance with a large shift from the free ion peak arises from the coordination of the sodium(I) ion in the O_3O_2 site of the complexes, resulting in a slow exchange at room temperature on the NMR timescale.

The slow exchange is confirmed by the peak at 0 ppm corresponding to the free ion, which originates from the presence of NaCl in the sample. The observed isotropic shift is very large as far as thulium(III), dysprosium(III) and terbium(III) complexes are concerned, whereas it is smaller for the ytterbium(III) complex; numerical values of these shifts are: [TmNa(**34**)(Cl)]: +270 ppm (r.t.), +360 ppm (−20 °C), [DyNa(**34**)(Cl)]: −158 ppm (r.t.), −200 ppm (−20 °C), [TbNa(**34**)(Cl)]: −258 ppm (r.t.), −352 ppm (−20 °C), [YbNa(**34**)(Cl)]: +50 ppm (r.t.), +61 ppm (−20 °C) [17].

The ^{23}Na NMR data in CD_3OD/D_2O (1:1) containing NaCl are comparable with those in CD_3OD, the most remarkable difference being a considerable broadening of the signal of the bound sodium ion due to the high Na_{bound}/Na_{free} exchange [17].

The crystal structure of [DyNa(**34**)(Cl){$(CH_3)_2CHOH$}] shows that the sodium ion is located in the O_2O_3 crown-like site of the macrocycle and reaches the coordination number of six by bonding five oxygen atoms from [**34**]$^{3-}$ and one n-propanol oxygen atom. The coordination geometry around the sodium ion has been described as a distorted pentagonal pyramid with the n-propanol oxygen atom as apex. The seven coordination of dysprosium ion is achieved by three nitrogen atoms, two phenolic oxygens that act as bridge, the pendant phenolic oxygen of the ligand and one chlorine ion. The coordination polyhedron around the dysprosium(III) ion is a distorted pentagonal bipyramid with the chloride ion and the phenolic pendant oxygen as apices. The total four positive charges of the two metal ions are neutralized by the negative charged three phenyl oxygens and by the chloride ion. As for other similar complexes, the molecule adopts a butterfly shape with the two benzene rings as wings (Fig. 5) [17].

Owing to the interesting lanthanide induced shift data of these complexes, structural data of the [DyNa(**34**)(Cl){$(CH_3)_2CHOH$}] complex have been compared with the similar [LnNa(**18**)(Cl)$_2$(CH_3OH)] (Ln = Nd^{III}, Eu^{III}, Gd^{III}, Yb^{III}) complexes that present a comparable ^{23}Na NMR shift. All complexes have shown that the sodium environment is always preserved with very similar coordination distances and angles, while some differences, as foreseen, are detected about the bond distances around the lanthanide ions. These in fact follow the constant decreasing of the ionic radii along the lanthanide series with a decrease of the coordination bond distances on going from neodymium(III) to ytterbium(III)

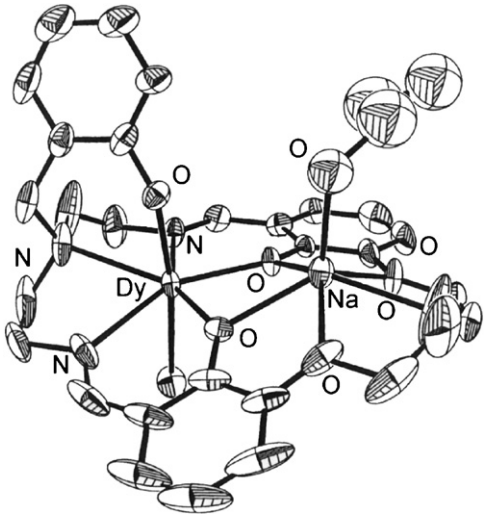

Fig. 5. Structure of [DyNa(**34**)(Cl)($CH_3CH_2CH_2OH$)].

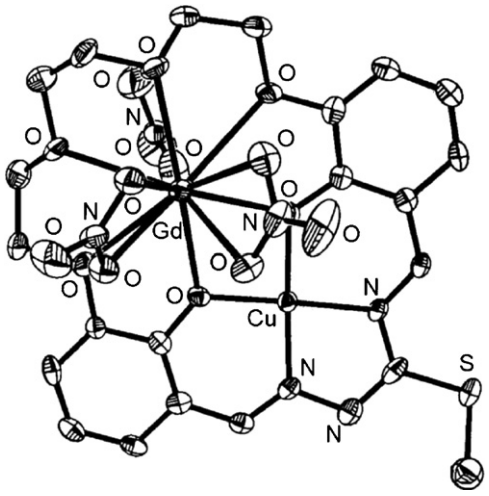

Fig. 6. Structure of [GdCu(**35**)(NO_3)$_3$].

complexes. Other differences with the structure described here are present in the bond angles of coordinated atoms and are mainly due to the geometrical constrains of the pendant phenolate group. The Ln···Na distances in the complexes of $[\mathbf{18}]^{2-}$ has a mean value 3.55 Å compared to the 3.496 Å of Dy···Na found ion [DyNa(**34**)(Cl){$(CH_3)_2CHOH$}] [17].

The reaction of H_2-**3b** with *S*-methylisothiosemicarbazide hydrochloride in the presence of $Ba(CF_3SO_3)_2$ as templating agent in methanol/tetrahydrofuran at 60 °C, followed by the addition of copper(II) acetate, yields $[CuBa(\mathbf{35})](CF_3SO_2)_2$ which, by further reaction with guanidinium sulphate, affords $[Cu(\mathbf{35})]\cdot 2H_2O$ [19,20].

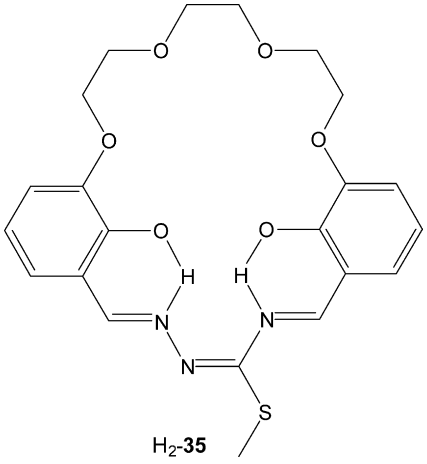

H_2-**35**

In [CuGd(**35**)(NO_3)$_3$], synthesized by the reaction of $[Cu(\mathbf{5})]\cdot 2H_2O$ with $Gd(NO_3)_3\cdot 6H_2O$ in dichloromethane/methanol solution, the copper(II) ion has a square planar geometry while the eleven coordinate gadolinium(III) ion is bound to five oxygen atoms from three nitrate ions, two acting as bidentate and the third as monodentate, and six oxygen atoms from the macrocyclic ligand (Fig. 6). [CuGd(**33**)(NO_3)$_3$] exhibits ferromagnetic $Cu^{II}\cdots Gd^{III}$ interaction ($J = 5\ cm^{-1}$) [20].

The condensation of H_2-**3b** and 3-methylisothiosemicarbazide hydroiodide in the presence of equimolar amounts of $K(CF_3SO_3)$ and $M(CH_3COO)_2\cdot nH_2O$ ($M = Ni^{II}$, Cu^{II}, Zn^{II}), yields [NiK(**35**)(I_3)], [NiK(**35**)(CF_3SO_3)], [CuK(**35**)(CF_3SO_3)(CH_3OH)] and [Zn_2K_2(**35**)$_2$(I)$_2$(CH_3OH)], respectively. To avoid the contemporary formation of [NiK(**35**)(I_3)] and [NiK(**35**)(CF_3SO_3)], the reaction mixture, resulted from H_2-**3b**, *S*-methylisothiosemicarbazide hydroiodide and $K(CF_3SO_3)$, was treated with $Ag(CF_3SO_3)$ and the precipitated AgI was removed by filtration. Subsequent addition of $Ni(CH_3COO)_2\cdot 4H_2O$ led exclusively to [NiK(**35**)(CF_3SO_3)] [21].

In [NiK(**35**)(I_3)] and [NiK(**35**)(CF_3SO_3)] the nickel(II) ion has a square planar N_2O_2 coordination geometry while the potassium ion is bound by two phenolic and four etheric oxygen atoms of the macrocycle. The major difference between the structures of the two complexes centers around the potassium ion: in [NiK(**35**)(I_3)] the potassium ion is linked to the polyiodide I_3^-, whereas in [NiK(**35**)(CF_3SO_3)] it is bonded to the trisulphate anion. In addition, in this last structure, the sulphur atoms of the neighboring metallomacrocycles are also involved in coordination to potassium. The Ni···K separations are similar in both structures (3.689 and 3.690 Å, respectively). In the crystals, π–π interactions occur resulting in infinite stacks along *a* axis in both structure (Fig. 7).

In [CuK(**35**)(CF_3SO_3)(CH_3OH)] the copper(II) ion is square planar. The potassium ion is eight coordinate on account of six oxygens of the macrocycle and two axially coordinated oxygens derived respectively from the monodentate triflate anion and the molecule of methanol, located on the different sides of the macrocycle. Another triflate oxygen and the methanol oxygen are involved in hydrogen-bonding with the neighboring complex resulting in the chain formation along *a*-axis. In the crystal lattice a nearly parallel arrangement of partially overlapped copper(II) bis(salicylidene)isothiosemicarbazidate moieties is realised [21].

[Zn_2K_2(**35**)$_2$(I)$_2$(μ-CH_3OH)] contains a CH_3OH ligand bridging the two potassium ions. Each potassium ion is coordi-

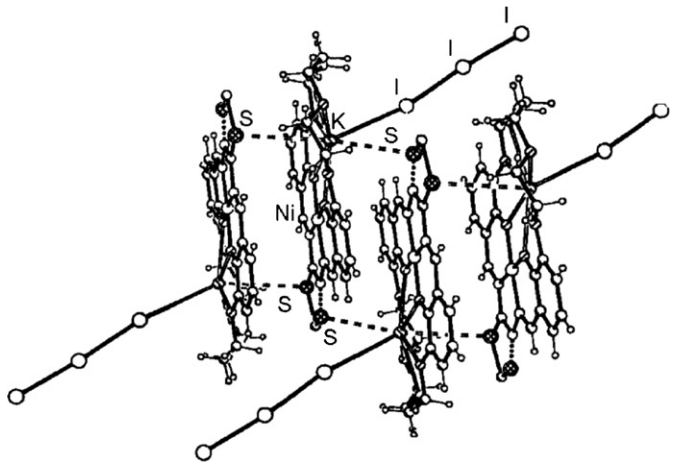

Fig. 7. Structure of [NiK(**35**)(I)$_3$].

nated by seven oxygen atoms, six from the macrocyclic ligand and one due to a bridging methanol molecule. The six oxygen atoms of the macrocycle are disposed at the vertices of a distorted hexagon. The coordination polyhedron of the zinc(II) ion is a distorted square pyramid, with the two salicylideneiminato groups of the macrocycle occupying the basal plane and the iodide anion the apical position. The zinc ion deviates out from the mean basal plane toward the iodide anion. The non-planarity of the coordination core leads to shallow boat conformation of the surrounding fragment (Fig. 8). In contrast to [ZnBa(**35**)(I)(CF_3SO_3)(CH_3OH)]$_2$·0.5H_2O, in which the barium(II) ion is located on one side of the macrocycle and the zinc(II) ion on the other, the zinc(II) and potassium(I) ions in [Zn_2K_2(**35**)$_2$(I)$_2$(CH_3OH)] are located on the same side of macrocyclic mean plane. As a result the Zn···K distance (3.475 Å) is shorter compared with the Zn···Ba distance (3.736 Å) in the Zn/Ba complex [21].

Magnetic susceptibility measurements and ESR spectra of [CuK(**35**)(CF_3SO_3)(CH_3OH)] indicate weak intermolecular ferromagnetic spin-spin interactions ($J = 0.8\ cm^{-1}$) which are mostly dipolar in origin [21].

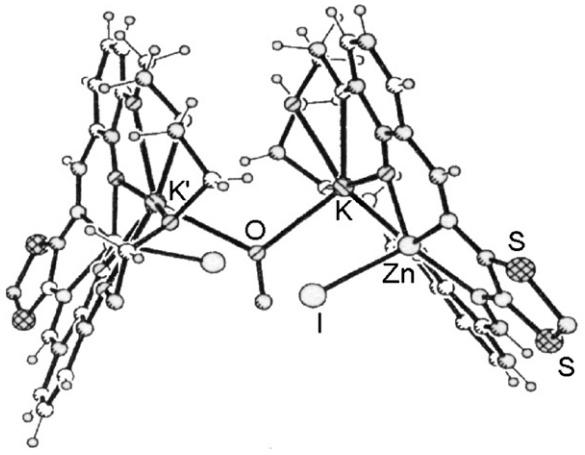

Fig. 8. Structure of [Zn_2K_2(**35**)$_2$(I)$_2$(CH_3OH)].

[Ba(H_2-**36**)](ClO_4) was obtained by the condensation of equimolar amounts of the diformyl precursor H_2-**3c** with 1,2-diaminobenzene in the presence of Ba(ClO_4)$_2$·*n*H_2O. The related disodium macrocycle, [Na_2(**36**)], synthesized by the transmetalation reaction of [Ba(H_2-**36**)](ClO_4)$_2$ with sodium sulphate, reacts with palladium acetate to afford a mixture, [Pd_2Na_2(**36**)$_2$(μ-H_2O)$_2$](ClO_4)$_2$·3CH_2Cl_2 and [Pd_2Na_2(**36**$^-$)$_2$]CH_3CN·2CH_3H_2O. The latter was revealed as an unusual metal-mediated electron delocalized complex [22].

The structure of [Pd_2Na_2(**36**)$_2$(μ-H_2O)$_2$](ClO_4)$_2$·3CH_2Cl_2 contains two stair-shaped macrocyclic dinuclear palladium(II)–sodium(I) complexes in parallel, which are connected by two bridging water molecules, forming a unique tetranuclear complex. The layered structure permits weak face-to-face π–π interactions between aromatic groups. Two non-coordinating perchlorate ions were found in the outer sphere of the complex. Each palladium(II) center has a distorted square planar array of two nitrogen and two phenolate oxygen atoms from the Schiff base cavity in a *cis* arrangement. However, the two sodium ions have quite different coordination environments: one is coordinated to four etheric oxygens atoms in the opposite side of the Schiff base moiety from one macrocycle in a bent arrangement, with the two ether oxygen donors remaining uncoordinated. The coordination is completed by two oxygens of two bridging water molecules, in such a way that this sodium ion shows six-coordination with an irregular geometry. The other sodium ion is bounded by two phenolate oxygen and two etheric oxygen atoms close to the Schiff base unit as well as two bridging water molecules such that the overall coordination geometry about the metal ion is also six coordinate. The intermetallic Pd···Na distances are 3.599 and 3.669 Å (Fig. 9a).

[Pd_2Na_2(**36**$^-$)$_2$]·2CH_2CN·2C_3H_6O is a dimer of a heterobinuclear complex with an imposed inversion symmetry. The non-planar skeleton of the macrocycle can be denoted as an approximate L-shape. In this complex no anion was found and the crystal structure provides an unusual electron delocalization of the Schiff base unit by metal-mediated electron transfer. The palladium(II) ions in a distorted square planar array show a very similar coordination environment to that of [Pd_2Na_2(**36**)$_2$(μ-OH_2)$_2$](ClO_4)$_2$·2CH_2C1_2. The sodium ion is above the mean plane of four coordinating oxygens. The Pd···Na intermetallic distance is 3.939 Å (Fig. 9b) [22].

H_2-**37** and H_2-**38** were prepared by the condensation of the diformyl-precursors H_2-**4a** or H_2-**4b** with 1,2-ethanediamine. Mass spectrometry indicated that some of the related macrocycle, deriving from a [2 + 2] condensation of H_2-**4a** and 1,2-ethanediamine, had been formed. No attempt was made to remove this component before the preparation of the metal complexes of H_2-**37** [23].

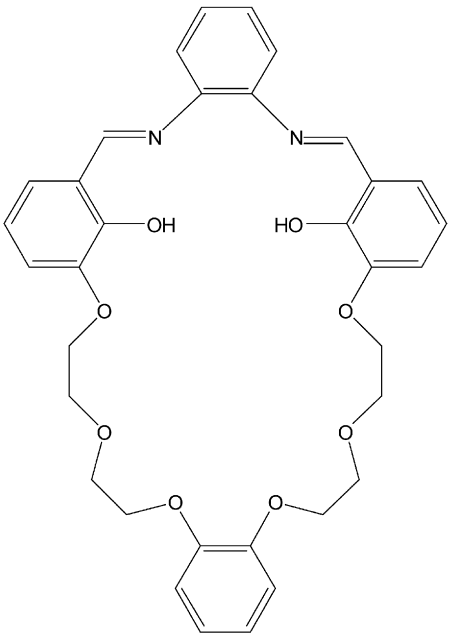

H_2-**36**

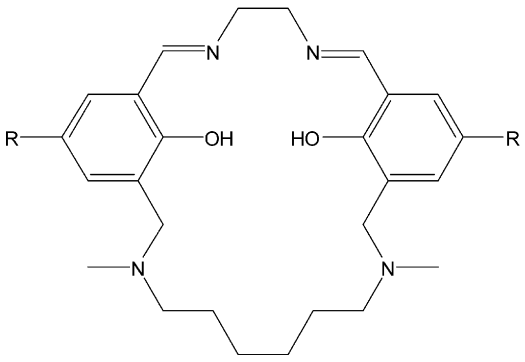

	R
H_2-**37**	$C(CH_3)_3$
H_2-**38**	C_9H_{13}

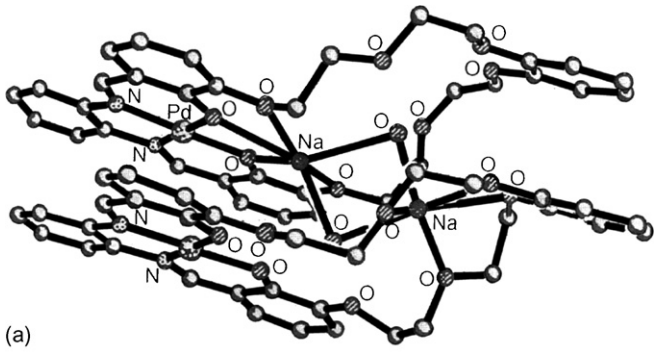

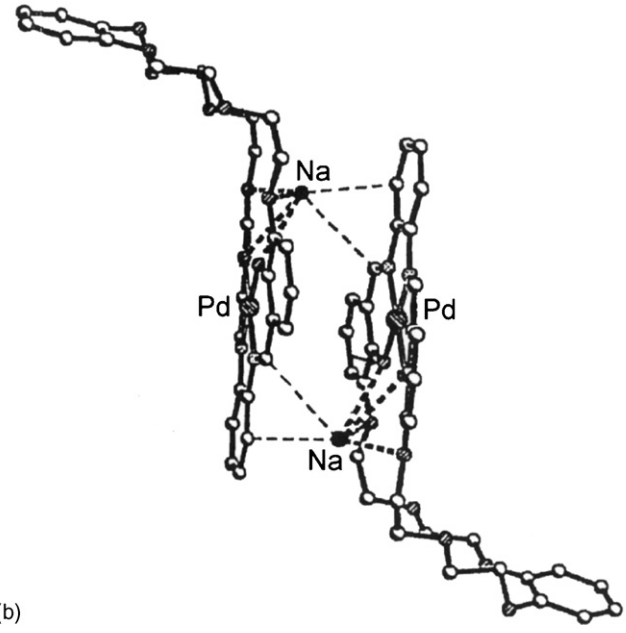

Fig. 9. Structure of $[Pd_2Na_2(\mathbf{36})_2(\mu\text{-}H_2O)](ClO_4)_2$ (a) and $[Pd_2Na_2(\mathbf{36}^{-})_2]$ (b).

$[M(H_2\text{-}\mathbf{37})](SO_4)\cdot H_2O$ and $[M(H_2\text{-}\mathbf{38})](SO_4)$ ($M = Cu^{II}$, Ni^{II}) have been prepared by reaction of methanolic solution of H_2-**37** or H_2-**38** with the appropriate metal(II) sulphate. [Cu(**38**)] was obtained as an oil by the condensation of H_2-**4b** and 1,2-ethanediamine using $Cu(CH_3COO)_2\cdot H_2O$ as template [23]. FAB-mass spectrometry and X-ray structure determinations confirmed the formation of complexes containing a zwitterionic form of the ligand in which the phenolic protons has been transferred to the nitrogen atoms of the hexamethylenediamine strap, and the complexation of the sulphate ion to these cationic sites rather than the metal center. Structural features associated with the assembly $\{[Ni(H_2\text{-}\mathbf{37})](SO_4)\cdot H_2O\}_2$ and $\{[Cu(H_2\text{-}\mathbf{37})](SO_4)\cdot H_2O\}_2$ are remarkably similar. Both are dimers with approximately planar $\{M^{II}(\text{Schiff base})\}$ units. The centers of the dimeric units are composed of two sulphate anions bridged by hydrogen-bonded water molecules. The sulphate anions interact strongly via electrostatic hydrogen-bondings with the protonated alkylammonium nitrogen atoms. These interactions lead to an approximately linear intermolecular N···S···N arrangements optimising the electrostatic component to bonding. The short intermolecular N···N separations make impossible for a sulphate ion to be included within the macrocyclic cavity defined by the hexamethylene strap (Fig. 10) [23].

The related macrocycle H_2-**38** with two multiply branched mixed isomer nonyl substituents and its copper sulphate complexes have sufficient solubility in a chloroform/butanol solution (95:5) to allow copper and sulphate loadings from aqueous solutions to be investigated [23]. The copper complex binds sulphate when contacted with aqueous solutions of pH < 7, and in the pH range 3–5 is consistent with more than 90% of the copper complex being present as $\{[Cu(H_2\text{-}\mathbf{38})\}(SO_4)$ in the organic phase. In contrast, the free ligand is less than 10% sulphate-loaded, as $[(H_4\text{-}\mathbf{38})(SO_4)]$ or $[(H_3\text{-}\mathbf{38})(HSO_4)]$, in this pH range, indicating that the copper center is needed to "template" the tertiary amine groups to provide an effective receptor for H_2SO_4 in chloroform/butanol. Such cooperativity of M^{2+} and SO_4^{2-} binding is potentially of great significance for tuning reagents to show high selectivities of metal sulphate transport.

Sulphate-loading, corresponding to the formation of the monosulphato complexes $\{[Cu(H_2\text{-}L)](SO_4)\}$, occurs at higher pH values for the macrocyclic system H_2-**38** than for linear analogues such as H_2-**39** and H_2-**40**. The pH values for 50% sulphate

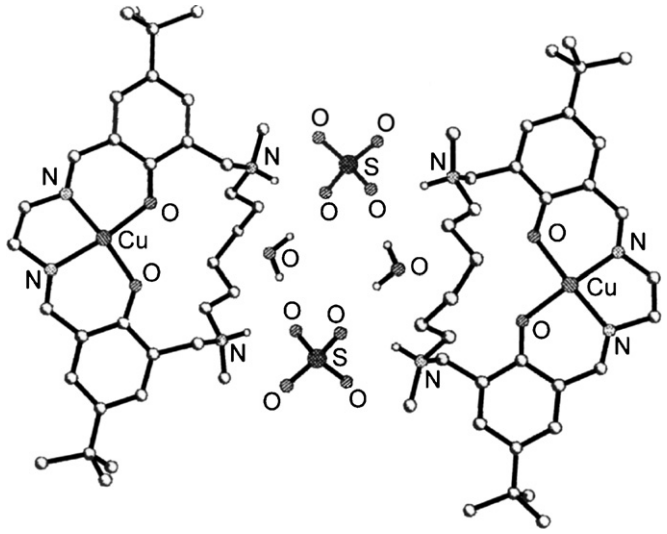

Fig. 10. Structure of $\{[Cu(H\text{-}\mathbf{37})](SO_4)\cdot H_2O\}_2$.

uptake by [Cu(**38**)] and of [Cu(**39**)] under identical conditions are 5.9 and 4.2, respectively.

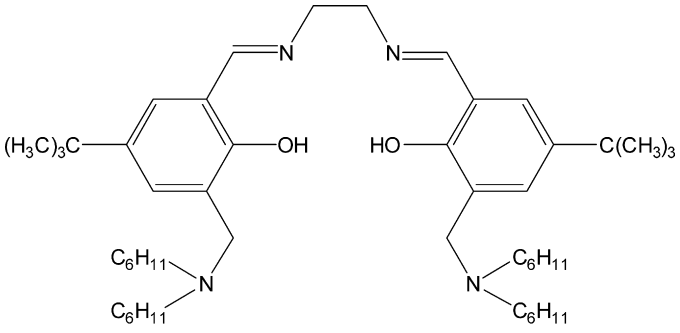

H_2-**39**

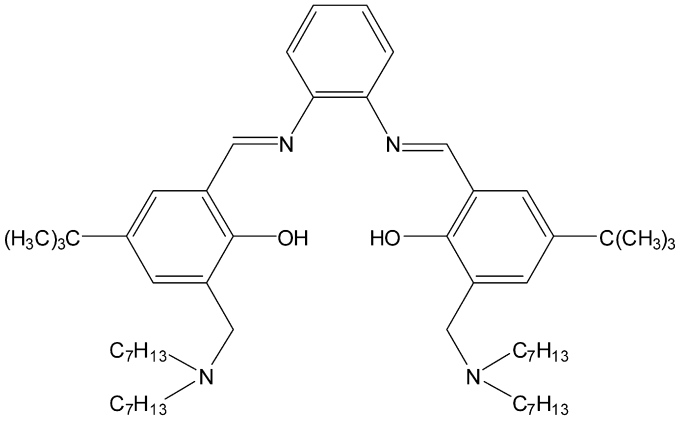

H_2-**40**

While the incorporation of the hexamethylene strap enhances sulphate binding in comparison with the acyclic complex [Cu(**39**)], the strength of metal-binding is decreased slightly. More than 85% of the copper is stripped when a chloroform solution of $\{[Cu(H_2\text{-}\mathbf{38})](SO_4)\}$ is contacted with dilute sulphuric acid of pH 1.2. Less than 70% of the copper had been stripped from $\{[Cu(H_2\text{-}\mathbf{39})](SO_4)\}$ at pH 1.2. This slight detuning of the metal binding site may arise from the hexamethylene strap imposing a distortion from a square planar arrangement of the N_2O_2 Schiff base donor set preferred by the copper(II) ion as is suggested by the X-ray structure determinations.

At pH $\simeq$ 4, >90% loading of $CuSO_4$ is possible without pH adjustment, and an efficient materials balance for a circuit will result if the copper is stripped with sulphuric acid at pH < 1.0. The slow rise of copper loading with increase of pH and the failure to load fully until the pH is >5.5 may be a feature of the reagent containing a significant quantity of the larger ring [2 + 2] condensation product. It was suggested that this will not so readily form the desired $CuSO_4$ complex, and 100% metal loading can only be achieved in the "metal only" form by deprotonation of the ligand at pH > 5.5 [23].

The condensation of H_2-**5** or H_2-**6** with 1,2-ethanediamine or 1,3-propanediamine in the presence of appropriate metal ions gives rise to simple or double metal ion migration and/or transmetalation reaction and ring contraction or expansion processes as already reported in a previous review [18].

The heterodinuclear $M^{II}Cu^{II}$ complexes $[CoCu(\mathbf{41})](ClO_4)_2\cdot CH_3CN$, $[NiCu(\mathbf{41})](ClO_4)_2$, $[ZnCu(\mathbf{41})](ClO_4)_2\cdot 0.5CH_3CN\cdot C_2H_5OH$, $[CoCu(\mathbf{42})(CH_3CN)_2\{(CH_3)_2CHOH\}](ClO_4)_2$, $[NiCu(\mathbf{42})](ClO_4)_2$, and $[ZnCu(\mathbf{42})](ClO_4)_2\cdot 1.5DMF$ have been obtained by the stepwise synthetic procedure from the reaction of the appropriate mononuclear copper(II) complex, [Cu(**L**)], with the desired transition metal(II) chloride, followed by substitution of chloride anions from $[MCu(\mathbf{L})(Cl)_2]$ with ClO_4^- by methathesis with $AgClO_4$ [24]. The corresponding portional $Cu^{II}M^{II}$ heterodinuclear isomers have been synthesized by transmetalation reaction of the related $Pb^{II}Cu^{II}$ complexes $[PbCu(L)](ClO_4)_2$, with the desired metal(II) sulphate. In the former complexes the copper(II) ion resides into the N(imine)$_2O_2$ chamber while in the latter one it lies in the N (amine)$_2O_2$ site (Scheme 4) [24].

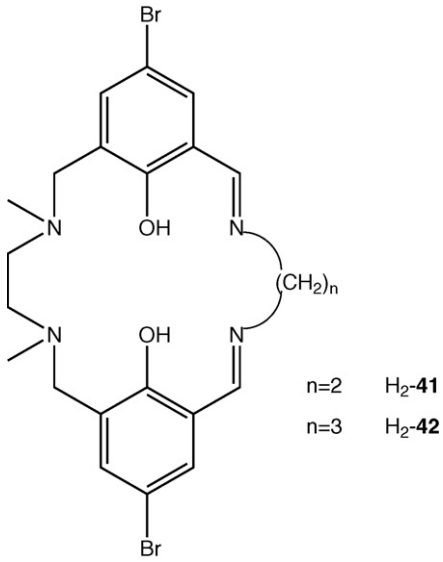

n=2 H_2-**41**

n=3 H_2-**42**

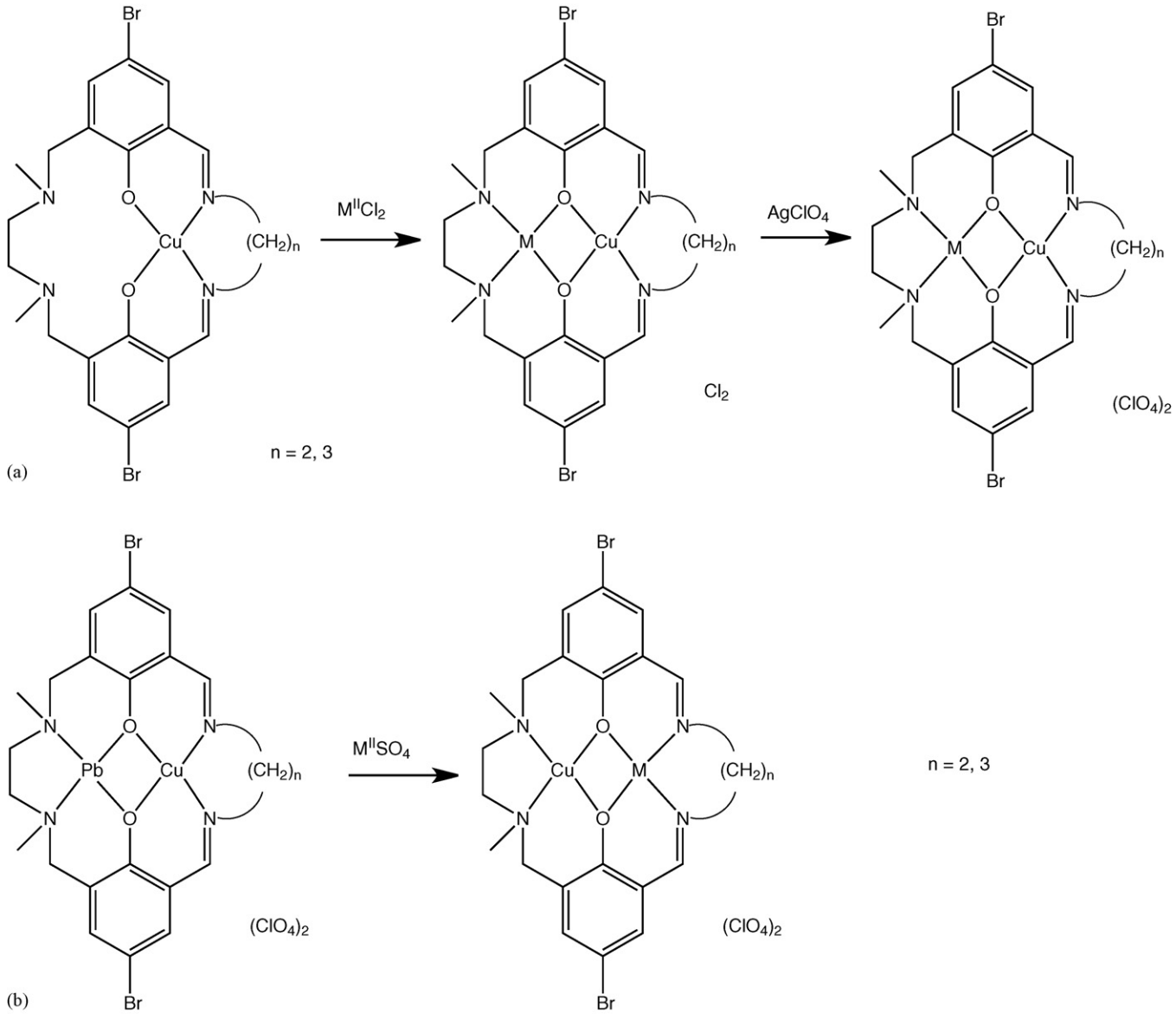

Scheme 4. Synthesis of the positional isomeric complexes $[M^{II}Cu^{II}(L)](ClO_4)_2$ (a) and $[Cu^{II}M^{II}(L)](ClO_4)_2$ (b) (H_2-L = H_2-**41**, H_2-**42**).

In $[CoCu(\mathbf{41})(CH_3CN)_3](ClO_4)_2$ the cobalt(II) ion resides in the aminic site and the copper(II) in the iminic one as found for the parent complex $[CoCu(\mathbf{41})(Cl)_2]$. The Co···Cu intermetallic separation, bridged by the two phenolic oxygen atoms, is 3.025 Å. The geometry about the copper(II) ion is square pyramidal with an acetonitrile nitrogen at the apex, the metal ion being displaced from the basal plane toward the apical acetonitrile nitrogen donor atom. The N_2O_2 donor set of the aminic site adopts a nonplanar chelating mode, providing a *cis*-β-octahedral geometry about the cobalt(II) ion together with two acetonitrile nitrogens in *cis*-positions (Fig. 11) [24].

In $[NiCu(\mathbf{41})(DMF)_2](ClO_4)_2$ the nickel(II) ion resides in the aminic site with a *cis*-β-octahedral configuration along with two dimethylformamide oxygens in *cis* positions. The copper(II) ion has a planar geometry in the iminic site. The Ni···Cu intermetallic separation is 2.959 Å (Fig. 12).

The X-ray structure of $[CoCu(\mathbf{42})(CH_3CN)]\{(CH_3)_2CHOH\}](ClO_4)_2$ demonstrates a dinuclear core with the cobalt(II) ion in the aminic site and the copper(II) ion in the iminic site, both metal ions being in a square pyramidal geometry. The Co···Cu intermetallic separation is 3.049 Å. The copper(II) and the cobalt(II) ions are displaced from their basal N_2O_2 plane respectively toward the axial 2-propanol oxygen and the axial acetonitrile nitrogen. The ethylene lateral chain in the aminic site assumes a gauche conformation, and the trimethylene chain in the iminic site assumes a chair conformation (Fig. 13) [24].

The magnetic behaviour of $[CoCu(\mathbf{41})(CH_3CN)](ClO_4)_2$ indicates an high spin cobalt(II) ion in the $N(amine)_2O_2$ site and an antiferromagnetic interaction within each molecule ($J = -8\,cm^{-1}$). The positional $Cu^{II}Co^{II}$ isomer has a magnetic moment of $3.22\mu_B$ at room temperature owing to the

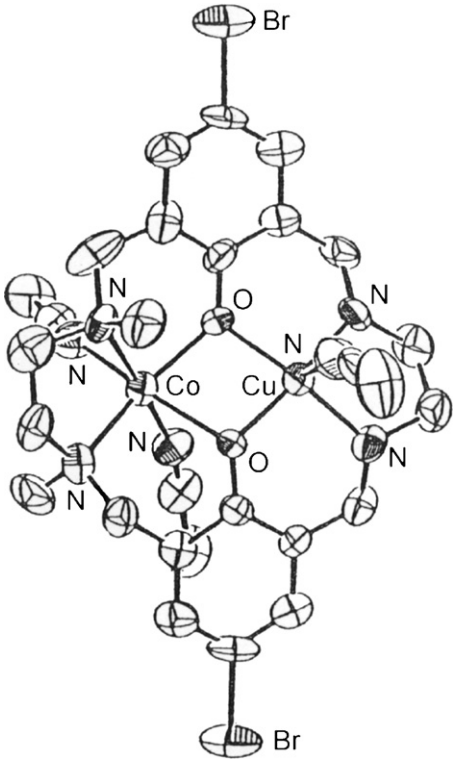

Fig. 11. Structure of $[CoCu(\mathbf{41})(CH_3CN)_3]^{2+}$.

presence of a low spin cobalt(II) ion in the $N(imine)_2O_2$ site. In $[NiCu(\mathbf{41})](ClO_4)_2$ an antiferromagnetic coupling operates ($J = -12\,cm^{-1}$)while the positional $Cu^{II}Ni^{II}$ isomer has a room temperature magnetic moment of $1.95\mu_B$ common for one unpaired electron because of the diamagnetic nature of the nickel(II) ion in the iminic site. Also in $[CoCu(\mathbf{42})(CH_3CN)\{(CH_3)_2CHOH\}](ClO_4)_2$ an antiferromagnetic coupling between copper(II) and cobalt(II) occurs ($J = -3.8\,cm^{-1}$). $[NiCu(\mathbf{42})](ClO_4)_2$ has a room-

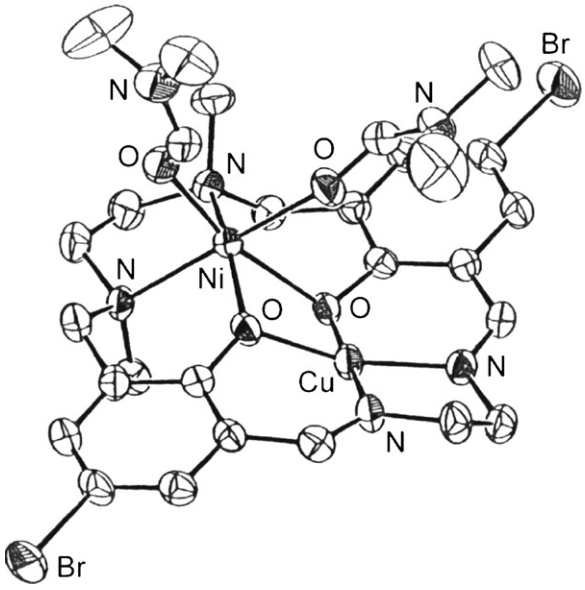

Fig. 12. Structure of $[NiCu(\mathbf{41})(DMF)_2]^{2+}$.

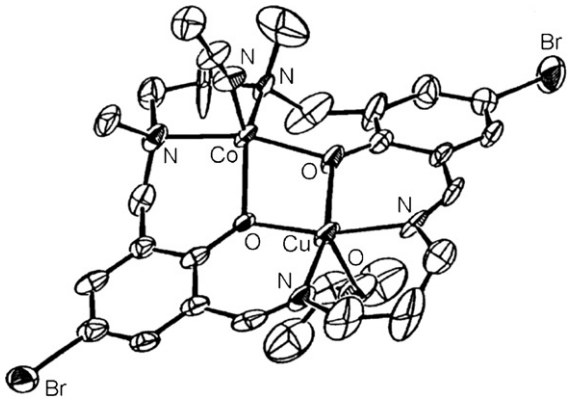

Fig. 13. Structure of $[CoCu(\mathbf{42})(CH_3CN)\{(CH_3)_2CHOH\}]^{2+}$.

temperature magnetic moment of $3.37\mu_B$, which decreases with decreasing temperature to $1.98\mu_B$ at 50 K. The magnetic analysis gives a coupling constant of $J = -57\,cm^{-1}$. A negatively larger exchange integral ($J = -97.0\,cm^{-1}$) was recognized for the isomer $[CuNi(\mathbf{42})](ClO_4)_2$. Thus, $[CoCu(\mathbf{42})](ClO_4)_2{\cdot}CH_3CN$, $[NiCu(\mathbf{41})](ClO_4)_2$ and $[NiCu(\mathbf{42})](ClO_4)_2$ are differentiated by magnetic studies from the related positional $Cu^{II}Co^{II}$, $Ni^{II}Cu^{II}$ and $Cu^{II}Ni^{II}$ isomers, while $[CoCu(\mathbf{42})(CH_3CN)\{(CH_3)_2CHOH\}](ClO_4)_2$ and the $Cu^{II}Co^{II}$ positional isomer could not be unambiguously differentiated. $[ZnCu(\mathbf{41})](ClO_4)_2$, $[ZnCu(\mathbf{42})](ClO_4)_2$ and the related $Cu^{II}Zn^{II}$ isomers have a magnetic moment common for one unpaired electron [24].

The band at 540–570 nm in the electronic spectra of $[CoCu(\mathbf{41})](ClO_4)_2$, $[NiCu(\mathbf{41})](ClO_4)_2$ and $[ZnCu(\mathbf{41})](ClO_4)_2$ in dimethylsulphoxide is attributed to a d–d band of the copper(II) ion in the iminic site. The positional $Cu^{II}Co^{II}$, $Cu^{II}Ni^{II}$ and $Cu^{II}Zn^{II}$ isomers show this d–d bond at longer wavelengths (646–670 nm). In the case of the $Cu^{II}Ni^{II}$ complex, an additional band is observed at 530 nm, characteristic of a low-spin nickel(II) ion [24].

The $Co^{II}Cu^{II}$, $Ni^{II}Cu^{II}$ and $Zn^{II}Cu^{II}$ complexes of $[\mathbf{42}]^{2-}$ show a d–d band due to the copper(II) ion at 634–643 nm. In the spectra of the $Cu^{II}Co^{II}$, $Cu^{II}Ni^{II}$ and $Cu^{II}Zn^{II}$ isomers in dimethylsulphoxide, one or two d–d bands are observed: 571 and 612 nm for the $Cu^{II}Co^{II}$ complex; 587 and 752 nm for the $Cu^{II}Ni^{II}$ complex, 639 nm for the $Cu^{II}Zn^{II}$ complex. Evidently, the spectra of the $Co^{II}Cu^{II}$ and $Ni^{II}Cu^{II}$ complexes with $[\mathbf{42}]^{2-}$ differ from those respectively of the $Cu^{II}Co^{II}$ and $Cu^{II}Ni^{II}$ isomers with $[\mathbf{42}]^{2-}$, though the $Zn^{II}Cu^{II}$ and $Cu^{II}Zn^{II}$ isomers cannot be differentiated by the visible spectra [24].

The $Co^{II}Cu^{II}$, $Ni^{II}Cu^{II}$ and $Zn^{II}Cu^{II}$ complexes of $[\mathbf{41}]^{2-}$ show a quasi-reversible couple at -1.16 ± 0.02 V (versus Ag/Ag) attributable to the Cu^{I}/Cu^{II} process at the iminic site. No reduction occurs for the Co^{II} and Ni^{II} ions in the aminic site at the available potential. In the case of the $Zn^{II}Cu^{II}$ complex the cyclic voltammogram changes with the repeat of sweep, with the decrease of the couple at -1.18 V with concomitant appearance of a cathodic peak near -0.7 V and an anodic peak near -0.6 V. This indicates instability of the complex on the electrode. The isomeric $Cu^{II}Co^{II}$, $Cu^{II}Ni^{II}$ and

$Cu^{II}Zn^{II}$ complexes show a reversible or quasi-reversible couple at -0.55 ± 0.07 V attributed to the Cu^{I}/Cu^{II} process in the aminic site. The reduction potentials for these latter complexes are higher than those of the former ones, indicating that the $\{CuN(amine)_2O_2\}$ chromophore is flexible enough to allow a distorted geometry preferred for the copper(I) ion. The cyclic voltammetry of the $Cu^{II}Co^{II}$ complex has an additional couple at -1.35 V attributable to the Co^{I}/Co^{II} process, and the cyclic voltammetry of $Cu^{II}Ni^{II}$ one has an additional couple at -1.76 V due to the Ni^{I}/Ni^{II} process [24].

The $Co^{II}Cu^{II}$, $Ni^{II}Cu^{II}$ and $Zn^{II}Cu^{II}$ complexes of $[\mathbf{42}]^{2-}$ show a quasi-reversible Cu^{I}/Cu^{II} couple at -0.96 ± 0.04 V, whereas the isomeric $Cu^{II}Co^{II}$, $Cu^{II}Ni^{II}$ and $Cu^{II}Zn^{II}$ complexes show the Cu^{I}/Cu^{II} couple at -0.64 ± 0.05 V. The complex $Co^{II}Cu^{II}$ shows no other reduction wave, but the $Cu^{II}Co^{II}$ isomer shows another reversible couple at -1.64 V attributable to the Co^{I}/Co^{II} process at the iminic site. The $Ni^{II}Cu^{II}$ complex shows an additional couple at -1.76 V attributable to the Ni^{I}/Ni^{II} process in the aminic site. In the case of the $Cu^{II}Ni^{II}$ isomer the Ni^{I}/Ni^{II} process in the iminic site is seen at -1.56 V. Thus, cyclic voltammetry is proved to be an effective technique for differentiating the isomeric $M^{II}Cu^{II}$ and $Cu^{II}M^{II}$ complexes [24].

It was also proved that a copper isomeric conversion in DMSO solution can occur. Thus, cyclic voltammetric measurements show that in the sweep down to 1.3 V, the $Co^{II}Cu^{II}$ complex with $[\mathbf{41}]^{2-}$ shows a good stability on the electrode except for a weaker couple near -0.6 V. In the sweep down to -2.2 V, however, the couple at -1.09 V decreases its intensity and is finally replaced with new two couples at -0.6 and -1.3 V. The resulting cyclic voltammogram is indeed that of the $Cu^{II}Co^{II}$ isomer, demonstrating the conversion of the $Co^{II}Cu^{II}$ complex into the $Cu^{II}Co^{II}$ one on the electrode. The result indicates that the $Co^{II}Cu^{I}$ species of $[\mathbf{41}]^{2-}$ is stable but the $Co^{I}Cu^{I}$ species is unstable to cause the site exchange of the metal ions. For the $Zn^{II}Cu^{II}$ complex with $[\mathbf{41}]^{2-}$ the redox wave at -1.18 V decreases with the repeat of sweep with concomitant appearance of a new couple near -0.65 V. The new redox wave is well compared to the Cu^{I}/Cu^{II} process of the $Cu^{II}Zn^{II}$ isomer, implying isomeric the conversion of the $Zn^{II}Cu^{II}$ complex into the $Cu^{II}Zn^{II}$ isomer [24].

A dimethylsulphoxide solution of the $Ni^{II}Cu^{II}$ complex with $[\mathbf{41}]^{2-}$, when heated at 70 °C, becomes green and shows a d–d band at 570 nm. The color of the solution changes to orange after it is heated at 70 °C for 12 h and shows an absorption band around 530 nm along with a weaker band at 670 nm. The spectrum of the orange solution is exactly the same as that of the $Cu^{II}Ni^{II}$ isomer, demonstrating the occurence of a thermal conversion of the $Ni^{II}Cu^{II}$ complex into the $Cu^{II}Ni^{II}$ one in solution. It must be emphasized that the $Ni^{II}Cu^{II}$ complex is stable at room temperature in dimethylsulphoxide at least for 1 week [24].

N,*N*′-Dimethyl-*N*,*N*′-ethylene-di-(5-bromo-3-formyl-2-hydroxybenzylamine), H_2-**5**, reacts with nickel(II) acetate and ethylenediamine in refluxing methanol and in 1:1:1 molar ratio to form the [1 + 1] macrocyclic complex [Ni(**41**)], where the nickel(II) ion resides in the $N(iminic)_2O_2$ site [25] as proved by the structure of $[Ni(H\text{-}\mathbf{41})](PF_6)\cdot 0.5H_2O$ (Fig. 14),

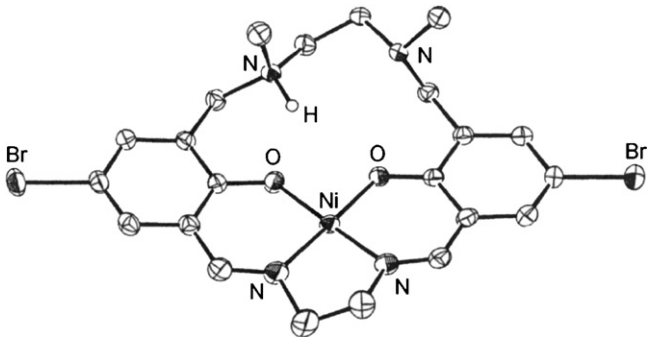

Fig. 14. Structure of $[Ni(H\text{-}\mathbf{41})]^{+}$.

unexpectedly obtained when [Ni(**41**)] was treated with KPF_6 in methanol (Fig. 14). [Ni(**41**)], however, proved not to be a good precursor for heterodinuclear $M^{II}Ni^{II}$ complexes because of its low solubility in common solvents. For example, in the reaction of [Ni(**41**)] with transition metal(II) chloride in methanol, the resulting product, $[MNi(\mathbf{41})(Cl)_2]$, was always contaminated with a large amount of intact [Ni(**41**)]. On the other hand, $[PbNi(\mathbf{41})(CH_3COO)_2]$, derived from [Ni(**41**)] by the reaction with $Pb(CH_3COO)_2\cdot 3H_2O$, was found to be considerably soluble in methanol. The transmetalation reaction using the desired metal(II) sulphate in the presence of KPF_6 afforded $[MNi(\mathbf{41})(CH_3COO)](PF_6)$ ($M = Co^{II}$, Ni^{II}, Cu^{II}, Zn^{II}) (Scheme 5) [25].

In $[PbNi(\mathbf{41})(CH_3COO)_2]$ the nickel(II) ion resides in the iminic site and assumes a nearly planar geometry. The lead(II) ion in the aminic site assumes an eight coordinate geometry together with two bidentate acetate groups (Fig. 15) [25].

$[CoNi(\mathbf{41})(CH_3COO)](PF_6)\cdot CH_3CN$ has a discrete heterodinuclear core with the cobalt(II) ion in the aminic site and the nickel(II) ion in the iminic site. The complex exists in two distinct forms, A and B, with respect to the configuration about one aminic nitrogen which is S in form A, but R in form B. The two methyl groups attached to the asymmetric aminic nitrogen atoms are situated *cis* in form A, but *trans* in form B. Fig. 16 shows the crystal structure of form A. The acetate group coordinates to the cobalt(II) ion as a chelating bidentate ligand, providing a distorted six coordinate geometry about the metal ion which is

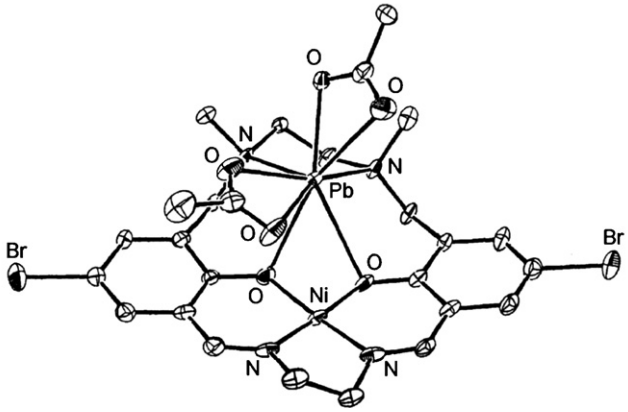

Fig. 15. Structure of $[PbNi(\mathbf{41})(CH_3COO)_2]$.

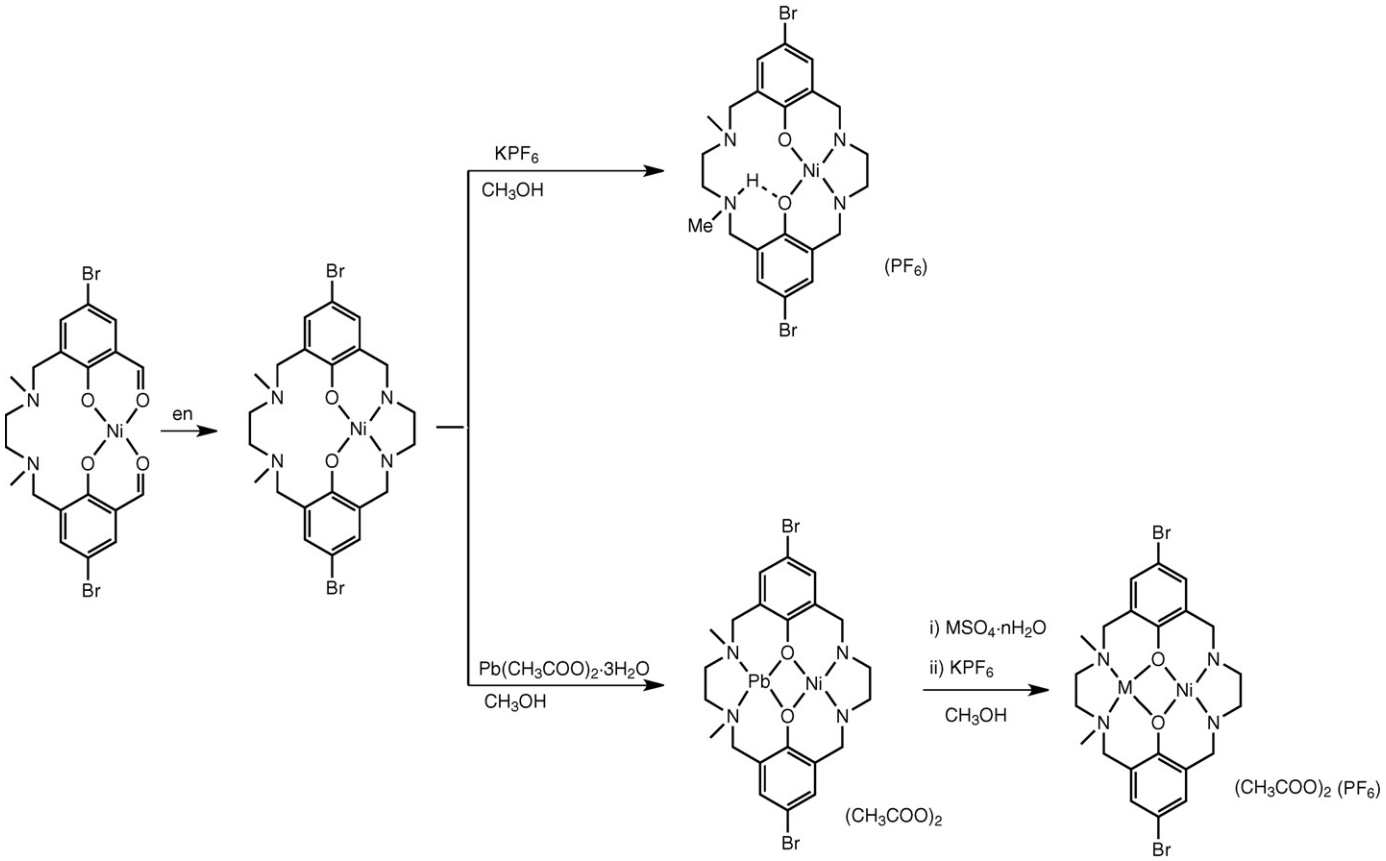

Scheme 5. Synthesis of $[M^{II}Ni(\mathbf{41})(CH_3COO)](PF_6)$ via transmetalation of $[Pb^{II}Ni^{II}(\mathbf{41})(CH_3COO)]$ with MSO_4 ($M = Co^{II}$, Ni^{II}, Cu^{II}, Zn^{II}).

displaced from the $N(amine)_2O_2$ plane toward the acetate ligand. The nickel(II) ion in the iminic site has a planar geometry. The Co···Ni intermetallic separation is 2.991 Å [25].

In $[Ni_2(\mathbf{41})(CH_3COO)](PF_6)$ the nickel(II) ion in the aminic site has a six coordinate geometry together with a bidentate acetate group and is displaced from the $N(amine)_2O_2$ plane toward the acetate group. The nickel(II) ion in the iminic site assumes a planar geometry [25]. $[CuNi(\mathbf{41})(CH_3CN)](PF_6)_2{\cdot}CH_3CN$ has a discrete heterodinuclear core with the copper(II) ion in the aminic site and the nickel(II) ion in the iminic site. The Cu···Ni separation is 2.820 Å. One acetonitrile molecule is bonded to the copper(II) ion providing a five coordinate geometry about the metal ion. The copper(II) ion is displaced from the basal $N(amine)_2O_2$ plane toward the acetonitrile nitrogen. The geometry about the nickel(II) ion is planar (Fig. 17) [25].

$[ZnNi(\mathbf{41})(CH_3COO)](PF_6){\cdot}CH_3CN$ has a discrete heterodinuclear core with a square pyramidal zinc(II) ion in the aminic site and a square planar nickel(II) ion in the iminic site, with a Ni···Zn intermetallic separation of 3.039 Å. The zinc(II) ion is displaced from the basal $N(amine)_2O_2$ plane toward the axial oxygen of the acetate group which acts as unidentate (Fig. 18) [25].

The above X-ray crystallographic results clearly indicate that the metal substitution reaction of $[PbNi(\mathbf{41})(CH_3COO)_2]$ with several metal(II) sulphates affords the corresponding $M^{II}Ni^{II}$ complexes. This differs from the metal substitution reaction of $[PbCu(\mathbf{L})](ClO_4)_2$ (H_2-**L** = H_2-**41**, H_2-**42**) with the same

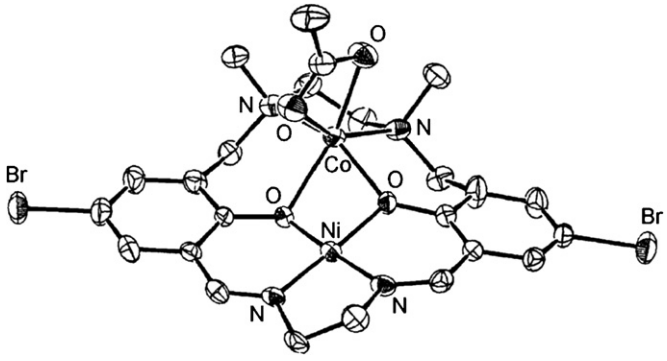

Fig. 16. Structure of $[CoNi(\mathbf{41})(CH_3COO)]^+$.

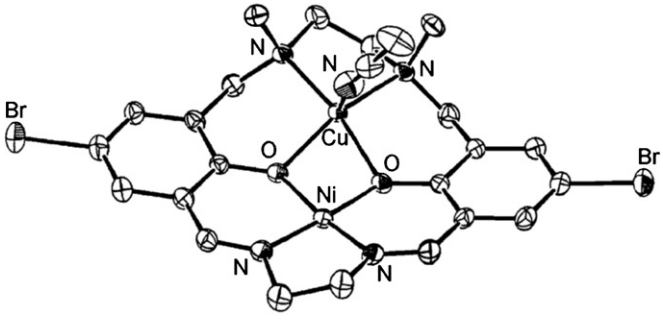

Fig. 17. Structure of $[CuNi(\mathbf{41})(CH_3CN)]^{2+}$.

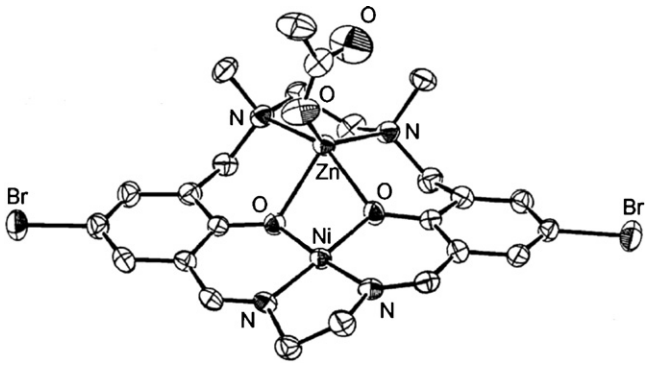

Fig. 18. Structure of $[ZnNi(\mathbf{41})(CH_3COO)]^+$.

metal(II) sulphates, where the copper(II) ion migrates from the iminic to the aminic site, affording the isomeric $Cu^{II}M^{II}$ complexes. It was supposed that $[PbCu(\mathbf{L})](ClO_4)_2$ binds the incoming metal(II) ion through the two phenolic oxygen atoms to form a di(μ_3-phenoxo) $Pb^{II}Cu^{II}M^{II}$ complex and then M^{II} moves to the iminic site with concomitant migration of Cu^{II} to the aminic site and release of the Pb^{II} from the aminic site. In the $Pb^{II}Ni^{II}$ analogue the metal substitution reaction may proceed by a dissociative mechanism, because the *cis* arrangement of the two *N*-methyl groups in the $Pb^{II}Ni^{II}$ precursor complex changes to the *trans* arrangement in $[CoNi(\mathbf{41})(CH_3COO)](PF_6)$ (form B) and $[Ni_2(\mathbf{41})(CH_3COO)](PF_6)$. The structure of $[PbNi(\mathbf{41})(CH_3COO)_2]$ indicates that the nickel(II) ion is strongly bound to the iminic site whereas the lead(II) ion is loosely bound to the aminic site. The structural features of the $Pb^{II}Ni^{II}$ complex can explain the facile substitution of the lead(II) ion in the aminic site for the incoming metal(II) ion while maintaining the nickel(II) ion in the iminic site [25].

While $[ZnNi(\mathbf{41})(CH_3COO)](PF_6)$ is diamagnetic, the room temperature magnetic moments of $[MNi(\mathbf{41})(CH_3COO)](PF_6)$ ($M = Co^{II}$, Ni^{II}, Cu^{II}) (4.98, 3.17 and 1.87 μ_B, respectively) are common for isolated cobalt(II), nickel(II) and copper(II) ions; the nickel(II) ion in the iminic site is diamagnetic in all these complexes [25].

The visible spectrum of $[MNi(\mathbf{41})(CH_3COO)](PF_6)$ in dimethylformamide shows a band at 520 nm, typical of planar nickel(II) ion in the iminic site. The $Co^{II}Ni^{II}$ complex shows a discernible shoulder near 1240 mm, due to a d–d band of the cobalt(II) ion. The $Ni_2{}^{II}$ complex shows two additional bands at 652 and 1030 nm attributable to the d–d components of the nickel(II) ion in the aminic site. The $Cu^{II}Ni^{II}$ complex has a distinct absorption band at 670 nm due to the copper(II) ion in the aminic site [25].

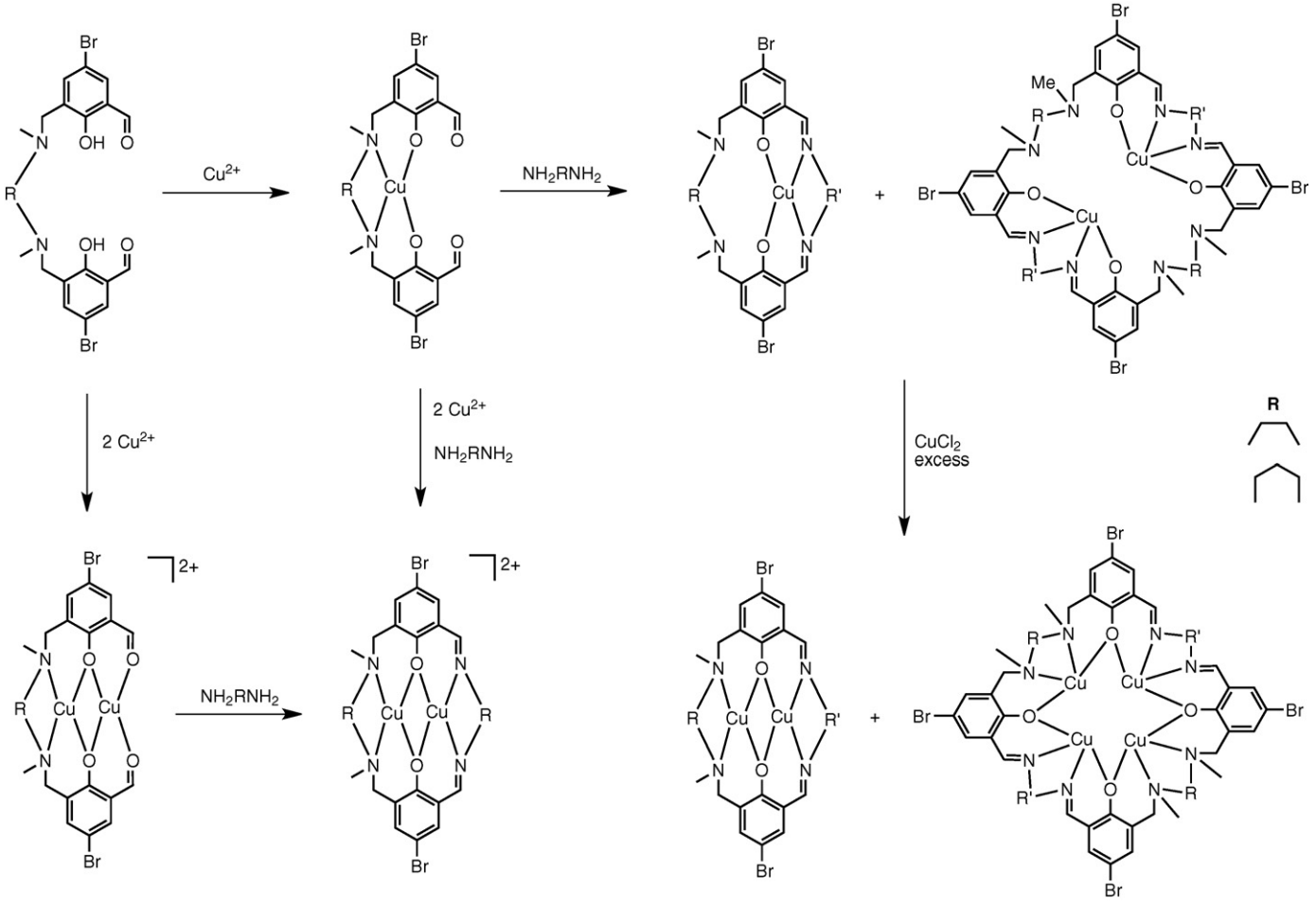

Scheme 6. Site migration and ring expansion in the synthesis of dinuclear and tetranuclear copper(II) complexes with asymmetric cyclic ligands.

Cyclic voltammetry of [MNi(**41**)(CH_3COO)](PF_6) shows a reversible or quasi-reversible couple at 1.29 V (versus Ag/Ag^+), attributable to the Ni^I/Ni^{II} redox process in the iminic site. The $Cu^{II}Ni^{II}$ complex shows two redox couples at −0.08 and −1.57 V; the former can be attributed to the Cu^I/Cu^{II} redox process at the aminic site. The high potential of the Cu^I/Cu^{II} process can be ascribed to the distorted $\{CuN_2O_2\}$ environment favourable for the copper(I) ion. The second couple at −1.57 V is assigned to the Ni^I/Ni^{II} process that occurs at low potential relative to those for the $Co^{II}Ni^{II}$, $Ni^{II}Ni^{II}$ and $Zn^{II}Cu^{II}$ analogues. This is because the reduction of the nickel(II) ion in [CuNi(**41**)(CH_3COO)](PF_6) accompanies a charge change of $\{Ni^{II}Cu^I/Ni^ICu^I\}$ and this change is energetically more difficult than the charge change of $\{M^{II}Ni^{II}/M^{II}Ni^I\}$ accompanied by the nickel(II) ion reduction of [MNi(**41**)(CH_3COO)](PF_6) (M = Co^{II}, Ni^{II}, Zn^{II}).

[CuNi(**41**)(CH_3COO)](PF_6) combines methylimidazole in dimethylformamide at the axial site of the nickel(II) ion to cause the spin conversion of the diamagnetic nickel(II) ion into the paramagnetic nickel(II) one. A strong antiferromagnetic interaction operates between the copper(II) and nickel(II) ions in the resulting methylimidazole adduct. The EPR spectrum for the spin-doublet ground state indicates that one unpaired electron exists on the molecular orbital comprised of d_z^2(Cu) and d_z^2 (Ni) and is delocalized over the two metal ions [25].

The [2 + 2] tetranucleating macrocyclic ligand H_4-**43**, containing N(amine)$_2O_2$ and N(imine)$_2O_2$ metal binding sites in an alternate fashion in a macrocyclic framework, was first obtained as [Cu_2(**43**)] together with [Cu(**41**)], which derives from a ring contraction the [2 + 2] macrocycle $[\mathbf{43}]^{4-}$ to the [1 + 1] macrocycle $[\mathbf{41}]^{2-}$, by the condensation of [Cu(**5**)] with ethylenediamine [26]. [Cu_2(**43**)] has been used to produce the mixed-metal $M^{II}{}_2Cu_2{}^{II}$ complexes, [M_2Cu_2(**43**)($Cl)_4$], of a deficient double cubane structure (M = Ni^{II}), or a dimer-of-dimers structure (M = Co^{II}, Zn^{II}) (Scheme 6) [27].

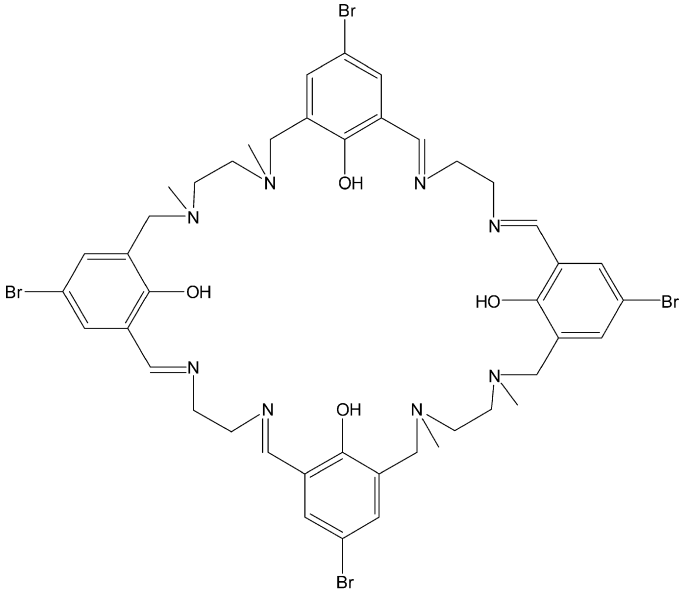

H_2-**43**

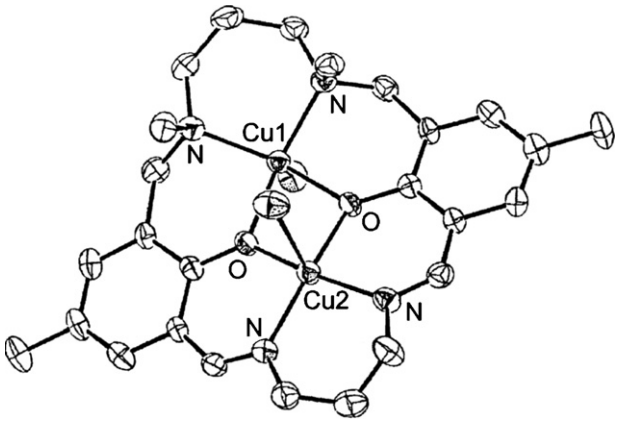

Fig. 19. Structure of [Cu_2(**44**)($Cl)_2$].

The reaction of the dinuclear acyclic copper complex [Cu_2(**6**)]($ClO_4)_2$ afforded preferentially the [1 + 1] condensation product, [Cu_2(**44**)]($ClO_4)_2$, when reacted with an α,ω-diamine, probably because the two formyl groups in [Cu_2(**6**)]($ClO_4)_2$ are fixed in close proximity so as to be efficiently cyclized with one diamine [28]. Instead, the green product, derived by the reaction of [Cu(**6**)], where the copper(II) ion is in the N(amine)$_2O_2$ site, with 1,3-diaminopropane was found to be a mixture of the [1 + 1] and [2 + 2] condensation products, [Cu(**44**)] and [Cu_2(**45**)], based on FAB mass spectrometric studies [29]. The mixture of [Cu(**44**)] and [Cu_2(**45**)], when treated with an excess of $CuCl_2$, gives a mixture of [Cu_2(**44**)($Cl)_2$] and [Cu_4(**45**)($Cl)_4$]. The tetranuclear less soluble complex deposits as a brown precipitate while [Cu_2(**44**)($Cl)_2$] was isolated as green crystals from the mother solution. FAB-mass spectrometry studies demonstrate that [Cu_4(**45**)($Cl)_4$] is a tetranuclear complex of $[\mathbf{45}]^{4-}$, affording peaks corresponding to $\{Cu_4(\mathbf{45})(Cl)\}^+$, $\{Cu_4(\mathbf{45})(Cl)_2\}^+$ and $\{Cu_4(\mathbf{45})Cl_3\}^+$ [29].

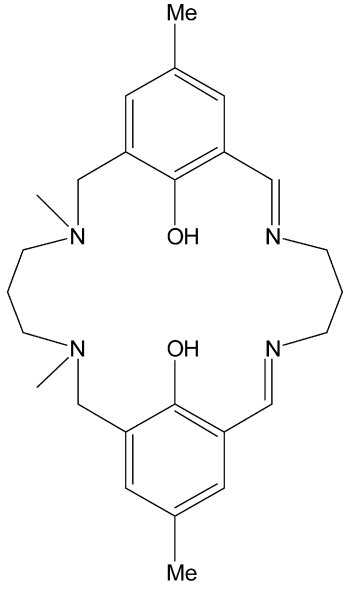

H_2-**44**

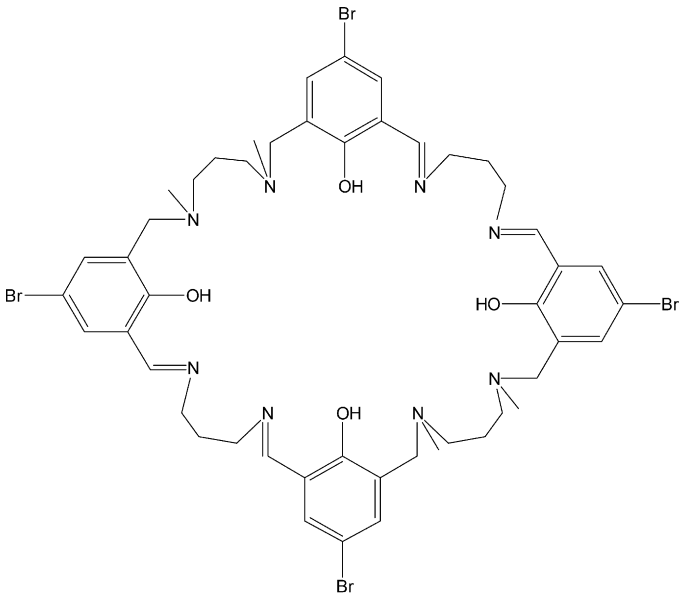

H_2-**45**

$[Cu_2(\mathbf{44})(Cl)_2]$ and $[Cu_4(\mathbf{45})(Cl)_4]$ were converted respectively into $[Cu_2(\mathbf{44})](ClO_4)_2$ and $[Cu_4(\mathbf{45})](ClO_4)_4$ by the treatment with $AgClO_4$; $[Cu_2(\mathbf{44})](ClO_4)_2$ was also obtained by the reaction of $[Cu_2(\mathbf{6})](ClO_4)_2$ and 1,3-diaminopropane. $[Cu_4(\mathbf{45})](ClO_4)_4$, when treated with excess NH_4Cl in methanol, reforms $[Cu_4(\mathbf{45})(Cl)_4]$ (Scheme 6) [29].

$[Cu_2(\mathbf{44})(Cl)_2]$ has the usual dinuclear structure with both copper(II) ions, 3.070 Å apart, in a square pyramidal geometry. Both copper(II) ions are displaced from the basal plane toward the apical chloride ions. The two chloride ligands are situated *trans* to each other with respect to the mean molecular plane (Fig. 19) [29].

The absorption spectrum of $[Cu_2(\mathbf{44})(Cl)_2]$ in methanol (two bands at 348 and 650 nm) resembles that of $[Cu_2(\mathbf{44})](ClO_4)_2$ in dimethylformamide (bands at 346 and 640), indicating that the axial chloride groups of $[Cu_2(\mathbf{44})(Cl)_2]$ are liberated in solution [29].

The magnetic moment of $[Cu_2(\mathbf{44})(Cl)_2]$ ($0.87\mu_B$ per Cu at room temperature) decreases with decreasing temperature to $0.17\mu_B$ at 2 K, implying a strong antiferromagnetic interaction between the two copper(II) ions ($J = -335\,cm^{-1}$). A slightly smaller exchange integral ($J = -270\,cm^{-1}$) was found for $[Cu_2(\mathbf{44})](ClO_4)_2$ [29].

$[Cu_4(\mathbf{45})(DMF)_2](ClO_4)_4\cdot(CH_3)_2CHOH\cdot 2DMF\cdot H_2O$, obtained when a dimethylformamide solution of $[Cu_4(\mathbf{45})(DMF)_2](ClO_4)_4$ was diffused with 2-propanol, has a dimer-of-dimers structure. Each $N(amine)_2O_2$ entity of the ligand accommodates one copper(II) ion in the usual tetradentate chelating mode, whereas each $N(imine)_2O_2$ entity presumes a spread shape to combine one copper(II) ion with its NO donor atoms and another copper(II) ion with the remaining NO donor atoms. The square pyramidal copper(II) ion in the aminic site is displaced from the basal plane toward the axial dimethylformamide oxygen. The other copper(II) ion resides in the $N(imine)_2O_2$ site in a planar four coordinate geometry. The Cu···Cu interatomic separation within each dimer is 3.090 Å and the Cu···Cu separation between dimers is 7.435 Å (Fig. 20) [29].

The magnetic moment of $[Cu_4(\mathbf{45})(Cl)_4]$ ($0.88\mu_B$ per Cu at room temperature) decreases with decreasing temperature to $0.18\mu_B$ at 2 K. Similarly, the magnetic moment of $[Cu_4(\mathbf{45})](ClO_4)_4$ ($0.64\mu_B$ at room temperature) decreases to $0.05\mu_B$ at 2 K. Although $[Cu_4(\mathbf{45})](ClO_4)_4$ has a dimer-of-dimers structure, the magnetic data can be rationalized according to the Bleaney Bowers equation and show an antiferromagnetic interaction ($J = -340\,cm^{-1}$) inside each dinuclear entity. Also $[Cu_4(\mathbf{45})(Cl_4)_4]$ has a tetranuclear core, consisting of two magnetically isolated dinuclear units where the two copper(II) ions interact antiferromagnetically [29].

The reflectance and absorption spectra of $[Cu_4(\mathbf{45})(Cl)_4]$ show Cl-to-Cu^{II} LMCT bands at ~480 and 475 nm and a d–d band at 600–1000 nm, indicating a tetranuclear core with

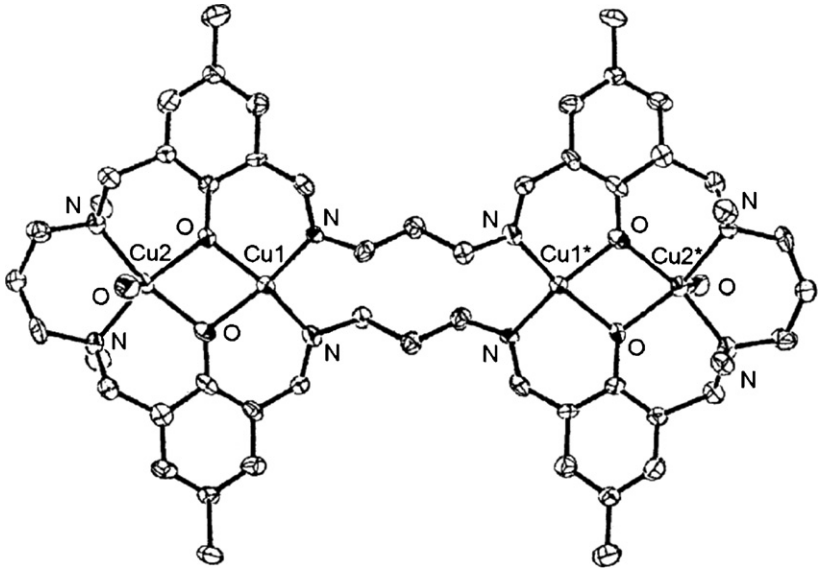

Fig. 20. Structure of $[Cu_4(\mathbf{45})(DMF)_2]^{2+}$ (only the oxygen atoms of the two dimethylformamide ligands are reported for clarity).

chloride ligations stable in methanol. A structure was proposed for $[Cu_4(\mathbf{45})(Cl)_4]$ which derives from the folded form of $[Cu_4(\mathbf{45})(ClO)_4]$ with Cu–Cl–Cu linkages [29]. This structure can explain the facile interconversion between $[Cu_4(\mathbf{45})](Cl)_4$ and $[Cu_4(\mathbf{45})](ClO_4)_4$ by the change the counter ion, and the strong chloride ligation in solution. The negligible magnetic interaction between the two dinuclear units through the chloride bridges is due to the absence of unpaired electron on the d_z^2 orbitals of the copper(II) ions [29].

The cobalt(II) complex of *N*,*N*′-dimethyl-*N*,*N*′-ethylenedi(5-bromo-3-formyl-2-hydroxybenzylamine), [Co(**5**)], when condensed with ethylenediamine in dimethylformamide in the presence of $Pb(ClO_4)_3{\cdot}3H_2O$, affords $[PbCo(\mathbf{41})(DMF)_4](ClO_4)_2$ which, by treatment with the appropriate metal(II) sulphate in acetonitrile and in the presence of sodium acetate, forms the heterodinuclear complexes $[FeCo(\mathbf{41})(\mu\text{-}CH_3COO)(CH_3OH)](ClO_4)$ and $[MCo(\mathbf{41})(\mu\text{-}CH_3COO)](ClO_4)$ ($M^{II} = Co^{II}$, Ni^{II}, Cu^{II}, Zn^{II}). As above reported, the similar transmetalation of the lead(II) ion in $[PbCu(\mathbf{41})](ClO_4)_2$ and $[PbCu(\mathbf{42})](ClO_4)_2$ by a transition metal(II) ion results in the migration of the copper(II) ion from the $N(imine)_2O_2$ to the $N(amine)_2O_2$ site to afford the isomeric $Cu^{II}M^{II}$ complexes [30]. Such metal migration is not the case in the transmetalation reaction of $[PbCo(\mathbf{41})(DMF)_4](ClO_4)_2$ with metal(II) sulphate [30].

The cobalt(II) ion, located in the $N(imine)_2O_2$ site of $[PbCo(\mathbf{41})(DMF)_4](ClO_4)_2$, completes its square pyramidal geometry by a dimethylformamide oxygen in the apical position. The metal ion is displaced from the basal N_2O_2 plane toward the dimethylformamide oxygen. The lead(II) ion in the $N(amine)_2O_2$ site reaches the eight coordinate geometry with four dimethylformamide oxygen atoms. One dimethylformamide molecule bridges the cobalt and lead ions through its oxygen atom. Also the lead ion is displaced from N_2O_2 plane. The intermetallic Co···Pb separation is 3.272 Å (Fig. 21) [30].

Owing to the presence of a bridging dimethylformamide between the lead(II) and cobalt(II) ions in $[PbCo(\mathbf{41})(DMF)_4](ClO_4)_2$, is likely that the transmetalation with $M^{II}SO_4$ proceeds by a mechanism differing from that of $[PbCu(\mathbf{41})](ClO_4)_2$ with $M^{II}SO_4$, which affords the $M^{II}Co^{II}$ complexes.

In $[FeCo(\mathbf{41})(\mu\text{-}CH_3COO)(CH_3OH)](ClO_4)$ the iron(II) ion in the $N(amine)_2O_2$ site and the cobalt(II) ion in the $N(imine)_2O_2$ site are bridged by an acetate group, giving rise to a {μ-acetato-di-μ-phenolato-iron(II)-cobalt(II)} core. The Fe···Co separation is 2.886 Å. The five coordinate square pyramidal iron(II) ion is displaced from the $N(amine)_2O_2$ mean plane toward one apical oxygen atom of the acetate group. The cobalt(II) ion in the $N(imine)_2O_2$ reaches an axially elongated octahedral geometry by a bridging acetate oxygen and a methanol oxygen at the axial sites (Fig. 22).

The crystals of $[MCo(\mathbf{41})(\mu\text{-}CH_3COO)](ClO_4)$ ($M = Co^{II}$, Ni^{II}, Cu^{II}, Zn^{II}) are isomorphous. The dicobalt(II) complex has a {μ-acetato-di-μ-phenolato-dicobalt(II)} core with a Co···Co intermetallic separation of 2.802 Å. The square pyramidal geometry around the cobalt(II) ion in the $N(amine)_2O_2$ site is

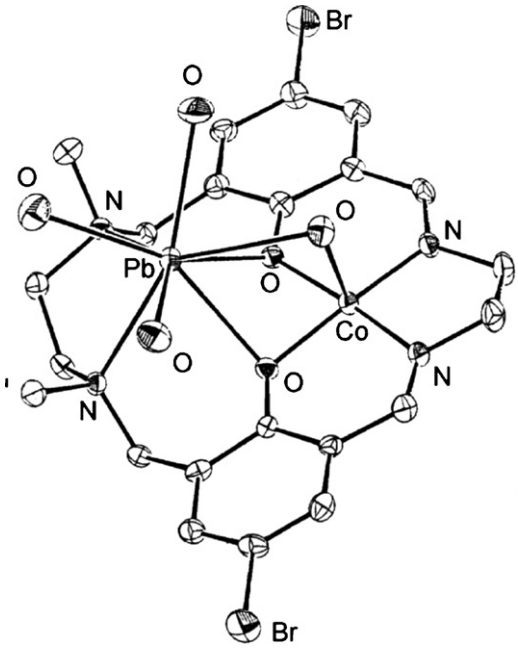

Fig. 21. Structure of $[PbCo(\mathbf{41})(DMF)_4]^{2+}$ (only the oxygen atoms of the four dimethylformamide ligands are reported for clarity).

completed by an axial acetate oxygen. The geometry around the other cobalt(II) ion in the $N(imine)_2O_2$ site is also square pyramidal, the metal ion being displaced from the mean basal N_2O_2 plane toward the other apical acetate oxygen (Fig. 23).

$[Zn^{II}Co^{II}(\mathbf{41})(\mu\text{-}CH_3COO)](ClO_4)$ contains a low spin cobalt(II) ion with the one unpaired electron in the d_z^2 orbital while the heterodinuclear complexes $[M^{II}Co^{II}(\mathbf{41})(\mu\text{-}CH_3COO)](ClO_4)$ exhibit antiferromagnetic interaction

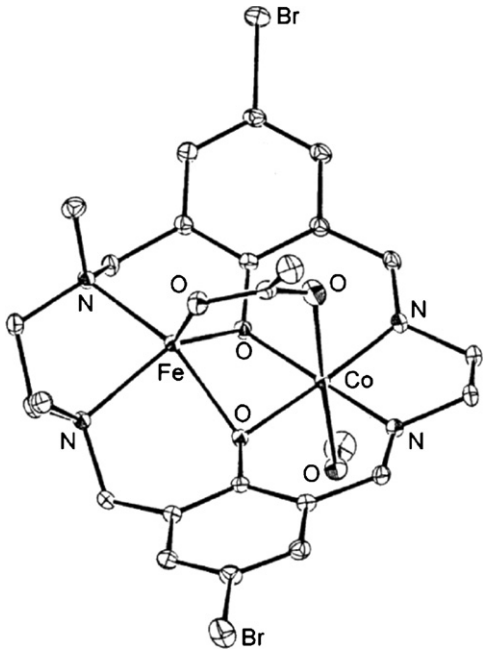

Fig. 22. Structure of $[FeCo(\mathbf{41})(CH_3COO)(CH_3OH)]^+$.

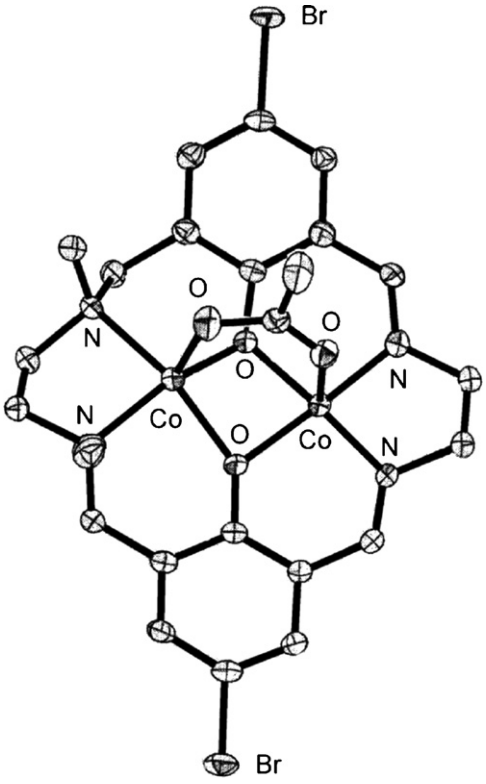

Fig. 23. Structure of $[Co_2(\mathbf{41})(CH_3COO)]^+$.

between the metal ions when M^{II} is Fe^{II} or Co^{II}, and ferromagnetic interaction when M^{II} is Ni^{II} or Cu^{II} [30].

The mononuclear macrocycle precursor [Cu(**46**)]·1.9NaCl, derived from the asymmetric macrocyclic compartmental ligand

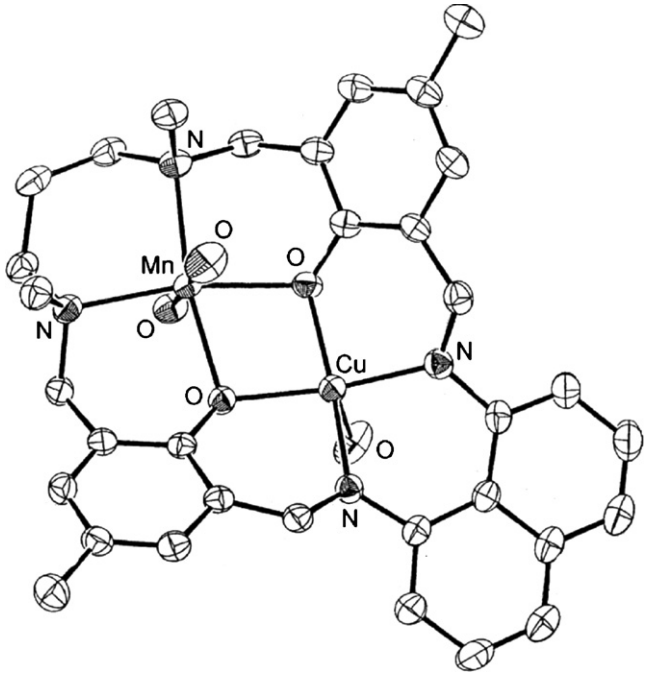

Fig. 24. Structure of $[MnCu(\mathbf{46})(DMF)_2]^{2+}$ (only the oxygen atoms of the two dimethylformamide ligands are reported for clarity).

H_2-**46** which has a $N(amine)_2O_2$ metal-binding site with a 1,3-trimethylene chain between the two aminic nitrogen atoms and a $N(imine)_2O_2$ site with a 1,8-naphthalene chain between the two iminic nitrogen atoms, affords the heterodinuclear complexes, $[M^{II}Cu^{II}(\mathbf{46})(DMF)_2](ClO_4)_2$ (M^{II} = Mn^{II}, Co^{II}, Ni^{II}, Zn^{II}) by reaction with the appropriate metal(II) perchlorate hexahydrate in a 1:1 molar ratio and in a methanol/dimethylformamide solution [31].

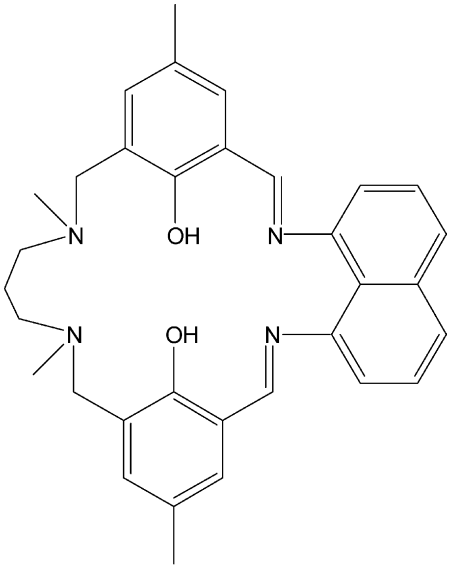

H_2-**46**

$[MnCu(\mathbf{46})(DMF)_2](ClO_4)_2$ has a discrete heterodinuclear core with the manganese(II) and the copper(II) ions, 3.144 Å apart, bridged by two phenolic oxygen atoms. The manganese(II) ion resides in the $N(amine)_2O_2$ site and reaches a six coordinate geometry with two dimethylformamide molecules at the axial positions. The copper(II) ion in the $N(iminic)_2O_2$ site has a five coordinate geometry with a perchlorate oxygen atom at the axial positional. The whole molecule has a saddle-like shape with a non-planar arrangement of the macrocyclic ligand about the two metal ions (Fig. 24). The crystal structures of the $Co^{II}Cu^{II}$, $Ni^{II}Cu^{II}$ and $Zn^{II}Cu^{II}$ complexes resemble that of the $Mn^{II}Cu^{II}$ one [31].

The visible spectra of these heterodinuclear $M^{II}Cu^{II}$ complexes are similar to each other and have two absorptions at 590 and 685 nm, attributed to d–d bands of the copper(II) ion in the iminic site. The d–d bands due to the cobalt(II) ion of the $Co^{II}Cu^{II}$ complex and the d–d bands due to nickel(II) ion of the $Ni^{II}Cu^{II}$ complex are concealed by the stronger copper(II) d–d bands. The spectrum of the $Co^{II}Cu^{II}$ complex has a discernible shoulder at −540 nm, possibly a d–d component of the pseudo octahedral cobalt(II) ion [31].

The cyclic voltammetry in dimethylformamide of these complexes, except the $Ni^{II}Cu^{II}$ one, show two reversible or quasi-reversible couples at −0.93 and −1.96 V (versus Ag/Ag^+) irrespective of the M^{II} in the aminic site. The former couple can be assigned to the Cu^{II}/Cu^{I} process. This wave is located at low potential relative to the Cu^{II}/Cu^{I}

reduction of related $M^{II}Cu^{II}$ complexes probably because the constrained $\{CuN_2O_2\}$ chromophore is hardly distorted to a non-planar configuration preferred for the copper(II) ion. The couple at ~ -1.96 V must be associated with the reduction of the naphthalene di-imine moiety of the ligand since such wave is not observed for $M^{II}Cu^{II}$ complexes of analogous macrocyclic ligands having an alkane bridge instead of the 1,8-naphthalene bridge. The CV of the $Ni^{II}Cu^{II}$ complex has another couple at -1.33 V attributable to the Ni^{I}/Ni^{I} process. In this complex the reduction wave of the ligand occurs at -2.10 V.

The effective magnetic moment of the $Mn^{II}Cu^{II}$ complex ($5.84\mu_B$ at room temperature) gradually decreases to $4.9\mu_B$ around 50 K, then it drops to $4.57\mu_B$ at 2.0 K. The result indicates that an antiferromagnetic interaction ($J = -30\,cm^{-1}$) operates between the manganese(II) and copper(II) ions. The effective magnetic moment of the $Co^{II}Cu^{II}$ complex ($4.67\mu_B$ at room temperature) decreases to $1.71\mu_B$ at 2.0 K, owing to the antiferromagnetic interaction operating between the cobalt(II) and copper(II) ions. However, the magnetic moment at 2.0 K lower than the value for $S_T = 1$, arises from an antiferromagnetic coupling between $S_{Co} = 3/2$ and $S_{Cu} = 1/2$, indicating that a secondary effect contributes to the temperature-dependence of the magnetic moment this complex. The decrease of the effective magnetic moment of the $Ni^{II}Cu^{II}$ complex from $3.40\mu_B$ at room temperature to $1.9\mu_B$ below 80 K indicates that a strong antiferromagnetic interaction operates between the nickel(II) and copper(II) ions which affords the thermal population only on the $S_T = 1/2$ ground state at liquid nitrogen temperature. The energy separation between the $S_T = 1/2$ ground state and the $S_T = 3/2$ upper state is 201 cm^{-1} [31].

The nickel(II) complexes $[Ni_2(\mathbf{L})](ClO_4)_2$ (H_2-**L** = H_2-**47**$\cdots H_2$-**51**), where the macrocyclic ligands contain two different N_2O_2 compartments, one with two piperazinyl nitrogens and two phenolic oxygens and the other with two azomethine nitrogens and two phenolic oxygens, were synthesized by condensation of the acyclic nickel(II) complexes [Ni(**7**)], derived from the reaction of 6,6′-piperazine-1,4-diyldimethylenebis(-2-formyl-4-X-phenol) (X = CH_3, Br) with nickel(II) acetate, with the appropriate diamines in the presence of $Ni(ClO_4)_2$ in a 1:1:1 molar ratio [32].

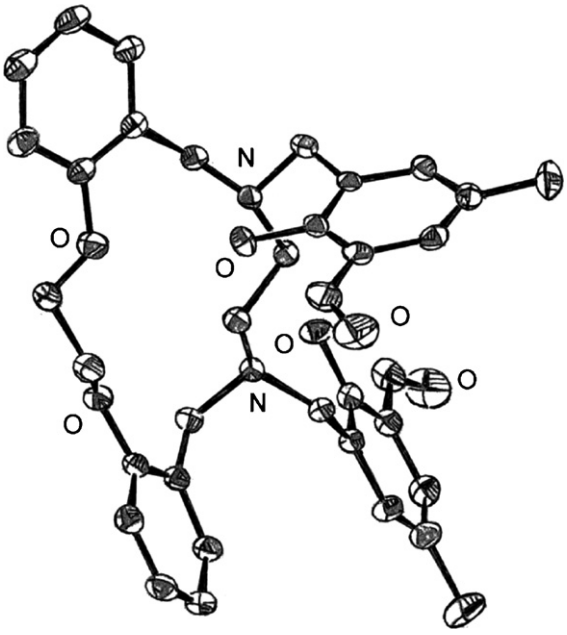

Fig. 25. Structure of $[H_3$-**8**$]^+$.

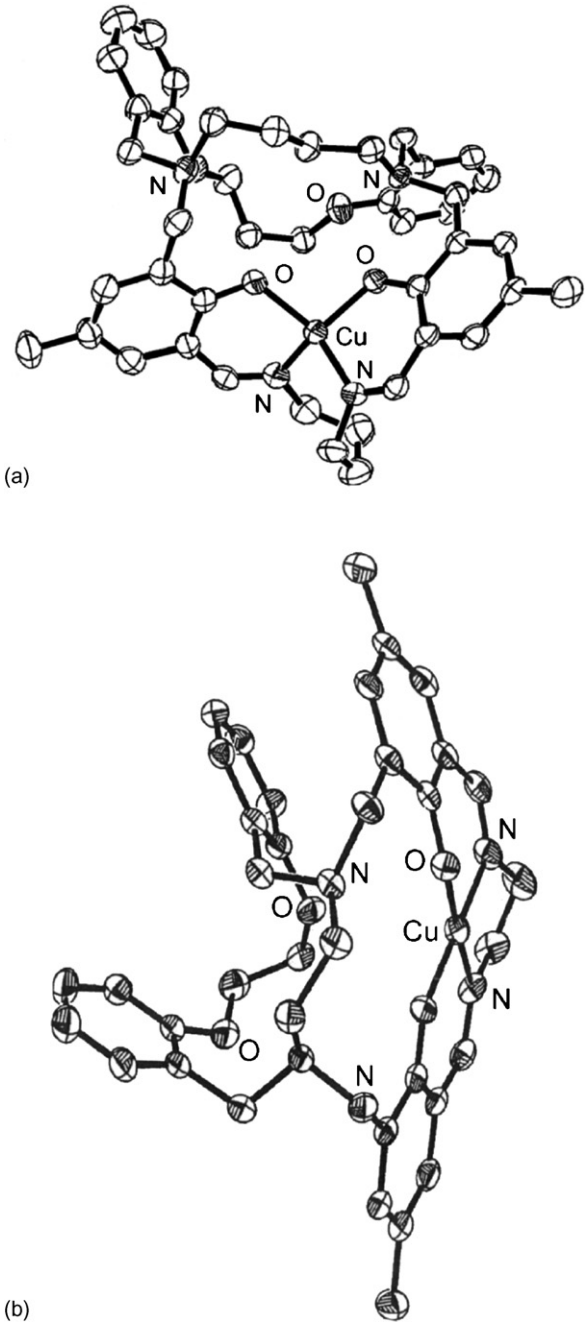

Fig. 26. Structure of $[Cu(H_2$-**54**$)]^{2+}$ (a) and $[Cu(H$-**55**$)]^+$ (b).

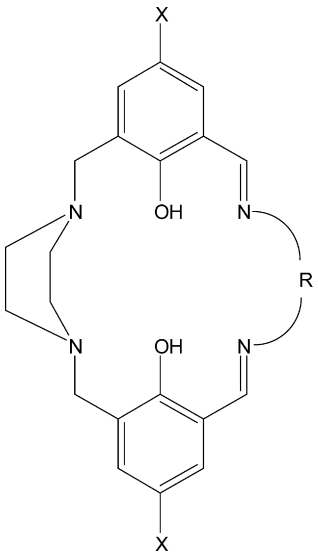

	R
H_2-**47**	-$(CH_2)_2$
H_2-**48**	-$(CH_2)_3$
H_2-**49**	-$(CH_2)_4$
H_2-**50**	-$(CH_2)_2$-NH-$(CH_2)_2$
H_2-**51**	

All these complexes undergo two quasi-reversible one electron transfer processes in the cathodic potential region (0 to −1.3 V) and two quasi-reversible one electron transfer processes in the anodic potential region (0 to +1.3 V). In both processes the first electron transfer process is shifted toward anodic potential region as the macrocyclic ring size increases. The reduction and oxidation processes also change with the substituent at the *para* position of the phenolic oxygen atoms [32].

The mononuclear copper(II) and nickel(II) complexes $[M(H_2\text{-}\mathbf{L})](ClO_4)_2$ (H_2-**L** = H_2-**52**···H_2-**60**) have been synthesized from the reaction of the appropriate formyl precursor (H_2-**8**···H_2-**13**) with the diamines, H_2N-R-NH_2 (R = $(CH_2)_n$ with n = 2,3,4;C_6H_4; $C_{10}H_6$) in the presence of $M(ClO_4)_2{\cdot}6H_2O$ (M = Ni^{II}, Cu^{II}) as templating agent. The correct nature of the diformyl precursor, obtained by reaction of the appropriate di-oxadiazamacrocycle with 3-chloromethyl-5-methylsalicylaldehyde, was established by X-ray diffractometry (Fig. 25) [33].

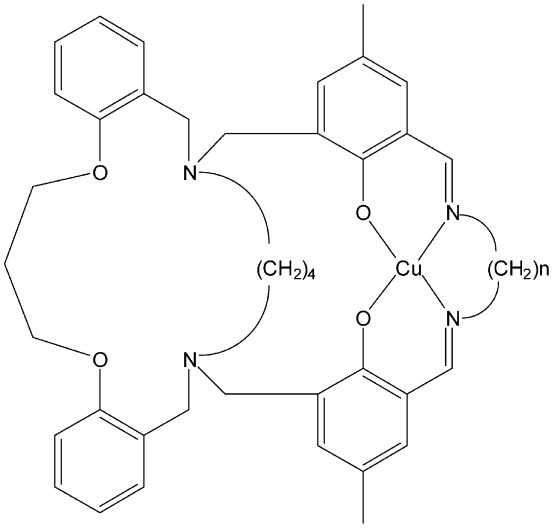

n	
2	H_2-**52**
3	H_2-**53**
4	H_2-**54**

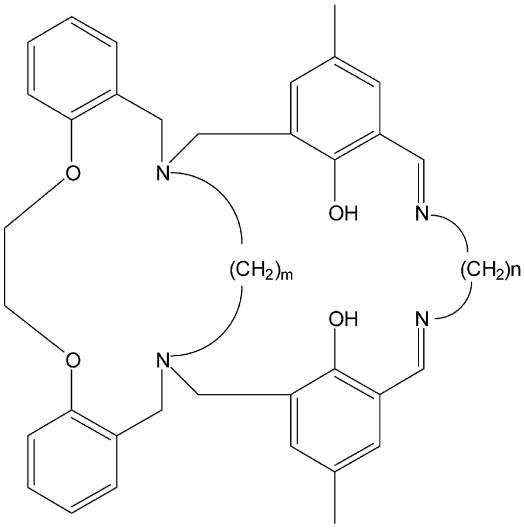

	m	n
H_2-**55**	2	2
H_2-**56**	2	3
H_2-**57**	2	4
H_2-**58**	3	2
H_2-**59**	3	3
H_2-**60**	3	4

The structure of [Cu(H$_2$-**54**)](ClO$_4$)$_2$·2CH$_3$CN shows the copper(II) ion is tetracoordinated by two imine nitrogen and two phenoxy oxygen atom in a distorted square planar geometry. Among the three compartments of H$_2$-**54**, the metal ion prefers to be encompassed by the N$_2$O$_2$ one containing phenolic oxygens and imine nitrogens. X-ray studies show the presence of perchlorate anions, acetonitrile solvent molecules and the protonation of tertiary nitrogen atoms (Fig. 26a) [33].

Also in [Cu(H-**55**)](ClO$_4$)·CH$_3$CN the copper(II) ion resides in the N$_2$O$_2$ chamber in a distorted square planar geometry. Two imine nitrogen and two phenoxy oxygen atoms were coordinated in the equatorial plane to the copper(II) ion. One of the tertiary nitrogen atoms is protonated. One perchlorate anion neutralizes the positive charge of the complex. The acetonitrile molecule is not coordinated to the copper(II) ion and occupies the crystal lattice as a free molecule (Fig. 26b) [34].

Voltammetry studies of [Cu(H$_2$-**L**)](ClO$_4$)$_2$ (H$_2$-**L** = H$_2$-**52**···H$_2$-**60**) in the potential range −0.2 to −1.3 and in dimethylformamide containing 10^{-1} M [N(Bu)$_4$](ClO$_4$) show one well defined quasi-reversible reduction wave at negative potential in the range −0.80 to −0.90 V due to Cu^{II}/Cu^{I} for all these dinuclear copper(II) complexes [Cu(H$_2$-**L**)](ClO$_4$)$_2$ in agreement with controlled potential electrolysis which indicates that the couple corresponds to one electron transfer process. The reduction potential of the copper complexes with H$_2$-**52** to H$_2$-**54** shifts toward anodic from −0.90 to −0.80 V, as the number of methylene group between imine nitrogens in chelate ring is increased. This, in turn, increasing the size of macrocycle and causing a higher flexibility and more distortion from planarity, tries to stabilize the copper(I) complex. The larger ΔE values observed have been attributed to the migration of the reduced copper(I) cation from the rigid Schiff base compartment to the adjacent, more flexible one, containing tertiary nitrogens which favours a tetrahedral geometry. Furthermore, the decrease in ΔE value as the chain length between two imine nitrogens increases, eases readily the tetrahedral geometry moving from the complexes of ligands H$_2$-**52** to H$_2$-**54**. Thus, a small variation of the ring size and/or rigidity of the ligand environment imposes a greater influence on structural and electrochemical properties of the complexes [33].

As ascertained by X-ray structural determinations of [Cu$_2$(**57**)](ClO$_4$)·2CH$_3$CN, the dinuclear copper(II) complexes [Cu$_2$(**L**)](ClO$_4$)$_2$·2CH$_3$CN (H$_2$-**L** = H$_2$-**55**···H$_2$-**60**), prepared by template reaction or by a step by step procedure in the presence of triethylamine, contain one distorted square pyramidal copper(II) ion in the N(amine)$_2$O$_2$ site with the basal plane occupied by two oxygen and two nitrogen atoms and the axial position by the oxygen atom of a perchlorate group. The other copper(II) ion lies in the Schiff base and has a distorted square planar arrangement. The two metal ions are present in the same macrocycle: the second metal ion also prefers to be encapsulated in the phenolic oxygen compartment, leaving the ether oxygen compartment free. The acetonitrile molecules are not coordinated to the copper(II) ions; they occupy the crystal lattice as free molecules (Fig. 27) [34].

The room temperature magnetic moment measurements (μ_{eff} = 1.45–1.55μ_B) and the broad ESR spectra convey the presence of antiferromagnetic coupling in these binuclear complexes, whereas the related mononuclear complexes show hyperfine splitting in ESR spectra and have magnetic moment values similar to the spin-only value (μ_{eff} = 1.69–1.72μ_B). A variable temperature magnetic susceptibility study of [Cu$_2$(**56**)](ClO$_4$)$_2$, indicates a $-2J$ value of 214 cm^{-1} [34].

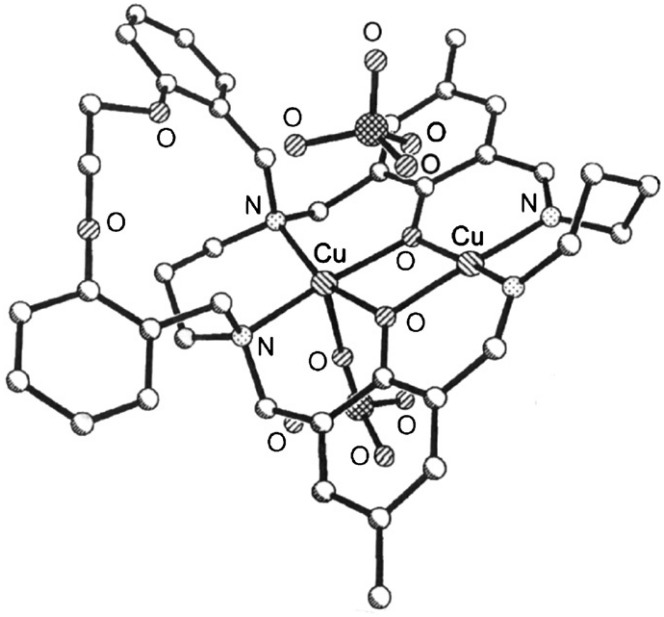

Fig. 27. Structure of [Cu$_2$(**57**)](ClO$_4$)$_2$.

Electrochemical investigations in dimethylformamide show one quasi-reversible reduction wave (E_{pc} = −0.78 to 0.87 V) for the mononuclear complexes and two quasi-reversible one-electron-transfer reduction waves (E^1_{pc} = −0.83 to 0.92 V, E^2_{pc} = −1.07 to −1.38 V) for the binuclear ones assigned to the Cu^{II}Cu^{II} ⇆ Cu^{II}Cu^{I} ⇆ Cu^{I}Cu^{I} processes [34].

The observed initial rate-constant values of catechol oxidation, using complexes as catalysts, range from 4.89×10^{-3} to 5.32×10^{-2} min^{-1} and are higher for binuclear complexes than for the corresponding mononuclear complexes. Kinetic studies also indicate that the binuclear complexes of ligand H$_2$-**58**···H$_2$-**60** have enhanced catalytic activities, in comparison to the activities of the complexes of ligand H$_2$-**55**···H$_2$-**57**. The increase in ring size makes the system more flexible as observed from electrochemical studies, and favours the catalysis. Hence, the rate-constant values of the complexes of H$_2$-**58**···H$_2$-**60** are found to be larger than those derived from H$_2$-**55**···H$_2$-**57**. From instance the rate constant value of the complex [Cu$_2$(**55**)](ClO$_4$)$_2$ (1.27×10^{-2} min^{-1}) is less than that of the complex [Cu$_2$(**56**)](ClO$_4$)$_2$ (4.66×10^{-2} min^{-1}) [34].

Similarly, the geometry around the copper(II) ion in the mononuclear complexes derived from H$_2$-**60a**···H$_2$-**60d** was proposed to be distorted square planar with one of the tertiary nitrogen atoms protonated, while in the related dinuclear copper(II) complexes one copper(II) ion is four coordinate and the other copper(II) ion is five coordinate. Conductivity measurements also vindicate that both mono and binuclear copper(II) complexes are 1:1 electrolytes [34].

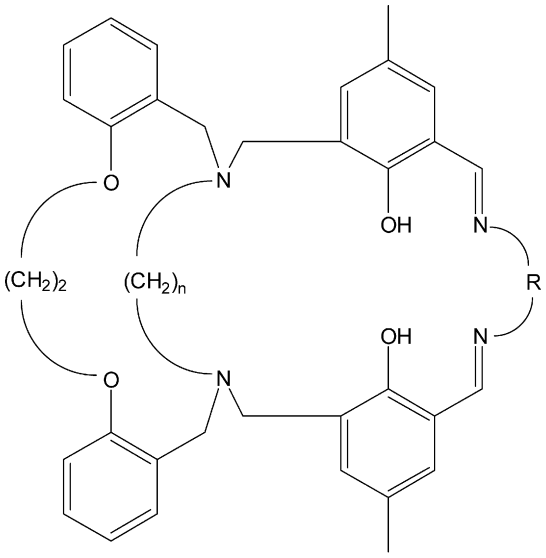

	n	R
H_2-**60a**	2	
H_2-**60b**	2	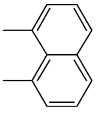
H_2-**60c**	3	
H_2-**60d**	3	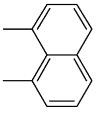

Electrochemical studies show one quasi-reversible reduction wave ($E_{pc} = -0.80$ to -0.88 V) for the mononuclear complexes and two quasi-reversible one electron transfer reduction waves ($E^1_{pc} = -0.84$ to -0.94 V, $E^2_{pc} = 1.25$ to -1.40 V) for the binuclear complexes are obtained. The comproportionation constants (K_{com}) for the equilibrium $Cu^{II}Cu^{II} + Cu^{I}Cu^{I} \leftrightarrows 2Cu^{II}Cu^{I}$ are: 6.07×10^7 for $[Cu_2(\mathbf{60a})(ClO_4)](ClO_4)$; 1.89×10^7 for $[Cu_2(\mathbf{62})(ClO_4)](ClO_4)$; 4.11×10^7 for $[Cu_2(\mathbf{60c})(ClO_4)](ClO_4)$; 1.28×10^6 for $[Cu(\mathbf{64})(ClO_4)](ClO_4)$. The decrease in K_{com} values for the complexes of $[\mathbf{60a}]^{2-}$ to $[\mathbf{60b}]^{2-}$ (6.07–1.89 $\times 10^7$) and of $[\mathbf{60c}]^{2-}$ to $[\mathbf{60d}]^{2-}$ (4.11×10^7 to 8.66×10^6) indicate that the stability of the mixed-valent species, formed as a result of the one electron reduction of complexes, decreases as the ring size increases. The increase in ring size produces more distortion of the geometry around the metal center and the added electron is localized in the first metal ion itself and its impact on the other metal ion is negligible. Thus, the lowered interaction between the two metal ions in the distorted geometry makes the reduction of the second metal ion easier [35].

Variable temperature magnetic susceptibility studies and the broad ESR spectra indicate an antiferromagnetic interaction in the binuclear complexes $[Cu_2(\mathbf{60a})(ClO_4)](ClO_4)$ and $[Cu_2(\mathbf{60b})(ClO_4)](ClO_4)$ ($-2J = 240$ and 219 cm^{-1}, respectively). Hyperfine splitting in ESR spectra is observed for the related mononuclear complexes and the magnetic moment value, at room temperature is close to the spin only value ($\mu_{eff} = 1.69$–$1.71\,\mu_B$ versus $\mu_{eff} = 1.35$–$1.42\,\mu_B$ in the dinuclear ones) [35]. The initial rate constant values of catechol oxidation using these complexes as catalysts have been found to span a domain ranging from 5.06×10^{-3} to 2.56×10^{-2} min^{-1} and the values are found to be higher for binuclear complexes than the corresponding mononuclear complexes. The catalytic activities of both mono- and binuclear complexes are found to increase as the macrocyclic ring size increases due to the intrinsic flexibility because of which the metal ion easily gets reduced and binds with the substrate and the same was supported by both spectral and electrochemical studies. The study implies that for mononuclear complexes the observed variation in the value of rate constant is very small when compared to the binuclear complexes. It can be stated that the planarity that is associated with the aromatic ring imparts the lesser catalytic efficiency due to the rigidity of the systems as observed in the case of electrochemical reduction of the complexes.

The observation on the comparison of catalytic activities of the complexes of H_2-**60a** and H_2-**60b** unambiguously evinces that the complexes of H_2-**60b** are accomplished with enhanced catalytic activity. The increase in flexibility due to increase in the ring size of macrocycle is the possible reason for the observed higher rate constant value for the complexes of H_2-**60b**. Spectral, electrochemical and catalytic studies support the distortion of the copper ion geometry that arises as the macrocyclic ring size increases [35].

$[Ni(H_2\text{-}\mathbf{L})](ClO_4)_2$, $[Ni_2(\mathbf{L})](ClO_4)_2$ and $[NiZn(\mathbf{L})](ClO_4)_2$ (H_2-**L** = H_2-**58**, H_2-**59**, H_2-**60**) have been prepared by a synthetic procedure similar to that employed for the analogous copper(II) complexes [34]. The nickel(II) ion in the cation $[Ni(H_2\text{-}\mathbf{58})]^{2+}$ coordinates into the N_2O_2 chamber and has a square planar geometry (Fig. 28) [36].

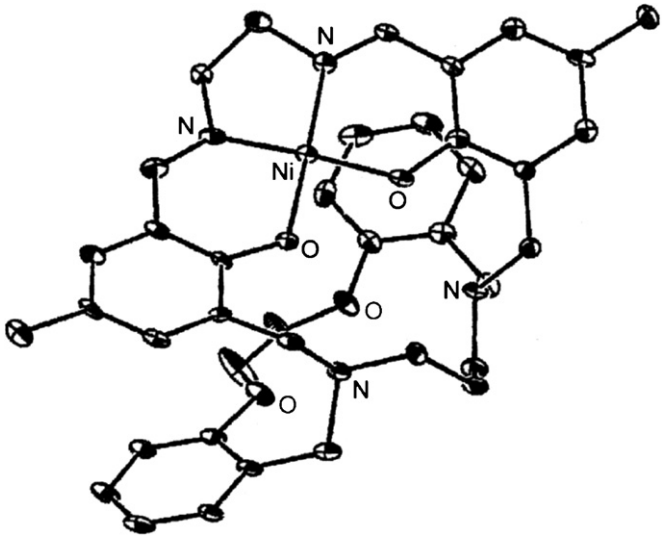

Fig. 28. Structure of $[Ni(H_2\text{-}\mathbf{58})]^{2+}$.

The cyclic voltammograms in dimethylformamide of the mononuclear nickel(II) complexes and the heterobinuclear $Zn^{II}Ni^{II}$ complexes in the potential range +1.4 to −2.0 V show irreversible redox processes while the homobinuclear nickel(II) complexes show quasi-reversible reduction and irreversible oxidation processes. Also for the nickel(II) complexes increase in the macrocyclic ring size, by the introduction of a methylene group in the alkyl chain of the diamines, produced distortion in the geometry of the complexes and shifts the reduction potentials anodically, favouring the reduction process [36].

The rate constants for the catalytic hydrolysis of 4-nitrophenyl phosphate catalyzed by these complexes were found to be higher for the homodinuclear Ni_2 and the heterodinuclear $Zn^{II}Ni^{II}$ complexes then the analogus mononuclear ones. This is due to the fact that the mononuclear complexes proceed via SN_1 type of reaction mechanism wherein, an external hydroxide anion coordinates to the metal ion, followed by its deprotonation

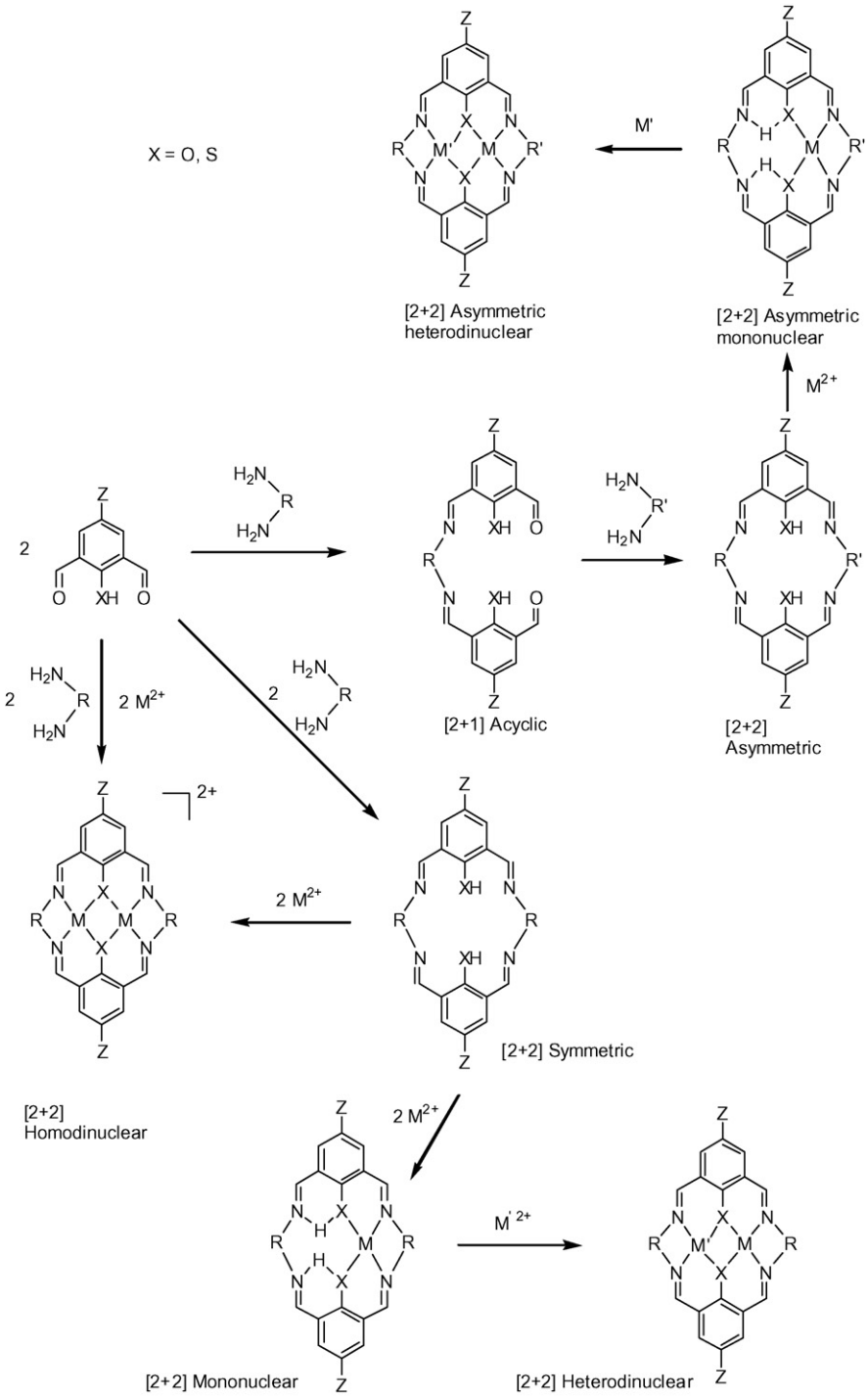

Scheme 7. Symmetric and asymmetric [2 + 2] macrocycles and related complexes.

and formation of an intermediate with the phosphate group and then cleavage of the bond to form the phenolate anion, along with hydroxylation of the phosphate group. The Ni^{II}_2 and $Zn^{II}Ni^{II}$ complexes follow a concerted SN_2 type of mechanism where the nucleophile OH^- adds to one of the nickel(II) ions and the phosphate is bound to the other metal ion. Here, bond formation and bond breakage, occur at the same time. This kind of mechanism requires two metal ions in close proximity. The mechanism of hydrolysis catalyzed by [ZnNi(**58**)]$(ClO_4)_2$ is similar to the one proposed for binuclear nickel(II) complexes. The rate constant was comparable with the binuclear nickel(II) complexes, but higher than the mononuclear complexes. Increase in the chelate ring size enhances the rate constant of hydrolysis fairly well by producing distortion in the geometry around the metal ion that enhances the accessibility of the metal ion for the bonding of phosphate and OH groups.

Kinetics of hydrolysis of 4-nitrophenyl phosphate catalyzed by the complexes showed pseudo first order processes with rate constants in the range $2 \times 10^{-5}\ s^{-1}$ for the mononuclear nickel(II) complexes and in the range $8 \times 10^{-4}\ s^{-1}$ for the homodinuclear nickel(II) and heterobinuclear zinc(II)–nickel(II) complexes [36].

The mononuclear and dinuclear nickel(II) complexes [Ni(H-**L**)]$(ClO_4)_2CH_2$ and [Ni_2(**L**)]$(ClO_4)_2$ (H_2-**L** = H_2-**52**, H_2-**53**, H_2-**54**, H_2-**60e**, H_2-**60g**) have been obtained by reaction of the diformyl-precursors H_2-**13** with the appropriate diamine in the presence of $Ni(ClO_4)_2 \cdot 6H_2O$ in a 1:1 and 2:1 molar ratio. Physico-chemical data indicate that the geometry around the nickel(II) ion is distorted square planar and in the mononuclear complexes, one of the tertiary nitrogen atoms is protonated. Conductivity measurements indicate that mononuclear and dinuclear nickel(II) complexes are 1:1 and 1:2 electrolytes, respectively [36].

Cyclic voltammetry and controlled electrolysis studies in CH_3CN indicate that the dinuclear nickel(II) complexes undergo two quasi-reversible one electron reduction in the potential ranges from −0.95 to −1.29 V and −1.32 to −1.67 V, assigned to the two redox processes $Ni^{II}Ni^{II} \leftrightharpoons Ni^{II}Ni^{I} \leftrightharpoons Ni^{I}Ni^{I}$ [36]. The reduction potential shifts anodically as the macrocyclic ring size increases from −0.89 to −0.82 V for the mononuclear nickel(II) complexes of H_2-**52** to H_2-**53** and H_2-**54** and from −1.01 to −0.91 V for those of H_2-**60e**, H_2-**60f**. This imparts more flexibility to the macrocycle and stabilizes the nickel(I) complexes. Also an electrochemical site migration of the nickel(I) ion occurs from the rigid imine nitrogen compartment to the flexible tertiary nitrogen compartment, which favours the tetrahedral geometry. This site migration process is easier as the macrocycle size increases [36].

The increase in macrocyclic ring size in the ligand framework has no influence on the electrochemical oxidation of the complexes. The quasi-reversible one electron oxidation processes occurring from 0 to 1.5 V are assigned to $Ni^{II}Ni^{II} \leftrightharpoons Ni^{II}Ni^{III} \leftrightharpoons Ni^{III}Ni^{III}$ [36].

The examination of kinetics of the hydrolysis of 4-nitrophenyl phosphate vindicates that the catalytic activities of the complexes are found to increase with macrocyclic ring size of the complexes [36].

The macrobicyclic heterobinuclear complexes [NiZn(**L**)]-$(ClO_4)_2$ (H_2-**L** = H_2-**60e**· · ·H_2-**60i**) have been synthesized from the corresponding mononuclear nickel(II) complexes [Ni(**L**)] with $Zn(ClO_4)_2$ in the presence of triethylamine as deprotonating agent. The nickel(II) ion lies in the N_2O_2 Schiff base in a square planar coordination environment [36]. Electrochemical and kinetic studies of the complexes have been carried out on the basis of macrocyclic ring size. Cyclic voltammetry and controlled electrolysis studies indicate that the nickel(II) metal ion in the heterobinuclear complexes undergo quasi-reversible one electron reduction and oxidation, whereas the zinc(II) metal ion does not undergo any reduction and oxidation [36]. The kinetics of hydrolysis of 4-nitrophenyl phosphate explores that the catalytic activities of the complexes are found to increase with macrocyclic ring size of the complexes. As the macrocyclic ring size increases, the spectral, electrochemical and catalytic studies of the complexes show variation due to distortion in the geometry of metal center. The catalytic activities of the complexes increase with increase in macrocyclic ring size. Macrocyclic ring size influences the spectral, electrochemical (reduction potential) and catalytic properties of the complexes [36].

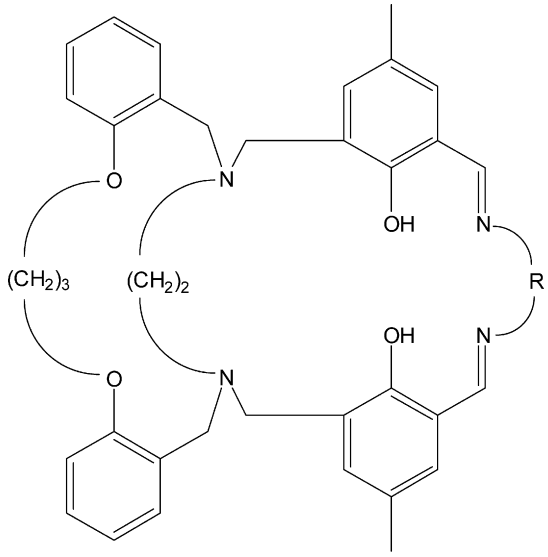

R

H_2-**60e**	-$(CH_2)_2$-
H_2-**60f**	-$(CH_2)_3$-
H_2-**60g**	-$(CH_2)_4$-
H_2-**60h**	
H_2-**60i**	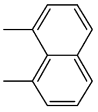

2.2. [2 + 2] symmetric and asymmetric Schiff base complexes, containing endogenous phenol- or thiophenol-XH (X = O, S) bridging groups and their evolution into higher homologues

Symmetric and asymmetric macrocyclic complexes with compartmental ligands bearing phenol or thiophenol bridging groups –XH (X = O, S) and their evolution into higher homologues or polymers have been primarily designed starting from the formyl precursors 2,6-diformyl-4-substituted phenol (CH_3, Cl, $C(CH_3)_3$) or 2,6-diformyl-4-substituted thiophenol (CH_3, $C(CH_3)_3$).

In the recent past a large variety of cyclic compartmental Schiff bases have been successfully proposed and extensively studied owing to their relatively easy synthesis and their versatility in the formation of stable complexes. The [2 + 2] symmetric macrocyclic compartmental ligands derive from the one pot condensation reaction of 2,6-diformyl-4-substituted phenol or -thiophenol and the appropriate amine H_2N-R-NH_2 in a 1:1 molar ratio. The asymmetric cyclic ligands have been prepared by a step by step procedure. On changing the head or the lateral units, these ligands have been conveniently diversified (Scheme 7) [1–5,37,38]. The best way for their preparation is to carry out the condensation reaction of appropriate formyl and amine precursors in the presence of a templating agent; nevertheless the possibility to obtain these compounds by self-condensation of appropriate precursors has been successfully experienced in the past. They are identical to the compounds obtained by demetalation of the related Schiff base complexes. Their cyclic nature was inferred especially by mass spectrometry and definitively demonstrated by single crystal X-ray structural determinations [4,5,39–41].

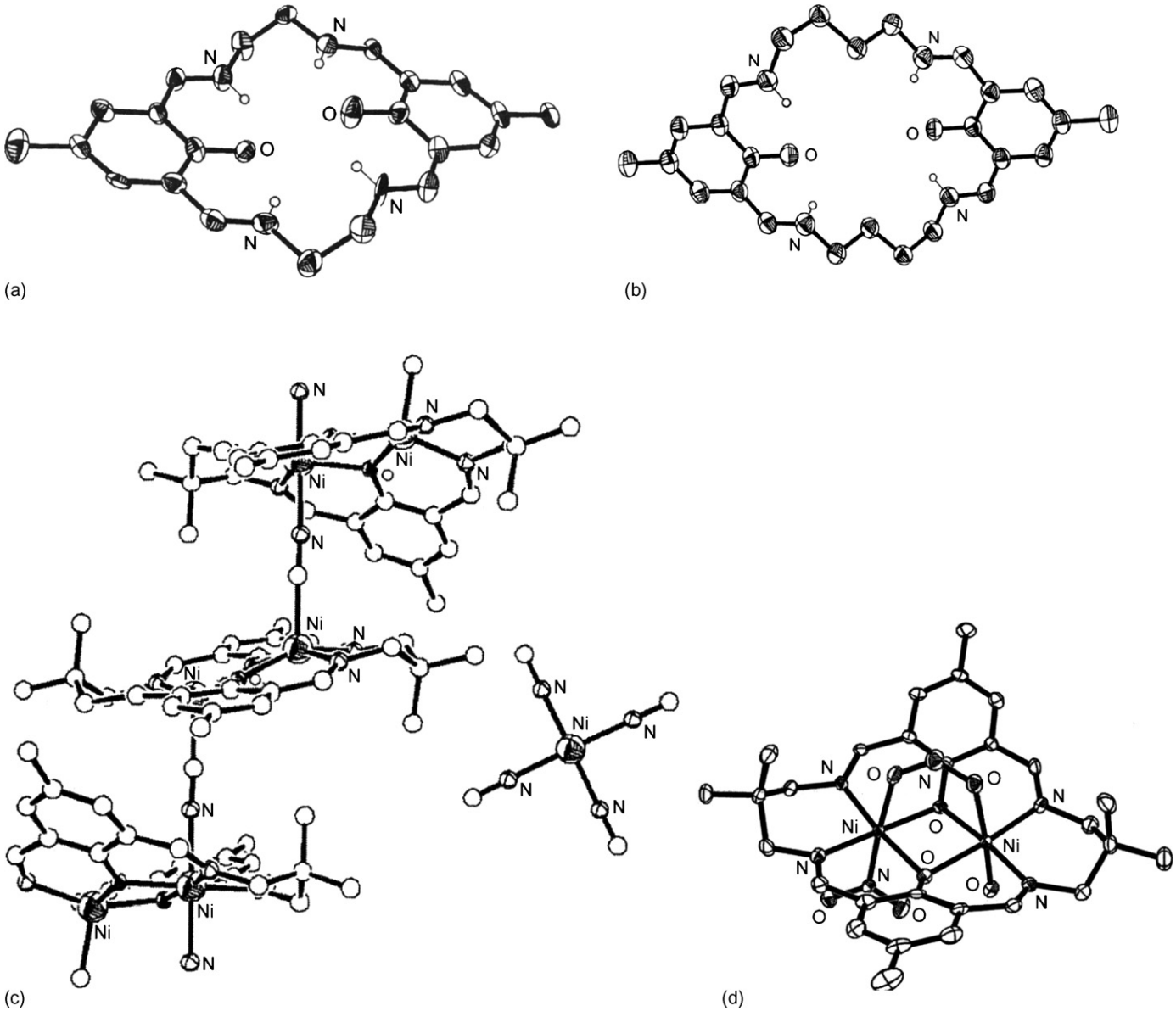

Fig. 29. Structure of $[H_4\text{-}\mathbf{61}]^{2+}$ (a), $[H_4\text{-}\mathbf{66}]^{2+}$ (b), $\{[Ni_6(\mathbf{71})_3(CN)_4][Ni(CN)_4]\}_n$ (c) and $[Ni_2(\mathbf{71})(\mu\text{-}NO_2)(NO_2)(H_2O)]$ (d).

2.2.1. Phenolate-based systems

On slow addition of a methanol solution of α,ω-diaminoalkane to a hot methanol solution containing 4-methyl(or *tert*-butyl)-2,6-diformyl(or diacyl)phenol, acetic acid and $NaClO_4$ in a 1:1:2:4 molar ratio the [2 + 2] macrocyclic compounds [H_4-**61**]$(ClO_4)_2\cdots$[H_4-**70**]$(ClO_4)_2$ separate out on standing at room temperature for several hours [42]. X-ray structural determinations of [H_4-**61**]$(ClO_4)_2$ and [H_4-**66**]$(ClO_4)_2$ (Fig. 29a and b) confirm the [2 + 2] cyclic nature of these complexes. The macrocyclic cations $[H_4\text{-}\mathbf{L}]^{2+}$ are stabilized by quite strong intramolecular hydrogen bonds involving the phenolic oxygens and the imino nitrogens. In these structures it appears more reasonable that all protons are transferred to the imino nitrogens, resulting in a symmetric N–H···O···H–N type of hydrogen bonding. Moreover, the ^{1}H NMR spectra of the macrocycles show the presence of a single peak due to the hydrogen-bonded protons, indicating it to be the symmetric type [42].

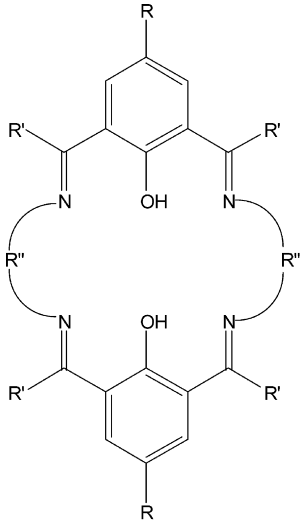

	R	R'	R''
H_2-**61**	CH_3	H	$(CH_2)_2$
H_2-**62**	CH_3	H	$CH_2CH(CH_3)$
H_2-**63**	CH_3	H	$(CH_2)_3$
H_2-**64**	CH_3	H	$(CH_2)_3$
H_2-**65**	$(CH_3)_3C$	H	$(CH_2)_3$
H_2-**66**	CH_3	H	$(CH_2)_4$
H_2-**67**	CH_3	H	$(CH_2)_6$
H_2-**68**	CH_3	H	$(CH_2)_8$
H_2-**69**	CH_3	H	$(CH_2)_9$
H_2-**70**	CH_3	H	$(CH_2)_{12}$

At room temperature, methanol, acetonitrile or nitromethane solutions of [H_4-**61**]$(ClO_4)_2\cdots$[H_4-**70**]$(ClO_4)_2$ on irradiation with light at 440 nm wavelength emit strong to very strong luminescence spectra with their peaks lying between 495 and 510 nm. [H_4-**67**]$(ClO_4)_2$ is the most fluorescence active. Addition of a base such as triethylamine to the CH_3CN solution of [H_4-L]$(ClO_4)_2$ causes quenching of fluorescence intensity, although for complete quenching about 25-fold of triethylamine is required. The product isolated under this condition has been characterized to be the macrocycle H_2-L in neutral form. Thus, the reaction of [H_4-**63**]$(ClO_4)_2$ or [H_4-**67**]$(ClO_4)_2$ with an excess of NEt_3 in dry CH_3CN affords H_2-**63** or H_2-**67** as a yellow sticky mass as confirmed by IR and NMR data. In addition the reaction of H_2-**63** with copper(II) salts forms the dinuclear complex $[Cu_2(\mathbf{63})(H_2O)_2](ClO_4)_2$ identical to that obtained from [H_4-**63**]$(ClO_4)_2$. Clearly, the macrocycle salts [H_4-**63**]$(ClO_4)_2$ on treatment with excess of triethylamine get deprotonated to the neutral macrocycles H_2-**63**. The requirement of excess base indicates the presence of strong intramolecular hydrogen bonding in the salts.

The neutral macrocycles H_2-**61**$\cdots H_2$-**70** are nonluminescent, but with the addition of an acid full recovery of the original luminescence can be achieved. Thus, reversible protonation/deprotonation of the tetraiminodiphenol macrocycles accompanied by manifold increase/decrease in fluorescence is the remarkable characteristic of this class of compounds [42].

Reaction of nickel chloride hexahydrate and a mixture of 2,6-diformyl-p-cresol with 2,2-dimethyl-1,3-propanediamine in methanol provided $[Ni_2(\mathbf{71})(H_2O)_2](Cl)_2\cdot H_2O$, which when reacted with a water solution of NaCN affords $[Ni_2(\mathbf{71})(CN)_2]\cdot 0.5H_2O$. The recrystallization of $[Ni_2(\mathbf{71})(CN)_2]\cdot 0.5H_2O$ in methanol over 2 months gives rise to $\{[Ni_6(\mathbf{71})_3(CN)_4]\cdot 5H_2O\cdot 8CH_3OH\}_\infty$ which consists of a packing of polymeric $[Ni_6(\mathbf{71})_3(CN)_4]^{2+}$ cations and $[Ni(CN)_4]^{2-}$ anions with five water and eight methanol molecules (Fig. 29c). The structure of the chain by cationic dinuclear complex $[Ni_6(\mathbf{71})_3(CN)_4]^{2+}$ shows that the two nickel(II) centers are bridged by the two phenolate oxygens as well as by CN^-. The central nickel ions are coordinated to carbon and nitrogen atoms derived from the bridging ligand, forming square pyramidal and octahedral geometries, respectively, and has N_2O_2 equatorial donors provided by the oxa-azamacrocyclic ligand. In the tetracyanonickelate moiety, the nickel ion is four coordinated by four cyanide–nitrogen atoms in a square-planar arrangement (Fig. 29c). The polar guest $[Ni(CN)_4]^{2-}$ methanol and water are accommodated among $[Ni_6(\mathbf{71})_3(CN)_4]^{2+}$ chains. The mean nonbonded Ni···Ni intermetallic separation in the polymeric complex is 3.159 Å [42].

Reaction of $[Ni_2(\mathbf{71})H_2O_2](Cl)_2\cdot H_2O$ with $NaNO_2$ in water provided $[Ni_2(\mathbf{71})(\mu\text{-}NO_2)(NO_2)(H_2O)]$ where the two nickel(II) centers are bridged by the two phenolate oxygens as well as by a nitrite ion. The metal centers, 3.013 Å apart, are six coordinate with irregular octahedral geometries and have N_2O_2 equatorial donors provided by $[\mathbf{71}]^{2-}$. The remaining apical position of one nickel(II) center is occupied by a water molecule, while that of the other nickel(II) ion by a nitrite nitrogen (Fig. 29d) [42].

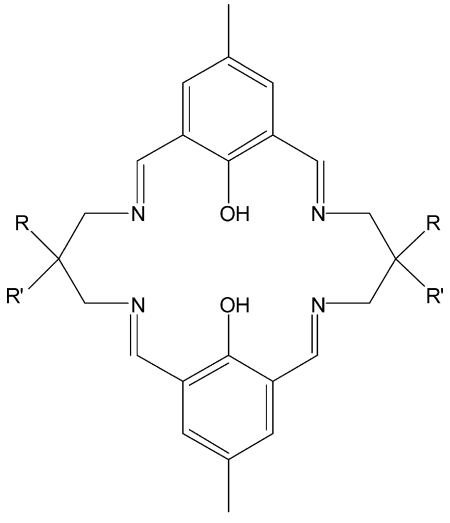

	R	R'
H_2-**71**	CH_3	CH_3
H_2-**71a**	H	OH

$[Cu_2(\mathbf{71a})(Cl)_2]\cdot 2H_2O$, $[Cu_2(\mathbf{71a})(\mu\text{-}CH_3COO)](CH_3COO)\cdot 6H_2O$, $[Cu_2(\mathbf{71a})(CH_3COO)_2(H_2O)_2]$ and $[Cu_2(\mathbf{71a})(H_2O)_2](HSO_4)_2$ have been prepared by condensation of 4-methyl-2,6-diformylphenol and 1,3-diamino-2-propanol in the presence of the appropriate copper(II) salt in a 1:1:1 molar ratio [42].

The structure of $[Cu_2(\mathbf{71a})(Cl)_2]\cdot 2H_2O$ corresponds to a binuclear copper(II) species with a Cu_2O_2 plane, which presents an inversion center. Each copper(II) ion shows a square pyramidal geometry, where the basal plane is formed by two nitrogen atoms from the macrocyclic ligand and two oxygen atoms, which are shared by both metallic atoms. The axial position is filled by a chloride ion [42].

$[Cu_2(\mathbf{71a})(\mu\text{-}CH_3COO)](CH_3COO)\cdot 6H_2O$ and $[Cu_2(\mathbf{71a})(\mu\text{-}CH_3COO)_2(H_2O)_2]$ cocrystallized together. In $[Cu_2(\mathbf{71a})(CH_3COO)_2(H_2O)_2]$ the two copper(II) ions are in a highly distorted octahedral environment: the two N_2O_2 donor set of the planar macrocycle form the basal plane while the axial ligands are a water molecule and a monodentate acetate ion. The OH groups of the amine fragments of $[Cu_2(\mathbf{71a})(\mu\text{-}CH_3COO)](CH_3COO)\cdot 6H_2O$ are axial and rest in a *trans* position with respect to the plane of the ligand. However, for $[Cu_2(\mathbf{71a})(Cl)_2]$ the same atoms are equatorial. $[Cu_2(\mathbf{71a})(\mu\text{-}CH_3COO)](CH_3COO)\cdot 6H_2O$ presents a folded macrocyclic ligand with a butterfly distortion. One acetate ligand bridges the copper(II) centers in a *syn–syn* mode; the other acetate is ionic [42].

In $[Cu_2(\mathbf{71a})(H_2O)_2](HSO_4)_2$ the copper(II) ions are square pyramidal with the basal plane defined by the two N_2O_2 donor sets of the macrocycle and the fifth position filled by an axial water ligand. Two $[HSO_4]^-$ act as counteranions [42].

$[Cu_2(\mathbf{71a})(Cl)_2]$ shows a very strong antiferromagnetic behaviour ($2J = -1015\ cm^{-1}$) while the antiferromagnetic coupling for $[Cu_2(\mathbf{71a})(\mu\text{-}CH_3COO)](CH_3COO)$ and $[Cu_2(\mathbf{71a})(CH_3COO)_2(H_2O)_2]$ was estimated to be $2J = -306$ and $-921\ cm^{-1}$, respectively. Finally in $[Cu_2(\mathbf{71a})(H_2O)_2](HSO_4)_2$ a strong antiferromagnetic interaction occurs [42].

The hydrolytic cleavage of the azomethine linkages has been studied with $[H_4\text{-}\mathbf{63}](ClO_4)_2$. In 1:1 acetonitrile–water mixture, the release of one molecule of 1,3-diaminopropane occurs, with the formation of the diiminiphenol oligomeric species $[H\text{-}\mathbf{72a}]_n$ together with the related [2 + 1] acyclic iminodialdehyde derivative $H_2\text{-}\mathbf{72}$. On the other hand, in 9:1 acetonitrile-water mixture only $H_2\text{-}\mathbf{72}$ forms. It thus appears that when a small amount of water is present in a solvent, the hydrolytic cleavage of $[H_4\text{-}\mathbf{L}](ClO_4)_2$ ($H_2\text{-}\mathbf{L} = H_2\text{-}\mathbf{61}\cdots H_2\text{-}\mathbf{70}$) occurs to the extent of releasing one molecule of diaminoalkane. However, with a larger amount of water, in addition to the above reaction, partial release of the dialdehyde and diamines occurs, which in turn undergoes oligomeric condensation reaction [42].

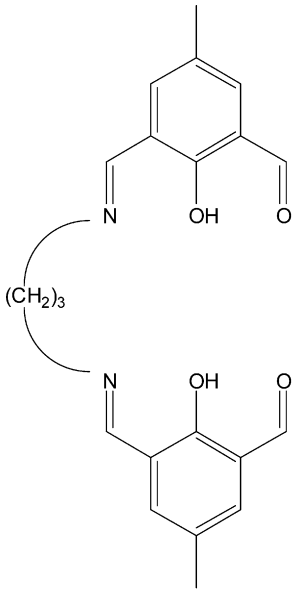

$H_2\text{-}\mathbf{72}$

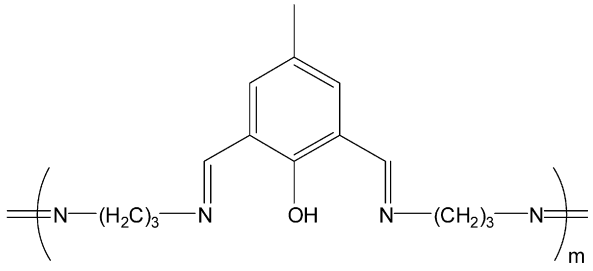

$[H\text{-}\mathbf{72a}]_n$

The symmetric cyclic ligands usually form homodinuclear complexes, although heterodinuclear complexation was observed using particular experimental conditions. This last complexation is generally favoured by the protonations of the nitrogens of one compartment, which makes the two sites no longer equivalent and hence accessible to two different and subsequent complexation reactions [5,37,38].

The ability to form heterodinuclear complexes is related to the possibility to synthesize stable mononuclear complexes to be used as ligands for further complexation or to have dinuclear systems capable to suffer a transmetalation process at one of the two chambers. Thus, the possibility to have two well defined and different recognition processes at the two adjacent sites of the compartmental systems is especially related to the use of asymmetric compartmental ligands. The presence of different donor atoms in the two chains, R and R′, in fact, allows a different recognition process at the two chambers [5,37,38].

Moreover, one chamber of these compartmental ligands can recognize a metal ion while the other chamber can give rise to a selective recognition process via the formation of hydrogen

bonding and/or complexation anions or organic molecule to the coordinated metal ion [7,42–50].

An example of heterodinuclear complexes derived from a [2 + 2] symmetric macrocycle is represented by [CuLa(**63**)$(NO_3)_3(H_2O)$] prepared by reaction of [Cu(**63**)] with $La(NO_3)_3{\cdot}6H_2O$ in warm methanol and in a 1:1 molar ratio [51]. This complex was especially prepared for testing its activity toward the hydrolysis of 4-nitrophenylphosphate (NPP) in H_2O/DMF (9:1). The activity of the $Cu^{II}La^{III}$ complex, compared with that of the mononuclear lanthanium(III), the dinuclear copper(II) and the mononuclear copper(II) complexes with H_2-**63** is higher, suggesting cooperatively functions in the NPP hydrolysis. Thus, the hydrolysis of phosphoester is significantly accelerated by the d,f-heterodinuclear complex, in line with the acceleration of hydrolysis by coexisting $FeCl_3$ and $LaCl_3$ previously reported [52,53]. Three possible mechanisms have been proposed: (i) a NPP coordination to the copper(II) and lanthanium(III) ions, followed by the attack of the hydroxide ion bound to the lanthanide(III) ion to the phosphorus nucleus; (ii) a nucleophilic attack by the hydroxide ion bound to the copper(II) ion; (iii) an attack of the hydroxide ion bound to lanthanide(III) to NPP coordinated to the same lanthanide(III) ion [51].

[CoNi(**74**)$(CH_3CN)_3$]$(ClO_4){\cdot}2CH_3OH{\cdot}0.5H_2O$ is an example of heterodinuclear complexes derived from an asymmetric compartmental ligand [54]. For the preparation of this complex, the related precursor complex [$Pb^{II}Co_2{}^{III}$(**74**)$_2$]$(ClO_4)_2{\cdot}2CH_3OH$ had to be prepared first by the cyclization of *N*,*N*′-ethylenedi(3-formyl-5-methylsalicylaldiminato)cobalt(II), [Co(**73**)], with 1,3-diaminopropane in the presence of $Pb(ClO_4)_2$. The $Pb^{II}Co_2{}^{II}$ complex subsequently was converted into the $Co^{II}M^{II}$ complexes (M = Ni^{II}, Zn^{II}, Mn^{II}, Fe^{II}, Cu^{II}) by the transmetalation reaction using one-half molar amount each of metal(II) sulphate and metal(II) perchlorate [54]. In the recent past by a similar procedure the $Cu^{II}M^{II}$ and $Ni^{II}M^{II}$ complexes of $[\mathbf{74}]^{2-}$ have been obtained [55–60]. The heterodinuclear complexation was detected by FAB mass spectra which show peaks due to $\{CoM(\mathbf{74})(ClO_4)\}^+$ and $\{CoM(\mathbf{74})\}^+$.

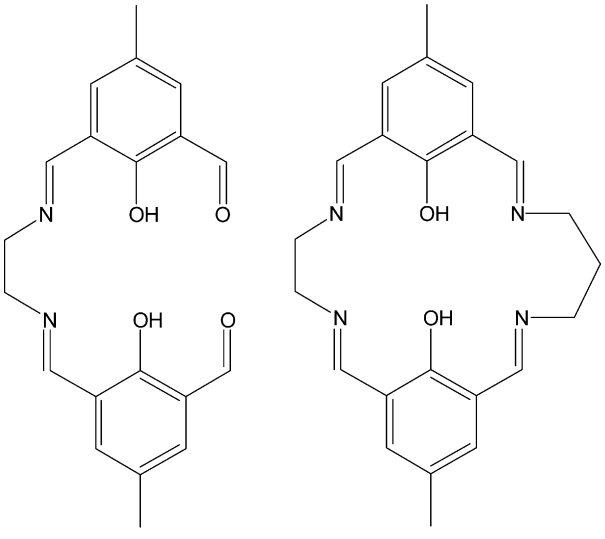

H_2-**73** H_2-**74**

In attempts to prepare the $Co^{II}M^{II}$ complexes by direct reaction of the mononuclear cobalt(II) complex of $[\mathbf{74}]^{2-}$ with the desired metal salt, a scrambling of metal ions occurred to afford a mixture of homodinuclear and heterodinuclear complexes. Thus, [$Co^{II}Mn^{II}$(**74**)(CH_3COO)(DMF)](ClO_4) has been derived from the related $Pb^{II}Co_2{}^{II}$ precursor complex by the transmetalation reaction of the lead(II) ion with manganese(II) ion in the presence of sodium acetate. In this complex, the acetate group bridges the two metal ions and contributes to the stabilization of the $Co^{II}Mn^{II}$ heterodinuclear core. Both $Co^{II}Ni^{II}$ and $Co^{II}Mn^{II}$ complexes are sensitive to O_2 in solution. [CoNi(**74**)]$(ClO_4)_2{\cdot}H_2O{\cdot}0.5CH_3CN$ and [NiCo(**74**)]$(ClO_4)_2{\cdot}H_2O$ are positional isomers when exogenous donating and solvating molecules are ignored [55–59]. Each of the $Co^{II}Ni^{II}$ and $Ni^{II}Co^{II}$ complexes are stabilized by macrocyclic effect not to cause scrambling of metal ions or isomerization in solution.

In [CoNi(**74**)$(CH_3CN)_3$]$(ClO_4)_2$ the cobalt(II) ion resides in the cavity with the ethylene lateral chain and the nickel(II) ion in the adjacent cavity with the trimethylene chain. The Co···Ni interatomic separation bridged by two phenolic oxygen atoms is about 3.0 Å. The nickel(II) ion has a pseudo octahedral geometry together with two acetonitrile molecules at the axial sites. The cobalt(II) ion has a square pyramidal geometry together with one acetonitrile molecule at the apex (Fig. 30) [54].

The $Co^{II}Zn^{II}$ complex has a magnetic moment of 2.7μ_B at room temperature, indicating a low-spin electronic structure. EPR spectra show that the cobalt(II) ion has one unpaired electron on its d_z^2 orbital. The magnetic moment of the $Co^{II}Ni^{II}$ complex, 3.71μ_B at room temperature, slowly increases with decreasing temperature to reach 3.97μ_B at 20 K and then decreases below this temperature. Such magnetic behaviour can be reasonably explained by the ferromagnetic interac-

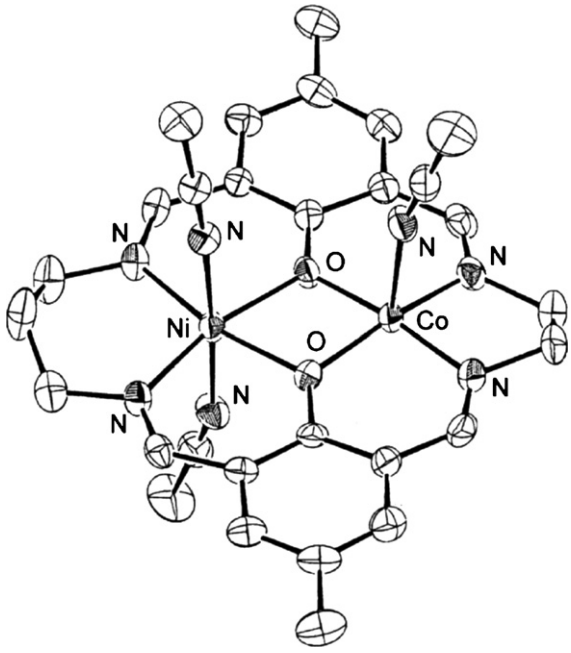

Fig. 30. Structure of [CoNi(**74**)$(CH_3CN)_3]^{2+}$.

tion between the cobalt(II) and nickel(II) centers ($J = 22\,cm^{-1}$) affording the $S_T = 3/2$ ground state. The drop in magnetic moment at low temperature may arise from a secondary effect such as the zero-field splitting of the $S_T = 3/2$ ground state. The ferromagnetic interaction in the $Co^{II}Ni^{II}$ complex is supported by EPR spectra: the complex is EPR silent at room temperature and shows three EPR signals at ∼1050, ∼2300 and ∼3100 G associated with the $S_T = 3/2$ ground state in a frozen dimethylformamide solution at liquid nitrogen temperature [54].

A change of the precursors induces different coordination shapes and hence higher metal aggregation: using 3-aminomethyl-5-salicylaldehyde or 2,6-diamonimethyl-4-methylphenol the macrocycles H_2-**75** and H_2-**76** and the related tetranuclear complexes have been prepared [61].

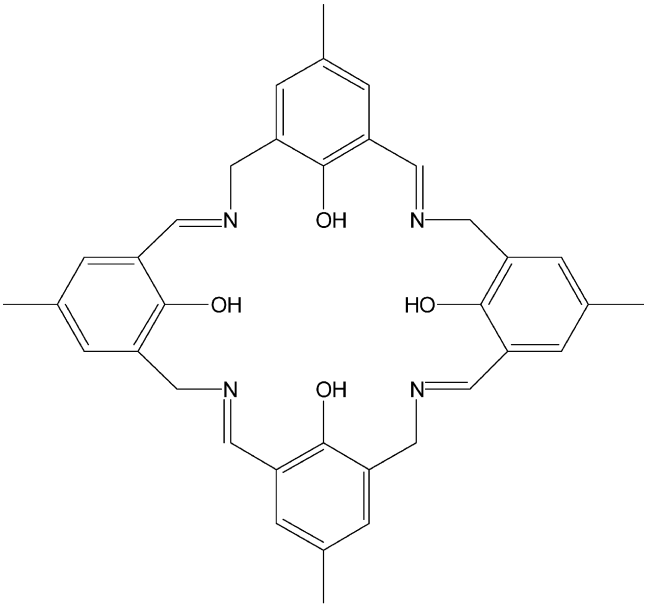

H_4-**75**

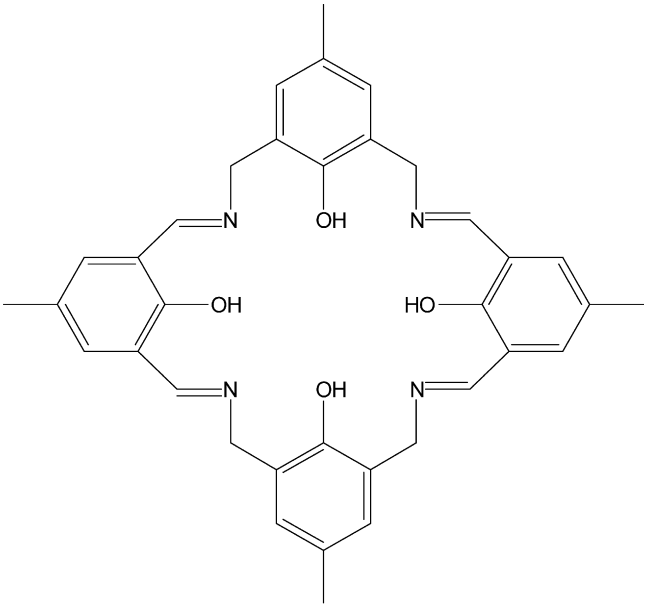

H_4-**76**

The autocondensation of 3-aminomethyl-5-methylsalicylaldehyde in the presence of nickel(II) salts afforded the tetranuclear $[Ni_4(\mathbf{75})(\mu_4\text{-}OH)(H_2O)_8](ClO_4)_3{\cdot}7H_2O$ and $[Ni_4(\mathbf{75})(\mu_4\text{-}O)(DMF)_4](ClO_4)_2$. The μ_4-hydroxo- and the μ_4-oxo-complexes were obtained by crystallization from water and dimethylformamide, respectively. The μ_4-oxo-complex can be converted into the related μ_4-hydroxo-species when suspended in a dilute perchloric acid and stirred at room temperature. This behaviour suggests that the μ_4-hydroxo- and the μ_4-oxo-complexes have a similar tetranuclear core [61].

The autocondensation of 3-aminomethyl-5-methylsalicylaldehyde in the presence of manganese(II) salts in open air gave the dinuclear complex $[Mn_2(H_2\text{-}\mathbf{75})(OH)(CH_3COO)_2(H_2O)](Br)$. Crystallographic studies demonstrate that the ligand $[\mathbf{75}]^{4-}$ has a cavity suitable for accommodating four nickel(II), producing a square Ni_4 core with a μ_4-hydroxo or μ_4-oxo-bridge at the center of the core. Such a tetranuclear square core must be difficult to produce with the smaller manganese(III) ions [61].

In $[Ni_4(\mathbf{75})(\mu_4\text{-}OH)(H_2O)_8](ClO_4)_3{\cdot}7H_2O$ the four nickel(II) ions are in a square arrangement with a μ_4-hydroxo group at the center of the square core. Each metal ion is bonded to a ONO donor set of the macrocyclic ligand and to the exogenous μ_4-hydroxo oxygen which is displaced from the plane defined by four nickel ions affording a hat-shape for the complex molecule. Each nickel(II) ion has a pseudo octahedral geometry with water molecules at the axial sites. The mean of the adjacent Ni···Ni distances is 3.01 Å and the mean of the diagonal Ni···Ni distances is 4.26 Å (Fig. 31a) [61].

In $[Mn_2(H_2\text{-}\mathbf{75})(OH)(CH_3COO)_2(H_2O)](Br)$ the macrocyclic ligand protonated at two imine nitrogen atoms, accommodates two manganese(III) ion using two ONO donor sets. The two manganese(III) ions are doubly bridged by hydroxide and acetate groups. One acetate group unidentately coordinates to one manganese(III) and one water molecule coordinates to another manganese affording a six-coordinate geometry for both manganese centers (Fig. 31b) [61].

The related macrocyclic ligand H_4-**76**, derived from the [2 + 2] condensation of 2,6-diformyl-4-methylphenol and 2,6-diaminomethyl-methylphenol was shown to afford μ_4-hydroxotetranickel(II) complexes of a $[Ni_4(\mathbf{76})(OH)(CH_3O{\cdot}H{\cdot}OCH_3)]^{2+}$ core of a bowl structure where the hydroxide group acts as a μ_4-bridge at the bottom group of the bowl and a pair of nickel(II) ions are bridged by methoxo group (two methoxo groups are hydrogen-bonded through proton). Thus, the tetranuclear nickel(II) core can be regarded as a dimer-of-dimers structure. The bowl structure of the tetranickel(II) complexes results from the flexibility of $[\mathbf{76}]^{4-}$, owing to the localization of the imine bonds in the macrocyclic framework. Obviously, the macrocyclic ligand $[\mathbf{75}]^{4-}$ is less flexible than $[\mathbf{76}]^{4-}$ due to the symmetric arrangement of the imine bonds in the macrocyclic framework [62].

The flexibility of H_2-**76** allowed less symmetrical bow-like ligand arrangement in $[Zn_4(\mathbf{76})(CH_3COO)_3(OH)]{\cdot}2.64CH_3OH{\cdot}2.5H_2O$ [62]. The Zn_4 group is markedly distorted from a square being no longer planar and having a short diagonal, 3.632 Å, and a long diagonal, 4.742 Å. A hydroxo group

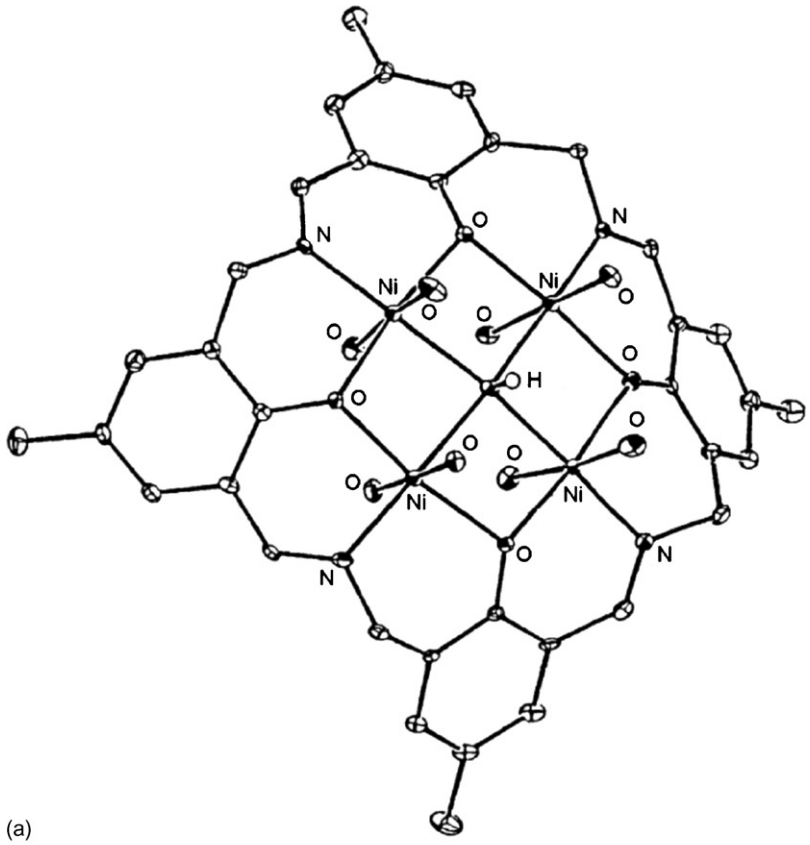

Fig. 31. Structure of $[Ni_4(\mathbf{75})(OH)(H_2O)_8]^{3+}$ (a) and $[Mn_2(H_2\text{-}\mathbf{75})(OH)(CH_3COO)_2(H_2O)]^{+}$ (b).

bridges the short diagonal but it also interacts less strongly with the other two zinc atoms. One acetate bridges the short diagonal on the side opposite to the hydroxo group and on the inside of the bowl. A second acetate bridges an edge of the Zn_4 cluster and the third acetate is monodentate but hydrogen bonded to the hydroxo group. One zinc ion is intermediate between four and five coordinate, two zinc(II) ions are five coordinate and the fourth one is six coordinate [62].

The reaction of manganese(II) acetate with 2,6-bis(aminomethyl)-4-methylphenol and 2,6-diformyl-4-methylphenol in the presence of lithium acetate and sodium perchlorate in boiling methanol followed by saturation of the solution with dioxygen after it had cooled to room temperature, gave brown crystals which, after being reexposed to the atmosphere, form $[Mn_2(H_2\text{-}\mathbf{76})(\mu\text{-}CH_3COO)(\mu\text{-}OH)(CH_3\text{-}OH)_2](ClO_4)\cdot 2H_2O$. The cation $[Mn_2(H_2\text{-}\mathbf{76})(\mu\text{-}CH_3COO)(\mu\text{-}OH)(CH_3OH)_2]^{2+}$ is situated around a crystallographic two-fold axis of symmetry passing through the bridging hydroxide and through the carbon–carbon bond of a bridging acetate. Each manganese ion has a tetragonally distorted six coordinated environment, indicative of a manganese(III) ion with a high-spin d^4 configuration [62].

In the tetranickel complexes with $[\mathbf{75}]^{4-}$ magnetic studies indicate a ferromagnetic interaction between the adjacent nickel(II) ions and an antiferromagnetic interaction between the diagonal nickel(II) ions ($J = 7.7\,cm^{-1}$, $J' = -28.5\,cm^{-1}$ for $[Ni_4(\mathbf{75})(\mu\text{-}OH)(H_2O)_8](ClO_4)_3$ and $J = 7.0\,cm^{-1}$, $J' = 27.0\,cm^{-1}$ for $[Ni_4(\mathbf{75})(\mu\text{-}O)(DMF)_4](ClO_4)_2$) [61]. In $[Ni_4(\mathbf{76})(\mu_4\text{-}OH)(CH_3O{\cdot}H{\cdot}OCH_3)](CH_3COO)_2$ the Ni_4 group behaves as an essentially noninteracting pair of Ni_2 units within which there is antiferromagnetic coupling with J values of $-33.3\,cm^{-1}$ (acetate) [62].

The cryomagnetic properties of the dimanganese(III) complex $[Mn_2(H_2\text{-}\mathbf{75})(OH)(CH_3COO)_2(H_2O)](Br)$ indicate a weak antiferromagnetic interaction between the manganese(III) ions [61]. Also for $[Mn_2(H_2\text{-}\mathbf{76})(\mu\text{-}CH_3COO)(\mu\text{-}OH)(CH_3OH)_2](ClO_4)_2{\cdot}2H_2O$ the magnetic of properties confirm the manganese(III) oxidation state; the magnetic moment per Mn is $4.61\mu_B$ at room temperature falling to $1.8\mu_B$ at 10 K, indicative of weak antiferromagnetic coupling ($J = -40\,cm^{-1}$) [62].

The [3 + 3] macrocycles H_6-**77** and H_6-**78** contain three tetradentate N_2O_2 binding sites organized in an equilateral triangle, as well as a pocket in the center that is surrounded by six phenolic oxygen atoms resembling [18]-crown-6. H_6-**77** (R = H), derived from the condensation of 3,6-diformylcatechol with 1,2-diaminobenzene, is insoluble in most solvents and takes about 2 weeks to synthesize [63]. On the contrary, the reaction of 3,6-diformylcatechol with 1,2-dihexyloxy-4,5-phenylenediamine afforded the red crystalline product H_6-**77** ($R = OC_6H_{13}$). This condensation reaction has been successively extended to the synthesis of the other [3 + 3] macrocycles derived from the appropriate 1,2-dialkyloxy-4,5-diphenylenediamine [63]. The structure of the macrocycles was verified by mass spectrometry and by NMR spectra which are consistent with the D_{3h} symmetry of the macrocycles in solution. Unlike H_6-**77** where (R = H) the macrocycles with peripheral alkoxy chains are soluble in a wide range of organic solvents such as chloroform and toluene [63].

The ESI-mass spectrum of H_6-**77** ($R = OC_6H_{13}$) shows the presence of not only the $[H_6\text{-}\mathbf{77}]^+$ ion, but also $[(H_6\text{-}\mathbf{77})+Na]^+$ and $[(H_6\text{-}\mathbf{77})_2+Na]^+$ and $[(H_6\text{-}\mathbf{77})_3+2Na]^+$ species; the sodium(I) ion is presumably a contaminant in the solvent or from the glass. When $NaBPh_4$ was added to a solution of H_6-**77**, the ESI-mass showed the three sodium complexes $[(H_6\text{-}\mathbf{77})+Na]^+$ $[(H_6\text{-}\mathbf{77})_2+Na]^+$ and $[(H_6\text{-}\mathbf{77})_3+2Na]^+$. It is most likely that these species are present in the solution before ionization. These observations corroborate the formation of Na^+ bridged dimers and trimers.

The data obtained from ESI-mass spectra, UV–vis and ^1H NMR spectroscopies suggest that small cations (i.e. alkali metal ions) induce the aggregation of the macrocycles H_6-**77** to form tubular assemblies. At low $[M^+]$:$[H_6\text{-}\mathbf{77}]$ ratios, intermediate species (e.g. dimers) are observed while at higher concentrations dynamic stacked structures are formed. It was proposed that in the tubular structure, the small cations are coordinated to the central phenolic oxygens of the macrocycle H_6-**78** rather than to the tetradentate N_2O_2 ligands [63].

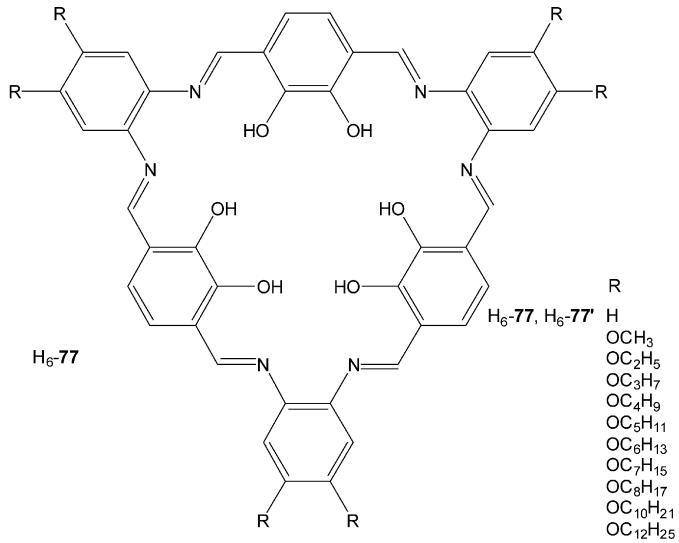

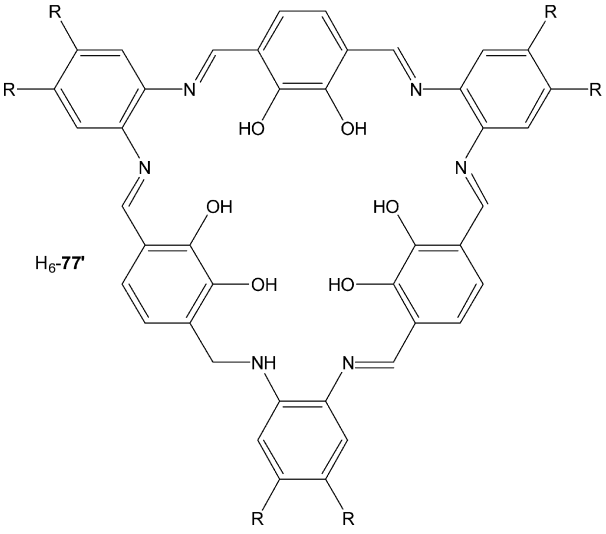

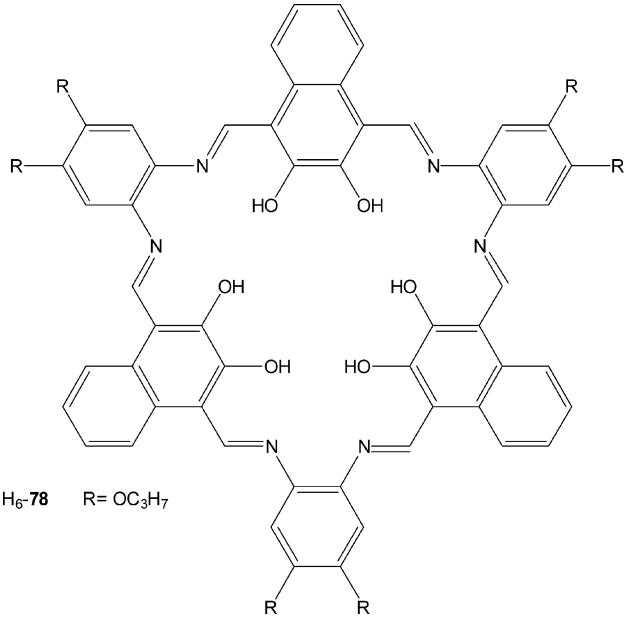

It was also verified that in the above [3 + 3] cyclocondensation of 2,6-diformylcatechol with 1,2-disubstituted-4,5-phenylenediamines the monoreduced macrocycles H_6-**77**′ also occur as confirmed by the X-ray structure of the compound with R = OC_6H_{13}. The compound is nonplanar with a single water molecule hydrogen-bonded to the center of the macrocycle. A plane of symmetry runs through the molecule, reflecting one-half of the macrocycle onto the other. The six hydroxyl groups of the macrocycle are tilted out of planarity with two of the diol moieties oriented upward and the third downward relative to the center of the macrocycle. Within the unit cell, the macrocycles are organized into planes, but the pores of the macrocycles are not aligned into channels [63].

Control experiments and deuterium labelling indicate that the macrocycle is reduced by a benzimidazoline generated during the reaction. Benzimidazolines may be convenient reagents for the mild and selective reduction of imines. On the basis of isolation of a benzimidazole by-product and deuterium labeling experiments, it was shown the [3 + 3] macrocycle is obtained by the reduction of 1,4-diformyl-1,2-dihydroxybenzene and 4,5-dialkoxy-1,2-diaminobenzene. Furthermore, it was observed that under certain conditions (50 °C acid catalyst) the major product in the synthesis of the macrocycle where R = $OC_{16}H_{33}$ is not the fully conjugated macrocycle, but instead the related monoreduced macrocycle [63].

Macrocycles incorporating naphthalene groups, have been also prepared by reaction of 1,4-diformyl-2,3-dihydroxynaphaline and 4,5-propoxy-1,2-diaminobenzene. The mass spectrum of the resulting macrocycle H_6-**78** shows the expected mass for the [3 + 3] Schiff base macrocycle. However, the IR and UV–vis spectra are substantially different for this extended macrocycle as compared to macrocycle H_6-**77** (R = OC_3H_7), suggesting a fundamental difference between these two systems [63]. H_6-**78** exists as a mixture but trautomer predominantly as the hexa-keto-enamine tautomer H_6-**78**′. This tautomerization breaks the conjugation in the macrocycle and renders it more flexible and thus more soluble. The formation of stable keto-enamines must be a sufficient driving force to overcome the aromatic stabilization of the second ring in naphtlalene [63].

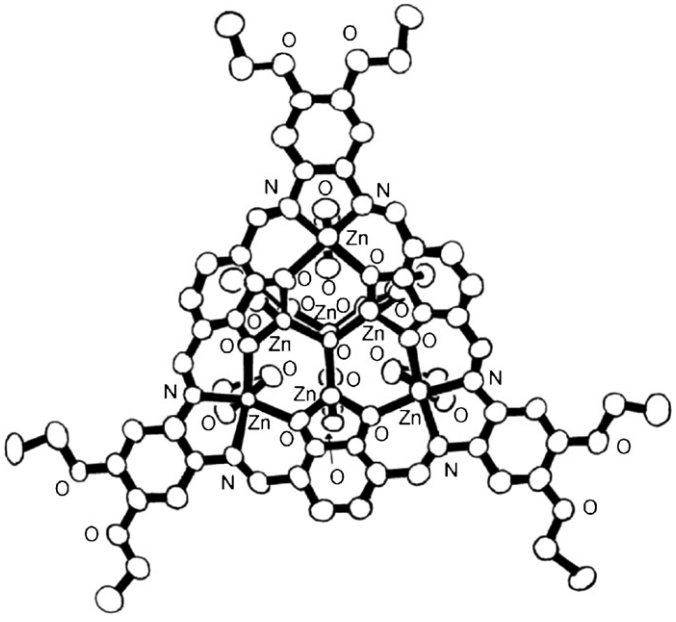

Fig. 32. Structure of [Zn_7(**77**)(μ-O)($\mu_{1,2}$-CH_3COO)$_3$($\mu_{1,1,2}$-CH_3COO)$_3$(DMSO)] (R = OC_2H_5).

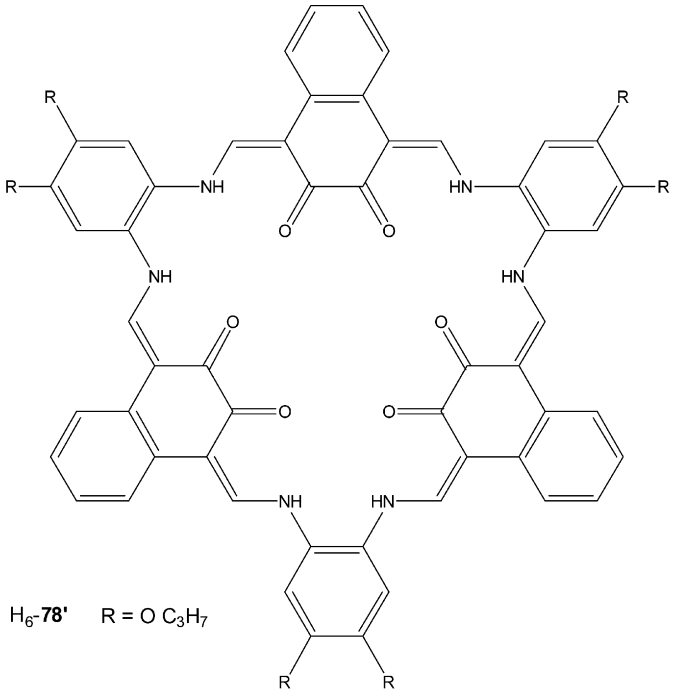

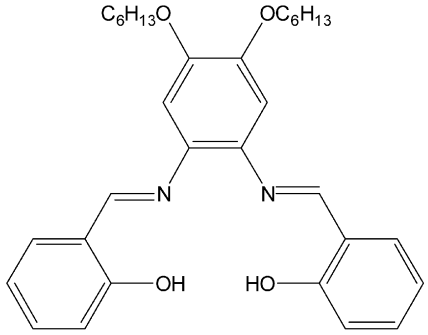

H_2-**79**

A control experiment, in which H_2-**79** was mixed with an excess of $NaBPh_4$ in $CDCl_3$, showed no change in color nor in its ^{1}H NMR spectrum, thus indicating that H_2-**79** does not incorporate $NaBPh_4$ in $CDCl_3$. In addition, the final [M^+]:[H_6-**79**] ratio was nearly 1:1 for each cation; a larger ratio would be expected if the cations were coordinating to the N_2O_2 pockets of each macrocycle. DFT calculations also indicate that a sodium ion has a strong affinity for binding to the phenolic oxygen atoms over the tetradentate N_2O_2 pockets offered by the macrocycle.

The Schiff base macrocycles H_6-**77** upon addition of small cations changes color and aggregates to form ionic assemblies.

H_6-**77** can behave like a crown ether, in which the phenolic oxygen atoms inside the macrocycle coordinate to small cations seated at the center of the macrocycle [63].

Reaction of the [3 + 3] macrocycles H_6-**77**, with an excess of $Zn(CH_3COO)_2$ yields the heptanuclear complexes $[Zn_7(\mathbf{77})(\mu\text{-}O)(\mu_{1,2}\text{-}CH_3COO)_3(\mu_{1,1,2}\text{-}CH_3COO)_3]$ as ascertained by their single crystal X-ray structure [63].

$[Zn_7(\mathbf{77})(\mu\text{-}O)(\mu_{1,2}\text{-}CH_3COO)_3 \quad (\mu_{1,1,2}\text{-}CH_3COO)_3(DMSO)]$ (R = OC_2H_5) has a bowl shape with nearly C_{3v} symmetry. The side of the bowl is formed by a trimetalated macrocycle with three zinc(II) ions in square pyramidal geometry. The metallomacrocycle adopts a cone shape as a result of the constrained geometry inside the macrocycle upon coordination to zinc(II) ions. Oxygen atoms in the interior of the shape-persistent macrocycle are further coordinated to a near-tetrahedral $[Zn_4O]^{6+}$ cluster that closes the bowl. The basic zinc acetate cluster is bridged by three μ-1,2 bidentate acetate ligands. Three tridentate acetate ligands bridge the zinc(II) ions in the macrocyclic N_2O_2 pockets with those at the base of the $[Zn_4O]^{6+}$ cluster. These ligands bridge in the very rare μ-1,1,2 fashion with monodentate and *syn–anti* bidentate bridges. The structure may be viewed as a cluster-capped trimetalated truncated-cone-shaped macrocycle. Overall, the molecule contains zinc(II) ions in tetrahedral, square pyramidal, and octahedral coordination geometries (Fig. 32) [63].

The complexes are stable for several months in solution. Also, a high-temperature ^{1}H NMR experiment of $[Zn_7(\mathbf{77})(\mu\text{-}O)(\mu_{1,2}\text{-}CH_3COO)_3(\mu_{1,1,2}\text{-}CH_3COO)_3]$ (R = OC_6H_{13}) in $(CDCl_2)_2$ showed no decomposition or dynamic motion in the complex at temperatures up to ca. 120 °C. Moreover, these molecules are insensitive to small quantities of water.

These multimetallic cluster complexes possess a concave surface of aromatic rings, creating a large void space. Interestingly, there is a dimethylsulphoxide molecule coordinated to one of the zinc(II) ions inside the bowl in the single-crystal structure of complex $[Zn_7(\mathbf{77})(\mu\text{-}O)(\mu_{1,2}\text{-}CH_3COO)_3(\mu_{1,1,2}\text{-}CH_3COO)_3(DMSO)]$ (R = OC_6H_{13}) but it is rapidly exchanging in solution, because the ^{1}H NMR spectrum of this heptazinc(II) complex in DMSO shows C_{3v} symmetry.

$[Zn_7(\mathbf{77})(\mu\text{-}O)(\mu_{1,2}\text{-}CH_3COO)_3(\mu_{1,1,2}\text{-}CH_3COO)_3]$ (R = OC_2H_5), which shows the same overall structure as $[Zn_7(\mathbf{77})(\mu\text{-}O)(\mu_{1,2}\text{-}CH_3COO)_3(\mu_{1,1,2}\text{-}CH_3COO)_3(DMSO)]$ (R = OC_2H_5) but with no solvent coordinated inside the bowl, is organized into pairs with the molecules arranged such that they nearly form a capsule in the solid state, where two of the molecules are oriented face-to-face, with ca. 60° rotation. The molecules are not interlocked but are separated by 6–7 Å with disordered solvent in the space between them [63].

Preliminary NMR studies of the Zn_7 complexes indicate that they aggregate in solution. Whereas their ^{1}H NMR spectra in $CDCl_3$, C_6D_6, and DMSO-d_6 are sharp, the spectra of these complexes in toluene-d_8 and xylenes-d_{10} are very broad, indicating short T_2 relaxation times that are characteristic of aggregates. Upon the addition of small (∼1%, v/v) quantities of coordinating solvents, the peaks in the ^{1}H NMR spectrum become sharp, as is expected for monomeric complexes. This suggests the possibility that the bowl-shaped compounds are assembling into dimers or larger aggregates in toluene and xylenes and that the aggregation is disrupted upon the addition of a solvent that can coordinate to the zinc(II) centers [63].

Finally the use of suitable bridging groups can favour the evolution of dinuclear complexes into oligomeric or polymeric species. The [2 + 2] Robson-type condensation reactions, involving one equivalent each of 2,6-diformyl-4-methylphenol, 1,3-diaminopropane and lead nitrate or lead perchlorate, produce the corresponding dilead(II)complexes $[Pb_2(\mathbf{63})(NO_3)_2]$ and $[Pb_2(\mathbf{63})(ClO_4)_2]$. When these reactions are carried out with half an equivalent of the metal salts these complexes are again obtained, although in a lower extent [64].

In $[Pb_2(\mathbf{63})(NO_3)_2]$ the metal centers are displaced from the basal plane of the flat macrocycle ligand in opposite directions. The lead(II) ions obtain a seven coordinate geometry due to three-fold coordination by the nitrate ions, two oxygen atoms stem from one nitrate group and the third oxygen atom stems from a second but symmetry-related nitrate group. This latter oxygen bridges two lead(II) ions from two different (but symmetry-related) $\{Pb_2(\mathbf{63})\}^{2+}$ units. Thus, one oxygen atom from each nitrate is bound to two lead ions, another oxygen atom to one lead, while the third oxygen atom is not involved in coordination. The whole structure then consists of parallel $\cdots(NO_3)_2\cdots[Pb_2(\mathbf{63})]\cdots(NO_3)_2\cdots$ chains (Fig. 33a) [64].

When one equivalent of lead perchlorate or lead nitrate is reacted with two equivalents of 2,6-diformyl-4-methylphenol and 1,3-diaminopropane in the presence of 2–3 equiv. of acetic acid, the imine protonated mononuclear complexes $[Pb(H_2\text{-}\mathbf{63})(ClO_4)](ClO_4)$ and $[Pb(H_2\text{-}\mathbf{63})(NO_3)_2]$ are obtained. In these complexes the protonation of the imine group prevents the formation of homodinuclear complexes [64]. These results parallel those obtained for the lead(II) complexes derived from the condensation of 2,6-diformyl-4-methylphenol and 1,5-diamino-2-hydroxypropane; the presence of two, one or none lead(II) ions in these [2 + 2] macrocyclic compounds is mainly governed by the protonation processes at the imine groups: the dinuclear complexes, originally formed, progressively demetalate forming the mononuclear derivatives and finally the free Schiff base [64].

The structure of $[Pb(H_2\text{-}\mathbf{63})(ClO_4)](ClO_4)$ has revealed that the lead(II) ion, occupying one of the compartments of the macrocycle, is bonded to the phenolate oxygens and to the imine nitrogens, The non-coordinated imine nitrogens are protonated and strongly hydrogen bonded to the phenolate oxygens. The N_2O_2 coordination set forming a trapezoid lies in a plane, while the metal center is considerably displaced from this plane. One perchlorate ion remains free, while the oxygen atoms belonging to the second perchlorate weakly interact with the metal center. Each of the three oxygen atoms are coordinated to three different but symmetrically equivalent lead units and each lead ion, in turn, is connected to three oxygen atoms from three different perchlorate groups. The process finally gives rise to association of six $[Pb(H_2\text{-}\mathbf{63})]^{2+}$ cations and six ClO_4^- anions producing the hexameric species $[\{Pb(H_2\text{-}\mathbf{63})(\mu\text{-}O_3ClO)\}_6]^{6+}$. The novel propeller-like architecture is built around a hexagonal frame provided by the lead ions. As a result of interaction with perchlorate oxygen, the lead center obtains a seven-fold coordination geom-

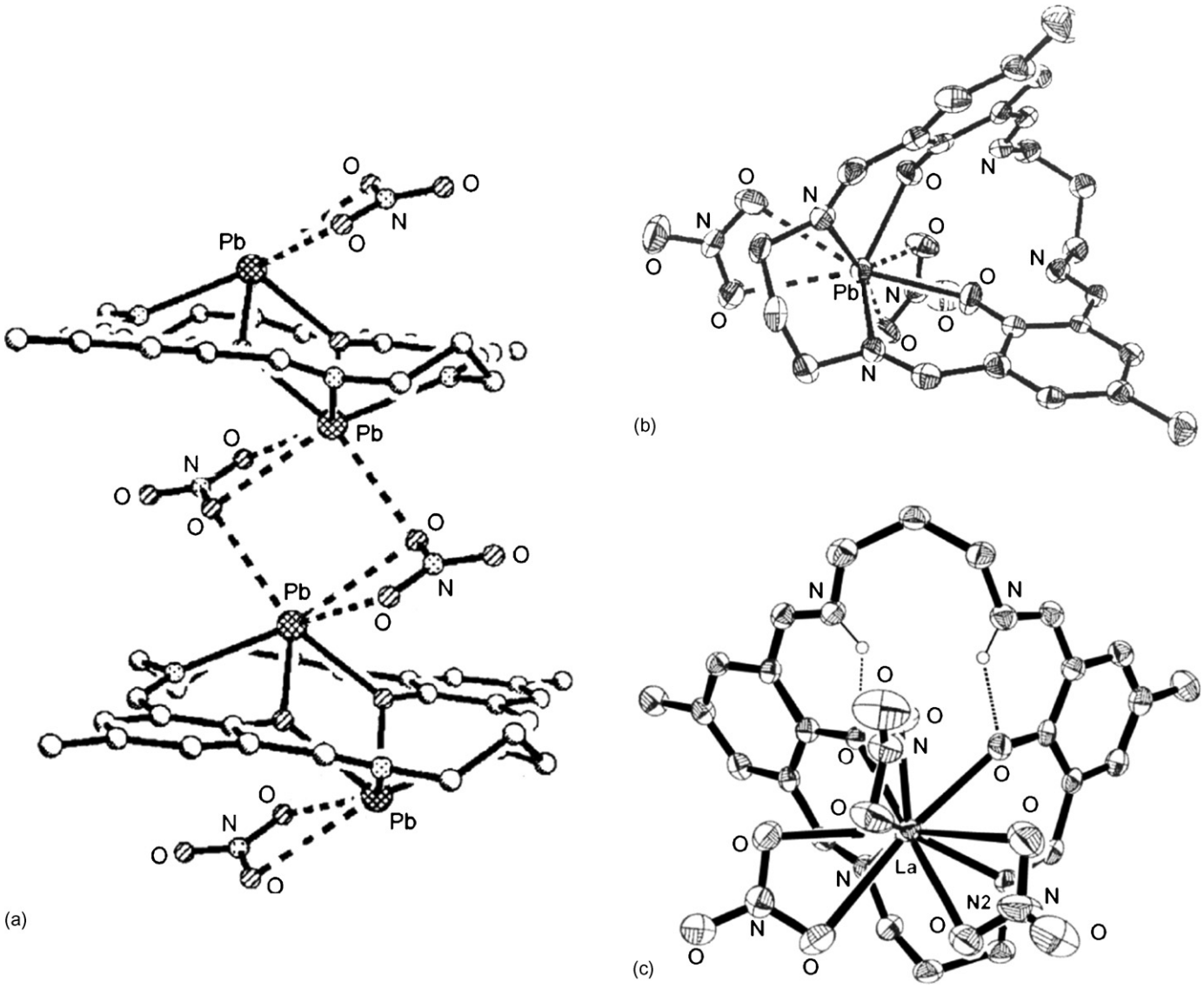

Fig. 33. Structure of $[Pb_2(\mathbf{63})(NO_3)_2]$ (a), $[Pb(H_2\text{-}\mathbf{63})(NO_3)_2]$ (b) and $[La(H_2\text{-}\mathbf{63})(NO_3)_3]$ (c).

etry. Another important consequence of this interaction is the adoption by the macrocyclic unit of a folded configuration [64].

In $[Pb(H_2\text{-}\mathbf{63})(NO_3)_2]$ the macrocyclic ligand is bound to the metal center in the same way as in $[Pb(H_2\text{-}\mathbf{63})(ClO_4)](ClO_4)$. The lead ion is additionally bound to the bidentate nitrate anions and, thus, acquires an eight coordinate N_2O_6 distorted dodecahedral geometry. No supramolecular association occurs in $[Pb_2(H_2\text{-}\mathbf{63})(NO_3)_2]$ presumably because of the attainment of eight coordinate geometry by the lead(II) ion. Similar to $[Pb(H_2\text{-}\mathbf{63})(ClO_4)](ClO_4)$, the protonated imines are hydrogen bonded to the adjacent phenolate oxygens (Fig. 33b) [64].

$[Pb(H_2\text{-}\mathbf{63})(ClO_4)](ClO_4)$ and $[Pb(H_2\text{-}\mathbf{63})(NO_3)_2]$ are convenient precursors for the preparation of mononuclear complexes of other metal ions which are kinetically either inert or labile in the oxidation states +2 and +3. For example $[Pt(H_2\text{-}\mathbf{63})](ClO_4)_2$, $[Rh(H_2\text{-}\mathbf{63})(Cl)(H_2O)](ClO_4)_2$ $[Ga(H_2\text{-}\mathbf{63})(Cl)(H_2O)](ClO_4)_2$ and $[Ln(H_2\text{-}\mathbf{63})(Cl)_2(H_2O)_2](ClO_4)$ have been obtained by the reaction between $[Pb(H_2\text{-}\mathbf{63})(ClO_4)](ClO_4)$ and the required metal chloride in acetonitrile. The precipitation of $PbCl_2$ acts as a driving force for the replacement reaction. The transmetalation reaction can also be carried out by using a relatively harder metal ion without recorse to precipitation of $PbCl_2$. Also $[Pb(H_2\text{-}\mathbf{63})(NO_3)_2]$, on treatment with an equivalent amount of $Ln(NO_3)_3{\cdot}nH_2O$ in methanol, affords the lanthanide(III) complexes $[Ln(H_2\text{-}\mathbf{63})(NO_3)_3]$ (Ln = Y, La–Er) and $[Ln(H_2\text{-}\mathbf{63})(NO_3)_2(H_2O)](NO_3)$ (Ln = Tm–Lu). The structural analyses of $[La(H_2\text{-}\mathbf{63})(NO_3)_3]$ and $[Ho(H_2\text{-}\mathbf{63})(NO_3)_3]$ have indicated that both compounds are isotypic. The lanthanide(III) ion occupies one of the compartments of H_2-**63** and is bonded to the phenolate oxygens and to the imine nitrogens. All the three nitrate ions are bound to the metal center in a bidentate mode and the lanthanide ion thereby achieves a ten coordinated configuration. The noncoordinated nitrogen atoms are protonated and are strongly hydrogen bonded to the phenolate oxygens. The coordination environment for the lanthanide(III) ion is a distorted bicapped square-antiprism (Fig. 33c) [64]. The structure of $[Lu(H_2\text{-}\mathbf{63})(NO_3)_2(H_2O)](NO_3)$ reveals that

H_2-**63** is bound to the lutetium(III) center in the same way as in $[Ln(H_2\text{-}\mathbf{63})(NO_3)_3]$ (Ln = La, Ho). However, unlike those two compounds, in the lutetium(III) complex only two nitrate ions are bound to the metal center. Indeed, one nitrate is coordinated in bidentate mode, while the second one is coordinated in unidentate fashion. A water molecule is also bound to the metal ion and thereby, the coordination number of the metal center is raised to eight [64].

NMR spectra in CD_3SO indicate that also in this solution the phenolic protons are shifted to the two uncoordinated imino nitrogens, which then get intramolecularly hydrogen-bonded to the metal-bound phenolate oxygens to give rise to a zwitterionic structure. Proton NMR spectra of these lanthanide(III) complexes show that, despite their structural differences in the solid state, all of them obtain the same configuration in dimethylsulphoxide. This indicates that all the nitrates in solution are probably dissociated and salvation of the macrocyclic complex cations takes place to the same extent. For the paramagnetic lanthanide(III) complexes contributions of contact and pseudocontact shifts to the lanthanide induced isotropic shifts (LIS) of the macrocycle protons have been separated and good agreement has been obtained between the calculated LIS values and the experimentally observed ones [64].

The samarium(III) and europium(III) complexes with H_2-**63** on photoexcitation at 400 nm exhibit well-resolved luminescence spectra at 77 K both in the solid state and a methanol–ethanol (1:4) glassy matrixy. For the terbium(III) and dysprosium(III) complexes with H_2-**63**, the observed luminescence peaks are less resolved and weak in intensity [64].

Furthermore, the metathetical reaction involving stoichiometric amounts of $[Pb(H_2\text{-}\mathbf{63})](ClO_4)_2$ and $RhCl_3{\cdot}xH_2O$ or $Na_2[Pd(Cl)_4]$ and excess $NaClO_4$ leads to the formation of $[Rh(H_2\text{-}\mathbf{63})(Cl_2](ClO_4){\cdot}3H_2O$ and $[Pd(H_2\text{-}\mathbf{63})](ClO_4)_2$. The palladium(II) complex, on reaction with a stoichiometric amount of a 3d metal perchlorate $M(ClO_4)_2{\cdot}6H_2O$(M = Mn, Fe, Co, Ni, Cu, Zn) and triethylarnine, affords the heterodinuclear complexes $[PdM(\mathbf{63})(H_2O)_2](ClO_4)_2$ (Mn–Ni), $[PdCu(\mathbf{63})](ClO_4)_2$ and $[PdZn(\mathbf{63})(H_2O)](ClO_4)_2{\cdot}H_2O$. If the above reaction is carried out with $Na_2[Pd(Cl)_4]$ and $NaClO_4$, the homodinuclear complex $[Pd_2(\mathbf{63})](ClO_4)_2$ is obtained. On the contrary the reaction of $[Rh(H_2\text{-}\mathbf{63})(Cl)_2](ClO_4){\cdot}3H_2O$ with the abovementioned metal perchlorates, failed to produce the desired $[RhM(\mathbf{63})(Cl)_2(H_2O)_n]^+$-type complexes. On the other hand, when the rhodium(III) complex is reacted with $Na_2[Pd(Cl)_4]$ and triethylamine in the presence of $NaClO_4$ or $[NH_4](PF_6)$ the mixed-metal complexes $[RhPd(\mathbf{63})(Cl_2)](X)$ ($X = ClO_4^-$, PF_6^-) complexes are readily obtained. This indicates that the *trans* axial chloride ions of $[Rh(H_2\text{-}\mathbf{63})(Cl)_2](ClO_4){\cdot}3H_2O$ sterically inhibit the entry of a second metal ion into the ligand compartment if the coordination number of the incoming metal ion exceeds four. In the case of palladium(II), no difficulty is encountered in obtaining $[RhPd(\mathbf{63})(C1)_2)]^+$ because of the square-planar geometry of the palladium center [64].

The dipalladium(II) complex $[Pd_2(\mathbf{63})](BF_4)_2$ has been prepared by reacting $[H_4\text{-}\mathbf{63})](BF_4)_2$ with palladium(II) chloride or acetate in acetonitrile in the presence of a 10-fold excess of triethylamine. Further, the heterodinuclear complex $[PdNi(\mathbf{63})(CH_3CN)_2](ClO_4)_2$ has been synthesized by reacting $[Ni(H_2\text{-}\mathbf{63})](ClO_4)_2{\cdot}H_2O$ with palladium(II) acetate in acetonitrile [64]. $[PdRh(\mathbf{63})(Cl)_2](PF_6)$ contains one palladium(II) and one rhodium(III) center, bridged by the two phenolate oxygens and separated by a distance of 3.150 Å. A significant deviation of the macrocycle from the planarity occurs; for the square planar palladium(II) center the basal plane is provided by the N_2O_2 donor atoms of $[\mathbf{63}]^{2-}$. Also the octahedral rhodium(III) ion is bound to the phenolate oxygens atoms and two imine nitrogen atoms of $[\mathbf{63}]^{2-}$ while two chloride ions occupy the *trans* axial position above and below the N_2O_2 equatorial plane (Fig. 34a) [64].

In $[PdCu(\mathbf{63})](ClO_4)_2$ the cation lies on a crystallographic inversion center and thus the N_2O_2 ring is planar with the two metal ions disordered over two sites (site occupation factor 0.5). The two metal centers are bridged by the two phenolate oxygens are separated by a distance of 3.083 Å. The basal plane for either of the metal atoms is formed by the N_2O_2 donor atoms (Fig. 34b) [63]. It should be noted that 0.5:0.5 disorder of the palladium(II) and copper(II) centers over two sites might as well indicate that $[PdCu(\mathbf{63})](ClO_4)_2$ is a 1:1 mixture of $[Pd_2(\mathbf{63})](ClO_4)_2$ and $[Cu_2(\mathbf{63})](ClO_4)_2$ rather than the mixed-metal complex $[PdCu(\mathbf{63})](ClO_4)_2$. However, the mass spectrum of $[PdCu(\mathbf{63})](ClO_4)_2$ provides clear evidence that it is a truly heterodinuclear complex [64].

$[Pd(H_2\text{-}\mathbf{63})](ClO_4)_2$, $[PdZn(\mathbf{63})](ClO_4)_2$ and $[Pd_2(\mathbf{63})](ClO_4)_2$ on excitation at 400 nm exhibit luminescence at room temperature at 505, 437, and 443 nm, respectively. Spectrofluorimetric titrations of $[Pd(H_2\text{-}\mathbf{63})]^{2+}$ with the acetate salts of zinc(II) or palladium(II) have shown that the formation of $[PdZn(\mathbf{63})]^{2+}$ and $[Pd_2(\mathbf{63})]^{2+}$ complex species are accompanied by blue shift of luminescence with increased and reduced emission intensities, respectively. Cyclic and square-wave voltammetric measurements in acetonitrile indicate for $[PdM(\mathbf{63})]^{2+}$ ($M = Ni^{II}$, Cu^{II}) reversible one-electron reduction with $E_{1/2} = -0.10$ V for $Pd^{II}Cu^{II}/Pd^{II}Cu^{I}$ and -0.80 V for $Pd^{II}Ni^{II}/Pd^{II}Ni^{II}$ versus Ag/AgC1. $[PdCo(\mathbf{63})]^{2+}$ undergoes irreversible reduction for cobalt(II) at -0.78 V [64].

$[Fe(H_2\text{-}\mathbf{63})(Cl)(H_2O)](ClO_4)_2{\cdot}2H_2O$ is obtained by the transmetalation of $[Pb(H_2\text{-}\mathbf{63})](ClO)_2$ with $FeCl_3{\cdot}6H_2O$, while the diaqua complex $[Fe(H_2\text{-}\mathbf{63})(H_2O)_2](ClO_4)_3{\cdot}2H_2O$ is prepared by reacting $Fe(ClO_4)_3{\cdot}6H_2O$ $[H_4\text{-}\mathbf{63}](ClO_4)_2$. In these compounds, H_2-**63** represents the zwitterionic state of the macrocycle where the two phenolic protons are transferred to two of the uncoordinated imine nitrogens. Both compounds $[Fe(H_2\text{-}\mathbf{63})(Cl)(H_2O)](ClO_4)_2{\cdot}2H_2O$ and $[Fe(H_2\text{-}\mathbf{63})(H_2O)_2](ClO_4)_3{\cdot}2H_2O$ upon treatment with one equivalent of aqueous alkali undergo dimerization to produce the oxo-bridged compound $[Fe_2(H_2\text{-}\mathbf{63})_2(\mu\text{-}O)(H_2O)_2](ClO_4)_4{\cdot}2H_2O$.

The aqua ligands of complexes $[Fe(H_2\text{-}\mathbf{63})(Cl)(H_2O)](ClO_4)_2{\cdot}2H_2O$, $[Fe(H_2\text{-}\mathbf{63})(H_2O)_2](ClO_4)_3{\cdot}2H_2O$, $[Fe_2(H_2\text{-}\mathbf{63})_2(\mu\text{-}O)(H_2O)_2](ClO_4)_4{\cdot}2H_2O$ get exchanged in acetonitrile. Reaction equilibria involving binding and exchange of the terminal ligands ($Cl^-/H_2O/CH_3CN$) in these complexes have been studied spectrophotometrically. The equilibrium constant (K_{aq}) for the aquation reaction $[Fe(H_2\text{-}\mathbf{63})(Cl)(H_2O)]^{2+} + H_2O \leftrightharpoons [Fe(H_2\text{-}\mathbf{63})(H_2O)_2]^{3+} + Cl^-$ in acetonitrile is 8.65(5) M,

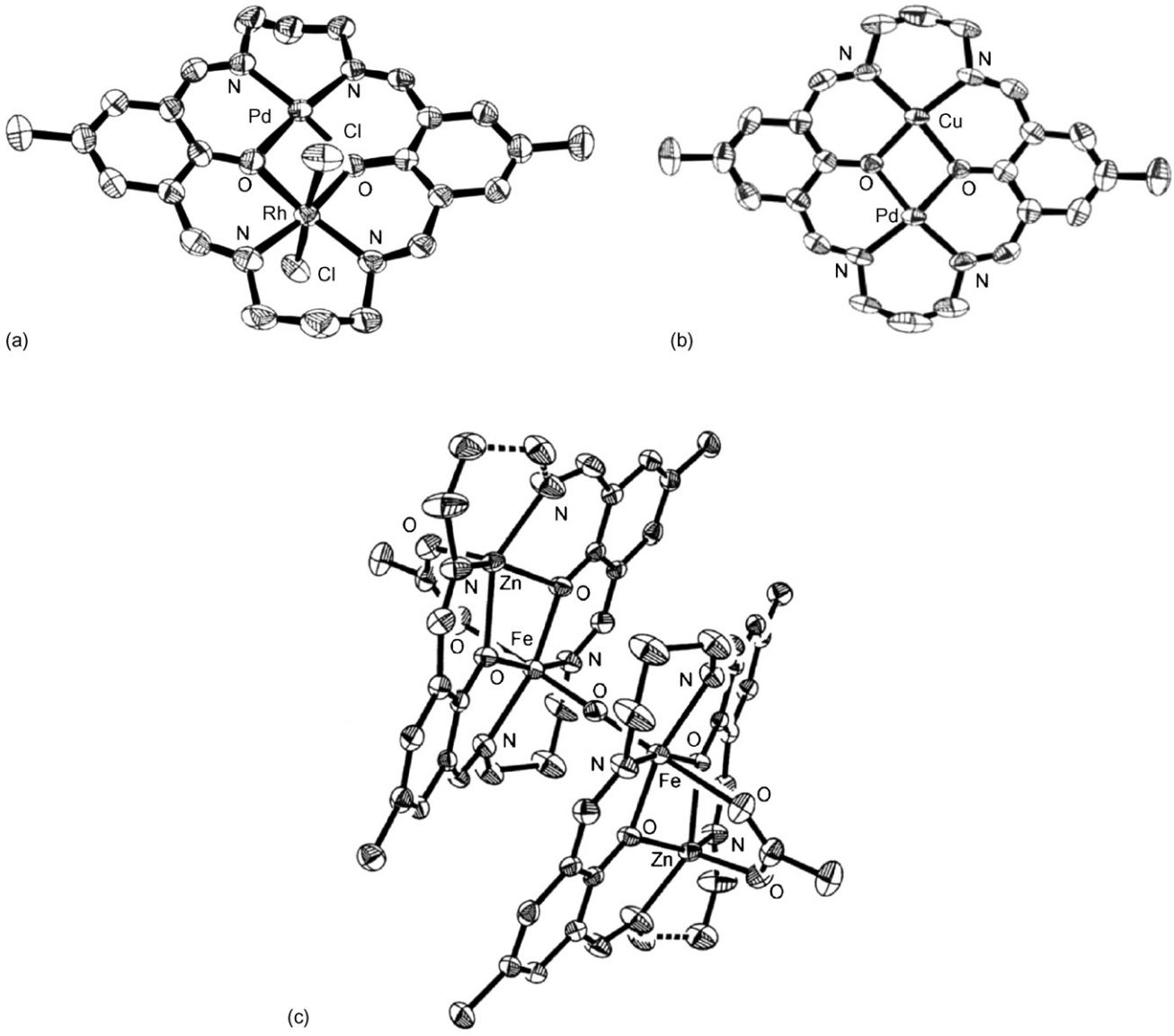

Fig. 34. Structure of $[PdRh(\mathbf{63})(Cl)_2]^{2+}$ (a), $[PdCu(\mathbf{63})]^{2+}$ (b) and $[Zn_2Fe_2(\mathbf{63})_2(\mu\text{-}CH_3COO)_2(\mu\text{-}O)]^{2+}$.

and the binding constant (K_{Cl^-}) for the reaction $[Fe(H_2\text{-}\mathbf{63})(Cl)(H_2O)]^{2+} + Cl^- \leftrightharpoons [Fe(H_2\text{-}\mathbf{63})(Cl)_2(H_2O)]^{+} + CH_3CN$ is 4.75(5) M. The pK_D value for the dimerization reaction $2[Fe(H_2\text{-}\mathbf{63})(H_2O)_2]^{3+} + 2OH^- \leftrightharpoons [Fe_2(H_2\text{-}\mathbf{63})_2(\mu\text{-}O)(H_2O)_2]^{4+} + 3H_2O$ in 1:1 acetonitrile–water is 9.38 [65].

When $[Fe(H_2\text{-}\mathbf{63})(Cl)(H_2O)](ClO_4)_2\cdot 2H_2O$ is reacted with one equivalent of $Zn(ClO_4)_2\cdot 6H_2O$ and an excess of sodium acetate, sodium pivalate, or bis(4-nitrophenylphosphate) (BNPP) (H_2-L), the corresponding carboxylate- or phosphate-bridged heterobimetallic tetranuclear complexes $[Zn_2Fe_2(\mathbf{63})_2(\mu\text{-L})(\mu\text{-O})](ClO_4)_2$ are obtained. The same complexes can also be prepared directly from the reaction of $[Fe_2(H_2\text{-}\mathbf{63})_2(\mu\text{-O})(H_2O)_2](ClO_4)_4\cdot 2H_2O$ with two equivalents of $Zn(ClO_4)_2\cdot 6H_2O$ and the sodium salts of the desired bridging anions [64]. The pseudo-first-order rate constant (k_{obs}) for the formation of $[Zn_2Fe_2(\mathbf{63})_2(\mu\text{-}CH_3COO)_2(\mu\text{-O})](ClO_4)_2$ at 25 °C from either $[Fe(H_2\text{-}\mathbf{63})(Cl)(H_2O)](ClO_4)_2\cdot 2H_2O$ or $[Fe_2(H_2\text{-}\mathbf{63})_2(\mu\text{-O})(H_2O)_2](ClO_4)_4\cdot 2H_2O$ with an excess of $Zn(CH_3COO)_2\cdot 2H_2O$ in 1:1 acetonitrile-water at pH 6.6 is found to be the same with $k_{obs} = 1.6(2) \times 10^{-4}\ s^{-1}$ [65].

The dinuclear or tetranuclear nature of these complexes have been determined by ESI-mass spectrometry in acetonitrile. In particular the species $[Fe(H_2\text{-}\mathbf{63})_2(\mu\text{-O})(ClO_4)_3]^+$, $[Fe_2(H_2\text{-}\mathbf{63})(H\text{-}\mathbf{63})(\mu\text{-O})(ClO_4)_2]^+$, $[Fe_2(H_2\text{-}\mathbf{63})_2(\mu\text{-O})(ClO_4)]^+$ have been detected for the diiron complex and $[Zn_2Fe_2(\mathbf{63})_2(\mu\text{-L})_2(\mu\text{-O})(ClO_4)]^+$ and $[Zn_2Fe_2(\mathbf{63})_2(\mu\text{-L})_2(\mu\text{-O})]^+$ (L = CH_3COO^-, $(NO_2\text{-}C_6H_4\text{-O})_2PCOO^-$) for the heterotetranuclear complexes.

In $[Fe_2(H_2\text{-}\mathbf{63})_2(H_2O)_2(\mu\text{-O})](ClO_4)_4\cdot 2H_2O$ the iron(III) center is six coordinated with a N_2O_2 basal plane and a water molecule is *trans*-axially disposed to the Fe–O–Fe linkage [65].

The cation of $[Zn_2Fe_2(\mathbf{63})_2(\mu\text{-}CH_3COO)_2(\mu\text{-O})](ClO_4)_2$ is comprised of two heterobimetallic macrocyclic units. The μ-oxygen atom lies on a crystallographic inversion center, and therefore the Fe–O–Fe bridge is exactly linear. In the asymmetric unit, the iron(III) and zinc(II) centers are triply bridged by the

two phenoxides of the macrocycle and an acetate ligand. Each of the metal centers is additionally coordinated by two imine nitrogens of the macrocycle. The iron(III) center thus obtains a distorted octahedral geometry, while the coordination environment around the zinc(II) ion is distorted square pyramidal. The N_2O_2 donor atom set around zinc(II) form an exact plane from which the metal ion is displaced toward the apical oxygen of the bridging acetate. The iron(III) ion is displaced from the least-squares basal plane of N_2O_2 toward the oxo ligand (Fig. 34c) [65]. Similarly, in $[Zn_2Fe_2(\mathbf{63})_2\{\mu\text{-}(NO_2C_6H_4)_2PCOO\}(\mu\text{-}O)](ClO_4)_2$ the oxygen atom, connecting the two hetero-bimetallic $Zn^{II}Fe^{III}$ units by the Fe–O–Fe linkage, lies on a crystallographic inversion center. Again, the zinc(II) and iron(III) centers are five and six coordinated, respectively. The intramolecular Fe···Zn distances in $[Zn_2Fe_2(\mathbf{63})_2(\mu\text{-}CH_3COO)_2(\mu\text{-}O)](ClO_4)_2$ (3.101 Å) and $[Zn_2Fe_2(\mathbf{63})_2\{\mu\text{-}(NO_2C_6H_4)_2PCOO\}_2(\mu\text{-}O)](ClO_4)_2$ (3.161 Å) are somewhat different.

Cyclic and square-wave voltammetric (CV and SWV) measurements have been carried out for $[Fe(H_2\text{-}\mathbf{63})(Cl)(H_2O)](ClO_4)_2\cdot 2H_2O$, $[Fe(H_2\text{-}\mathbf{63})(H_2O)_2](ClO_4)_3\cdot 2H_2O$, $[Fe_2(H_2\text{-}\mathbf{63})_2(\mu\text{-}O)(H_2O)_2](ClO_4)_4\cdot 2H_2O$ and $[Zn_2Fe_2(\mathbf{63})_2(\mu\text{-}CH_3COO)_2(\mu\text{-}O)](ClO_4)_2$ in acetonitrile. The variation of the solvent composition (acetonitrile-water) has a profound effect on the $E_{1/2}$ and ΔE_p values. The binding of an additional chloride ion to an iron(III) center in $[Fe(H_2$-

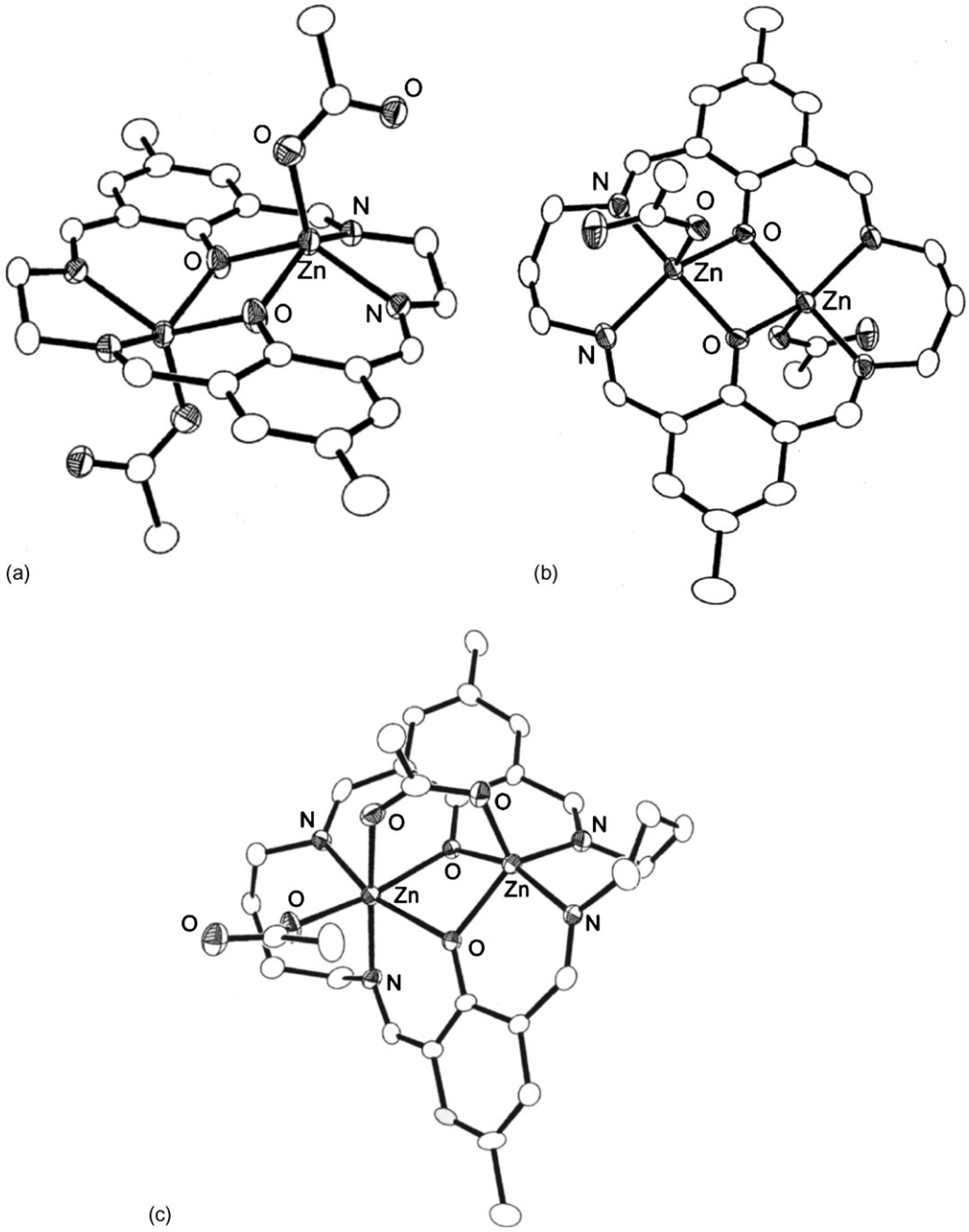

Fig. 35. Structure of $[Zn_2(\mathbf{61})(CH_3COO)_2]$ (a), $[Zn_2(\mathbf{63})(CH_3COO)_2]$ (b) and $[Zn_2(\mathbf{66})(\mu\text{-}CH_3COO)(CH_3COO)]$ (c).

63)(Cl)(H_2O)](ClO_4)$_2$·2H_2O, [Fe(H_2-**63**)(H_2O)$_2$](ClO_4)$_3$·2H_2O and [Fe_2(H_2-**63**)$_2$(μ-O)(H_2O)$_2$](ClO_4)$_4$·2H_2O is accompanied by a remarkable shift of $E_{1/2}$ to more negative values. The observation of quasi-reversible CV for complexes containing a Fe^{III}–O–Fe^{III} unit ([Fe_2(H_2-**63**)$_2$(μ-O)(H_2O)$_2$](ClO_4)$_4$·2H_2O and [Zn_2Fe_2(**63**)$_2$(μ-CH_3COO)$_2$(μ-O)](ClO_4)$_2$) indicates that in the electrochemical time scale unusual Fe^{III}–O–Fe^{II} is produced. The ^{1}H NMR spectra of [Fe_2(H_2-**63**)$_2$(μ-O)(H_2O)$_2$](ClO_4)$_4$·2H_2O and [Zn_2Fe_2(**63**)$_2$(μ-L)$_2$(μ-O)](ClO_4)$_2$ exhibit hyperfine-shifted signals in the range 0–90 ppm with similar features. The metal-hydrogen distances obtained from T_1 measurements are in good agreement with the crystallographic data. Variable-temperature (2–300 K) magnetic susceptibility measurements carried out for [Fe_2(H_2-**63**)$_2$(μ-O)(H_2O)$_2$](ClO_4)$_4$·2H_2O and [Zn_2Fe_2(**63**)$_2$(μ-CH_3COO)$_2$(μ-O)](ClO_4)$_2$ indicate strong antiferromagnetic exchange interaction ($H = -2J\,S_1 \cdot S_2$) between the high-spin iron(III) centers in the Fe–O–Fe unit with $J = -114$ and $-107\ cm^{-1}$, respectively [65].

[Zn_2(**61**)(CH_3COO)$_2$], [Zn_2(**63**)(CH_3COO)$_2$] and [Zn_2(**66**)(μ-CH_3COO)(CH_3COO)], were synthesized by the addition of the appropriate diamine to a mixture of Zn(CH_3COO)$_2$·2H_2O and 2,6-diformyl-4-methylphenol in $CHCl_3$/CH_3OH. The formation of the required [2 + 2] macrocycles was confirmed by FAB-mass spectrometry [66].

[Zn_2(**61**)(CH_3COO)$_2$] lies across a crystallographic inversion center. The zinc(II) ions, 3.183 Å apart, are disposed in an *anti* arrangement and are displaced in opposite directions from the plane of the donor atoms. Each metal ion has a distorted square pyramidal geometry, supported by an N_2O_3 donor set, i.e. two bridging phenoxy oxygens, two imine nitrogens and a monodentate acetate oxygen (Fig. 35a) [66].

The structure of [Zn_2(**63**)(CH_3COO)$_2$]·2$CHCl_3$ was found to be analogous to that of [Zn_2(**61**)(CH_3COO)$_2$]·2$CHCl_3$, each zinc(II) ion having an analogous N_2O_3 donor set: two bridging phenoxy oxygens, two imine nitrogens and a monodentater acetate oxygen. The zinc(II) ions are disposed out of the plane of the donor set of the macrocycle with an intermetallic distance of 3.313 Å. Increasing the size of the cavity in the macrocycle decreases the mismatch between the cavity size and cationic diameter, while increases the distance between the zinc(II) ions, decreasing their displacement out of the plane of the macrocycle. The Zn···Zn distance and the displacement of the zinc(II) ions from the N_2O_2 plane of the ligand (0.532 Å) are in accord with parameters observed in [Zn_2(**63**)(N_3)$_2$] (Fig. 35b) [67].

Although changing the diamine used in the template condensation had little effect on the structure on going from the –(CH_2)$_2$– linked to the –(CH_2)$_3$– linked macrocycles, increasing the length of the hydrocarbon chain from –(CH_2)$_3$– to –(CH_2)$_4$– had a more pronounced effect. [Zn_2(**66**)(μ-CH_3COO)(CH_3COO)]·$CHCl_3$ is again a [2 + 2] macrocyclic complex containing two zinc(II) ions and two acetate moieties but the macrocycle adopts a twisted conformation to allow one acetate ligand to bridge the two metal centers. The intermetallic distance (3.120 Å) is shorter than in the related complexes with [**61**]$^{2-}$ and [**63**]$^{2-}$ and the acetate binding to zinc(II) ions is also altered. [Zn_2(**66**)(μ-CH_3COO)(CH_3COO)]·$CHCl_3$ contains one six and one five coordinate zinc(II) ion, the coordination geometry of the former being distorted octahedral with an N_2O_4 donor set provided by two bridging phenoxy oxygens, two imine nitrogens, a monodentate acetate oxygen and an oxygen from a bridging acetate. The geometry of the five coordinate zinc(II) center is very similar to that of the zinc(II) ions found in [Zn_2(**61**)(CH_3COO)$_2$] and [Zn_2(**63**)(CH_3COO)$_2$], being distorted square pyramidal with an N_2O_3 donor set provided by two bridging phenoxy oxygens two imine nitrogens and an oxygen from a bridging acetate (Fig. 35c) [66,67].

Surprisingly, the product deriving from the reaction of two equivalents of Zn(CH_3COO)$_2$·2H_2O with one equivalent of [H_4-**80**](PF_6)$_2$ is not binuclear but the mononuclear [Zn(H_2-**80**)(CH_3CN)](PF_6)$_2$. The synthesis of [Zn(H_2-**80**)(CH_3CN)](PF_6)$_2$ is reproducible even when excess Zn(CH_3COO)$_2$·2H_2O is used [65,66]. In [Zn(H_2-**80**)(CH_3CN)](PF_6)$_2$ the zinc(II) ion adopts a square pyramidal geometry and is bound to two imine nitrogens, two phenoxy oxygens and the nitrogen of an axially ligated CH_3CN molecule. The macrocycle [**80**]$^{2-}$ adopts a stepped conformation (Fig. 36a).

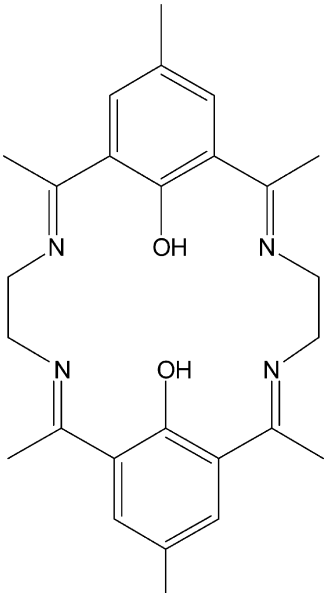

H_2-**80**

Reaction of [H_4-**63**](PF_6)$_2$ with Zn(CH_3COO)$_2$·2H_2O in CH_3CN affords [Zn_2(**63**)(μ-CH_3COO)](PF_6); the FAB-mass spectrum is consistent with the coordination of two zinc(II) ions within the macrocyclic ligand as confirmed by the X-ray structure. The complex contains two zinc(II) ions, 3.038 Å apart, in a distorted square pyramidal geometry, provided by two bridging phenoxy oxygens, two imine nitrogens and an oxygen from a bridging acetate. The ligand is not planar (Fig. 36b) [66].

Template reaction of 2,6-diacetyl-4-methylphenol, $ZnCl_2$ and 1,2-diaminoethane afforded [Zn_2(**80**)(Cl)$_2$]. The same complex was obtained when the template reaction was performed using Zn(NO_3)$_2$·6H_2O or Zn(CH_3COO)$_2$·2H_2O, followed by anion metathesis with KCl. Each zinc(II) center is five coordinate and adopts a distorted square pyramidal geometry with

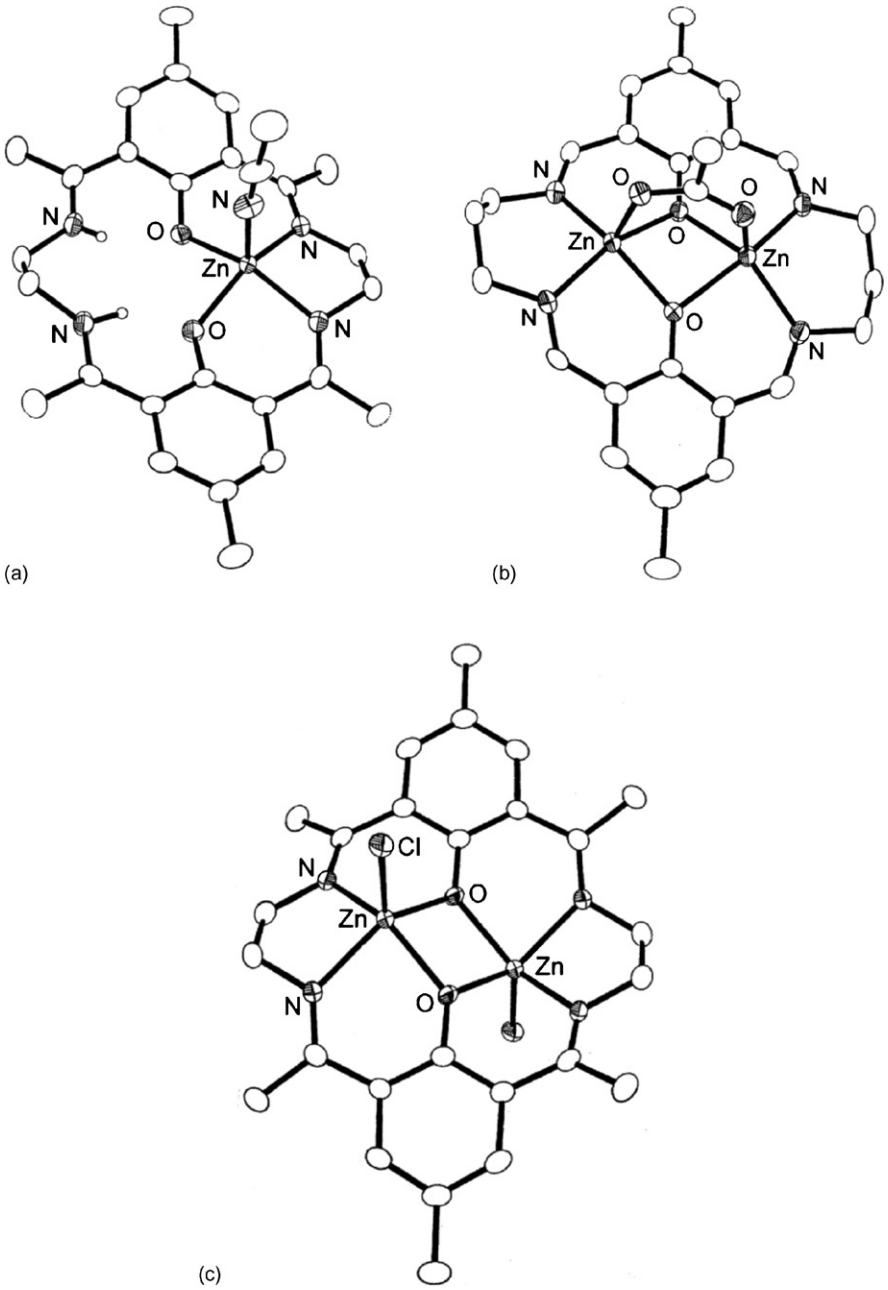

Fig. 36. Structure of $[Zn(H_2\text{-}\mathbf{80})(CH_3CN)]^{2+}$ (a),$[Zn_2(\mathbf{63})(\mu\text{-}CH_3COO)]^{+}$ (b) and $[Zn_2(\mathbf{80})(Cl)_2]$ (c).

coordination to two imine nitrogens, two bridging phenoxy oxygens and an axial chloride ligand. The symmetry equivalent zinc(II) ions lie in opposite directions out of the N_2O_2 mean plane, with a Zn···Zn separations of 3.229 Å. The coordination spheres of $[Zn_2(\mathbf{61})(CH_3COO)_2]$ and $[Zn_2(\mathbf{80})(Cl)_2]$ are closely related and are very similar to the 1,2-cyclohexanediamine bridged macrocyclic complex [65]. This suggests that the N_2O_2 compartments of the C_2-bridged macrocyclic ligands are too small to accommodate the zinc(II) centers as in all these compounds the metal ion is ca. 0.78 Å out of the N_2O_2 plane (Fig. 36c) [66].

The zinc(II) complexes with the macrocycles $[H_4\text{-}\mathbf{L}](ClO_4)_2$ ($H_2\text{-}\mathbf{L} = H_2\text{-}\mathbf{61}$, $H_2\text{-}\mathbf{63}$, $H_2\text{-}\mathbf{66}$) have been synthesized either by metal template condensation reaction or using the preformed ligands. The cavity sizes of the macrocyclic ligands markedly influence the composition of the zinc(II) complexes formed. Thus, when 2 equiv. of 2,6-diformyl-4-methyl-phenol and 1,2-diaminoethane are reacted in the presence of 1 equiv. of $Zn(ClO_4)_2{\cdot}6H_2O$ in methanol, the mononuclear complex $[Zn(H_2\text{-}\mathbf{61})](ClO_4)_2$ is obtained. A similar mononuclear complex, however, is not obtained when 1,3-diaminopropane or 1,4-diaminobutane is used as amine precursors. On the other hand, the reaction involving equimolar amounts of 2,6-diformyl-4-methyl-phenol, $Zn(ClO_4)_2{\cdot}2H_2O$, and 1,2-diaminoethane or 1,3-diaminopropane produces the dizinc(II) complex $[Zn_2(\mathbf{61})](ClO_4)_2$ or $[Zn_2(\mathbf{63})(H_2O)_2](ClO_4)_2$, while the same reaction carried out with 1,4-diaminobutane affords the metal-free macrocycle $[H_4\text{-}\mathbf{66}](ClO_4)_2$. Again,

$[Zn_2(\mathbf{63})(H_2O)_2](ClO_4)_2$ is readily obtained by treating $[H_4\text{-}\mathbf{63}](ClO_4)_2$ in acetonitrile with $Zn(ClO_4)_2{\cdot}2H_2O$ and triethylamine in a 1:2:4 ratio, albeit similar reactions with $[H_4\text{-}\mathbf{61}](ClO_4)_2$ and $[H_4\text{-}\mathbf{66}](ClO_4)_2$ fail to produce the corresponding dizinc(II) complexes. The dinuclear complex $[Zn_2(\mathbf{66})(\mu\text{-}CH_3COO)](ClO_4)$ is obtained by reacting $[H_4\text{-}\mathbf{66}](ClO_4)_2$ with $Zn(CH_3COO)_2{\cdot}2H_2O$ in acetonitrile, even as the same reaction with $[H_4\text{-}\mathbf{63}](ClO_4)_2$ produces the acetate-free diaqua complex $[Zn_2(\mathbf{63})(H_2O)_2](ClO_4)_2$ [67].

The carboxylate-bridged compounds $[Zn_2(\mathbf{63})(\mu\text{-}RCOO)](ClO_4){\cdot}2H_2O$ have been prepared by reacting $[Zn_2(\mathbf{63})(H_2O)_2](ClO_4)_2$ with an excess of RCOONa (R = CH_3, C_6H_5, *p*-$CH_3C_6H_4$, *p*-$OCH_3C_6H_4$, *p*-ClC_6H_4, *p*-$NO_2C_6H_4$) in methanol. Interestingly, the reaction between $[Zn_2(\mathbf{63})(\mu\text{-}C_6H_5COO)_2](ClO_4)_2$ and benzoic acid in acetonitrile has led to the isolation of an unusual compound of composition $[Zn_2(\mathbf{63})(\mu\text{-}C_6H_5COO)(C_6H_5COO)(H_3O)](ClO_4)$. This compound can be deprotonated to produce the dibenzoate bridged complex $[Zn_2(\mathbf{63})(\mu\text{-}C_6H_5COO)_2]{\cdot}H_2O$ when treated in acetonitrile with 1 equiv. of aqueous sodium hydroxide [67].

Crystals of $[Zn_2(\mathbf{63})(H_2O)_2](ClO_4)_2$ contain two independent molecules per asymmetric unit. The cation is centrosymmetric with its center of inversion at the middle of the $\{Zn_2(\mu\text{-phenoxide})_2\}$ plane. In this compound the macrocyclic ligand is flat. The metal centers are displaced from the basal plane in the opposite direction and their square pyramidal geometry is completed by coordination with a water molecule,

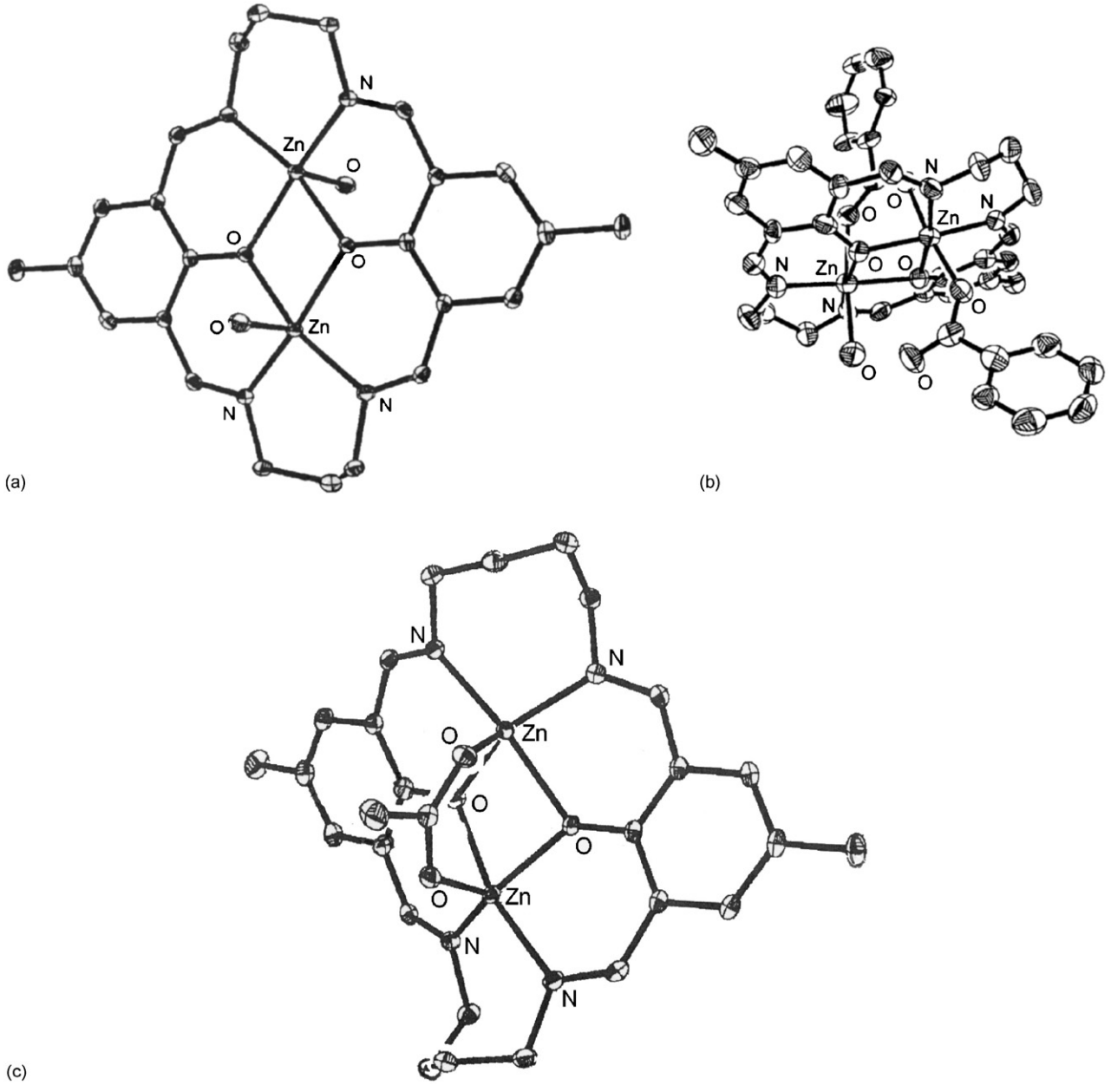

Fig. 37. Structure of $[Zn_2(\mathbf{63})(H_2O)_2]^{2+}$ (a), $[Zn_2(\mathbf{63})(\mu\text{-}C_6H_5COO)(C_6H_5COO)(H_2O)]^{+}$ (b) and $[Zn_2(\mathbf{66}\ (\mu\text{-}CH_3COO)]^{+}$ (c).

the equatorial plane being formed by the N_2O_2 donor set of each coordination chamber of the macrocyclic ligand. The Zn···Zn separations is 3.171 Å (Fig. 37a) [67].

The two metal centers in $[Zn_2(\mathbf{63})(\mu\text{-}C_6H_5COO)(C_6H_5COO)(H_3O)](ClO_4)$ are triply bridged by the two phenolate oxygens of the macrocyclic ligand and a benzoate group. Both the metal centers are hexacoordinated, the sixth coordination position of one zinc(II) ion is occupied by a monodentate benzoate, while that of the other zinc(II) ion is occupied by a water molecule. The macrocyclic ligand adopts a puckered configuration. The equatorial N_2O_2 donor atoms do not deviate from their mean planes; one zinc(II) ion is displaced above while the other zinc(II) ion lies below the basal plane. The two metal centers are separated from each other by 3.098 Å. One zinc(II) ion has a regular octahedral geometry while considerable distortion in the geometry of the other six coordinate zinc(II) ion occurs (Fig. 37b) [67]. The structural parameters seem to exclude protonation of the macrocyclic ligand donor atoms and also of the carboxylate moieties. There are, therefore, two possibilities, namely either the water molecule is protonated, that is $[Zn_2(\mathbf{63})(\mu\text{-}CH_3COO)(C_6H_5COO)(H_3O)](ClO_4)$, or the proton is associated with the perchlorate anion, that is, $[Zn_2(\mathbf{63})(\mu\text{-}C_6H_5COO)(C_6H_5COO)(H_2O)]\cdot HClO_4$. The geometric parameters for a $[Zn{-}OH_3]^+$ interaction seems to be the more likely case [67].

The structure of $[Zn_2(\mathbf{66})(\mu\text{-}CH_3COO)](ClO_4)$ consists of two five coordinate zinc centers, bridged by two phenoxide oxygens and the acetate moiety. The equatorial N_2O_2 donor atoms about the two metal ions slightly deviate from the mean plane. The two metal centers, in turn, are displaced in the same direction from the mean N_2O_2 planes. They are in a distorted square pyramidal geometry at a Zn···Zn distance of 3.038 Å (Fig. 37c) [67].

The binding of zinc(II) ion with the macrocyclic ligands $[H_4\text{-}\mathbf{L}](ClO_4)_2$ ($H_2\text{-}\mathbf{L} = H_2\text{-}\mathbf{61}$, $H_2\text{-}\mathbf{63}$, $H_2\text{-}\mathbf{66}$), whose cavity sizes increase progressively, have been studied by spectrophotometric and spectrofluorimetric titrations. In particular, titrations of $[H_4\text{-}\mathbf{61}](ClO_4)_2$ with $Zn(CH_3COO)_2\cdot 2H_2O$ indicate that two stepwise reaction equilibrium takes place with the formation respectively of $[Zn(H_2\text{-}\mathbf{61})]^{2+}$ and $[Zn_2(\mathbf{61})]^{2+}$. The same reactions occurs when $[H_4\text{-}\mathbf{63}](ClO_4)_2$ was employed; in this case, however the equilibrium constants are more overlapping. This explains the failure to isolate $[Zn(H_2\text{-}\mathbf{63})](ClO_4)$ while $[Zn(H_2\text{-}\mathbf{61})](ClO_4)$ can be obtained. Finally the same titration experiments using $[H_4\text{-}\mathbf{66})](ClO_4)_2$ indicate simultaneous occupation of the two cavity of the macrocycle with the formation of $[Zn_2(\mathbf{66})(\mu\text{-}CH_3COO)]^+$ [67].

The photoluminescence behaviour of the complexes $[Zn_2(\mathbf{63})(\mu\text{-}RCOO)](ClO_4)\cdot 2H_2O$ ($R = CH_3$, C_6H_5, $p\text{-}CH_3C_6H_4$, $p\text{-}CH_3OC_6H_4$, $p\text{-}ClC_6H_4$, $p\text{-}O_2C_6H_4$) indicates that the intensities of the luminescence spectra vary with the donor ability of the carboxylate; it is maximum for the *p*-methyl derivative and minimum for the *p*-nitro derivative. The equilibrium constants (*K*) involving the binding of acetate/benzoate and the carboxylate moiety of the amino acids glycine L-alanine, L-histidine, L-valine or L-proline with $[Zn_2(\mathbf{63})(H_2O)_2]^{2+}$, determined in aqueous solution by spectrofluorimetric titrations, lie in the range $(1\text{–}8)\times 10^5$ indicating that the amino acids are quite effective in binding with the zinc ion fluorophore through their carboxylate unit.

The zinc-induced fluorescence enhancement of the macrocyclic ligand $[H_4\text{-}\mathbf{63}](ClO_4)_2$, which can be considered as a photoinduced charge-transfer fluorophore, is significant. The internal charge transfer, that occurs from the phenolate donor site to the protonated imino acceptor site of the ligand at 440 nm, undergoes a blue shift to 370 nm on formation of the dizinc(II) complex $[Zn_2(\mathbf{63})(H_2O)_2]^{2+}$. Consequently, the luminescence band of the ligand at 510 nm is also markedly blue-shifted to 435 nm with considerable enhancement of intensity. The 70-fold increase in luminescence intensity of $[Zn_2(\mathbf{63})(H_2O)_2]^{2+}$ relative to $[H_4\text{-}\mathbf{63}](ClO_4)_2$ is further augmented with the formation of the carboxylate-bridged complexes $[Zn_2(\mathbf{63})(\mu\text{-}RCOO)]^+$ [67].

Single crystals of $[\{M^{III}(CN)_4(phen)\}_2\{Ni^{II}_2(\mathbf{63})(H_2O)_2\}]\cdot 2CH_3CN$ ($M = Fe^{III}$, Cr^{III}; phen = phenanthroline) were grown by a slow diffusion of an aqueous solution of $Li[M(CN)_4(phen)]$, generated by the metathesis reaction of $[P(Ph_4)][Fe(CN)_4(phen)]\cdot 2H_2O$ or $[P(Ph_4)[Cr(CN)_4(phen)]\cdot H_2O\cdot CH_3OH$ with $LiClO_4$ in a 1:1 molar ratio in acetonitrile, into an acetonitrile solution of $[Ni_2(\mathbf{63})(H_2O)_2](ClO_4)_2$, prepared by the reaction of aqueous solutions of $[Ni_2(\mathbf{63})(H_2O)_2(Cl)_2]$ and silver perchlorate in a 1:2 molar ratio in the dark [68].

The tetranuclear entity is constituted by a central $[Ni_2(\mathbf{63})(H_2O)_2]^{2+}$ dinuclear motif to which two peripheral $[M(CN)_4(phen)]^-$ units are connected through one of the four cyanide groups. The macrocyclic ligand $[\mathbf{63}]^{2-}$ is almost flat, enclosing two distorted octahedral nickel(II) centers, bridged by phenoxide oxygen atoms. Each nickel(II) ion has two imine nitrogen and two phenoxide oxygen atoms forming the strictly planar N_2O_2 equatorial donor set whereas a water molecule and a cyanide-nitrogen fill the axial positions. The nickel ion is shifted from the N_2O_2 basal plane toward the axial nitrogen atom. An inversion center is located in the middle of Ni_2O_2 plane. The two nickel ions are separated by 3.098 and 3.101 Å, respectively, in the $Ni^{II}_2Fe^{III}_2$ and in the $Ni^{II}_2Cr^{III}_2$ complex. Two mononuclear cyano-containing complexes act as monodentate ligands toward the $[Ni_2(\mathbf{63})(H_2O)_2]^{2+}$ unit through one of the cyano groups. This leads to cyano-bridged heterometallic $Ni^{II}_2Fe^{III}_2$ and $Ni^{II}_2Cr^{III}_2$ tetranuclear units. The iron(III) and chromium(III) ions are coordinated by two nitrogen and four cyanide carbon atoms in a distorted octahedral geometry. The shortest intermolecular M···M distances are 7.161 and 7.020 Å, while the Ni···M distances are 6.025 and 6.118 Å, respectively, in the Ni_2Fe_2 and Ni_2Cr_2 complex. Graphite-like interactions through the phenanthroline ligand occur, the interplanar phenanthroline–phenanthroline separations being 3.51 Å in the Ni_2Fe_2 complex and 3.53 Å in the Ni_2Cr_2 one. These interactions lead to chains growing along the c axis, the intrachain $M^{III}\cdots M^{III}$ separations being 8.853 Å in the Ni_2Fe_2 complex and 8.971 Å in the Ni_2Cr_2 one [68].

The magnetic data, collected in the temperature range 1.9–290 K, show for $[Ni_2(\mathbf{63})(H_2O)_2](ClO_4)_2$ an antiferromagnetic behaviour ($J = -61\ cm^{-1}$). An overall antiferromagnetic

behaviour is observed for the Ni_2Fe_2 and Ni_2Cr_2 complexes with a low-lying singlet spin state. The values of the intramolecular magnetic couplings are $J_{Fe–Ni} = +17.4\,cm^{-1}$ and $J_{Ni–Ni} = -44.4\,cm^{-1}$ for the Ni_2Fe_2 complex and $J_{Cr–Ni} = +11.8\,cm^{-1}$ and $J_{Ni–Ni} = -44.6\,cm^{-1}$ for the Ni_2Cr_2 one [68].

The mononuclear and dinuclear nickel(II) complexes of H_2-**81** were successfully prepared by template condensation of 1*R*,2*R*-diphenylethylenediamine with 2-diformyl-4-methylphenol. Reaction of the dialdehyde and the diamine with 0.5 equiv of nickel(II) perchlorate produced the yellow mononuclear complex $[Ni(H_2\text{-}\mathbf{81})](ClO_4)_2$, whereas the reaction with 1 equiv. of $Ni(ClO_4)_2$ with the addition of $N(Et)_3$, creating a more basic condition, yielded the brown dinickel product $[Ni_2(\mathbf{81})](ClO_4)_2$ [68].

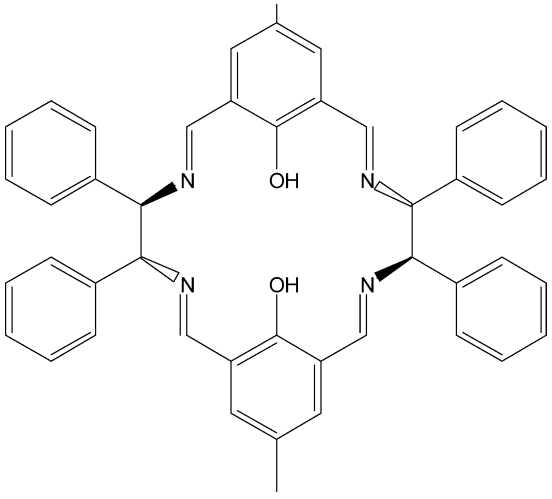

H_2-**81**

In the mononuclear complex, the nickel(II) ion occupies one N_2O_2 cavity, binding with two imine groups and two phenolic oxygen atoms. The geometry of the metal ion is planar and the whole macrocycle adopts a saddle-like conformation. The macrocycle is not deprotonated [68]. Upon deprotonation of the two phenol groups, the macrocyclic ligand can bind a second metal ion forming a homo- or heterodinuclear complex.

In $[Ni_2(\mathbf{81})](ClO_4)_2{\cdot}2CH_3CN$ the nickel(II) ions, 2.865 Å apart, occupy two chiral cavities with each metal ion bound to four macrocyclic donors in the basal plane. The conformation of the macrocycle is very similar to that found in $[Ni(H_2\text{-}\mathbf{81})](ClO_4)_2$ and the dicationic complex possesses an overall D_2 symmetry (Fig. 38) [68].

Zinc(II) perchlorate can also serve as an effective template for the formation of H_2-**81**; in the presence of 0.5 equiv. of $Zn(ClO_4)_2$, the mononuclear complex $[Zn(H_2\text{-}\mathbf{81})](ClO_4)_2{\cdot}2CH_3OH$ was obtained. Deprotonation of the two phenol groups, followed by charging with the second zinc ion, gives rise to the dizinc complex $[Zn_2(\mathbf{81})](ClO_4)_2$ [68].

The crystal structure of $[Zn(H_2\text{-}\mathbf{81})](ClO_4)_2{\cdot}2CH_3OH$ contains two different species, which interact with one or two methanol molecules along the axial direction of the mononuclear zinc(II) complex, respectively, giving rise to an octahedral and square pyramidal coordination environment around the zinc(II) ion (Fig. 39) [68].

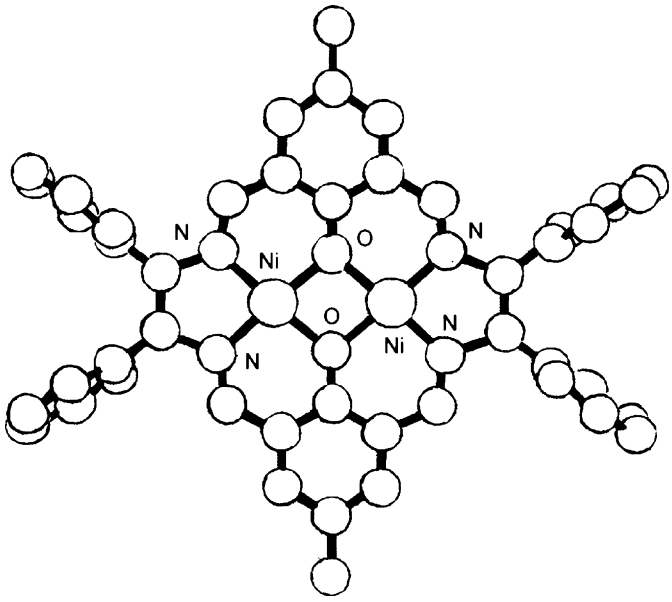

Fig. 38. Structure of $[Ni_2(\mathbf{81})]^{2+}$.

The coordination of copper(II) ion to H_2-**81** is much stronger than that of nickel(II) and zinc(II) ions. Irrespective of whether base was introduced, the product is always the dicopper(II) complex $[Cu_2(\mathbf{81})](ClO_4)_2{\cdot}2CH_3CN$. The crystal structure reveals a dinuclear structure, bearing two copper(II) centers bridged by two phenolic oxygen. Each four coordinate copper(II) ion is entrapped in one N_2O_2 coordination compartment of the macrocycle. On each side of the molecular platform a coordinated CH_3CN molecule and a ClO_4^- anion were observed [68].

The extension of the template condensation approach in the synthesis of the related [2 + 2] macrocycle H_2-**82** from *R*-1,1′-binapthalenyl-2,2′-diamine and 2,6-diformyl-4-methylphenol proved unsuccessful. The ESI-mass spectrum of the resulting solution indicated that no [2 + 2] compound could be identified but a mixture of the acyclic [1 + 1] and [2 + 1] ligands [68].

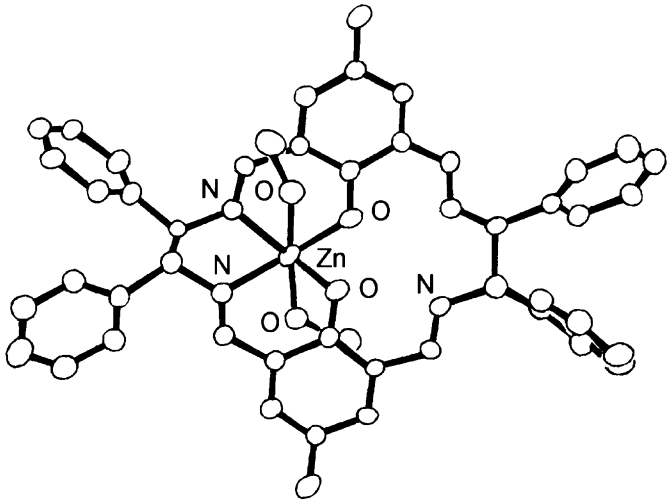

Fig. 39. Structure of $[Zn(H_2\text{-}\mathbf{81})(CH_3OH)_2]^{2+}$.

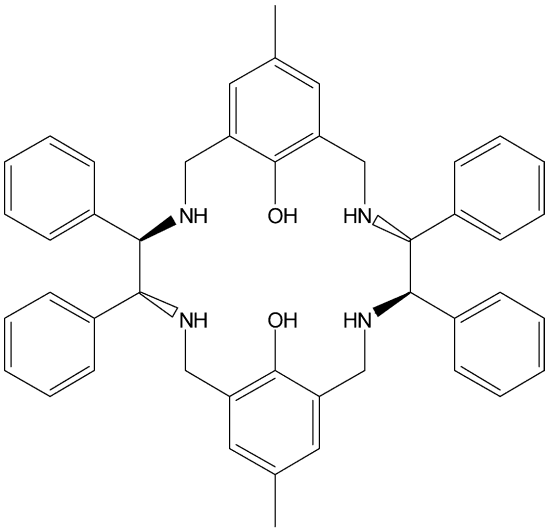

H_2-**81a**

Template effects of nickel(II), copper(II) and zinc(II) ions were observed in the construction of the mono- and dinuclear complexes of H_2-**83**···H_2-**85** [68,69]. The reaction of 1*R*,2*R*-1,2-diaminocyclohexane with 2,6-diformylphenol or its substituted derivatives in the presence of $Cu(ClO_4)_2$ gave the dinuclear complexes $[Cu_2(\mathbf{L})](ClO_4)_2{\cdot}4CH_3OH$ (H_2-**L** = H_2-**83**···H_2-**85**). $[Cu_2(\mathbf{84})](ClO_4)_2{\cdot}4CH_3OH$ contains two copper(II) centers, 2.888 Å apart, each coordinated in a N_2O_2 compartmental. Each copper(II) ion adopts a square pyramidal geometry with a coordinated methanol molecule in the axial position (Fig. 40) [68].

This approach was studied to include the syntheses of the air-sensitive dinuclear manganese(II), iron(II) and cobalt(II) complexes. These metal ions were found to be effective in forming the corresponding dinuclear complexes which in turn react with O_2 to afford the dioxygen adducts. Oxidation of the dicobalt(II) complex $[Co_2(\mathbf{84})]^{2+}$ occurred in air when a Lewis acid (i.e. acetic acid) was added dropwise. This led to the isolation of the chiral tetranuclear cobalt(III) complex $[Co_4(\mathbf{84})_2(OH)_2(CH_3COO)_2](ClO_4)_4{\cdot}4CH_3OH$. The complex can be described as a dimer of dimer structure constructed via the efficient spontaneous self-assembly of two tetra-Schiff base scaffolds and two hydroxyl groups (Fig. 41) [68].

With larger templating metal ions, such as cadmium(II), lead(II) and lanthanum(III), only mononuclear macrocyclic complexes can be successfully prepared. This behaviour is significantly different from that observed in the highly template dependent synthesis of traditional Robson-type Schiff base macrocyclic complexes. For example, magnesium(II) may result in a tetranuclear complex, whereas copper(II) creates a dinuclear complex. This behaviour can be related directly to the structural features of the linear diamine which lacks structural rigidity and chirality. In the synthesis of lead(II) complexes of $[\mathbf{84}]^{2-}$, the addition of 1 equiv of $Pb(SCN)_2$ results in the formation of the mononuclear complex $[Pb(H_2\text{-}\mathbf{84})](SCN)_2{\cdot}2CH_3OH$. The use of more lead(II) salt does not alter the reaction: the mononuclear complex is always obtained. The structure of $[Pb(H_2\text{-}\mathbf{84})](SCN)_2$ reveals entrapment of a lead(II) cation in one coordination compartment of the macrocycle H_2-**84**. The lead(II) ion is tetracoordinate, bound to two phenolate oxygens and two diamine nitrogens in a distorted square plane environment (Fig. 42) [68].

The preparation of the free Schiff bases H_2-**81**, H_2-**83**, H_2-**84** and H_2-**85** by self-condensation of the two precursors lead to oligomers. On the contrary the same condensation in the presence of $Pb(CH_3COO)_2$ in methanol, followed by reduction of the resulting yellow Schiff bases with $NaBH_4$ at 0 °C, afforded the desired reduced polyamine macrocycles H_2-**81a**, H_2-**83a**, H_2-**84a** and H_2-**85a**. The dicopper(II) complexes with these reduced polyamine were readily prepared by reacting the corresponding macrocycle with 2 equiv. of copper(II) salts in CH_3OH [68].

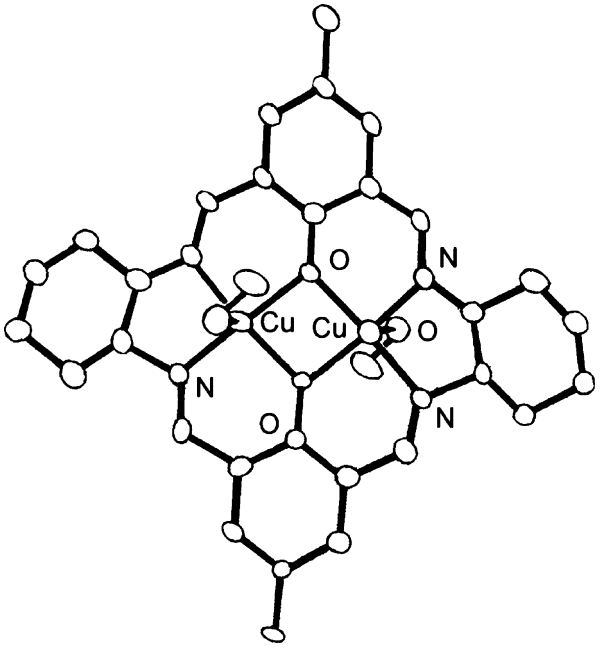

Fig. 40. Structure of $[Cu_2(\mathbf{84})(CH_3OH)_2]$.

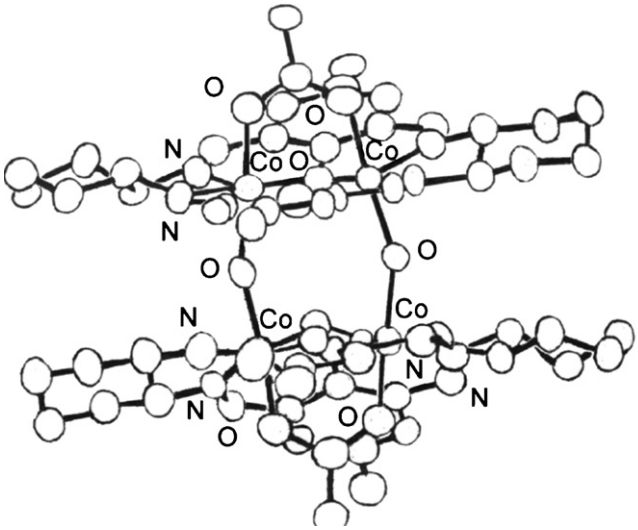

Fig. 41. Structure of $[Co_4(\mathbf{84})_2(OH)_2(CH_3COO)_2]^{4+}$.

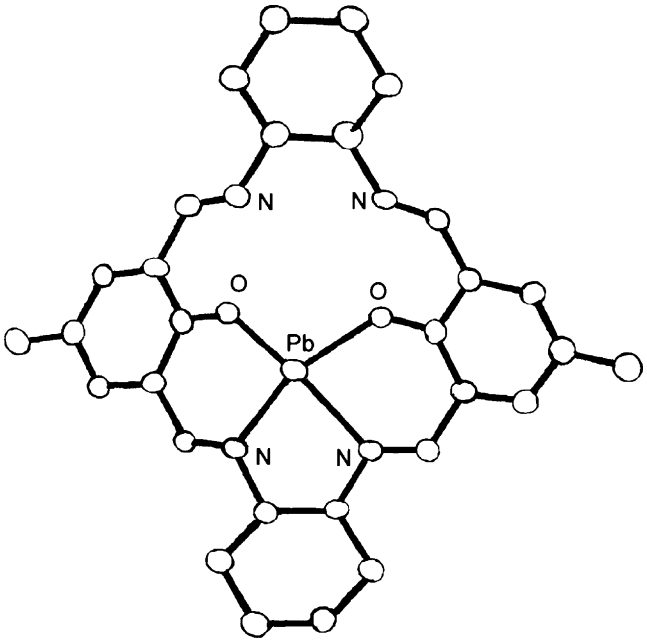

Fig. 42. Structure of $[Pb(H_2\text{-}\mathbf{84})]^{2+}$.

The oxidative coupling of 2-naphthol was employed as a model reaction to compare the catalytic activity and enantioselectivity of the dicopper(II) complexes of $[\mathbf{81}]^{2-}$, $[\mathbf{83}]^{2-}$, $[\mathbf{84}]^{2-}$ and $[\mathbf{85}]^{2-}$ with those of $[\mathbf{81a}]^{2-}$, $[\mathbf{83a}]^{2-}$, $[\mathbf{84a}]^{2-}$ and $[\mathbf{85a}]^{2-}$. All reaction were carried in the presence of the catalysts (10 mol%) in CCl_4 at 0 °C with molecular oxygen as oxidant. The use of the complex $[Cu_2(\mathbf{84})]^{2+}$ resulted in a yield of 79% and a moderate enantioselectivity of 82% ee. When $[Cu_2(\mathbf{84a})]^{2+}$ was used slightly increases in the ee value (86%) and the yield (84%) were observed. In general, polyaza complexes are more robust than their corresponding Schiff base complexes in terms of reproducibility and stability. Catalytic efficiency seems to be insensitive to the bulk of the peripheral groups. At higher temperatures, the reaction rate increases, but lower enantioselectivitites are observed. For instance, the ee value for $[Cu_2(\mathbf{84})]^{2+}$ decreased by 37% when the temperature was increased from 0 to 20 °C. Increased bulk of the diamino residues does not significantly affect the enantioselectivity. Furthermore, the control compound [Cu(**86**)] with one metal center and a C_2 symmetry, synthesized by condensation of 2 equiv. of salicylaldehyde with 1*R*,2*R*-diphenylethylenediamine in the presence of copper(II) ions, leads to a low enantioselectivity at 0 °C (only 19% ee). These results suggest that a rigid dinuclear platform is essential for high enantioselectivity. The copper(II) complex mediated oxidative coupling can proceed through three mechanistic pathways: homolytic coupling of two radical species, radical insertion of one aryl into the C–H bond of another aryl, and reaction of an anion with a carbocation. For the coupling reaction mediated by $[Cu_2(\mathbf{84})]^{2+}$, a substrate molecule may undergo ligand exchange with CH_3OH on one copper(II) ion to form a copper(II)–substrate complex, which is followed by the generation of a radical intermediate, which results from one-electron transfer from the substrate to the copper(II) ion. Simultaneously, the same process may occur on the other copper(II) center. Minimization of steric interactions between the radical intermediates and the axial hydrogen atoms of the chiral cyclohexyl rings should favour the orientation of the system which should produce the S product, 2,2′-dinaphtol [68].

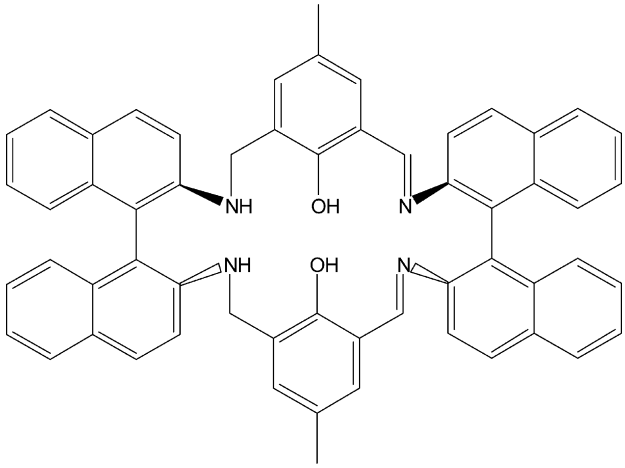

H_2-**82**

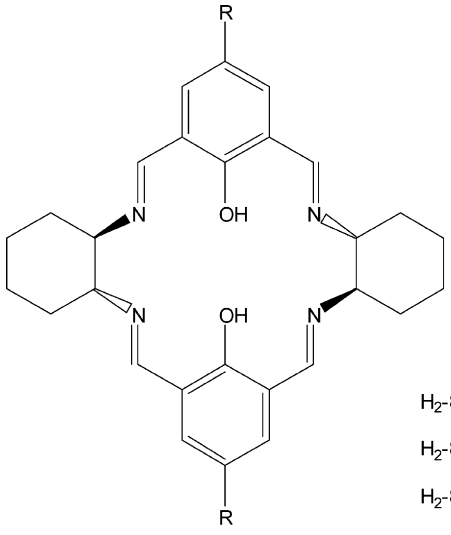

	R
H_2-**83**	H
H_2-**84**	CH_3
H_2-**85**	$C(CH_3)_3$

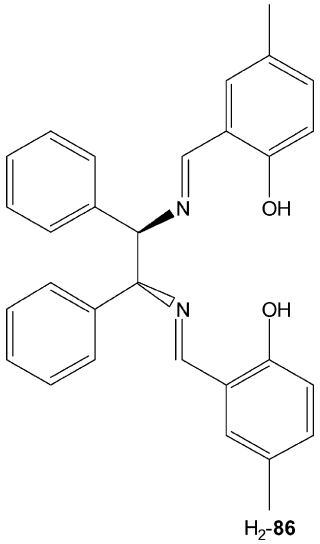

H_2-**86**

The [3 + 3] chiral Schiff bases H_3-**87** and H_3-**88** have been prepared in the presence of an excess of alkaline and even alkaline earth metal ions [68]. H_3-**87** shows a vaselike tridimensional conformation, where the lower rim of the vase consists of methyl-substituted benzene fragments, and the upper rim contains the benzene rings from the diphenylethylenediamines. This represents an overall C_3 symmetry (Fig. 43a) [68].

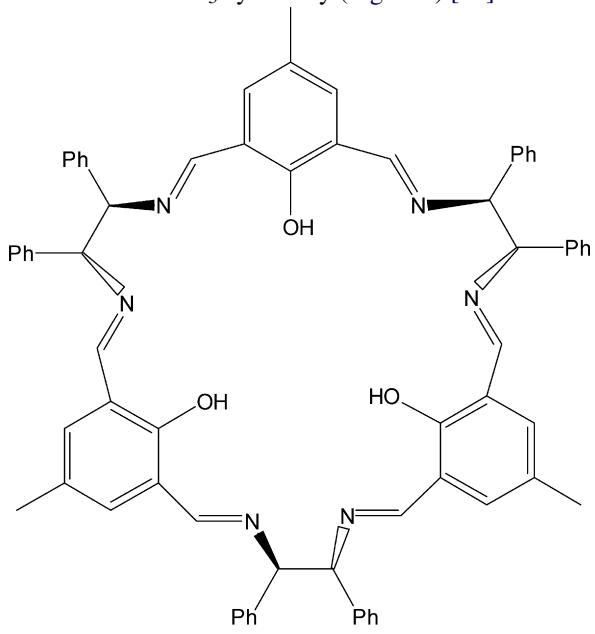

H_2-**87**

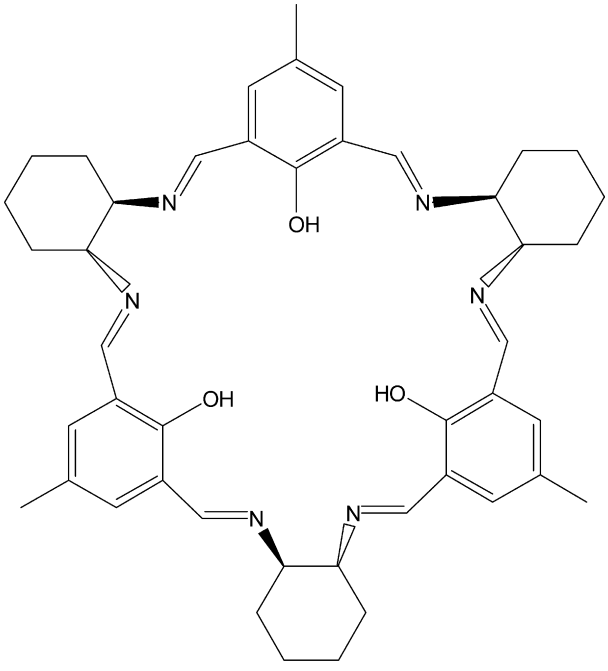

H_3-**88**

While condensation reaction of dialdehydes with linear diamines generally affords polymeric Schiff base products including the [1 + 1], [2 + 2], [3 + 3] and [4 + 4] macrocycles and other polymeric Schiff base compounds depending upon the reactants and the template conditions [17,18], by using a rigid dialdehyde and a rigid chiral diamine the self-assembly of [3 + 3] chiral macrocycle was highly efficient (<95%). [3 + 3] Cyclocondensation reactions have been successfully achieved by condensation of equimolecular amounts the appropriate dicarboxaldehydes, (1,3-diformyl-3-methylbenzene, 1,3-diformyl-5-methylbenzene, 1,3-diformyl-2,4,6-trimethylbenzene, 1,4-diformyl-2,5-dimethylbenzene, 1,4-diformyl-2,5-dimethoxybenzene, 1,4-diformyl-2,3-dimethoxybenzene, 1,3-diformyl-2,4,6-trimethoxybenzene, 1,1-dimethoxy-2,2′-diformyl-4,4′-dimethylbiphenyl, 3,3′-diformylbiphenyl, 9,10-diformylantracene) with (1*R*,2*R*)-diaminocyclohexane in dichloromethane followed by recrystallization of the crude products (sometime contaminated by the [2 + 2] omologues) from toluene or ethylacetate. Reduction of these Schiff bases to the corresponding [3 + 3] polyamine derivatives was achieved in CH_3OH using $NaBH_4$ as reducing agents [69].

Ring contraction from [3 + 3] to [2 + 2] macrocycles occurs for some of these Schiff bases when refluxed in CH_2Cl_2 for a long period of time (from 12 h up to 72 h). Other condensation reactions give rise only to the [2 + 2] macrocycles; this occurs, for instance, when 9-ethyl-3,6-diformyl carbazole was used as formyl precursor [69]. All compounds adopt a conformation of the highest possible symmetry in solution. However, dynamic interchange of conformation was observed. All the macrocycles are enantiomerically pure. Most remarkably due to the generality of this macrocyclization procedure, it is possible to synthesize macrocycles with varying ring sizes and tunable lipophilic cavities. Thus, it is possible to functionalize the macrocycle and change its electronic properties by variation of the dialdehyde component.

The reaction of 2,6-diformyl-4-methylphenol and *trans*-(1*R*,2*R*)-diaminecyclohexane in methanol at room temperature results in the facile formation of the [3 + 3] condensed optically active, chiral macrocyclic Schiff base H_3-**88** instead of the related [2 + 2] macrocycle H_2-**84**. Its [3 + 3] entity was inferred by FAB-mass spectrometry and confirmed by an X-ray analysis on crystals obtained during attempted crystallization of the related europium(III) complex from dimethylformamide [69]. The macrocycle is of approximate C_3 symmetry and the aromatic rings form a cone-like cavity resembling calixarenes (Fig. 43b). The phenolic hydroxyl groups are positioned at the narrower rim of the cavity, while the methyl groups form the broader rim. In that respect the structure is different from the structure obtained from calculations that predicted a vase-shape molecule with methyl groups positioned on the narrower rim and smaller diameter of the cavity. The crystal structure H_3-**88** confirms the predicted *s-trans* conformation of the diimine fragment [69].

Reduction of H_3-**88** by $NaBH_4$ resulted in the formation of the related [3 + 3] hexaazamacrocyclic derivatives H_3-**88a** as indicated by FAB mass spectrometry and ascertained by an X-ray structural determination on a crystal grown from benzene [69] (Fig. 43c). The molecular three-fold symmetry coincides with the crystallographic three-fold axis. The three phenolic-OH groups projected inside the cavity generate three equivalent N_2O_2 sub-cavities. The macrocycle is stabilized by

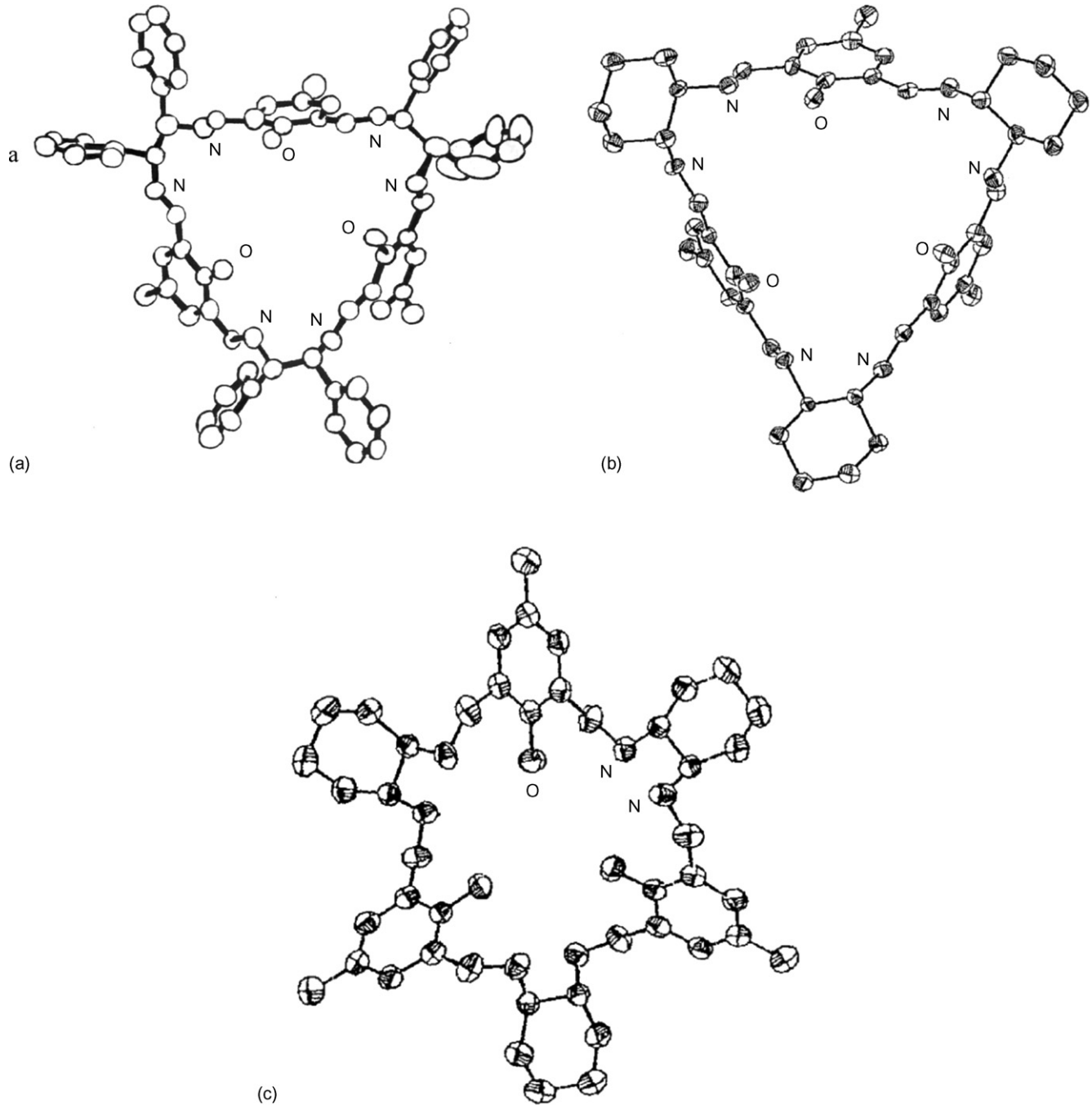

Fig. 43. Structure of H_3-**87** (a), H_3-**88** (b) and H_3-**88a** (c).

intramolecular hydrogen bonding. The macrocycle has an internal hydrophilic cavity, capable of forming hydrogen bonds and an external hydrophobic periphery. The molecules are extended in the *ab* plane with the mean plane of the molecule perpendicular to the *c*-axis. Each molecule is surrounded by six molecules leading to a trigonal network structure. The organization of the molecules in the ab plane is governed by the hydrophobic interaction between the methyl groups of formyl moiety and methylene groups of amine moiety and is not assisted by any other observable interactions. The stacking in the *c*-axis is maintained by intermolecular N–H···N hydrogen bonding and supported by weak C–H···O interactions leading to a channel like structure. The three-dimensional trigonal assembly of the macrocycle is maintained by hydrophobic interactions in the *ab* plane and hydrogen bonding along the *c*-axis [69].

The geometry of these sub-cavities appears suitable for metal complexation as the two nitrogen and two oxygen atoms provide appropriate coordination sites. H_3-**88**, when reacted with $LnX_3 \cdot nH_2O$ (Ln = La, Ce, Eu, Yb, Lu; X = NO_3^-, Cl^-, CH_3COO^-) under a variety of conditions, gives rise to lanthanide(III) complexes, as confirmed by the paramagnetically shifted lines in ^{1}H NMR spectra of europium(III) and ytterbium(III) derivatives. The incorporation of the lanthanide(III) ions into the macrocycle is also confirmed by ESI-mass spectra;

for example the product, derived from the reaction of H_3-**88** with europium(III) chloride in the presence of three equivalents of triethylamine, gives rise to peaks corresponding to the $[Eu(H\text{-}\mathbf{88})]^+$ and $[Eu(H_2\text{-}\mathbf{88})]^+$ species. The NMR and ESI-mass data suggest that H_3-**88** forms lanthanide(III) complexes similar to that of the H_3-**88a** macrocycle. Unfortunately the NMR spectra could not be assigned and analyzed due to broadening and overlapping of signals. Moreover, the complexation of the lanthanide(III) ions by H_3-**88** is further complicated by the possibility of hydrolysis of the Schiff base macrocycle. Unlike the spectra of the complexes with H_3-**88a**, the NMR spectra of the lanthanide(III) complexes with H_3-**88** are time dependent. Upon standing for several days new complexes are generated, that may indicate rearrangement of H_3-**88** to the corresponding [2 + 2] macrocycle H_2-**84**, as observed in the case of complexation by transition metal ions.

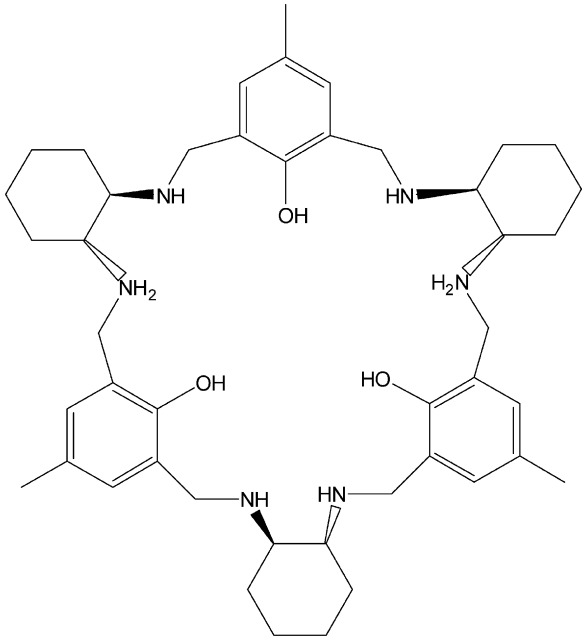

H_3-**88a**

The reaction, in fact, of the preformed [3 + 3] Schiff base H_3-**88** with metal(II) salts (1:3 ratio) in hot methanol gives rise to a macrocyclic ring contraction with the consequent formation of the [2 + 2] macrocyclic complexes $[M_2(\mathbf{84})(X)_2]$ ($M = Cu^{II}$, Ni^{II}, Fe^{II}, Co^{II}, Mn^{II}). Crystals of $[Zn_2(\mathbf{84})(Cl)_2]$ (Fig. 44a), obtained from a slow evaporation of a $CHCl_3/CH_3CN$ solution, show the phenoxo groups serve as bridges between the metal centers. Each metal ion has square pyramidal geometry bridged by two oxo groups and coordinated by two imine nitrogens. The fifth axial coordination position is occupied by a chloride anion in axial position. The Zn···Zn distance is 3.19 Å. The macrocycle is planar and the metal ions are located above and below the plane formed by the N_2O_2 donors [69].

Analogously, in $[Cu_2(\mathbf{84})(\mu\text{-}CH_3COO)](ClO_4)\cdot CH_3CN$ (Fig. 44b) the two copper centers, strongly antiferromagnetic interacting each other, are bridged by two phenolic oxygens and are coordinated by two imine nitrogens. An acetate group forms a bridge between the two copper ions. The geometry around each copper ion is square pyramidal with the ligand N_2O_2 donor atoms forming the basal plane with acetate oxygen at the apical position. The two copper ions are above the N_2O_2 plane toward the acetate groups. The Cu···Cu distance is 2.872 Å [69].

$[Cu_2(\mathbf{84})(\mu\text{-}CH_3COO)](ClO_4)\cdot CH_3CN$, shows two stepwise one-electron reduction peaks in negative potential at −0.63 and −1.25 V in acetonitrile corresponding to $Cu^{II}Cu^{II} \leftrightarrows Cu^{I}Cu^{II}$ and $Cu^{I}Cu^{II} \leftrightarrows Cu^{I}Cu^{I}$.

In the diamagnetic complex $[Ni_2(\mathbf{84})](ClO_4)_2\cdot CH_3CN\cdot CH_3OH$ (Fig. 44c) the nickel environments are square planar generated by two imine nitrogens and two bridging oxygen atoms from the ligand. The nickel ions are in the plane of N_2O_2 compartment at a Ni···Ni, distance of 2.80 Å. The complex has two uncoordinated perchlorate anions and a methanol and an acetonitrile molecule in the crystal lattice [69].

H_3-**88a** reacts with transition metal salts in dry methanol under nitrogen atmosphere and in a 1:3 molar ratio to form the homotrinuclear complexes $[Zn_3(\mathbf{88a})(CH_3COO)](ClO_4)_2\cdot 3CHCl_3\cdot H_2O$, $[Zn_3(\mathbf{88a})(CH_3COO)](ClO_4)\cdot(PF_6)\cdot 5CH_3OH\cdot H_2O$ and the heterotrinuclear complex $[Zn_2Cu(\mathbf{88a})(CH_3COO)](ClO_4)_2\cdot 3CHCl_3\cdot H_2O$ [69]. The copper content in the heterotrinuclear Zn_2Cu complex and its magnetic moment of $\mu = 1.60\mu_B$, a shoulder d–d transition band (in CH_3CN) at 632 nm, and a reversible cyclic voltammetric redox couple at −1.00 V (Cu^{II}/Cu^{I}) are consistent with the presence of one distorted tetrahedral copper ion [69].

In $[Zn_3(\mathbf{88a})(\mu\text{-}CH_3COO)](ClO_4)_2\cdot 3CHCl_3\cdot H_2O$ (Fig. 45a) the *trans* geometry of the cyclohexyldiamine moiety and the flexibility offered by the –CH_2–NH– linkage together with the large size of the macrocyclic ring influences the macrocycle to twist to accommodate three metal ions in its cavity. The complex has a central Zn_3O_3 coordination core where the zinc ion and phenoxo oxygen atoms are alternate to each other, constituting a cyclic six membered ring. Each zinc(II) ion is coordinated by two bridging phenoxo oxygens and two amino nitrogens of the macrocycle. Two zinc(II) ions, 3.348 Å apart, are bridged vertically by an external acetato group in a distorted trigonal bipyramidal geometry. A distorted tetrahedral geometry around the third zinc(II) ion occurs. The interatomic distances between this zinc(II) and the other two metal ions are 3.298 and 3.568 Å, respectively [69].

The basic cationic structure of the other trinuclear complexes is very similar to $[Zn_3(\mathbf{88a})(\mu\text{-}CH_3COO)](ClO_4)_2\cdot 3CHCl_3\cdot H_2O$. In $[Zn_2Cu(\mathbf{88a})(\mu\text{-}CH_3COO)](ClO_4)_2\cdot 3CHCl_3\cdot H_2O$ the replacement of one zinc(II) ion with a copper(II) ion produces the same distorted tetrahedral geometry around the copper(II) ion, which is separated from the two zinc(II) ions by 3.327 and 3.535 Å, respectively [69].

The stability of the Zn_3 and Zn_2Cu complexes toward water was investigated by NMR spectra. Retention of ^1H NMR (d_6-DMSO) signals corresponding to the ligand and acetate bridge of $[Zn_3(\mathbf{88a})(CH_3COO)](ClO_4)\cdot(PF_6)\cdot 5CH_3OH\cdot H_2O$ in 0.5 μl of water indicates the stability of the complex in DMSO/H_2O [69].

Investigations into mimicking the hydrolytic activity of $[Zn_3(\mathbf{88a})(CH_3COO)](ClO_4)\cdot(PF_6)\cdot 5CH_3OH\cdot H_2O$ and

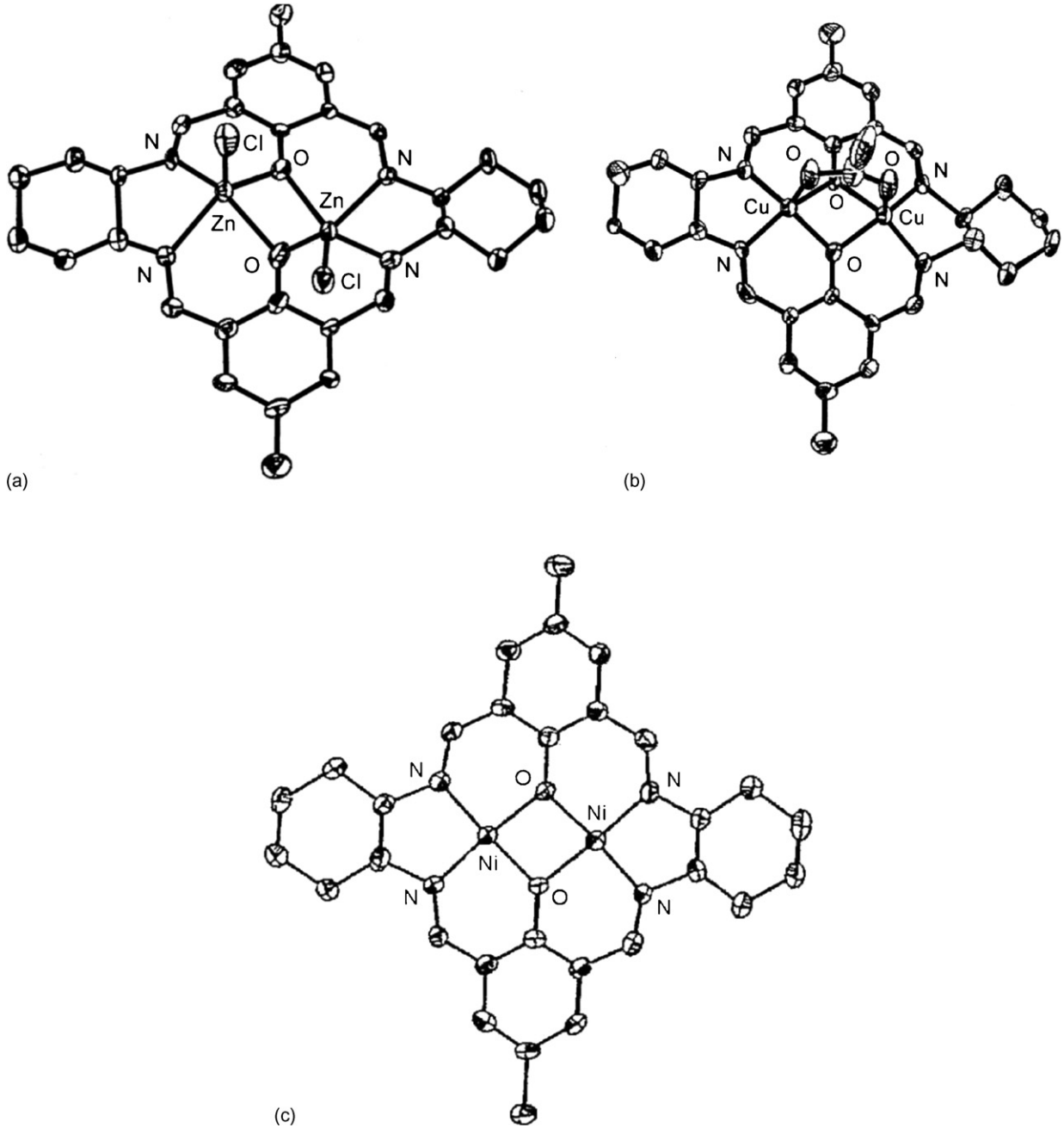

Fig. 44. Structure of $[Zn_2(\mathbf{84})(Cl)_2]$ (a), $[Cu_2(\mathbf{84})(\mu\text{-}CH_3COO)]^{+}$ (b) and $[Ni_2(\mathbf{84})]^{2+}$ (c).

$[Zn_2Cu(\mathbf{88a})(\mu\text{-}CH_3COO)](ClO_4)_2\cdot 3CHCl_3\cdot H_2O$ in DMSO were conducted on calf thymus (CT) DNA. Both of the complexes were found to be effective in the cleavage of CT DNA. The effects of complex concentration and temperature on DNA cleavage were significant. The results suggest that DMSO does not induce any changes in DNA, At 37 °C, low concentrations of the complexes (100 μM) did not cleave DNA as effectively, whereas three- or five-fold concentrations of the complex completely hydrolyzes the DNA. At an elevated temperature (50 °C), DNA was completely hydrolyzed irrespective of the concentrations of $[Zn_3(\mathbf{88a})(CH_3COO)](ClO_4)\cdot(PF_6)\cdot 5CH_3OH\cdot H_2O$ whereas $[Zn_2Cu(\mathbf{88a})(\mu\text{-}CH_3COO)](ClO_4)_2\cdot 3CHCl_3\cdot H_2O$ was found to be highly active only at high concentrations. The high activity of $[Zn_3(\mathbf{88a})(CH_3COO)](ClO_4)\cdot(PF_6)\cdot 5CH_3OH\cdot H_2O$ indicates the active role of the Zn_3 ions in catalytic processes [69].

Crystals of $[Eu(H_4\text{-}\mathbf{88a})(NO_3)_2](NO_3)_2\cdot 5CH_3OH$, obtained upon standing of methanol solutions containing H_3-**88a** and excess of $Eu(NO_3)_3\cdot 6H_2O$, are unstable and readily lose solvent molecules. The composition of the crystals indicates that the europium(III) ion is complexed by the protonated form of the macrocycle $[H_4\text{-}\mathbf{88a}]^{+}$. The compound crystallizes with the complex cation $[Eu(H_4\text{-}\mathbf{88a})(NO_3)_2]^{2+}$, two nitrate anions and five methanol molecules in the asymmetric unit. One of solvent molecule is partially disordered. In this complex the macrocycle acts as pentadendate ligand; the europium(III) ion

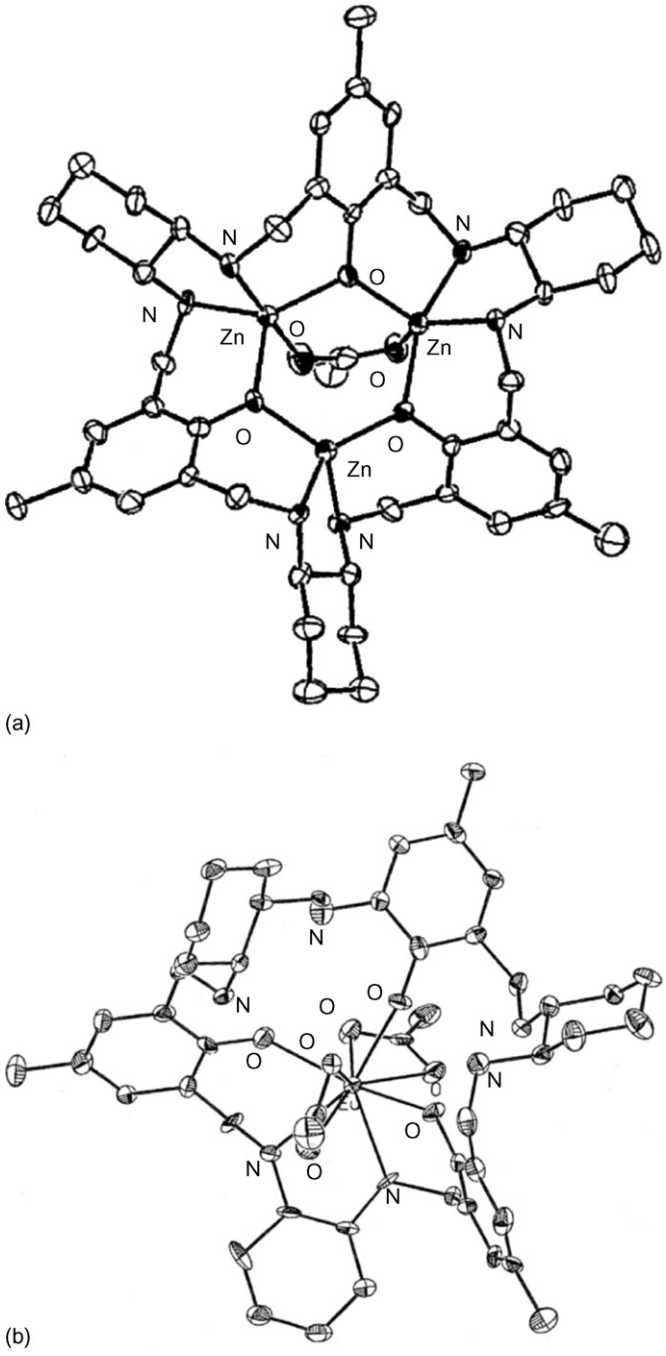

Fig. 45. Structure of $[Zn_3(\mathbf{88a})(\mu\text{-}CH_3COO)]^{2+}$ and $[Eu(H_4\text{-}\mathbf{88a})(NO_3)_2]$ (b).

is coordinated by three phenolic oxygen and two amine nitrogen atoms. The coordination sphere of the metal ion is completed by two bidendate nitrate anions bound in axial positions on two sides of the macrocycle (Fig. 45b). The coordination sphere of europium(III) defines a highly irregular polyhedron; the regular arrangement of coordinating atoms is prevented by the constraints imposed by the macrocycle. In the complex the macrocycle, strongly distorted in comparison with the free ligand, adopts a highly irregular saddle-type conformation, reflecting both helical twist and considerable folding of the macrocycle [69].

The ability of H_3-**88a** to bind lanthanide(III) ions is clearly confirmed by NMR spectra of the paramagnetic Ce(III), Eu(III), Dy(III) and Yb(III) derivatives generated in solution. These spectra also indicate formation of a variety of complexes by given lanthanide(III) ions. The results are strongly dependent on solvent, the kind of counteranion, amount of the added lanthanide(III) ion and amount of the added base. The rich variety of species, detected in solution by NMR, reflects the various possible coordination modes of H_3-**88a**, various protonation states of the ligand and various sets of axial ligands. The spectra of D_2O or D_2O/CD_3OD solutions of $[Eu(H_4\text{-}\mathbf{88a})(NO_3)_2](NO_3)_2$ are concentration dependent and exhibit additional signals due to uncomplexed protonated ligand. This indicates that $[Eu(H_4\text{-}\mathbf{88a})(H_2O)_n]^{4+}$ partially dissociates in aqueous solutions to $[Eu(H_2O)_n]^{3+}$ and $[H_4\text{-}\mathbf{88a}]^+$. The partial dissociation of the complexes is also visible in the ^1H NMR spectra of D_2O solutions of the related Sm(III), Dy(III), Yb(III) and Lu(III) complexes. The ^1H NMR spectral pattern of the europium(III) complex, generated in solution, allows to propose that the europium(III) ion is bound within the macrocycle in aqueous solution, the macrocycle is of C_2 symmetry and only one diaminocyclohexane fragment is involved in coordination. As the solid state molecular structure of the europium(III) complex is not of C_2 symmetry, it follows that the macrocycle is flexible and in solution conformational changes (fast on the NMR time scale) result in an effective, time-averaged C_2-symmetric structure. In the case of the diamagnetic lutetium(III) derivative, obtained by adding different amount of $LuCl_3{\cdot}6H_2O$ to H_3-**88a** in D_2O/CD_3OD, NMR data reveal the presence of a dynamic process corresponding to migration of Lu(III) within the macrocycle and this migration does not proceed through a dissociative mechanism [69]. The ability of H_3-**88a** to bind lanthanide(III) ions is also confirmed by ESI-mass spectra of methanol solutions. The spectra show peaks corresponding to $[Ln(H_2\text{-}\mathbf{88a})(NO_3)]^+$, $[Ln(H\text{-}\mathbf{88a})]^+$ and $[H_4\text{-}\mathbf{88a}]^+$, both for the isolated complexes $[Ln(H_4\text{-}\mathbf{88a})(NO_3)_2](NO_3)_2{\cdot}nH_2O$, and for the solutions containing H_3-**88a** and lanthanide(III) nitrates. When the europium(III) or ytterbium(III) complexes $[Ln(H_4\text{-}\mathbf{88a})(NO_3)_2](NO_3)_2{\cdot}nH_2O$ are titrated with NaOH, the ^1H NMR signals of the starting complexes disappear and broad, unresolved signals are obtained. The observed spectral changes result from formation of complexes with the deprotonated ligand $[\mathbf{88a}]^{3-}$ and not from dissociation of the lanthanide ion from the macrocycle.

$Na[La(\mathbf{88a})(NO_3)]{\cdot}3H_2O$, $Na[Ce(\mathbf{88a})(NO_3)]$ and $Na_2[Pr(\mathbf{88a})(NO_3)(OH)]{\cdot}4H_2O$ have also been obtained by addition of NaOH. It is unlikely that the broad spectra observed would arise from species containing symmetrically bound lanthanide(III) ion in the center of the macrocycle. Additionally, ESI-MS reveals formation of dinuclear complexes when H_3-**88a** is reacted with two equivalents of lanthanide(III) ions (Ln = La, Ce, Pr, Eu) in the presence of NaOH or acetate. For instance the acetate derivative, obtained from the reaction of two equivalents of $Eu(CH_3COO)_3{\cdot}4H_2O$ with H_3-**88a**, shows signals corresponding to $[Eu_2(\mathbf{88a})(CH_3COO)]^{2+}$, $[Eu_2(H\text{-}\mathbf{88a})(CH_3COO)_2]^{2+}$ and $[Eu_2(\mathbf{88a})(CH_3COO)_2]^+$, respectively. The ^1H NMR spectra of the acetate derivatives are

very complicated, indicating the presence of two species of low symmetry, and their COSY spectra indicate that more than one diaminocyclohexane unit is involved in complexation.

Reaction of two equivalents of the praseodinium(III) ion with H_3-**88a** in the presence of NaOH results in the formation of the dinuclear complex $Na_3[Pr_2(\mathbf{88a})(NO_3)_2(OH)_2]_2NO_3{\cdot}5H_2O$. Binding of the two praseodinium(III) ions to the macrocycle is indicated by ESI-mass spectra that exhibit signals corresponding to $[Pr(H\text{-}\mathbf{88a})]^+$, $[Pr(\mathbf{88a})(NO_3)]^+$, $[Pr_2(\mathbf{88a})(NO_3)_2]^+$ and $[Pr_2(H\text{-}\mathbf{88a})(NO_3)_3]^+$. Single crystals of this complex have been obtained by diffusion of water into a methanol solution of the complex or slow evaporation of a methanol water solution Although the crystals were twinned and too small to obtain a satisfactory solved molecular structure, the data obtained show coordination of two praseodinium(III) ions within the macrocycle. In fact a tetranuclear complex, consisting of two dinuclear macrocycle units bridged by two nitrate bridges, occurs [69].

The mode of binding of two lanthanide ions by macrocycle $[\mathbf{88a}]^{3-}$ displayed by this structure is fully in accord with ^{1}H NMR spectrum of the complex which is in agreement with different coordination environments of the two praseodinium(III) ions. The NMR spectral pattern indicates that the binding of the second lanthanide(III) ion makes the macrocycle less flexible so the conformational averaging of C_1-symmetric structure to the C_2-symmetric structure, discussed above for the $[Eu(H_4\text{-}\mathbf{88a})(NO_3)_2](NO_3)_2$ complex, is no longer possible [69].

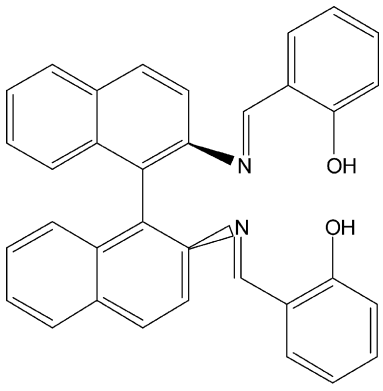

H_2-**89**

R-1,1′-Binaphthalenyl-2,2′-diamine does not form the corresponding trimeric macrocycle by direct condensation. The open Schiff base H_2-**89**, prepared to mimic the local geometry around *R*-1,1′-binaphthalenyl-2,2′-diamine, shows the affiliated phenol groups are constrained to remain on each side of the pivot due to the energy barrier that exists in the chiral diamine. The failure of the self-assembly process can be explained by the restricted rotation around the aryl–aryl bond [68].

H_3-**87**, when reacted with copper(II), nickel(II) or zinc(II) salts, gives rise to the cleavage of the trimeric macrocycle and the formation of the dinuclear complexes $[M_2(\mathbf{81})]^{2+}$. The ring contraction product is considered to be the thermodynamic stable product [68]. Surprisingly, however, reaction of the Schiff base salt, $[Na_3(\mathbf{87})]$, with nickel(II) perchlorate can produce $[Ni(H\text{-}\mathbf{87})]$, $[Ni_2(\mathbf{87})](ClO_4)$ and $[Ni_3(\mathbf{87})](ClO_4)_3$, depending on the ligand/metal ion ratio. Molecular modeling study shows that the energy-minimized conformation of the complexes is highly distorted and the vaselike confirmation cannot be maintained. Upon binding with the metal ions, one of the three phenol groups of the macrocyclic ligand reverses its direction. Successful preparation of these compounds was confirmed by ESI-mass spectra. Spectrophotometric titrations show $[Na_3(\mathbf{87})]$ binds with nickel(II) in three steps before reaching saturation. This behaviour indicates the critical role protons play in the rearrangement of the macrocycle in coordination with metal ions [68].

$\{[Fe_2(\mathbf{63})(CH_3COO)]_2(O)_2\}(PF_6)_2$, obtained as dark brown crystals by the [2 + 2] condensation of 2,6-diformyl-4-methylphenol and 1,3-diaminopropane in presence of iron(III) acetate as templating agent and $[NH_4](PF_6)$ in ethanol consists of two dinuclear $\{Fe_2(\mathbf{63})(CH_3COO)\}$ units, two oxo ligands and two PF_6^- ions. In each dinuclear unit the macrocyclic ligand accommodates two iron(III) ions with a Fe···Fe separation of 3.078 Å. An acetate group in the *syn*,*syn* mode bridges the two iron ions. Two $\{Fe_2(\mathbf{63})(CH_3COO)\}$ units are combined by oxide ions, producing a tetranucelar core of a face-to-face type (Fig. 46a) [70]. The powdered sample of the complex has a subnormal magnetic moment of 1.84μ_B at room temperature and the moment decreases with lowering temperature to reach a plateau value of 0.53μ_B near 30 K. The cryomagnetic property of the complex is well reproduced using $J = -101\ cm^{-1}$, $J' = -11\ cm^{-1}$ where J' is the exchange integral in the dinuclear unit and J is the exchange integral between the dinuclear units [70].

Reaction of equimolar amounts of 2,6-diformyl-4-*tert*-butylphenol and 1,3-diaminopropane with an excess of aqueous HBr in CH_3OH followed by the addition of excess $[NH_4](PF_6)$ affords an orange precipitate which, by recrystallization from acetonitrile/diethyl ether, produces $[H_4\text{-}\mathbf{65}](PF_6)_2$. Treatment of $[H_4\text{-}\mathbf{65}](PF_6)_2$ in CH_3CN with five equivalents of $N(Et)_3$ results in a rapid change of color from orange to yellow leading to the formation of the free [2 + 2] macrocycle H_2-**65**, which has a zwitterionic structure [71].

Co^{II}, Ni^{II}, Cu^{II}, Zn^{II}, Cd^{II}, Ag^{I}, Pb^{II} extraction and transport by H_2-**65** from an aqueous source phase (30 ml) at pH 4.7 into an aqueous receiving phase (30 ml) at pH 3, across a $CHCl_3$ phase (50 ml) was studied in order to determine whether H_2-**65** would act as a double-loaded extractant for the selective binding of two metal(II) ions centers, thus affording a more efficient extraction via a 2:1 metal:ligand protocol. Transport was performed against a back gradient of protons; under the conditions employed H_2-**65** yielded highly selective transport of the copper(II) ion after 24 h [71]. A parallel two-phase extraction experimental was performed in which the conditions employed mirrored those used for the three-phase transport system with the aqueous phase containing equimolar concentrations of the above seven metal ions. The results confirm that after 24 h significant selectivity for the copper(II) ion was again apparent with 81% of the copper(II) ion initially present in the aqueous phase being extracted into the $CHCl_3$ phase together with a minor amount of zinc(II) ion (3.7%) and traces of the cadmium(II) ion. H_2-**65** is seen to be an efficient extraction reagent (approximately 85% of the ligand sites are occupied under the conditions employed)

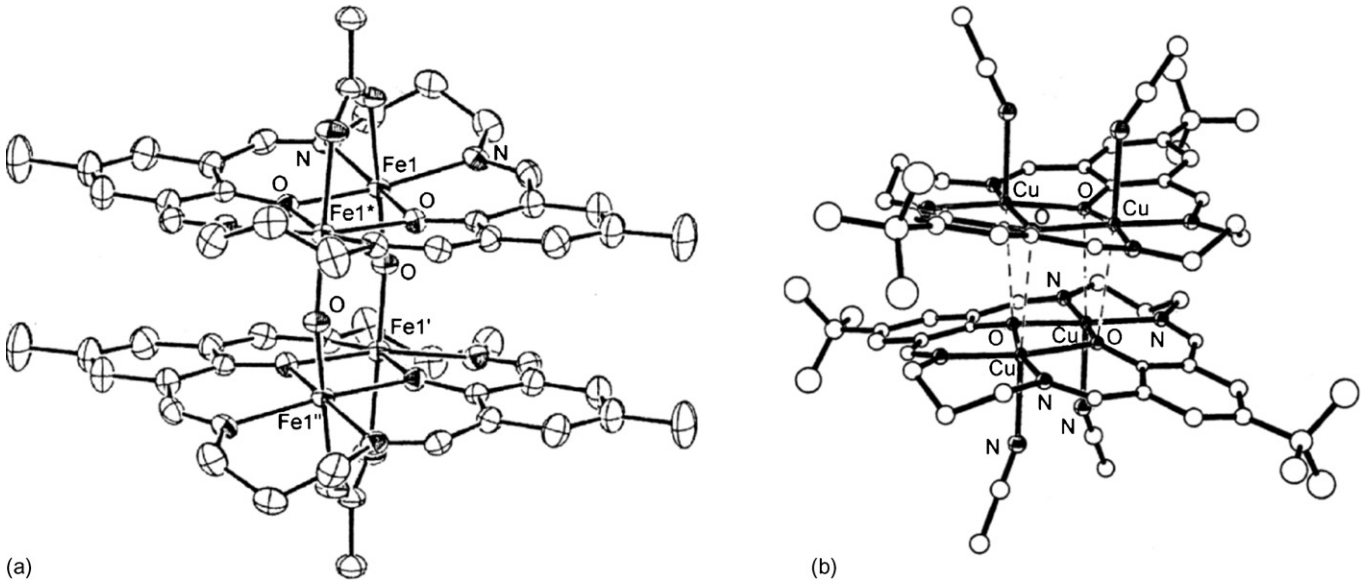

Fig. 46. Structure of $\{[Fe_2(\mathbf{63})(CH_3COO)]_2(O)_2\}^{2+}$ (a) and $\{[Cu_2(\mathbf{65})(CH_3CN)_2]_2\}^{4+}$ (b).

showing high specificity for the copper(II) ion, thus paralleling the behaviour observed for the corresponding transport system [71].

When 2 equiv. of $Cu(CH_3COO)_2{\cdot}H_2O$ were treated with 1 equiv of $[H_4\text{-}\mathbf{65}](PF_6)_2$ and excess $N(Et)_3$ in CH_3CN/C_2H_5OH was added, $\{[Cu_2(\mathbf{65})(CH_3CN)_2](PF_6)_2\}_2$ was isolated. The structure confirms a highly unusual tetranuclear structure incorporating a distorted Cu_4O_4 cubane core. The Cu· · ·Cu separation is 3.119 Å within each Cu_2O_2 unit with each copper(II) ion in a tetragonally distorted octahedral environment. The coordination sphere about each copper(II) ion is completed by a long-range interaction to the phenoxy oxygen atom from the macrocycle in the other half of the cluster. While the long-range interactions between the two Cu_2O_2 units in each dimer are too long to be

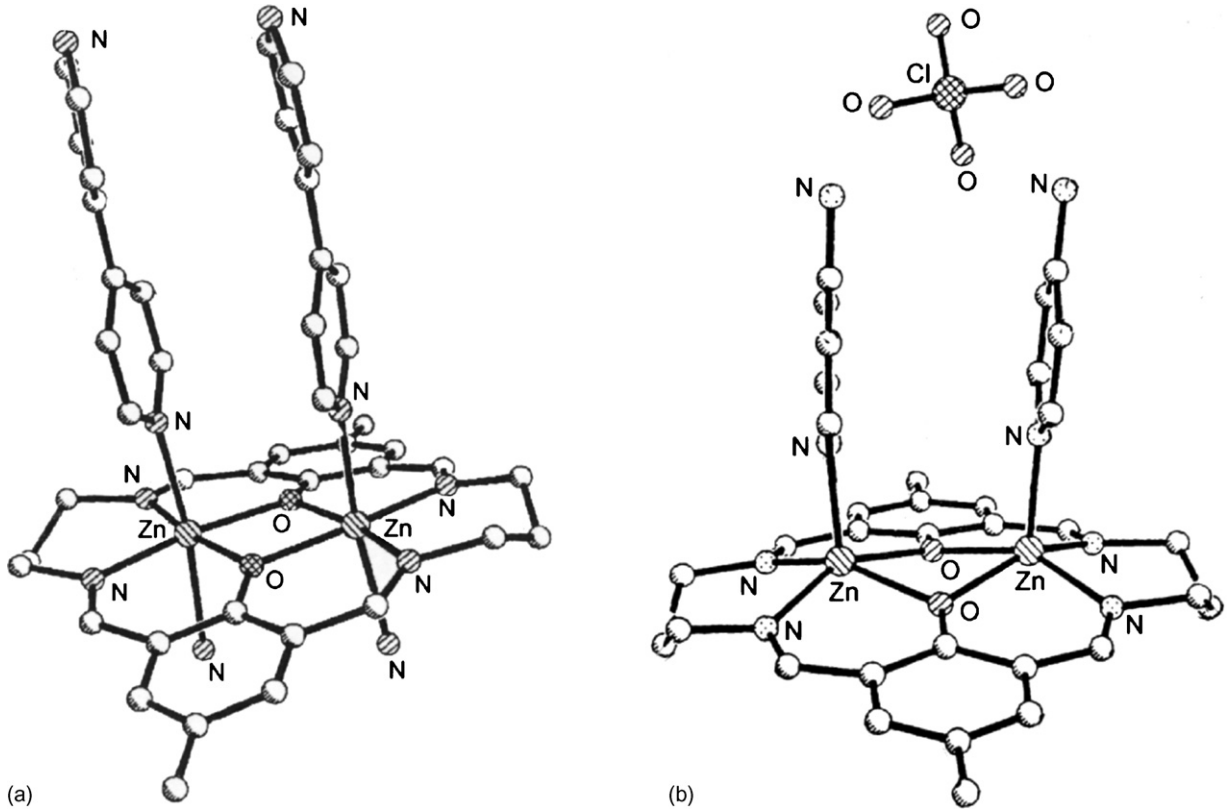

Fig. 47. Structure of $[Zn_2(\mathbf{63})(4,4\text{-dipy})_2]^{2+}$ (a) and $[Zn_2(\mathbf{63})(4\text{-ampy})](ClO_4)]^{+}$ (b).

regarded as genuine bonds, these interactions cause each macrocycle to deviate noticeably from planarity (Fig. 46b) [71]. In solution the formation of discrete solvated $[Cu_2(\mathbf{65})]^{2+}$ units was proposed, although aggregation in relatively non-polar solutions cannot be discounted [71].

The coordination environment around each zinc(II) ion in $[Zn_2(\mathbf{63})(4,4'\text{-bipy})_2](ClO_4)_2$ (bipy = bipyridine), prepared by refluxing $[Zn_2(\mathbf{63})(H_2O)_2](ClO_4)_2$ with 4,4′-bipyridine in a 1:2 molar ratio in CH_3CN/C_2H_5OH for 1 h and then partially evaporating the solution and cooling to room temperature, is a distorted octahedron with the two apical positions occupied by the bridging 4,4′-bipyridine ligand (Fig. 47a). The crystal structure exhibits an infinite 1D molecular ladder motif composed of 4,4′-bipyridine molecules with two zinc ions inside each dinuclear unit in very close proximity (<3.2 Å). $[Zn_2(\mathbf{63})(4,4'\text{-bipy})_2](ClO_4)_2$ has rectangular hydrophobic cavities where the 4,4′-bipyridine ligands connect the zinc(II) ions to serve as the side rails (long sides) and where the phenoxy oxygen atoms on the ring link the zinc(II) ions to act as the rungs (short sides) [72]. $[Zn_2(\mathbf{63a})(4,4'\text{-bipy})_2](ClO_4)_2$, where H_2-**63a** is the [2 + 2] macrocycle derived from the condensation of 2,6-diformyl-4-chlorophenol and 1,3-diaminepropane, possesses almost the same molecular ladder motif as $[Zn_2(\mathbf{63})(4,4'\text{-bipy})_2](ClO_4)_2$ [72].

Similarly, 4-aminopyridine (4-ampy) reacts with $[Zn_2(\mathbf{63})(H_2O)_2](ClO_4)_2$ to form $[Zn_2(\mathbf{63})(4\text{-ampy})_2](ClO_4)_2$, where the two 4-aminopyridine molecules are linked but amino groups are uncoordinate. Each zinc(II) ion on the macrocyclic framework has been bound to one 4-aminopydine molecule, preferably resulting in a pyramidal rather than an octahedral coordination environment around the metal ion. The axial position is occupied by the pyridine nitrogen atom due to its stronger coordination ability than that of the amino group and water molecule. The amino group is naked uncoordinatedly, and no ladder motifs have been yielded. Two pyridine rings are set at the same direction of the macrocycle which is slightly bent. Two pyridine planes are assembled in a nearly parallel way via π–π interactions, forming a concavity structure. A perchlorate group acts as a bridge to link two amino species in the way of N–H···O bonding, generating a large hydrogen bond cycle (Fig. 47b) [72].

When pyridine-4 carboxylate sodium salt (4-$NaOOCC_5H_4N$) was reacted with $[Zn_2(\mathbf{63})(4,4'\text{-bipy})_2](ClO_4)_2$, the tetranuclear array $[Zn_4(\mathbf{63})_2(4\text{-}OOCC_5H_4N)_2]$ was obtained [73]. The X-ray structure of this complex shows that two zinc(II) ions in a macrocyclic framework have a five-coordinating configuration analogous to that of $[Zn_2(\mathbf{63})(4\text{-ampy})_2]^{2+}$ except that one apical position is taken up by one nitrogen atom and the other by one oxygen atom of the 4-carboxylate pyridine ligand. Each 4-carboxylate pyridine group acts as a bridge to link two macrocyclic units by coordination bonding to form a wheel-like molecule, with two substituted pyridine groups placed at a reverse position. An approximate parallelogram consisting of a tetranucelar zinc(II) unit has been formed: two pyridine rings are parallel to each other via π–π interactions. The Zn···Zn distance in the two macrocyclic subunits is 3.182 Å. The resulting cavity is so small that no guest species or molecules can be accommodated (Fig. 48) [72].

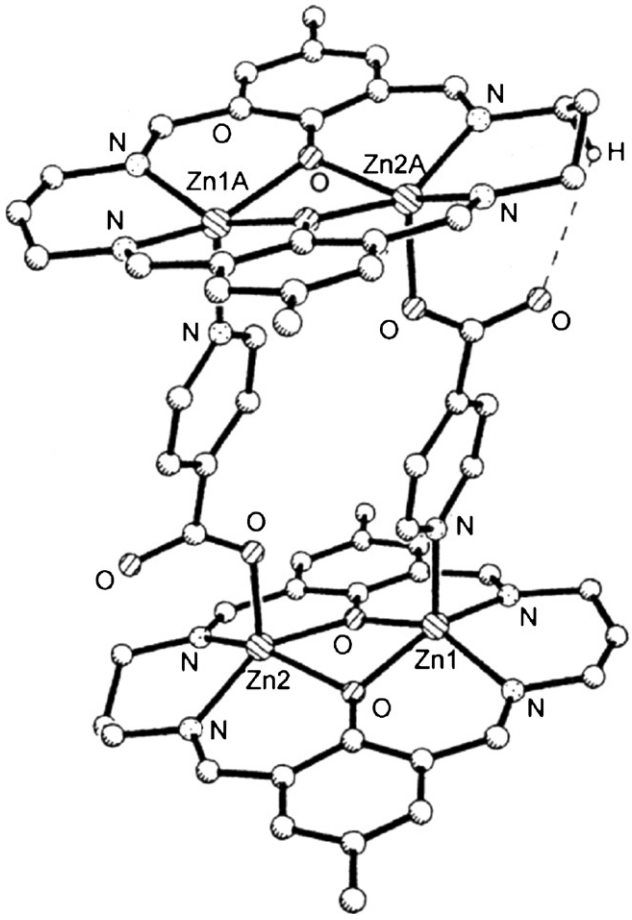

Fig. 48. Structure of $[Zn_4(\mathbf{63})(4\text{-}OOCC_5H_4N)_2]$.

The dinuclear complex $[Cu_2(\mathbf{63})(Cl)_2]$ reacts in methanol with acetylenedicarboxylic acid and triethylamine in a 1:1:1 molar ratio to lead a linear coordination polymer, the binuclear nodes being connected through the dicarboxylate linkers [73]. The copper(II) ions are quadruply bridged, two preexisting phenoxo oxygen atoms arising from the macrocyclic ligand, and two carboxylato groups, exhibiting the classical *syn–syn* bridging mode. Each copper(II) ion is hexacoordinate, with an elongated octahedral geometry. The apical positions are occupied by the carboxylato oxygen atoms. The distance between the quadruply bridged copper(II) ions is 3.052 Å, while the distance between the copper(II) ions belonging to two neighboring platforms is 10.21 Å (Fig. 49) [73].

The heterotrinuclear complex $[\{CuMn(\mathbf{90})(H_2O)\}\{Cr(phen)(C_2O_4)_2\}](ClO_4)\cdot H_2O$ was prepared by self-assembly of $[CuMn(\mathbf{90})](ClO_4)_2\cdot H_2O\cdot CH_3OH$ with $K[Cr(C_2O_4)_2(phen)]$ in water [73]. A key intermediate in the synthesis of this complex is $[CuPb(\mathbf{90})](ClO_4)_2\cdot H_2O$, which is obtained in a stepwise manner, starting from 2,6-diformyl-*p*-cresol [73]. Its transmetalation reactions with transition metal sulphates, led to a series of $Cu^{II}M^{II}$ binuclear complexes (M = Mn, Fe, Co, Ni, Zn) [73].

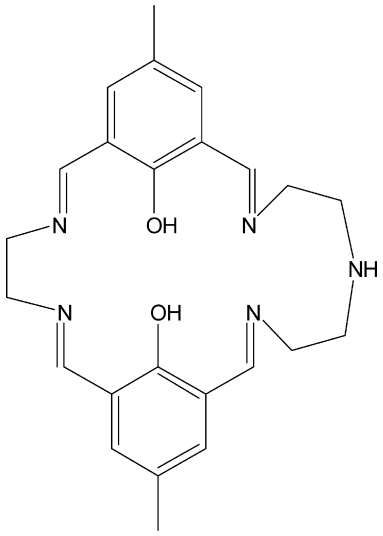

H_2-**90**

During the synthesis of the CuMn precursor, single crystals of the CuPb derivative [CuPb(**90**)]$(ClO_4)_2$ were obtained [73]. The structure consists of discrete binuclear units, perchlorate anions and crystallization water molecules (Fig. 50a). The copper(II) ion resides within the smallest compartment, N_2O_2, of the binucleating ligand, while the lead(II) ion is bound at the five coordination site. The two metal ions are bridged by the phenolic oxygen atoms, with an intermetallic distance of 3.506 Å. The copper(II) ion exhibits a square pyramidal geometry, with two nitrogen and two phenoxo oxygen atoms from the organic ligand forming the basal plane. One perchlorate ion is coordinated to the apical position. This perchlorate ion is simultaneously weakly coordinated to the lead ion from the same binuclear unit. The bulky lead(II) ion is hosted into the larger compartmental of the macrocyclic ligand. Pairs of [CuPb(**90**)$(ClO_4)]^+$ ions are connected through two perchlorate ions which bridge the lead ions. The coordination number of the lead ion is then eight. The resulting supramolecular pairs further interact through π–π stacking interactions established between the phenyl rings of the organic ligands forming supramolecular chains. The corresponding acetate derivative displays a 1D polymeric structure, with CuPb heterodinuclear nodes connected through acetate double bridges [73].

The crystallographic investigation of the trinuclear complex reveals two crystallographically independent $[\{CuMn(\mathbf{90})(H_2O)\}\{Cr(phen)(C_2O_4)_2\}]^+$ entities and uncoordinated perchlorate anions (Fig. 50b). The copper(II) and manganese(II) ions are hosted into the compartments of the macrocyclic ligand. The copper(II) ion exhibits a square pyramidal geometry. The apical position is occupied by an oxalate oxygen atom, arising from the $[Cr(phen)(C_2O_4)_2]^-$ ion, which acts as a monodentate ligand through one oxalato group. The manganese(II) ion is hexacoordinated by two phenoxo oxygens atoms, two nitrogens arising from the imino groups, one secondary amine nitrogen, and one aqua ligand. It results in a strongly distorted octahedral geometry. The Mn···Cu distances within the two independent units are 3.166 and 3.184 Å, while the Cr···Cr distances across the oxalate bridge are 6.603 and 6.658 Å. The octahedral coordination about the manganese(III) ions resembles that found in similar $[Cr(C_2O_4)_2(phen)]^-$ moieties [73].

The cryomagnetic investigation of the CuMnCr trinuclear complex reveals an antiferromagnetic interaction between the copper(II) and the manganese(II) ions within the compartmental ligand ($J = -39\ cm^{-1}$) while the interaction between the copper(II) and the chromium(III) ions across the oxalato bridge is negligible [73].

By employing the heterobinuclear complex [CuZn(**90**)]$(ClO_4)_2$ as a starting material and bis(4-pyridyl)ethylene (bpete) as a linker, the heterotetranuclear complex $[Cu_2Zn_2(\mathbf{90})_2(bpete)_2](ClO_4)_4{\cdot}4.5CH_3OH$ was synthesized with the metal ions located in the corners of a rectangle [74]. The copper(II) and the zinc(II) ions are diagonally disposed. The copper(II) ions are pentacoordinated with a square pyramidal geometry, in which the apical position is occupied by the nitrogen atom arising from the bpete linker. The basal plane is formed by two nitrogen atoms arising from the Schiff base ligand, and two phenoxo oxygen atoms. The zinc ions are coordinated by two imino nitrogens and two phenoxo

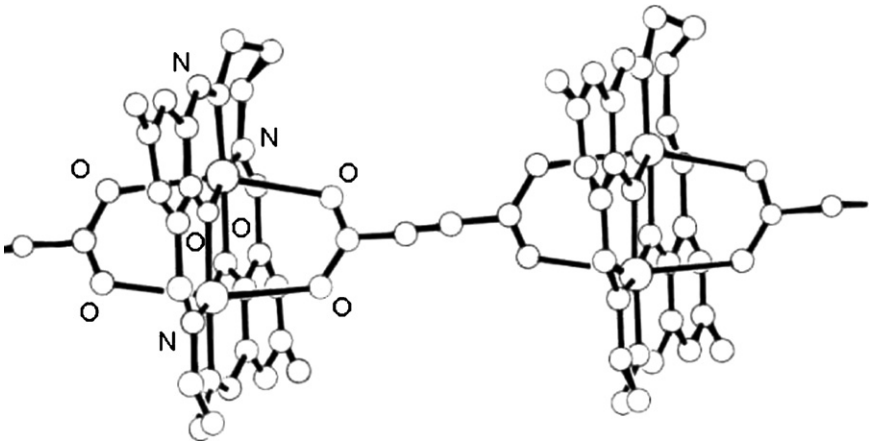

Fig. 49. Structure of $[Cu_2(\mathbf{63})(acetylenedicarboxylate)]_n$.

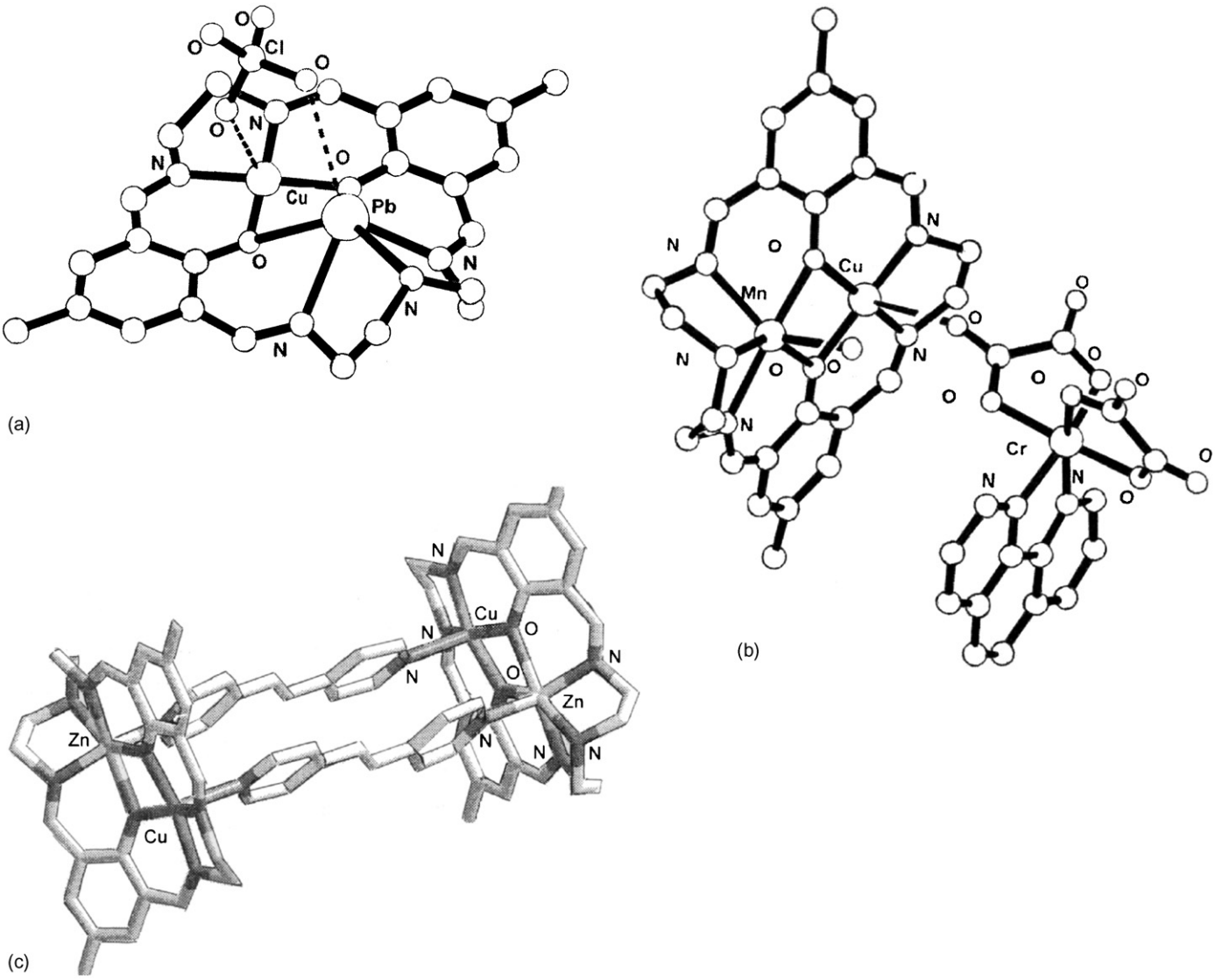

Fig. 50. Structure of $[CuPb(\mathbf{90})(ClO_4)]^+$ (a), $[\{CuMn(\mathbf{90})(H_2O)\}\{Cr(phen)(C_2O_4)_2\}]^+$ (b) and $[Cu_2Zn_2(\mathbf{90})(bpete)_2]^{4+}$ (c).

oxygens arising from the Schiff base and one nitrogen atom from the bpete bridge. The secondary amine nitrogen can be considered as being semi-coordinated. The Cu···Zn in distance each dinuclear unit is 3.198 Å while the distance between the diagonally disposed metal ions are: Cu···Cu = 13.84 Å and Zn···Zn = 14.28 Å (Fig. 50c) [73].

The diformyl precursor 2,2′-dihydroxy-5,5′-di-*tert*-butyl-3,3′-dialdehyde, derived by oxidation of the related dialcohol derivative with MnO_2, reacts with 1,3-diamino-2-hydroxypropane in the presence of the appropriate metal(II) salt to form $[M_2(H_4\text{-}\mathbf{91})(Cl)](Cl)\cdot n$S (M = Cu^{II}, Zn^{II}, Ni^{II}; S = CH_3OH; H_2O, n = 1–4), $[M_2(H_4\text{-}\mathbf{91})(H_2O)_n](ClO_4)_2\cdot mH_2O$ (M = Co^{II}, Ni^{II}; n = 1–3; m = 2, 3), $[M_2(H_4\text{-}\mathbf{91})(NO_3)(H_2O)_2](NO_3)\cdot nH_2O$ (M = Ni^{II}, Zn^{II}; n = 1–3) and $[Mn_2(H_2\text{-}\mathbf{91})(Cl)_2(C_2H_5OH)_2]\cdot 6H_2O$ [74]. The subsequent crystallization from ethanol or dimethylformamide affords the same complexes although with a different set of coordinated or solvate molecules. If an ethanol solution of $[Zn_2(H_4\text{-}\mathbf{91})(NO_3)(H_2O)_2](NO_3)\cdot 3H_2O$ is exposed to air for several days the nitrate anions appear to be slowly replaced by a carbonate anion, yielding a complex analysing as $[Zn_2(H_4\text{-}\mathbf{91})(CO_3)(H_2O)_4]$. In the isomorphous complexes $[M_2(H_4\text{-}\mathbf{91})(Cl)](Cl)$ (M = Cu^{II}, Zn^{II}) the metal ions are each coordinated to two imine groups, two phenol oxygen atoms and a bridging chloride ion. The geometry at the metal ions, respectively, 3.999 and 3.656 Å apart, is square pyramidal with a chloride ligand as the apical donor. The macrocycle adopts a saddle conformation (a hyperbolic paraboloid) with the basal planes about each metal ion severely inclined to each other. This shape is maintained by two strong hydrogen bonds linking adjacent phenol oxygen atoms. This structure is consistent with loss of one proton from each methylenediphenol unit, resulting in a phenol–phenolate interaction. The pendant alcohol groups are not involved in bonding to the metal ions but they form hydrogen bonds to the non-coordinated chloride ion forming one-dimensional chains through the lattice (Fig. 51a) [74].

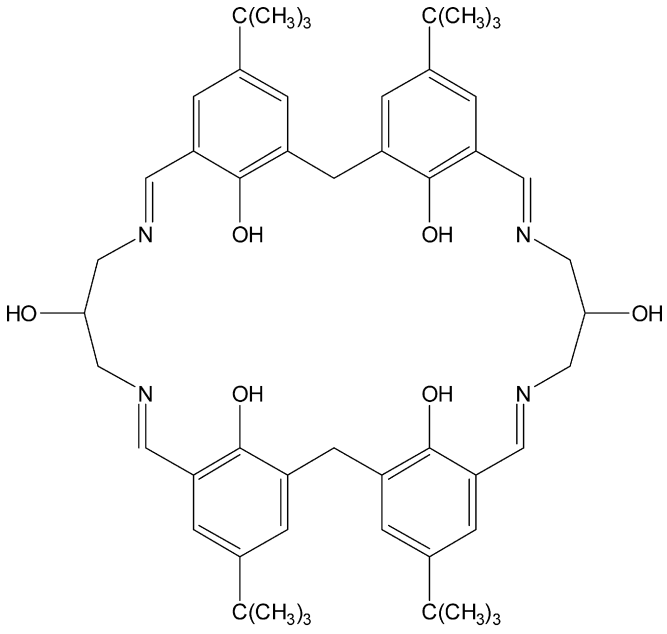

H_6-**91**

$[Ni_2(H_4$-**91**$)(Cl)](Cl)\cdot 4H_2O$ has been supposed to contain the same chloro bridged structure, probably with water as sixth ligand to each nickel ion [74].

The dicobalt(II) and dinickel(II) complexes $[M_2(H_4$-**91**$)(H_2O)(C_2H_5OH)_2](ClO_4)_2\cdot 4C_2H_5OH$ are also isomorphous. In the cations $[M_2(H_4$-**91**$)(H_2O)(C_2H_5OH)_2]^{2+}$ the chloro bridge has been replaced by water and the metal ions are six coordinate. The additional ethanol ligands lie within folds of the macrocycle and do not alter the overall shape of the macrocyclic cation, which is similar to that found in $[M_2(H_4$-**91**$)(Cl)](Cl)$. The macrocycle remains diprotonated and the phenols are linked by short hydrogen bonds. The guest water molecule is hydrogen bonded to two ethanol molecules. Hydrogen bonding involving the pendant alcohols, perchlorate anions, coordinated and lattice ethanol, links the cations into chains which run along the *b*-axis [74].

The nitrato-bridged dinickel(II) and dizinc(II) complexes $[Ni_2(H_4$-**91**$)(NO_3)(DMF)_2](NO_3)\cdot 2DMF\cdot H_2O$ and $[Zn_2(H_4$-**91**$)(NO_3)(C_2H_5OH)](NO_3)$ again show short hydrogen bonds across the monodeprotonated 2,2′-methylenediphenol units and overall saddle conformation. These structures are not isomorphous. In $[Ni_2(H_4$-**91**$)(NO_3)(DMF)_2]^+$ (Fig. 51b) the nitrate acts as a *syn*,*anti*-1,3-bridge. The nickel ions are six-coordinate (the sixth ligand being a DMF molecule in each case) and have quite regular geometry. The Ni···Ni distance is 4.604 Å. In the dizinc(II) cation $[Zn_2(H_4$-**91**$)(NO_3)(C_2H_5OH)]^+$ one of the metal ions is six coordinate (with ethanol as the sixth ligand) and the other is five coordinate. The bound nitrate ion is disordered 60:40 over two positions, the major one is bound in the same way as $[Ni_2(H_4$-**91**$)(NO_3)(DMF)_2](NO_3)$ but the minor component is monodentate, coordinated only to the five coordinate zinc ion. The cations are linked into chains by hydrogen bonding involving the pendant alcohols, the uncoordinated nitrate anion and the coordinated ethanol molecule [74].

In $[Mn_2(H_2$-**91**$)(Cl)_2(DMF)(DMSO)]\cdot 1.5DMF\cdot 0.3(C_2H_5)_2O$ (Fig. 51c) the six coordinate manganese(III) ions, each having chloride and a solvent molecule (DMF or DMSO) as the non-macrocyclic ligands, are well separated and there is no exogenous bridge linking them. The saddle-shape of the macrocycle has been lost and the phenolate groups in each methylenediphenolate are rotated with respect to one another so that one is tilted above the plane of the macrocycle and the other is tilted below. As a consequence of this, the metal ions also lie one on each side of the macrocyclic plane. Hydrogen bonding between one of the coordinated chloride ions and a pendant alcohol links the molecules into zigzag chains. The different in conformation of the dimanganese(III) complex with respect to that of the other complexes derived from H_6-**91** can be ascribed to the complete deprotonation of the 2,2′-methylenediphenol groups in the dimanganese(III) complex. This, in turn, is due to the higher oxidation state of the Mn(III) ion; it is a better Lewis acid than the other metal(II) ions. The structures of the $\{M_2(H_4$-**91**$)\}$ skeletons of the other complexes are almost superimposable; changing the non-macrocyclic ligands or even the coordination number of the metal ions has very little effect. This suggests that their conformation is controlled primarily by the two intramolecular phenol–phenolate hydrogen bonds and that the bridging ligand is simply occupying the preformed cleft resulting from the hydrogen-bonding [74].

Reaction of 1,3-diamino-2-ol and 5,5′-di-*tert*-butyl-3,3′-methanediyldibenzaldehyde with two equivalents of $Cu(NO_3)_2\cdot 6H_2O$ yields the green tetracopper product $[Cu_4(H_2$-**91**$)(OH)_2(H_2O)(C_2H_5OH)](NO_3)_2$ on short reflux. The tetranuclear complex converts into the brown tricopper species $[Cu_3(H_2$-**91**$)(NO_3)](NO_3)\cdot 3DMF$ on recrystallization from *N*,*N*-dimethylformamide [74].

The structure of each complex has been investigated by X-ray crystallography. The tricopper(II) complex $[Cu_3(H_2$-**91**$)(NO_3)](NO_3)\cdot 3DMF$ is dark brown, presumably because of charge transfer between the fully deprotonated phenolate groups and the copper(II) ions. Two copper(II) ions occupy the two N_2O_2 sites while the third copper(II) ion the central O_2O_2 site, with each metal ion bound to four macrocyclic donors in its basal plane. The planes of the two external copper(II) ions are inclined to that at the internal copper(II) ion. A coordinated nitrate counterion lies within the concave curve of the three copper(III) sites. The nitrate is disordered between two related positions; one site involves a single atom bridge between Cu1 and Cu2 and a three atom bridge between Cu2 and Cu3, while the minor site provides a single atom bridge between Cu3 and Cu2 with a three atom bridge linking Cu2 and Cu1. The conformation of the macrocycle is very similar to that in $[Cu_2(H_4$-**91**$)(Cl)](Cl)\cdot 1.6(C_2H_5)_2O\cdot C_2H_5OH$ (Fig. 52a) [74].

In $[Cu_4(H_2$-**91**$)(OH)_2(H_2O)(C_2H_5OH)](NO_3)_2$ the copper(II) ions occupy four equivalent sites. As observed in $[Cu_2(H_4$-**91**$)(Cl)](Cl)\cdot 1.6(C_2H_5)_2O\cdot C_2H_5OH$ each adjacent pair of phenols is monodeprotonated and linked by a hydrogen bond. The overall conformation of the tetranuclear complex is, however, very different from that of $[Cu_2(H_4$-**91**$)(Cl)](Cl)\cdot 1.6(C_2H_5)_2O\cdot C_2H_5$ and $[Cu_3(H_2$-**91**$)(NO_3)](NO_3)\cdot 3DMF$. The saturated portions of the ring are

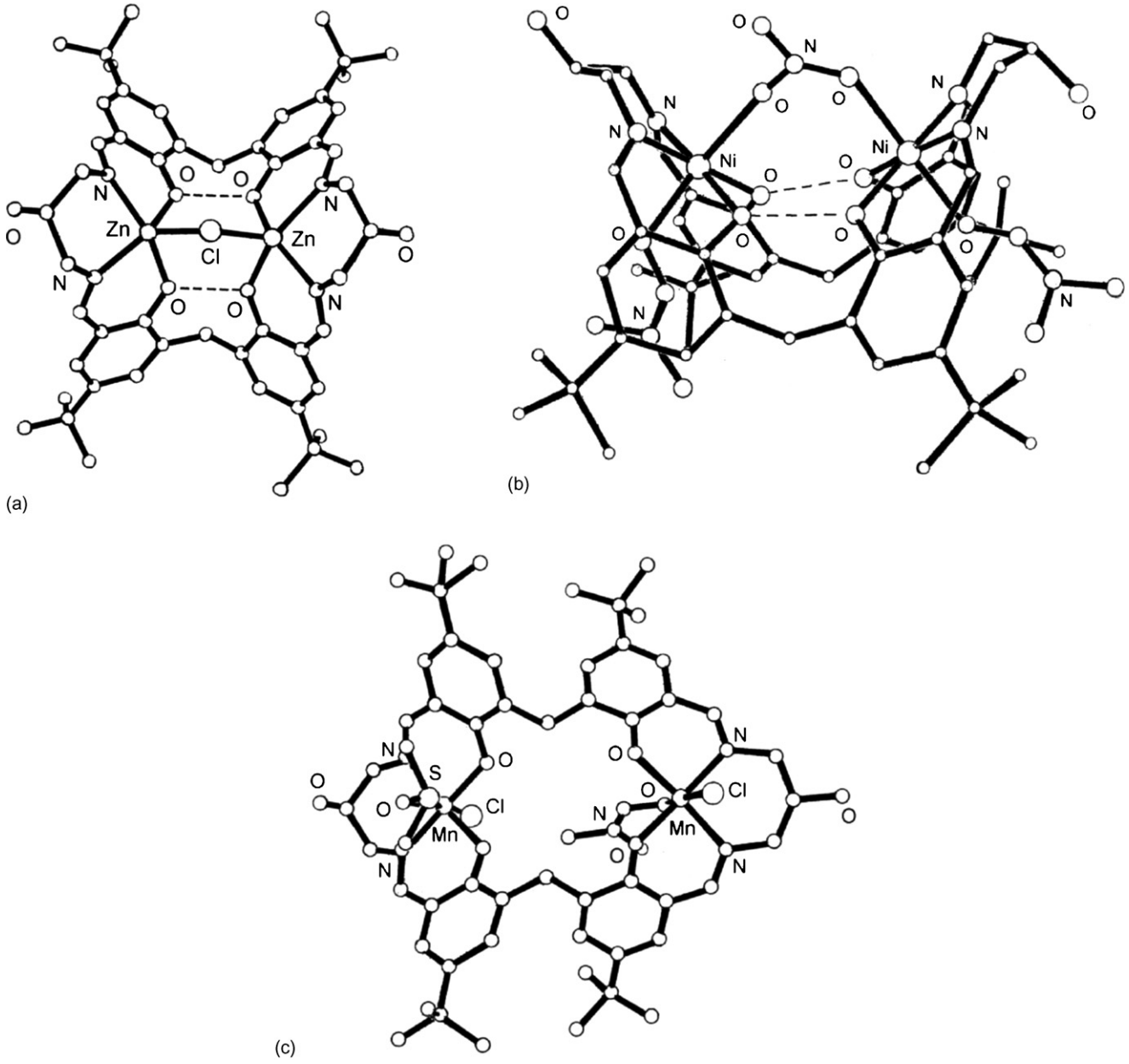

Fig. 51. Structure of $[Zn_2(H_4\text{-}\mathbf{91})(\mu\text{-}Cl)]^+$ (a), $[Ni_2(H_4\text{-}\mathbf{91})(NO_3)(DMF)_2]^+$ (b) and $[Mn_2(H_2\text{-}\mathbf{91})(Cl)_2(DMF)(DMSO)]$ (c).

fully extended to allow each alkoxo group to bridge two copper(II) ions and the macrocycle is sharply folded down its long axis, with each half approximately planar. Each copper(II) ion has a square pyramidal geometry; the base comprises macrocyclic phenoxo, alkoxo, and imine donors as well as an exogenous μ_2-hydroxo group (Fig. 52b) [74].

The most striking feature of this series of complexes is the variation in nuclearity within the same ligand system. This effect is linked to the variation in the extent of deprotonation of the ligand, the orientation of the phenol groups, and the overall shape of the macrocyclic host. The currently available investigations suggest that the dicopper complex is only isolated in the presence of a good coordinating anion which is also large enough to fit the cavity defined by the hydrogen-bonding interactions of the ligand. When NO_3^-, ClO_4^-; or BF_4^- were used, the initial product of the template reaction was the tetracopper complex, irrespective of the stoichiometry of the template reaction [74].

The ligands H_4-**91a–d** (a = R=C_6H_4, b = C_6H_{10}, c = $(CH_2)_2$, d = $(CH_2)_3$) have been prepared by reaction in $CHCl_3/CH_3OH$ of 3,3′-methylenebis(salicylaldehyde) with the appropriate diamine in the presence of boric acid as template agent and in a 2:2:1 molar ratio. The resulting precipitate does not need further purification. Neither the metal-templated method, such as nickel(II) and lanthanum(III) ions, nor the high dilution method formed the pure desired product, while the macrocycles obtained from these methods included [2 + 2] condensation products as deduced from mass spectroscopic analysis and ^1H NMR spectra in $CDCl_3$. Furthermore, these last measurements

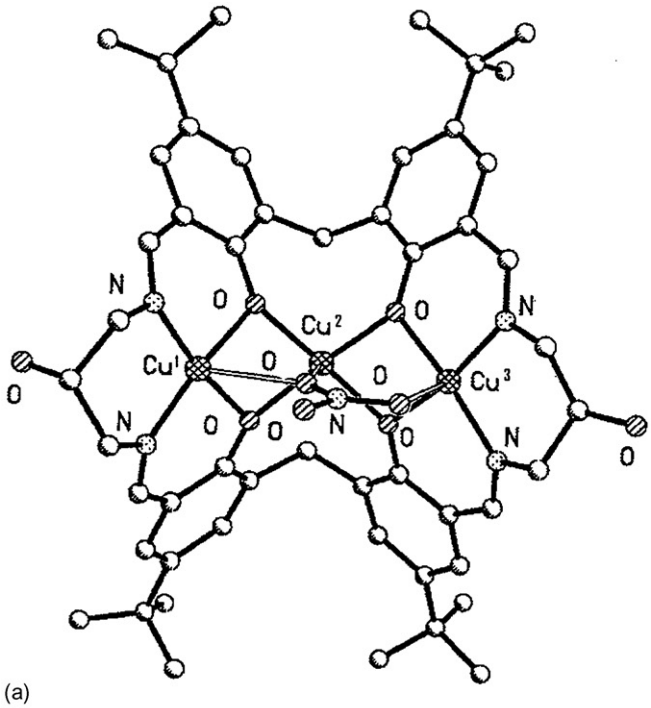

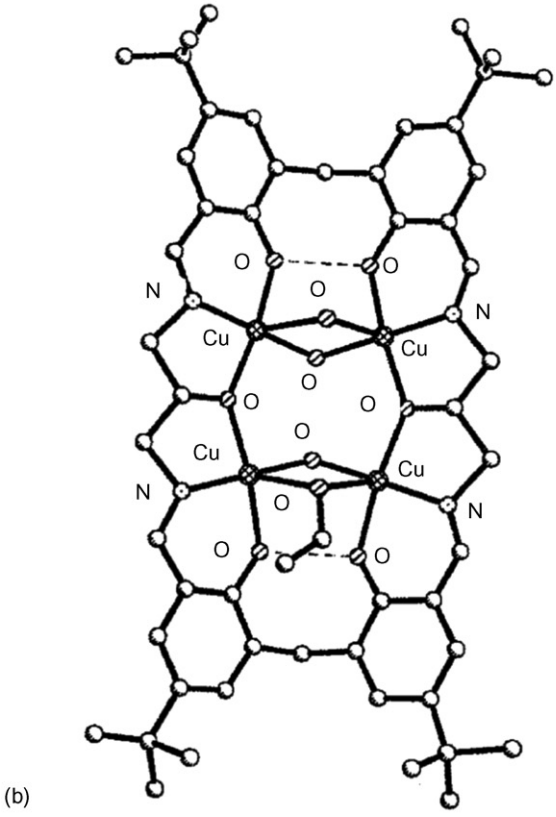

Fig. 52. Structure of $[Cu_3(H_2\text{-}\mathbf{91})(NO_3)]^+$ (a) and $[Cu_4(H_2\text{-}\mathbf{91})(OH)_2(H_2O)(C_2H_5OH)]^{2+}$ (b).

show the macrocycles are highly stable in solution, where remain unchanged over 1 month. When *p*-toluenesulphonic acid in place of boric acid was used, the formation of these ligands did not proceed effectively [74].

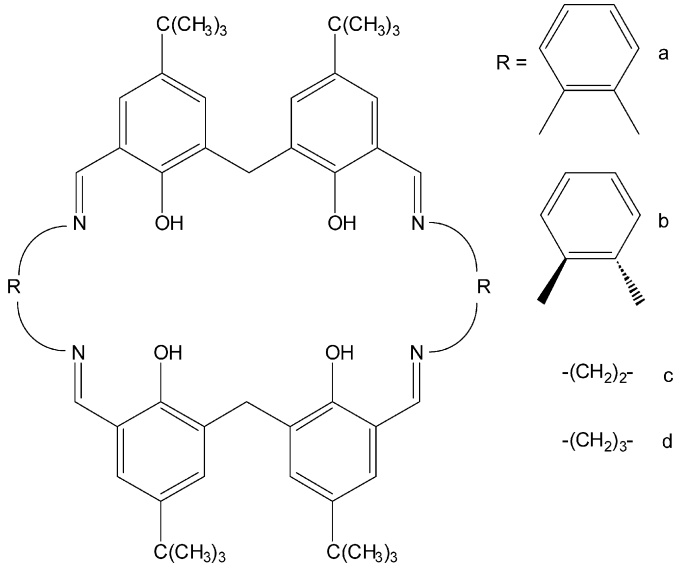

H_4-**91a-d**

The [2 + 2] cyclic nature of these ligands was ascertained by a single crystal X-ray analysis of H_4-**91a** (Fig. 53a). The macrocycle contains two adjacent N_2O_2 metal binding sites; thus, it coordinates the cobalt(II), nickel(II), copper(II) ions forming the related homodinuclear complexes $[M_2^{II}(\mathbf{91a})]$, when reacted with the appropriate metal(II) acetate hydrate in $CHCl_3/CH_3OH$ in a 1:2 molar ratio. The dicobalt(II) complex was obtained under nitrogen atmosphere [74]. The dinuclear nature of these complexes was inferred by FAB mass spectrometry. The complexes have similar electronic spectra and a comparable electrochemical behaviour. Cyclic voltammograms of the dicobalt(II) complex in dimethylformamide show the reaction $Co^{II}Co^{II} \leftrightharpoons Co^{I}Co^{I}$ and $Co^{III}Co^{III} \leftrightharpoons Co^{II}Co^{II}$ occur respectively are −1.10 and +0.10 V versus Ag/AgCl, respectively [74]. The redox behaviour suggests that the dicobalt complex $[Co_2(\mathbf{91a})]$ has two discrete square planar structures [74].

The one pot synthesis of the diamagnetic low-spin d_6 state $[Co_2^{III}(\mathbf{91a})(H_2N\text{-}R\text{-}NH_2)_2](CF_3SO_3)_2$ was achieved by reacting in $CHCl_3/CH_3OH$ and in air H_4-**91a** and $Co(CH_3COO)_2{\cdot}4H_2O$, followed by the addition at room temperature of the appropriate diamine and $Na(CF_3SO_3)$ or $Na(ClO_4$ in a 1:3.6:2.7:1.1 molar ratio [74]. The [2 + 2] dinuclear nature of these complexes, indicated by ^1H NMR and ESI-mass analyses, was confirmed by single crystal X-ray structural determinations of $[Co_2(\mathbf{91a})\{H_2N(CH_2)_8NH_2\}_2](CF_3SO_3)_2$ and $[Co_2(\mathbf{91a})\{H_2NCH_2(CH_2OCH_2)_2CH_2NH_2\}_2](CF_3SO_3)_2$ [74]. The dinucleating ligand $[\mathbf{91a}]^{4-}$ holds two cobalt ions at each N_2O_2 coordinating site and two diamine molecules were intramolecularly coordinated at each cobalt ion and occupy the four axial positions of the distorted octahedral complex. The Co···Co intramolecular nonbonded distance is 7.53 and 7.44 Å, respectively. It is noteworthy that each salicylaldiminato residue is bent to a symmetric umbrella but away from each other to reduce the steric

strain of the two octahedral coordination centers (Fig. 53b) [74].

The cyclic voltammogram of $[Co_2^{III}(\mathbf{91a})\{NH_2CH_2(CH_2\text{-}CH_2)_4CH_2NH_2)_2\}_2]^{2+}$ in the potential range between 0.60 and −1.60 V versus Ag/AgCl in a dimethylformamide solution reveals no oxidative wave, while a first reductive wave occurs at −80 V, due to $[Co^{III}Co^{III}(\mathbf{91a})(diamine)_2] \rightarrow [Co^{II}Co^{III}(\mathbf{91a})]+2(diamine)$. The reduction of the dicobalt(III) complex results in the loss of its axial diamine ligands in weakly coordinating solvents. The second reduction potential, due to the $\{Co^{II}Co^{II}(\mathbf{91a})\} \leftrightharpoons \{Co^{I}Co^{I}(\mathbf{91a})\}$ process, shows a reversible behaviour at −1.10 V versus Ag/AgCl. Upon reveals of the scan direction, the thus-formed four-coordinate cobalt(II) complex is reoxidized to the dicobalt(III) one, i.e. $[Co^{II}Co^{II}(\mathbf{91a})] \rightarrow [Co^{III}Co^{III}(\mathbf{91a})]$ at 0.30 V versus Ag/AgCl, which has much higher potentials because of the absence of a donating axial diamine at both cobalt centers. Then, in a rapid consecutive reaction (coordination of diamine), the six-coordinate complex with a doubly bridged structure will be reformed. In this way, the irreversible $Co^{III}Co^{III} \rightarrow Co^{II}Co^{II}$ redox couple is accompanied by the dissociation of the axial diamine. These structural changes were followed by UV–vis spectroscopy.

The doubly bridged dicobalt complex $[Co_2^{III}(\mathbf{91a})\{NH_2CH_2(CH_2OCH_2)_4CH_2NH_2\}]^{2-}$ shows UV–vis absorption at 351, 370, 408, and 485 nm in dimethylformamide. During the electrolysis at −0.90 V versus Ag/AgCl, the spectrum was changed to a new spectrum with four isosbestic points at 343, 384, 463 and 560 nm. The final spectrum showed absorption maxima at 304, 347, and 415 nm, which were characteristic of those of the dicobalt(II) complex in dimethylformamide. After electrolysis at −0.90 V versus Ag/AgCl, the potential was subsequently changed to 0.50 V versus Ag/AgCl. The spectrum was changed to the starting one with the same isosbestic points. The recovered species was characterized by ESI-mass analysis as the original doubly bridged complex. These reversible changes were repeated over fine times without decomposition of the complex. These results strongly suggested that these doubly bridged dicobalt complex should act as a redox-switchable molecular container [74].

A peculiar [2 + 2] cofacial Schiff base complex is represented by the diamanganese(III) complex $[Mn_2(\mathbf{91e})(C_2H_5OH)_2(H_2O)_2](SbF_6)_2$, prepared via condensation of 5,5-(9,9-dimethylxanthene-4,5-diyl)bis(salicylaldehyde) with (1*R*,2*R*)-1,2-cyclohexanediamine in the presence of $Mn_2Cl_2{\cdot}4H_2O$ and NaOH in methanol followed by addition of $Ag(SbF_6)$ to the not isolated complex $[Mn_2(\mathbf{91e})(Cl)_2]$, whose existence was inferred by ESI-mass spectra [74]. The diformyl precursor was obtained by two-fold lithiation of 9,9-dimethylxanthene followed by the boronation and hydrolysis to afford 9,9-dimethylxanthene-4,5-diboronic acid which, by palladium-catalyzed cross coupling reaction with 2 equiv. of 5-bromosalicylaldehyde, gave the designed dialdehyde whose two salicylaldehyde moieties are almost parallel and anchored by 9,9-dimethylxanthene-4,5-diylunit to form a U-shaped molecule [74].

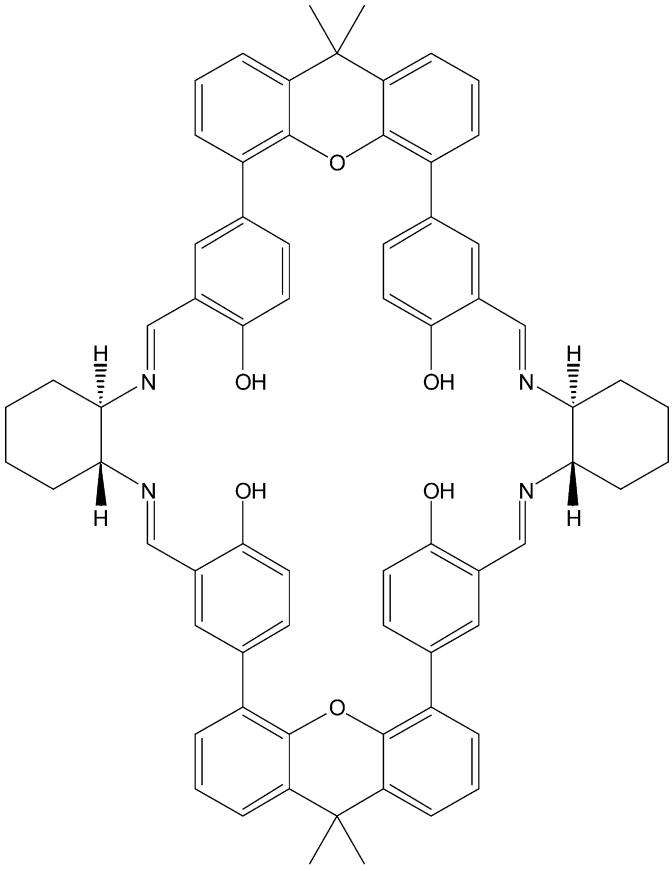

H_4-**91e**

In $[Mn_2(\mathbf{91e})(C_2H_5OH)_2(H_2O)_2](SbF_6)_2$ two manganese(III) Schiff-base units in the cationic dimanganese complex are connected by two 9,9-dimethylxanthene-4,5-diyl spacers to form a macrocyclic structure. Each manganese center is surrounded by a N_2O_2 donor set from the Schiff base ligand and two oxygen atoms of ethanol and water molecules at the axial positions. The cofacial two manganese(III) Schiff base units are aligned as an *anti* manner. The two manganese centers are separated by 5.093 Å [74].

An asymmetric oxidation of methyl phenyl sulphide by PhIO revealed that $[Mn_2(\mathbf{91e})(C_2H_5OH)_2(H_2O)_2](SbF_6)_2$ catalyzed the reaction to give methyl phenyl sulphoxide in a moderate chemical yield (65%), but the enantioselectivity was extremely low (6% ee). Interestingly, addition of 4-(dimethylamino)pyridine to the reaction system improved the enantioselectivity to 22% ee [74].

2.2.2. *Thiophenolate-based systems*

The previous work on this topic was comprehensively reviewed [4] and consequently not included here.

2,6-Diformyl-4-methylthiophenol was conveniently prepared purified and stored as the dimethylthiocarbamate derivative. This was hydrolyzed to the thiophenol derivative in situ by NaOH, and the resulting product was engaged in coordination/condensation reaction without separation [75].

Template reactions of cobalt(II) and cobalt(III) salts with 2,6-diformyl-4-methylthiophenol and 1,3-diaminopropane under a

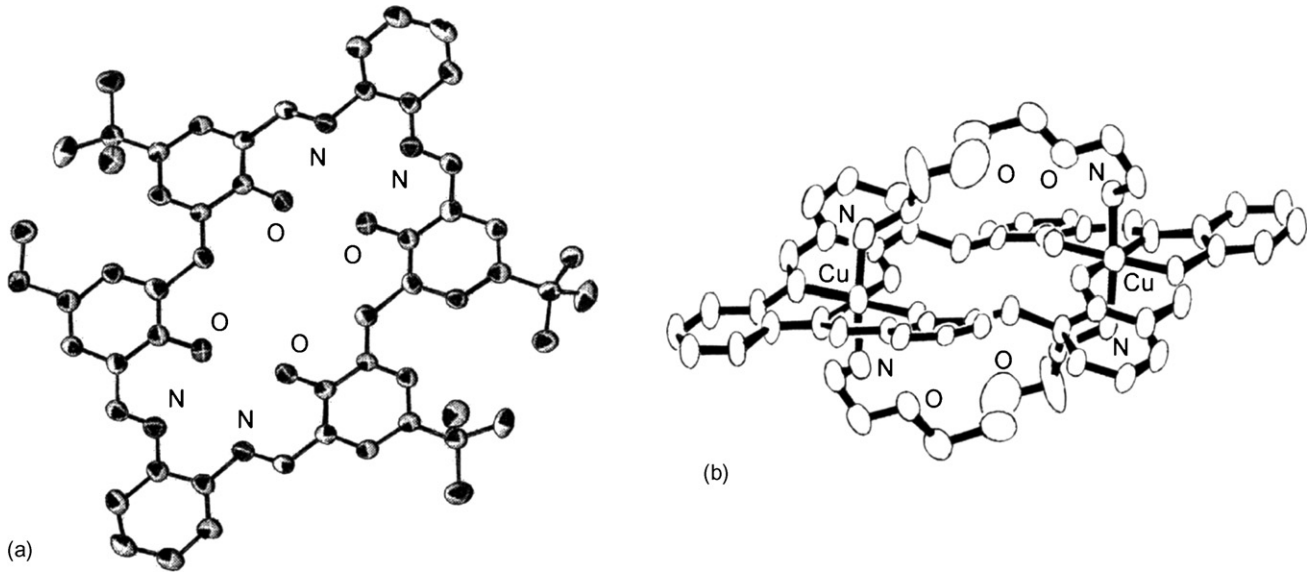

Fig. 53. Structure of H_4-**91a** (a), and $[Co_2(\mathbf{91a})\{H_2NCH_2(CH_2OCH_2)_2CH_2NH_2\}]^{2+}$ (b).

range of conditions generally do not afford the metal complexes in a pure tractable form. Higher yields of up to 60% can be obtained, however, by trasmetalation reactions of the analogous zinc(II) complex. Thus, reaction of $[Zn_2(\mathbf{92})(CH_3COO)](PF_6)$ with $Co(CH_3COO)_2{\cdot}4H_2O$ in CH_3CN in the presence of $[NH_4](PF_6)$ under aerobic conditions affords the red diamagnetic complex $[Co_2(\mathbf{92})(\mu\text{-}CH_3COO)(CH_3COO)(NH_3)](PF_6)_2$ whose solid state structure, entirely consistent with the structure proposed in solution on the basis of IR and NMR data, shows two octahedral cobalt(III) centers, each bound to the N_2S_2 donor set provided by the macrocyclic ligand and to a bridging acetate ion. The coordination sphere of one cobalt(III) center is completed by a monodentate acetate ion while the remaining site on the other center is occupied by NH_3 molecule. The macrocyclic ligand adopts a folded conformation, with the bridging acetate ion located within the cleft of the macrocycle (Fig. 54) [75].

Cyclic voltammetry of $[Co_2(\mathbf{92})(\mu\text{-}CH_3COO)(CH_3COO)(NH_3)](PF_6)_2$ displays two reversible one-electron reductions (confirmed by coulometry) in CH_3OH (0.3 M $[N(Bu)_4](PF_6)$, carbon electrode, 293 K) at $E_{1/2} = -0.76$ and 0.96 V versus Fc/Fc^+, assigned to the formation of $Co^{III}Co^{II}$ and $Co^{II}Co^{II}$ species, respectively [75].

$[Ni_2(\mathbf{92})](ClO_4)_2$, derived from the condensation of 2,6-diformyl-4-methylthiophenol, and 1,3-diaminopropane in the presence of $Ni(ClO_4)_2{\cdot}6H_2O$ shows a reversible oxidation at $E_{1/2} = +0.55$ V versus Fc/Fc^+ assigned as a predominantly metal-based oxidation process, i.e. resulting in a Ni^{II} Ni^{III} species. Coulometric studies confirm the oxidation to be a one-electron process and UV–vis spectroelectrochemistry at 273 K demonstrates a fully reversible $[Ni^{II}{}_2(\mathbf{92})]^{2+} \leftrightarrows [Ni^{II}Ni^{III}(\mathbf{92})]^{3+}$ couple. Furthermore, the cyclic voltammogram of chemically prepared $[Ni_2(\mathbf{92})]^{3+}$ is identical to that of the starting materials $[Ni_2(\mathbf{92})]^{2+}$ [75].

Multi-frequency EPR spectroscopy on Ni-labelled samples of $[Ni_2(\mathbf{92})]^{3+}$ confirms significant charge-delocalization between the nickel(III) center and thiolate donors in the $Ni^{II}Ni^{III}$ complex [75].

The Schiff base condensation of (*S*)-(2,6-diformyl-4-*tert*-butylphenyl)dimethylthiocarbamate and 1,3-diaminopropane, via metal-promoted concurrent sulphur deprotection in the presence of nickel(II), palladium(II) or zinc(II) salts, can be controlled to yield either [2 + 1] mononuclear acyclic, [2 + 2] or [4 + 4] dinuclear and [4 + 4] tetranuclear complexes by the choice of metal cation, counterion and solvent. In addition hexanuclear complex comprising three [2 + 2] units linked by μ_3-thiolate bridges between three of the six metal ions was isolated using zinc(II) perchlorate [75].

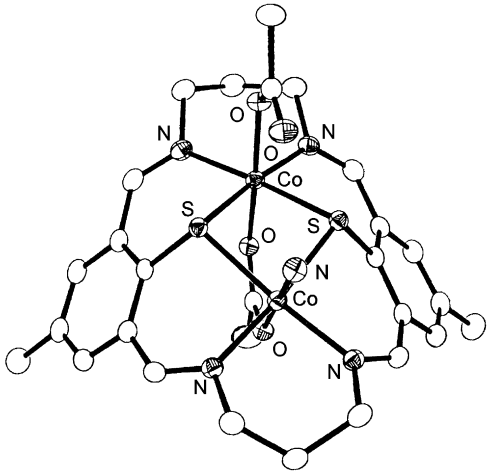

Fig. 54. Structure of $[Co_2(\mathbf{92})(\mu\text{-}CH_3COO)(CH_3COO)(NH_3)]^{2+}$.

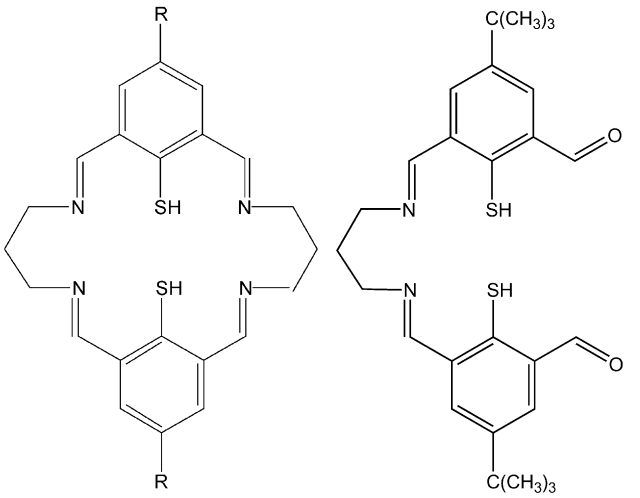

	R
H_2-**92**	CH_3
H_2-**92a**	$C(CH_3)_3$

H_2-**92b**

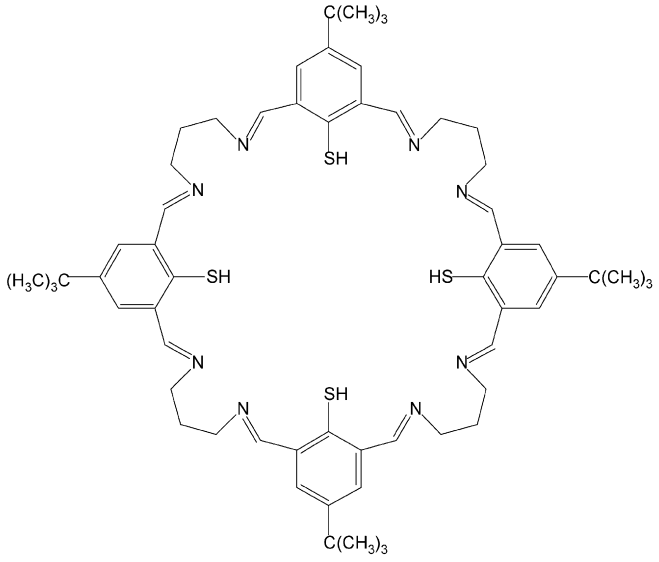

H_4-**92c**

When equimolar amounts of the protected thiophenol dialdehyde, 1,3-diaminopropane and nickel(II) perchlorate are reacted in methanol or acetonitrile the [2 + 2] dinuclear complexes [Ni_2(**92a**)](ClO_4)$_2$ was obtained, while the same reaction in dimethylformamide affords the acyclic [2 + 1] complex [Ni(**92b**)], which reacts with 1,3-diaminopropane in methanol to form the [4 + 4] dinuclear macrocyclic complex [Ni_2(**92c**)]. Furthermore, the [2 + 1] acyclic nickel(II) complex [Ni(**92b**)] evolves into the mononuclear diacetal form in methanol. The same diformyl and amine precursors, under comparable experimental conditions, using palladium(II) dichloride as template and a 2:3:1 molar ratio, forms the [2 + 1] acyclic complex [Pd(**92b**)] in acetonitrile; on the contrary, the dinuclear [4 + 4] complex [Pd_2(**92c**)] is obtained when a 1:2:1 stoichiometry was employed. FAB-mass spectra account of these results [75].

For the reactions incorporating the zinc(II) ion, the outcome is influenced by the identity of the counteranion. Thus, if zinc(II) nitrate is used as the starting salt, nitrate remains coordinated to the metal ion, leading to precipitation of the [4 + 4] tetranuclear complex [Zn_4(**92c**)(NO_3)$_4$]. In the presence of the less strongly coordinating perchlorate, the [2 + 2] macrocycle is formed, similar to the reactions observed with the nickel(II) ion in methanol or acetonitrile. When this reaction mixture is allowed to crystallize slowly under ambient conditions, carbon dioxide is fixed from the atmosphere to form the hexanuclear [Zn_6(**92a**)$_3CO_3$](ClO_4)$_4$. ESI-MS spectra furnish conditions mild enough to observe the carbonated hexanuclear species [75].

In each of the dinuclear nickel(II) complexes [Ni_2(**92a**)](ClO_4)$_2$·2CH_3CN, [Ni_2(**92a**)](ClO_4)$_2$·2CH_3OH and [Ni_2(**92a**)](ClO_4)$_2$·0.5DMF·0.5CH_3OH, the [Ni_2(**92a**)]$^{2+}$ cation displays a "V-shaped" (*syn*) conformation, in which the sulphur atoms of the thiophenolate groups lie to the same side of the plane defined by the four nitrogen atoms of the macrocycle. The nickel(II) ions are square planar [75].

In the [2 + 1] acyclic complex [Pd(**92b**)], whose structure is very similar to that of the nickel(II) analogue, the metal ion is square planar [75].

The structure of [Pd_2(**92c**)]·3DMF is also closely comparable to the analogous nickel(II) complex [Ni_2(**92c**)]·$x$$H_2O$. The two square planar palladium(II) ions occupy opposed N_2S_2 coordination site in the [4 + 4] macrocycle. The complex as a whole resembles an extended ring, folded *via* the =N–(CH_2)$_3$–N= linkages to form an approximate "V-shaped" conformation (Fig. 55a) [75].

[Zn_4(**92c**)(NO_3)$_4$]·5CH_3CN adopts a conformation dramatically different from those of the dinuclear nickel(II) and palladium(II) complexes. The macrocycle is folded to form a cylinder-like arrangement in which the zinc(II) cations are coordinated to two nitrogen atoms and one not bridging sulphur atom. The metal ions in each case adopt an essentially tetrahedral coordination geometry, with the nitrate group occupying the fourth coordination site. The nitrate anions form either monodentate or bidentate arrangements. Two crystallographically distinct complexes exist, displaying slightly different conformations. In one complex, two of the zinc(II) cations are brought relatively closer together (ca. 8.0–8.2 Å) across the macrocycle compared to the other pair (ca. 9.2–9.4 Å), so that one end of the cylinder is relatively more open than the other, and the overall arrangement approaches a bowl. Acetonitrile molecules lie within the bowl. In the second crystallographically distinct macrocycle, the cross-complex separation between zinc(II) cations is comparable (ca. 9.1 Å) at both ends, so that the macrocycle resembles more closely a regular cylinder. In this case, two acetonitrile molecules are threaded through the cylinder: thus, the bowl shape can become more cylindrical to accommodate the acetonitrile molecules. The folding of the macrocycle in [Zn_4(**92c**)(NO_3)$_4$], compared to the extended ring conformation in the dinuclear nickel(II) and palladium(II) complexes, can be viewed as a requirement for coordination of the two additional zinc(II) cations: a dinuclear complex comparable to that of nickel(II) and palladium(II) must fold if its previously uncoordinated nitrogen atoms are to wrap around the two additional zinc(II) cations. It is clear that such an arrangement cannot accommodate a

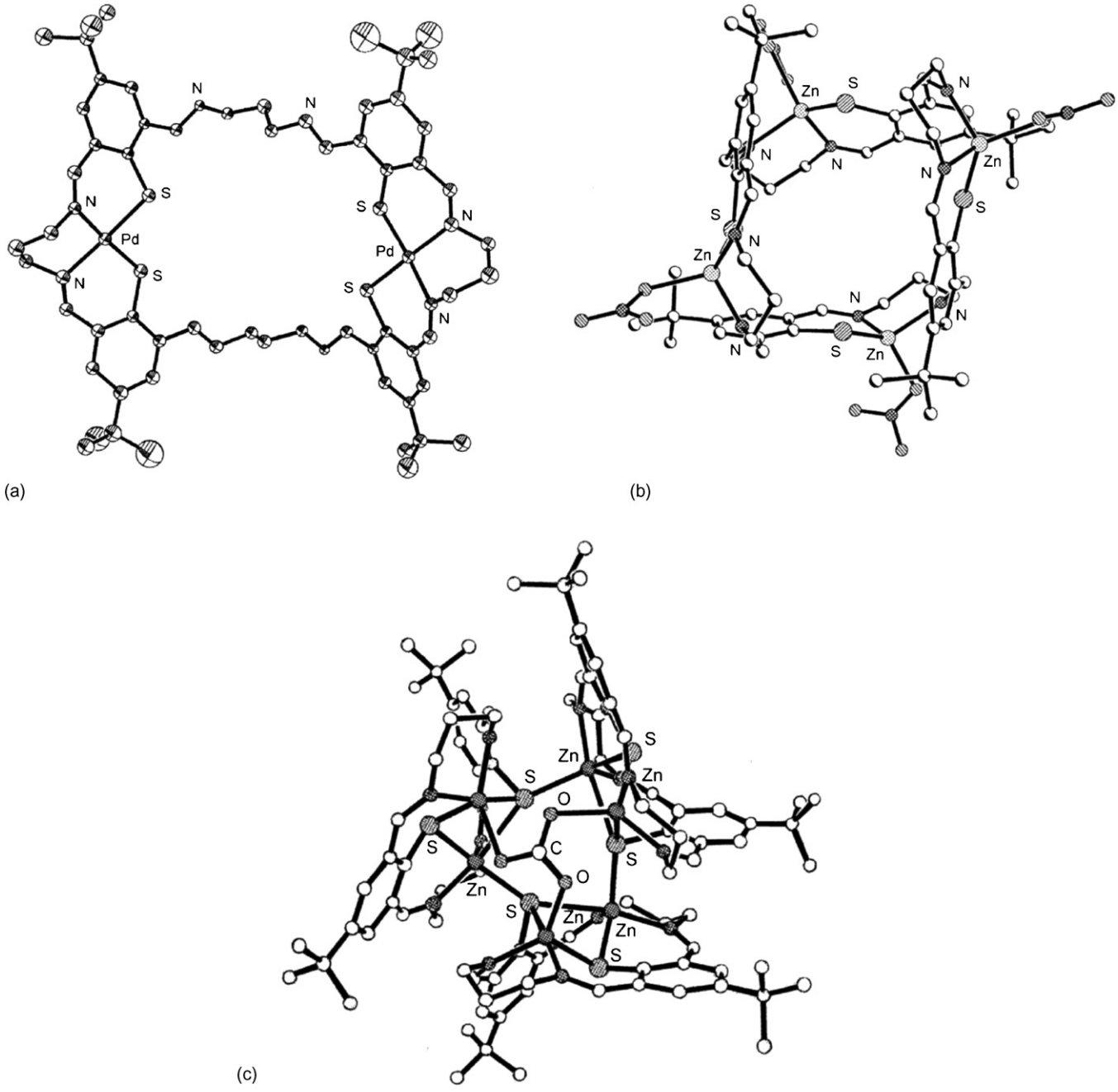

Fig. 55. Structure of $[Pd_2(\mathbf{92c})]$ (a), $[Zn_4(\mathbf{92c})(NO_3)_4]$ (b) and $[Zn_6(\mathbf{92a})_3(CO_3)]^{4+}$ (c).

metal cation in a square-planar geometry, which may offer some rationalization for the absence of tetranuclear nickel(II) and palladium(II) complexes of $[\mathbf{92c}]^{4-}$ (Fig. 55b) [75].

The hexanuclear complex $[Zn_6(\mathbf{92a})_3(CO_3)](ClO_4)_4{\cdot}4H_2O$ consists of three distinct $[Zn_2(\mathbf{92a})]^{2+}$ units, linked via further Zn–S bonds. The coordination geometry around three of the six zinc(II) cations resembles trigonal bipyramidal, with the two sulphur atoms and two nitrogen atoms of a given $[Zn_2(\mathbf{92a})]^{2+}$ unit occupying two equatorial and two axial positions, and the sulphur atom from an adjacent $[Zn_2(\mathbf{92a})]^{2+}$ unit occupying one equatorial position. The sulphur atoms of the thiophenolate rings, that bridge between these two zinc(II) centers, adopt μ_3-coordination in an approximate trigonal planar arrangement. The three zinc(II) cations and three sulphur atoms form a six membered Zn_3S_3 ring that is approximately planar and very close to three-fold symmetric. The remaining three zinc(II) cations lie in second plane, that is close to parallel to the plane of the Zn_3S_3 ring, with an approximate perpendicular separation of ca. 2.6 Å. The triangular arrangement of these zinc(II) cations is distorted, with one Zn···Zn distance (4.817 Å) significantly longer than the other two (4.450 and 4.539 Å). The coordination geometry around the zinc(II) ions is again approximately trigonal bipyramidal, with the two sulphur atoms and two nitrogen atoms of a given $[Zn_2(\mathbf{92a})]^{2+}$ unit occupying two equatorial

and two axial positions. The remaining equatorial coordination site is occupied by oxygen from a μ_3-carbonate anion that lies approximately within the upper Zn_3 plane. The geometry of the three individual $[Zn_2(\mathbf{92a})]^{2+}$ units in $[Zn_6(\mathbf{92a})_3(CO_3)]^{4+}$ differs from that observed in the isolated $[Ni_2(\mathbf{92a})]^{2+}$ units of $[Ni_2(\mathbf{92a})](ClO_4)_2$: the sulphur atoms of the thiophenolate groups lie on opposite sides of the plane defined by the four nitrogen atoms of the macrocycle, giving rise to an *anti* conformation (Fig. 55c) [75].

Transmetalation of [Zn(**93a**)] with $Co(CH_3COO)_2{\cdot}4H_2O$ in the presence of $[NH_4](PF_6)$ affords the cobalt(III) complex $[Co_2(\mathbf{93a})_2(\mu\text{-}CH_3COO)](PF_6)$ whose X-ray structure is in agreement with the spectroscopic data observed in solution, suggesting that the dinuclear structure is stable in solution even in coordinating solvents as CH_3CN. Although both metal ions exhibit the same coordination environment, the *cis* configuration adopted by the tetradentate ligand accounts for the various signals observed in the ^1H NMR spectrum. The overall structures of $[Co_2(\mathbf{92})(\mu\text{-}CH_3COO)(CH_3COO)(NH_3)](PF_6)_2$ and $[Co_2(\mathbf{93a})_2(\mu\text{-}CH_3COO)](PF_6)$ are similar [75].

Cyclic voltammetry of $[Co_2(\mathbf{93a})_2(\mu\text{-}CH_3COO)](PF_6)$ gives rise to only irreversible redox processes, reflecting the loss of redox stability on going from the macrocyclic chelate $[\mathbf{91}]^{2-}$ to the polychelate $[\mathbf{93}]^{2-}$, even though the resultant complexes have very similar coordination spheres [75].

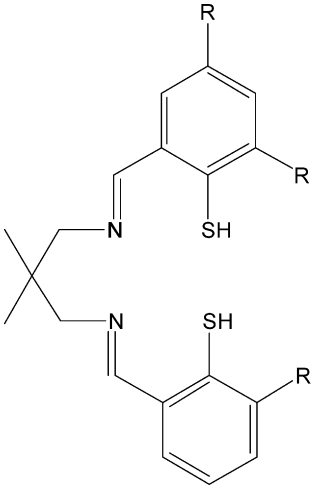

	R
H_2-**93a**	H
H_2-**93b**	$C(CH_3)_3$

Interestingly, reaction of [Zn(**93b**)] with $Co(CH_3COO)_2{\cdot}4H_2O$ in $CHCl_3$ affords the corresponding mononuclear complex [Co(**93b**)(CH_3COO)], which shows octahedral coordination at the cobalt(III) ion with an acetate anion binding as a *cis*-chelate. The ligand $[\mathbf{93b}]^{2-}$ binds to the metal center in a folded manner, the inherent steric hindrance of the ligand inhibiting the formation of dinuclear complex products. This observation is further confirmed by the formation of mononuclear complexes of $[\mathbf{93b}]^{2-}$ and related hindered ligands with square-planar nickel(II), copper(II) and palladium(II) ions and tetrahedral zinc(II) ions [75].

The [2 + 2] symmetric macrocyclic aminodiphenol or dithiophenol derivatives are readily obtained by reducing the related imino derivatives with $NaBH_4$ (Scheme 3) [42]. They have a higher stability as they do not suffer the hydrolitic processes encountered with the Schiff base analogues, a great flexibility, maintaining an appreciable capability to form complexes with transition metal ions. The availability of these polyamine systems allows a useful comparison between Schiff bases and their reduced analogues about the different recognition processes in consequence of the change from imine to amine groups inside the two adjacent coordinating sites. Generally, these macrocyclic polyamine derivatives have been stored as the white hydrate solid H_2-L·*n*HX (X = Cl, Br), derived from the reaction of the appropriate macrocycle with HCl or HBr [42].

When the direct condensation of the appropriate formyl and amine precursors followed by reduction of the resulting Schiff bases does not form the desired polyamine compound, the Schiff base formation in the presence of the appropriate template ions as Ba^{II}, Pb^{II}, or Cd^{II} followed by a reductive demetalation by $NaBH_4$ was successfully tested [5].

2.3. [2 + 2] Macrocyclic polyamine derivatives with endogenous phenolate or thiophenolate XH (X = O, S) bridging groups

2.3.1. Phenolate-based systems

The non-template synthetic approach has been used for the preparation of the macropolycyclic ligand H_2-**95** from the related Schiff base H_2-**94** [76]. The direct condensation of equimolecular amounts of 1,4-bis(2-aminoethyl)-1,4,7-triazacyclononane with 2,6-diformyl-4-methylphenol in methanol affords the cofacial [2 + 2] macropolycycle H_2-**94**, as demonstrated by ^1H and ^{13}C NMR spectroscopy and FAB-mass spectrometry. The macrocyclic polyamine precursor was synthesized by reaction of 1-(*p*-tolylsulphonyl)-1,4–7-triazacyclononane with 2 equiv. of N-(*p*-tolylsulphonyl)-aziridine, with subsequent detosylation of the resulting product with concentrated sulphuric acid. The reduction of H_2-**94** was achieved using a mixture of sodium cyanoborohydride and sodium borohydride in CH_3OH to give H_2-**95**·$4H_2O$ [76]. The X-ray structure determination of $[H_8\text{-}\mathbf{95}](ClO_4)_6{\cdot}8H_2O$, grown by slow evaporation of an aqueous solution of H_2-**95**·$4H_2O$ saturated with $NaClO_4$ and containing a drop of concentrated $HClO_4$, confirms the formation of the cation $[H_8\text{-}\mathbf{95}]^{6+}$, which has all six secondary nitrogen-donors protonated (Fig. 56). The crystal packing involves extensive hydrogen bonds between the perchlorate counteranions, the water molecules, the protonated secondary amines, and the phenolic OH groups. Only two water molecules sit within the macrocyclic cavity of $[H_8\text{-}\mathbf{95}]^{6+}$; all the other water molecules and the perchlorate anions lie outside the ring cavity [76].

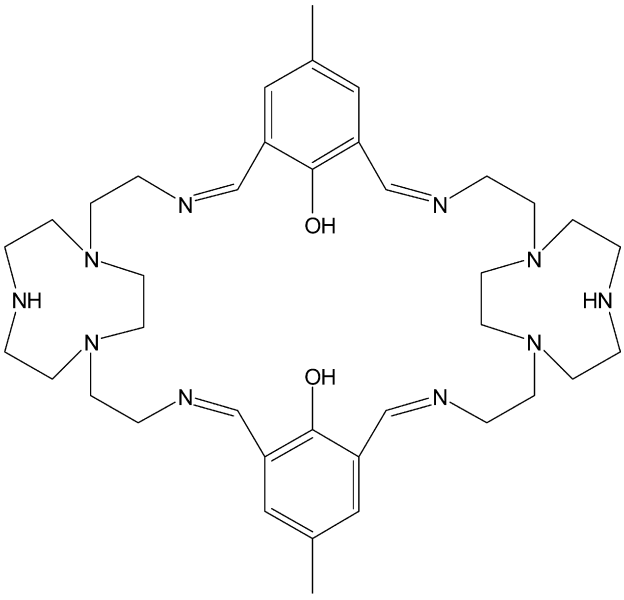

H_2-**94**

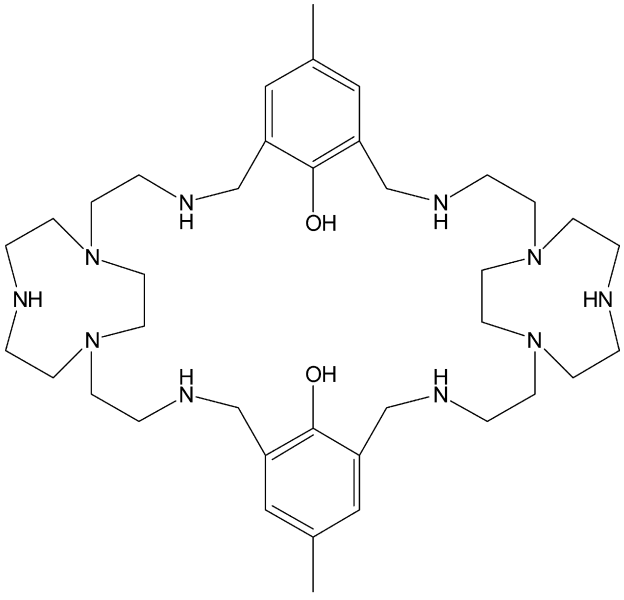

H_2-**95**

The protonation constants of H_2-**95** and the thermodynamic stabilities of the 1:1 and 2:1 (metal:ligand) complexes with copper(II), zinc(II) and lead(II) ions have been investigated by means of potentiometric measurements in aqueous solutions. The first two protonation equilibria involve the *p*-cresol functions, while the third and the fourth protonation steps take place on amine groups. In particular the third and fourth protonation steps occur on the two separated 1,4-bis-(2-aminoethyl)-1,4,7-triazacyclononae units. Similar considerations apply to subsequent protonation equilibria, leading to the conclusion that in the cationic species $[H_8$-**95**$]^{6+}$ the six positively charged ammonium groups are equally distributed between the two pentaamine compartments of the ligand. Thus, $[H_8$-**95**$]^{6+}$ contains six NH_2^+ functions separated by an unprotonated amine group. Such a disposition would reduce the electrostatic repulsion

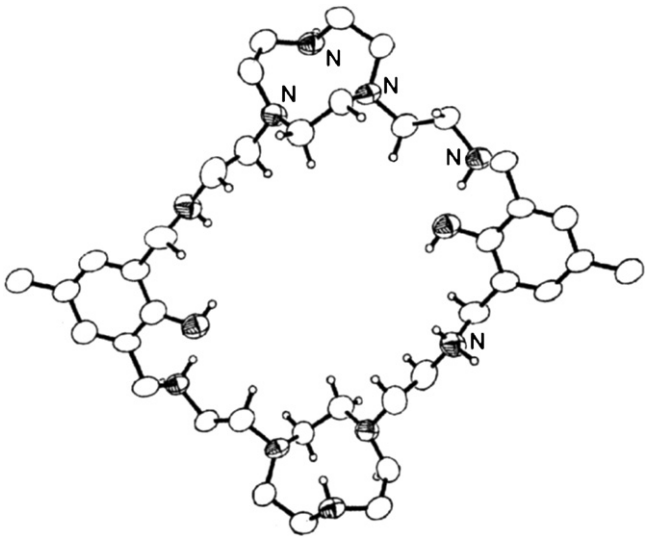

Fig. 56. Structure of $[H_8$-**95**$]^{6+}$.

between the charged ammonium functions. This suggestion is corroborated by the crystal structure of $[H_8$-**95**$](ClO_4)_6 \cdot 8H_2O$. The mononuclear [M(**95**)] complexes show remarkably high stability suggesting that, along with the large number of nitrogen donors available for metal binding, deprotonated phenolic functions are also involved in binding the metal ion. In these complexes the metal resides in one of the two 1,4-bis(2-aminoethyl)-1,4,7-triaazacyclononane moieties, while the other, which is not involved in binding to the metal ion, can be readily protonated. The mononuclear complexes show a marked tendency to encapsulate a second metal ion in aqueous solution; both mono- and dinuclear complexes are formed even with a 1:1 metal:ligand ratio [76]. The mononuclear species [M(**95**)] (M = Cu^{II}, Zn^{II}, Cd^{II}, Pb^{II}) forms several protonated complexes in aqueous solution. [Pb(**95**)] can bind up to four protons, while the remaining mononuclear complexes can also form pentaprotonated species. For all the systems investigated, binuclear species are largely prevalent from slightly acidic to alkaline pH values in aqueous solution containing the ligand and the metal ion in 1:2 molar ratio. Protonated mononucelar complexes are only present at acidic pH and then only in low concentrations. The formation of complexes $[M_2(H_2$-**95**$)]^{4+}$ occurs at neutral or slightly acidic pH and is generally followed by metal-assisted deprotonation of the phenolic groups to give $[M_2(H$-**95**$)]^{3+}$ and $[M_2($**95**$)]^{2+}$ in weakly basic solutions [76].

The binuclear complexes $[Cu_2($**95**$)](BF_4)_2 \cdot 1/2CH_3CN$, $[Zn_2(H$-**95**$)](ClO_4)_3 \cdot 1/2CH_3CN$, $[Cd_2($**95**$)](NO_3)_2 \cdot 2CH_3CN$, and $[Pb_2($**95**$)](ClO_4)_2 \cdot 2CH_3CN$ were obtained from the reaction of H_2-**95** with the appropriate metal salt in CH_3CN at room temperature [76]. Crystals suitable for X-ray diffraction analysis were obtained for the dicopper(II), dizinc(II) and dilead(II) complexes by slow diffusion of Et_2O vapor into CH_3CN solutions of the microcrystalline products. In $[Cu_2($**95**$)](BF_4)_2 \cdot 1/2CH_3CN$ each copper(II) ion bound to an N_4O donor set within a slightly distorted square pyramidal environment. For each metal ion, the basal positions of the pyramidal coordination sphere are occupied by the two tertiary nitrogen donors of the [9]-ane-N_3

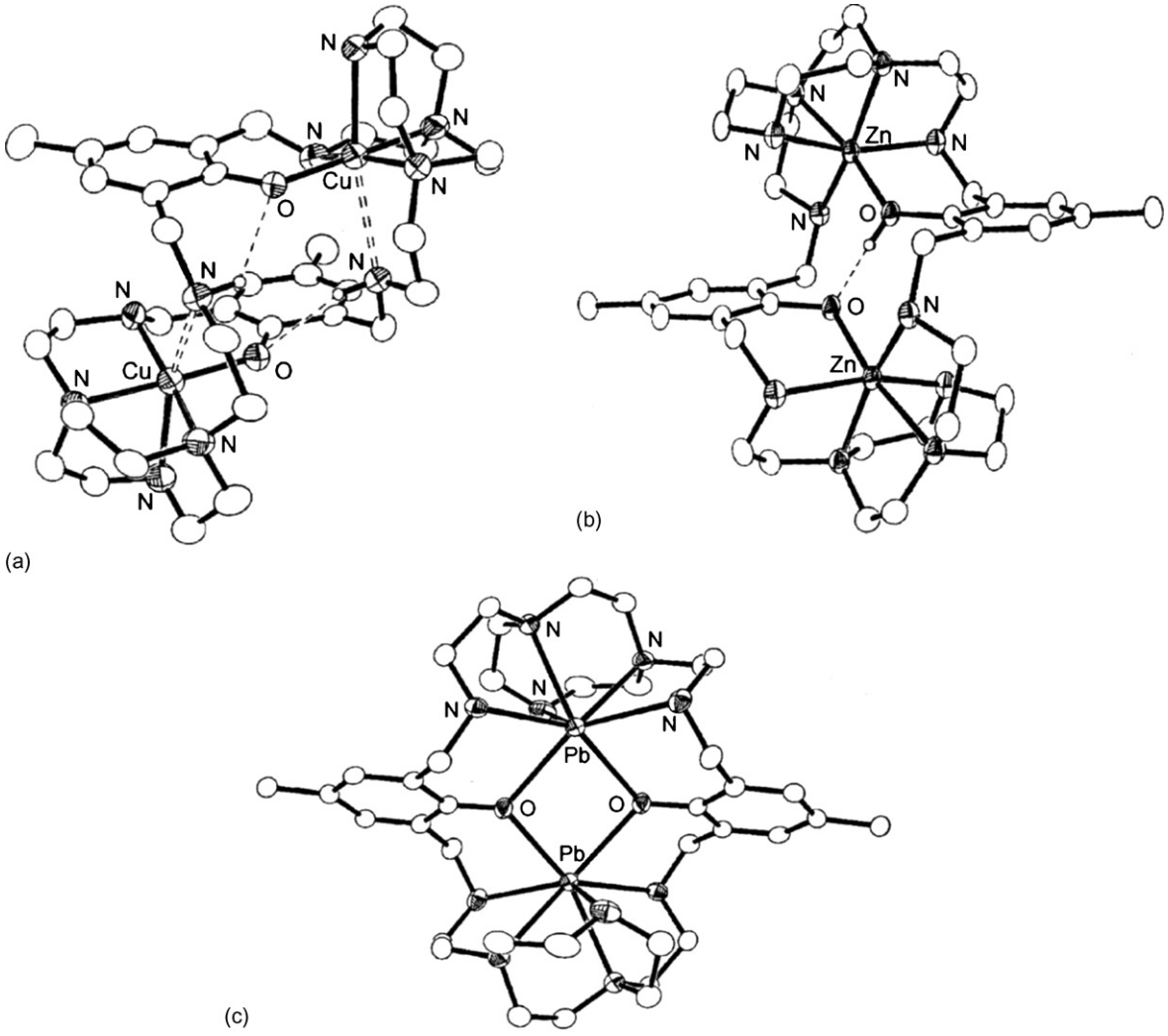

Fig. 57. Structure of $[Cu_2(\mathbf{95})]^{2+}$ (a), $[Zn_2(H\text{-}\mathbf{95})]^{3+}$ (b) and $[Pb_2(\mathbf{95})]^{2+}$ (c).

moiety, one secondary nitrogen donor from the aliphatic chain of the macropolycyclic ligand and one *p*-cresolate oxygen. The two metal centers are displaced out of the mean N_3O coordination planes in the direction of the apical secondary nitrogen donor. The overall N_5O coordination around each metal center is completed by a long interaction involving the remaining two secondary nitrogen donors of the anionic macropolycyclic ligand $[\mathbf{95}]^{2-}$. The two N_5O compartments of the macropolycycle act, therefore, as isolated donor sets with the *p*-cresolate oxygens not bridging metal ions. In fact, each oxygen donor is involved in a strong hydrogen bond with the secondary nitrogen donor from the adjacent N_5O compartmental that weakly interacts with the metal center. These intramolecular hydrogen bonds force the donor atoms of $[\mathbf{95}]^{2-}$ to assume a peculiar disposition with the *p*-cresolate oxygens twisted in opposite directions and each pointing toward an individual metal ion. As a result, the *p*-cresolate oxygen donors cannot bridge the copper(II) centers, which are, therefore, segregated within their own N_5O-donor compartments (Cu···Cu distance 5.954 Å). Interestingly, the mean planes of the two benzene rings of the macropolycycle are almost parallel, but quite distant from each other (Fig. 57a) [76]. This might reflect the greater flexibility of $[\mathbf{95}]^{2-}$ as compared with the related Schiff base polycycle $[\mathbf{94}]^{2-}$; indeed in the crystal structure of the binuclear complex $[Cd_2(\mathbf{94})](NO_3)_2{\cdot}2CH_3CN$, the two *p*-cresolate rings are involved in a moderately strong face to face π–π interaction characterized by a perpendicular distance of 3.342 Å between the mean planes of the aromatic rings [76].

In $[Zn_2(H\text{-}\mathbf{95})](ClO_4)_3{\cdot}(1/2)CH_3OH$ each six coordinate zinc(II) ion is bonded to an N_5O donor set within a slightly distorted octahedral environment. Only one of the two *p*-cresolate-OH groups of the macropolycycle is deprotonated and is involved in a strong intramolecular hydrogen-bond with the remaining –OH function. Thus, the two N_5O-donating compartments of $[H\text{-}\mathbf{95}]^{-}$, although acting as isolated donor sets, are connected by Zn–O···H–O–Zn bridge with a Zn···Zn distance of 5.572 Å (Fig. 57b) [76].

In $[Pb_2(\mathbf{95})](ClO_4)_2{\cdot}2CH_3OH$ the two lead(II) centers lie within the two N_5O donating compartments of $[\mathbf{95}]^{2-}$ and are bridged by the *p*-cresolate oxygen atoms with an interatomic Pb···Pb distance of 3.942 Å [76]. The structure of $[Pb_2(\mathbf{95})](ClO_4)_2{\cdot}2CH_3OH$ can be compared with that of the

binuclear complex $[Y_2(\mathbf{94})(OH)]^{3+}$ in which the two eight coordinate yttrium(III) ions are bridged not only by the two *p*-cresolate oxygen donors but also by a hydroxyl group, with the donor atoms evenly distributed about the coordination sphere [76]. In $[Pb_2(\mathbf{95})]^{2+}$ each lead(II) ion is coordinated to seven donor atoms, but some of these bonds are weaker than others: while one *p*-cresolate oxygen and the secondary nitrogen-donor from the [9]-ane-N_3 moiety are more strongly bound to the metal center, the other *p*-cresolate oxygen and the remaining nitrogen donors are at longer distances. The coordination sphere at each lead(II) center has been described as a distorted monocapped trigonal prism (Fig. 57c) [76].

On going from the dicopper(II) to the dizinc(II) and the dilead(II) complexes, the macropolycyclic ligand gradually adopts a more extended conformation. This can be qualified from the relative disposition of the two *p*-cresolate groups. In the dilead(II) complex these groups are almost coplanar and face each other, allowing the oxygen donors to be shared between the two metal centers. On going to the dicopper(II) and the dizinc(II) complexes, the two *p*-cresolate groups move to occupy parallel planes, approaching a situation in which they are stacked. This movement leads to a gradual segregation of the two metal centers, and is supported by the formation of intramolecular hydrogen bonds involving the phenolate oxygens and the amine donors. An important role is played by the stereoelectronic requirements of the metal centers, by their dimensions, and by the flexibility of the large ring ligand [76].

Also asymmetric macrocyclic polyamines have been designed and synthesized; for instance H_2-**96** and H_3-**97**, containing the 1,1′-bis(2-phenol) function, have been prepared using a template reaction (Scheme 10), which requires the preliminary formation of a cadmium Schiff base complex of the appropriate acyclic polyamine with two terminal primary amines (i.e. 1,8-diamino-3,6-azadiazaoctane or the polyamine derivative H_2-**98** was synthesized according to Scheme 8) and 3,3′-diformyl-1,1′-bis(2-phenol) as cycling reagents. The cyclic polyamine ligands are obtained after the reduction of the imine functions and demetalation of the cyclic Schiff base cadmium complexes with H_2-**96a** and H_2-**97a**. The same synthetic pathway, by substituting the diphenol-diformyl precursor with a different diformyl reagent, can be followed for the preparation of a wide range of macrocyclic polyamine derivatives [77].

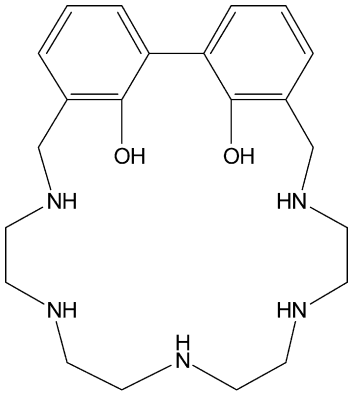

H_2-**96**

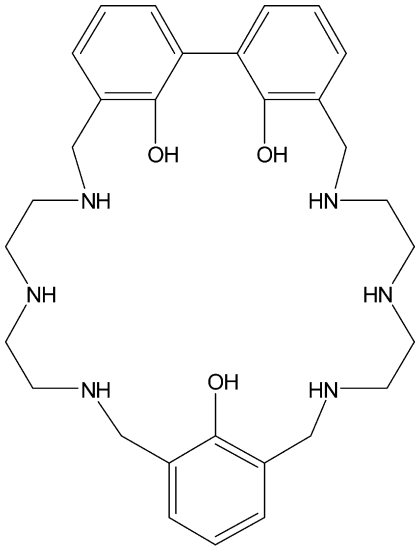

H_3-**97**

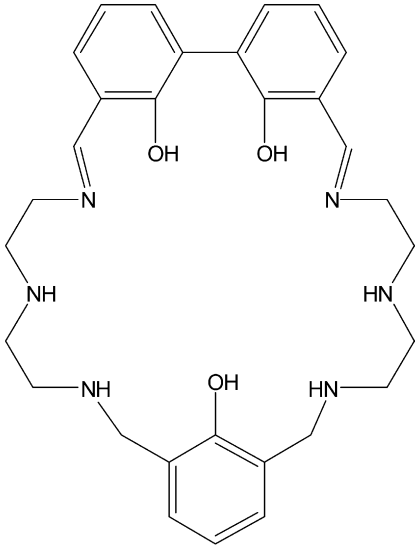

H_3-**97a**

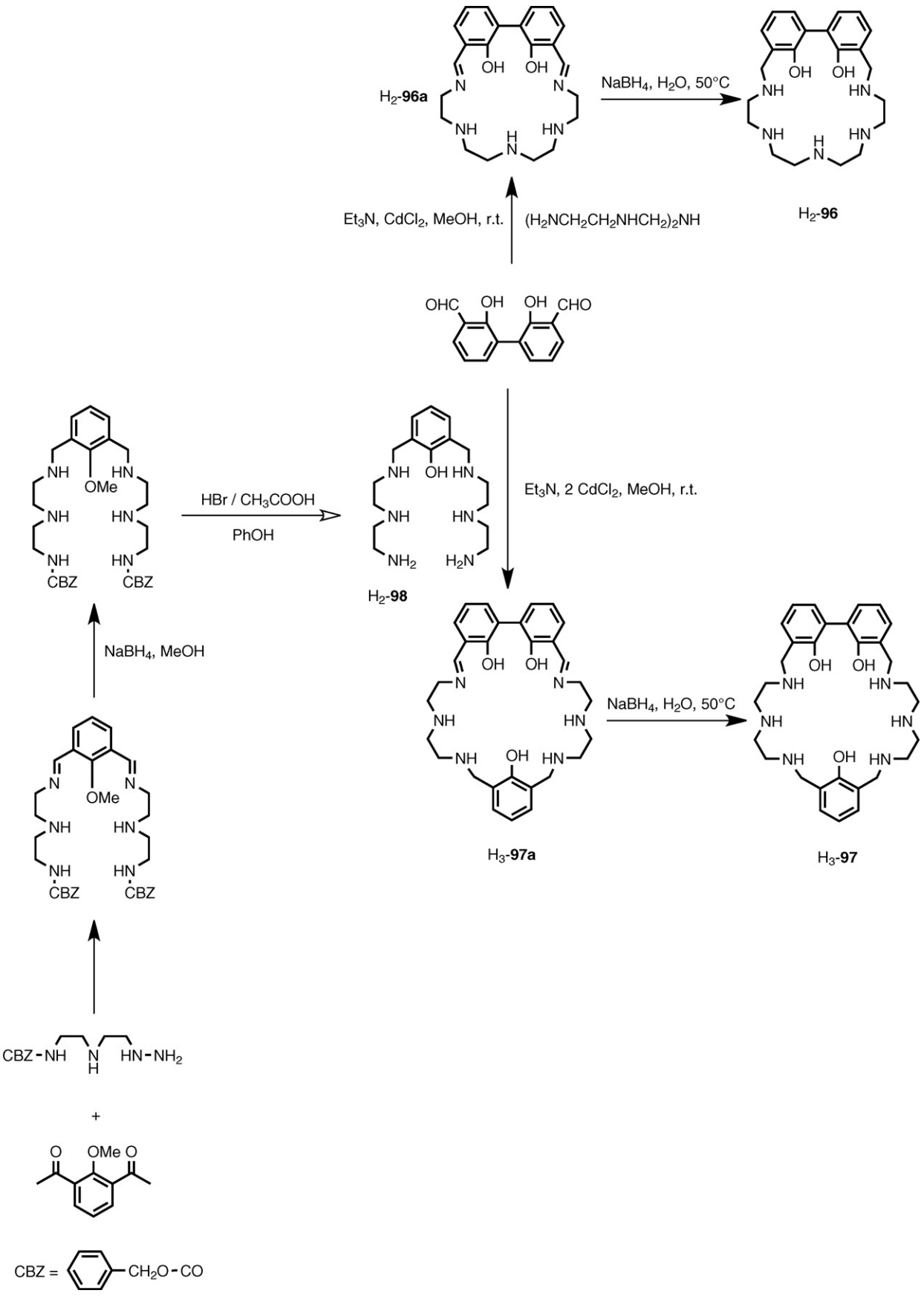

Scheme 8. Synthesis of asymmetric macrocyclic polyamines.

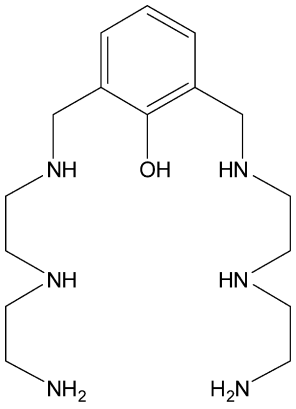

H_2-**98**

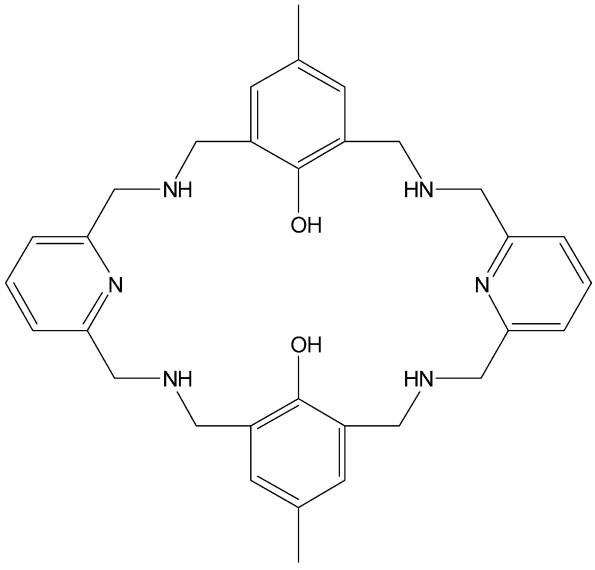

H_2-**99**

[Cu_2(**99**)$(Cl)_2$], derived from the reaction of H_2-**99** with $CuCl_2$ in anhydrous ethanol and in a 1:2 molar ratio, forms [Cu_2(**99**)(Cl)](ClO_4) when treated in water with $NaClO_4$. The complex contains a pair of copper(II) ions, entrapped in the macrocycle. Each copper(II) ion is five coordinate with three nitrogen atoms and one phenolate oxygen at equatorial plane and a bridged chloride ion at axial position. Each copper(II) ion and the related N_3O donor atoms are almost coplanar. The macrocyclic ligand is folded to a chair conformation to meet the requirement of coordinated copper(II) ions. Each chloride anion links two copper(II) ions in two neighboring macrocyclic complexes, resulting in a zigzag coordination polymer chain. The 1D chains are held together through weak $\pi\cdots\pi$ interactions between the pyridyl rings in one chain and phenoxy rings in adjacent chains [78].

This kind of complexation is much different from those of the mononuclear [Zn(H_2-**99**)]$(NO_3)_2\cdot 5H_2O$ and the heterodinuclear [ZnCd(**99**)$(Cl)_2$] complexes. In [Zn(H_2-**99**)]$(NO_3)_2$, both phenolate oxygen atoms and three nitrogen atoms on one side of the macrocycle are coordinated to the zinc(II) ions while in [ZnCd(**99**)$(Cl)_2$], the zinc(II) ion has almost the same coordination conformation as that in [Zn(H_2-**99**)]$(NO_3)_2\cdot 5H_2O$, except one phenolate oxygen bridging the zinc and cadmium ions, while the cadmium(II) ion is coordinated with the remaining three nitrogen atoms, one bridging phenolate oxygen atom and two chloride anions [78,79].

[Cu_2(**100**)(Br)](Br), prepared by the reaction of methanolic solutions H_2-**100** and $CuBr_2\cdot 2H_2O$ in the presence of $N(Et)_3$, reacts with imidazole or methylimidazole to form [Cu_2(**100**)(μ-Im)]$(Br)_2\cdot 5CH_3OH$ or [Cu_2(**100**)(μ-CH_3-Im)]$(Br)_2\cdot 5.5CH_3OH$ [80].

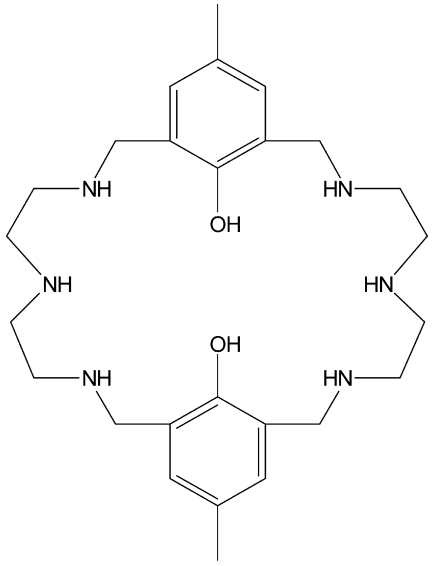

H_2-**100**

In [Cu_2(**100**)(Br)](Br), the conformation of the macrocycle is distorted owing to the specific binding of the two phenol groups which act as monodentate toward one copper(II) ion. The Cu···Cu separation is approximately 6.0 Å. Each copper(II) ion resides into one of the two N_3O coordination moieties which are situated on each side of the molecule. One copper(II) ion is pentacoordinate with a bromide ion filling the fifth coordination site, while the other copper(II) ion is tetracoordinate (Fig. 58).

In the similar copper(II) complex [Cu_2(**100**)$(Cl)_2$], the two five coordinated copper(II) ions reside equally at the N_3O_2 sites and are bridged by the two phenolate oxygens with an intermetallic separation of 3.46 Å (Fig. 59). The two structures suggest that the phenolic oxygen atoms may be interchangeable between the μ-bridged and unbridged binding fashion in solution state. Consequently, the cavity size and the distance of the two metal centers may readily change and, significantly, this property provides these metal complexes an ability to recognize, accept and release the substrate by enlarging and contracting the macrocyclic ligand [80].

IR and UV–vis measurements confirm that the [Cu_2(**100**)(μ-Im)]$(Br)_2\cdot 5.5CH_3OH$ or [Cu_2(**100**)(μ-CH_3Im)]$(Br)_2\cdot 5.5CH_3OH$ have a μ-Im or a μ-CH_3-Im bridged dinuclear structure with $[\mathbf{100}]^{2-}$ as a supporting molecule. The two five coordinate copper(II) ions sit in a distorted square pyramidal environment [80].

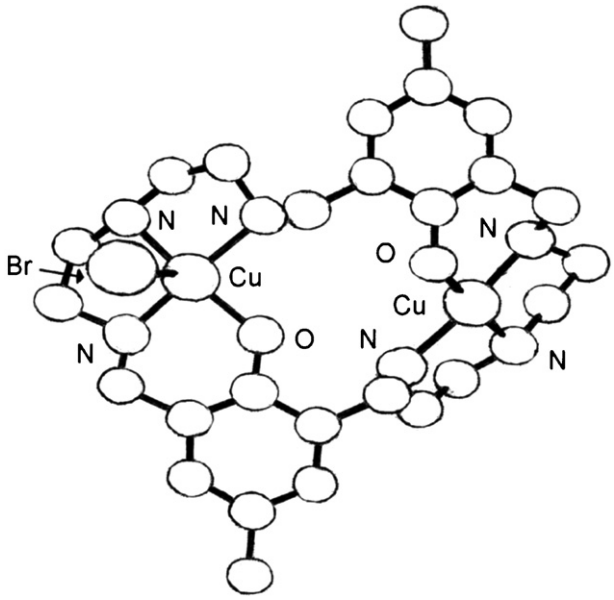

Fig. 58. Structure of $[Cu_2(\mathbf{100})(Br)]^+$.

Potentiometric investigations indicate that $[Cu_2(\mathbf{100})(\mu\text{-}CH_3\text{-}Im)]^{2+}$ is more stable than $[Cu_2(\mathbf{100})(\mu\text{-}Im)]^{2+}$ and they both are more stable than $[Cu_2(\mathbf{100})]^{2+}$. $[Cu_2(\mathbf{100})(\mu\text{-}CH_3\text{-}Im)]^{2+}$ is the predominant compound in the range of pH 6–12. By comparison, $[Cu_2(\mathbf{100})(\mu\text{-}Im)]^{2+}$ is less stable and can be changed into $[Cu_2(\mathbf{100})]^{2+}$ by releasing the bridging ligand [80].

The catalytic oxidation of cathecol by these complexes follows the order $[Cu_2(\mathbf{100})(\mu\text{-}Im)]^{2+} > [Cu_2(\mathbf{100})(\mu\text{-}CH_3\text{-}Im)]^{2+} > [Cu_2(\mathbf{100})(Br)]^{2+}$. The presence of one additional methyl group on position 2 of the imidazole ring leads to a low catalytic activity (about 50%) as the highest conversion was reached after the same reaction time. This decrease of oxidative rate (ca. 1:2) may be due to the difference in the ligand basicity. Imidazole ligand has a pK_a of 7.0, which is greater than the pK_a of methyl-imidazole of 7.9. The more basic the ligand, the greater the ability to take the proton from the catechol.

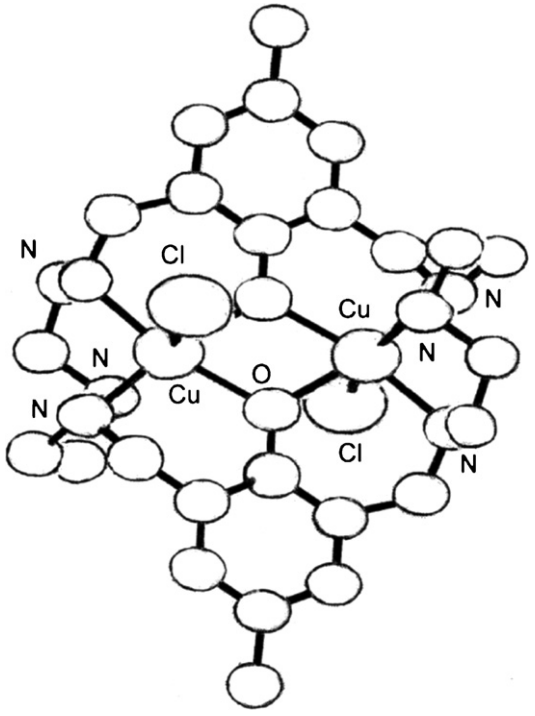

Fig. 59. Structure of $[Cu_2(\mathbf{100})(Cl)_2]$.

The important role of imidazole is to occupy and eliminate from the catalyst host and thus provide a bis-coordination site to the substrate dianion. It can also serve as a proton donor to the $\{Cu_2(O_2)\}$ adduct in the following steps, leading to the formation of H_2O and reforming the imidazolate-bridge.

UV–vis and ESR studies support a mechanism that involves a $\{Cu^I(O_2)Cu^I\}$ as the intermediate. The initial stage for catechol oxidation involves the equilibrium between $[Cu_2(\mathbf{100})(\mu\text{-}Im)]^{2+}$ and $[Cu_2(\mathbf{100})]^{2+}$. By releasing the μ-Im ligand as illustrated by potentiometric titration and visible spectral studies, an active form of $[Cu_2(\mathbf{100})]^{2+}$ was formed, which favours the binding of the catecholate substrate to the $Cu^{II}Cu^{II}$ center. This process can be promoted by the intermediate base Im as well as the stronger bases $N(Et)_3$ and $NaOC_2H_5$. The following consequences involve the reduction of the catalytic center and the oxidation of the substrate. Under anaerobic conditions only stoichiometric reaction could be achieved and the catalytic cycle could only be fulfilled when the dioxygen participated in the reaction. Although the $\{Cu_2(O_2)\}$ intermediate was not isolated, the co-existence of $Cu^{II}Cu^{II}$ and $\{Cu^I(O_2)Cu^I\}$ species are strongly supported by the UV–vis spectra and ESR results [80].

$[Cu_2(\mathbf{100})](Br)(Cl)\cdot 3H_2O$, prepared by the reaction of $H_2\mathbf{100}\cdot 6HBr$ with $CuCl_2\cdot 2H_2O$ in the presence of $N(Et)_3$ and in a 1:2:4 molar ratio affords, by the addition of CH_3COONa or $Na_2C_2O_4$ $[Cu_2(\mathbf{100})(\mu\text{-}CH_3COO)](ClO_4)\cdot 4H_2O$ and $[Cu_2(\mathbf{100})(\mu\text{-oxalate})]\cdot 2CH_3OH\cdot H_2O$, respectively. These complexes are stable in dimethylformamide and behave as 1:2, 1:1 and non-electrolytes, respectively. Moreover, according to IR and UV–vis spectra, the complexes have a μ-acetate or μ-oxalate bridged dinuclear structure [82].

In $[Cu_2(\mathbf{100})](Br)(Cl)\cdot 3H_2O$ the two copper(II) ions reside equally at the N_3O_2 sites of the pyramidal geometry and are bridged by phenolic oxygens with an intermetallic separation of 3.46 Å. The Cu_2O_2 moiety is nearly coplanar and perpendicular to the aromatic moieties. In this complex a significant antiferromagnetic spin-exchange ($J = -210\,cm^{-1}$) operates between the two copper(II) ions [82].

Titration experiments show that $[Cu_2(\mathbf{100})]^{2+}$ is the dominant specie for $[Cu_2(\mathbf{100})](Br)(Cl)$ and for $[Cu_2(\mathbf{100})(\mu\text{-}CH_3COO)](ClO_4)$. For the $H_2\text{-}\mathbf{100}\text{:}Cu^{II}\text{:}H_2C_2O_4$ system, a dinuclear complex can form, which maintains the coordinate oxalate group.

The catalase-like activity ($2H_2O_2 \rightarrow 2H_2O + O_2$) of these complexes was tested by measuring the dioxygen evolution and the amount of residual H_2O_2 [81]. For $[Cu_2(\mathbf{100})](Br)(Cl)\cdot 3H_2O$, the rapid dioxygen evolution rate was reached after the reaction was initiated and slowed down as the reaction proceeded, attributable at least partially to

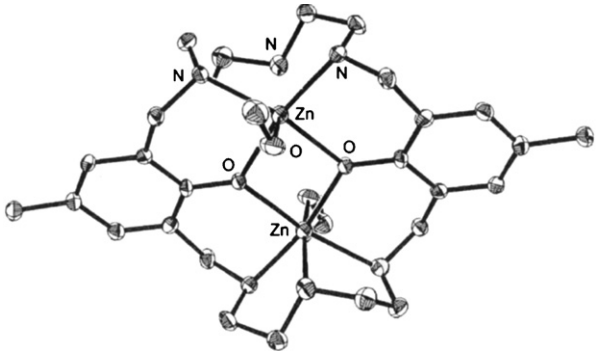

Fig. 60. Structure of $[Zn_2(\mathbf{100})(CH_3OH)_2]^{2+}$.

destruction of the complex. When the catalytic process ceased, the evolved dioxygen gas corresponds to 100% decomposition of hydrogen peroxide, implying that the catalysts are efficient toward peroxide dismutation. The evolution profile indicates that no slow catalytic process or lag phase occurs at the initial stage, in this point being different from those of the $Mn^{II}Mn^{II}$ model complex systems [82].

$[Cu_2(\mathbf{100})](Br)(Cl)\cdot 3H_2O$ and $[Cu_2(\mathbf{100})(\mu\text{-}CH_3COO)](ClO_4)$ have a high catalytic rate while $[Cu_2(\mathbf{100})(\mu\text{-}C_2O_4)]$ is much less reactive; this is due to the liability of the CH_3COO^- bridge while the oxalate ion remains coordinated to the metal ions, this depressing the catalytic reactivity.

The observed steady state molecularities for $[Cu_2(\mathbf{100})](Br)(Cl)\cdot 3H_2O$ show that the reaction rate is first order in $[Cu_2(\mathbf{100})]^{2+}$ and zero order in $[H_2O_2]$. No induction period was needed before vigorous evolution of dioxygen occurred. ESR and UV–vis spectra studies support a mechanism involving a $\{Cu^I(O_2)Cu^I\}$ intermediate, which was isolated and verified by IR and elemental analysis. As a result, a catalytic mechanism of H_2O_2 dismutation by this complex system was proposed. The initial stage for catalase activity starting with $[Cu_2(\mathbf{100})(\mu\text{-}CH_3COO)](ClO_4)$ involves an equilibrium with water and possibly a dissociation process of the acetate bridge from $[Cu_2(\mathbf{100})(\mu\text{-}CH_3COO)](ClO_4)$. An active form of $[Cu_2(\mathbf{100})(H_2O)_2]^{2+}$ species favours the binding of hydrogen peroxide to the $Cu^{II}Cu^{II}$ center by displacement of the bound water. UV–vis and ESR data support the formation of this yellow-colored, ESR silent Cu^ICu^I intermediate. Hence, one H_2O_2 molecule reduces two copper(II) ions by releasing one O_2 molecule. Subsequently, the dicopper(I) center was coordinated by another H_2O_2 molecule and, consequently, the complex was restored to its initial active form [81].

The dizinc complex $[Zn_2(\mathbf{100})(CH_3OH)_2](Br)_2$, derived from the reaction of H_2-**100** (obtained by neutralizing $[H_8\text{-}\mathbf{100}](Br)_6$ with KOH), with $Zn(ClO_4)_2\cdot 6H_2O$ in methanol, contains two slightly distorted octahedral zinc(II) ions bridged by phenolic oxygens with an intermetallic separation of 3.146 Å. Each zinc(II) ion is coordinated with three nitrogen atoms of the macrocyclic ligand and two oxygen atoms of phenolate groups, while the sixth coordination site is occupied by a methanol oxygen (Fig. 60) [83].

Potentiometric titrations in 75/25 ethanol/water solutions show that in the 1:1 H_2-**100**:Zn^{II} system the mononuclear–monohydroxo complex $[Zn(\mathbf{100})(OH)]^-$ begins to form at pH 9.90 and gradually increases the concentration as the pH goes up. The dinuclear complex $[Zn_2(H\text{-}\mathbf{100})]^{3+}$ is present at 40% in the pH range of 5–8 even though the conditions were favourable for the mononuclear species. This indicates that the zinc(II) ions have strong tendency to form dinuclear complexes with H_2-**100**. In the 1:2 H_2-**100**:Zn^{II} system, three kinds of mononuclear species were found in the pH range lower than 6. $[Zn_2(H\text{-}\mathbf{100})]^{3+}$ dominates in solution from pH 6 to 9 and reaches the highest concentration at pH 7.5 (98%). In this intermediate two zinc ions were coordinated to two deprotonated phenolic oxygen and form square bridged core with one positive proton located on one of the amine groups. The dinuclear-hydroxo species start to form at pH higher than 9.5.

The dinuclear complexes $[Zn_2(\mathbf{100})]^{2+}$ and $[Zn(\mathbf{100})(OH)]^+$ play crucial roles in hydrolytic reaction of tris(4-nitrophenyl)phosphate (TNP). It was proposed that $[Zn(\mathbf{100})(OH)]^+$ can act as a nucleophile to attack the phosphate ester to initiate the hydrolitic reaction and $[Zn_2(\mathbf{100})]^{2+}$ stabilizing the formation of the intermediate $[Zn_2(\mathbf{100})(BNP)]$ (BNP = bis(4-nitrophenyl)phosphate) due to its suitable Zn···Zn distance [83].

$[H_8\text{-}\mathbf{100}](Br)_6\cdot 6H_2O$, after neutralization with KOH, when reacted under stirring for 2 h with a methanol solution of $CdBr_2\cdot 4H_2O$ in a 1:1 molar ratio followed by addition of 1 equiv. of $Ni(ClO_4)_2\cdot 6H_2O$, affords $[Ni_2(\mathbf{100})(H_2O)][Cd(Br)_4]$ instead of the heterodinuclear CdNi complex [84]. In the homodinuclear nickel(II) unit, two different coordination environments occur: the five coordinate square pyramidal dinuclear species $[Ni_2(\mathbf{100})]^{2+}$ and the six coordinate dinuclear species $[Ni_2(\mathbf{100})(H_2O)_2]^{2+}$. In $[Ni_2(\mathbf{100})]^{2+}$ each nickel(II) ion is coordinate in the equatorial plane by the N_2O donor set of the macrocycle and the oxygen atom of the other chamber, while one apical position is filled by the remaining nitrogen donor of the macrocycle. Furthermore, a bromide ion of the $[Cd(Br)_4]^{2-}$ entity fills the remaining apical position. Therefore, the molecular aggregation is $\{[Ni_2(\mathbf{100})][Cd(Br)_4]\}$. In $[Ni_2(\mathbf{100})(H_2O)_2]^{2+}$, there are two six coordinate nickel(II) centers, each of which is bonded to a tetradentate N_3 diethylenetriamine metal-binding domain of the ligand. A terminal water molecule and two bridging phenolic oxygen atoms occupy the remaining coordination sites on each metal ion. This motif has been described as a distorted octahedron. $[Cd(Br)_4]^{2-}$ serves not only as a counter ion but also as hybrid bridge to connect two separate coordination entities and form infinite chains [84].

The asymmetric macrocycle H_2-**101** forms a number of protonated or hydroxo mononuclear, homodinuclear, heterodinuclear complexes with copper(II), nickel(II), cadmium(II), zinc(II) and lead(II) ions. Their stability constants and species distribution as a function of pH have been determined. The pH potentiometric studies show that the dinuclear complexes are formed via the mononuclear chelates in which two kinds of coordination patterns were observed: in one coordination pattern the metal ion coordinates to the N_3O donor set of one coordination site of macrocycle, while in the other the whole N_3O_2

donor set of one site of the macrocycle is bonded to the metal ion [85].

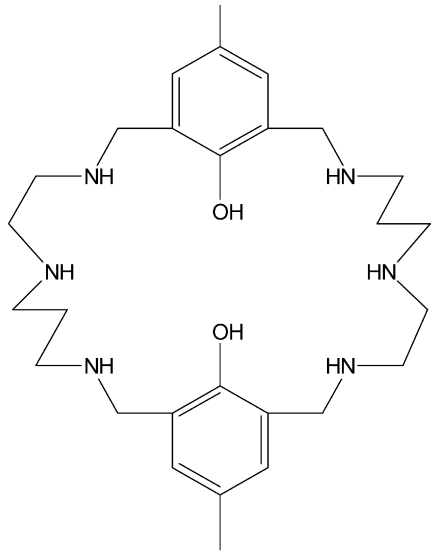

H_2-**101**

In the 2:1 H_2-**101**:M^{II} systems the mononuclear species predominate in acidic solution while the dinuclear species predominate in basic solution except the cases of copper(II) and nickel(II). Homodinuclear copper(II) complexes are present at pH 4 where the second copper(II) occupies the other coordination sites of the macrocycle [86]. In the nickel(II) systems no mononuclear complexes were found in species distribution diagrams and the two nickel(II) ions enter into the cavity of the macrocyclic ligand spontaneously. Thermodynamically, the diprotonated dinuclear complex $[Ni_2(H_2\text{-}\mathbf{101})]^{4+}$ is the most stable in the pH range from 5 to 8 [85].

The dinuclear nickel(II) complex $[Ni_2(\mathbf{101})](ClO_4)_2$ has a center of symmetry with each nickel(II) ion strongly coordinated by the two amino nitrogen atoms and two bridged phenolic oxygen atoms at equatorial positions, and by one nitrogen atom and, more weakly, by one oxygen from perchlorate anion to the axial positions. Therefore, the overall coordination geometry around the nickel(II) ions is an elongated octahedron (Fig. 61) [85]. This structure is different form that of $[Cu_2(\mathbf{101})(Br)_2]\cdot 2CHCl_3\cdot 2CH_3OH$ [86] and $[Co_2(\mathbf{101})(NO_3)_2]\cdot 12H_2O$ [85] where no bridged M_2O_2 core was formed; in the dicopper(II) and dicobalt(II) complexes the metal ions were separately situated in two compartments of the macrocycle, with two anions as auxiliary ligands to complete the five or six coordinated polyhedron. This type of coordination may also hold in the mononuclear protonated copper(II) and cobalt(II) complexes of $[H_4\text{-}\mathbf{101}]^{2+}$, where only one phenol group coordinates to the metal center and the positive charges are well delocalized on the other side of the amino nitrogen atoms [85,86].

Titrations of solutions containing Cu^{II} and M^{II} ions ($M = Cd^{II}$, Co^{II}, Fe^{II}, Zn^{II}, Ni^{II}) with $[H_8\text{-}\mathbf{101}]^{6+}$ in 1:1:1 ratios show that heterodinuclear complexes form. The affinity of second metal ions increases in the order $Cd^{II} < Ni^{II} < Co^{II} < Zn^{II} < Fe^{II}$ in the Cu^{II} hosting system. The

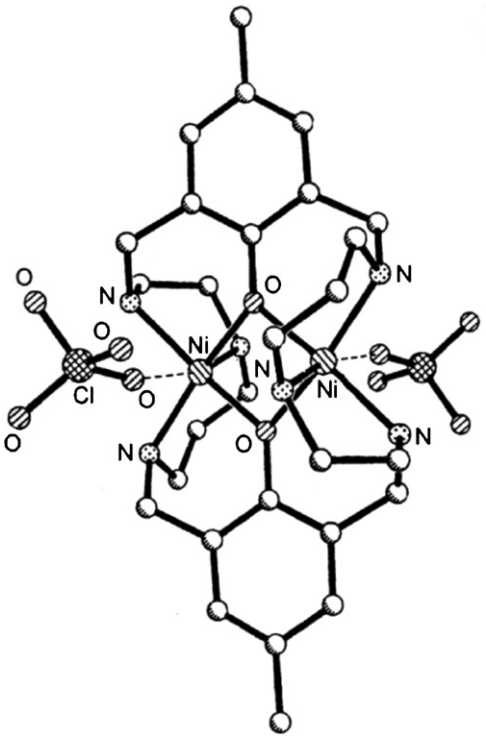

Fig. 61. Structure of $\{[Ni_2(\mathbf{101})](ClO_4)_2\}$.

stability constants of the heterodinuclear complexes are greater than those of homodinuclear complexes, indicating that these heterodinuclear complexes are more stable than corresponding homodinuclear complexes. The heterodinuclear complexes are formed with high yields in broad pH regions (6–10 for $Cu^{II}Zn^{II}$ and $Cu^{II}Fe^{II}$ systems with 90% content; 7–9 for $Cu^{II}Co^{II}$ system with 60% content; 8–11 for $Cu^{II}Cd^{II}$ system with 80% content; 10–12 for $Cu^{II}Ni^{II}$ system with 90% content). The hydroxo species $[CuM(\mathbf{101})(OH)]^{+}$ and $[CuM(\mathbf{101})(OH)_2]$ are detected in four mixed systems, not including the $Cu^{II}Ni^{II}$ case, as the content of $[CuM(\mathbf{101})]^{2+}$ decreases [85].

$[Fe_2(\mathbf{101})(CO_3)_2]\cdot 12H_2O$ was obtained by reaction of a water solution of $[H_8\text{-}\mathbf{101}](Br)_6$, neutralized till pH 6 with KOH, with $Fe(ClO_4)_2\cdot 6H_2O$ and Na_2CO_3 in a 1:2:1 molar ratio [87]. In this complex two pseudo-octahedral iron(II) ions are located in separated compartments and each of them is six coordinate, being bonded to three nitrogens, one phenolic oxygen and two carbonate oxygens. The Fe···Fe separation is 5.23 Å (Fig. 62) [87].

Potentiometric equilibrium studies indicate that a variety of protonated, mononuclear and dinuclear complexes are formed with iron(II) and iron(III) from pH 2 through 12 in aqueous solution. The stability constants and species distribution as a function of pH of the 1:1, 1:2 and 1:1:1 [H_2-**101**:Fe^{II}, H_2-**101**:Fe^{III} or H_2-**101**:Fe^{II}:Fe^{III}] complexes were determined in KCl supporting electrolyte ($\mu = 0.100$ M) at 25 °C. The data obtained from solutions containing H_2-**101**·6HBr and Fe^{2+} show that for the mononuclear systems the species $[Fe^{II}(H_4\text{-}\mathbf{101})]^{4+}$, $[Fe^{II}(H_3\text{-}\mathbf{101})]^{3+}$, $[Fe^{II}(H_2\text{-}\mathbf{101})]^{2+}$, $[Fe^{II}(H\text{-}\mathbf{101})]^{+}$, $[Fe^{II}(\mathbf{101})]$ were identified. $[Fe^{II}(\mathbf{101})]$ begins to dominate when the pH is higher than 8 and reaches its higher concentration at a more alka-

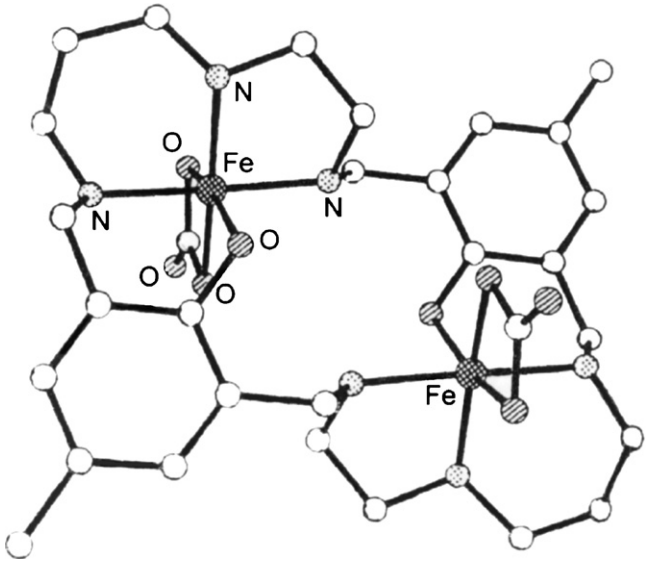

Fig. 62. Structure of $[Fe_2(\mathbf{101})(CO_3)_2]$.

line area. In the dinuclear system, the species $[Fe_2^{II}(\mathbf{101})]^{2+}$, $[Fe_2^{II}(\mathbf{101})(OH)]^{3+}$ and $[Fe_2^{II}(\mathbf{101})(OH)_2]^{2+}$ dominate in the range pH 6–12. Dinuclear complexes easily form hydroxo-bridged hydrolytic species. For the H_2-**101**:Fe^{III} 1:1 and 1:2 systems it was observed that the mononuclear $[Fe^{III}(H_4$-**101**$)]^{5+}$complex predominates from pH 3 to 5. The other two mononuclear complexes $[Fe^{III}(H_3$-**101**$)]^{4+}$ and $[Fe^{III}(H_2$-**101**$)]^{3+}$ exist at more basic region (pH 4–7) with the percentage around 4.6–5.7%. Then the other iron(III) ion enters into the macrocyclic cavity to form the protonated dinuclear iron(III) complex $[Fe_2^{III}(H_2$-**101**$)]^{6+}$ and $[Fe_2^{III}(H$-**101**$)]^{5+}$; both of them reach their maximum concentration (68.4%) at pH 5.2 and (31.7%) at pH 6.2, respectively. Neutral dinuclear iron(III) complexes start to form from pH > 5 and reaches its highest concentration at pH 7.2 (78.6%). The first water molecule coordinates with iron(III) ion and forms a hydroxo complex $[Fe_2^{III}(OH)(\mathbf{101})(OH)]^{3+}$ when pH is higher than 7. It overlaps with neutral dinuclear species and reaches its maximum concentration 76.7% at pH 9. Between pH 9 and 11, the second and third water molecules coordinate with iron(III) ions to form $[Fe_2^{III}(\mathbf{101})(OH)_2]^{2+}$ and $[Fe_2^{III}(\mathbf{101})(OH)_3]^{+}$. Above pH > 7–12, the hydrolytic species, $[Fe_2^{III}(\mathbf{101})(OH)]^{3+}$, $[Fe_2^{III}(\mathbf{101})(OH)_2]^{2+}$,$[Fe_2^{III}(\mathbf{101})(OH)_3]^{+}$ are formed successively. The μ-oxo bridged diiron(III) complexes and their further hydrolytic species become the main components in aqueous solutions at high pH.

H_2-**101** has stronger affinity for the iron(III) ion than for the iron(II) ion. Therefore, heterodinuclear complexes containing different valence ions were expected to form in 1:1:1 systems. Titration curves of the 1:1:1 H_2-**101**:Fe^{III}:Fe^{II} system show the initial formation of the mononuclear $[Fe^{III}(H_4$-**101**$)]^{5+}$complex which predominates in acidic solution, and an inflection at $a = 8$ indicative of the formation of mixed-valence $[Fe^{III}Fe^{II}(\mathbf{101})]^{3+}$ complex. In addition, the $[Fe^{III}Fe^{II}(\mathbf{101})(OH)]^{2+}$, $[Fe^{III}Fe^{II}(\mathbf{101})(OH)_2]^{+}$ and the corresponding μ-oxo species $[Fe^{III}Fe^{II}(\mathbf{101})(\mu\text{-}O)(OH)_2]^{-}$ are also identified.

Thus, H_2-**101** contains six nitrogens able to act as donor atoms in complexes. However, they are arranged as two subunits separated by two phenolic bridging donor groups. It is expected that a mononuclear complex $[Fe^{III}(H_2$-**101**$)]^{3+}$ will be formed by the coordination of the iron(III) ion to one of the subunits. When the pH is raised, the remaining amino groups deprotonate and the iron(II) ion coordinates μ-hydroxo bridged species and further hydrolytic mixed-valence species are subsequently formed in alkaline solution. According to the K_{com}, the mixed-valent complex is more stable than the single-valent dinuclear complexes [87].

The dinuclear iron(II) complex easily forms μ-peroxo adduct at 1 atm oxygen atmosphere with the oxygenation constant $\log K[O_2] = 7.74$, when the titration of the H_2-**101**:Fe^{II} was carried out under 1 atm purified oxygen. Three dinuclear oxygen complexes have formed successively with increasing pH values. $[Fe^{II}(\mathbf{101})(O_2)]^{4+}$ reaches its highest concentrations 76.83% at pH 5.8 and 7.7, respectively. When the pH increases >7, $[Fe_2^{II}(\mathbf{101})(OH)(O_2)]$ becomes the major species in the pH range from 7 to 10, and the maximum concentration appears at pH 9.6 at a value of 77.3%. After that point, its distribution decreases and dihydroxo complex: $[Fe_2^{III}(\mathbf{101})(OH)_2(O_2)]$ forms and increases with the pH, then reaches highest concentration of 94.0% (pH 12). The diiron(II) complex can be irreversibly oxidizes to the mixed $Fe^{II}Fe^{III}$ complex, which is not further oxidized to the $Fe^{III}Fe^{III}$ complex [87].

Condensation of equimolar amounts of 2,6-diformyl-4-methylphenol and triethylenetetraamine in the presence of $Pb(SCN)_2$ as a template leads to the [2 + 2] Schiff base which, by hydrogenation with sodium tetrahydroborate, forms the corresponding saturated [30]-membered octaazamacrocycle H_2-**102**. The final treatment with H_2SO_4 removes the lead ions, and allows the extraction of the macrocyclic ligand with organic solvents. The macrocycle was separated as the octabromide salt $[H_{10}$-**102**$](Br)_8$ [88].

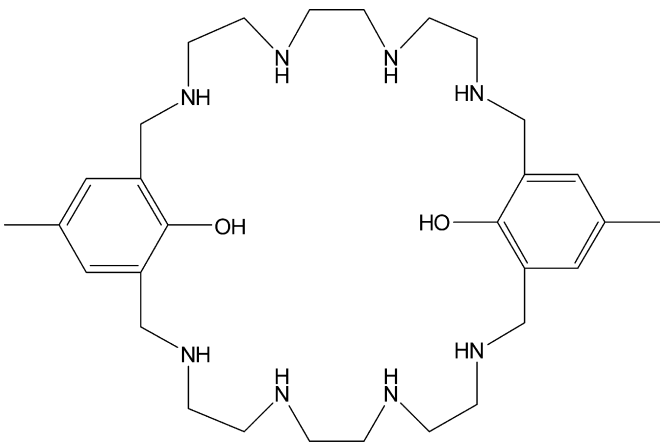

H_2-**102**

At pH < 2, the ligand exists in the fully deprotonated form, $[H_{10}$-**102**$]^{8+}$. As the pH is increased, the ligand loses its protons from amino nitrogens to become $[H_9$-**102**$]^{7+}$, $[H_8$-**102**$]^{6+}$, $[H_7$-**102**$]^{5+}$, $[H_6$-**102**$]^{4+}$, $[H_5$-**102**$]^{3+}$, $[H_4$-**102**$]^{2+}$, $[H_3$-**102**$]^{+}$ and H_2-**102** species, respectively. The neutral ligand H_2-**102** reaches

its maximum concentration at pH 10.6 (68.2%). When the pH is above 10.5, one of the two phenolic hydrogen begins to be deprotonated to form [H-**102**]$^{-}$, which reaches its maximum concentration (51.7%) at pH 11.6. Under more alkaline conditions, the other phenolic hydrogen deprotonates to the free ligand dianion [**102**]$^{2-}$ (pH > 12) [88].

Potentiometric titrations, carried out to determine the stability constants of the complexes formed by H_2-**102** and copper(II) and nickel(II), were run in 1:1 and 2:1 (M^{II}:H_2-**102**) systems. For the 1:1 systems, the hexaprotonated mononuclear copper complex [Cu(H_6-**102**)]$^{6+}$ is formed from pH 2.2 and reaches its highest concentration (59.9%) at pH 3.1. The most interesting feature of this system is the predominant species are penta-, tri- and diprotonated complexes, which are present at higher concentrations than any other component between pH 2.5 and 9.5. The maxima for [Cu(H_5-**102**)]$^{5+}$, [Cu(H_3-**102**)]$^{3+}$, [Cu(H_2-**102**)]$^{2+}$ are 83.3% at pH 6.6 and 84.4% at pH 8.7, respectively. The fully deprotonated complex, [Cu(**102**)], forms from pH 9.0 to 12.0, with stepwise deprotonation of ligand [88].

The nickel(II) ion enters into the coordination cavity of H_2-**102** around pH 4. The first species formed in solution are [Ni(H_4-**102**)]$^{4+}$. As the pH increases, the ligand is deprotonated stepwisely, and forms the tri-, di-, monoprotonated species, respectively. In basic solutions two hydrolytic species occur and overlap with unprotonated mononuclear species [Ni(**102**)] [88].

For the 2:1 Cu^{II}:H_2-**102** systems, the titration curve shows that the mononuclear species [Cu_2(H-**102**)]$^{3+}$ is formed at low pH. The species distribution diagram based on the stability constants reveals that, prior to the formation of the monoprotonated dinuclear complex [Cu_2(H-**102**)]$^{3+}$, the mononuclear chelates [Cu(H_6-**102**)]$^{6+}$ and [Cu(H_5-**102**)]$^{5+}$ exist and overlap with dinuclear species. [Cu_2H-**102**]$^{3+}$ is the principle species from pH 5 to 8. The other two dinuclear species [Cu_2(H-**102**)]$^{2+}$ and [Cu_2(**102**)(OH)]$^{+}$ become the major component after pH 9.5 [88].

For the 2:1 Ni^{II}:H_2-**102** system, there is only one mononuclear species [Ni(H_4-**102**)]$^{4+}$ observed in small percentage when pH is lower than 5, then four dinuclear chelates were formed successively. The first water molecule binds with [Ni_2(**102**)]$^{2+}$ and forms [Ni_2(**102**)(OH)]$^{+}$ when pH is above 7. [Ni_2(**102**)(OH)$_2$] become very significant after pH 10 [88].

In the 2:1 M^{II}:H_2-**102** systems, two metal ions were suggested to enter into the cavity separately and located into the two compartments without formation of μ-oxo bridged core, as observed also in the solid state structure of [Cu_2(**102**)](ClO$_4$)$_2$·3CH$_3$OH·2H$_2$O, where the two copper(II) ions are located in separate compartments and each of them is five coordinate in a square pyramidal coordination polyhedron, being bonded to four nitrogen donors from triethylenetetraamine units of the macrocycle and one phenolic oxygen. The macrocyclic ligand serves as the N_4O donor for each copper ion (Fig. 63). The intramolecular Cu···Cu separation is 5.361 Å [88], which is comparative to [Cu_2(**100**)](Cl)(Br) (5.36 Å) [89] and shorter than [Cu_2(**100**)(Br)$_2$]·2CHCl$_3$·2CH$_3$OH (5.814 Å) [86] and [Cu_2(**103**)(Br)$_2$]·CH$_3$OH (6.005 Å) [90]. The macrocyclic skeleton of [**102**]$^{2-}$ is very flexible to be folded when the two copper ions intercalate into the macrocyclic cavity, which

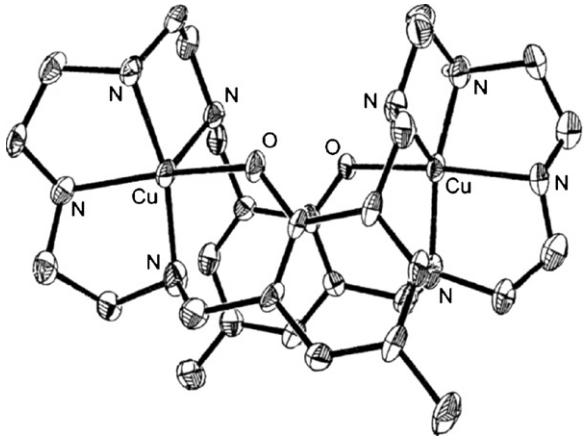

Fig. 63. Structure of [Cu_2(**102**)]$^{2+}$.

can effectively reduce the repulsion of each of the two copper ions. The macrocycle skeleton adopts a twisted conformation [88].

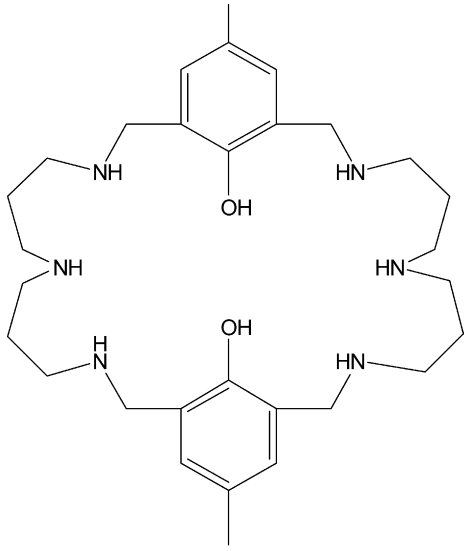

H_2-**103**

In [Ni_2(**102**)(H_2O)$_2$](ClO$_4$)$_2$·3H$_2$O each nickel(II) ion is coordinated in a slightly distorted octahedral geometry to four amino nitrogens, one phenolic oxygen and one oxygen from a water molecule. The equatorial plane is composed of N_2O_2 donor set of the macrocycle while the other nitrogen and a water oxygen atoms occupied two apex positions. The distance between two nickel ions is 5.515 Å, indicating that no Ni_2O_2 bridged core occurs (Fig. 64) [88].

Thus, in the dicopper(II) and dinickel(II) complexes with [**102**]$^{2-}$ the metal ions were separately situated in two compartments of the macrocycle. This type of coordination mode may also apply to the mononuclear protonated copper(II), nickel(II), complexes of [**102**]$^{2-}$, where only one phenol group coordinates to the metal center. The positive charges are well delocalized on the other side of the amino nitrogen atoms. As mentioned above, the phenol groups start to deprotonate when pH is higher than 8. It is possible for the protonated mononuclear complex (such

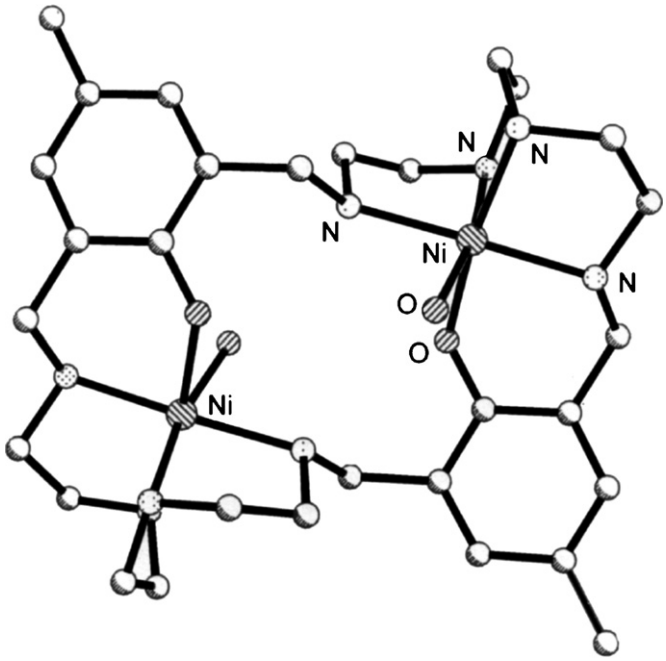

Fig. 64. Structure of $[Ni_2(\mathbf{102})(H_2O)_2]^{2+}$.

as $[M(H_4\text{-}\mathbf{102})]^{4+}$, $[M(H_3\text{-}\mathbf{102})]^{3+}$) to have one deprotonated phenol in their coordination environment [88].

The dinuclear copper complexes of $[\mathbf{102}]^{2-}$ were found to have cleavage ability toward supercoiled DNA in the presence of hydrogen peroxide. EPR and UV spectroscopic results suggested that this cleavage might occur via Cu_2-peroxo intermediate without the involvement of hydroxyl radicals [88].

Potentiometric experiments, run in a 1:1 and 1:2 H_2-**103**:M^{II} molar ratio (M^{II} = Co^{II}, Pb^{II}, Cu^{II}, Ni^{II}), show all the metal ions combine easily with the macrocycle to form the deprotonated $[M(\mathbf{103})]$ and $[M_2(\mathbf{103})]^{2+}$, the multiprotonated $[M(H_n\text{-}\mathbf{103})]^{n+}$ and $[M_2(H_n\text{-}\mathbf{103})]^{(n+2)+}$ as well as hydroxy bridged complexes in concentrations depending on the pH of the solution. In the 1:1 H_2-**103**:M^{II} systems, the successive protonation constants of mononuclear copper(II), cobalt(II), nickel(II) and lead(II) complexes $[M(H_i - \mathbf{103})]^{i+}$ $(i = 1-3)$ are close, whereas the formation constants of the mononuclear complexes $[M(\mathbf{103})]$ are different. The stability constants of mononuclear complexes show that the affinity of the ligand for metal ions decreases in the order $Cu^{II} > Ni^{II} > Co^{II} > Pb^{II}$, and the order of stability of Co^{II} and Ni^{II} are close, that of Pb ^{II} is lower and of Cu^{II} it is much higher. It can be explained that the mononuclear complexes $[M(\mathbf{103})]$ of all four metal ions have similar successive protonation formation and four metal ions have different reactivities toward to the ligand. The hydrolysis of $[M(\mathbf{103})]$ to $[M(\mathbf{103})(OH)]^-$ occurs in the lead(II) and nickel(II) systems [91].

For 1:2 H_2-**103**:M^{II} systems, stable dinuclear species are formed at pH 8–10. Unlike the 1:1 system only monoprotonated species of dinuclear complexes can be found in the system, whereas $[M_2(\mathbf{103})]^{2+}$ has a tendency to form hydroxy-bridged complexes [91].

The potentiometric titrations of 1:2 $[H_8\text{-}\mathbf{103}]^{6+}$:$Co^{II}$ in an atmosphere of oxygen show the predominant species are all oxygenated complexes: $[Co_2(H_2\text{-}\mathbf{103})(O_2)]^{2+}$ reaches its maximum at pH 6; $[Co_2(\mathbf{103})(O_2)]$ is the predominant species from pH 6.5 to 10.5, then $[Co_2(\mathbf{103})(O_2)(OH)]$ forms.

The potentiometric titrations of 1:1:1 molar ratio $[H_8\text{-}\mathbf{103}]^{6+}$:$Co^{II}$:$M^{II}$ (M = Cu^{II}, Ni^{II}, Pb^{II}), carried out under Ar gas and dioxygen, show that the stability constants of homodinuclear complexes are two orders of magnitude more than those of the heterodinuclear complexes. It can be explained that the homodinuclear cobalt(II) complexes form an intramolecular dioxygen species and the other forms the intermolecular dioxygen complexes. Thus, the stability constants of these intermolecular dioxygen complexes are nearly half of those of the intramolecular dioxygen species, except the $[CoCu(\mathbf{103})(OH)_2]$ in higher pH range. Comparison of the neighboring effect of these M^{II} ions shows that Ni^{II} has the smallest effect of the three. The effect increases in the order $Ni^{II} > Cu^{II} > Pb^{II} > Co^{II}$ [91].

Similarly to the analogous copper(II) and zinc(II) complexes also in $[Ni_2(\mathbf{103})(Br)_2]$, obtained by slow evaporation of a methanol solution of H_2-**103** and Ni^{II} in a 1:2 molar ratio at pH > 8, the nickel(II) ions have a distorted square pyramid geometry. Each metal ion is coordinated by two phenolate bridging groups and three nitrogen donors of one side of the macrocycle. Two phenolate groups and two amino nitrogens form the basal plane with another amino nitrogen from the ligand occupying the apical position. The copper(II), nickel(II) and cobalt(II) ions in related heterodinuclear macrocyclic complexes with $[\mathbf{74}]^{2-}$ have distorted square pyramid conformations, while the lead(II) ions has a six coordinate geometry. The donor atoms of the macrocycle on the basal square plane of copper(II) complex are N_3O, those of other three metal ions complexes are N_2O_2 [92]. Macrocyclic heterodinuclear $Pb^{II}Co^{II}$ complexes with a similar asymmetric Schiff base have been reported, which can take dioxygen reversibly at 0° in dimethylformamide giving rise to is a μ-peroxo dimer [93].

The $Co^{II}Co^{II}$ complexes with $[\mathbf{103}]^{2-}$ have larger oxygenation constants since they form intramolecular oxygenated species. The sixth apical vacant position of two cobalt(II) ions can accept one molecule of dioxygen. For the related heterodinuclear complexes, the oxygenated complexes would be intramolecular species; the lead(II) ions having a six coordinate geometry would stimulate the neighboring cobalt(II) ion to accept dioxygen in its sixth vacant position to turn into six-coordinate geometry. Although the nickel(II) ion has a similar square pyramid conformation to the cobalt(II) ion, they are separate entities and the nickel(II) ion is not helpful to the cobalt(II) ion in its oxygenation [91].

H_2-**104**, obtained by condensation of 2,6-diformyl-4-methylphenol with 1,5-diamino-3-oxapentane in the presence of $Pb(SCN)_2$ followed by reduction of the resulting [2 + 2] Schiff base complexes with $NaBH_4$ in methanol, gives rise to the related dinuclear copper(II) complex $[Cu_2(\mathbf{104})](ClO_4)_2$ when reacted with $Cu(ClO_4)_2{\cdot}6H_2O$ in methanol [94]. $[\mathbf{104}]^{2-}$ binds the two copper(II) ions by way of its 2,2-oxobisethylamine moieties, which provide two nitrogen and one oxygen donors to each metal ion. The coordination set around each copper ion is completed

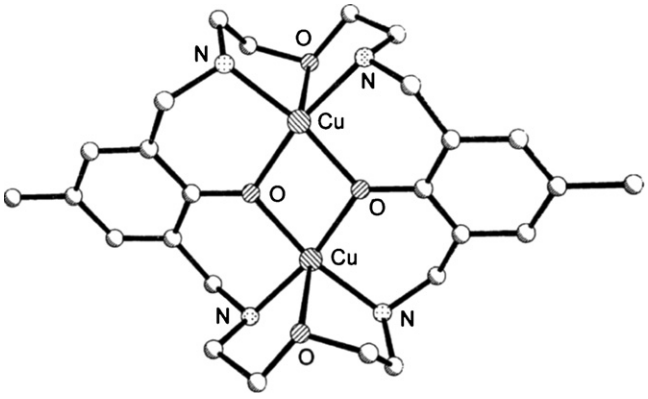

Fig. 65. Structure of $[Cu_2(\mathbf{104})]^{2+}$.

by the coordination of two phenolate oxygen atoms in equatorial positions. The formation of the Cu_2O_2 bridged core greatly enhances the stability of the complex. The oxygen atom locates in an apical position, thus resulting in a distorted square pyramidal geometry. The macrocyclic ligand serves as the N_2O_3 donor to each copper ion (Fig. 65) [94].

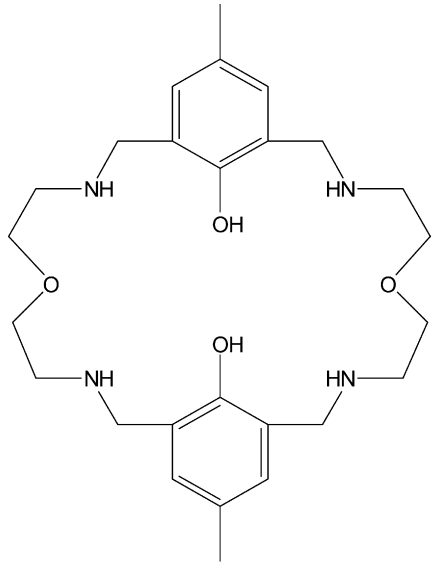

H_2-**104**

The coordination properties of H_2-**104** toward copper(II) ions were studied in aqueous 0.1 M KCl solution with direct potentiometric titration. The experiments were run in a 1:1 and 1:2 (H_2-**104**:Cu^{II} systems). Both 1:1 and 1:2 H_2-**104**:Cu^{II} systems start at lower pH than the ligand itself, because copper ions strongly bind to fully protonated ligand and substitute protons. For the 1:1 system, diprotonated mononuclear copper complex formed from pH 3 and reaches its highest percentage (90.1) at pH 7.1, coexisting with the dinuclear species $[Cu_2(\mathbf{104})]^{2+}$ at lower pH.

For the system containing 1:2 Cu^{II}:H_2-**104** molar ratio only one mononuclear protonated species is formed only at very low pH range and never becomes a major component in solution. The fully deprotonated dinuclear complex $[Cu_2(\mathbf{104})]^{2+}$ also starts form pH > 3.5, as pH raised above 4.0, becomes predominant species and reaches its maximum concentration (95.7%) at pH 5.9. From then on to pH 12, $[Cu_2(\mathbf{104})]^{2+}$ maintains its highest concentration. No hydroxo copper(II) complex species are found in the whole titration range investigated [94].

It was shown that the magnesium templated reaction of 2, 6-diformyl-4-methylphenol and 1,2-diaminoethane produces the large [4 + 4] Schiff base macrocycle H_4-**105a** as a magnesium complex and that this could be converted into the metal-free amine analogue H_4-**105** by reduction with sodium borohydride followed by careful workup [5].

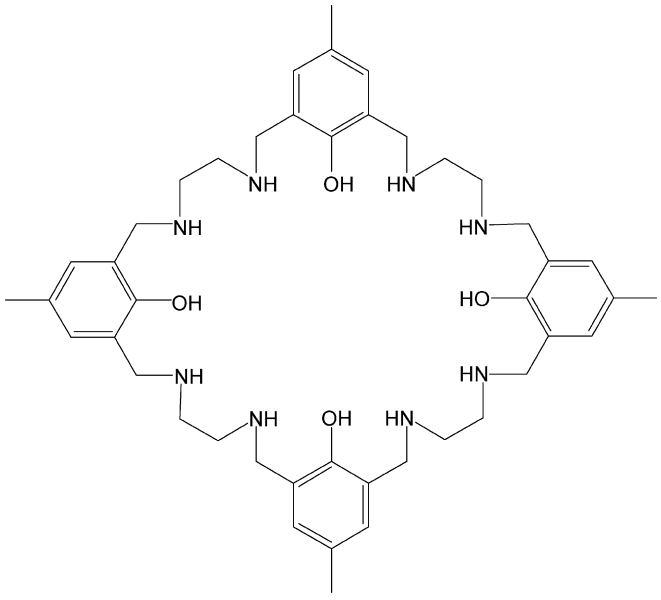

H_4-**105**

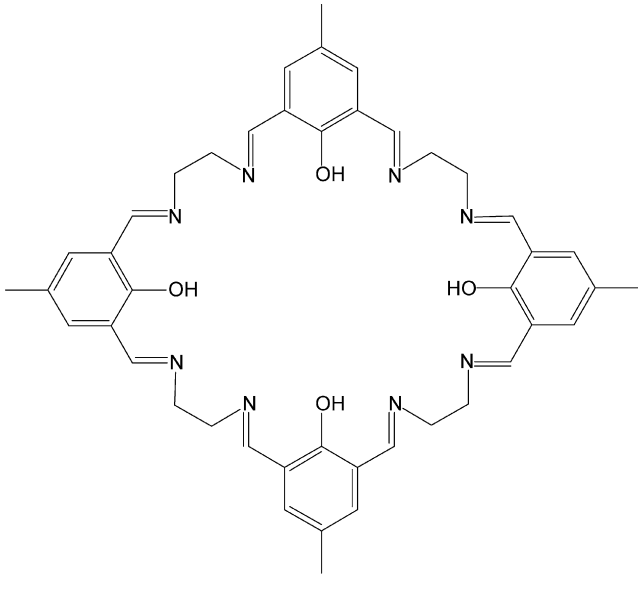

H_4-**105a**

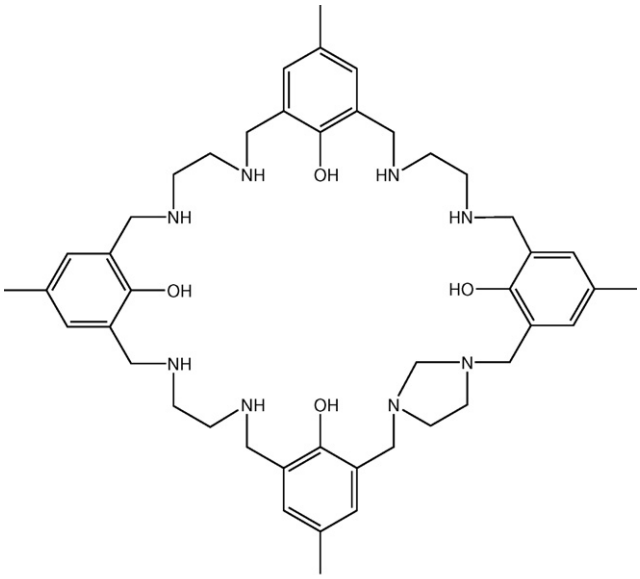

H_4-**105'**

The reaction of H_4-**105** with both iron(III) and iron(II) salts in methanol yields the tetranuclear iron(III) complex $[Fe_4(\mathbf{105'})_2(OH)_2(OCH_3)_2]$, as either $[Fe_4(\mathbf{105'})_2(OH)_2(OCH_3)_2]\cdot 10H_2O\cdot 8CH_3OH$ or $(H_5O_2)[Fe_4(\mathbf{105'})_2(OH)_2(OCH_3)_2](Cl)\cdot H_2O\cdot 10CH_3OH$, containing the modified macrocycle $[\mathbf{105'}]^{4-}$. Freshly distilled methanol was used to eliminate the possibility of contamination of this solvent by formaldehyde. $[Fe_4(\mathbf{105'})_2(OH)_2(OCH_3)_2]$ was initially prepared from a 4:1 reaction of $Fe(NO_3)_3\cdot 9H_2O$ with H_4-**105**, in 23% yield based on the limiting reagent H_4-**105**. Comparable yields were obtained using a 4:1 ratio with $FeCl_2\cdot 4H_2O$ (26%) and $FeCl_3\cdot 6H_2O$ (25%). When iron(II) chloride was used in the stoichiometric 2:1 ratio a similar yield of $[Fe_4(\mathbf{105'})_2(OH)_2(OCH_3)_2]$ (22%) was obtained. Finally, when a stoichiometric amount of formaldehyde was introduced to the 2:1 iron(II) chloride reaction $[Fe_4(\mathbf{105'})_2(OH)_2(OCH_3)_2]$ was obtained in a higher yield (43%). This indicates with the suggestion that formaldehyde is involved in the reaction mechanism by which H_4-**105** in converted into H_4-**105'** [95].

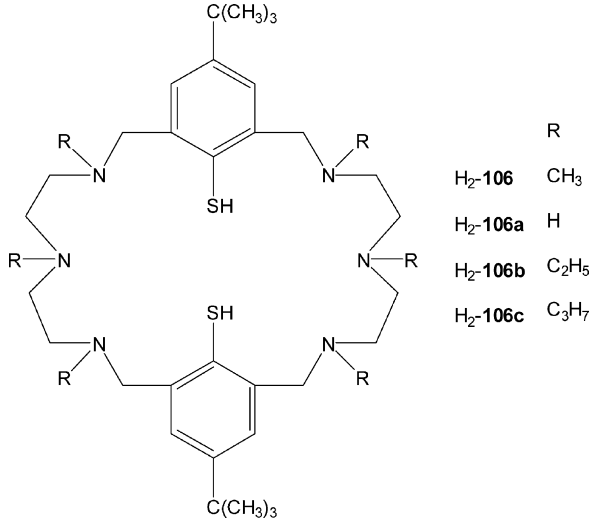

	R
H_2-**106**	CH_3
H_2-**106a**	H
H_2-**106b**	C_2H_5
H_2-**106c**	C_3H_7

For both complexes $[Fe_4(\mathbf{105'})_2(OH)_2(OCH_3)_2]\cdot 10H_2O\cdot 8CH_3OH$ and $(H_5O_2)[Fe_4(\mathbf{105'})_2(OH)_2(OCH_3)_2](Cl)\cdot 3H_2O\cdot 10CH_3OH$ the centrosymmetric complex molecule comprises two macrocyclic ligands, each containing two well separated high-spin iron(III) centers; no mixed-valence complexes are formed. The two diiron macrocycles are linked by hydroxy and methoxy bridges to give two dinuclear $[Fe_2^{III}(\mu\text{-}OH)(\mu\text{-}OCH_3)]^{4-}$ units. Overall, this gives a structure containing two $\{Fe(OH)(CH_3O)Fe\}$dimers sandwiched by two $[\mathbf{105'}]^{4-}$ macrocycles. The intradimer Fe···Fe separation is similar in both structures (3.150 and 3.173 Å). The phenolic oxygens are all deprotonated, and the conformations of the complex molecules in the two structures are very similar. As is frequently observed in cases where iron salts are used in reactions where no attempts are made to exclude either air or water, dinuclear $\{Fe^{III}(OR)_2Fe^{III}\}^{4+}$ units form easily, and in this case serve as a means for joining together two of the modified $[\mathbf{105'}]^{4-}$ macrocycles (Fig. 66). Two adjacent phenolate oxygens and the two intervening amino nitrogens coordinate to a iron(III) ion, with one nitrogen and one oxygen *trans* to the methoxo and hydroxo bridges, respectively. In a similar manner, the remaining two phenolate oxygens, together with the two nitrogens that lie between them (and are thus diametrically opposite to the other coordinated nitrogens in the macrocyclic ring) coordinate to the iron(III) ion of the inversion-related dinuclear unit.

In both complexes $[Fe_4(\mathbf{105'})_2(OH)_2(OCH_3)_2]\cdot 10H_2O\cdot 8CH_3OH$ and $(H_5O_2)[Fe_4(\mathbf{105'})_2(OH)_2(OCH_3)_2](Cl)\cdot 3H_2O\cdot 10CH_3OH$, one of the two uncoordinated 1,2-diaminoethane moieties in the macrocycle, that has been transformed into a five membered imidazolidine ring by the insertion of a methylene carbon between the two nitrogens. A series of hydrogen bonds results in a fairly compact structure for the complex molecule. The bonding arrangement in the complex means that these two dinuclear iron(III) units are effectively isolated with the shortest interdimer Fe···Fe distance being over 8 Å. The magnetic susceptibility data have been interpreted in terms of two isolated antiferromagnetically coupled iron(III) dimers ($J = -23.75$ K) [95].

2.3.2. Thiophenolate-based system

In previous reviews [4,5] the synthesis of the macrocyclic ligand H_2-**106a** and its permethylated derivative H_2-**106** was reported, together with the related dinickel(II) complexes $[Ni_2(\mathbf{106a})(\mu\text{-}Cl)](ClO_4)$ and $[Ni_2(\mathbf{106})(\mu\text{-}Cl)](ClO_4)$ [5,96].

H_2-**106a** was obtained by a [1 + 2] condensation between the appropriate tetraaldehyde and 1,5-diamino-3-azapentane in $C_2H_5OH/CHCl_3$ followed by reduction of the resulting Schiff base with $NaBH_4$. The reductive methylation of the resulting macrocycle with formaldehyde and formic and gave the permethylated derivative. Both the unmethylated and permethylated thioethers have been converted into the corresponding thiophenols H_2-**106a** and H_2-**106** by using sodium in liquid ammonia as reducing agent (Scheme 9) [96].

$[Ni_2(\mathbf{106a})(\mu\text{-}Cl)](ClO_4)$, obtained by the reaction of $NiCl_2\cdot 6H_2O$ with H_2-**106a**·6HCl in methanol using $N(Et)_3$ as base (2:1:8 molar ratio), consists of a cofacial bioctahedral

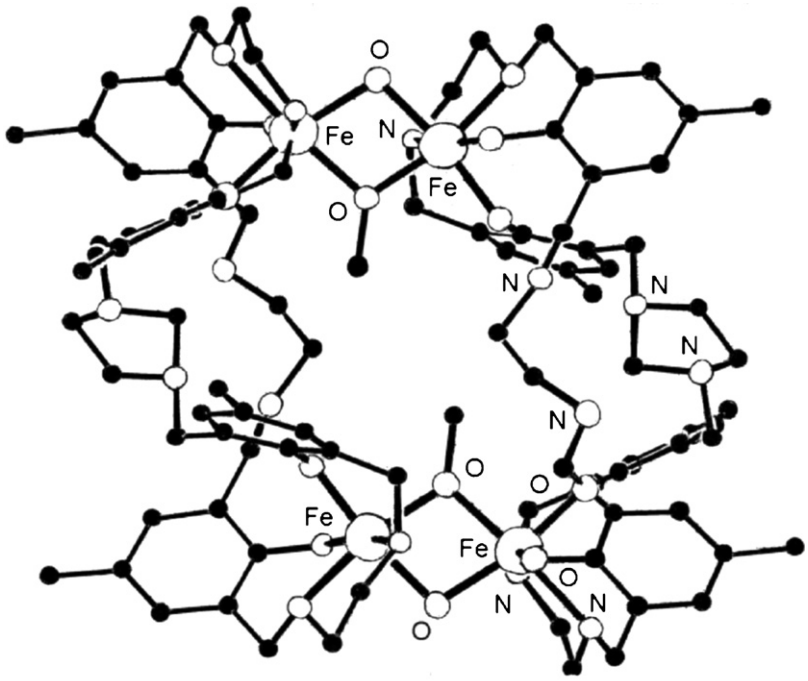

Fig. 66. Structure of $[Fe_2^{III}(\mathbf{105'})(\mu\text{-}CH_3O)(\mu\text{-}OH)]_2$.

species. The chloride coligand is found in a bridging position [96]. The structure of $[Ni_2(\mathbf{106})(\mu\text{-}Cl)](ClO_4)$, prepared under similar reaction conditions, may be simply derived from that of $[Ni_2(\mathbf{106a})(\mu\text{-}Cl)](ClO_4)$ by replacing the six NH hydrogen atoms by methyl groups [96].

Binding studies demonstrate that utilization of the permethylated ligand H_2-**106** in place of H_2-**106a** drastically alters the ease of substitution of the bridging halide substituent, presumably because of the more hydrophobic microenvironment about the μ-Cl, function in $[Ni_2(\mathbf{106})(\mu\text{-}Cl)](BPh_4)$. Thus, while the latter reacts with $[N(Bu)_4](OH)$ in acetonitrile to produce the μ-OH complex $[Ni_2(\mathbf{106})(\mu\text{-}OH)](BPh_4)$, $[Ni_2(\mathbf{106a})(\mu\text{-}Cl)](ClO_4)$ was found to be unreactive. Even the addition of a halide scavenger such as $Pb(ClO_4)_2$ did not lead to substitution of the Cl^- ion. $[Ni_2(\mathbf{106})(\mu\text{-}OH)](BPh_4)$ is isostructural with $[Ni_2(\mathbf{106})(\mu\text{-}Cl)](BPh_4)$. The OH group replaces the μ-Cl ligand, demonstrating that the substitution reaction takes place without gross structural changes of the parent complex. The separation of the nickel ions has decreased to 3.037 Å. The hydroxo unit is not involved in hydrogen bonding interactions [96].

Methanolic solutions of $[Ni_2(\mathbf{106})(\mu\text{-}Cl)](ClO_4)$ or $[Ni_2(\mathbf{106})(\mu\text{-}OH)](ClO_4)$ fix CO_2 from air at room temperature forming $[Ni_2(\mathbf{106})(\mu\text{-}CH_3OCOO)](ClO_4)$. $[Ni_2(\mathbf{106})(\mu\text{-}H_2O)]^{2+}$ and $[Ni_2(\mathbf{106})(\mu\text{-}HCO_3)]^+$ have been proposed as two subsequent intermediates in the formation of $[Ni_2(\mathbf{106})(\mu\text{-}CH_3OCOO)](ClO_4)$. The structure of $[Ni_2(\mathbf{106})(\mu\text{-}HCO_3)](BPh_4)$ supports this proposal. In the solid state the $HCO^-{}_3$ groups bridges the two nickel(II) centers in a symmetric way this complex shows a vaselike structure (type B) while in $[Ni_2(\mathbf{106})(\mu\text{-}Cl)](ClO_4)$ and $[Ni_2(\mathbf{106})(\mu\text{-}OH)](ClO_4)$ a calyx-like structure (type A) was observed (Scheme 9) [96].

$[Co_2^{II}(\mathbf{106})(\mu\text{-}Cl)](ClO_4)$, obtained with a synthetic procedure similar to that employed for the preparation of $[Ni^{II}{}_2(\mathbf{106})(\mu\text{-}Cl)](ClO_4)$ [96], reacts smoothly with 1.5 equiv. of sodium acetate or sodium cinnamate in methanol at room temperature to produce upon addition of $LiClO_4{\cdot}3H_2O$, or $NaBPh_4$, $[Co_2^{II}(\mathbf{106})(\mu\text{-}CH_3COO)](X)$ or $[Co_2^{II}(\mathbf{106})(\mu\text{-}C_6H_5CH{=}CHCOO)](X)$ ($X = ClO_4^-$, BPh_4^-), respectively [96]. The compounds exhibit good solubility in acetonitrile while are only sparingly soluble in alcohols. Unlike the chloro bridged complex $[Co_2^{II}(\mathbf{106})(\mu\text{-}Cl)](ClO_4)$, all are stable in air, even in solution. The addition of an excess of bromine to solutions $[Co_2^{II}(\mathbf{106})(\mu\text{-}CH_3COO)](ClO_4)$ and $[Co_2^{II}(\mathbf{106})(\mu\text{-}C_6H_5CH{=}CHCOO)](ClO_4)$ in acetonitrile at 0 °C, followed by recrystallization of the resulting solid from C_2H_5OH/CH_3CN, was found to form $[Co_2^{III}(\mathbf{106})(\mu\text{-}CH_3COO)](ClO_4)_3$ and $[Co_2^{III}(\mathbf{106})(\mu\text{-}C_6H_5CH{=}CHCOO)](ClO_4)_3$, respectively. The oxidation of $[Co_2^{II}(\mathbf{106})(\mu\text{-}CH_3COO)](ClO_4)$ with iodine produces the mixed $Co^{II}Co^{III}$ complex $[Co^{II}Co^{III}(\mathbf{106})(\mu\text{-}CH_3COO)](I_3)_2$. The reaction of the Co_2^{II} complexes with the related Co_2^{III} ones in CH_3CN gives rise to the mixed-valent $Co^{II}Co^{III}$ complexes $[Co^{II}Co^{III}(\mathbf{106})(\mu\text{-}CH_3COO)](ClO_4)_2$ or $[Co^{II}Co^{III}(\mathbf{106})(\mu\text{-}C_6H_5CH{=}CHCOO)](ClO_4)_3$, which are air stable and can be stored for several days at room temperature without noticeable decomposition [97].

The reactivity of $[Co_2^{II}(\mathbf{106})(\mu\text{-}Cl)](ClO_4)$ is very similar to that of $[Ni_2^{II}(\mathbf{106})(\mu\text{-}Cl)](ClO_4)$. Thus, the preparation of $[Co_2^{II}(\mathbf{106})(\mu\text{-}CH_3OCOO)](ClO_4)$ and $[Co_2^{II}(\mathbf{106})(\mu\text{-}C_6H_5OCOO)](ClO_4)$ can be accomplished by treatment of $[Co_2^{II}(\mathbf{106})(\mu\text{-}Cl)](ClO_4)$ with the corresponding alcohol in the presence of air or by transesterification of the alkyl carbonate species [97].

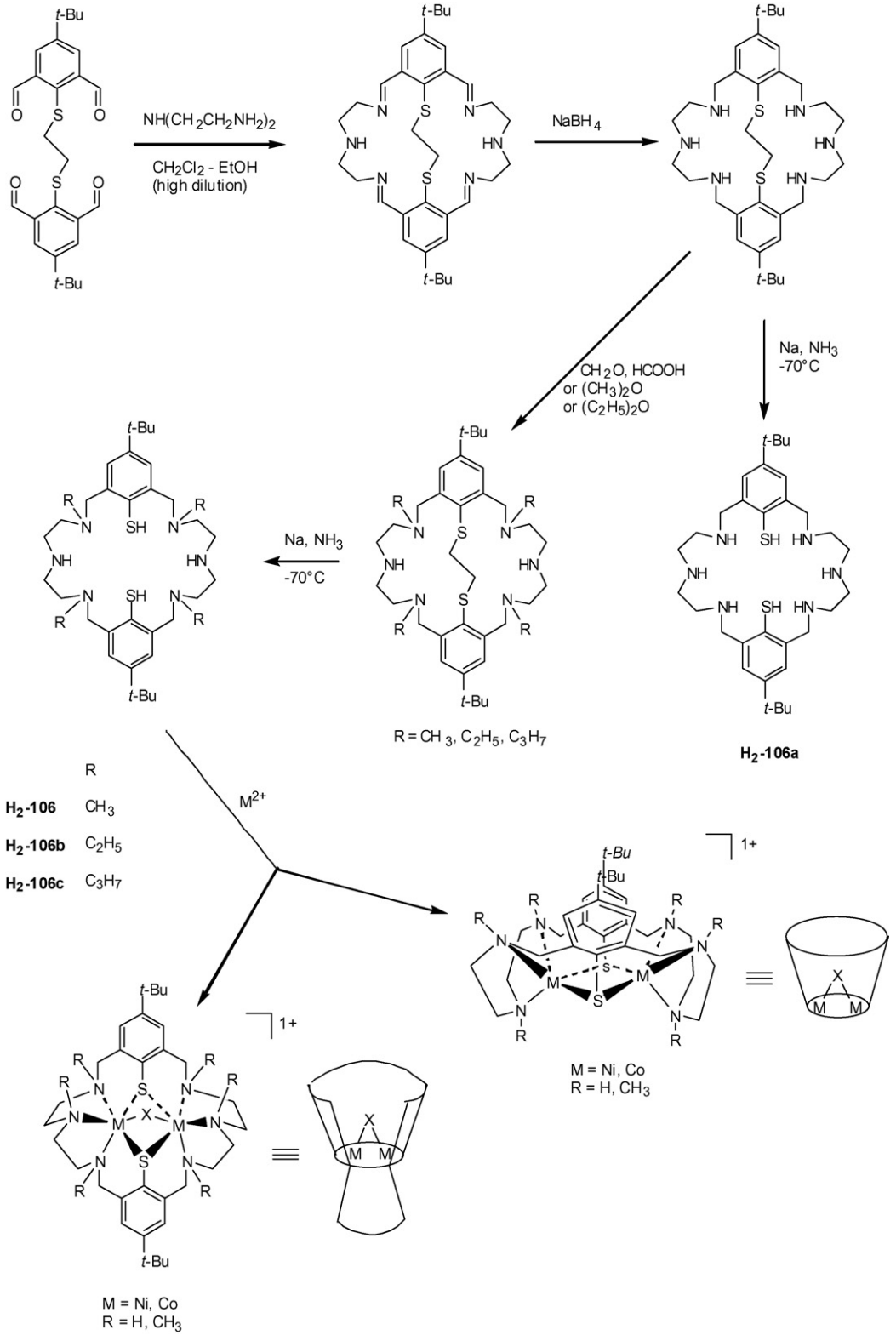

Scheme 9. Preparation of the dithiophenol macrocycles and related complexes together with a schematic representation of the corresponding metal complexes A and B (X = exogenous bridging group).

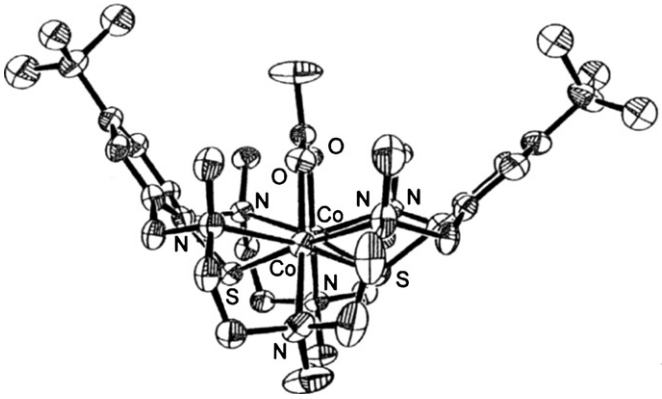

Fig. 67. Structure of $[Co_2^{II}(\mathbf{106})(\mu\text{-}CH_3COO)]^+$.

The bridging methyl carbonate group in complex $[Co_2^{II}(\mathbf{106})(\mu\text{-}CH_3OCOO)](ClO_4)$ is, unlike the carboxylate complexes, a potentially hydrolyzable substrate. Treatment of $[Co_2^{II}(\mathbf{106})(\mu\text{-}CH_3OCOO)](ClO_4)$ with an excess of bromine, produces the Co_2^{III} complex $[Co_2^{III}(\mathbf{106})(\mu\text{-}CH_3OCOO)](ClO_4)_3$ in good yields. Likewise, oxidation of $[Co_2^{II}(\mathbf{106})(\mu\text{-}CH_3OCOO)](ClO_4)$ with $[Co_2^{III}(\mathbf{106})(\mu\text{-}CH_3OCOO)](ClO_4)_3$ yields the mixed-valent $Co^{II}Co^{III}$ complex $[Co^{II}Co^{III}(\mathbf{106})(\mu\text{-}CH_3OCOO)](ClO_4)_2$[97]. The oxidations are chemically reversible: thus, addition of suitable reducing agents such as $NaBH_4$ to either the Co_2^{III} or the $Co^{II}Co^{III}$ species reforms the parent $Co^{II}Co^{II}$ complexes [97].

The structures of $[Co_2^{II}(\mathbf{106})(\mu\text{-}CH_3COO)](BPh_4)\cdot CH_3CN$, $[Co^{II}Co^{III}(\mathbf{106})(\mu\text{-}CH_3COO)](I_3)_2$, $[Co^{II}(\mathbf{106})(\mu\text{-}C_6H_5CH{=}CHCOO)](BPh_4)\cdot 2CH_3CN$, $[Co^{II}Co^{III}(\mathbf{106})(\mu\text{-}C_6H_5CH{=}CHCOO)](ClO_4)_2\cdot C_2H_5OH$, $[Co_2^{III}(\mathbf{106})(\mu\text{-}C_6H_5CH{=}CHCOO)](ClO_4)_3\cdot CH_3CN\cdot 3H_2O$, and $[Co^{II}Co^{III}(\mathbf{106})(\mu\text{-}CH_3OCOO)](ClO_4)_2\cdot 2CH_3OH\cdot H_2O$ are similar to one another.

In $[Co_2^{II}(\mathbf{106})(\mu\text{-}CH_3COO)](BPh_4)\cdot CH_3OH$ the structure of the cation $[Co_2^{II}(\mathbf{106})(\mu\text{-}CH_3COO)]^+$ is of the type B of Scheme 9, where X is by an acetate group, bridging in a symmetrical μ-1,3 fashion the two cobalt(II) centers, at a distance of 3.448 Å. The idealized symmetry is C_5 with a mirror plane passing through the two S atoms and the carboxyl carbon atom of the acetate group. Both cobalt ions are six coordinate with considerably distorted pseudo-octahedral geometry (Fig. 67). The analogous dimanganese(II), diiron(II), dinickel(II) and dizinc(II) complexes are isostructural [97].

Also in $[Co^{II}(\mathbf{106})(\mu\text{-}C_6H_5CH{=}CHCOO)](BPh_4)\cdot 2CH_3CN$ the cinnamate ion bridges the six coordinate cobalt(II) ions in a symmetrical μ-1,3 fashion. The substituents at the carbon–carbon double bond are in a *trans* position. The cinnamate ion is not planar [97].

The crystal structure of $[Co^{II}Co^{III}(\mathbf{106})(\mu\text{-}CH_3COO)](I_3)_2$ consists of discrete $[Co^{II}Co^{III}(\mathbf{106})(\mu\text{-}CH_3COO)]^{2+}$ cations and I_3^- anions. When the different oxidation states in the cobalt ions in the $Co^{II}Co^{III}$ dication are neglected, the complex can be regarded as isostructural with its parent dicobalt(II) complex. Thus, oxidation of $[Co_2^{II}(\mathbf{106})(\mu\text{-}CH_3COO)](BPh_4)$ does not affect its overall bowl-shaped structure and occurs without loss of the bridging coligand. The different metal–ligand bond lengths for the two cobalt centers reflect the different oxidation state [97].

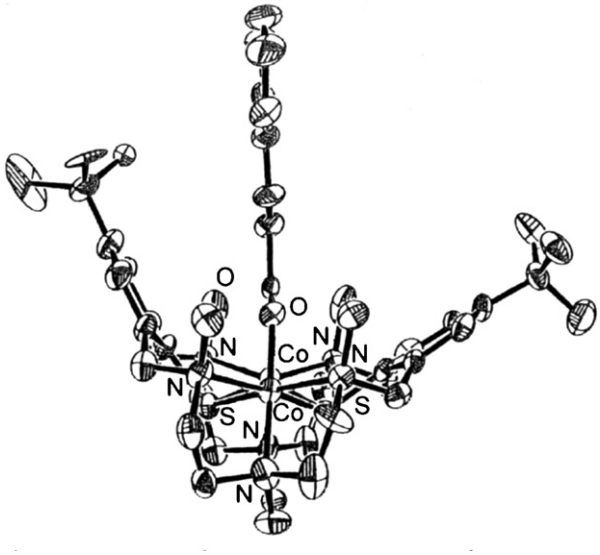

Fig. 68. Structure of $[Co_2^{III}(\mathbf{106})(\mu\text{-}C_6H_5CH{=}CHCOO)]^{3+}$.

The crystal structure of $[Co^{II}Co^{III}(\mathbf{106})(\mu\text{-}C_6H_5CH{=}CHCOO)](ClO_4)_2$ reveals the presence of discrete $[Co^{II}Co^{III}(\mathbf{106})(\mu\text{-}C_6H_5CH{=}CHCOO)]^{2+}$ dications. There are two essentially identical molecules in the asymmetric unit. Unlike $[Co^{II}(\mathbf{106})(\mu\text{-}C_6H_5CH{=}CHCOO)](BPh_4)$, the cinnamate ion bridges the two cobalt ions in an asymmetric manner. The bond distances show that one metal ion can be regarded as a d^7 high spin cobalt(II) ion and the other metal ion as a d^6 low spin cobalt(III) ion [97].

The X-ray structure analysis of $[Co_2^{III}(\mathbf{106})(\mu\text{-}C_6H_5CH{=}CHCOO)](ClO_4)_3$ confirms unambiguously that the overall structure of the parent complexes is retained in all three oxidation states (Fig. 68). The cinnamic ion is almost planar, in contrast to the twisted conformations found in the two reduced forms. Clearly the binding mode of the carboxylate ligand is a function of the oxidation state of the two metal ions [97].

Crystals of $[Co^{II}Co^{III}(\mathbf{106})(\mu\text{-}CH_3OCOO)](ClO_4)_2$ consist of $[Co^{II}Co^{III}(\mathbf{106})(\mu\text{-}CH_3COO)]^{2+}$ cations and well separated ClO_4^- anions. The metal ligand bond lengths compare well with those observed for the $Co^{II}Co^{III}$ complexes $[Co^{II}Co^{III}(\mathbf{106})(\mu\text{-}CH_3COO)](I_3)_2$ and $[Co^{II}Co^{III}(\mathbf{106})(\mu\text{-}C_6H_5CH{=}CHCOO)](ClO_4)_2$ [97].

The cyclic voltammogram in CH_3CN solution with $[N(Bu)_4](PF_6)$ as the supporting electrolyte reference of $[Co_2^{II}(\mathbf{106})(\mu\text{-}CH_3COO)](ClO_4)$ displays two reversible redox waves at $E^1_{1/2} = +0.22\,V$ ($\Delta E_p = 122\,mV$) and $E^2_{1/2} = +0.60\,V$ ($\Delta E_p = 150\,mV$) versus SCE. The cyclic voltammograms of $[Co^{II}Co^{III}(\mathbf{106})(\mu\text{-}CH_3COO)](ClO_4)_2$ and $[Co_2^{III}(\mathbf{106})(\mu\text{-}CH_3COO)](ClO_4)_3$ using the same experimental conditions, are identical within experimental error. Thus, the reversible oxidation at E^1 is assigned to the one electron oxidation of the $Co^{II}Co^{II}$ complex to the mixed-valent $Co^{II}Co^{III}$ complex $[Co^{II}Co^{III}(\mathbf{106})(\mu\text{-}CH_3COO)](ClO_4)_2$, and the second redox wave at E^2 is assigned to the oxidation of the

mixed-valent $Co^{II}Co^{III}$ complex to the fully oxidized $Co^{III}Co^{III}$ form $[Co_2{}^{III}(\mathbf{106})(\mu\text{-}CH_3COO)](ClO_4)_3$. The cyclic voltammograms of $[Co^{II}(\mathbf{106})(\mu\text{-}C_6H_5CH{=}CHCOO)](ClO_4)$ and $[Co_2{}^{II}(\mathbf{106})(\mu\text{-}CH_3COO)](ClO_4)$, show, as expected, only very small differences each other. Again, the cyclic voltammograms of their oxidized derivatives are identical within experimental error [97].

The carboxylato and methyl carbonato bridged dicobalt complexes with $[\mathbf{106}]^{2-}$ are redox-active species that undergo two stepwise one-electron-oxidation processes. All three members of each series are cleanly obtained by chemical oxidation of the parent $Co^{II}Co^{III}$ forms by using mild oxidants. The monooxidized complexes are mixed-valent $Co^{II}Co^{III}$ compounds with localized high spin $Co^{II}(d^7)$ and low spin $Co^{III}(d^6)$ ions. The fully oxidized forms represent diamagnetic $Co_2{}^{III}$ species with low spin d^6 configurations for both Co^{III} ions. The metal centered redox reactions do not affect the overall bowl-shaped structure of the parent complexes, the coligands remain in a bridging position, and the solid state structures are retained in the solution state. Infrared spectral changes that occur upon oxidation of the complexes suggest that the substrates are more susceptible to nucleophilic attack by the solvent or other reagents [97].

The dinickel(II) complexes $[Ni_2(\mathbf{106})(\mu\text{-}X)](Y)_n$ ($n=1$ for $X=Cl^-$, $NO_3{}^-$, $NO_2{}^-$, $N_3{}^-$, pyrazolate, $C_6H_5COO^-$, CH_3COO^-; $n=2$ for X = hydrazine, pyridazine, phtalazine; $Y=ClO_4{}^-$, $BPh_4{}^-$, $NO_3{}^-$, $N_3{}^-$) have been prepared by treatment of $[Ni_2(\mathbf{106})(\mu\text{-}Cl)](ClO_4)$, with a two- to five-fold excess of the sodium salt of the corresponding anion or neat hydrazine hydrate in the case of the related complex in aqueous methanolic solution. Electronic spectra in acetonitrile indicate octahedral environments about the two metal ions. Furthermore, each complex retains the coligand and the bioctahedral structure. This is also confirmed by cyclic voltammetry in CH_3CN using a standard calomel electrode (SCE). Two oxidative processes have been observed at very positive potentials assigned to the $Ni^{II}Ni^{II} \leftrightarrow Ni^{III}Ni^{II}$ and $Ni^{III}Ni^{II} \leftrightarrow Ni^{III}Ni^{III}$ processes [98].

In all these dinickel(II) complexes the macrocycle adopts the conical calixarene-like conformation above reported for the acetato-bridged complex $[Ni_2(\mathbf{106})(\mu\text{-}CH_3COO)](ClO_4)$. In this nearly C_{2v}-symmetric structure, the two nickel atoms are coordinated in a square pyramidal fashion by the two fac-$N_3(\mu\text{-}S)_2$ donor sets of the doubly deprotonated macrocycle $[\mathbf{106}]^{2-}$. Upon coordination of the exogenous coligands, distorted octahedral environments result or the two metal atoms. The structures of the dinuclear subunits are similar but not identical within the series. For example, the Ni···Ni distance varies from 3.392 to 3.683 Å. The metal···metal separations correlate with the nature of bridging ligands. Complexes having multiple atom bridges such as $\mu_{1,3}$-carboxylate display longer Ni···Ni distances than complexes with $\mu_{1,3}$-bridges, such as $NO_2{}^-$.

All coligands (X in Scheme 9) act as $\mu_{1,n}$ ($n=2$ or 3) bidentate: the nitrate ion coordinates in a symmetrical $\mu_{1,3}$-fashion, while the nitrite ion bridges in the $\mu_{1,2}$-NO nitro-form, the $N_3{}^-$ ion joints two nickel(II) centers in an end-to-end motif ($\mu_{1,3}$-$N_3{}^-$), the hydrazine ligand adopts a *cis* (eliptic) conformation (Fig. 69a) while pyrazolate, pyrazine and phtalazine bind to the $[Ni_2(\mathbf{106})]^{2+}$ fragment as bidentate bridges through their two ring nitrogens. Consequently, the Ni···Ni distances are nearly identical in these three compounds (average value is 3.394 Å). Finally, the benzoate ion chelates the two nickel(II) ions in a symmetric $\mu_{1,3}$-fashion, as observed for the similar acetate group [98].

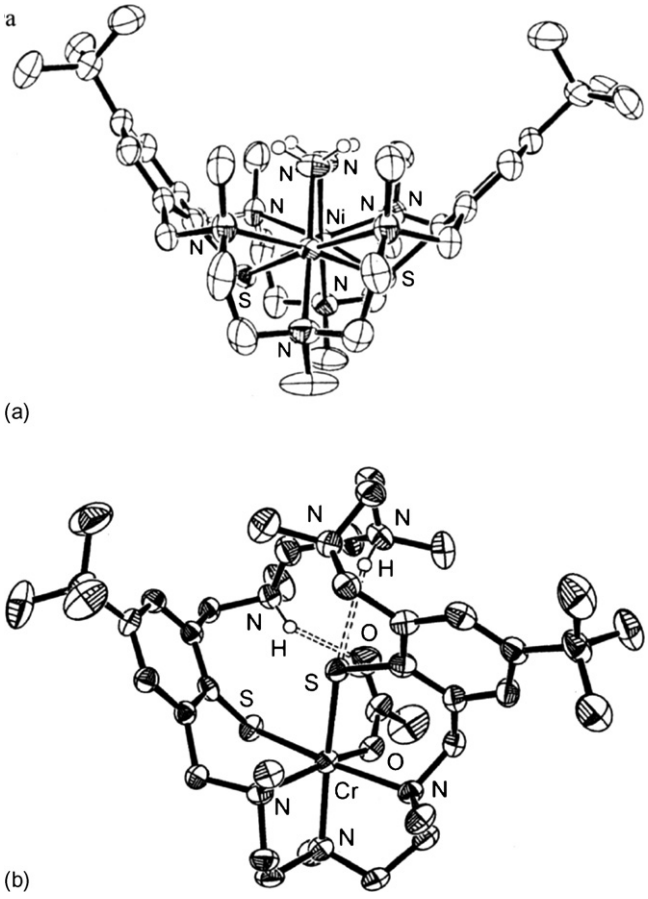

Fig. 69. Structure of $[Ni_2(\mathbf{106})(\mu\text{-}N_2H_2)]^{2+}$ (a) and $[Cr(H_2\text{-}\mathbf{106})(CH_3COO)]^{2+}$ (b).

Exchange experiments to estimate the relative binding affinities of the coligands carried out at ambient temperature in acetonitrile/ethanol (1:1) using a ten-fold excess of the coligand Y, according to the reaction $[Ni_2(\mathbf{106})(\mu\text{-}X)]^{n+} + Y \leftrightarrow [Ni_2(\mathbf{106})(\mu\text{-}Y)]^{n+} + X$, after 5 h it gave the following relative binding affinities: pyrazine ~ phthalazine < nitrate < hydrazine < nitrite < pyrazolate < azide < acetate < benzoate. The $\{Ni_2(\mathbf{106})\}^{2+}$ system binds anionic ligands preferentially over neutral species. This can be readily explained by the Coulomb attraction between the positively charged $\{Ni_2(\mathbf{106})\}^{2+}$ subunit and the negatively charged coligands.

All these complexes show ferromagnetic intramolecular exchange interactions (J ranges from 3.5 to 7.9 cm^{-1}). In contrast, the azido bridge in $[Ni_2(\mathbf{106})(\mu_{1.3}\text{-}N_3)]^+$ results in an antiferromagnetic exchange interaction ($J=-46.7\,cm^{-1}$) [98].

Treatment of a methanolic solution of [H_8-**106**]$(Cl)_6$ with solid $CrCl_2$ in the presence of $N(Et)_3$ in a 1:2:8 molar ratio, followed by the addition of CH_3COONa in air, gave a dark green solution, which upon addition of $LiClO_4$ afforded [Cr(H_2-**106**)(CH_3COO)]$(ClO_4)_2$. The chromium(III) ion is in a distorted octahedral environment, being coordinated by two sulphur and three nitrogen atoms of the macrocycle and a monodentate acetate ion. Two of the remaining three amine nitrogens are protonated. The coordinated diethylene triamine unit binds facially; this places the remaining donors in a *cis*-orientation to each other. The structure is further stabilized by intramolecular hydrogen bonding interactions (Fig. 69b) [98].

Treatment of $[\mathbf{106}]^{2-}$ with 2 equiv. of $Mn(CH_3COO)_2{\cdot}4H_2O$ resulted in a colorless solution, from which upon addition of $LiClO_4$ colorless crystals of [Mn_2(**106**)(CH_3COO)](ClO_4) precipitated. Similarly, the reaction of $[\mathbf{106}]^{2-}$ with $Fe(CH_3COO)_2$, prepared in situ from $FeCl_2$ and CH_3COONa, in the presence of $LiClO_4$ gave [Fe_2(**106**)(CH_3COO)](ClO_4). The same synthetic procedure, using $NaBPh_4$ instead of $LiClO_4$ gave rise to the corresponding complexes [M(**106**)(CH_3COO)](BPh_4) [98].

Both complexes display no absorptions in the 430–1600 nm range indicative of high-spin d^5 (Mn^{II}) and d^6 (Fe^{II}) configurations. The IR spectra indicate that the macrocycle $[\mathbf{106}]^{2-}$ forms an isostructural series of bioctahedral [M^{II}(**106**)(CH_3COO)](X) cations (M = Mn^{II}, Fe^{II}, Co^{II}, Ni^{II}, Zn^{II}; X = ClO_4^-, BPh_4^-). It is supported by the crystal structures [$Mn_2{}^{II}$(**106**)(μ-CH_3COO)](BPh_4) and [$Fe_2{}^{II}$(**106**)(μ-CH_3COO)](BPh_4). $[\mathbf{106}]^{2-}$ adopts a bowl-shaped "calixarene-like" conformation. The metal ions are in a strongly distorted octahedral N_3S_2O environment, being coordinated by two sulphur and three facially oriented nitrogen atoms of the macrocycle and a symmetrically bridging acetate ion to give a $\{N_3M^{II}(SR)_2(CH_3COO)M^{II}N_3\}$ core [98].

The cyclic voltammetry of the Mn_2 complex exhibits two waves, one at $E^1_{1/2} = +0.60$ V (versus SCE) with a peak to peak separation of 180 mV and one at $E^1_{1/2} = +1.19$ V with a peak-to-peak separation of 130 mV. The CV of the $Fe_2{}^{II}$ complex is very similar, but the two redox waves are observed at less anodic potentials at $E^1_{1/2} = +0.32$ V (versus SCE) and at $E^1_{1/2} = +1.0$ V, respectively. Thus, as observed also for the Co_2 and Ni_2 complexes, the divalent Mn^{II} and Fe^{II} oxidation states are enormously stabilized over their trivalent ones. The dizinc complex displays a single, irreversible redox wave at $E = +0.88$ V versus SCE. Since the two zinc(II) ions are redox inactive, the anodic peak can only be assigned to a ligand-centered redox reaction. It is very likely that this process corresponds to the oxidation of the thiophenolate sulphur atoms yielding a zinc-bound thiyl radical. These data show that for the other dinuclear complexes the metal centered oxidation $M^{II}M^{II}/M^{II}M^{III}$ occurs. The further oxidation processes above 0.90 V are believed to be largely ligand centered in nature [98].

The temperature dependent magnetic susceptibility measurements reveal the magnetic exchange interactions in [$M^{II}{}_2$(**106**)(CH_3COO)](ClO_4) to be relatively weak.

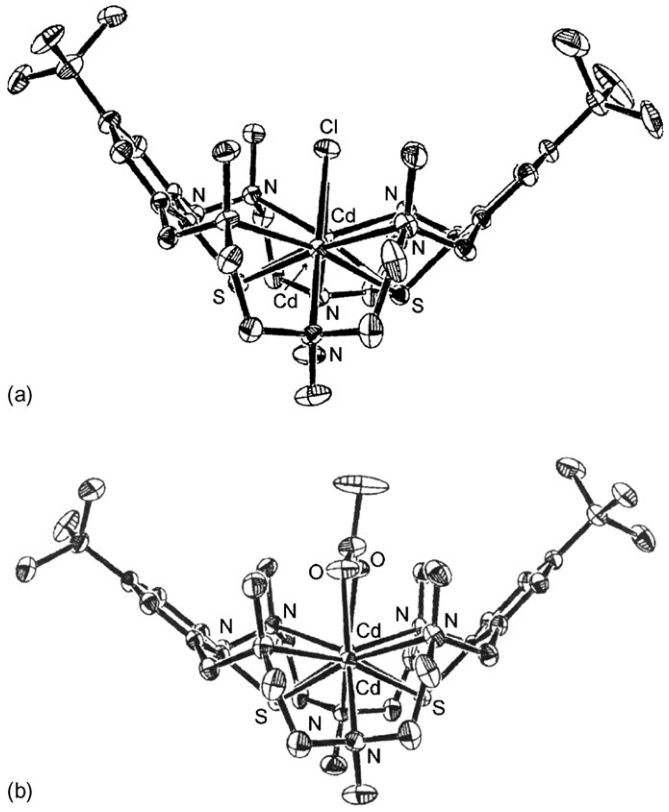

Fig. 70. Structure of [Cd_2(**106**)(μ-Cl)]$^+$ (a) and [Cd_2(**106**)(μ-CH_3COO)]$^+$ (b).

Intramolecular antiferromagnetic exchange interactions are present in the $Mn_2{}^{II}$, $Fe_2{}^{II}$, and $Co_2{}^{II}$ complexes, where $J = -5.1$, -10.6 and $-2.0\,cm^{-1}$, respectively. In contrast, in the dinickel complex a ferromagnetic exchange interaction is present ($J = +6.4\,cm^{-1}$) [98].

The complexation reactions of H_2-**106**$\cdot 6H_2O$ with $CdCl_2$, $Cd(CH_3COO)_2$, $Hg(CH_3COO)_2$ and $Pb(CH_3COO)_2$, carried out in methanol in the presence of $N(Et)_3$, produces, upon addition of an excess $LiClO_4$, [Cd_2(**106**)(μ-Cl)](ClO_4), [Cd_2(**106**)(μ-CH_3COO)](ClO_4), [Hg_2(**106**)]$(ClO_4)_2$ and [Pb_2(**106**)]$(ClO_4)_2$. [Cd_2(**106**)(μ-CH_3COO)](ClO_4) was also accessible from [Cd_2(**106**)(μ-Cl)](ClO_4) and sodium acetate. [Cd_2(**106**)(μ-Cl)](ClO_4) fixes carbon dioxide from air to give the methyl carbonate complex [Cd_2(**106**)(μ-CH_3OCOO)](ClO_4) [99].

[Cd_2(**106**)(μ-Cl)]$(BPh_4)\cdot 1.5\ CH_3OH$ exhibits idealized C_{2v} symmetry as was established by NMR spectroscopy. The cadmium(II) ions are coordinated in a distorted octahedral fashion by three facially oriented nitrogen atoms, two bridging thiophenolate sulphur atoms and a bridging halide ion. The macrocycle adopts a conical calixarene-like conformation which differs from the alternative partial cone conformation seen in the related complexes [M_2(**106**)(μ-Cl)]$^+$ (M = Co^{II}, Ni^{II}, Zn^{II}) [97,98,100]. The preference of the latter for adopting the partial cone conformation is presumably due to the smaller ionic radii of these metal ions and presumably also due to the rigid nature of the [24]-membered macrocycle (Fig. 70a) [99].

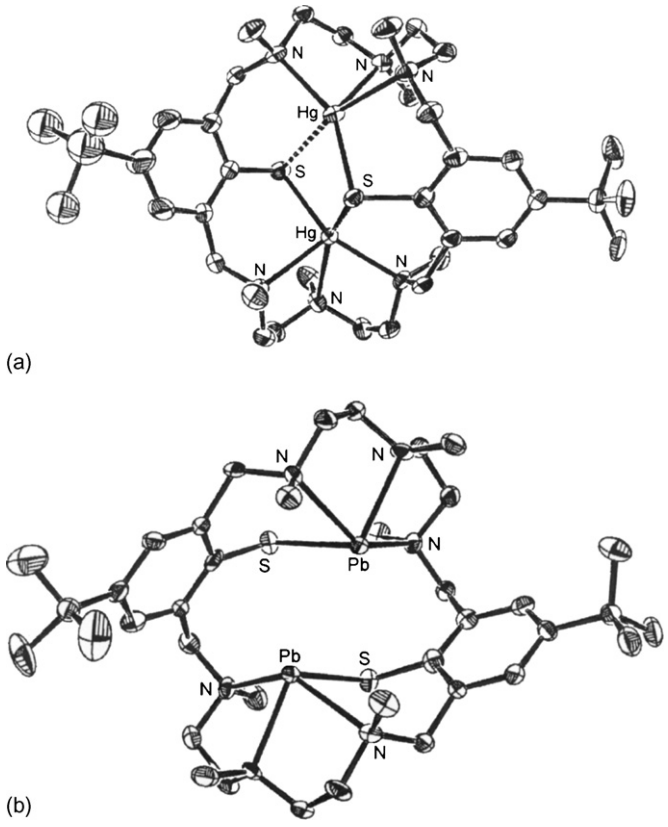

Fig. 71. Structure of $[Hg_2(\mathbf{106})]^{2+}$ (a) and $[Pb_2(\mathbf{106})]^{2+}$ (b).

$[Cd_2(\mathbf{106})(\mu\text{-}CH_3COO)](BPh_4)\cdot 2CH_3CN\cdot CH_3OH$ is isostructural with $[Zn_2(\mathbf{106})(\mu\text{-}CH_3COO)]^+$ [96]. The hexaazadithiophenolate ligand $[\mathbf{106}]^{2-}$ assumes a bowl-shaped calixarene-like conformation which is typical for carboxylato-bridged complexes of this macrocycle [97,98]. The acetate ion bridges the two cadmium ions in a symmetrical fashion with a Cd···Cd distance of 3.402 Å. It is deeply buried in the binding cavity of the $[Cd_2(\mathbf{106})]^{2+}$ fragment. As a consequence, its methyl protons are positioned above the center of the two phenyl rings in the shielding region (Fig. 70b) [99].

In $[Hg_2(\mathbf{106})](BPh_4)_2\cdot CH_3CN$ the dication bears no additional coligands and has an intramolecular Hg···Hg separation of 3.725 Å. The mercury(II) ions are surrounded by three nitrogen and two sulphur donor atoms from $[\mathbf{106}]^{2-}$ in highly irregular N_3S_2 coordination environments (Fig. 71a) [99].

Also in $[Pb_2(\mathbf{106})](ClO_4)_2\cdot CH_3CN$ the coordination environment of each lead(II) ion consists of three tertiary amine donors and one thiophenolate sulphur atom. The coordination geometry has been described as distorted square pyramidal, with the lead ion sitting above the plane formed by the four donor atoms. The empty space above the lead(II) ion on the apex of the pyramid is indicative of a stereochemically active lone pair (Fig. 71b) [99].

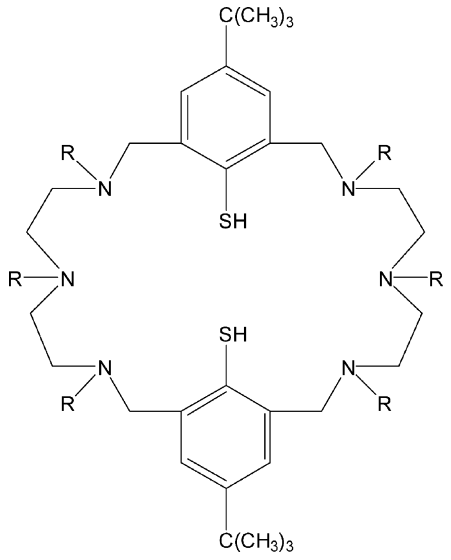

	R
H_2-**106**	CH_3
H_2-**106a**	H
H_2-**106b**	C_2H_5
H_2-**106c**	C_3H_7

The *N*-alkylated hexaazamacrocyclic dithiophenolic ligands H_2-**106b** and H_2-**106c** have been prepared by acylation of the related polyamine H_2-**106a** with the appropriate anhydride $(CH_3CO)_2O$ or $(C_2H_5CO)_2O$, followed by reduction of the resulting amides by $LiAlH_4$ in refluxing tetrahydrofuran to the corresponding polyamine. The final deprotection of the thioether functions, archived by sodium in liquid ammonia, affords the designed macrocyclic ligand which could be readily isolated as the hydrochloride salts $[H_8\text{-}\mathbf{L}](Cl)_6$ (Scheme 9) [100].

The preparation of $[M(H_2\text{-}\mathbf{L})](ClO_4)_2$ ($M = Ni^{II}$, Zn^{II}; $H_2\text{-}\mathbf{L} = H_2\text{-}\mathbf{106}$, H_2-**106c**) was achieved by addition of the metal(II) chloride hydrate to the desired macrocycle in methanol, followed by $LiClO_4$: salt metathesis of $[Ni(H_2\text{-}\mathbf{L})](ClO_4)_2$ with $NaBPh_4$ in methanol forms $[Ni(H_2\text{-}\mathbf{L})](BPh_4)_2$ [100].

In $[Ni(H_2\text{-}\mathbf{106})](ClO_4)_2$ the metal ion is five coordinate in a distorted square pyramidal geometry, formed by three nitrogen and two sulphur donors of one of the two N_3S_2 adjacent chambers of H_2-**106**. The two hydrogen atoms, bonded to the benzylic amine nitrogens, are intramolecularly hydrogen bonded to the thiolate sulphur atoms [100].

The configuration of $[Ni(H_2\text{-}\mathbf{106})](BPh_4)_2$, $[Ni(H_2\text{-}\mathbf{106c})](BPh_4)_2$ and $[Zn(H_2\text{-}\mathbf{106})](ClO_4)_2$ is very similar to that of $[Ni(H_2\text{-}\mathbf{106})](ClO_4)_2$. The $NH^+\cdots S^-$ hydrogen bonding is more significant in $[Ni(H_2\text{-}\mathbf{106c})](BPh_4)_2$: the longer *n*-propyl groups of $[\mathbf{106c}]^{2-}$ create a more lipophilic microenvironment about the $NH^+\cdots S^-$ functions which, in turn, results in a lower local dielectric constant that strengthens the electrostatic interaction in $[Ni(H_2\text{-}\mathbf{106c})](BPh_4)_2$ [100].

The mononuclear complexes $[M(H_2\text{-}\mathbf{106})](ClO_4)$ can be readily converted into the homodinuclear ones $[M_2(\mathbf{106})(CH_3COO)](ClO_4)$ when treated with the appropriate metal(II) acetate hydrate in the presence of triethylamine [100]. The reaction of $[Zn(H_2\text{-}\mathbf{106})](ClO_4)_2$ with $Cd(CH_3COO)_2\cdot 2H_2O$ and triethylamine in methanol produced a non-statistical 1:1:8 mixture of $[Zn_2(\mathbf{106})(\mu\text{-}CH_3COO)]^+$, $[Cd_2(\mathbf{106})(\mu\text{-}CH_3COO)]^+$ and $[ZnCd(\mathbf{106})(CH_3COO)]^+$: ^1H NMR investigations indicate that the spectrum of the ZnCd complex is different from that of the Zn_2 and Cd_2 one.

Furthermore, ESI-mass spectra show the presence of the cation $[ZnCd(\mathbf{106})(CH_3COO)]^+$ [100].

H_2-**106b** and H_2-**106c** react with $NiCl_2{\cdot}6H_2O$ and $N(Et)_3$ in a 1:2:8 molar ratio in methanol to afford $[Ni_2(\mathbf{106b})(\mu\text{-}Cl)](ClO_4)$ and $[Ni_2(\mathbf{106c})(\mu\text{-}Cl)](ClO_4)$ after stirring the reaction solution respectively for 3 days and 1 week at room temperature [100]. As observed for the related complex $[Ni_2(\mathbf{106})(\mu\text{-}Cl)](ClO_4)$, the bridging halide ions in $[Ni_2(\mathbf{106b})(\mu\text{-}Cl)](ClO_4)$ and $[Ni_2(\mathbf{106c})(\mu\text{-}Cl)](ClO_4)$ prove quite labile. Thus, the reactions of the respective complexes $[Ni_2(L)(\mu\text{-}Cl)](ClO_4)$ (H_2-L = H_2-**106b**, H_2-**106c**) with sodium acetate proceed smoothly and yield green solutions, which depositate green crystals of $[Ni_2(L)(\mu\text{-}CH_3COO)](ClO_4)$. The same compounds can also be directly synthesized from the respective ligands and $Ni(CH_3COO)_2{\cdot}6H_2O$ [100].

$[Ni_2(\mathbf{106b})(\mu\text{-}CH_3OCOO)](ClO_4)$ was obtained by a carbonation reaction in air of the green μ-hydroxo species $[Ni^{II}{}_2(\mathbf{106b})(\mu\text{-}OH)]^+$ prepared in situ from $[Ni_2(\mathbf{106b})(\mu\text{-}Cl)](ClO_4)$ and NaOH; the conversion of the methyl carbonate complex $[Ni_2(\mathbf{106b})(\mu\text{-}CH_3OCOO)](ClO_4)$ into the ethyl carbonate species $[Ni_2(\mathbf{106b})(\mu\text{-}C_2H_5OCOO)](ClO_4)$ was accomplished by a transesterification reaction with neat ethanol [100].

$[Ni_2(H\text{-}\mathbf{106b})](ClO_4)_3$ forms rather unexpectedly during attempts to prepare $[Ni_2(\mathbf{106b})(\mu\text{-}OCH_3)](ClO_4)_2$ by reaction of $[Ni_2(\mathbf{106b})(\mu\text{-}Cl)](ClO_4)$ with $Pb(ClO_4)_2$ in methanol. This complex does not bear coligands and reforms $[Ni_2(\mathbf{106b})(\mu\text{-}Cl)](ClO_4)$ when treated with $[N(Et)_4](Cl)$ in methanol. Also it produces $[Ni_2(\mathbf{106b})(\mu\text{-}CH_3COO)](ClO_4)$ upon addition of CH_3COONa [100].

The transformation of $[Ni_2(\mathbf{106b})(\mu\text{-}Cl)](ClO_4)$ into $[Ni_2(\mathbf{106b})(\mu\text{-}CH_3COO)](ClO_4)$ involves a conformational change of the macrocycle from a conical calix-arene-like conformation to a partial cone one (i.e. from type A to type B of Scheme 9). This requires an inversion of the configurations of the tertiary nitrogen donor atoms. However, this can only proceed by dissociation of the metal-nitrogen bonds. The crystal structure of $[Ni_2(H\text{-}\mathbf{106b})](ClO_4)_3$ reveals such non-coordinating nitrogen donor atoms. Thus, $[Ni_2(\mathbf{106b})](ClO_4)_3$ is presumably an intermediate in the above substitution reactions [100].

The acetato-bridged dizinc complex $[Zn_2(\mathbf{106b})(\mu\text{-}CH_3COO)](ClO_4)$ was obtained by the direct reaction of $[H_8\text{-}\mathbf{106b}](Cl)_6$ with $Zn(CH_3COO)_2{\cdot}2H_2O$ and $N(Et)_3$ in methanol. Attempts to prepare a chloro-bridged complex such as $[Zn_2(\mathbf{106b})(\mu\text{-}Cl)](ClO_4)$ were unsuccessful [100].

Similarly, $[Co_2(\mathbf{106b})(\mu\text{-}Cl)](ClO_4)$, prepared by reaction of $[H_8\text{-}\mathbf{106b}](Cl)_6$ and $CoCl_2{\cdot}6H_2O$ in the presence of $N(Et)_3$ in a 1:2:8 molar ratio in methanol, gives rise to $[Co(\mathbf{106b})(\mu\text{-}CH_3COO)](ClO_4)$ when treated with CH_3COONa in methanol [100].

The structures of $[Co^{II}(\mathbf{106})(\mu\text{-}Cl)]^+$ and $[Co_2(\mathbf{106})(\mu\text{-}CH_3COO)]^+$ have been shown to be of calix-type (type A) and vase-type (type B), respectively. On the basis of spectroscopic similarities, analogous structures are likely for the complexes supported by $[\mathbf{106b}]^{2-}$. This is confirmed by the X-ray structure determination of $[Co_2(\mathbf{106b})(\mu\text{-}CH_3COO)](BPh_4)$ [100].

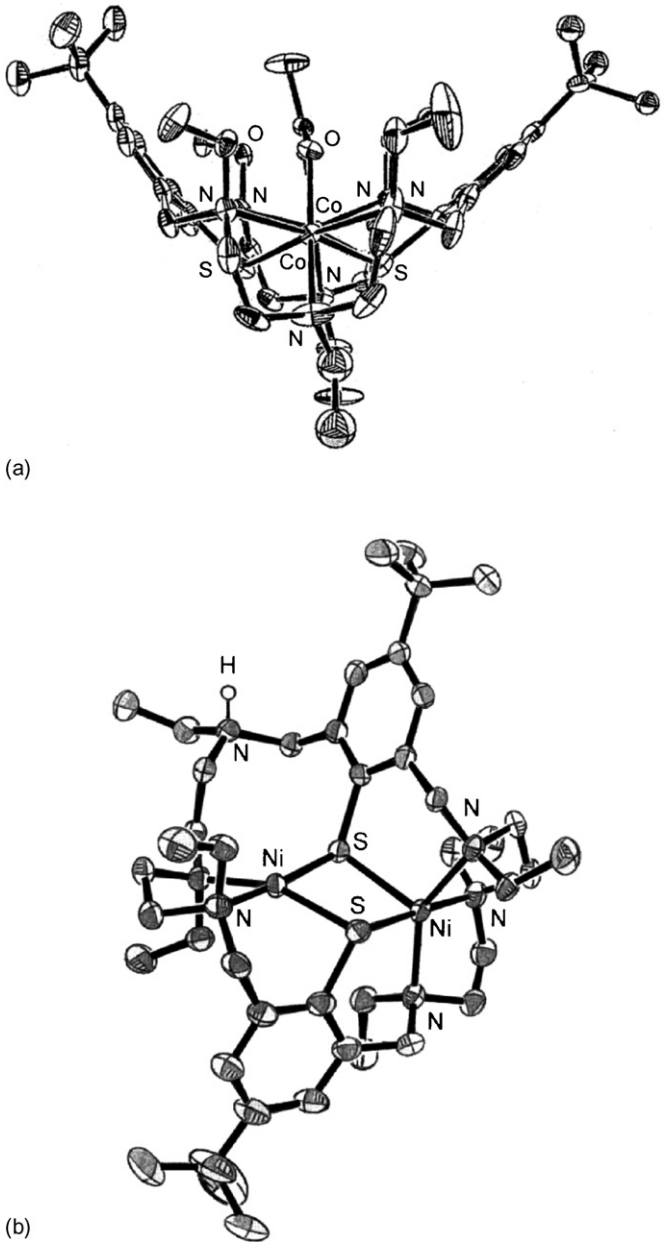

Fig. 72. Structure of $[Co_2{}^{II}(\mathbf{106b})(\mu\text{-}CH_3COO)]^+$ (a) and $[Ni_2(H\text{-}\mathbf{106b})]^{3+}$ (b).

All these complexes are stable in air both in solution and in the solid state. The perchlorate salts are very soluble in a range of common polar organic solvents (CH_3CN, C_2H_5OH, CH_3OH). The complexes with the longer alkyl chains also exhibit some solubility in apolar solvents such as cyclohexane or toluene.

The overall structures of these complexes are very similar to the corresponding complexes of the parent permethylated ligand system $[\mathbf{106}]^{2-}$. Furthermore, the structures of $[Ni_2(\mathbf{106c})(\mu\text{-}CH_3COO)](ClO_4)$, $[Ni_2(\mathbf{106b})(\mu\text{-}C_2H_5COO)](ClO_4)$, $[Zn_2(\mathbf{106b})(\mu\text{-}CH_3COO)](ClO_4)$ and $[Co_2(\mathbf{106b})(\mu\text{-}CH_3COO)](ClO_4)$ are very similar each other (Fig. 72a). The macrocycles adopt the conformation of type B of Scheme 9, previously reported for $[Ni_2(\mathbf{106})(\mu\text{-}CH_3COO)](ClO_4)$. In each case, the two metal ions are coordinated in a square pyramidal fashion by the two fac-

$N_3(\mu\text{-}S)_2$ donor sets of the doubly deprotonated macrocycles. The coordination of the exogenous coligands generates distorted octahedral environments for the metal ions. The central $\{N_3M(\mu\text{-}S)_2(\mu\text{-}RCOO)MN_3\}$ cores are very similar [100].

The structure of $[Ni_2(H\text{-}\mathbf{106b})](ClO_4)_3\cdot 3CH_3OH\cdot H_2O$ confirms that this complex bears no coligands and features two differently coordinated nickel(II) ions (Fig. 72b). One nickel ion is coordinated in a distorted planar fashion by two *cis*-oriented nitrogen ion and two bridging thiophenol are sulphur atoms. The other nickel ion is five coordinate. The protonated amine donor is out of range of bonding interaction with the metal ions and points away from them. The coordination geometry of the four coordinate nickel ion is significantly distorted from square planar toward tetrahedral. The coordination environment around the five coordinate nickel ion is distorted trigonal bipyramidal. The Ni···Ni separation is 3.319 Å. The two nickel(II) ions are almost completely surrounded by the apolar N-ethyl substituents from the macrocycle. This steric crowding about the coordinatively unsaturated dinickel site might explain its higher stability relative to the very unstable trication $[Ni_2(H\text{-}\mathbf{106})]^{3+}$

Thus, H_2-**106b** and H_2-**106c**, the N-alkylated variants of H_2-**106** bearing ethyl and propyl groups in place of the methyl functions, support the formation of dinuclear complexes with a bowl-shaped structure. The binding pocket of the complexes expands to a more conical, calixarene-like cavity upon going from the $[\mathbf{106}]^{2-}$ to the $[\mathbf{106b}]^{2-}$ or $[\mathbf{106c}]^{2-}$ ligand system. The rate of the substitution reactions and the ability to fix small molecules is not drastically altered by the longer alkyl chains. Finally, H_2-**106b** and H_2-**106c** allow for the stabilization of reactive intermediates. The use of the longer alkyl chains expands the binding pocket of the complexes to a more conical, calixarene-like cavity and has allowed for the isolation of the trication $[Ni_2(H\text{-}\mathbf{106b})]^{3+}$, which is an intermediate in the substitution reactions of $[Ni_2(\mathbf{106b})(\mu\text{-}Cl)](ClO_4)$. The complex $[Ni_2(H\text{-}\mathbf{106b})]^{3+}$ reveals a new coordination mode of the supporting ligand with adjacent four and five coordinate nickel(II) ions. Its higher stability is presumably a consequence of the increased steric crowding imposed by the longer alkyl chains of $[\mathbf{106b}]^{2-}$. These results demonstrate that these highly functionalized ligand systems allow the stabilization of reactive intermediates [100].

2.4. [2 + 2] macrocyclic Schiff base complexes and related polyamine derivatives, containing =N–N= or =N–NH– endogenous bridging groups

The diformyl derivatives more recently used (3,6-diformylpyridazine, 1H-pyrazole-3,5-dicarboxylaldehyde and 2,5-diacetyl-1H-1,2,4-triazole) contain the neutral or negatively charged =N–N= or –N–N$^-$– groups, which can bridge two metal ions. Their synthetic procedure was already reported in recent reviews [3,5,102]. These precursors form [2 + 2] macrocyclic Schiff bases when reacted with the appropriate polyamine $H_2N\text{-}R\text{-}NH_2$ using the self-condensation or template procedure.

2.4.1. Pyridazine-based systems

Earlier work has comprehensively reported in excellent papers [4,5]. Under particular conditions the larger [4 + 4] macrocycles or their complexes have been obtained. For instance, the condensation of 3,6-diformylpyridazine with 1,3-diaminopropane in the presence of lead(II) perchlorate as templating agent gives rise to [4 + 4] or [2 + 2] macrocyclic complexes depending on the reaction conditions employed: a 2:2:1 ratio results in the formation of the [4 + 4] complex $[Pb_2(\mathbf{107})](ClO_4)_4$ whereas a 1:1:1 ratio forms the [2 + 2] complex $[Pb_2(\mathbf{108})](ClO_4)_4$, as confirmed also by X-ray structural investigations [101]. Furthermore, the [4 + 4] complex suffers a ring contraction to the corresponding [2 + 2] macrocyclic complex when transmetalation reaction of $[Pb_2(\mathbf{107})](ClO_4)_4$ with transition metal ions was carried out. This reaction clearly shows that $[Pb_2(\mathbf{107})](ClO_4)_4$ is an excellent starting complex for the preparation of [2 + 2] complexes with transition metal ions otherwise hardly accessible (Scheme 10) [101]. For instance, $[Co_2(\mathbf{108})](ClO_4)_4$ has been prepared in good yield by transmetalation of $[Pb_2(\mathbf{107})](ClO_4)_4$ with four equivalents of $Co(ClO_4)_2\cdot 6H_2O$. Direct reaction of the macrocycle components, 3,6-diformylpyridazine and 1,3-diaminopropane, using cobalt(II) as a template ion, failed to produce the dicobalt complex [102].

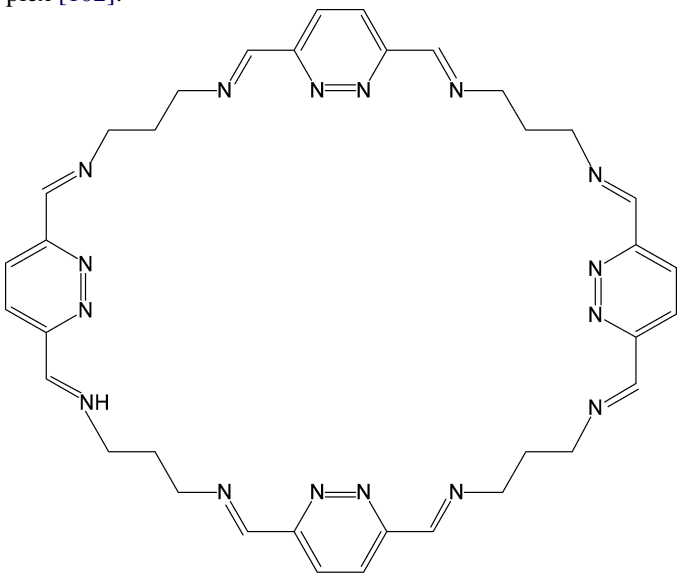

107

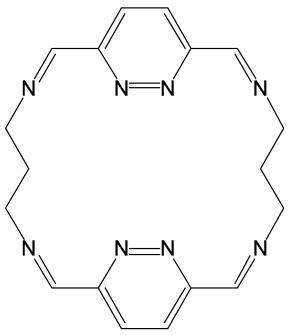

108

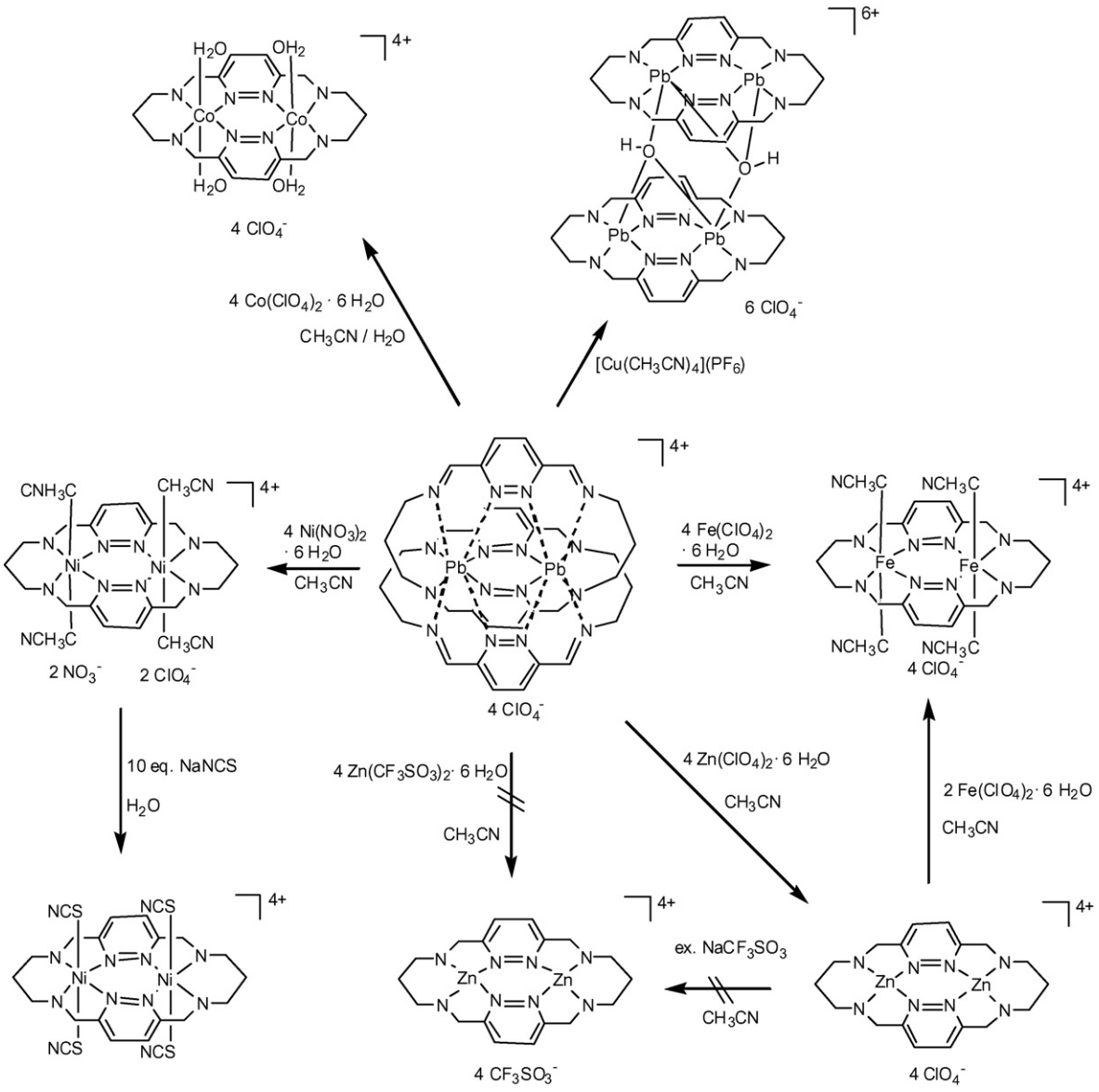

Scheme 10. Transmetalation of $[Pb^{II}(\mathbf{108})](ClO_4)_4$.

The addition of small quantity of water (∼9% by volume) to an acetonitrile solution of $[Co_2(\mathbf{108})](ClO_4)_4$, changes the color form deep red to bright orange. Slow diffusion of diethyl ether into this orange solution gives $[Co_2(\mathbf{108})(H_2O)_4](ClO_4)_4{\cdot}H_2O{\cdot}2CH_3CN$. In this complex both cobalt(II) centers are in a distorted octahedral environment, the six donor atoms consisting of two pyridazine and two imine nitrogens from the macrocycle and two water oxygens. The cobalt(II) ions sit almost exactly in the N_4 basal plane. There is an extensive hydrogen-bonding network between the water molecules coordinated with the cobalt ions, the perchlorate anions and the various solvent molecules present in the unit cell (Fig. 73a) [102].

The reaction of $[Co_2(\mathbf{108})(H_2O)_4](ClO_4)_4$ with $Na_2S_2O_6$ gives $[Co_2(\mathbf{108})(H_2O)_4](S_2O_6)_2{\cdot}4H_2O$, which affords $[Co_2(\mathbf{108})](S_2O_6)_2$ when dried in vacuo. The structure of $[Co_2(\mathbf{108})(H_2O)_4](S_2O_6)_2{\cdot}4H_2O$ demonstrates the non-coordinating nature of the dithionate anion. Both cobalt(II) ions are in an octahedral environment, the six donor consisting of four nitrogen donors of two pyridazine and two imine donors from the macrocycle and two water oxygens [102].

Additions of two equivalents of NaN_3 to $[Co_2(\mathbf{108})](ClO_4)_4$ results in the isolation of the orange-brown diazide complex $[Co_2(\mathbf{108})(N_3)_2](ClO_4)$. Similarly, reaction of the deep red tetraacetonitrile adduct $[Co_2(\mathbf{108})(CH_3CN)_4](ClO_4)_4$, in CH_3CN with appropriate anions affords $[Co_2(\mathbf{108})(NCO)_3](ClO_4)$, $[Co_2(\mathbf{108})(NCS)_2(SCN)_2]$ and $[Co_2(\mathbf{108})(Cl)_2](ClO_4)_2$. In the case of the formation of the $[Co_2(\mathbf{108})(NCO)_3](ClO_4)$, the addition of three equivalents of NaOCN to $[Co_2(\mathbf{108})(CH_3CN)_4](ClO_4)_4$ resulted in the crystallization of the desired product. Other amounts of NaOCN gave

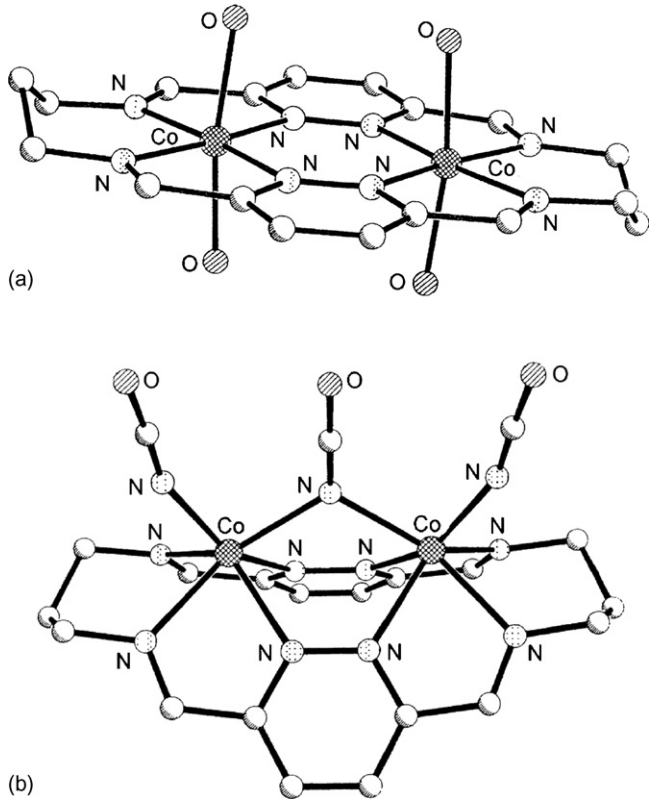

Fig. 73. Structure of $[Co_2(\mathbf{108})(H_2O)_4]^{4+}$ (a) and $[Co_2(\mathbf{108})(NCO)_3]^{+}$ (b).

$[Co_2(\mathbf{108})(NCO)_3](ClO_4)$ contamined with $[Co_2(\mathbf{108})](ClO_4)_4$ or excess NaOCN. In the case of $[Co_2(\mathbf{108})(NCS)_2(SCN)_2]$, a large excess of NaNCS was needed to ensure complete reaction, although some of the tetrathiocyanate complex was formed even when only two equivalents of NCS^- were present. $[Co_2(\mathbf{108})(Cl)_2](ClO_4)_2$ was formed from $[Co_2(\mathbf{108})(NCO)_3](ClO_4)$ by adding a stoichiometric amount of $[N(Et)_4](Cl)\cdot 4H_2O$. The coordinated and uncoordinated water molecules are involved in an extensive hydrogen-bonding network with the dithionate anions [102].

Orange crystals of $[Co_2(\mathbf{108})(NCO)_3](ClO_4)$ are marginally suitable for X-ray diffractions studies, however the overall structure of the complex is perfectly clear (Fig. 73b). While the bowled shape of the ligand **108** is unusual, it has been observed before for the manganese(II) thiocyanate complex of **108** [102].

The magnetic behaviour of $[Co_2(\mathbf{108})(H_2O)_4](ClO_4)_4$, $[Co_2(\mathbf{108})(H_2O)_4](S_2O_6)_2\cdot 4H_2O$, $[Co_2(\mathbf{108})(N)_3](ClO_4)_4$ and $[Co_2(\mathbf{108})(NCO)_3]ClO_4$ is typical of high-spin ($S = 3/2$) dinuclear cobalt(II) complexes exhibiting weak antiferromagnetic exchange with small negative $2J$ values (-7 to $-20\,cm^{-1}$). $[Co_2(\mathbf{108})](ClO_4)_4$, $[Co_2(\mathbf{108})](ClO_4)_4\cdot 4CH_3CN$ and $[Co_2(\mathbf{108})(NCS)_2(SCN)_2]$ are rare examples of binuclear complexes displaying simultaneous spin crossover ($3/2 \leftrightarrow 1/2$) at high temperatures and antiferromagnetic exchange of the low spin d^7–d^7 ions at low temperatures ($2J = -10$ to $-14\,cm^{-1}$) [102].

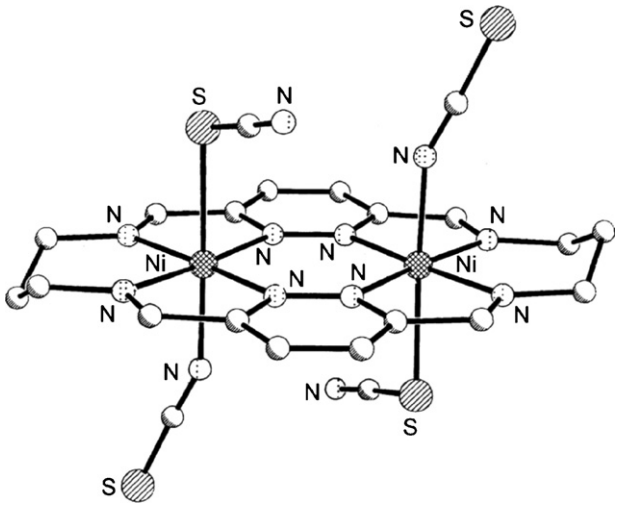

Fig. 74. Structure of $[Ni_2(\mathbf{108})(NCS)_2(SCN)_2]$.

Treatment of $[Pb_2(\mathbf{107})](ClO_4)_4$ with four equivalents of $Ni(NO_3)_2\cdot 6H_2O$ leads to the expected ring contraction from the [4 + 4] to the [2 + 2] macrocycle with the formation of $[Ni_2(\mathbf{108})(CH_3CN)_4](ClO_4)_2(NO_3)_2$ which, by reaction with an excess of sodium thiocyanate in water, turns into $[Ni_2(\mathbf{108})(NCS)_2(SCN)_2]$ [103]. The compound possesses a center of inversion located in the plane of the macrocycle between the two metal centers. Each nickel(II) ion is octahedrally coordinated in an almost planar macrocycle. The axial positions are occupied by thiocyanates, one of which is nitrogen bound, the other one sulphur bound. The differing coordination modes adopted by the thiocyanates are consistent with the two ν C≡N IR bands observed. The Ni···Ni distance is 3.817 Å (Fig. 74) [103].

Attempts to make a copper(I) complex of **108** by treatment of $[Pb_2(\mathbf{107})](ClO_4)_4$ with $[Cu(CH_3CN)_4](PF_6)$ give rise to few crystals which show that, though ring contraction from the [4 + 4] to the [2 + 2] macrocycle has occurred, the expected transmetalation of the lead(II) ions by copper(II) ions does not occur. Instead, the doubly hydroxo-bridged dimeric dilead(II) complex, $[Pb_4(\mathbf{108})_2(\mu_3\text{-}OH)_2](ClO_4)_6\cdot 2CH_3CN$ forms. The X-ray structure confirms a doubly μ_3-hydroxo-bridged dimers of complex dications, with the macrocycle being significantly folded. Both lead ions are located above their respective N_4 mean planes. However, the two lead centers are coordinated in different coordination patterns. Each of them bonds to four nitrogen donors, but while one lead ion only bonds to one hydroxide ion, the other lead ion possesses two hydroxide ions in its coordination sphere. The oxygen atom of the hydroxide ion bridges three lead ions in an almost symmetrical pattern. There are several weak lead-perchlorate interactions present in the structure (Fig. 75) [103]. It must be noted that Cu_2^{II}, Cu^ICu^{II}, Cu_2^I and Cu_4^I complexes of **108** were reported earlier [4,5].

$[Zn_2(\mathbf{108})](ClO_4)_4$ was prepared by transmetalation of $[Pb_2(\mathbf{107})](ClO_4)_4$ with $Zn(ClO_4)_2\cdot 6H_2O$. Attempts to form the potentially less explosive triflate analogue, $[Zn_2(\mathbf{108})](CF_3SO_3)_4$, by either a transmetalation reac-

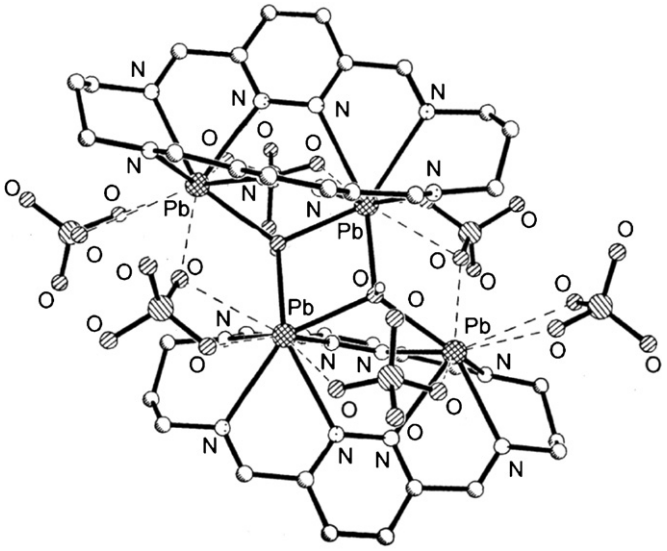

Fig. 75. Structure of $[Pb_4(\mathbf{108})_2(\mu_3\text{-}OH)_2](ClO_4)_6$.

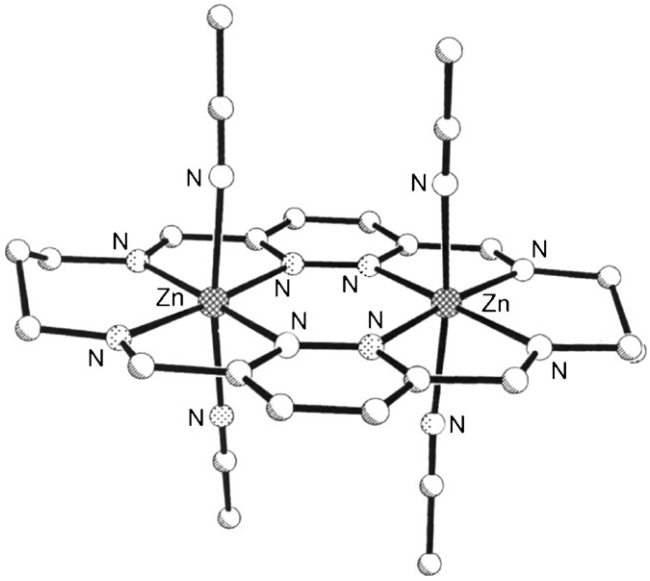

Fig. 76. Structure of $[Zn_2(\mathbf{108})(CH_3CN)_4]^{4+}$.

tion on $[Zn_2(\mathbf{108})](ClO_4)_4$ or a metathesis reaction on $[Zn_2(\mathbf{108})](ClO_4)_4$, were unsuccessful: in both cases only $[Zn_2(\mathbf{108})](ClO_4)_4$ was isolated, albeit in reduced yield. In contrast, the template synthesis of $[Zn_2(\mathbf{108})](CF_3SO_3)_4$ from 3,6-diformylpyridazine and 1,3-diaminopropane in the presence of $Zn(CF_3SO_3)_2{\cdot}6H_2O$ was successful. Analogously, transmetalation of $[Pb_2(\mathbf{107})](ClO_4)_4$ with four equivalents of $Fe(ClO_4)_2{\cdot}6H_2O$ leads to the formation of the low spin iron(II) complex $[Fe_2(\mathbf{108})(CH_3CN)_4](ClO_4)_4$, which slowly decomposes in solution due to hydrolysis and oxidation. This prevents the obtainment of the pure diiron(II) complex [103].

The structure of $[Zn_2(\mathbf{108})(CH_3CN)_4](ClO_4)_4$ reveals the presence of four bound CH_3CN molecules. Drying under vacuum removes these coordinated molecules form the complex, a feature not uncommon for the dinuclear complexes with the macrocycle **108**. The zinc(II) centers are in a distorted octahedral donor environment. The Zn···Zn separations in the two independent molecules are 3.826 and 3.823 Å. The macrocyclic ligand is nearly undistorted with the metal centers sitting almost exactly in their respective N_4 macrocyclic basal planes. The donors are all nitrogen atoms, consisting of two pyridazine and two imine donors form the macrocycle and two coordinated CH_3CN molecules (Fig. 76) [103].

The macrocyclic Schiff base complex $[Ba_2(\mathbf{108a})(ClO_4)_4(H_2O)]$ was synthesized by the reaction of 3,6-diformylpyridazine, N^1-(2-aminoethyl)-N^1-(methylene-2-pyridyl)-ethane-1,2-diamine and barium perchlorate in a 2:2:2 molar ratio in acetonitrile at room temperature. Unlike for $[Pb_2(\mathbf{108})](ClO_4)_4$, using lead(II) ions to template the **108a** macrocyclic ring formation proved unsuccessful. This is presumably due to the significantly bigger ionic radius of the barium(II) ion (1.34 Å versus 1.20 Å of the lead(II) ion) which enables it to better stabilize the larger **108a** macrocyclic ring through the thermodynamic template effect. Also in contrast to the synthesis of **108**, there was no indication of the formation of a [4 + 4] product and even the alteration of the molar ratio of 3,6-diformylpyridazine, the functionalized polyamine and $Ba(ClO_4)_2$ to 2:2:1 had no effect on the outcome [104].

$[Ba_2(\mathbf{108a})(ClO_4)_4(H_2O)]$ (Fig. 77a), contains two barium(II) ions doubly bridged by the pyridazine moieties of the macrocycle and additionally by a single water molecule (Ba···Ba 4.955 Å). The environment around the barium centers is not closely related to a regular polyhedron and each barium ion is surrounded by ten donors consisting of six nitrogen donors (comprised of one nitrogen of each pyridazine, two imine nitrogens, one tertiary amino nitrogen, one pyridyl nitrogen from the macrocycle) and four oxygen donors from two perchlorate anions (one η^2, the other η^1 with a hydrogen bridge to a water hydrogen atom) and one water molecule. The **108a** macrocyclic ring is not as flat and rigid as **108** is in most of its complexes [104].

It was impossible to prepare pure homodinuclear complexes with d-transition metal ions by a similar template procedure. $[Cu_2^{II}(\mathbf{108a})](ClO_4)_4{\cdot}2CH_3CN$, $[Fe_2^{II}(\mathbf{108a})(CH_3CN)_2](ClO_4)_4$ and two manganese complexes with the same formula $[Mn_2^{II}(\mathbf{108a})(CH_3CN)(H_2O)](ClO_4)_4$ were synthesized by a transmetalation reaction of $[Ba_2(\mathbf{108a})(ClO_4)_4(H_2O)]$ with two molar equivalents of the desired transition metal perchlorate at room temperature in acetonitrile. An immediate color change was observed in all cases, blue for $[Cu_2(\mathbf{108a})](ClO_4)_4$, dark green for $Fe_2(\mathbf{108a})(CH_3CN)_2](ClO_4)_4$ and yellow for $[Mn_2(\mathbf{108a})(CH_3CN)(H_2O)](ClO_4)_4$. No precipitate formed during these reactions as all these complexes have good solubility in acetonitrile. In all cases, single crystals, suitable for X-ray structure determinations were obtained over 3 days by slow diethyl ether vapour diffusion into the reaction solution at ≃+4 °C [104].

In $[Cu_2^{II}(\mathbf{108a})](ClO_4)_4{\cdot}2CH_3CN$ (Fig. 77b), due to its different coordination preferences and its much smaller ionic radius

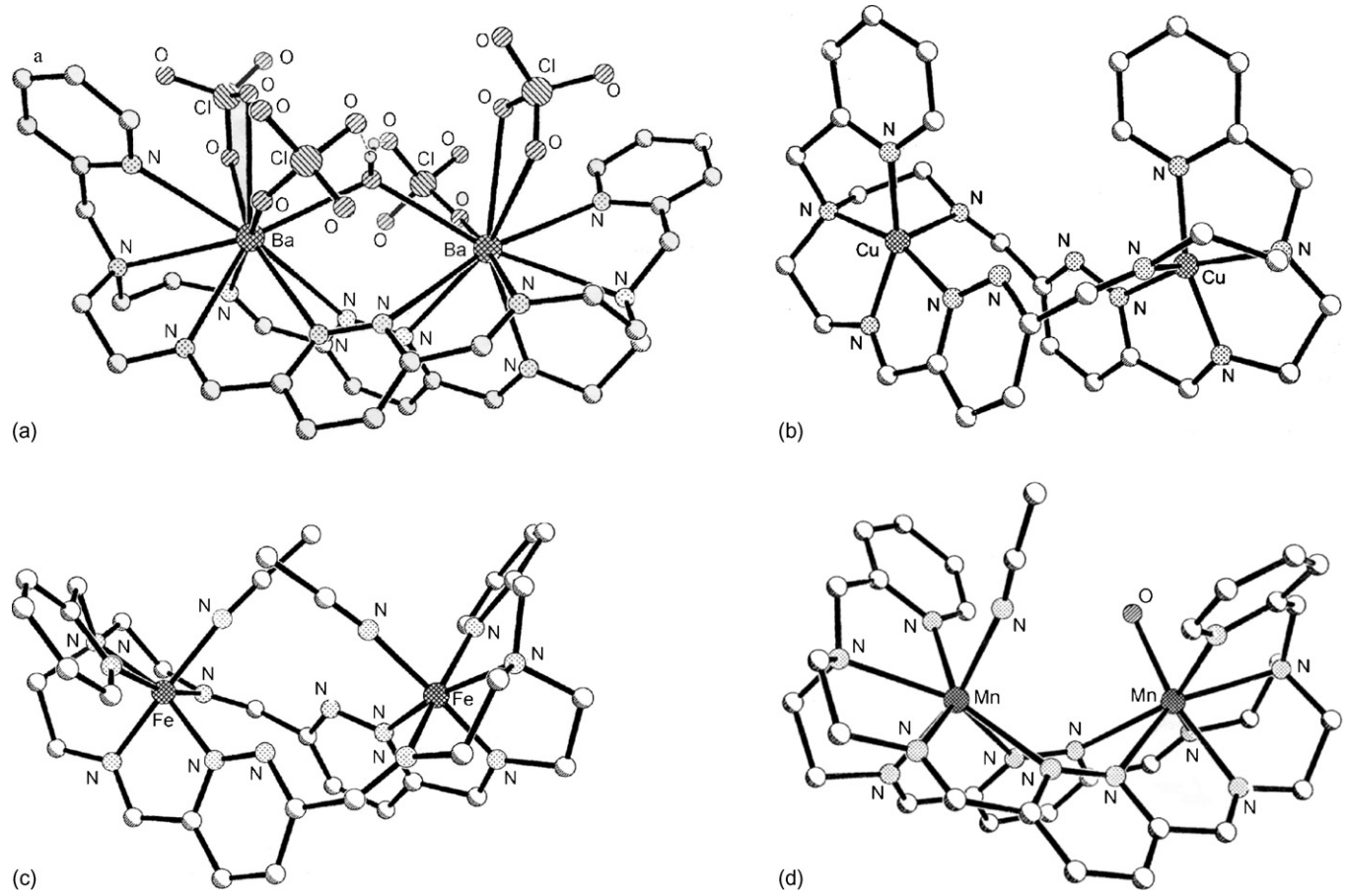

Fig. 77. Structure of $[Ba_2(\mathbf{108a})(ClO_4)_4(H_2O)]$ (a), $[Cu_2(\mathbf{108a})]^{4+}$ (b), $[Fe_2^{II}(\mathbf{108a})(CH_3CN)_2]^{4+}$ (c) and $[Mn_2^{II}(\mathbf{108a})(CH_3CN)(H_2O)]^{4+}$ (d).

compared to the barium(II) ion, each copper center is in a N_5 square pyramidal environment which is only slightly trigonally distorted. All ten of the nitrogen donors are provided by **108a**. In each case the four equatorial nitrogen donors are provided by a pyridazine ring, an imine, a tertiary amine and a pyridine ring of the macrocycle while the apical site is occupied by an imine nitrogen atom. To achieve this the macrocyclic framework folds, providing a cleft-like structure. The Cu···Cu separation (5.937 Å) is almost 1 Å longer than the distance between the barium centers in $[Ba_2(\mathbf{108a})(ClO_4)_4(H_2O)]$, reflecting the non-bridging mode of the pyridazine rings in $[Cu_2(\mathbf{108a})](ClO_4)_4$ [104].

In $[Fe_2^{II}(\mathbf{108a})(CH_3CN)_2](ClO_4)_4$ (Fig. 77c) both iron(II) centers are surrounded by six nitrogen donors in a distorted octahedral environment. Each set comprises one pyridazine nitrogen, two imine nitrogens, one tertiary amino nitrogen, one pyridyl nitrogen, all from the macrocycle, and one nitrogen from a coordinated acetonitrile molecule. The Fe···Fe distance (5.740 Å) lies between the Ba···Ba and the Cu···Cu distances in $[Ba_2(\mathbf{108a})(ClO_4)_4(H_2O)]$, and $[Cu_2(\mathbf{108a})](ClO_4)_4$. It is significantly longer than the distance between the doubly pyridazine bridged barium(II) ions in $[Ba_2(\mathbf{108a})(ClO_4)_4(H_2O)]$, as expected given that in $[Fe_2(\mathbf{108a})(CH_3CN)_2](ClO_4)_4$ the pyridazine moieties do not bridge the metal ions. The two pendant pyridyl arms are positioned on different sides due to the combination of the preference of the iron(II) ions for an octahedral geometry and the placement of the coordinated acetonitrile molecules [104].

The yellow plates and orange needles, both of which have the formula $[Mn_2^{II}(\mathbf{108a})(CH_3CN)(H_2O)](ClO_4)_4$, show a remarkably similar geometry of the cations overall structure $[Mn_2(\mathbf{108a})(CH_3CN)(H_2O)]^{4+}$. Every manganese(II) ions is seven coordinate with a distorted pentagonal bipyramidal geometry. In both cases **108a** provides a total of twelve nitrogen donors, comprising two pyridine nitrogens, four pyridazine nitrogens, two tertiary amine nitrogens and four imine nitrogens, to the two encircled manganese(II) ions. In each case one of the apical sites is occupied by one of these imine nitrogen donor atoms and the other apical site one manganese(II) ion by one nitrogen donor atom from a coordinated acetonitrile molecule whereas in the other manganese(II) ion by one oxygen donor atom from a water molecule. Both hydrogen atoms of this water molecule form hydrogen bonds to two of the four perchlorate counter ions. In contrast to the dicopper(II) and diiron(II) complexes with **108a**, the structures of both manganese(II) complexes reveal double pyridazine bridging of the metal ions. The distance between the manganese(II) ions (4.520 and 4.370 Å) is significantly shorter than the metal···metal separations observed in the unbridged dicopper(II) and diiron(II) complexes (Fig. 77d) [104].

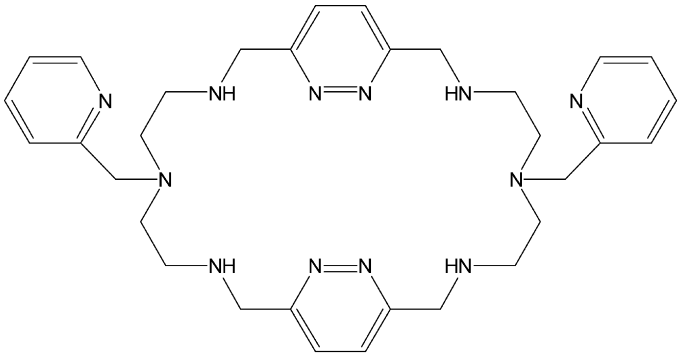

108a

2.4.2. Pyrazolate-based systems

The macrocycles H_2-**109**···H_2-**114** have been obtained, according to the above reported procedure, by the [2 + 2] condensation of 1H-pyrazol-3,5-dicarbaldehyde with the corresponding α,ω-diamine, followed by hydrogenation of the resulting Schiff base imine bonds [105–107]. The α,ω-diamine precursors were synthesized by protection of the primary amino groups of 1,5-diamino-3-azapentane through treatment with phthalic anhydride, followed by alkylation of the resulting secondary amino group of 1,5-diphthalimido-3-azapentane with benzyl, phenethyl, or octyl bromide. Finally, the phthalimido groups of the *N*-alkyl substituted intermediates were removed by treatment with hydrazine to afford the desired amines [105,106].

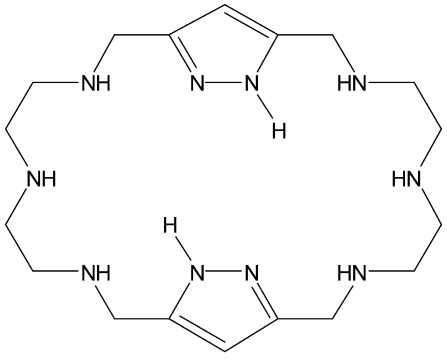

H_2-**109**

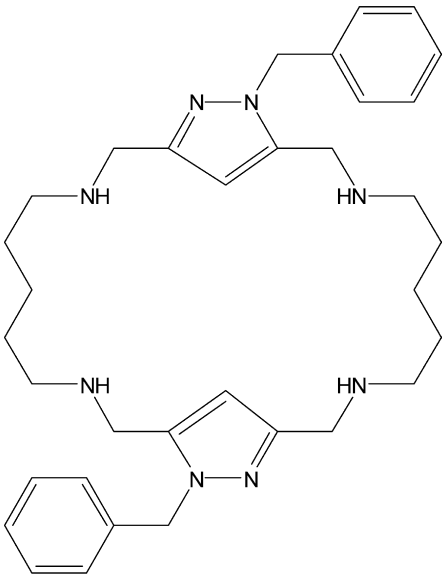

110

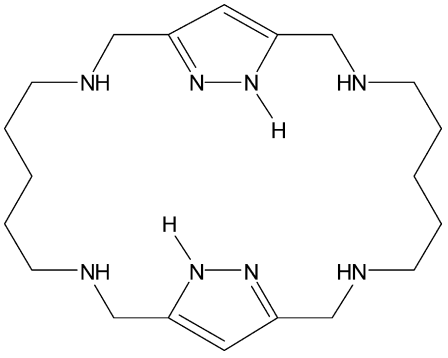

H_2-**111**

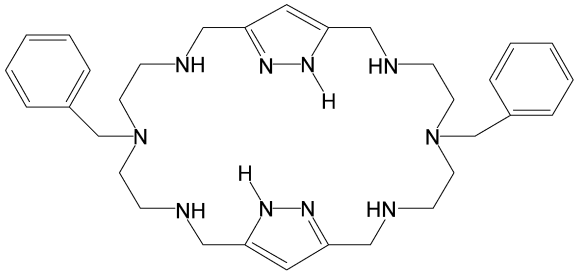

H_2-**112**

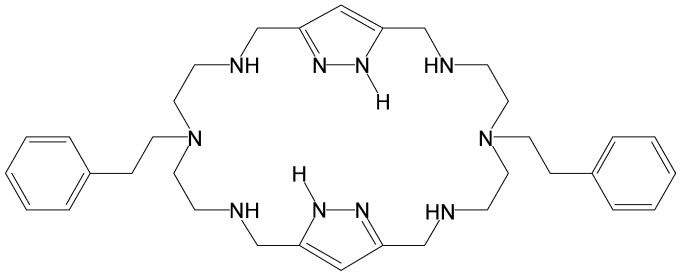

H_2-**113**

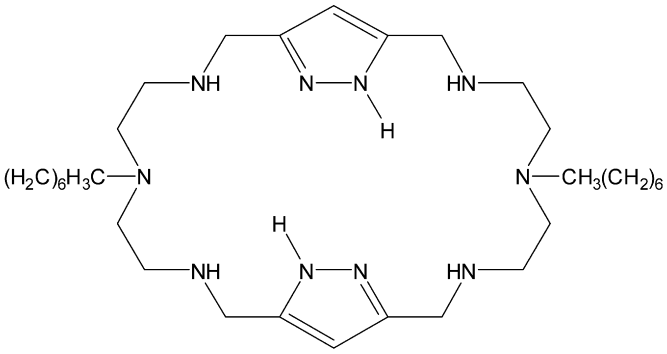

H_2-**114**

The structures of all these cyclic polyamines have been established by mass spectrometry and ^{1}H and ^{13}C NMR data of both the free ligands H_2-**109**···H_2-**114** and their corresponding hydrochloride salts $[H_8$-**109**$](Cl)_6$, $[H_6$-**110**$](Cl)_4$, $[H_8$-**111**$](Cl)_6$, $[H_8$-**112**$](Cl)_6$, $[H_8$-**113**$](Cl)_6$ and $[H_8$-**114**$](Cl)_6$ [107].

The interactions of these pyrazole-containing macrocyclic receptors with L-glutamate in aqueous solution has been studied by potentiometric techniques. The potentiometric results show that H_2-**112** containing benzyl groups in the central nitrogens of the polyamine side chains is the receptor displaying the larger interaction at pH 7.4 ($K_{eff} = 2.04 \times 10^4$). The presence of phenethyl groups H_2-**113** or H_2-**114** instead of benzyl groups of H_2-**112** in the central nitrogens of the chains produces a drastic decrease in the stability ($K_{eff} = 3.51 \times 10^2$ for H_2-**113**, $K_{eff} = 3.64 \times 10^2$ for H_2-**114**). The studies show the relevance of the central polyaminic nitrogen in the interaction with glutamate. H_2-**109** and **110** with secondary nitrogens in this position present significantly larger interactions than H_2-**111**, which lacks an amino group in the center of the chains. The NMR and modeling studies suggest the important contribution of hydrogen bonding and π-cation interaction to adduct formation. Furthermore, association constants of H_2-**112** with L-aspartate show a 15-fold selectivity of L-glutamate over L-aspartate at pH 7.4 [107].

Addition of copper(II) perchlorate to an aqueous solution of H_2-**111** in a 2:1 molar ratio, followed by evaporation of the solvent, yields $[Cu_4(\mathbf{111})_2(H_2O)_2(ClO_4)_2](ClO_4)_2{\cdot}2H_2O$ [108]. In contrast with $[\mathbf{109}]^{2-}$, which formed discrete binuclear $[Cu_2(\mathbf{109})]^{2+}$ species [109], the molecular features of $[\mathbf{111}]^{2-}$ favour an arrangement in which two molecules of $[\mathbf{111}]^{2-}$ are connected together by four copper(II) ions. Each one of the four metal centers is bound by a secondary nitrogen and two pyrazole nitrogen atoms belonging to different macrocyclic subunits forming the base of a strongly distorted square pyramid. All the pyrazole fragments are deprotonated and behave as exobidentate ligands. The severely distorted axial positions are occupied by an oxygen of a perchlorate anion and by one water molecule (Fig. 78). The other perchlorate anions in the structure that are acting as counter ions display strong disorder. The Cu···Cu distance is 3.967 Å.

The cage displays a rectangular prismatic shape with two opposite faces defined by the two metal ion binuclear

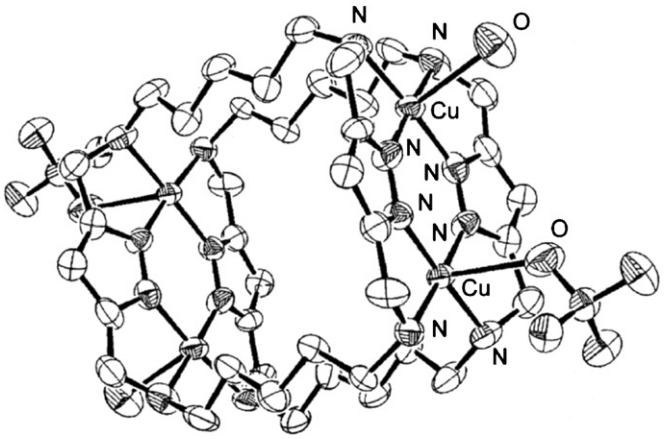

Fig. 78. Structure of $[Cu_4(\mathbf{111})_2(H_2O)_2(ClO_4)_2]^{2+}$.

coordination sites. This coordination faces would be interconnected by four edges constituted by the pentamethylene chains of the two receptors, which should afford a significant hydrophobic character to the cage interior. None of the water molecules or chloride anions are placed within the cage. The different cages do not show interconnections through hydrogen bonds or other intermolecular forces. The hydrophobic edges of different cages show a separation of >4.5 Å [109].

Although there are not yet definite proofs, this molecular arrangement seems to be also preserved in aqueous solution. Potentiometric studies suggest the formation of the very stable red species $[Cu_4(\mathbf{111})_2]^{4+}$ that would quantitatively be formed in solution above pH 5.5 for a Cu^{2+}:H_2-**111** = 2:1 molar ratio. The formation of this compound implies the deprotonation of the pyrazole moieties in solution with a significant increase in the acidity of the pyrazole fragments induced by the coordination of the copper(II) ions as already observed for H_2-**109** and H_3-**115** [104,108–112].

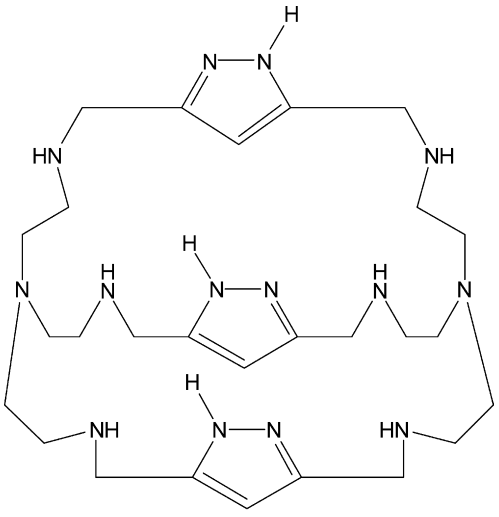

H_3-**115**

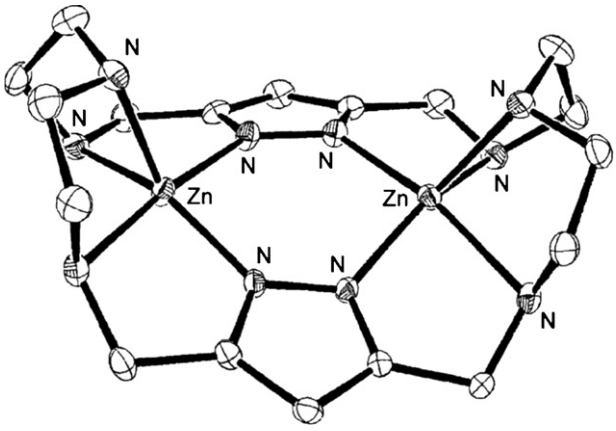

Fig. 79. Structure of $[Zn_2(\mathbf{109})]^{2+}$.

The in situ deprotonation of ligands H_2-**109** and H_3-**115** upon addition of NaOH, as well as the formation of zinc(II) pyrazolate complexes was observed by NMR in DMSO-d_6/D_2O mixtures [112,113]. The treatment of the neutral ligands H_2-**109**, **110** and H_3-**115** with $Zn(ClO_4)_2{\cdot}6H_2O$ in methanol and in a molar ratio M:H_2-L = 2:1, affords $[Zn_2(\mathbf{109})](ClO_4)_2$, $[Zn_2(\mathbf{110})](ClO_4)_4{\cdot}6H_2O$ and $[Zn_2(H\text{-}\mathbf{115})](ClO_4)_2{\cdot}4H_2O$ as indicated by FAB-mass measurements [112]. Thus, in the case of H_2-**109** and H_3-**115**, the zinc(II) coordination induces the deprotonation of the pyrazole ring to afford the pyrazolate bridging ligand without the need to add a base. On the other hand, considering that the structure of **110** corresponds to a constitutional isomer in which the 1-benzylpyrazole substituents are in positions opposite each other displaying C_2 symmetry and taking into account the crystal structure of the analogous copper(II) complex $[Cu_2(\mathbf{110})](ClO_4)_4{\cdot}4H_2O$, it is reasonable to assume that in the zinc(II) complex $[Zn_2(\mathbf{110})](ClO_4)_4{\cdot}4H_2O$ the nitrogen atoms of the pyrazole rings are also involved in the coordination of the metal ions [112].

The structure of $[Zn_2(\mathbf{109})](ClO_4)_2$ shows that each zinc(II) ion is coordinated by three nitrogen atoms from one of the polyamine chain and by one nitrogen atom from each one of the pyrazole units which are deprotonated and behave as bridging η^1: η^1-bis(monodentate) pyrazolate ligands (Fig. 79). The coordination geometry around the metal ions can be defined as midway between a strongly distorted square pyramid and a trigonal bipyramid. In order to achieve such a coordination geometry, the central part of the chains are forced to move in the same direction giving something of a boat-like shape. The Zn···Zn distance (3.99 Å) is close to those found for the copper(II) complexes of $[\mathbf{109}]^{2-}$ and $[H\text{-}\mathbf{115}]^{2-}$ [113].

As already observed in the systems $\{Cu^{II}\text{-}H_2\text{-}\mathbf{109}\}$ and $\{Cu^{II}\text{-}H_3\text{-}\mathbf{115}\}$ [115], the copper(II) coordination causes the ready deprotonation of the pyrazole moities without requiring any addition of base [110,111].

The preparation of H_2-**116** was performed by a [2 + 2] condensation of 3,5-pyrazoledicarbaldehyde with *N*-(3-aminopropyl)-1,3-propanediamine in methanol at room temperature, followed by in situ reduction of the resultant Schiff base with $NaBH_4$. After careful purification firstly by chromatography and then by crystallization from toluene, H_2-**116** was isolated as a pure solid. The disodium dipyrazolat salt $[Na_2(\mathbf{116})]$ was obtained by refluxing the free ligand H_2-**116** with 2 equiv. of NaOH in CH_3OH [113].

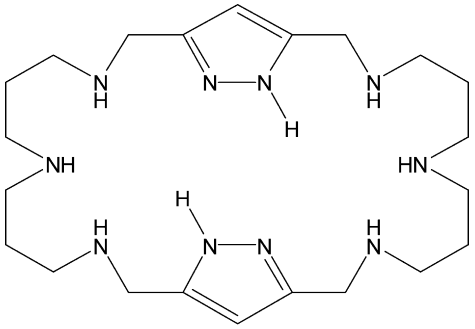

H_2-**116**

Treatment of $[Na_2(\mathbf{116})]$ with 2 equiv. of $Cu(ClO_4)_2{\cdot}6H_2O$ or $Zn(ClO_4)_2{\cdot}6H_2O$ affords $[Cu_2((\mathbf{116}))](ClO_4)_2$ and $[Zn_2((\mathbf{116}))](ClO_4)_2$, respectively. Again FAB-MS spectra corroborate the formation of these dinuclear complexes [113].

The acid–base behaviour, the copper(II) coordination chemistry and dopamine recognition capabilities of a series of pyrazole-containing polyamine macrocycles of different topologies [104,110–112] were recently reviewed [5]. These studies have been extended to the copper(II) and zinc(II) complexes with the pyrazole-containing macrocycle H_2-**116** in order to study the effect of the propylenic chains on the acid–base behaviour and on the copper(II) and zinc(II) coordination chemistry in aqueous solution. In these studies copper(II) and zinc(II) complexes derived from the ligands H_2-**109**,**110** and H_3-**115** have been taken into consideration, discussing the influence of the hydrocarbon chain length on the coordination features of these complexes [113].

pH-Metric titrations indicate that H_2-**116** shows six protonation steps in the pH range 2–11. In the absence of metal ions, the pyrazole moieties are not involved in acid–base processes in this pH range. With copper(II), H_2-**116** forms mononuclear $[Cu(H_x\text{-}\mathbf{116})]^{(x+2)+}$ complexes with $x = 0$, 1, 2 and 3 and dinuclear $[Cu_2(H_x\text{-}\mathbf{116})]^{(x+4)+}$ complexes with $x = 1$–3. The extent of formation of each one of these complexes depends on pH, M/**106** molar ratio and concentration. The zinc(II) complexes display remarkably lower stabilities than the copper(II) analogues.

In all the Zn/L systems, formation of mono- and dinuclear complexes can be observed and for the Zn/H_3-**115** system even a trinuclear species $[Zn_3(H\text{-}\mathbf{115})]^{4+}$ was detected. The degree of protonation of the mononuclear complexes reaches a value of 3 for $[Zn(H_5\text{-}\mathbf{109})]^{5+}$ and $[Zn(H_6\text{-}\mathbf{115})]^{5+}$ and only of 1 for $[Zn(H_3\text{-}\mathbf{110})]^{3+}$ and $[Zn(H_3\text{-}\mathbf{116})]^{3+}$. The degree of protonation of the dinuclear zinc(II) complexes varies between 0 and −3. In the case of the $\{Zn(H_2\text{-}\mathbf{109})\}$ system, it has not been possible to identify any nondeprotonated species [113].

A comparison with copper(II) shows that for zinc(II), the deprotonation of pyrazole is shifted approximately two units to higher pH values as a result of the poorer inductive effect exerted by this metal ion. Taking into account the crystal struc-

ture of $[Zn_2(\mathbf{116})](ClO_4)_2$ and the spectroscopic data, it is likely that in $[Zn_2(H\text{-}\mathbf{116})]^{3+}$ and $[Zn_2(\mathbf{116})]^{2+}$ both pyrazole groups are deprotonated. In $[Zn_2(H\text{-}\mathbf{116})]^{3+}$ one of the central nitrogen atoms of the bridging chain will be protonated. In the case of H_2-**109** the species $[Zn_2(H\text{-}\mathbf{109})]^{3+}$ cannot be detected and the only dinuclear species found in solution is $[Zn_2(\mathbf{109})]^{2+}$. For the cryptand H_3-**115** the situation is analogous to that of H_2-**109** and the species $[Zn_2(H_2\text{-}\mathbf{115})]^{3+}$ can be postulated as having the two pyrazole in the noncoordinating bridge will be non-deprotonated and one of the amino groups in this region will be protonated. Such a situation has already been observed in the crystal structure of the analogous copper(II) complex of H_3-**115** [111]. Finally, in the ligand **110** with N-benzylated pyrazole spacers, the main species in solution at neutral pH, is $[Zn_2(\mathbf{110})]^{4+}$. Deprotonation of the coordinated water molecules to give hydroxo species requires higher pH values. Thus, addition of copper(II) and zinc(II) ions results in deprotonation of the pyrazole moieties which act as a bis(monodentate) η^1: η^1 ligands. This induced deprotonation occurs at higher pH values than in the complex of the analogous ligand H_2-**109** containing diethylenetriamine bridges [113].

The crystallographic data of $[Cu_2(\mathbf{116})](ClO_4)_2$, collected at 150 K to depress disorders, show the coordination geometry around each copper(II) ion is an irregular, axially elongated, square pyramid. The base of the pyramid is formed by the two secondary nitrogen atoms of the polyamine bridges closer to the heterocycle and by two nitrogen atoms of two different pyrazolate units which act as η^1: η^1 bis(monodentate) anionic bridging ligands. The Cu···Cu distance is 3.96 Å which is almost identical to those found in the crystal structures of $[Cu_2(\mathbf{109})](ClO_4)_2$ and $[Cu_2(H_2\text{-}\mathbf{115})](ClO_4)_3\cdot 2H_2O$. The axial elongation observed in this complex is much smaller than those previously reported for $[Cu_2(\mathbf{109})](ClO_4)_2$ and $[Cu_2(H_2\text{-}\mathbf{115})](ClO_4)_3\cdot 2H_2O$. The complex again adopts a boat-shaped conformation with the side-chains folded toward the same side of the macrocyclic cavity (Fig. 80a) [113].

The crystallographic data of $[Zn_2(\mathbf{116})](ClO_4)_2$, also recorded at 150 K because of similar disorder to that found in the analogous copper(II) complex, show the coordination geometry around each zinc(II) ion is a distorted square pyramid. Analogous to the structure of $[Cu_2(\mathbf{116})](ClO_4)_2$, the base of pyramid is formed by the two secondary nitrogen atoms of the polyamine bridge closer to the heterocycle and by two nitrogen atoms of two different pyrazolate units which act as η^1: η^1 bis(monodentate) anionic bridging ligands. Zn···Zn distance is again 3.96 Å. The conformation of the whole molecule is again boat-shaped with the central part of both chains folded toward the same side of the macrocyclic plane (Fig. 80b) [112].

A different behaviour was observed by direct treatment of the neutral ligand H_2-**116** with $Cu(ClO_4)_2\cdot 6H_2O$ in methanol, to that previously described using the disodium dipyrazolate salt $[Na_2(\mathbf{116})]$ as a starting material. Thus, treatment of methanolic solution of H_2-**116** (2.5×10^{-2} M) with $Cu(ClO_4)_2\cdot 6H_2O$ in a 1:2 molar ratio at room temperature gave a blue precipitate which, after being vacuum-dried at 100 °C, afforded the blue solid $[Cu_2(H_2\text{-}\mathbf{116}](ClO_4)_4\cdot 2H_2O$. After redissolving this blue solid in boiling water for 5 min, a red solid slowly

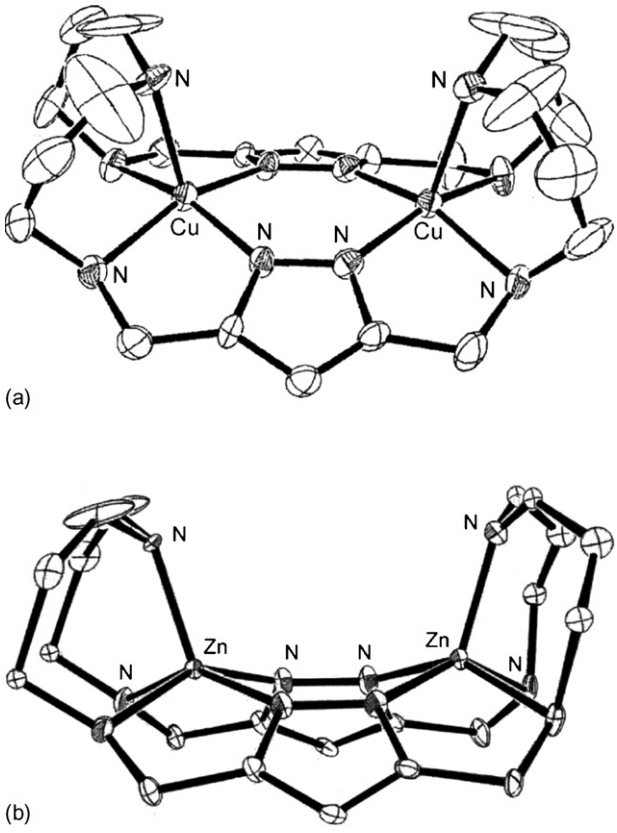

Fig. 80. Structure of $[Cu_2(\mathbf{116})]^{2+}$ (a) and $[Zn_2(\mathbf{116})]^{2+}$ (b).

and unexpectedly crystallized. After being vacuum-dried at 100 °C, this resulted in the reddish brown complex $[Cu_2(H_2\text{-}\mathbf{116}](ClO_4)_4\cdot 2H_2O$, with identical analytical data to the blue precursor mentioned above [113].

This can be explained if both the blue and the red forms of this complex correspond to dinuclear copper(II) dipyrazolate species which share the characteristic feature of having the two sp^3 nitrogen atoms located at the center of the side chains protonated and, in contrast to $[Cu_2(\mathbf{116})](ClO_4)_2$, thereby not directly coordinated to the metal atoms, The coordination of the metal ions causes the release of the protons from the pyrazole fragments which are captured by the basic central nitrogen atoms of the bridges.

The color changes observed has been tentatively attributed to the presence of the two water molecules which are bound in a different manner in both complexes. In the blue form they would be coordinated to the metal ion occupying the axial positions of the pentacoordinate environment. In the red form the coordination environment around each copper(II) would be square-planar and the water molecules would not occupy the first coordination sphere of the metal ion. In both cases the water molecules might be stabilized through $^+NH\cdots OH_2$ hydrogen bonds with the two protonate sp^3 nitrogen atoms located in the center of the side chains. These types of monohydrated ammonium groups were previously reported in the crystalline structure of the dinuclear copper(II) ion complex $[Cu_2(H\text{-}\mathbf{115})](ClO_4)_2\cdot(HClO_4)\cdot 2H_2O$, where one of the aliphatic nitrogen atoms of the noncoordinated

bridge is protonated and hydrogen-bonded to a water molecule [111].

In the red complex $[Cu_2(H_2\text{-}\mathbf{116})](ClO_4)_4\cdot 2H_2O$, the conformational change produced would be induced by the treatment of the starting precursor blue form with boiling water [113].

Starting form a more concentrated methanol solution of H_2-**116** (6.0×10^{-2} M) under similar reaction conditions and in the presence of 2 equiv. of $Cu(ClO_4)_2\cdot 6H_2O$ at room temperature a bright green solid precipitated which, after being vacuum dried at 100 °C, gave a trinuclear copper complex consistent, according to the analytical and mass spectrometry data, with the formula $[Cu_3(\mathbf{116})](ClO_4)_4\cdot 2CH_3OH$ [113].

The magnetic data of $[Cu_2(\mathbf{116})](ClO_4)_2\cdot 2H_2O$ and of $[Cu_2(H_2\text{-}\mathbf{116})](ClO_4)_4$ indicate an antiferromagnetic interaction between the copper(II) ions with singlet spin ground states. The pathway for magnetic exchange is propagated throughout the bridging pyrazolate ligands. From the molecular structure of $[Cu_2(\mathbf{116})](ClO_4)_2$ it was concluded that the unpaired electron in each metal center is clearly described by a $d_{x^2-y^2}$ magnetic orbital which is coplanar with the pyrazolate skeleton. The significant overlap between these magnetic orbitals accounts for the strong antiferromagnetic coupling observed. Although the crystal structure of the red $[Cu_2(H_2\text{-}\mathbf{116})](ClO_4)_4\cdot 2H_2O$ is not available, the very close magnetic behaviour of the blue and red copper(II) complexes indicates a similar exchange pathway. This again supports the suggestion that deprotonation of the pyrazolate rings has occurred in both structures [113].

2.4.3. Triazolate-based systems

The coordination chemistry of earlier non-crystallographically characterized, triazole macrocycle Schiff base systems was reviewed [102]. 3,5-Diacetyl-1,2,4-trizole was obtained by oxidation of the corresponding (*S*,*S*)-3,5-bis(1-hydroxyethyl)-1,2-, 4-triazole with CrO_3 in H_2SO_4, followed by the extraction with CH_2Cl_2 of the crude product [114].

$[Pb_2(\mathbf{117})](ClO_4)_2$ was formed by the addition of $Pb(ClO_4)_2\cdot 6H_2O$ to a solution of 3,5-diacetyl-1H-1,2,4-triazole and NaOH in refluxed methanol followed by the dropwise addition of a methanolic solution of 1,3-diaminopropane and extraction of the resulting precipitate with acetonitrile [115].

The structure reveals a perchlorate-bridged dimer of complexes dications, with the macrocycle bonded to the lead in the expected manner (Fig. 81): the triazolate head units doubly bridge the two metal ions and along with the imine nitrogen atoms provide an N_4 donor set to each lead ion. The macrocycle is significantly folded. Both lead(II) ions are pulled out of the respective N_4 mean planes, which direct the metal ions away from each other [115].

The dicobalt(II) complex $[Co_2{}^{II}(\mathbf{117})(Cl)_2]$ was prepared by transmetalation of $[Pb^{II}{}_2(\mathbf{117})](ClO_4)_2$ with a stoichiometric amount of $CoCl_2\cdot 6H_2O$ in acetonitrile and subsequent reaction with two equivalents of $[N(Et)_4](Cl)$ [115,116]. The addition of $CoCl_2$ leads to $PbCl_2$ precipitating out of the reaction mixture. The further addition of chloride anions provides axial ligands for the complexed cobalt centers. After centrifuging to remove the $PbCl_2$, the dark red solution was concentrated and diffused with diethyl ether, yielding dark red–violet crystals. The structure of this complex shows that the cobalt(II) centers are five coordinate being bonded to four nitrogen atoms in the equatorial plane and a chloride ion in the apical position. The Co···Co distance is 4.280 Å. The macrocycle is significantly bent. The bond length for the first coordination sphere are consistent with the presence of high-spin cobalt(II) centers (Fig. 82a) [115].

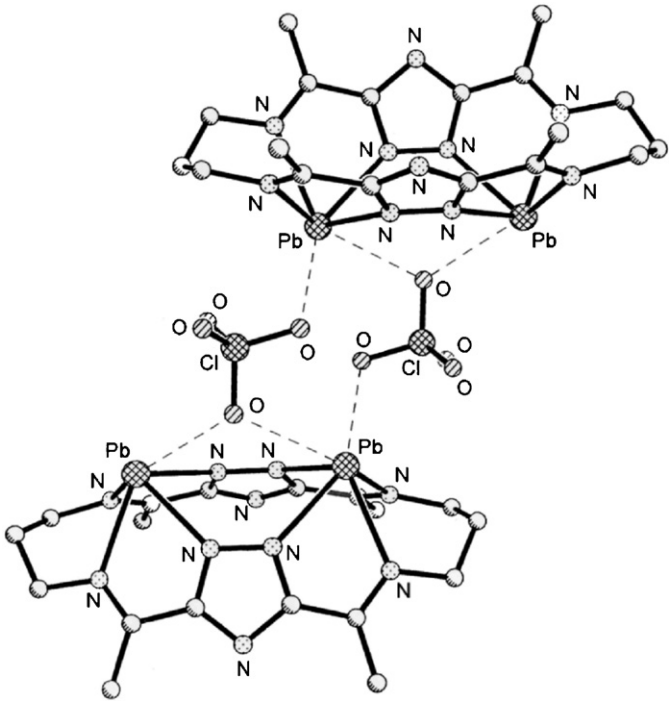

Fig. 81. Structure of $[Pb_4(\mathbf{117})_2(ClO_4)_2]^{2+}$.

In an attempt to recrystallize $[Co_2(\mathbf{117})(Cl)_2]$ from nitromethane in air, some red crystals of $[Co_2{}^{III}(\mathbf{117})(Cl)_2(CH_2NO_2)_2]$ grew slowly and spontaneously. The structure determination reveals two octahedral cobalt(III) centers separated by 3.808 Å. The two cobalt(III) centers are small enough to fit into the coordination sites of the macrocycle without folding it. The whole macrocycle is very flat with only the middle carbon atom of each of the two propylene lateral group being significantly out of the macrocycle mean plane. Each cobalt(III) ion is coordinated by the four nitrogen atoms in the equatorial plane and a chloride and the carbon atom of a nitromethane molecule that has lost a proton. In forming $[Co_2(\mathbf{117})(Cl)_2(CH_2NO_2)_2]$ clearly the cobalt(II) ions have been oxidized to the cobalt(III) ions and some of the nitromethane solvent has, in the absence of added base, lost a methyl proton and coordinated to the cobalt center forming a Co–C bond. In $[Co_2(\mathbf{117})(Cl)_2(CH_2NO_2)_2]$ the two chloride ligands are *trans* to each other while in $[Co_2(\mathbf{117})(Cl)_2]$ they are *cis* (Fig. 82b) [115].

$[Cu_2(\mathbf{117})(CH_3CN)_2](ClO_4)_2$ was prepared by transmetalation of $[Pb_2(\mathbf{117})](ClO_4)_2$ with two equivalents of $Cu(ClO_4)_2\cdot 6H_2O$ in CH_3CN. The lead(II) ion was completely removed as $Pb(SCN)_2$ by addition of four equivalents of NaSCN and the copper complex was readily crystallized from the resulting dark green solution by diethyl ether diffusion [115]. The structure proves that the transmetalation has occurred and the two lead ions have been replaced by two copper ions. Both copper(II) centers are five coordinate and are bridged by the two

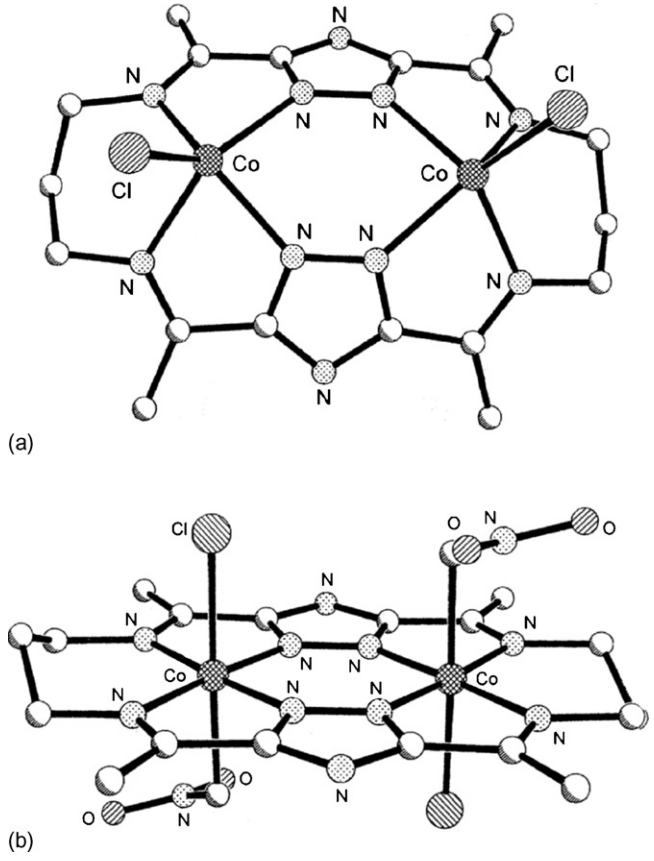

Fig. 82. Structure of $[Co_2^{II}(\mathbf{117})(Cl)_2]$ (a) and $[Co^{III}(\mathbf{117})(Cl)_2(CH_3NO_2)_2]$ (b).

triazolare units of the macrocyclic framework. The macrocycle also contributes a further two imine nitrogen donors to each copper center to complete the N_4 equatorial base. The axial position of each copper(II) center is occupied by a coordinated acetonitrile solvent molecule. The copper(II) coordination geometry is distorted square pyramidal, similar to the closely related pyridazine-bridged complex $[Cu_2^{II}(\mathbf{108})(CH_3CN)_2]^{4+}$. The copper ions are pulled out of the N_4 basal plane. The macrocycle unit is significantly folded. The Cu···Cu separation is 4.066 Å (Fig. 83a) [115].

$[Cu_2^{II}(\mathbf{117})(NCS)_2]$ was prepared though the same synthetic procedure by adding 8.00 equiv. of NaSCN per macrocycle to the transmetalation solution. After filtration to remove the $Pb(SCN)_2$, diethyl ether diffusion into the green acetonitrile solution afforded green crystals of the dicopper(II) complex [117]. The X-ray structure determination of $[Cu_2^{II}(\mathbf{117})(NCS)_2]$ shows that the fifth axial donor atom of each copper(II) ion in the macrocycle unit is the nitrogen of a thiocyanate ion. The copper ions have distorted square pyramidal geometry and are pulled out of the N_4 basal planes. There is again a significant fold in the macrocycle. The thiocyanate donors are slightly asymmetrically located above the basal planes toward imine donors on opposite corners of the macrocycle unit. The Cu···Cu separation is 4.075 Å. There are no significant intermolecular interactions in the crystal lattice (Fig. 83b) [115].The addition of 4.67 equiv. of NaSCN per macrocycle to the acetonitrile transmetalation reaction solution gave the dark blue complex $[\{Cu_2^{II}(\mathbf{117})\}_3(NCS)_2](ClO_4)_4$, obtained by diffusion of diethyl ether into the acetonitrile filtrate. The trimeric complex cation is constructed from three $\{Cu_2^{II}(\mathbf{117})\}$ units and two thiocyanate bridges. The sulphur donors of the thiocyanate ions each bridge two copper centers from different macrocycles, while the nitrogen donors coordinate to the copper centers in the single remaining macrocycle unit. The copper ions have distorted square pyramidal geometries, each with the basal N_4 plane comprised of two imine and two thioazolate nitrogen donors. The fifth donor atom for two copper(II) ions is the nitrogen atom of a bridging thiocyanate ion, giving an N_5 donor set, while for the remaining four copper atoms it is the sulphur of a bridging thioacyanate ion, giving an N_4S donor set. The copper(II) ions are pulled out of the N_4 plane; the Cu···Cu separations range from 4.027 to 4.061 Å (Fig. 83c) [115].

When 5.00 equiv. of NaSCN per macrocycle are added to the acetonitrile transmetalation reaction, blue green block crystals of $\{[Cu_2^{II}(\mathbf{117})(NCS)][Cu_2^{II}(\mathbf{117})(SCN)](ClO_4)_2{\cdot}H_2O\}_n$ are obtained by diethyl ether diffusion into the acetonitrile filtrate. In addition blue green crystals of the polymeric product $\{[Cu_2^{II}(\mathbf{117})(NCS)](ClO_4){\cdot}DMF\}_n$ were recovered from the same solution, when treated with diethylether followed by recrystallization of the resulting compound from a dimethylformamide-diethylether solution [115].

In $\{[Cu_2^{II}(\mathbf{117})(NCS)][Cu_2(\mathbf{117})(SCN)](ClO_4)_2{\cdot}H_2O\}_n$·the polymeric structure results from the 1,3-bridging thiocyanate ions. The bridging arrangement of the thiocyanate ligands has resulted in two distinct types of dicopper(II) tri-azolate macrocycles in the polymer repeating unit. In the first type of complex fifth donor atoms are the sulphur atoms of the 1,3-bridging thiocyanate ions (S-bound form) whereas in the second type of complex the fifth donor atoms are the nitrogens of these thiocyanate ions (N-bound form). $[\mathbf{117}]^{2-}$ provides two imine nitrogen and two triazolate nitrogen donors to the basal plane of each copper ion which has distorted square pyramidal geometry. The macrocycles are significantly folded. Within the macrocycles the respective Cu···Cu separations are 4.050 for the S-bound macrocycle and 4.081 Å for the N-bound macrocycle. The polymer chains are arranged in double layers with the thiocyanate 'faces' toward each other and then the alkyl faces of each double layer facing, separated by a channel of perchlorate and water molecules. The chains are staggered within double layers and between double layers (Fig. 84a) [115].

In contrast to $\{[Cu_2^{II}(\mathbf{117})(NCS)][Cu_2^{II}(\mathbf{117})(SCN)](ClO_4)_2{\cdot}H_2O\}_n$, the structure of $\{[Cu_2^{II}(\mathbf{117})(NCS)](ClO_4){\cdot}DMF\}_n$ is an alternative polymeric isomer arising from a different combination of the 1,3-bridging modes of the two thiocyanate ions. The complex consists of only one type of macrocycle, with one N-bound and one S-bound thiocyanate ion, in the polymer repeat unit. The polymer chains are arranged in layers with adjacent chains separated by a channel of perchlorate counterions and dimethylformamide solvent molecules. Successive layers are staggered. The thiocyanate ions are all in the same direction along the chain. This results in each macrocycle unit having one copper atom with an S-bound thiocyanate as the fifth donor atom, giving an N_4S donor set and the other an N-bound thiocyanate, giving an N_5 donor set. Both copper

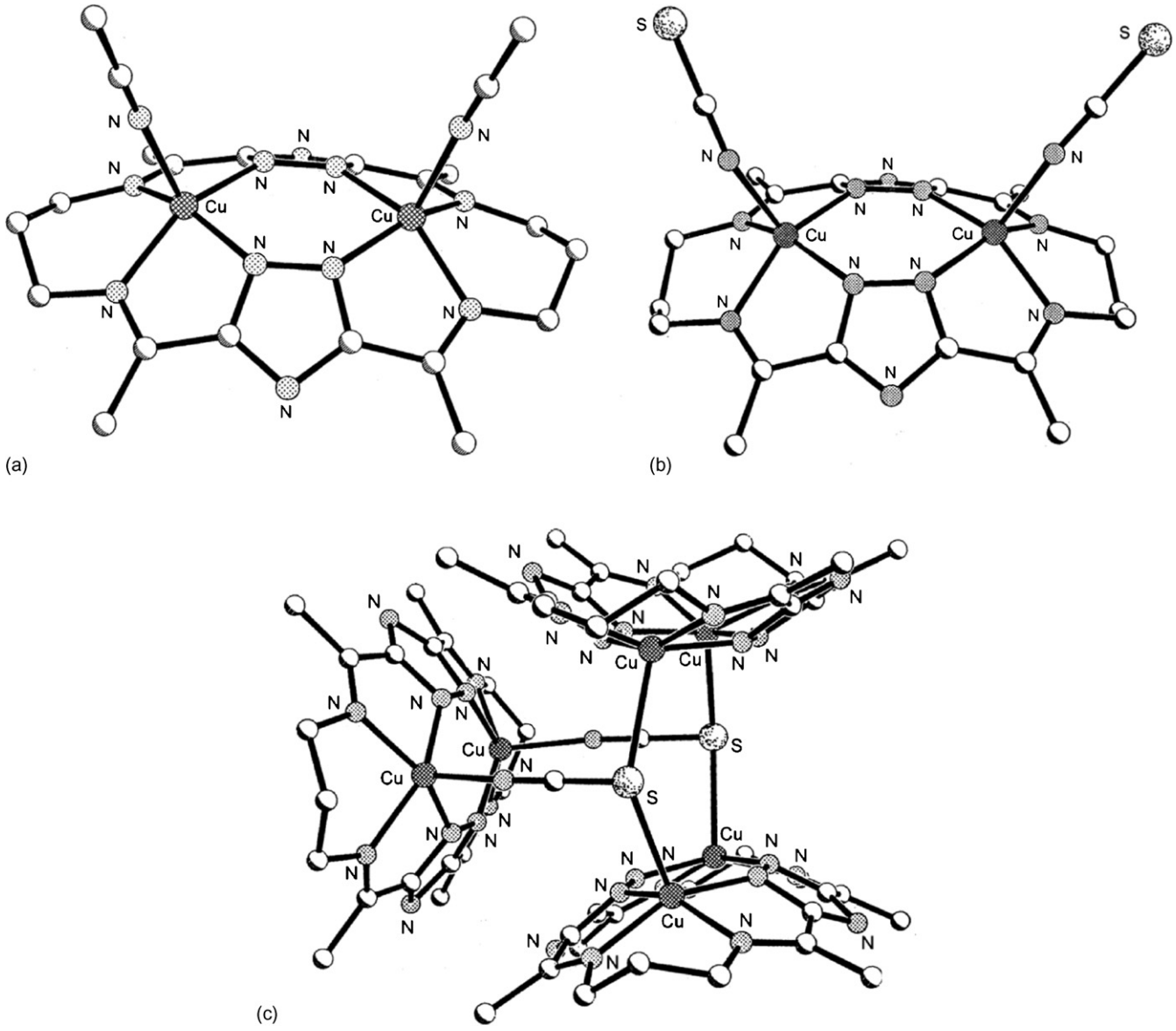

Fig. 83. Structure of $[Cu_2(\mathbf{117})(CH_3CN)_2]^{2+}$ (a), $[Cu_2(\mathbf{117})(NCS)_2]$ (b) and $\{[Cu_2(\mathbf{117})]_3(NCS)_2\}^{4+}$ (c).

ions have distorted square pyramidal geometry and are pulled out of the N_4 basal plane toward the axial thiocyanate donor (Fig. 84b) [115].

Due to the different orientation of the thiocyanate ions in $\{[Cu_2^{II}(\mathbf{117})(NCS)][Cu_2^{II}(\mathbf{117})(SCN)](ClO_4)\cdot H_2O\}_n$ and $\{[Cu_2^{II}(\mathbf{117})(NCS)](ClO_4)\cdot DMF\}_n$, the geometry of the polymer chains is different. In $\{[Cu_2^{II}(\mathbf{117})(NCS)][Cu_2^{II}(\mathbf{117})(SCN)](ClO_4)_2\cdot H_2O\}_n$, the unit with two sulphur donors is bent away from the nitrogen bound unit because of the preference of sulphur for a bent angle. In $\{[Cu_2^{II}(\mathbf{117})(NCS)](ClO_4)\cdot DMF\}_n$ each unit has one sulphur donor and one nitrogen donor, resulting in a zigzag chain. If the polymers are considered to be in a square tube, in $\{[Cu_2^{II}(\mathbf{117})(NCS)][Cu_2^{II}(\mathbf{117})(SCN)](ClO_4)\cdot H_2O\}_n$ the macrocycle units occupy adjacent sides, whereas in $\{[Cu_2^{II}(\mathbf{117})(NCS)](ClO_4)\cdot DMF\}_n$ they occupy opposite sides [115].

The polymeric structural motif observed in $\{[Cu_2^{II}(\mathbf{117})(NCS)](ClO_4)\cdot DMF\}_n$ has also been observed in the acetonitrile solvate, $\{[Cu_2^{II}(\mathbf{117})(NCS)](ClO_4)\cdot CH_3CN\}_n$ prepared by redissolving $\{[Cu_2^{II}(\mathbf{117})(NCS)](ClO_4)\cdot DMF\}_n$ in acetonitrile and growing crystals by vapour diffusion of diethyl ether. The polymer chains of $\{[Cu_2^{II}(\mathbf{117})(NCS)](ClO_4)\cdot CH_3CN\}_n$ is constructed in the same manner as that in the dimethylformamide solvate, with bridging thiocyanate ions alternating between nitrogen and sulphur donors. The polymer chains are arranged in layers with chains separated by perchlorate counterions and acetonitrile solvent molecules. Further layers are staggered slightly and the overall packing of the polymer chains is the same as in the previous structure. The Cu···Cu separation 4.053 Å is effectively the same as in the dimethylformamide solvate (4.043 Å). The macrocycle is folded [115].

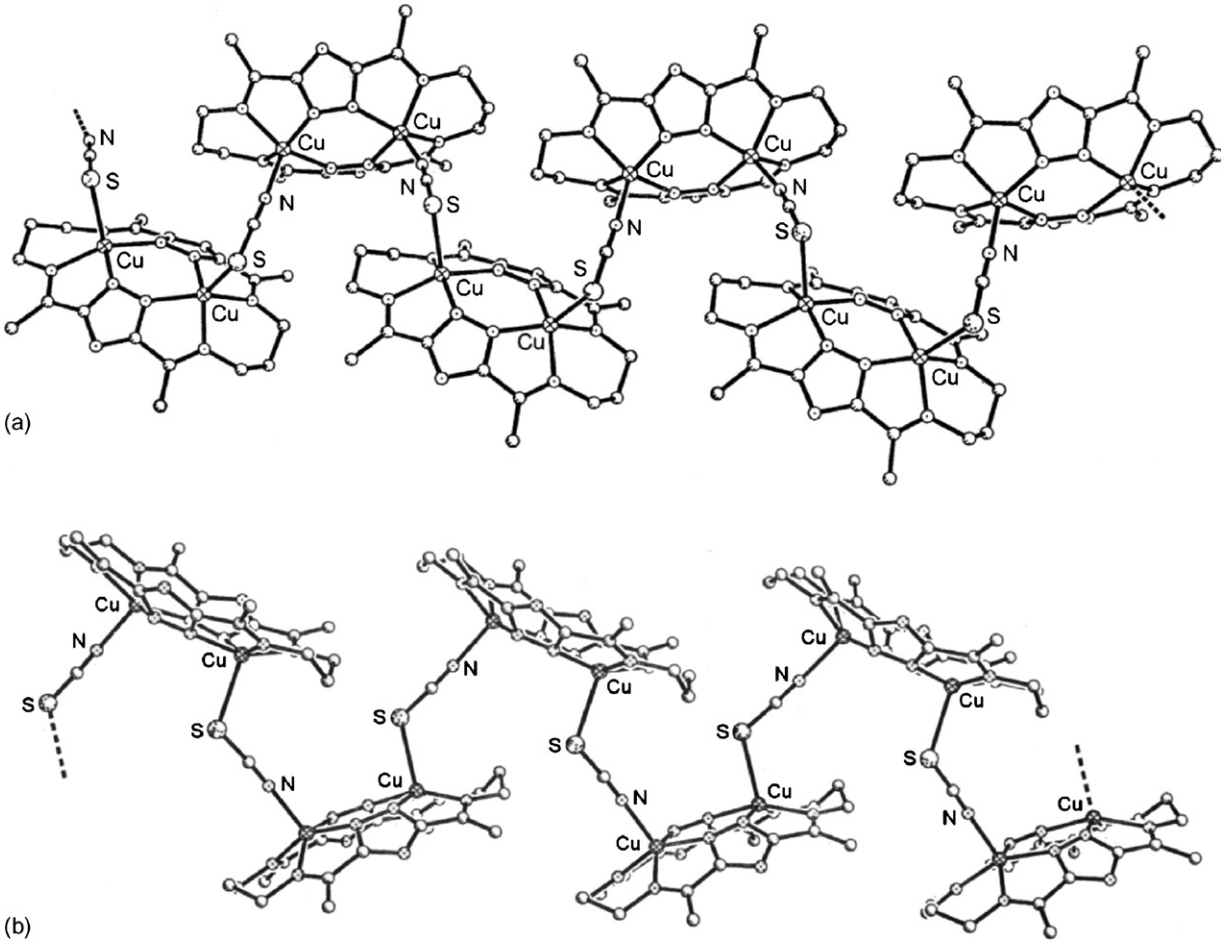

Fig. 84. Structure of $\{[Cu_2(\mathbf{117})(NCS)][Cu_2(\mathbf{117})(SCN)]\}^{2+}{}_n$ (a) and $\{[Cu_2(\mathbf{117})(NCS)]^{+}\}_n$ (b).

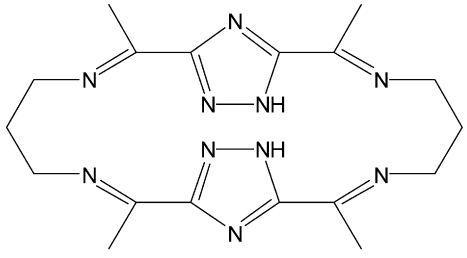

H_2-**117**

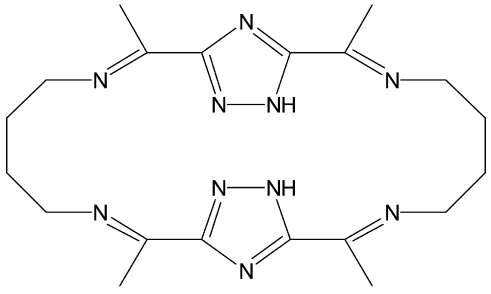

H_2-**118**

Attempts to prepare the metal-free macrocycle H_2-**118** were unsuccessful, so the template method was followed to synthesize it from the 3,5-diacetyl-1H-1,2,4-triazole and 1,4-diaminobutane. The direct synthesis of a copper complex from the triazole and amino components, i.e. using copper(II) ions as templates, was not successful. Rather, the use of lead(II) ions as templates proved to be the best way to obtain comparatively good yield of pure macrocyclic complex. Specifically, the addition of lead(II) perchlorate hexahydrate and 1,4-diaminobutane to a solution of 3,5-diacetyl-1H-1,2,4-triazole, in the presence of stoichiometric amounts of base to deprotonate the triazole head unit, yields the white crystalline complex $[Pb_2(\mathbf{118})](ClO_4)_2$, as indicated by the FAB-mass spectrum [115].

Orange blocks crystals of the air stable, six coordinate dicobalt(II) macrocyclic complex $[Co_2{}^{II}(\mathbf{118})(H_2O)_3(CH_3CN)](ClO_4)_2{\cdot}H_2O{\cdot}2CH_3CN$ were obtained by adding two equivalents of $CoCl_2{\cdot}6H_2O$ to $[Pb_2(\mathbf{118})](ClO_4)_2$ in refluxing acetonitrile, filtering the solution to remove the resulting $PbCl_2$ and finally diffusing diethyl ether into the filtrate. The FAB mass spectrum shows that a dicobalt complex of $[\mathbf{118}]^{2-}$ has formed. The complex is a 2:1 conductor in acetonitrile. The addition of two equivalents of NaOCN to $[Co_2{}^{II}(\mathbf{118})(H_2O)_3(CH_3CN)](ClO_4)_2{\cdot}H_2O{\cdot}2CH_3CN$ results in the formation of red–purple crystals of $[Co_2{}^{II}(\mathbf{118})(NCO)_2]$. The complex is a non-conductor in acetonitrile [118].

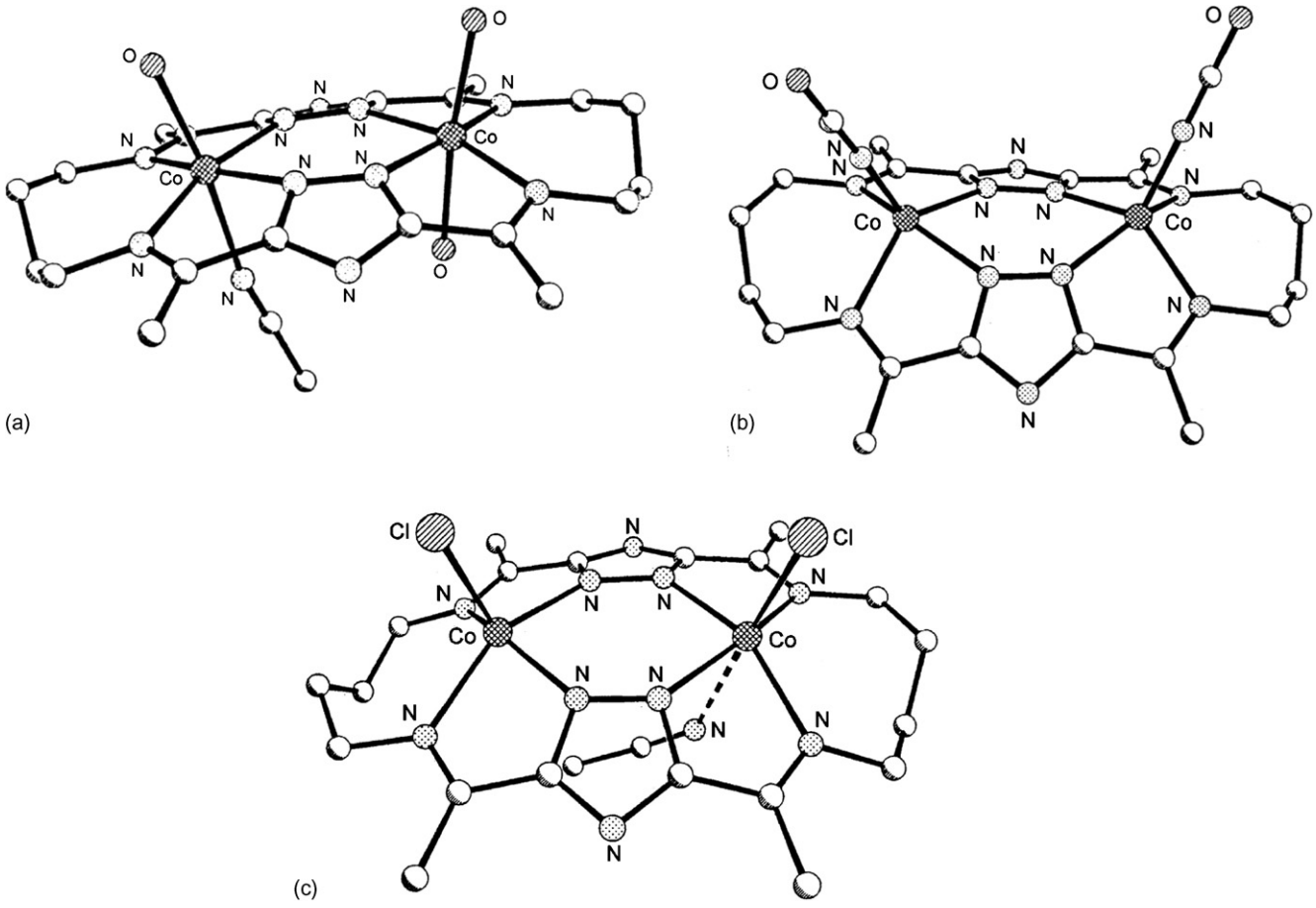

Fig. 85. Structure of $[Co_2(\mathbf{118})(H_2O)_3(CH_3CN)]^{2+}$ (a), $[Co_2(\mathbf{118})(NCO)_2]$ (b) and $[Co_2(\mathbf{118})(Cl)_2]$ (c).

Similarly, the addition of two equivalents of $[N(Et)_4](Cl)$ to $[Co_2^{II}(\mathbf{118})(H_2O)_3(CH_3CN)](ClO_4)_2{\cdot}H_2O{\cdot}2CH_3CN$ leads to the formation of $[Co_2^{II}(\mathbf{118})(Cl)_2]{\cdot}1.5CH_3CN$ as red crystals. The ESI-mass spectrum indicates that it is a dicobalt complex of the ligand $[\mathbf{118}]^{2-}$ containing chloride. Again, it is a non-conductor in acetonitrile. After about 2 weeks time at room temperature in air, a red sample of $[Co_2(\mathbf{118})(Cl)_2]{\cdot}1.5CH_3CN$ turned into the orange $[Co_2^{II}(\mathbf{118})(H_2O)_3(Cl)_2]{\cdot}2H_2O$ complex, which is a non-conductor in acetonitrile [115].

The structure of $[Co_2^{II}(\mathbf{118})(H_2O)_3(CH_3CN)](ClO_4)_2{\cdot}H_2O{\cdot}2CH_3CN$ (Fig. 85a) reveals that both cobalt(II) ions are six coordinate with four equatorial donors supplied by the triazolate macrocycle $[\mathbf{118}]^{2-}$ and one axial donor provided from a water molecule; the remaining axial site is occupied by a further water molecule in one cobalt(II) ion and by an acetonitrile molecule in the other cobalt(II) ion. The macrocycle is somewhat domed. Both cobalt(II) ions are raised up out of their respective N_4 mean planes of the macrocycle toward the respective water oxygens [115].

The X-ray structure of the red–purple crystals of $[Co_2(\mathbf{118})(NCO)_2]$, grown from acetonitrile/diethyl ether solution, reveals that the complex contains five coordinate cobalt(II) ions. The four equatorial donors are supplied by the macrocycle while the single axial donor is a cyanate ion. The five coordinate cobalt ions are displaced from their respective N_4 mean planes of the macrocycle toward the cyanate ions (Fig. 85b).

In $[Co_2(\mathbf{118})(Cl)_2]{\cdot}1.5CH_3CN$ there are two very similar dicobalt complexes in the asymmetric unit. The cobalt(II) ions are five coordinate with the axial positions occupied by two chloride anions. The cobalt ions are raised out of their respective N_4 mean planes of the macrocycle toward the chloride anions (Fig. 85c) [115].

The complexes show an irreversible electrochemistry. These results and the observed air stability of these cobalt(II) complexes have been ascribed to the distorted geometries imposed by the macrocycle as, for example, cobalt(III) would not be expected to be as accommodating as the high-spin cobalt(II) ions are. In the air stable dicobalt(II) complexes the macrocycle contains two high-spin cobalt(II) centers which are weakly antiferromagnetically coupled ($2J = -3.0$, -0.4, $-3.5\,cm^{-1}$ for $[Co_2^{II}(\mathbf{118})(H_2O)_3(CH_3CN)](ClO_4)_2{\cdot}H_2O{\cdot}2CH_3CN$, $[Co_2(\mathbf{118})(NCO)_2]$ and $[Co_2(\mathbf{118})(Cl)_2]{\cdot}1.5CH_3CN$, respectively) [115].

2.5. [2 + 2] Macrocyclic ligands without endogenous bridging groups and related complexes

This class of ligands derive from the [2 + 2] condensation of diformyl precursors which do not bear endogenous bridging

groups; thus the communication between the two compartments, where present, must arise from exogenous bridges. The diformyl precursors used for the synthesis of these macrocycles are bis(2-formyl)phenyltelluride, bis(2-formyl)phenylselenide, 2,5-diformylpyridine, substituted-5,5′-diformyldipyrrole, 2,5-disubstituted-1,3-diformylbenzene, 1,4-diformylbenzene, 2-2′-diformyl-diphenyle while the amine precursors are the diamines H_2N R NH_2 (R = aliphatic or aromatic chain) and the triamines $H_2N(CH_2)_nNR(CH_2)_nNH_2$ (R = H, CH_3; $n = 2, 3$).

The papers, dealing with the Schiff bases and related complexes, published in these last years, are here reviewed. However, most of the recent work regards the chemical behaviour of the related [2 + 2] polyamine macrocycles, obtained by reduction of the Schiff bases or by reductive demetalation of their complexes with $NaBH_4$.

2.5.1. Selenium or tellurium-containing macrocycles

Metal free condensation of equimolar amounts bis(2-formyl)phenyltelluride or bis(2-formyl)phenylselenide with the appropriate primary diamine H_2N-R-NH_2 in CH_3CN at room temperature affords the [2 + 2] macrocyclic Schiff bases **119a–d** which, by reduction with $NaBH_4$ in methanol at °C, give rise to the related [2 + 2] polyamine macrocycles **120a–d**. The [2 + 2] cyclic nature of these compounds was inferred by FAB mass spectra and confirmed by X-ray structural determinations [116]. The reduced polyamines have been collected as hydrobromide derivatives (Fig. 86a–d).

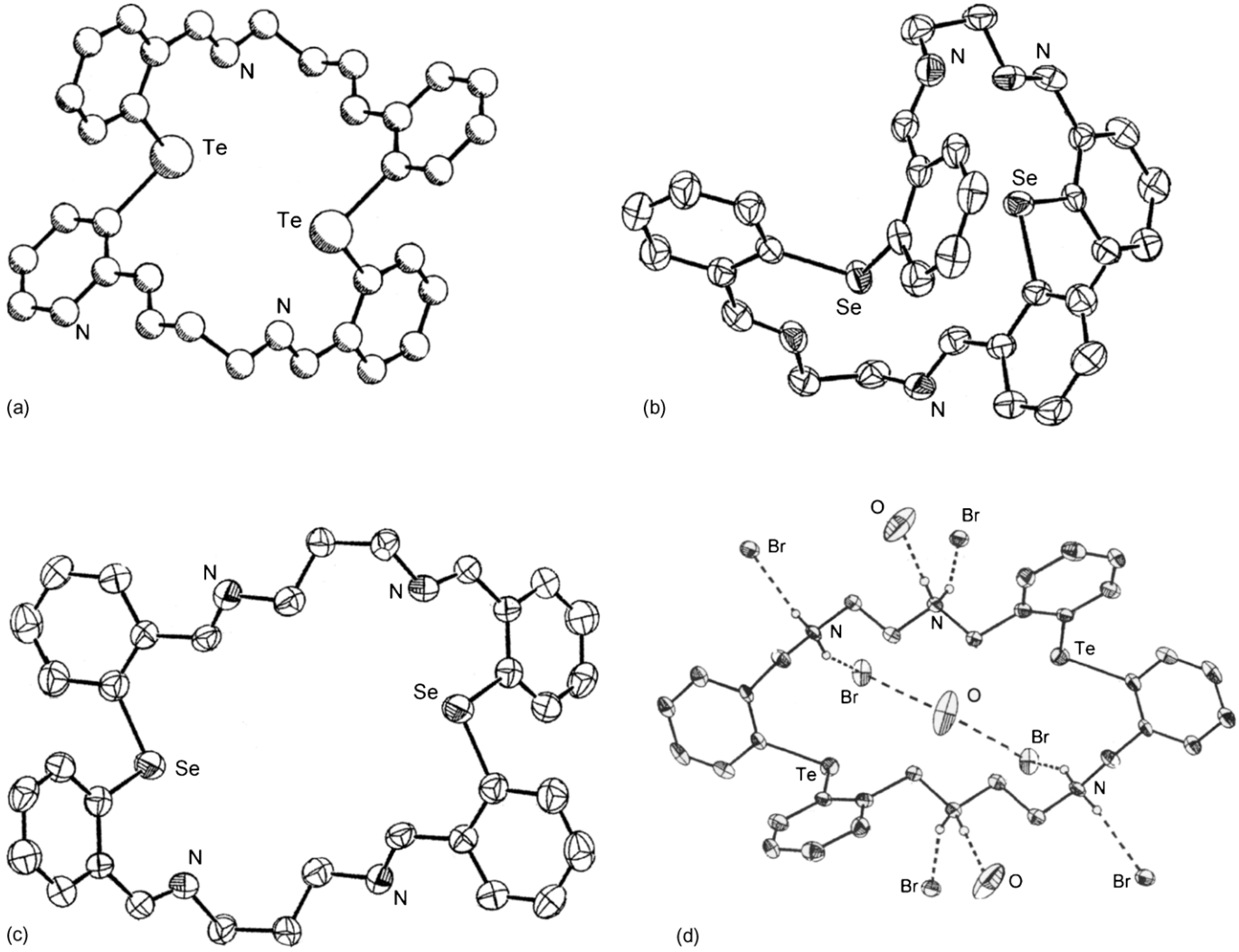

Fig. 86. Structure of **119a** (a), **119b** (b), **119d** (c) and [H_4-**120a**]$(Br)_4 \cdot 3H_2O$ (d).

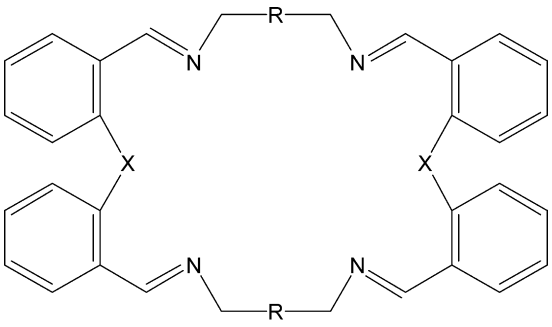

	X	R
119a	Te	-$(CH_2)_2$-
119b	Se	-$(CH_2)_2$-
119c	Se	-$(CH_2)_3$-
119d	Se	-$(CH_2)_2NH(CH_2)_2$-

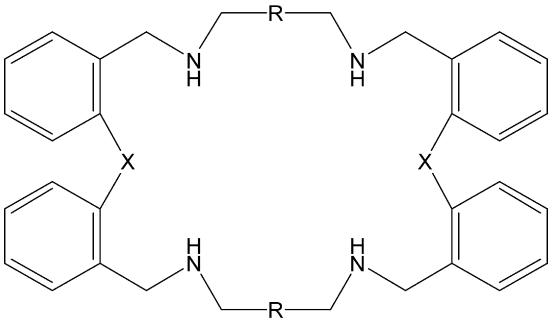

	X	R
120a	Te	-$(CH_2)_2$-
120b	Se	-$(CH_2)_2$-
120c	Se	-$(CH_2)_3$-
120d	Se	-$(CH_2)_2NH(CH_2)_2$-

These macrocycles form mononuclear and/or dinuclear complexes when reacted with copper(II), nickel(II), palladium(II) mercury(II), mercury(I) or lead(II) ions. In some cases the complexes with the [2 + 2] Schiff bases evolve into hydrolyzed compounds while the [2 + 2] polyamine complexes are stable [116].

Refluxing $Hg(CH_3COO)_2$ with **120d** in CH_3OH, followed by the addition of $[NH_4](PF_6)$, afforded white crystals of $[Hg_2(\mathbf{120d})](PF_6)_2$. Attempted syntheses of this complex using mercurous chloride or mercuric chloride produced black and white products, respectively, which were difficult to characterize due to the solubility problems. Also, the complexation reaction with mercurous acetate afforded a mixture of products. $[Hg_2(\mathbf{120d})](PF_6)_2$ is insoluble in most of the organic solvents and only partially soluble in CH_3CN [116]. The structure shows a Hg_2^{2+} cation trapped inside the macrocycle **120d**, bonded through six nitrogen atoms. The nitrogen atoms around the mercurous cation are arranged in an antiprismatic manner. The Hg···Hg distance is 2.535 Å (Fig. 87a) [116].

Reaction of **120d** with either 1 or 2 equiv. of $Pb(CH_3COO)_2{\cdot}4H_2O$ in refluxing methanol afforded, after recrystallization of the crude product form acetonitrile/diethylether, $[Pb_2(\mathbf{120d})(CH_3COO)_2](PF_6)_2$ [116]. The geometry around each lead(II) ion is a distorted octahedron. The two metal ions and the bridging oxygen atoms form a central four membered Pb_2O_2 ring. Each acetate ion acts as a chelating ligand toward one metal ion and is bridging between the two metal ions through one of its oxygen atoms. Each lead(II) ion coordinates to three nitrogen atoms. The Pb···Pb distance is 4.481 Å (Fig. 87b). No interaction occurs between the lead(II) ions and the selenium atoms. It is interesting to note that the corresponding lead(II) complexation with the corresponding azathia macrocycle shows lead(II) coordination to both sulphur and nitrogen atoms [116].

2.5.2. *Pyridine-based macrocycles*

2,6-Diformylpyridine and 2,6-diacetylpyridine have been used in macrocycle formation for a very long time and adequately reviewed [3–5]; only the must recent material is covered here.

The condensation of 2,6-diformylpyridine, derived by oxidation of 2,6-hydroxymethylpyridine with MnO_2 in CH_2Cl_2 [117] with the appropriate diamine gives rise to the [2 + 2] condensation Schiff base tetraimines, which can be reduced to the related [2 + 2] polyamine derivatives, generally recovered as tetraprotonated bromide hexaimine derivatives [2 + 2]. Both Schiff bases and related polyamine derivatives form mononuclear (but also dinucelar) complexes with the metal ion encapsulated inside the N_6 moiety [5].

When this macrocyclic moiety is conveniently enlarged, the coordination of two metal ions inside the macrocyclic cavity becomes feasible. This, for instance, occurs with the [2 + 2] macrocycles **121a** and **121b**, prepared in good yield by the condensation in acetonitrile of 2,6-pyridinedicarbaldehyde and bis(3-aminopropyl)amine or 3,3-diamine-*N*-methyldipropylamine in a 1:1 molar ratio followed by the reduction of the Schiff base. The some compounds were also synthesized using the lead(II) ion as the template ion, although at much lower yield because this metal ion was hard to remove from the complex. The pure macrocycles were obtained as salts by precipitation of the hexaprotonated hydrochloride [117].

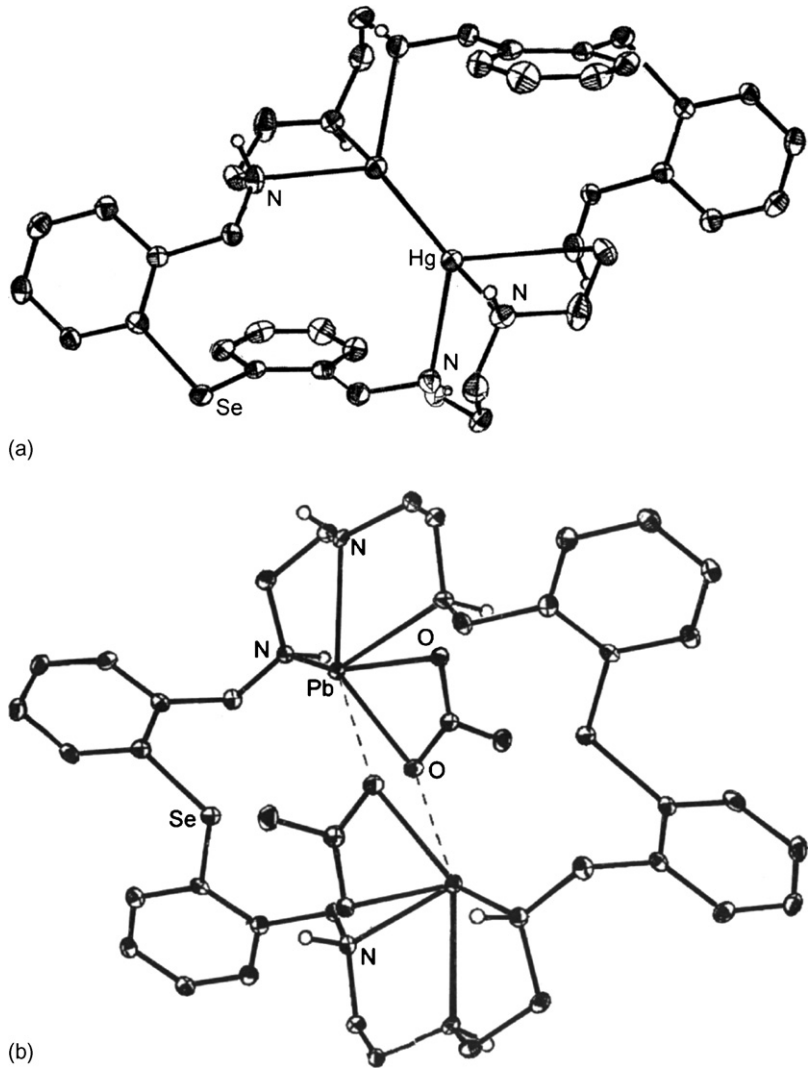

Fig. 87. Structure of $[Hg_2(\mathbf{120d})]^{2+}$ (a) and $[Pb_2(\mathbf{120d})(CH_3COO)_2]^{2+}$ (b).

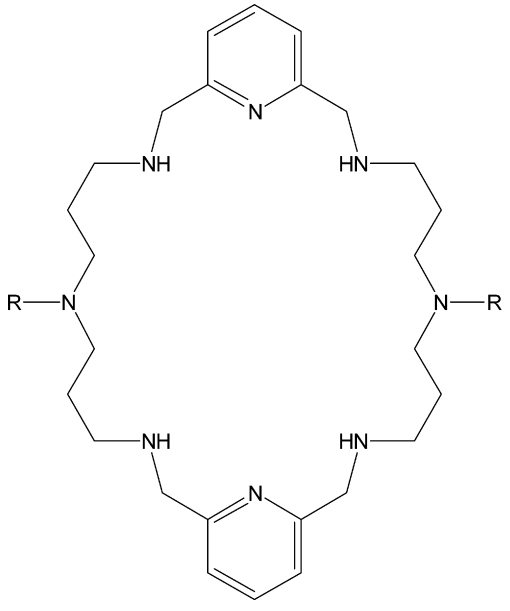

	R
121a	H
121b	CH_3

The protonation constants of the *N*-methyl-derivative **121b** and the stability constants of the related nickel(III), copper(II), zinc(II), cadmium(II) and lead(II) complexes were determined at 25 °C in 0.10 mol dm^{-3} KNO_3. The high overall basicity of this macrocycle is ascribed to the weaker repulsion between protonated contiguous charged ammonium sites separated by propyl chains. These studies together with NMR, UV–vis and EPR spectroscopies indicated the presence of mononuclear and dinuclear species. Several complexes were found in solution with the divalent metal ions studied: the mononuclear $[M(\mathbf{121b})]^{2+}$, $[M(H_i\text{-}\mathbf{121b})]^{(i+2)}$ ($i = 1$–4), $[M(\mathbf{121b})(OH)]^{+}$ and the dinuclear complexes $[M_2(\mathbf{121b})]^{4+}$, $[M_2(H_j\text{-}\mathbf{121b})]^{(4+j)+}$ ($j = 1$, 2), $[M_2(\mathbf{121b})(OH)_k]^{(4-k)+}$ ($k = 1$, 2). It was impossible to determine the constant corresponding to the formation of $[Zn_2(\mathbf{121b})]^{4-}$ (or other dinuclear protonated complexes) due to the immediate hydrolysis and the formation of $[Zn_2(\mathbf{121b})(OH)]^{3+}$ and $[Zn_2(\mathbf{121b})(OH)_2]^{2+}$ which start to form at pH $\simeq$ 7. The stability constant corresponding to $[Pb(\mathbf{121b})]^{2+}$ was also not available, due to the much more stable $[Pb_2(\mathbf{121b})]^{4+}$ and the two hydrolyzed

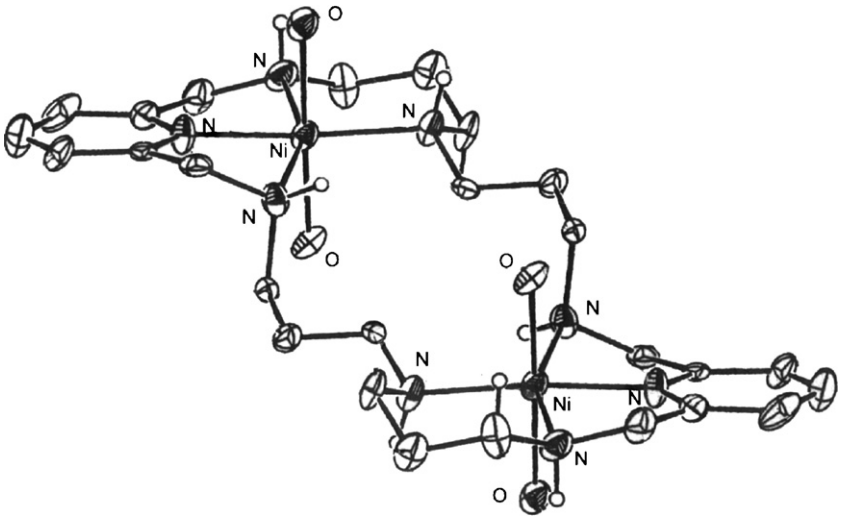

Fig. 88. Structure of $[Ni_2(\mathbf{121a})(H_2O)_4]^{4+}$.

species, $[Pb_2(\mathbf{121b})(OH)]^{3+}$ and $[Pb_2(\mathbf{121b})(OH)_2]^{2+}$ being formed even at a 1:1 ratio. Accurate values for the constants of the two hydrolyzed species, $[Ni_2(\mathbf{121b})(OH)]^{3+}$ and $[Ni_2(\mathbf{121b})(OH)_2]^{2+}$ could not be determined due to precipitation.

In $[Ni_2(\mathbf{121a})(H_2O)_4](Cl)_4{\cdot}3H_2O$, prepared by reaction of **121a** with $NiCl_2{\cdot}6H_2O$ in water, each nickel(II) center displays a distorted octahedral coordination with the equatorial plane defined by four sequential nitrogen atoms of the macrocycle (Fig. 88). The axial positions are occupied by two oxygen atoms from water molecules. The macrocycle adopts a ladder type conformation with each pyridil ring slightly tilted relatively to the N_4 equatorial coordination plane. The two pyridine rings are parallel. The metal is barely out of the N_4 coordination macrocyclic cavity. The Ni···Ni distance within the macrocycle is 6.991 Å [117].

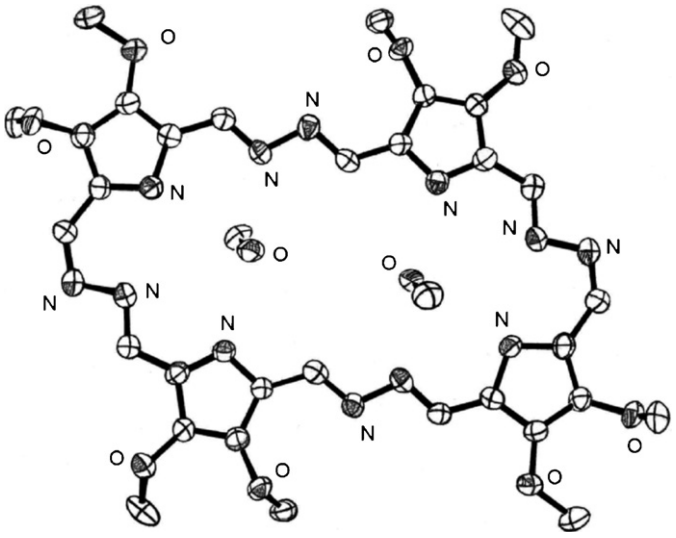

Fig. 89. Structure of $\{\mathbf{122a}{\cdot}2CH_3OH\}$.

2.5.3. Pyrrole-based macrocycles

It was reported that the reaction of 3,4-dialkylated-2,5-diformylpyrrole with 4,5-difunctionalized-1,2-diaminobenzene in the presence of excess $UO_2(CH_3COO)_2$ gives rise to the related mononuclear [2 + 2] macrocyclic uranyl(VI) complexes [118]. However, the use of hydrazine gives rise to the larger [4 + 4] condensation products **122a** which were synthesized by the acid-catalyzed condensation of 3,4-($C_nH_{2n+1}O$)-2,5-diformylpyrrole with one equivalent of hydrazine ($n = 1$, 6, 10, 14). These hydrazinophyrins are dark red in solution with high extinction coefficients typical of fully conjugated expanded porphyrins [118].

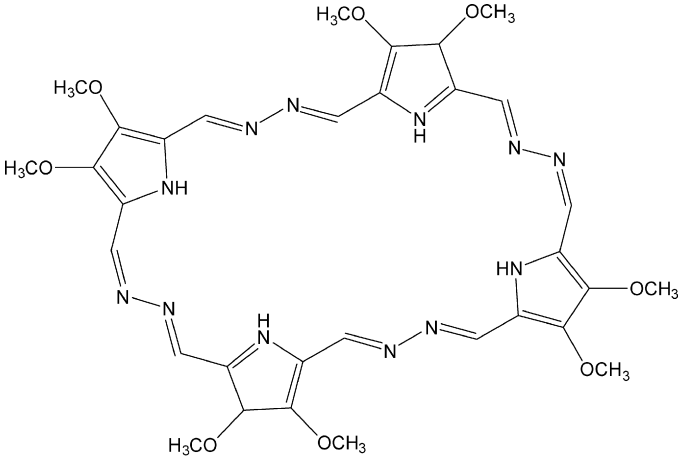

122a

The structure of **122a** ($n = 1$) (Fig. 89) revealed the presence of two molecules of methanol bound inside the central macrocyclic cavity. As expected for a fully conjugated system, the macrocycle is planar, the hydrazine units in the macrocycle are all in a *trans* configuration, while the system as a whole possesses C_2 symmetry. ^{1}H NMR spectroscopy indicates that **122a** ($n = 1$) and its homologues ($n = 6$, 10, 14) retain C_2 symmetry in solution. The protonated forms of **122a** ($n = 1$) are able to

bind anions, such as chloride, with high affinity in aprotic media [118].

Similarly, the condensation of 2,2′-dibenzyl-5,5′-diformylpyrrole with 1,3-propanediamine in the presence of $Mn(CH_3COO)_2$ gives rise to the dimanganese(II) complex $[Mn_2(\mathbf{122b})(CH_3COO)_2(H_2O)]$. The [2 + 2] macrocyclic Schiff base $[\mathbf{122b}]^{2-}$ is in the dipyrromethane form, which means that the diformyldipyrromethane reactant oxidizes during the course of the Schiff base reaction. Upon complex formation, two of the pyrrole nitrogens deprotonate resulting in a dianionic ligand. The structure (Fig. 90) reveals a dinuclear metal site with a Mn···Mn separation of 5.40 Å. Each dipyrromethane fragment is coordinated to a manganese ion in a planar fashion and the two planes are almost perpendicular to each other. One acetate forms a *cis*, *anti* bridge between the two metal ions, while the other is weakly chelated to one of the manganese(II) ions. Additionally, one water molecule is bound to one manganese(II) ion which, thus, maintains a distorted octahedral geometry. The other manganese(II) ion forms a distorted pseudo-seven coordinate complex. The complex catalyzes the disproportionation of H_2O_2 making it a functional model for diamanganese catalase [118].

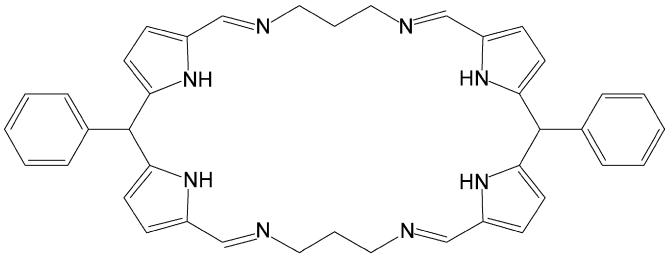

H_2-**122b**

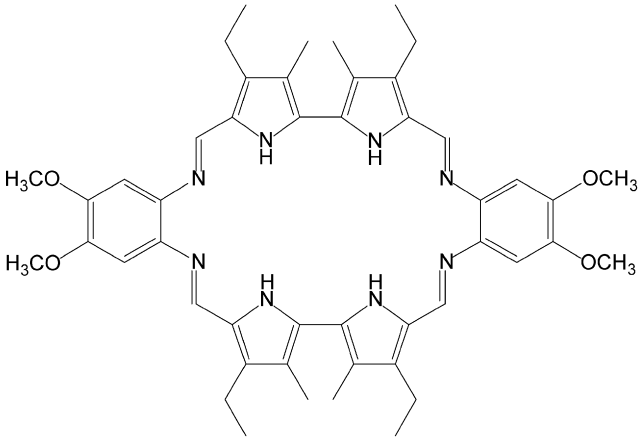

H_4-**122c**

4,4′-Diethyl-5,5′-diformyl-3,3′-dimethyl-2,2′-bipyrrole reacts with 1,2-diamino-4,5-dimethoxybenzene under nitric acid catalyzed conditions to form $[H_6$-**122c**$](NO_3)_2$, which precipitates from the reaction mixture after several minutes in near quantitative yield. The neutral ligand H_4-**122c** was obtained by dissolving this salts in CH_2Cl_2 and adding a few drops of triethylamine. Attempts to prepare H_4-**122c** using other acids were also made. In all cases, the yields of H_4-**122c** were substantially lower than if HNO_3 were used [118]. The X-ray structure of H_4-**122c**, obtained by redissolving in CH_2Cl_2 and layering with methanol H_4-**122c**, revealed a 2:1 complex of methanol (Fig. 91). The methanol molecules lie above and below the macrocycle. The bipyrrole hydrogens are hydrogen bound to the methanol oxygens. The methanol hydrogen is also involved in a bifurcated hydrogen bond with the imine nitrogen atoms [118].

The expanded porphyrin is formally in its unprotonated neutral free-base form. IR and NMR experiments show that hydrogen bonding remains also in CH_2Cl_2. Ethanol, trifluoroethanol, phenol and catechol can also be bound to H_4-**122c**, however with a preference for 1:1 compounds. These data support the hypothesis that certain expanded porphyrins, such as H_4-**122c**, may be used to chelate neutral substrates both in solution and in the solid state. The high affinity observed for the complexation of certain substrates (e.g. phenol, catechol) suggests that a generalized expanded porphyrin approach could provide the basis for an interesting way to the recognition and binding of neutral substrates, including those substrates such as catecholamines and carbohydrates of obvious biological importance.

H_4-**122c**, obtained by adding $N(Et)_3$ to a suspension of the diprotonated nitrate salt $[(H_6$-**122c**$)](NO_3)_2$ in CH_2Cl_2 or alternatively washing the same suspension in CH_2Cl_2 with a saturated aqueous solution of $NaHCO_3$, reacts with nickel(II), copper(II), or zinc(II) acetate at room temperature in CH_2Cl_2/CH_3CN to give $[M_2(H_4$-**122c**$)(CH_3COO)_4]$ as indicated by mass spectrometry and ascertained by single crystal X-ray analysis for $[Ni_2(H_4$-**122c**$)(CH_3COO)_4]$, where the two nickel(II) ions lie in a distorted octahedral geometry and are coordinated to the macrocycle by the iminic nitrogens. The pyrrolic nitrogens do not participate in metal complexation. The hydrogen atoms of the bipyrrolic nitrogens are hydrogen-bound to the donor oxygens of the four acetate conditions. The acetate ions also coordinate to the nickel(II) centers in three distinct binding modes: a bidentate acetate group coordinates one nickel(II) ion, a bridging acetate group binds to both nickel(II) ions and, finally, two monodentate acetates bind to the other nickel(II) ion. Each nickel(II) ion is also coordinated to a water molecule. The Ni···Ni distance is 5.375 Å (Fig. 92a) [118].

$[(H_6$-**122a**$)](NO_3)_2$, when reacted with the copper(I) mesitylene reagent $[Cu_5(Mes)_5]$, in tetrahydrofuran at room temperature under argon, gives rise to $[Cu_2(H_4$-**122c**$)(NO_3)_2]$. In this complex the macrocycle lies around a crystallographic inversion center and each copper(I) ion coordinates two imine donors of the macrocycle and one oxygen of the nitrate counterion, leading to a distorted T-shaped planar arrangement of these atoms. The coordination planes, containing the copper(I) ions and the nitrate anions, are tilted above and below the average plane of the macrocycle such that each counterion interacts with only one metal center. The Cu···Cu distance is 5.296 Å (Fig. 92b.).

The structures of the dinickel(II) or dicopper(I) complexes indicate that macrocycle H_4-**122c** can support both monovalent and divalent cations in a similar coordination mode, involving

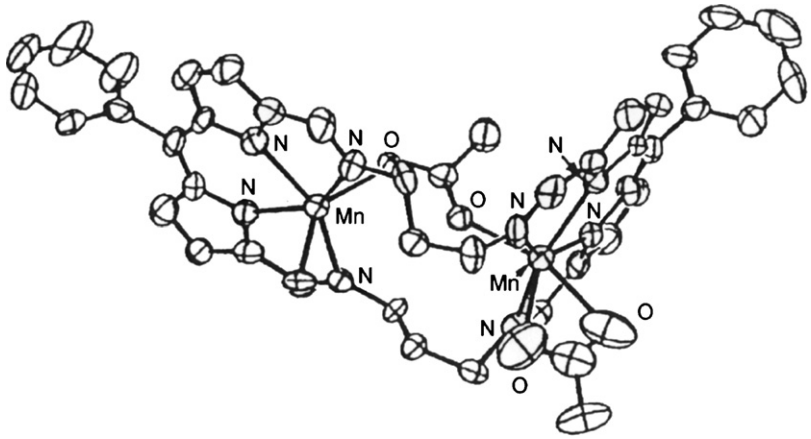

Fig. 90. Structure of $[Mn_2(\mathbf{122b})(CH_3COO)_2(H_2O)]$.

the imine nitrogens but not the pyrrolic nitrogens. However, this is not the only binding mode available to H_4-**122c**: when crystals of $[Cu_2^{I}(H_4\text{-}\mathbf{122c})(NO_3)_2]$ are dissolved in CH_2Cl_2, layered with n-pentane and exposed to air, the oxidation of the copper(I) centers to copper(II) and the production of the complex $[Cu_2^{II}(H_2\text{-}\mathbf{122c})(NO_3)_2]$ occur. The two additional anionic ligands, which are required by the charge balance of the complex, are provided by the macrocycle itself. Indeed, the ligand undergoes a dramatic distortion in order to coordinate to each copper(II) ion not only via the two imine nitrogen atoms but also through a pyrrolic nitrogen. As a consequence, the metal ions lie in a distorted square pyramidal environment that includes a bridging nitrate ion. The fifth coordination site is occupied by the second nitrate counterion for one copper(II) ion and by a water molecule for the other copper(II) ion. The Cu···Cu distance is 5.289 Å (Fig. 92c).

Efforts to obtain $[Cu_2(H_2\text{-}\mathbf{122c})(NO_3)_2]$ directly by treatment of $[H_6\text{-}\mathbf{122c}](NO_3)_2$ with $Cu(NO_3)_2$ failed; instead, $[Cu_2(H_2\text{-}\mathbf{122c})(NO_3)_4]$ appears to be obtained.

As expected from the large separation between the metal centers in these complexes, no evidence of a magnetic coupling was seen in solution at room temperature. Additionally, magnetic susceptibility SQUID data were consistent with a paramagnetic behaviour of these complexes in the temperature range 5–300 K [118].

5,5-Dimethyl-1,9-diformyldipyrromethane reacts in dry methanol with 1,3-diaminopropane or 1,4-diaminobutane in the presence of the appropriate nickel(II) or copper(II) acetate and $N(Et)_3$ to form the corresponding [2 + 2] macrocyclic Schiff base complexes $[M_2(\mathbf{122d})]$ or $[M_2(\mathbf{122e})]$ [119].

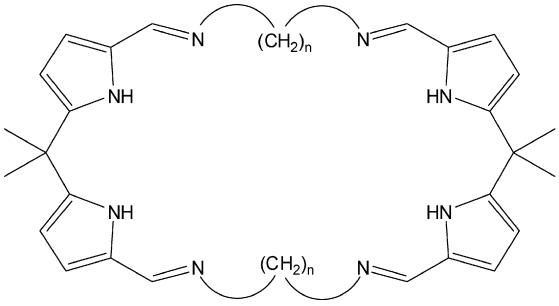

The X-ray structures of $[Cu_2(\mathbf{122d})]\cdot 2CH_2Cl_2$, $[Cu_2(\mathbf{122e})]\cdot 2CH_2Cl_2$, $[Ni_2(\mathbf{122d})]\cdot 2CHCl_3$ and $[Ni_2(\mathbf{122e})]\cdot 3CHCl_3$

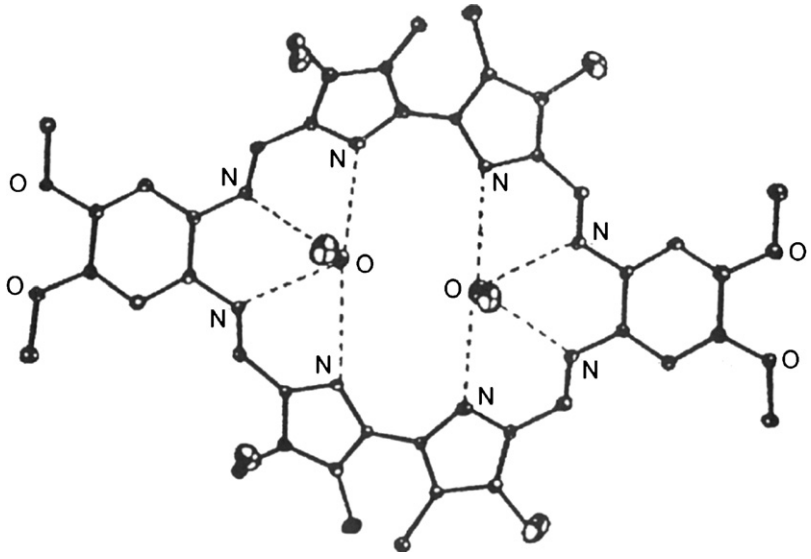

Fig. 91. Structure of $\{H_4\text{-}\mathbf{122c}\cdot 2CH_3OH\}$.

(Fig. 93a–d) reveal that they all consist of neutral dimetallic macrocycles with each metal center in a square planar N_4 geometry. Each copper(II) or nickel(II) ion is bound by two deprotonated pyrrole nitrogen atoms of one dipyrromethane unit and to two adjacent imine nitrogen atoms. In [Cu_2(**122d**)] the macrocycle is folded resulting in a L-shape conformation. Replacement of the two propylene lateral linkers in [Cu_2(**122d**)]·2CH_2Cl_2 by the two longer, butylene lateral linkers in [Cu_2(**122e**)]·2CH_2Cl_2 makes the latter macrocycle more flexible than the former, and it therefore adopts a different conformation, stretching out into a tep-like conformation. Hence, unsurprisingly, the intramolecular Cu···Cu separation is significantly longer, at 8.323 Å, than it is in [Cu_2(**122d**)]·2CH_2Cl_2 (6.506 Å) [118]. In [Ni_2(**122d**)]·2$CHCl_2$ and [Ni_2(**122e**)]·3$CHCl_3$ the macrocycles adopt the same conformation of the copper(II) analogues. The Ni···Ni separation is 6.682 Å in [Ni_2(**122d**)] and 8.3235 Å in [Ni_2(**122e**)]. NMR spectra of the dinuclear(II) complexes show that in $CDCl_3$ they are highly symmetric and diamagnetic [119].

The expanded pyrrole-containing Schiff base macrocycles H_4-**122f**···H_6-**122l** have been prepared by condensation under suitable conditions of the appropriate substituted diformyl-dipyrrole and functionalized and 1,2-diaminobenzene precursors. For example, the addition of *p*-toluenesulphonic acid to a stirred mixture of the appropriate dipyrrol-dialdehydes and 1,2-diaminobenzene in methanol cleanly generates the [2 + 2] Schiff-base condensation products H_4-**122f** and H_4-**122g**, respectively, in high yield as orange, microcrystalline solids. Electrospray mass spectrometry of the reaction mixture showed that no higher order cyclization products are present [118].

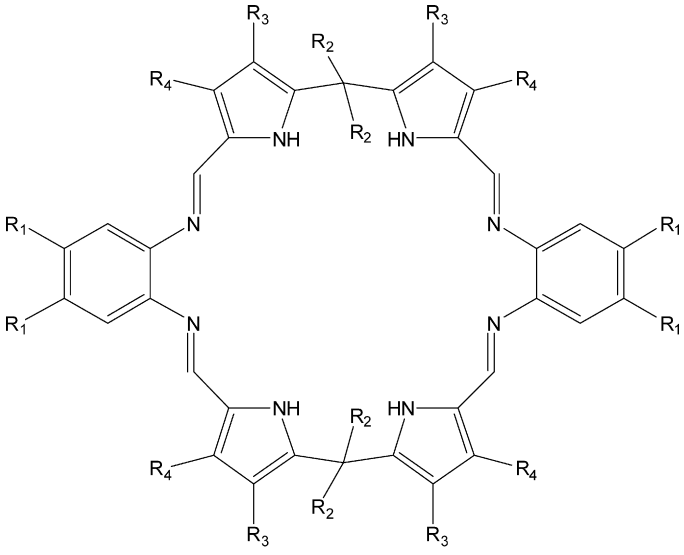

	R_1	R_2	R_3	R_4
H_4-**122f**	H	CH_3	H	H
H_4-**122g**	H	C_6H_5	H	H
H_4-**122h**	OCH_3	CH_3	H	H
H_4-**122i**	H	H	CH_2CH_3	CH_3

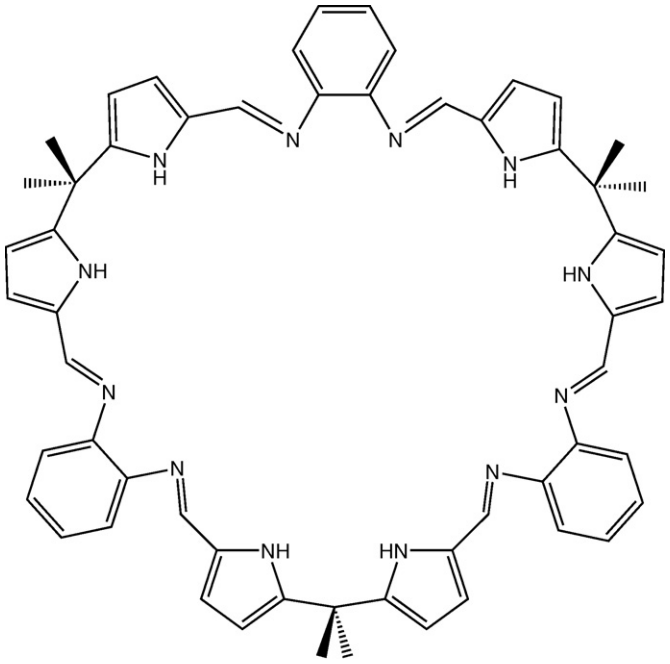

H_6-**122l**

The X-ray crystal structure of the salt [H_8-**122f**](${CH_3C_6H_4SO_3}_4$ confirms [2 + 2] cyclization has occurred. The tetraprotonated macrocycle adopts a bowl-like conformation with one *p*-toluenesulphonato group hydrogen bonded to iminopyrrole units. Two further *p*-toluensulphornato groups interact with the remaining iminopyrrole units (Fig. 94a) [118].

According to the metal ion used they can give rise to mononuclear or homodinuclear complexes. Thus, the reaction between the free-base macrocycle H_4-**122f** and the uranyl(VI) amide [$UO_2(THF)_2\{N(SiMe_3)_2\}_2$] in THF at low temperature resulted in the rapid and sole formation of the mononuclear uranyl complex [UO_2(H_2-**122f**)(THF)]. The diuranyl(VI) complex [$(UO_2)_2$(**122f**)] was not observed, even when the reaction was carried out at elevate temperature [120].

In [UO_2(H_2-**122f**)(THF)] one N_4-donor set of [H_2**122f**)]$^{2-}$ is flexible enough to accommodate successfully the linear uranyl(VI) ion, which adopts the usual five coordination in the equatorial plane. The second N_4-donor compartment remains metal free. The expanded coordination site is occupied by THF, which complete the approximate pentagonal bipyramidal geometry at the metal ion [118]. The THF molecule adopts a highly unusual, slightly asymmetric sandwiched position between the two aryl rings that bridge the two N_4-donor compartments. The presence of the rigid, bridging aryl groups between the two donor compartments has resulted in a bent structural motif, prescribing a well-defined, monometallic cleft with one oxo group of the linear uranyl ion located within the cleft and the other exo. An appreciable hydrogen bonding interaction occurs between the pyrrolic hydrogens and the uranyl oxygen (Fig. 94b) [120].

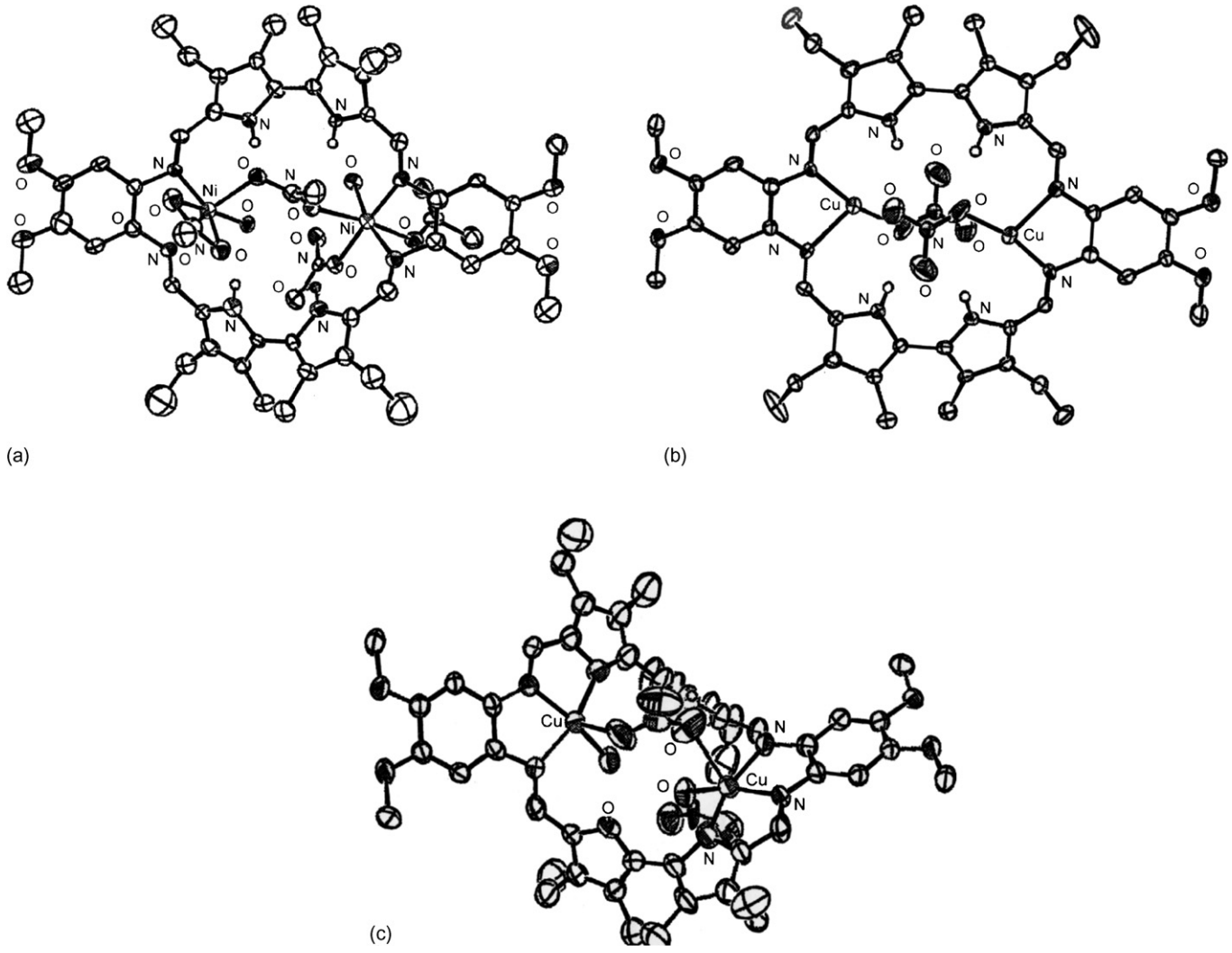

Fig. 92. Structrure of $[Ni_2(H_4\text{-}\mathbf{122c})(CH_3COO)_4]$ (a), $[Cu_2^{I}(H_4\text{-}\mathbf{122c})(NO_3)_2]$ (b) and $[Cu_2^{II}(H_2\text{-}\mathbf{122c})(NO_3)_2]$ (c).

The reaction between $[UO_2(H_2\text{-}\mathbf{122f})(THF)]$ and excess pyridine results in THF substitution and the formation of the mono-pyridine adduct $[UO_2)(H_2\text{-}\mathbf{122f})(py)]$. No reaction was observed between $[UO_2(H_2\text{-}\mathbf{122})(THF)]$ and either 2,2-bipyridine or benzophenone. The X-ray structure of $[UO_2(H_2\text{-}\mathbf{122f})(py)]$ was shows a hinged molecular topology similar to $[UO_2(H_2\text{-}\mathbf{122f})(THF)]$ but with pyridine π-stacked between the aryl-bridged hinge instead of THF [120].

Addition of triethylamine to a stirred mixture of $Pd(CH_3COO)_2$ and H_4-**122f** or H_4-**122g** in CH_2Cl_2 results in the clean generation of the orange dipalladium compounds $[Pd_2(\mathbf{122f})]$ and $[Pd_2(\mathbf{122g})]$, respectively. The ESI-mass spectrum of the reaction medium of $[Pd_2(\mathbf{122f})]$ showed only one signal at 872 *m/z* with the correct isotopic pattern for $[Pd_2(\mathbf{122f})]$ [120].

The X-ray structures of both complexes are very similar. They show the two palladium(II) ions are both coordinated by diiminodipyrrolide donor compartments in square planar geometries. The presence of the rigid *o*-aryl spacer between the donor compartments has a profound effect on the overall molecular geometry with face-to-face stacking of the *o*-aryl groups enforcing a unique wedge-like arrangement of the two PdN_4 square planar. The Pd···Pd distance is 3.76 Å (Fig. 94c). The solid state structure of these complexes appears to be retained in solution [120].

Preliminary results suggest that the dicobalt(II) complexes of H_4-**122f** and H_4-**122g** react spontaneously with O_2; thus, reaction between $Co(CH_3COO)_2$ and H_4-**122f** and NEt_3 in air forms the oxo-complex $[Co_2(O)(\mathbf{122f})]$ as the sole product according to ESI mass spectra [120].

The reaction of H_4-**122f**···H_4-**122i** with $FeCl_2$, $FeCl_3$ or $Fe(acac)_3$ in the presence of base failed. Also the reaction of $[Fe(CH_3CN)_6][(Au(Cl)_4)]_2$ or $[Fe(CH_3CN)_6](BF_4)_2$ with these macrocycles was not successful. On the contrary, either the desired free base H_4-**L** (H_4-**L** = H_4-**122f**, H_4-**122h**, H_4-**122i**) or its bis-HCl salt $[H_6\text{-}\mathbf{L}](Cl)_2$ and (H_4-**L** = H_4-**122h**, H_4-**122i**) and the diiron(II) tetramesitylene $[Fe_2(Mes)_4]$, when dissolved in THF at −78 °C and then allowed to warm to room temperature, give a dark brown solution which, stirred overnight and then evaporated to dryness, forms respectively the μ-oxo complexes $[Fe_2(\mathbf{L})(O)]$ and $[Fe_2(H_2\text{-}\mathbf{L})(O)(Cl)_2]$ [118].

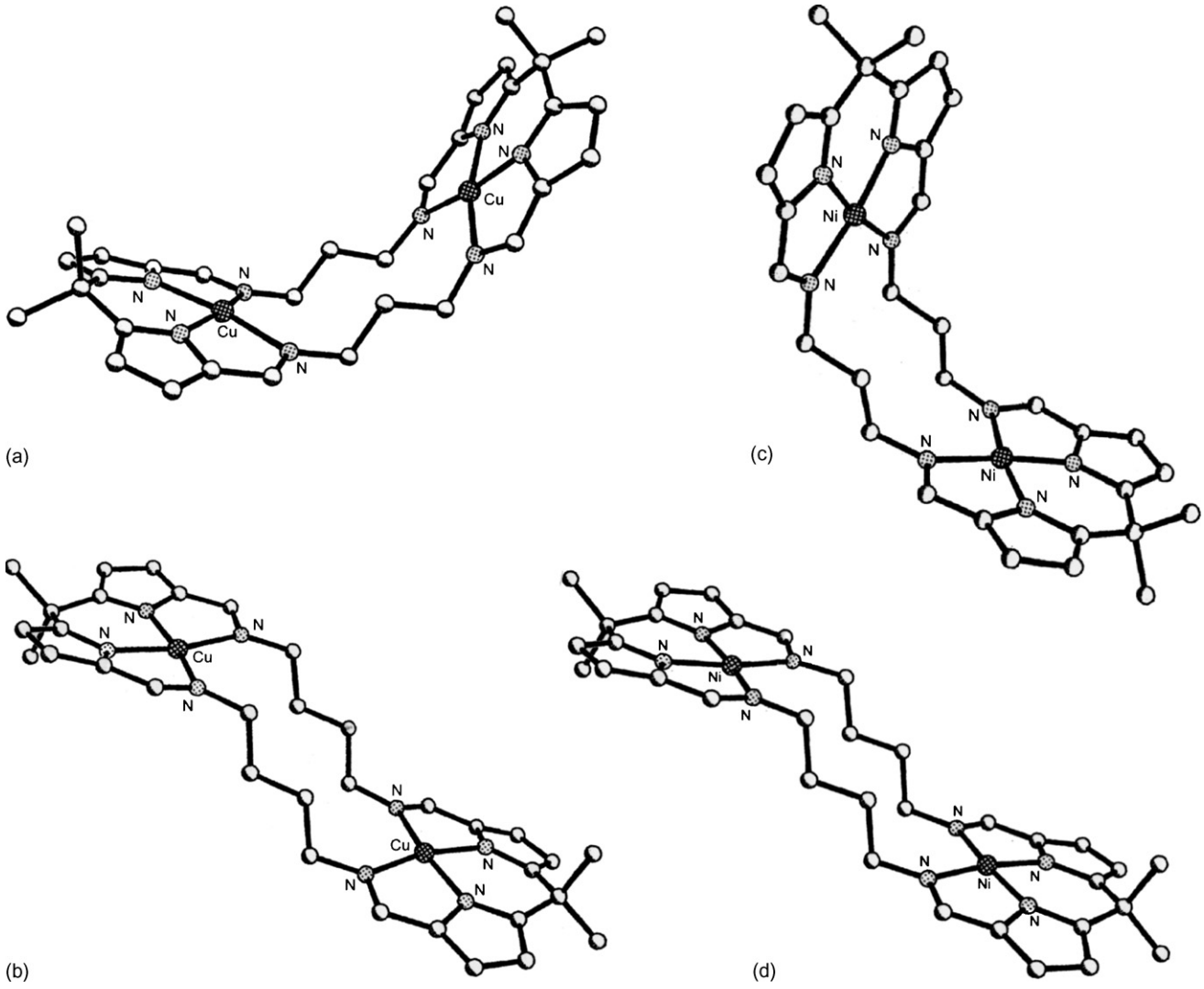

Fig. 93. Structure of [Cu_2(**122d**)] (a), [Cu_2(**122e**)] (b), [Ni_2(**122d**)] (c) and [Ni_2(**122e**)] (d).

In these complexes each ligand is bound by two iron(III) ions containing a single μ-oxo bridge. However, the nature of this binding differs when the complexes are formed from the free base macrocycles rather than from the HCl salts. In the case of complexes derive from the free macrocycle (Fig. 95 a and b) the ligand is significantly folded about the axis containing the two sp^3 carbon atoms. As a result, two phenylene rings of each macrocycle are stacked relative to one another, this yields a crystallographic mirror plane which bisects the Fe–O–Fe angle in [Fe_2(**122f**)(O)] and the approximate mirror planes found in [Fe_2(**122h**)(O)] and [Fe_2(**122i**)(O)] (the latter two structures have substituents which break the overall symmetry). In this conformation, each iron(III) ion of the central Fe–O–Fe moiety is coordinate to one dipyrromethane unit, through each pyrrole nitrogen and to two phenylene diimine units, through one imine nitrogen from each phenylene diimine. In these complexes each iron center is five coordinate with a geometry that has been described as being a distorted square pyramid (Fig. 95a) [118].

In contrast to these complexes, the presence of HCl in the starting macrocycle vastly alters the binding mode of Fe(III) in the resulting complexes. Like [Fe_2(**L**)(O)], the complexes [Fe_2(H_2-**L**)(O)Cl_2] are five coordinate μ-oxo diiron(III) complexes. However, the metal coordination environment is not the same. In [Fe_2(H_2-**L**)(O)Cl_2] each iron ion of an Fe–O–Fe moiety is coordinated to one phenylene diimine unit through each imine nitrogen, one pyrrole nitrogen from a dipyrromethane unit, and one chloride anion. In this conformation, the geometry for each iron ion in [Fe_2(H_2-**122h**)(O)Cl_2] and [Fe_2(H_2-**122i**)(O)Cl_2] is a distorted trigonal bipyramid. Unlike the complexes [Fe_2(**L**)(O)] which are characterized by a bent Fe–O–Fe group, the complexes [Fe_2(H_2-**L**)(O)Cl_2], contain an almost linear Fe–O–Fe group. These differences are also reflected in the Fe···Fe distances (3.639 and 3.651 Å, respectively) (Fig. 95 c and d) [118].

H_4-**122f** reacts with excess copper(I) mesitylene [$Cu_5(Mes)_5$] in tetrahydrofuran at room temperature under argon to form a dark brown solution presumably, containing one or more coordinated copper(I) species, which stirred overnight at room temperature followed by subsequent air oxidation gave the bis-copper(II) complex [Cu_2^{II}(**122f**)] as dark green crystals after

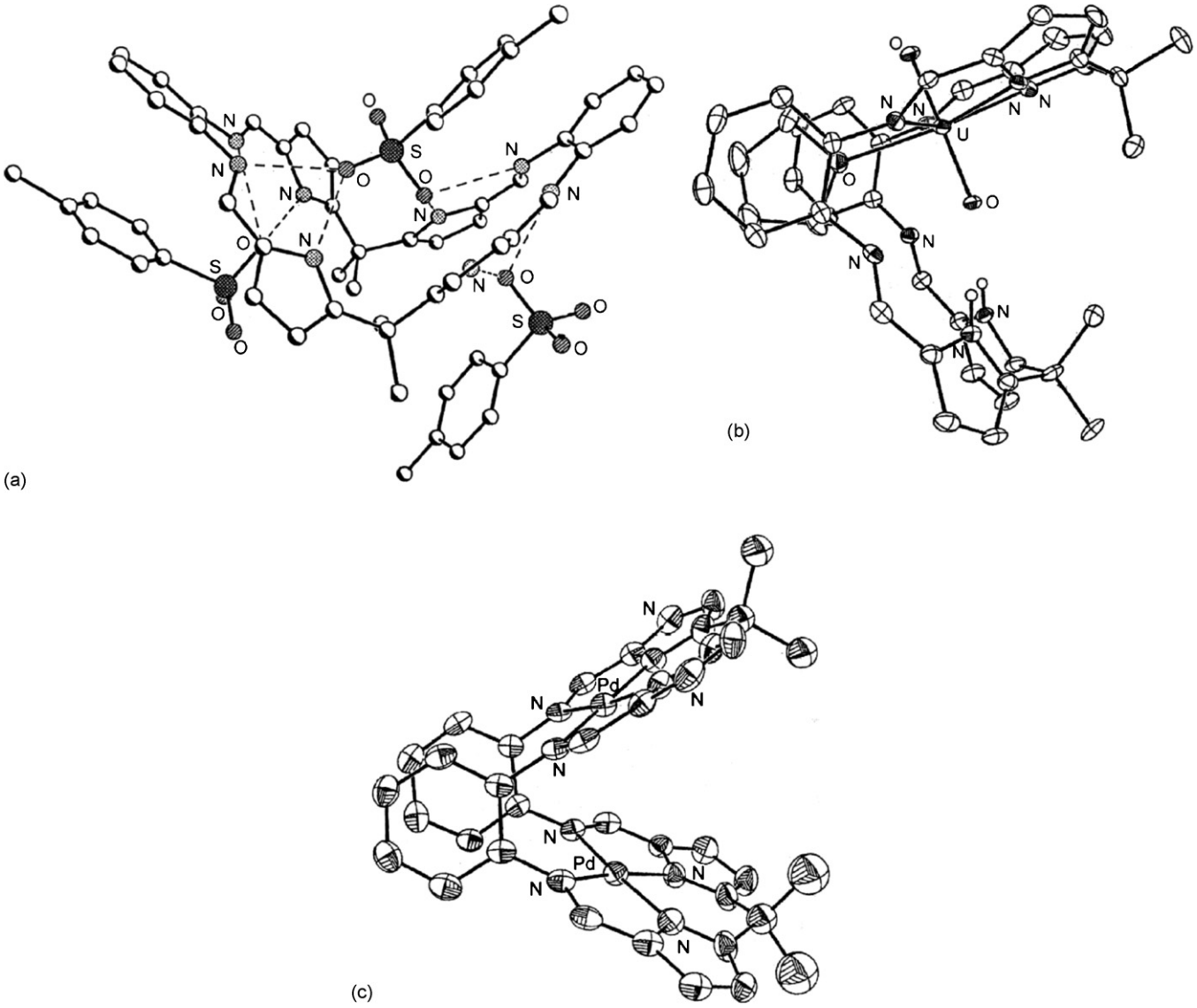

Fig. 94. Structure of $\{[H_8\text{-}\mathbf{122f}](CF_3C_6H_4SO_3)_4\}$ (a), $[UO_2(H_2\text{-}\mathbf{122f})(THF)]$ (b) and $[Pd_2(\mathbf{122f})]$ (c).

subjecting the crude product to recrystallization by slow diffusion of hexanes into a methylene dichloride solution. In $[Cu_2(\mathbf{122f})]$ the geometry about each copper(II) center is square planar; each copper(II) center is bound to one of the pyrrole nitrogen atoms from each of the two dipyrromethane units and to one of the imine nitrogen atoms from each of the phenylenediimine units. The Cu···Cu distances is 3.4.73 Å [118] (Fig. 96a).

The addition of 2 equiv. of HCl to 1 equiv. of H_4-**122f** in CH_2Cl_2, followed by evaporation of the solvent and the addition of 1 equiv. of $[Cu_5(Mes)]_5$ and 20 ml of dry oxygen free THF, gives rise to a yellow–brown solution. This, stirred overnight at room temperature and evaporated to dryness, separates a brown powder which, redissolved in THF and layered with *n*-pentane gives air-sensitive yellow–brown crystals of the dinuclear copper(I) complex $[Cu_2^{I}(H_4\text{-}\mathbf{122f})(Cl)_2]$. By a similar procedure also $[Cu_2^{I}(H_4\text{-}\mathbf{122i})(Cl)_2]$ was obtained. The structures of these complexes (Fig. 96b and c) correspond to bimetallic copper(I) complexes with each copper ion bound to two nitrogen atoms from a single phenylenediamine unit and to, at least, one chloride ion. In $[Cu_2^{I}(H_4\text{-}\mathbf{122i})(Cl)_2]$ there are two bridging chloride groups and the geometry around each copper(I) ion a distorted tetrahedron [118]. The flexibility of the macrocycle allows the ligand to fold and bring the two copper(I) ions close together, resulting in a Cu···Cu distance of 3.290 Å [118].

Mass spectrometric analyses of $[Cu_2(H_4\text{-}\mathbf{122f})(Cl)_2]$ and $[Cu_2(H_4\text{-}\mathbf{122i})(Cl)_2]$, after dissolution in CH_2Cl_2 and exposition to air, confirmed that the copper ions remained coordinated to the macrocycles after air oxidation [118]. Crystals, isolated from the oxidation reaction of $[Cu_2^{I}(H_4\text{-}\mathbf{122f})(Cl)_2]$, contain exactly the same connectivity found in $[Cu_2^{II}(\mathbf{122f})]$. In $[Cu_2(H_4\text{-}\mathbf{122f})(Cl)_2]$ the macrocycle supports the coordination of two copper(I) cations by acting as a bis-bidentate ligand through the two phenylene diimine units. However, upon air oxidation the macrocycle becomes a bis-tetradentate ligand and coordinates

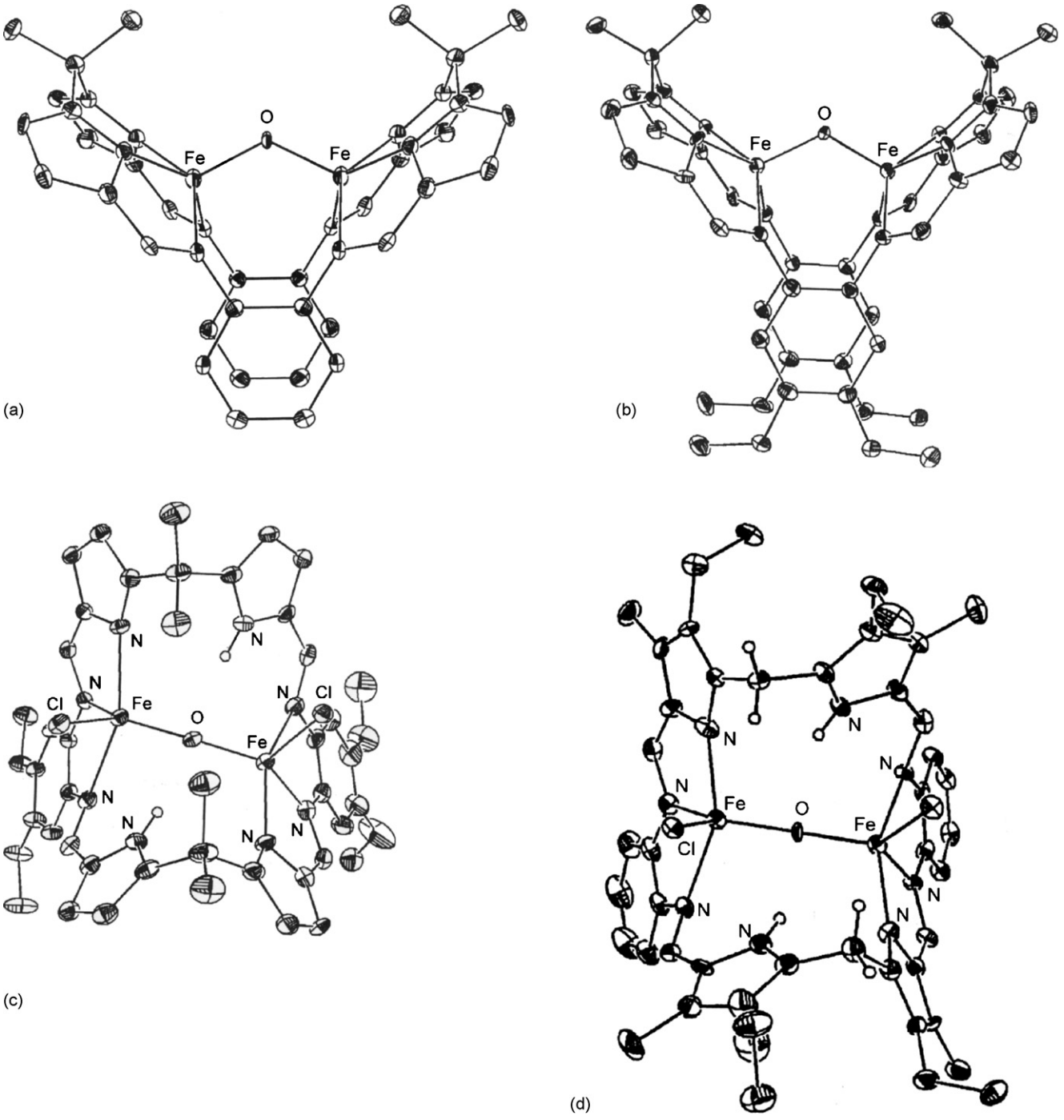

Fig. 95. Structure of [Fe_2(**122f**)(O)](a), [Fe_2(**122h**)(O)] (b), [Fe_2(H_2-**122h**)(O)$(Cl)_2$] (c) and [Fe_2(H_2-**122i**)(O)$(Cl)_2$] (d).

each copper(II) cation through the pyrrole nitrogen atoms of a dipyrromethane unit and one imine nitrogen atom from each phenylenediimine unit [118].

SQUID magnetic susceptibility of [Cu_2(**122f**)] provide evidences for antiferromagnetic coupling ($-J = 41\ cm^{-1}$) between the two copper(II) centers [118].

The reaction between equimolar amounts of H_4-**122f** and $Zn(CH_3COO)_2{\cdot}2H_2O$ in boiling $CHCl_3$ results in the formation of [Zn_3(H_6-**122l**)$(CH_3COO)_6$]. While no molecular ion for the trinuclear complex was observed in the ESMS spectrum, the peak at *m/z* 907 can be assigned to the metal free product H_6-**122l**. The X-ray structure of confirms that the [2 + 2] macrocycle H_4-**122f** has indeed been expanded to the new [3 + 3] macrocycle H_6-**122l** on reaction with $Zn(CH_3COO)_2{\cdot}2H_2O$. The six iminopyrrole units are linked alternatively to three rigid *o*-aryl spacers and three sp^3-hybridized meso-$C(CH_3)_2$ groups, thus precluding the full conjugation of the molecule and forming a [39]-membered organic macrocycle. Each zinc(II) ion is bound to two imine nitrogen centers and to two acetate groups; two zinc(II) ions are in a tetrahedral geometry as the acetate ligands are monodentate, while for third zinc(II) ion the combination of mono- and bidentate acetate coordination results in a distorted

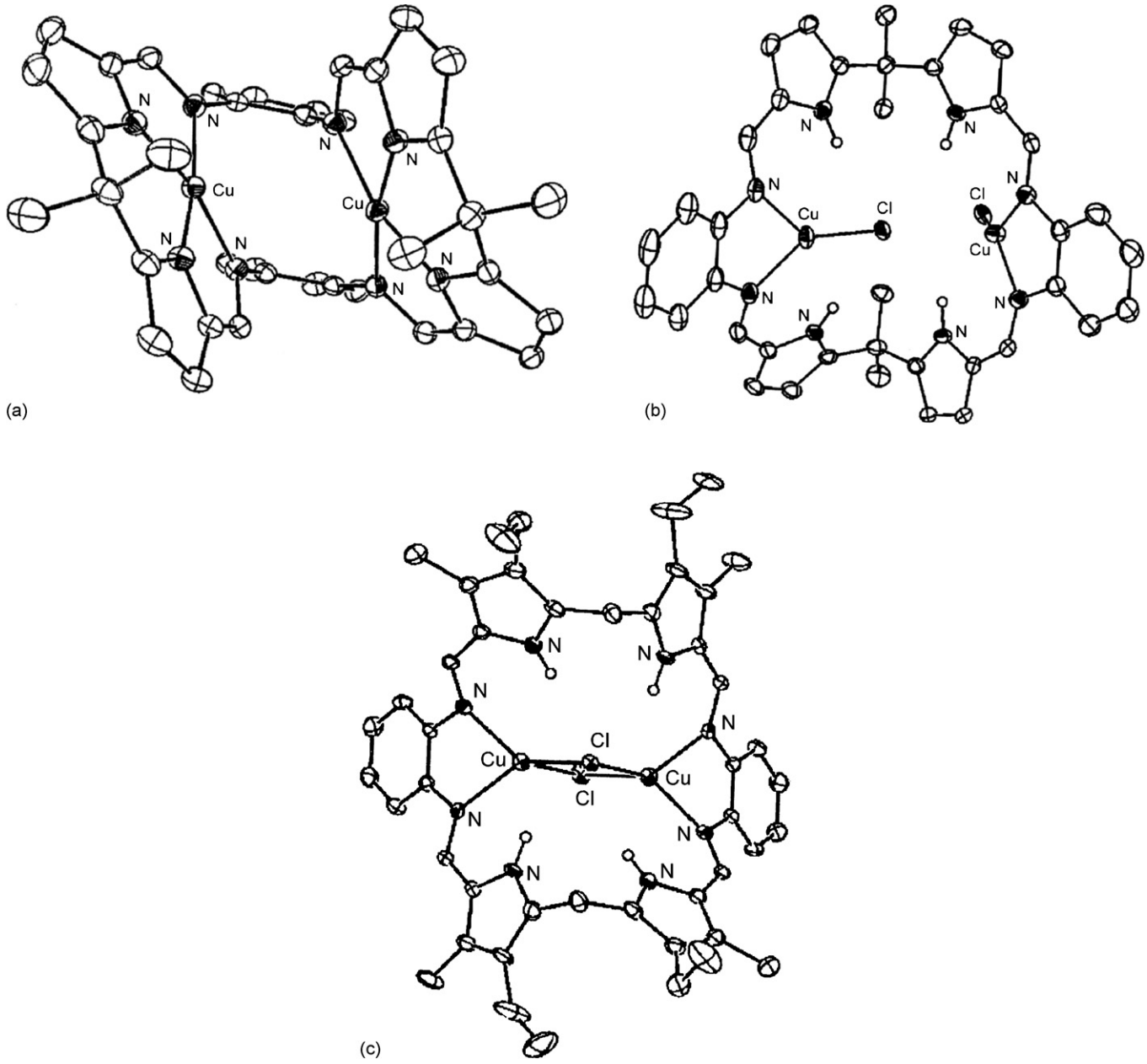

Fig. 96. Structure of $[Cu^{II}_2(\mathbf{122f})]$ (a), $[Cu^{I}_2(H_4\text{-}\mathbf{122f})(Cl)_2]$ (b) and $[Cu^{I}_2(H_4\text{-}\mathbf{122i})(\mu\text{-}Cl)_2]$ (c).

trigonal bipyramidal geometry. The macrocycle itself is not planar as the flexibility at the dipyrromethane meso-carbons promotes an overall wedge-shape in which three acetate groups are endo- to the cleft, with the remainder exo. The wedge topology appears to be stabilized by intra- and intermolecular hydrogen-bonding interactions between the oxygen atoms of the acetate groups and the acidic protons of both the pyrrolic groups and chloroform solvent of crystallization (Fig. 97a) [118].

Protonation of $[Zn_3(H_6\text{-}\mathbf{122l})(CH_3COO)_6]$ by a variety of acids results in the isolation of the protonated [2 + 2] species $[H_4\text{-}\mathbf{122f}]\cdot 4HX$ ($HX = CH_3C_6H_4SO_3H$, CF_3COOH, CH_3COOH). However, the reaction between $[Zn_3(H_6\text{-}\mathbf{122l})(CH_3COO)_6]$ and Na_2S resulted in the clean formation of H_6-**122l** as a yellow powder that was readily separated by extraction from ZnS and $Na(CH_3COO)$ by-products. While H_6-**122l** is stable against contraction in the solid state, rapid (ca. 10 min.) and complete conversion into H_4-**122f** is observed in solution [120].

Attempts to reduce H_6-**122l** to a more stable amine analogue using borohydride were unsuccessful and yielded H_4-**122f** only. Some insight into the structures and relative stabilities of H_4-**122f** and H_6-**122l** was gained from conformational calculations that showed that while both macrocycles adopt global minimum conformations of similar energy, the calculated structure of H_6-**122l** adopts a more twisted conformation that, as a consequence, may result in its lack of stability with respect to contraction [120].

The reaction between H_4-**122f** and $Cd(CH_3COO)_2\cdot 2H_2O$ in boiling $CHCl_3$ did not generate any [3 + 3] macrocyclic product, but instead resulted in the formation of the [2 + 2] macrocyclic product $[Cd_2(H_4\text{-}\mathbf{122f})(CH_3COO)_4]$ as indicated by ESI and

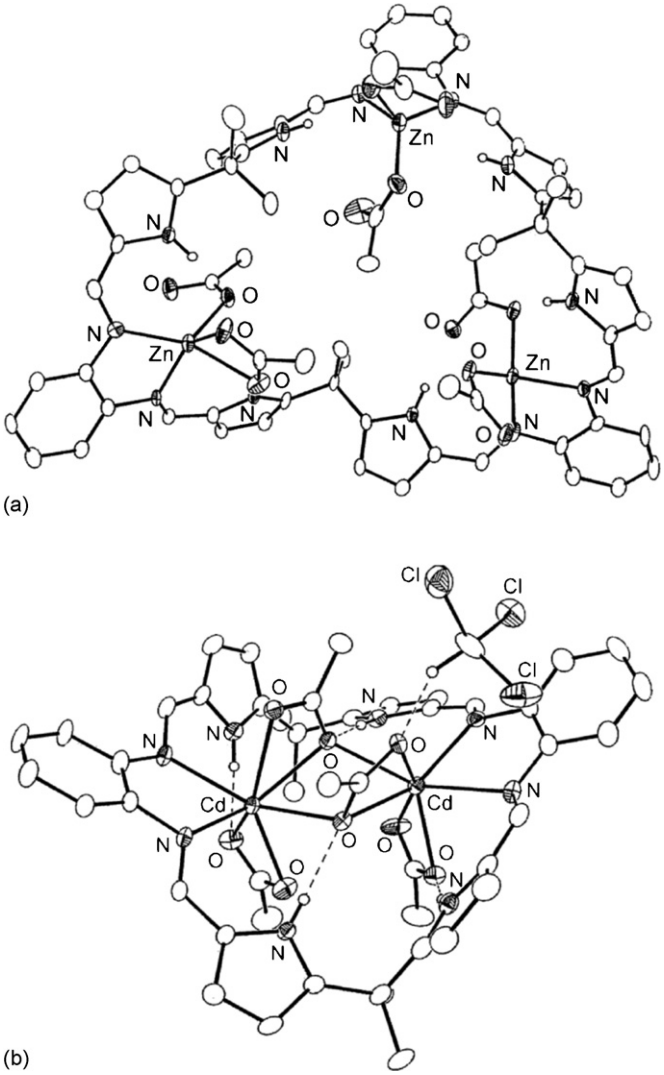

Fig. 97. Structure of $[Zn_3(H_6\text{-}\mathbf{122l})(CH_3COO)_6]$ (a) and $\{[Cd_2(H_4\text{-}\mathbf{122f})(CH_3COO)_4]\cdot CHCl_3\}$ (b).

FAB-mass spectrometric measurements, which showed peaks at *m/z* 605 due to $[H_4\text{-}\mathbf{122f}]^+$ and 826 at *m/z* attributed to $[Cd_2(H_4\text{-}\mathbf{122f})]$ and by ^{1}H NMR spectroscopy which shows Cd-coupling to the imine H(J_{CdH} 30.3 Hz), consistent with complexation of the cadmium(II) ions to the imine nitrogen, a coordination mode that is further corroborated by the presence of hydrogen-bonded pyrrolic NH resonances at 12.2 ppm [120]. The structure shows that the cadmium(II) acetates are bound to the macrocycle H_4-**122f** via imine nitrogens only, while the pyrrolic nitrogens remain protonated. A unique cadmium(II) acetate environment is observed that consists of symmetric terminal- and, significantly, bridging-bidentate acetate coordination (Fig. 97b) [120]. In a similar manner to $[Zn_3(H_6\text{-}\mathbf{122l})(CH_3COO)_6]$, close interactions between the pyrrolic nitrogen and acetate oxygen atoms occur in $[Cd_2(H_4\text{-}\mathbf{122f})(CH_3COO)_4]$ and are consistent with the presence of intramolecular hydrogen-bonding.

Analogously, the reaction between H_4-**122f** and $Zn(BF_4)_2\cdot 2H_2O$ in boiling $CHCl_3$ does not result in macrocycle expansion, but instead generates the [2 + 2] macrocyclic

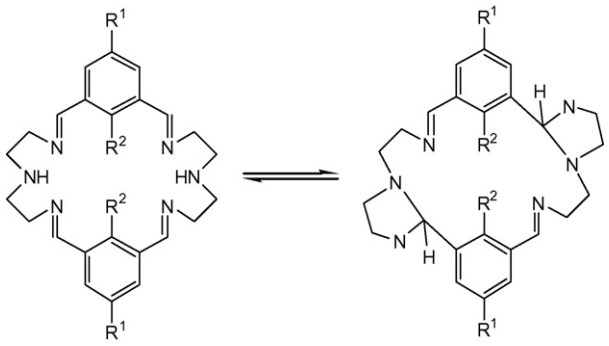

Scheme 11. Ring contraction and ring expansion of cyclic Schiff bases.

complex $[Zn_2(H_4\text{-}\mathbf{122f})](BF_4)_4$ whose ^{1}H NMR spectrum shows the presence of pyrrolic NH resonances (δ 10.7 ppm) and ESI-mass spectrometry data, showing a peak at *m/z* 605 attributable to $[H_4\text{-}\mathbf{122f}]^+$, confirm the formation of a [2 + 2] structure [120].

2.5.4. Benzine-based macrocycles

The macrocyclic compounds **123a**···**123d** were prepared as crystalline solids by the condensation of bis(2-

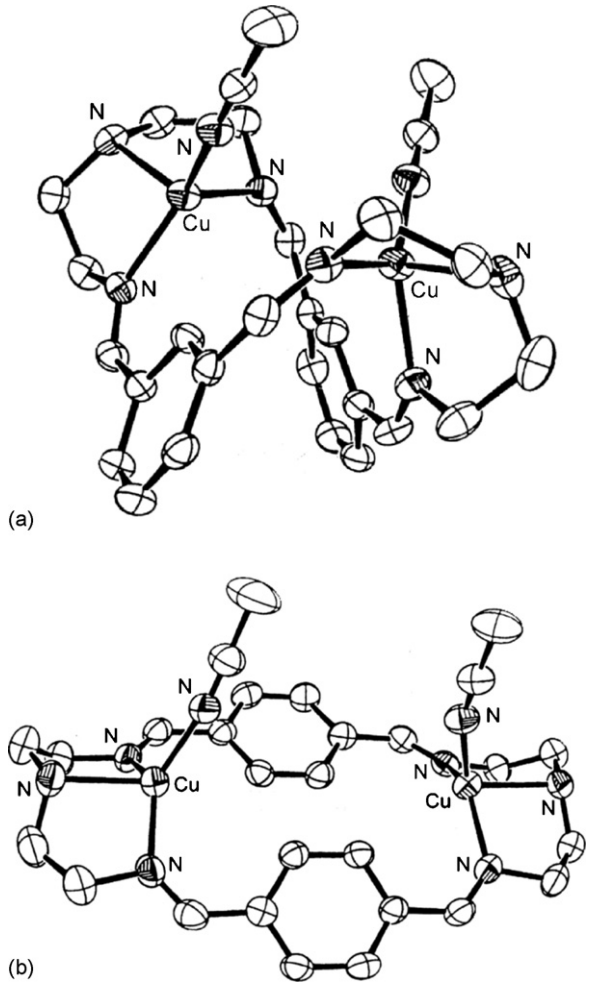

Fig. 98. Structure of $[Cu_2(\mathbf{123a})(CH_3CN)_2]^{2+}$ (a) and $[Cu_2(\mathbf{123d})(CH_3CN)_2]^{2+}$ (b).

aminoethyl)amine with the appropriate aromatic dialdehyde under dilute conditions. The products were characterized by a combination of different mass spectrometry techniques and by IR and NMR spectroscopy. The ^{1}H NMR spectra of **123a**···**123c** suggest the existence of isomers in solution due to the facile nucleophilic attack of an NH group to one of the neighboring imine fragments, leading to the reversible formation of [18]-membered diimine imidazolimine macrocycles (Scheme 11). According to ^{1}H and ^{13}C NMR studies in CD_3CN, DMSO or DMF at 25 °C, **123b** exists predominantly in the form of the [18]-membered di-imidazolidine isomer, while for **123a** and **123c** no preference has been found between the [24]-tetraimine isomer and the [18]-membered diimine one [119,120]. Similar ring expansion and ring contraction processes have been extensively discussed in previous reviews [5].

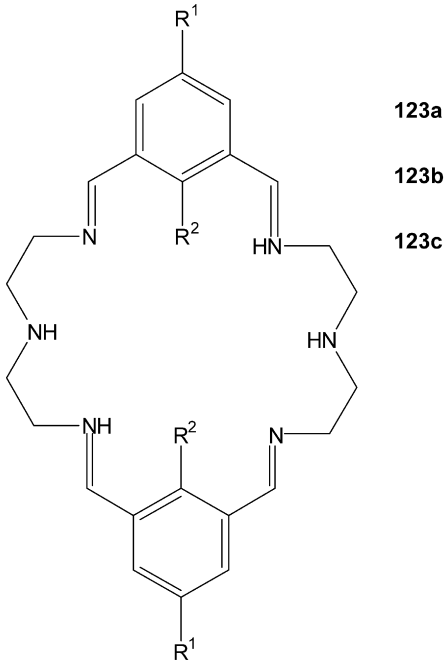

	R^1	R^2
123a	H	H
123b	$C(CH_3)_3$	H
123c	H	CH_3

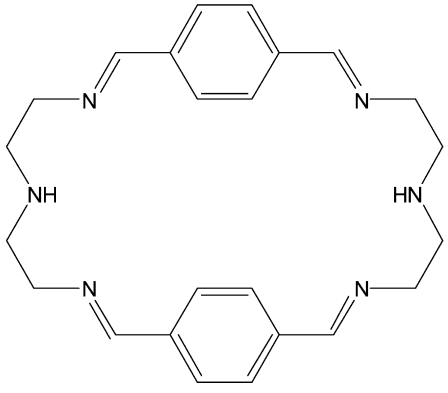

123d

The complexes $[Cu_2(\mathbf{L})(CH_3CN)_2](X)_2$ (**L** = **123a**···**123c**, $X = ClO_4^-$, $CF_3SO_3^-$) were obtained by the addition of in situ generated copper(I) perchlorate or copper(I) triflate to the appropriate ligand in CH_2Cl_2 followed by recrystallization of the resulting product from an acetonitrile/diethyl ether solution.

The structure of $[Cu_2(\mathbf{123a})(CH_3CN)_2](ClO_4)_2$ and $[Cu_2(\mathbf{123c})(CH_3CN)_2](CF_3SO_3)_2$ confirms in both cases the coordination of two copper(I) ions to the hexadentate macrocycle. Additionally, a coordinated acetonitrile molecule completes the distorted tetrahedral coordination geometry of the copper centers. In the case of $[Cu_2(\mathbf{123a})(CH_3CN)_2](ClO_4)_2$ the *meta*-substituted aromatic spacer units afford a C_2-symmetric arrangement of both copper(I) containing subunits relative to each other leading to a short Cu···Cu distance of 4.28 Å. Thereby, the two copper centers are pointing toward each other, enforced by a pocket-like orientation of the macrocyclic ligand array (Fig. 98a) [119]. $[Cu_2(\mathbf{123d})(CH_3CN)_2](CF_3SO)_2$ contains two tridentate metal binding sites that are separated by *para*-substituted aromatic spacer units. This leads to a linear arrangement of the two copper sub-structures with a larger Cu···Cu distance of 6.86 Å. The copper(I) centers in $[Cu_2(\mathbf{123d})(CH_3CN)_2](CF_3SO_3)_2$ are oriented to the same side of the plane defined by the macrocycle. The two triflate anions show no direct interactions with the metal centers (Fig. 98b) [121].

Dioxygen bubbling at room temperature into the orange acetonitrile/dichloromethane/methanol solution of $[Cu_2(\mathbf{123a})(CH_3CN)_2](ClO_4)_2$ gradually developed a green solution. After workup, green prismatic crystals of $[Cu_2(\mathbf{123a})(OCH_3)_2](ClO_4)_2$ have been isolated by recrystallization from acetonitrile. Single crystal X-ray analysis indicates this complex to be a dinuclear bis(μ-methoxy) copper(II) complex still bearing the initial macrocyclic ligand. The cation shows a chiral C_2-symmetry around the dinuclear copper(II) core. The geometry around each copper(II) core is distorted square planar with a Cu···Cu separation of about 3.03 Å. The $\{Cu_2(\mu\text{-}OCH_3)\}^{2+}$ core unit forms an ideal plane which is located perpendicular to the macrocyclic pocket structure (Fig. 99a) [121].

The reaction of $[Cu_2(\mathbf{123b})(CH_3CN)_2](ClO_4)_2$ with dioxygen in dichloromethane proved to be even faster than $[Cu_2(\mathbf{123a})(CH_3CN)_2](ClO_4)_2$. The nonsymmetric complex $[Cu_2(\mathbf{123e})(OH)](ClO_4)_2$, which was isolated in high yield, is the product of an intramolecular oxygenation reaction bearing bridging phenoxide and hydroxy units. Each copper(II) ion adopts a slightly distorted square pyramidal coordination environment. One imine and one amine nitrogen, and one phenolic and one hydroxo oxygen atom form the basal equatorial plane. In contrast to $[Cu_2(\mathbf{123a})(OCH_3)_2](ClO_4)_2$, the two axial imine donors are deposited *cis* with respect to the Cu_2O_2 plane, which leads to the unusual U-form of the macrocyclic ligand system (Fig. 99b) [121].

An electrophilic attack of the μ-η^2-η^2-peroxo moiety to the aryl part of the ligand is proposed for the formation of such hydroxylation products. This suggestion is supported by the observation that tert-butyl substitution at the 5-position of the aromatic spacer unit increases the rates of the C–H activation process in the 2-position and leads to higher yields of the insertion product $[Cu_2(\mathbf{123e})(OH)](ClO_4)_2$. It is further found that a lower reaction temperature or addition of toluene inhibits the

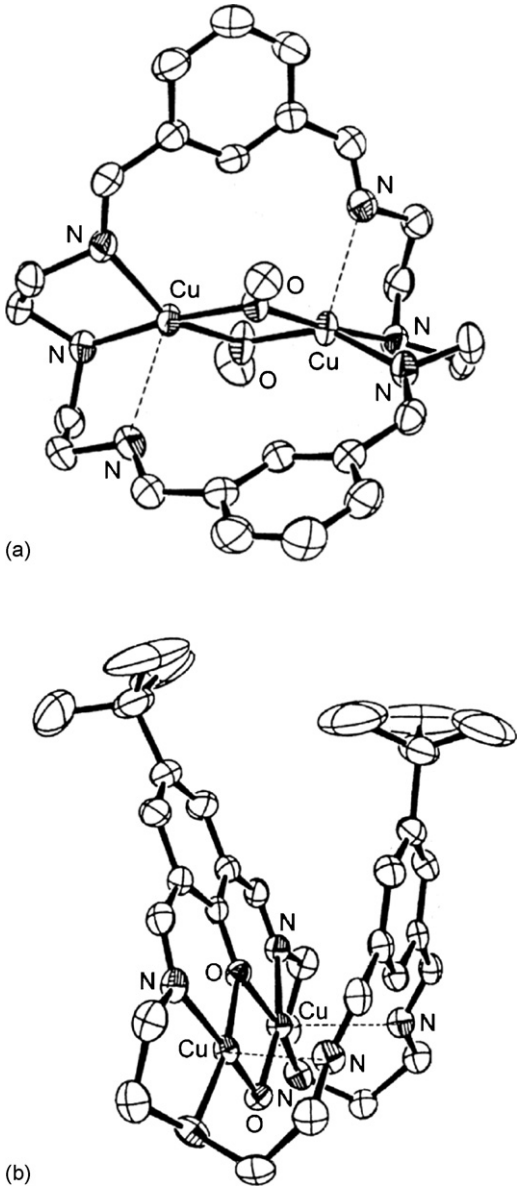

Fig. 99. Structure of $[Cu_2(\mathbf{123a})(\mu\text{-}OCH_3)_2]^{2+}$ (a) and $[Cu_2(\mathbf{123e})(OH)]^{2+}$ (b).

hydroxylation reaction. However, the presence of benzyl alcohol increases the ratio of $[Cu_2(\mathbf{123e})(OH)](ClO_4)_2$ to the rest of oxidation products up to 88%. The increase of the proton donor ability of the reaction medium favours the formation of the hydroxylation products [121].

$[Cu_2(\mathbf{123c})(CH_3CN)_2](ClO_4)_2$, bearing methyl substituents on the aromatic rings of the macrocycle frame, shows a completely different reactivity with dioxygen than $[Cu_2(\mathbf{123a})(CH_3CN)_2](ClO_4)_2$ and $[Cu_2(\mathbf{123b})(CH_3CN)_2](ClO_4)_2$. The reaction of $[Cu_2(\mathbf{123c})(CH_3CN)_2](ClO_4)_2$ with dioxygen was also performed on a synthetic scale in dichloromethane at room temperature. The color of the solution changed gradually to yellow-greenish and a solid of the same color developed as in the cases of $[Cu_2(\mathbf{123a})(CH_3CN)_2](ClO_4)_2$ and $[Cu_2(\mathbf{123b})(CH_3CN)_2](ClO_4)_2$. After workup, a yellow-greenish powder was isolated, which shows the existence of a $[Cu_2(\mathbf{123c})(O_2)]^{2+}$ fragment by means of mass spectrometry. Unfortunately, all attempts to purify the products by crystallization failed, due to the poor solubility in suitable solvents. The analysis of products obtained after hydrolysis by addition of 4N HCl and subsequent extraction with dichloromethane gave the original dialdehyde, 4-hydroxy-2-methylisophtalaldehyde and the tetraaldehyde 1,3,1′,3′-tetraformyl-2,2′-dimethylphenyl coupling product. Thus, the introduction of 2-methyl substituents in H_2-**123c** has not blocked the binding of dioxygen but has effectively inhibited the intramolecular hydroxylation reactions. The formation of 4-hydroxy-2-methylisophtalaldehyde might be explained assuming that an intermolecular hydroxylation process occurs. If an electrophilic attack is suggested for this process, the hydroxylation should happen in the 5-position of the aromatic unit. Thus, the 4-hydroxy-2-methylisophtalaldehyde and even the coupling product are most likely formed via a free radical process before or during acidic decomposition [121].

Compared to the oxygenation activity of $[Cu_2(\mathbf{L})(CH_3CN)_2](ClO_4)_2$ ($\mathbf{L} = \mathbf{123a}\cdots\mathbf{123c}$) the *para*-substituted copper(I) complex $[Cu_2(\mathbf{123d})(CH_3CN)_2](ClO_4)_2$ is completely inert to dioxygen. No oxygenation or even decomposition was observed in solution or in the solid state after exposure to dioxygen. This surprising effect becomes clear by comparing the Cu···Cu distances in the *meta*-bridged complex $[Cu_2(\mathbf{123a})(CH_3CN)_2](ClO_4)_2$ and the linear *para*-bridged complex $[Cu_2(\mathbf{123d})(CH_3CN)_2](ClO_4)_2$. The *para*-substituted aromatic units restrict the free location of the two copper(I) centers relative to each other and leads to a separation of the copper centers (Cu···Cu = 6.86 Å). This implies that no dioxygen can be activated. The *meta*-aromatic bridges force the two copper(I) centers into a chiral, pocket-like arrangement with a short Cu···Cu distance (4.28 Å) allowing both copper centers to bind and activate the dioxygen molecule simultaneously [121].

The magnetic susceptibilities of $[Cu_2(\mathbf{123a})(OCH_3)_2](ClO_4)_2$ and $[Cu_2(\mathbf{123e})(OH)](ClO_4)_2$ were determined from 2 to 400 K (or 300 K). $[Cu_2(\mathbf{123a})(OCH_3)_2](ClO_4)_2$ shows a remarkable antiferromagnetic behaviour over the whole temperature range, due to the coupling of two copper(II) ions in the same molecule, where the superexchange is mediated by the bridging methoxy group. The effective magnetic moment for copper (μ_{eff}/Cu) is about $1.2\mu_B$ in solid state. A value of $-2J = 587\ cm^{-1}$ is obtained at room temperature, indicating a strong coupling between the two copper ions even at this temperature [119]. The magnetic behaviour of $[Cu_2(\mathbf{123e})(OH)](ClO_4)_2$, significantly different from that of $[Cu_2(\mathbf{123a})(OCH_3)_2](ClO_4)_2$ despite the relative similar Cu···Cu distance, suggests that the copper ions are essentially independent centers or, at best, very weakly coupled. In the low temperature range, the molar susceptibility of $[Cu_2(\mathbf{123e})(OH)](ClO_4)_2$ is in a good agreement with the Curie–Weiss law as indicated by the linear relation of $1/\chi$ over T below 100 K [121].

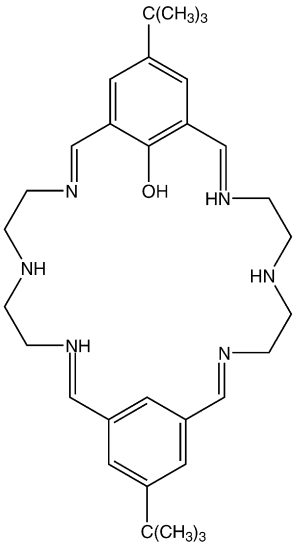

H-**123e**

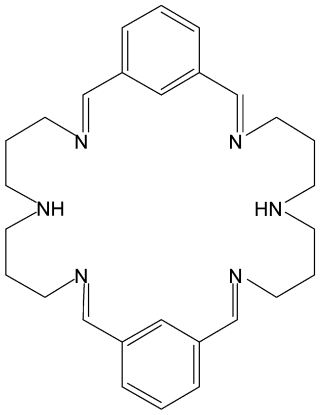

124

The ring enlarged [28]-membered macrocyclic Schiff base **124** has been prepared by condensation of 1,3-diformylbenzene and bis(3-aminopropyl)amine. The same condensation, using $[Cu(CH_3CN)_4](ClO_4)$ as templating agent under inert conditions, afforded $[Cu_2(\mathbf{124})](ClO_4)_2$ where each copper(I) ion is coordinated in a distorted trigonal planar manner by two imine donors and one amine donor. In contrast to $[Cu_2(\mathbf{123a})(CH_3CN)_2](ClO_4)_2$, no acetonitrile molecules are coordinated in $[Cu_2(\mathbf{124})](ClO_4)_2$ as additional coligands. The phenyl rings in this complex are coplanar to each other and therefore provide a large cavity in which the two copper(I) ions are included. The copper(I) ions are separated from one another by 7.700 Å and shifted out of the N_3 plane (Fig. 100) [121].

Furthermore, the reaction of $[Cu_2(\mathbf{124})](ClO_4)_2$ in methanol with dioxygen does not give rise to intramolecular aromatic ring hydroxylation. The final reaction product, not characterized in detail, was proposed to be a bis(μ-methoxy)-bridged dicopper(II) complex. A kinetic analysis of the reaction of $[Cu_2(\mathbf{124})](ClO_4)_2$ with dioxygen in methanol or acetone proved to be complex with several reaction steps detected. Under the conditions employed, no reactive dioxygen intermediate could be detected [121].

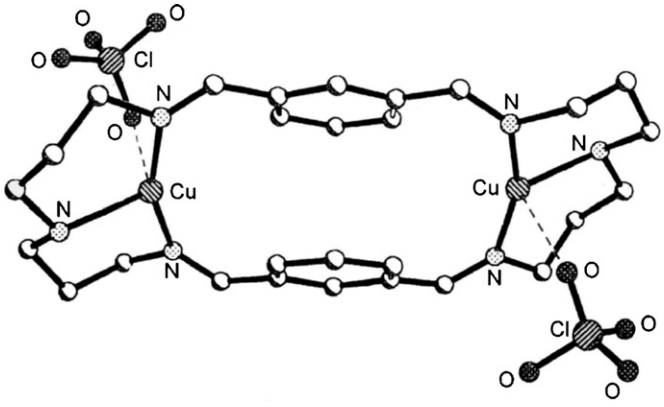

Fig. 100. Structure of $[Cu_2(\mathbf{124})](ClO_4)_2$.

Electrochemical studies of $[Cu_2(\mathbf{123a})(CH_3CN)_2](ClO_4)_2$ in dichloromethane show a broad irreversible oxidation wave at +0.56 V which disappears upon addition of varying equivalents of copper(I) salt to be replaced by a new irreversible oxidation wave (to copper(II) for the copper(I) complex at +0.12 V accompanied by a number of irreversible reduction waves on the return scan at −0.011, −0.34 and −1.31 V. In dichloromethane the height of the +12 V wave increases linearly with the equivalents of Cu^I added up to a sharp break leveling off at exactly 2.0 equiv., indicating that a single complex, the copper(I) species $[Cu_2(\mathbf{123a})(CH_3CN)_2](ClO_4)_2$, is relevant over all ratios of Cu^I to **123a** in this solvent. However, in acetonitrile different behaviour is observed, with more than 2.0 equiv. of copper(I) ion required to maximize the height of the +0.12 V wave of the dicopper(I) species. The growth of the peak with copper(I) ion concentration is now curved without the appearance of a sharp break. It was proposed that acetonitrile competes with $[Cu_2(\mathbf{123a})(CH_3CN)_2](ClO_4)_2$ for coordination to the copper(I) ion, thus setting up an equilibrium between $[Cu_2(\mathbf{123a})(CH_3CN)_2](ClO_4)_2$ and $[Cu(CH_3CN)_x]^+$ quite feasible since acetonitrile is known to be an effective ligand for the copper(I) ion. Furthermore, this finding correlates with the observation that intramolecular aromatic ring hydroxylation is suppressed in acetonitrile [121].

All attempts to isolate a stable dicopper(II) complex with **123a** under different conditions and using various anions failed. The reaction of $Cu(ClO_4)_2$ in dry methanol with **123a** precipitated the bluish-green, moisture sensitive, solid $[Cu_2(\mathbf{123a})](ClO_4)_4$, with infrared evidences of weak ClO_4^- coordination. This and other related complexes rapidly turn bright blue in the air, due to formation of copper(II)-bis-(2-aminoethyl)amino complexes as a result of hydrolysis of the macrocyclic ligand. The isolation of solid $[Cu_2(\mathbf{123a})(X)_2](X)_2$ ($X = Cl^-$ or NO_3^-) has also been claimed but in the absence of crystal structure this result must be confirmed [120]. From one of these reactions for example the chloride-bridged copper(II) complex $[Cu_2(dien)_2(Cl)_2](SO_3CF_3)_2$ where dien is bis-(2-aminoethylamino, diethylenetriamine) was isolated and identified by X-ray determination. Also a dinuclear copper(II) complex of **124** was postulated to form by reacting $CuCl_2$ with **124** in methanol, but characterization of this compound was not reported; however, the product $[Cu_2(dpt)_2(Cl)_2]Cl_2$ (dpt = dipropylenetriamine) of the quantitative hydrolysis of this complex was described [121].

The stability and kinetics of formation of nickel(II) complexes with the macrocyclic ligand **125**, derived form the reduction of **123a** with $NaBH_4$, have been studied in water solution. The equilibrium studies indicate the formation of several mono- and dinuclear complexes. However, only mononuclear species are formed in presence of ligand excess, whereas the complete conversion of **125** in binuclear complexes can be achieved in the presence of metal excess. The stability data and the electronic spectra suggest a similar coordination environment of the metal centers in all complexes, each nickel(II) ion being coordinated to three of the amine groups in the ligand.

At pH close to 7, complex formation occurs in a single kinetic step both for the mono- and the dinuclear species, which indicates that coordination of both metal ions to the macrocycle occurs with statistically controlled kinetics. The resolved rate constant for reaction of the nickel(II) ion with the protonated forms of the ligand are close to those found for related open-chain polyamines of similar steric requirements thus showing that the macrocycle is flexible enough to allow a rapid structural reorganization during the complex formation processes [122].

Potentiometric equilibrium studies, UV–vis spectrophotometric and voltammetric measurements were carried out to determine the binding of 4-methoxy-1,2-phenylendiamine (DMA) with the dicobalt(II) complexes $[Co_2(\mathbf{125})](ClO_4)_2$ in the absence and presence of dioxygen [122]. Potentiometric measurements show that the $[H_6\text{-}\mathbf{125}]^{6+}$ gives rise to two buffer regions: one near pH 4.0 and the other in the pH range 7.5–11, showing the neutralization of two macrocycle protons in the first buffer and four protons in the second. Neutralization of the macrocyclic ligand therefore occurs in the pH range from 3 to 11. The same potentiometric titrations in the presence of cobalt(II) in a **125**:Co^{II} 1: 2 ratio indicate that, after a consumption of 2 mol of KOH ($a > 2$) per mol of ligand the complexation, reaction of Co^{II} and **125** occurs. The titration is finished at pH near 8.5, where precipitation occurs which makes it impossible to continue the experiment. In the presence of O_2, oxygen complexes start to appear at pH values above 5 and it was possible to titrate the system until pH 11 due to stabilization of μ-peroxo in the cavity of the dinuclear complexes. This dinuclear μ-peroxo complex is stabilized by the presence of 4-methoxy-1,2-phenylendiamine. The species distribution curves for the $\{Co^{II}(\mathbf{125})(O_2)\}$ system in the absence and presence of 4-methoxy-1,2-phenylendiamine as a function of pH indicate that the monohydroxo dioxygen species $\{Co_2(\mathbf{125})(OH)(O_2)\}^+$, appears in aqueous solution at pH values above 7, reaching a maximum of 68% at pH 8.4. The formation of the dihydroxo species $\{Co_2(\mathbf{125})(OH)_2(O_2)\}$ begins to occur at pH 8, forming 88.4% at pH 10.5. The dioxygen complex with the diamine $\{Co_2(\mathbf{125})(O_2)(DAM)\}^{2+}$ is formed at pH value 7.8 and the monohydroxo species $\{Co_2(\mathbf{125})(OH)(O_2)(DAM)\}^+$ reaches a maximum at pH value 9.3 [123]. UV–vis studies show a charge-transfer absorption band for the dinuclear complex $[Co_2(\mathbf{125})](ClO_4)_2$ with the maximum at 297 nm at pH 8.1. In the presence of dioxygen the formation of the $\{Co_2^{II}(\mathbf{125})(\mu\text{-}O_2)\}$ species begins to occur at pH 8.1, and the formation of this complex is completed after 5 h, as indicated by the increasing charge-transfer band at 297 nm. The diamine coordinates with the dicobalt center of the dioxygen complex at pH 8.9. Finally, after 2 h of reaction with diamine, another shoulder at 420 nm is probably due to the product of the oxidation reaction that may take place since the reductant aromatic diamine and the oxidant μ-peroxo are close to each other bonded to the bimetallic center in the cavity of the macrocycle [123].

The reduction potential for the dioxygen dicobalt complex was measured by cyclic voltammetry with a working platinum electrode in aqueous solution containing 0.1 mol l^{-1} KCl as the supporting electrolyte in the range −0.8 to +0.8 V. The cyclic voltammogram shows an irreversible cathodic reduction peak at −0.50 V versus Fe^{II}/Fe^{III}, due to the peroxide bridge in the complex cavity. The process is irreversible most probably because the bridge is broken down. The two peaks at 0.13 and 0.33 V are attributed to the oxidation of the diamine [123].

The reaction of **125**·6HBr with $Ni(CH_3COO)_2{\cdot}4H_2O$ in H_2O at pH ≅ 7 and in a 1:2 molar ratio affords, after the addition of $NaClO_4$, $[Ni_2(\mathbf{125})(CH_3COO)_2(H_2O)_2](ClO_4)_2$. The similar reaction of **126**·6H_2O with $Cu(CH_3COO)_2{\cdot}2H_2O$ affords $[Cu_2(\mathbf{126})(\mu\text{-}CO_3)(H_2O)_2]_2(ClO_4)_4{\cdot}8H_2O$ [123]. Furthermore, **126**·6HBr reacts with $Ni(NO_3)_2{\cdot}6H_2O$ in a 1:1 molar ratio to yield, after cation-exchange chromatography, a complex with possible composition $[Ni_2(\mathbf{126})(H_2O)_6](ClO_4)_4$ which, recrystallized from DMF, forms $[Ni_2(\mathbf{126})(DMF)_6](ClO_4)_4{\cdot}4H_2O$ $[Cu_2(\mathbf{126})(CH_3COO)_2](BF_4)_2$ derives from the reaction of $Cu(CH_3COO)_2{\cdot}2H_2O$ with **126** in methanol in the presence of $NaBF_4$ while $[Cu_2(\mathbf{125})(\mu\text{-Im})(Br)]_2(Br)_4{\cdot}6H_2O$ is obtained when **125**·6HBr and $CuBr_2$ are reacted in water at pH 8, followed by the addition of imidazole in a 1:2:1 molar ratio [124].

In these complexes two metal centers are bound per ligand. In $[Ni_2(\mathbf{125})(CH_3COO)_2(H_2O_2)](ClO_4)_2$, $\{[Cu_2(\mathbf{126})(CH_3COO)(Br)](ClO_4)_2\}_n$, $[Cu_2(\mathbf{126})(\mu\text{-}CO_3)(H_2O)_2]_2(ClO_4)_4{\cdot}8H_2O$, $[Cu_2(\mathbf{126})(CH_3COO)_2](BF_4)_2$ and $[Cu_2(\mathbf{125})(\mu\text{-Im})(Br)]_2(Br)_4{\cdot}6H_2O$, the N_3 subunits of **125** or **126** coordinate meridionally to the metal centers, while in $[Ni_2(\mathbf{126})(DMF)_6](ClO_4)_4{\cdot}2H_2O$ each N_3 subunit of **126** adopts a facial coordination mode. The binuclear cations $[Ni_2(\mathbf{125})(CH_3COO)_2(H_2O)_2]^{2+}$ and $[Ni_2(\mathbf{126})(DMF)_6]^{4+}$ have chair-like conformations, with the distorted octahedral nickel(II) coordination sphere completed by terminal water and a bidentate acetate ligand in $[Ni_2(\mathbf{125})(CH_3COO)_2(H_2O)](ClO_4)_2$ and three DMF ligands in $[Ni_2(\mathbf{126})(DMF)_6](ClO_4)_4{\cdot}2H_2O$ (Fig. 101a and b). The copper(II) centers in $\{[Cu_2(\mathbf{126})(CH_3COO)(Br)](ClO_4)_2\}_n$, $[Cu_2(\mathbf{126})(\mu\text{-}CO_3)(H_2O)_2]_2(ClO_4)_4{\cdot}8H_2O$, $[Cu_2(\mathbf{126})(CH_3COO)_2](BF_4)_2$ and $[Cu_2(\mathbf{125})(\mu\text{-Im})(Br)]_2(Br)_4{\cdot}6H_2O$ generally reside in square planar environments, although a weakly binding ligand enters the coordination sphere in some cases, generating a distorted square pyramidal geometry. The binuclear $\{Cu_2(\mathbf{126})\}$ units in $[Cu_2(\mathbf{126})(CH_3COO)_2](BF_4)_2$, $\{[Cu_2(\mathbf{126})(CH_3COO)(Br)](ClO_4)_2\}_n$, and $[Cu_2(\mathbf{126})(\mu\text{-}CO_3)(H_2O)_2]_2(ClO_4)_4{\cdot}8H_2O$ adopt similar bowl-shaped conformations, stabilized by H-bonding interactions between pairs of amine groups from **126** and a perchlorate or tetrafluoroborate anion. In $\{[Cu_2(\mathbf{126})(CH_3COO)(Br)](ClO_4)_2\}_n$ the binuclear units are linked through acetate groups, bridging in a *syn–anti* fashion, to produce a zigzag polymeric chain structure (Fig. 101c), while $[Cu_2(\mathbf{126})(\mu\text{-}CO_3)(H_2O)_2]_2(ClO_4)_4{\cdot}8H_2O$ incorporates a tetrameric cation consisting of two binuclear units linked via a pair of carbonate bridges (Fig. 102a). $[Cu_2(\mathbf{125})(\mu\text{-Im})(Br)]_2(Br)_4{\cdot}6H_2O$ features an imidazolate bridge between the two copper(II) centers bound by **125.** Pairs of $[Cu_2(\mathbf{125})(\mu\text{-Im})]^{3+}$ units are then weakly linked through a pair of bromide anions (Fig. 102b) [124].

$[H_6\text{-}\mathbf{126}](Br)_6$ reacts with $Cu(ClO_4)_2{\cdot}6H_2O$ in methanol and in presence of $N(Et)_3$ in a 1:2: 6 molar ratio to form $[Co_2(\mathbf{126})](ClO_4)_4{\cdot}2HBr{\cdot}H_2O$ [124]. A similar reaction

in the presence of Na_2CO_3, $NaOCH_3$ or C_6H_5COONa affords the tetranuclear complexes $[Cu_4(\mathbf{126})_2(\mu\text{-}CO_3)_2](ClO_4)_4{\cdot}4H_2O$, $[Cu_4(\mathbf{126})_2(\mu\text{-}OCH_3)_2](ClO_4)_6{\cdot}6H_2O$ or $[Cu_4(\mathbf{126})_2(C_6H_5COO)_2](Br)_6{\cdot}H_2O$ [124]. In $[Cu_4(\mathbf{126})_2(\mu\text{-}CO_3)_2](ClO_4)_4{\cdot}4H_2O$ the cation $[Cu_4(\mathbf{126})_2(\mu\text{-}CO_3)_2]^{4+}$ contains two dinuclear copper(II) units in a layer-to-layer arrangement. In each dinuclear unit the two copper(II) ions are connected by a macrocyclic ligand, with a Cu···Cu separation of 7.23 Å. The two parallel layers are bis-bridged by two CO_3^{2-} groups. The copper ions in each dimer are equivalent; their geometry is square pyramidal with the three amine nitrogens and one oxygen at the nearly same basal plane and a CO_3^{2-} oxygens at the axial site. The copper(II) ions are nearly coplanar (Fig. 102c) [125].

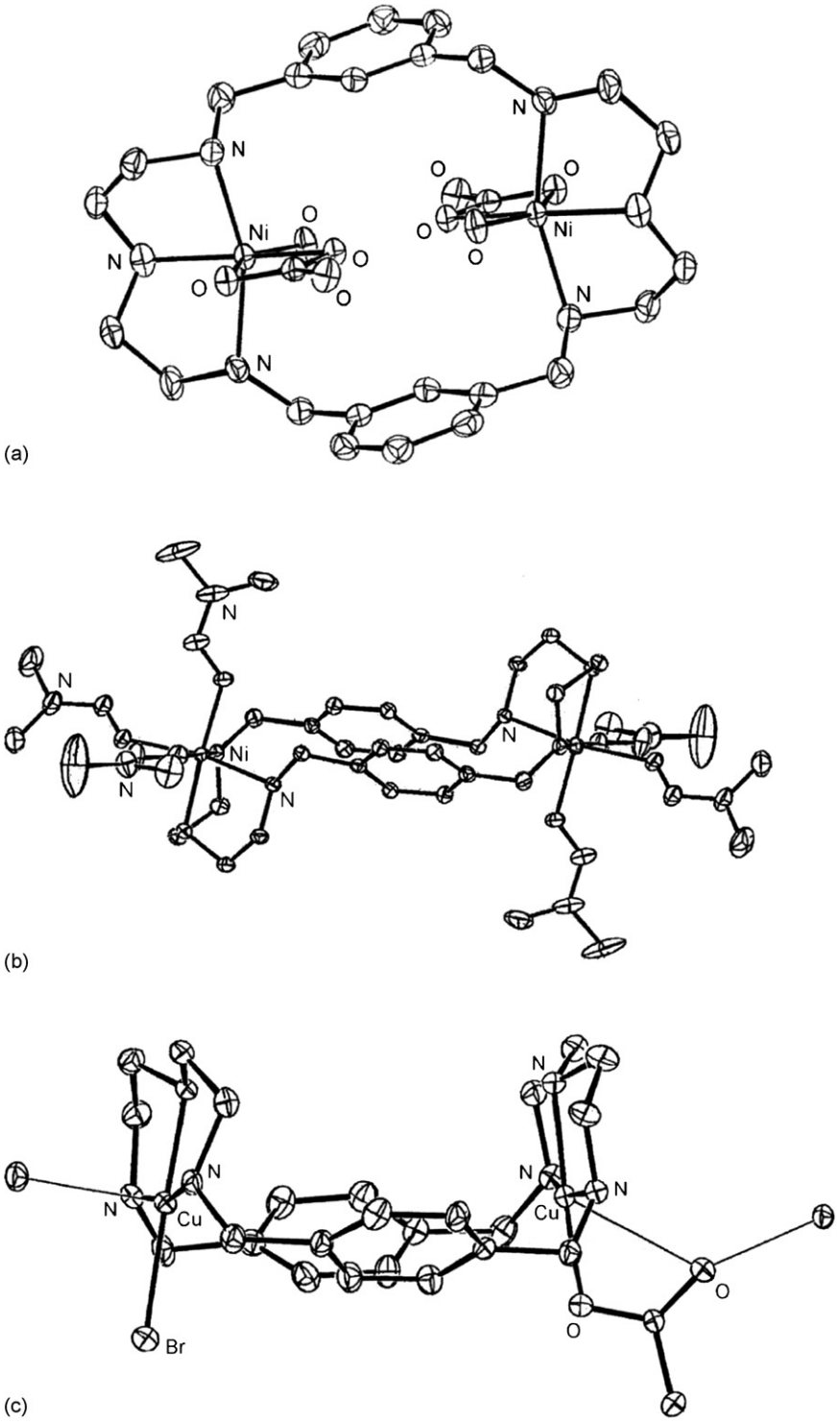

Fig. 101. Structure of $[Ni_2(\mathbf{125})(CH_3COO)_2(H_2O)_2]^{2+}$ (a), $[Ni_2(\mathbf{126})(DMF)_6]^{4+}$ (b) and $[Cu_2(\mathbf{126})(CH_3COO)_2(Br)]^{2+}$(c).

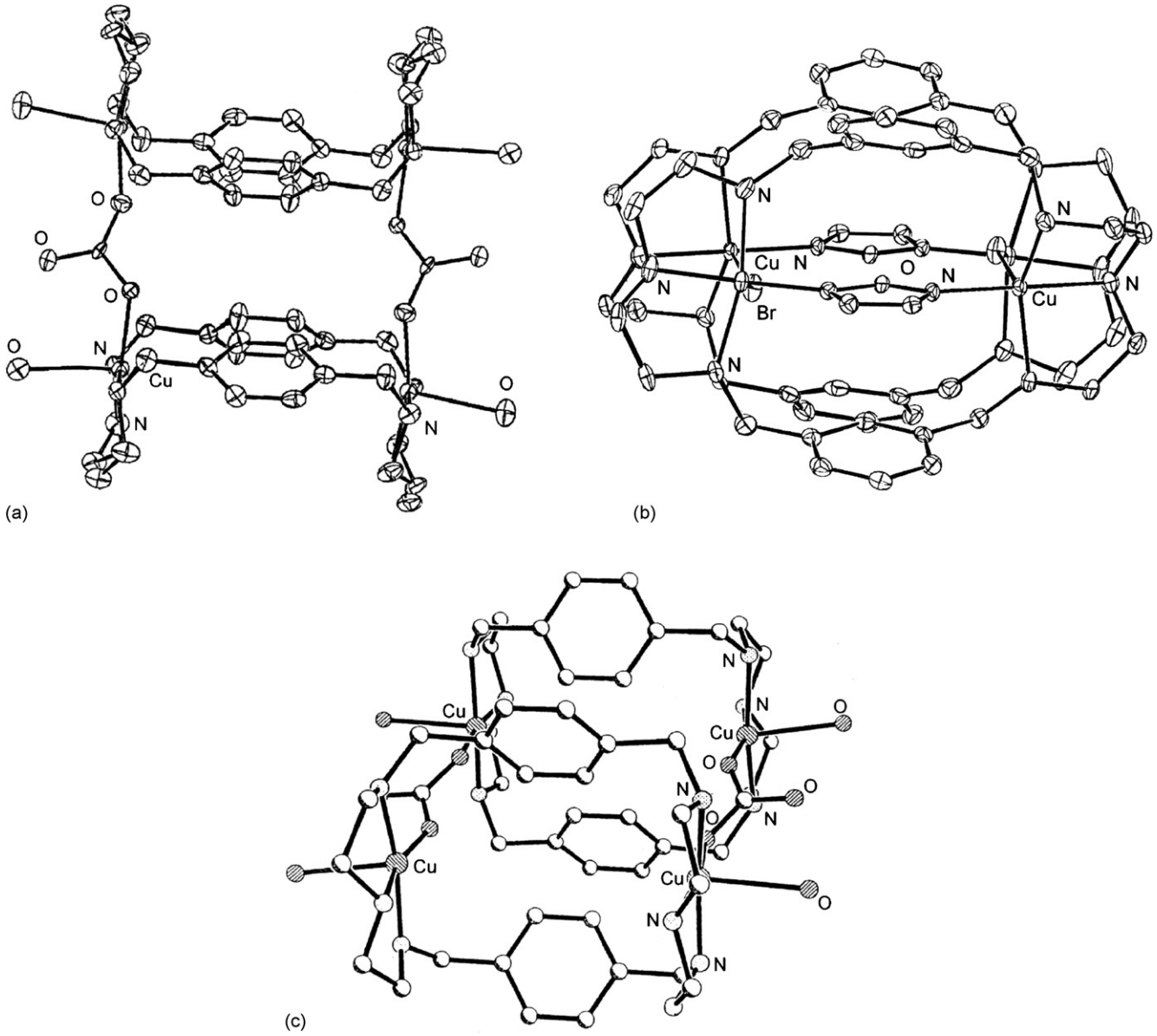

Fig. 102. Structure of $[Cu_4(\mathbf{126})_2(\mu\text{-}CO_3)_2(H_2O)_4]^{4+}$ (a), $[Cu_4(\mathbf{125})_2(\mu\text{-}Im)_2(Br)_2]^{4+}$ (b) and $[Cu_4(\mathbf{126})_2(\mu\text{-}CO_3)_2]^{4+}$ (c).

As a first approximation the magnetic interaction between the two copper(II) ions in each macrocycle can be neglected due to the large separation. Consequently, an interdimer antiferromagnetic interaction ($J = -254\,cm^{-1}$) was estimated [125].

These tetranuclear copper(II) complexes were used to test their influences on the oxidation reaction of 2,6-dimethylphenol (DPM) to polyphenylene ether (PPE) and/or 3,3′-5,5′-tetramethyl-4,4′-diphenoquinone (DPQ) under basic conditions [124]. The O_2 up-take curves of these complexes show that the most effective catalyst is the tetranuclear complex, where the μ-OCH_3 is the bridging group. It gives the maximum reaction rate of PPE. As the basicity order of the bridging ligand is $C_6H_5COO^- < CO_3^{2-} < CH_3O^-$, it shows that the deprotonation process of phenol by basic ligand is critical in the whole catalytic process.

With the increase of the base to complex ratio, the reaction rate of the coupling reaction increases dramatically. But after approximately 4:1, the reaction rate is improved only slightly, and the selectivity of PPE decreases significantly, even though the substrate is converted more quickly.

More phenolic ions will be produced when more $NaOCH_3$ is added. The only possible explanation is that the phenoxonium cations produced were consumed by the phenolic anions. Subsequently, radicals thus formed lead to PPE or to the by-product DPQ by C—O and C—C coupling, respectively.

During the oxygen uptake, $NaOCH_3$ was used as catalyst. It may also bridge the copper(II) ions to form dimer-of-dimer structures in the reaction process. Since methoxide is a strong base, it will be completely protonated in reaction with an excessive amount of the substrate, phenol. Thus, even in the presence of an excess of $NaOC_2H_5$, compared to the $\{Cu^{II}(\mu\text{-alkoxo})\}$ compound, complexes cannot form. Instead, bis-μ-phenolic tetranuclear structures form with promotion of $NaOC_2H_5$. The bridged phenolate is readily attacked after it is oxidized to the

corresponding phenoxonium cation. This attack may come from a free phenolic anion in the solution system or by an inner-layer one.

The bis-μ-alkoxo bridged dicopper(II) complex with **125** only gives the product DPQ. The only structural difference between **125** and **126** complexes is the distance between two copper(II) centers. In searching the possibility of intramolecular μ-X-type of binding of the dicopper(II) complex with **126**, several small bridging anions as CH_3O^-, CH_3COO^- and $C_6H_5COO^-$ have been used to prepare single crystals but the experimental results were negative. The individual coordination of each $C_6H_5COO^-$ ligand to each copper(II) ion is due to the large separation between the copper ions. This phenomenon strongly supports that the C–O coupling reaction comes from the dimer-of-dimer structures, which is necessary for the chain growth process. The product H_2-DPQ was suggested to be formed by C–C coupling of a resonance form with a high density of unpaired electron at *para* position of the phenoxy radical, and thus was oxidized to DPQ. In the catalytic cycle, the phenoxonium cations coexist with phenolic anions. It was supposed that the phenoxy radicals were formed through one electron transfer process between these two species. To verify these hypothesis, the effect of radical scavenger DMS was tested and shows that it reduces the reaction rate significantly. By C–O coupling, anion and cation quinone ether is formed. The chain growth is initiated form the bridged phenoxonium. After tautomerization, the low degree of polymerized phenol is replaced by another phenolate anion, or remain coordinated to the dicopper(II) motif to increase its chain.

The function of the additional $NaOC_2H_5$ in the catalytic cycle was clarified in terms of reaction rate and selectivity. As more phenolic anion is formed, it will promote the phenol coupling step. However, at high concentration, it competes with the phenoxonium intermediates and thus induces the formation of the by-product DPQ. The formation of PPE and DPQ are synergic in the whole reaction. Thus, a tetracopper(II) structure is critical in oxidative coupling of DMP, and the by-product DPQ is inevitable in this alkoxo promoted process. Experimental results indicate that some chemical reagents can stabilize the intermediate of phenoxonium cation and thus increase the PPE selectivity to nearly 100% [125].

Potentiometric experiments, carried out for the system Cu^{II}:**126**:CO_3^{2-} = 1:2:1 to determine the stability constants for the formation of mono-, di- and tetranuclear complexes, indicate the prevalence of tetracopper(II) species at the basic region. It was also observed that the steady rates of H_2O_2 dismutation follow the formation of the tetranuclear complex $[Cu_4(\mathbf{126})_2(\mu\text{-}CO_3)_2](ClO_4)_4$; with a 1.0 mM solution of $[Cu_4(\mathbf{126})_2(\mu\text{-}CO_3)_2]^{4+}$ it would take 3 days for 100 turnovers at pH 6.04. It would take only 85 min for 100 turnovers at pH 7.11 and a mere 22 min at pH 8.69. In the initial stage of the proposed mechanism, a lag phase for O_2 production was observed, this phenomenon was ascribed to the slow reduction of Cu^{II} to Cu^{I} which in turn to initiate the rapid catalytic cycles. The partially negatively charged hydrogen peroxide molecule was proposed to coordinate the two copper(II) ions between two dinuclear entities. This suggestion is under the consideration that

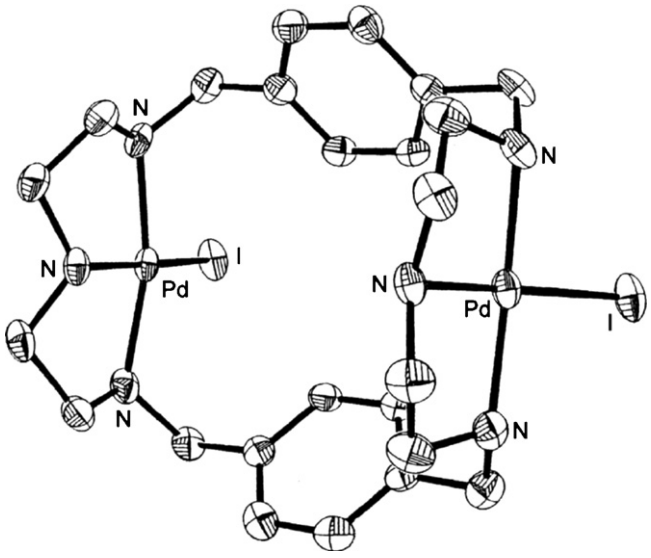

Fig. 103. Structure of $[Pd_2(\mathbf{126})(I)_2]^{2-}$.

the copper···copper separation in one dinuclear entity is too large (7.23 Å) for the formation of the bridged H_2O_2 intermediates. Since the formation constant of the tetranuclear complex is much higher ($\log K = 13.59$), it precludes the possibility of the binuclear complex catalyzed mechanism. In addition, $CuCl_2$ served as a parallel control for all experiments and no significant reaction rate was observed for the simple copper(II) salt. In the catalytic process, by reducting one of the bridged Cu_2^{II} dimers cooperatively, one O_2 molecule was released. Consequently, two H_2O_2 molecules are bridged between the Cu_2^{I} and Cu_2^{II} within the hetero-macrocycle and the steady disproportionation rate was reached at this stage. The redox process is undertaken consecutively within the tetranuclear structure to complete the catalytic cycle [126].

$[Pd_2(\mathbf{126})(Cl)_2](Cl)_2$, obtained by refluxing a methanol solution of **126** and $PdCl_2$ in a 1: 2,6 molar ratio, followed by storage of the resulting solution in a refrigerator overnight, forms $[Pd_2(\mathbf{126})(I)_2](I)_2$ and $[Pd_2(\mathbf{126})(Cl)_2](NO_3)_2$ by methatesis respectively with an excess of KI or 2 equiv. of $AgNO_3$ [127].

In $[Pd_2(\mathbf{126})(I)_2](I)_2$ each palladium(II) ion is coordinated by three nitrogen atoms and one iodide ion in a somewhat distorted square planar geometry. The free macrocycle **126**·$5H_2O$ adopts a chair conformation but $[Pd_2(\mathbf{126})(I)_2](I)_2$ adopts a boat-like conformation. The distance between the two palladium(II) ions is 6.85 Å. The ionic iodide ions lie on the two-fold axis and interact with two nitrogen atoms to form weak H···I bond inside the channel formed by the rings of the polyamine column. The coordinated iodide ions also engage in hydrogen bonding with the coordinated amino group in the symmetry related molecule, to form a one-dimensional chain along the c axis (Fig. 103) [127].

The structure of $[Pd_2(\mathbf{126})(Cl)_2](NO_3)_2{\cdot}H_2O$ resembles that of $[Pd_2(\mathbf{126})(I)_2](I)_2$. The two coordination moieties are virtually planar. The palladium(II) configuration in $[Pd_2(\mathbf{126})(Cl)_2](NO_3)_2{\cdot}H_2O$ is closer to square planar than that in $[Pd_2(\mathbf{126})(I)_2](I)_2$. The distance between the two palladium(II) ions is 6.763 Å, slightly shorter that in

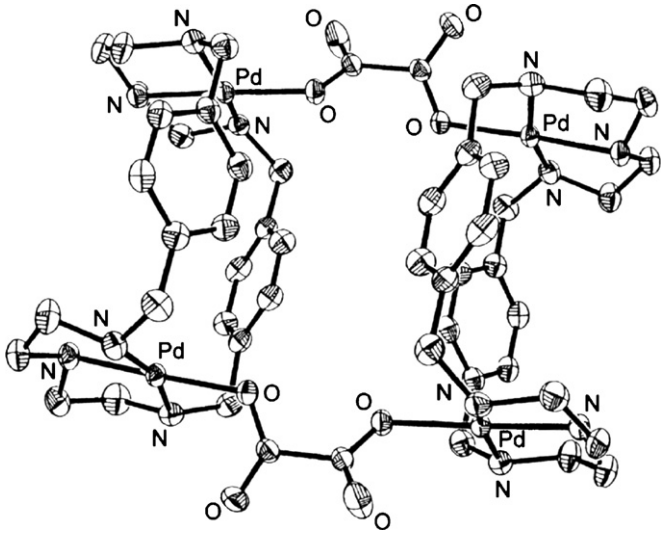

Fig. 104. Structure of $[Pd_4(\mathbf{126})_2(\mu\text{-}C_2O_4)_2]^{4+}$.

$[Pd_2(\mathbf{126})(I)_2](I)_2$. The macrocyclic ligand in this complex also adopts a boatlike conformation. In the structure, one oxygen atom of a nitrate anion is inserted into the two N_3Cl planes and also interacts with two nitrogen atoms via hydrogen bonds. The two chloride ligands form hydrogen bond with the amino groups of symmetry-related molecules. This hydrogen bonding makes the complex molecules form one-dimensional chains along the a axis as in $[Pd_2(\mathbf{126})(I)_2](I)_2$. The multiple hydrogen bonds involving water, nitrate anions and amino groups of the ligands act as the driving force for the self-assembly of the chain structure [127].

The aqua complex cations $[Pd_2(\mathbf{126})(H_2O)_m(NO_3)_n]^{(4-n)+}$ ($n = 0$–4), formed from $[Pd_2(\mathbf{126})(I)_2](I)_2$ and $[Pd_2(\mathbf{126})(Cl)_2](Cl)_2$ by treatment with 4 equiv. of $AgNO_3$ in aqueous solution, when mixed with an aqueous solution of diethyl oxalate in a molar ratio of 1:1 for 2 days at 40 °C give rise to $[Pd_4(\mathbf{126})_2(C_2O_4)_2](NO_3)_4{\cdot}6H_2O$, a tetranuclear complex that may be considered a product of a [2 + 2] condensation of two binuclear complexes. In this molecule, there are two identical moieties, each containing one macrocyclic ligand and two palladium(II) ions. Each palladium(II) ion is bonded to three nitrogen atoms from the same lateral arm of the ligand and an oxygen atom of the oxalate bridging ligand. The two moieties are connected by two oxalate anions, each spanning a pair of palladium(II) ions. The mean deviation of the palladium(II) ions from the N_3O coordination planes ($\simeq$0.07 Å) confirms that the configuration geometry of the palladium(II) ions in $[Pd_4(\mathbf{126})_2(C_2O_4)_2](NO_3)_4{\cdot}6H_2O$ is close to square planar. Both macrocyclic polyamine ligands adopt boat-like conformations. The Pd···Pd distances inside each dinuclear entity are 6.73 and 6.72 Å, respectively. The whole molecule looks like a box. In the crystal, there are many hydrogen bonds involving the disordered water molecule, disordered NO_3^- ions, the amino groups and the bridging oxalate anions. These hydrogen bonds array the boxes into a one-dimensional chain. The chains are also connected via two kinds of π–π stacking to form a two-dimensional structure (Fig. 104) [127].

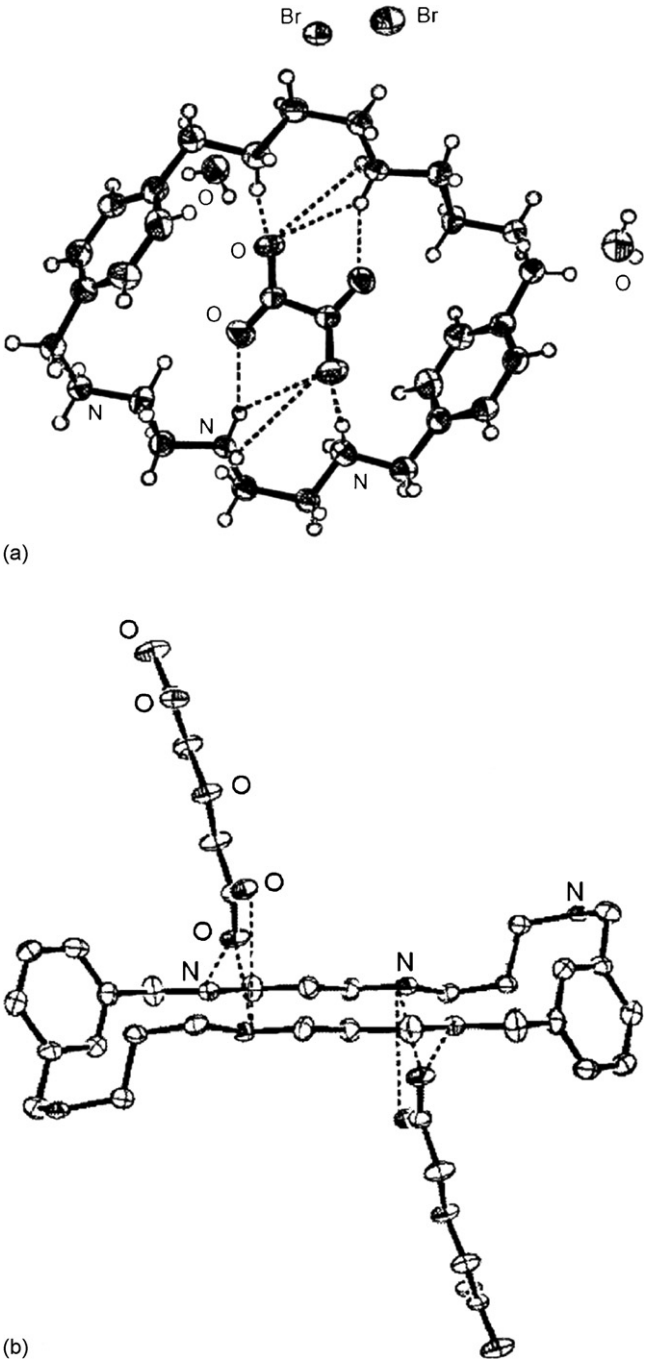

Fig. 105. Structure of $[(H_6\text{-}\mathbf{126})(ox)]^{4+}$ (a) and $[(H_2\text{-}\mathbf{127})(od)_2]^{2+}$ (b).

Mixing equimolar amounts of $[H_6\text{-}\mathbf{126}](Br)_6$ and disodium oxalate (Na_2ox) in water generates colorless crystals of $[(H_6\text{-}\mathbf{126})(ox)](Br)_4{\cdot}2H_2O$, after a slow diffusion of this solution with ethanol at room temperature. $[(H_6\text{-}\mathbf{127})(od)_2](Br)_2{\cdot}6H_2O$ is prepared by mixing $[H_6\text{-}\mathbf{127}](Br)_6$ and oxydiacetate (od^{2-}) with molar ratio 1:2 in water, adjusting the acidity to pH 5, and allowing water to evaporate slowly for a few days.

The centrosymmetric cation part of $[(H_6\text{-}\mathbf{126})(ox)](Br)_4$ can be considered as the initial $[H_6\text{-}\mathbf{126}]^{6+}$ ligand bonded to the oxalate dianion within its macrocyclic cavity, with the inversion center situated in the middle of the oxalate C–C bond. The

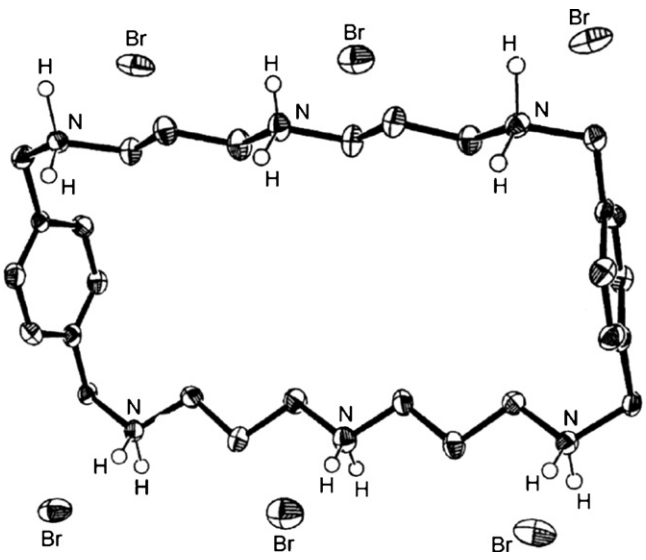

Fig. 106. Structure of $[H_6$-**128**$](Br)_6$.

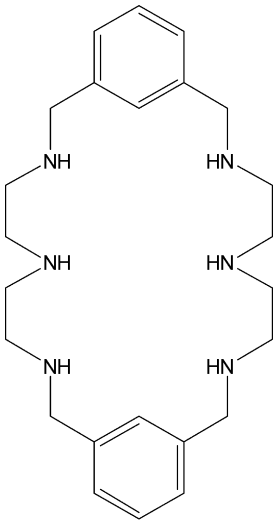

125

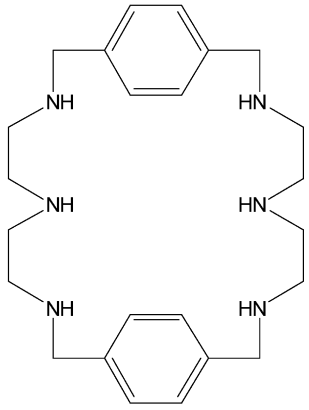

126

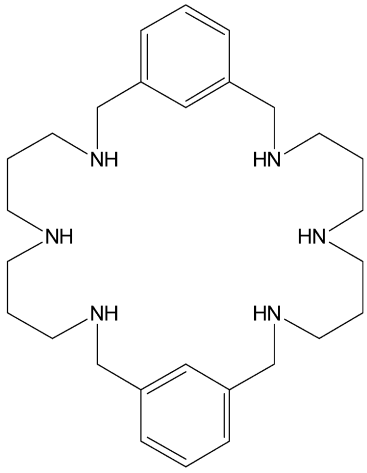

127

oxalate is placed inside the cavity, so that two oxygen atoms are directed upward with regard to the plane of the cavity and the other two downward. The oxalate is strongly bonded to the macrocyclic ligand through electrostatic interactions and also through a network of hydrogen bonds with its carboxilate groups (Fig. 105a) [128].

The centrosymmetric cation part of $[(H_6$-**127**$)(od)_2](Br)_2$ can be considered as the initial $[H_6$-**127**$]^{6+}$ macrocycle bonded to the oxydiacetate dianion, with the inversion center situated in the center of the macrocyclic cavity. The $[H_6$-**127**$]^{6+}$ moiety is forming a sort of a chair mostly flat except for the ends where the N_3 secondary amines are situated at the upper and lower positions with regard to the mentioned cavity plane. Two oxydiacetate/macrocyclic moiety are vertically located above and below the cavity and are strongly bonded through electrostatic interactions and hydrogen bonding. This generates a pseudochain along the x axis since each diacetate is bridging two symmetrically related macrocyclic moieties. The chains are interacting one another along the y axis through weak hydrogen-bonded water molecules that act as bridging units and along the z axis through hydrogen bonds between the central oxygen of the diacetate, and the N_3 atoms of the macrocycle. Finally, the bromide counterions are also weakly interacting with the water molecules (Fig. 105b) [128].

128 was prepared by literature procedures or slight modifications thereof while its corresponding hexabromide salt was synthesized by treating **128** with 48% HBr. According to X-ray diffraction analysis, $[(H_6$-**128**$)](Br)_6$, has a plane of symmetry perpendicular to the ligand cavity that contains the two central amine atoms. The macrocyclic cavity can be described as a $12.4 \times 5.8\ Å^2$ rectangle which is roughly 12% larger than for the related *meta* isomer $[(H_6$-**127**$)]^{6+}$ ($12.8 \times 4.9\ Å^2$), due to the increase of the two member ring units from [28] for **127** to [30] for **128** (Fig. 106) [131].

125···**128** differ one another in the aromatic substitution that can be *meta* or *para* and in the number of methylenic units linking the secondary amines. **125**, possessing *meta* substitution and two methylenic units, is the receptor having the smallest cavity whereas **128**, which possesses *para* substitution and three methylenic units, has the largest cavity. Assuming an extended conformation of all the carbon and nitrogen sp^3 atoms, which is the conformation presented by **127** in its X-ray structure [128], the relative site of their cavities can be calculated normalized to **125**, which is the ligand with the smallest cavity. In this way isomeric ligands are 12% larger in the *para* case since the cavity increases by two member ring units with respect to the *meta*; ligands with the same aromatic substitution but differing in the number of methylenic units increase their cavity size by 20%, due now to the increase in four member ring units of the cavity. From a topologic viewpoint the *meta* ligands have a rectangular shape whereas the *para* substituted are closer to a square. From the acid–base point of view the isomeric ligands have practically the same protonation constants.

The increase in four methylenic units increases the basicity by about 10 orders of magnitude; this influences the zones of predominance of the different protonated species of each ligand. Thus, for **128** the pentaprotonated species, $[H_5\text{-}\mathbf{128}]^{5+}$ does not start to form significantly up to pH higher than 5 whereas for **126** at pH 2 the abundance of $[H_5\text{-}\mathbf{126}]^{5+}$ is already 9%.

The host-guest interaction between **125**···**128** and oxalic acid (H_2ox) and oxydiacetic acid (H_2od) has been investigated by potentiometric equilibrium methods. Ternary complexes are formed in aqueous solution as a result of hydrogen bond formation and Coulombic interactions between the host and the guest. In the $[(H_6\text{-}\mathbf{126})(ox)]^{4+}$ complex those bonding interactions reach a maximum yielding a log *K* of 6.08. The most salient features of these systems are the following: (i) **125** and **126** bind oxalate significantly much more stronger than oxydiacetate; this is clearly manifested for the {**125**:ox:od} competitive system, where a selectivity of 92.5% in favour of the {**125**–ox} complexation against the {**125**–od} is obtained at pH 2.8; (ii) no isomeric effect is found when comparing binding capacities of oxalate with two isomeric ligands such as **125** and **126** since their affinity to bind the substrate is relatively similar; (iii) **127** and **128** have a similar behaviour as that observed for **125** and **126** except that due to the increase in cavity size the differentiation becomes smaller; (iv) the less basic ligands with two methylenic units **125** and **126** bind stronger to the substrate than **127** and **128** with three methylenic units even though their relative predominance depends on pH [128].

The oxalic and oxydiacetic acids differ in size and molecular flexibility. While oxalic acid can be considered a very rigid molecule, oxydiacetic acid can be considered as highly flexible due to the three sp^3 atoms linking the carboxylic groups. For the {L-ox} systems (L = **125**, **126**) over the pH range 2–7 the predominant species are $[(H_i\text{-L})(ox)]^{(i-2)+}$ rather than the individual species derived from protonation of the ligand and substrates. This range is reduced to 4–6.5 for **127** and **128** ligands that contain three methylenic units. In all cases the more abundant species are the $[(H_6\text{-L})(ox)]^{4+}$; **125** and **126** reach a maximum abundance of nearly 90% at pH 3.0, whereas for 127 and 128 the maximums are shifted to pH 5.0 and the abundance is lowered to 60%.

The recognition constant values obtained for the isomeric **127** and **128** ligands containing three methylenic units bonding the amines lay within the range of host-guest interactions with cyclic and acyclic receptors and carboxylic acids reported in the literature [129]. However, the recognition constants obtained for the **125** and **126** ligands with regard to the oxalate anion are the highest reported in the literature [129].

For the {**125**-ox-od} competitive system, [(H-**125**)(ox)] species predominate over [(H-**125**)(od)] within the pH range 2–7, as a consequence of the higher binding constants found for the {**125**-ox} system with respect to the {**125**-od} system. The {**126**-ox-od} system parallels that of the **125** just described, where the **126** ligand display higher affinity for the oxalate substrate than for the oxydiacetate.

The stronger affinity of oxalate over oxyadiacetate for either the **125** or **126** ligand receptors is attributed to the fact that oxalate is capable to better accommodate into the macrocyclic cavity of the ligand than oxyadiacetate and its rigidity produces an even stronger Coulombic and hydrogen-bonding interactions in agreement with the X-ray structure above reported.

When a comparison is made of the behaviour of oxalate with the two isomeric ligands **125** and **126**, it is found that the affinities are relatively similar. This means that different cavity topology presented by the **125** (rectangular) and **126** (squared) does not substantially affect the overall bonding. This can be understood if one takes into consideration, that as shown in the X-ray structure, the oxalate due to its rigidity only binds to the ligand receptor through four of the six secondary amines, Given the relative flexibility of the ligand receptors, the four-way bonding can take place with comparable restrains for the two isomers and thus bind in a very similar manner.

For the {**127**-ox-od} and {**128**-ox-od} competitive systems, the behaviour parallels that of their analogous ligands **125** and **126** bearing only two methylenic units within secondary amines, respectively, but with a lower degree of differentiation. The decrease in recognition capacity is due to an increase of the macrocyclic cavity dimension of the **127** and **128** ligands that produces a much poorer fit.

Finally, the less basic ligands containing two methylenic units **125** and **126** bind stronger to the substrates than those containing three methylenic units **127** and **128**. It has been observed that [(H-**126**)(ox)] predominates over a much larger pH range than the corresponding [(H-**128**)(ox)]. There are pH zones where the selectivity of one ligand for a substrate is very high: for instance at pH 3.3 the selectivity of the **125** ligand over **127** for the oxalate substrate is 95.6%. This behaviour had previously been observed for similar ligands but interacting with phosphate and nucleotide type substrates. These results show that the appropriate ligand design allows to modulate the topology and flexibility of a receptors cavity and thus allows one built up tailored molecules for specie substrates. In this particular case it has been shown how the appropriate hexaazamacrocyclic ligand, under the right conditions, can strongly and selectively bind to oxalate, a rigid substrate, and generate much weaker interactions with another flexible dicarboxylic acid like oxydiacetic [130].

The protonation constants of **128** and its host-guest interactions with monophosphate (Ph) and pyrophosphate (Pp) have been investigated by potentiometric equilibrium methods. Ternary complexes are formed in aqueous solution as a result of hydrogen bond formation and Coulombic interactions between the host and the guest. The highest equilibrium constant for the ternary recognition systems {**128**/Pp/H} corresponds to the formation of the species $[(H_6\text{-}\mathbf{128})(Pp)]^{2+}$. This complex can be formally described as a $[(H_6\text{-}\mathbf{128})]^{6+}$ positive cation bonded to a $[Pp]^{4-}$ anion by Coulombic forces and hydrogen bonds. In this complex the Coulombic interactions and hydrogen bonding reach a maximum as **128** shows a stronger preference (selectivity) for pyrophosphate substrate over the monophosphate one as a consequence of the much stronger formation constants with pyrophosphate. An analysis of the isomeric effect is also carried out by comparing the {**128**-S} versus {**127**-S} systems. In the best case, a selectivity of over 88% is achieved for the diphosphate complexation when using the *meta* isomer over the *para*, due solely to the size and shape of the receptors cavity [131].

The results obtained for the formation of anionic complexes with the diphosphate substrate clearly indicate that the **127** is capable of stronger recognition of this substrate compared to its isomeric **128**. This recognition capacity, given the similarity in the chemical nature of **127** and **128**, arises only because of the different shape and/or size of the cavity of those two ligands. Thus, the **127**, which has a smaller and more rectangular cavity than its isomer **128**, is capable of better fitting the diphosphate substrate and thus ends up forming much more stronger complexes. This is further corroborated by the behaviour of those two ligands with regard to the monophosphate substrate. In this particular case, the substrate binds to the ligands in a very similar manner, since the smaller size of the monophosphate substrate cannot be discriminated by the large cavities of those hexaaza-macrocyclic ligands [131].

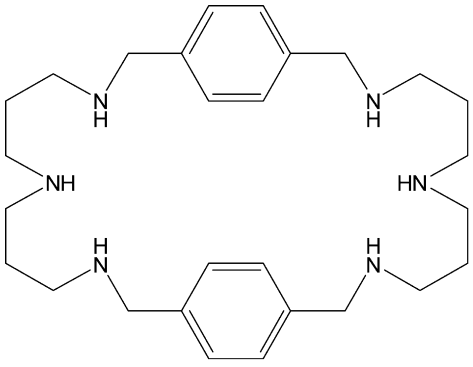

128

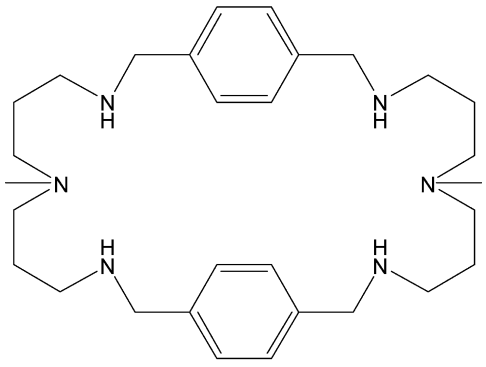

129

129 was synthesized through the condensation of *N*,*N*-bis(3-aminopropyl)methylamine with terephthaldialdehyde at 0 °C, in acetonitrile, followed by the reduction of the obtained Schiff-base with $NaBH_4$ in ethanol at room temperature [132]. The presence of the methyl group appended to the central tertiary amine prevents the formation of the aminal ring, which leads to the contracted macrocycle form occuring when the imine group of the extended Schiff-base macrocycle is attacked by the nearby secondary amine function [133,134]. The crystal structure of **129** is built from an asymmetric unit composed of one discrete molecule and one half solvent water molecule. The macrocycle exhibit a conformation with both phenyl rings almost parallel. The conformation adopted is stabilized by π–π

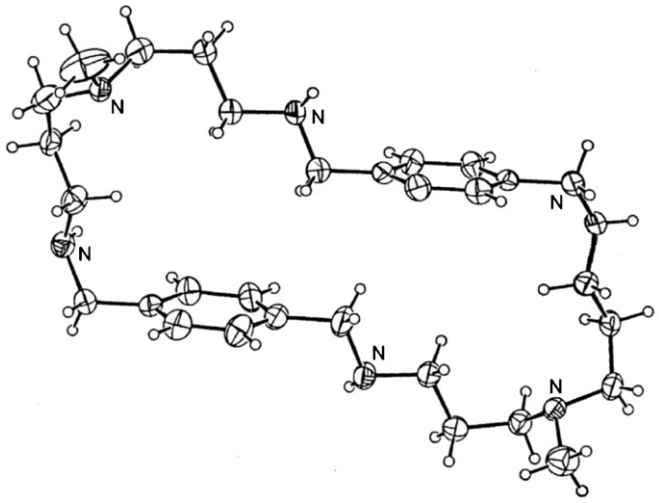

Fig. 107. Structure of **129**.

stacking interactions. In the crystal structure the molecules of **129** are self-assembled via N–H···N bonding interactions into a 1D network. The hydrogen bonds comprise the concomitant interaction of four neighboring **129** molecules which give rise to the formation of eight membered centrosymmetric rings constructed via two independent N–H···N bonds. The oxygen atom of the lattice of water is also involved in the hydrogen bonding network bridging two adjacent **129** molecules (Fig. 107) [132].

The protonation constants of **129** and the stability constants of the related copper(II) and zinc(II) complexes, were determined in water–methanol (9:1 v/v) at 25 °C with ionic strength 0.10 mol dm^{-1} in KCl. The potentiometric and spectroscopic studies (especially NMR) of zinc, cadmium and lead complexes and the EPR of the copper complexes indicate the formation of only dinuclear complexes. For the dizinc complex the maximum percentage to the dinuclear complex occurs at pH 7.8 and after pH 8.5 hydroxo-complexes are the main species, the $[Zn_2(\mathbf{129})(OH)]^{3+}$ complex being the dominant species above pH 8.

The association constant of the dinuclear copper(II) complex with anions (thiocyanates, terephthalate and glyphosate) and neutral molecules (1,4-benzenedimethanol, *p*-xylylenediamine and terephthalic acid) were determined at 20 °C in methanol. The structural preferences of **129** and of the related dinuclear copper(II) complexes with a variety of bridging ligands were evaluated theoretically by molecular mechanics calculations and molecular dynamics using quenching techniques. The association constants determined for the ternary complexes involving the studied substrates are not markedly different, but the lowest values were found for SCN^-, and a clear preference is apparent for the terephthalate anion and glyphosate.

Solution studies as well as the modeling studies show that for **129**, in spite of the presence of two *p*-xylyl rigid spacers, the dipropyltriamine linkages confer enough steric flexibility to the macrocycle such that several conformations with similar energies can be adopted.

These conformations can be stabilized by π–π interactions between the two aromatic rings ranging form edge-to-face to

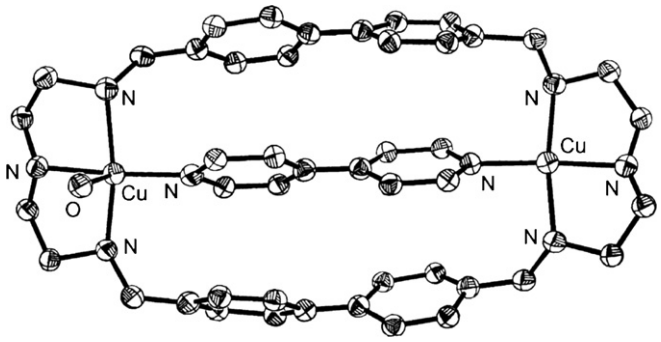

Fig. 108. Structure of $[Cu_2(\mathbf{130})(4,4'\text{-bipy})(H_2O)]^{4+}$.

face-to-face. Additionally the aromatic rings offer two distinct sites to encapsulate two metal centers. Theoretical studies and EPR spectroscopy indicate unequivocally that a wide range of distances (6.85–10.11 Å) between the two metal centers is possible. However, the fitting of the complex to short Cu···Cu distances result in a considerable increase of steric energy. When a bridge substrate is inserted into the macrocycle cavity, the Cu···Cu distance changes specifically in order to fit the stereo-electronic requirements of the substrate. Moreover, the comparison of the values of formation constants where the ternary species and the Cu···Cu distances suggests that higher constants correspond to a critical Cu···Cu distance, smaller values of the distance lead to lower formation constants, indicating that the complexes loses conformational energy to fold to the right position for the coordination of small substrates. In other words, the dinuclear copper complex of **129** has enough flexibility to accommodate bridged ligands with different sizes [132].

The reaction of **130** with $Cu(ClO_4)_2{\cdot}6H_2O$ and 4,4′-bipyridine in H_2O/CH_3CN and in a 2:1:1 molar ratio affords $[Cu_2(\mathbf{130})(4,4'\text{-bipy})(H_2O)](ClO_4)_4{\cdot}3H_2O$ [135] with a binuclear copper(II) center, in which the two copper(II) ions, 10.95 Å apart, are bridged by a 4,4′-bipyridine molecule. In addition, one copper(II) ion is five coordinate in a distorted square pyramidal geometry by three nitrogen atoms from a diethylenetriamine unit of **130** and an oxygen atom from a water molecule, while no water molecule is coordinated to the other copper(II) ion which is four coordinate. Each pyridyl group is sandwiched between two phenyl planes; this gives rise to face-to-face π–π interactions. The macrocyclic cationic units are further connected by perchlorate anions through hydrogen bonds (Fig. 108) [135].

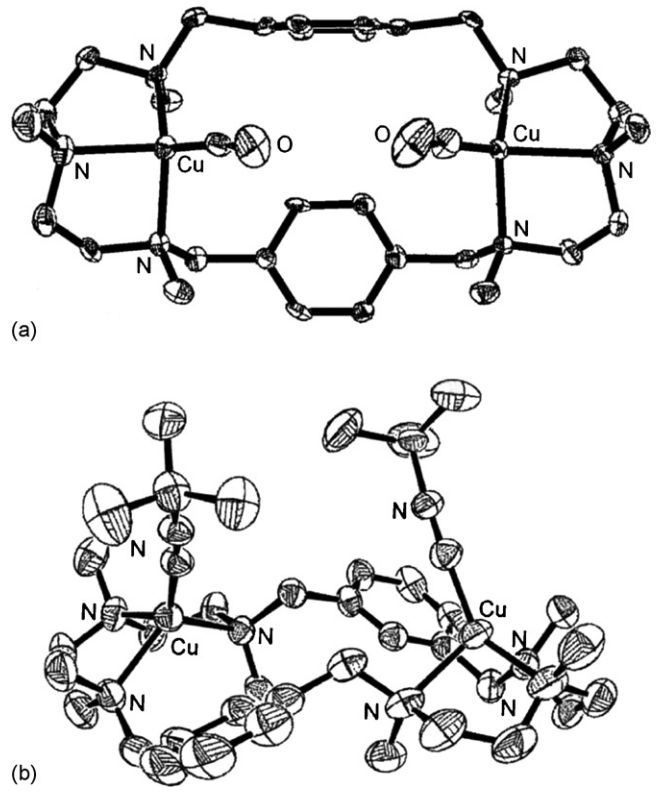

Fig. 109. Structure of $[Cu_2(\mathbf{131})(CO)_2]^{2+}$ (a) and $[Cu_2(\mathbf{132})(tert\text{-}BuNC)(PPH_3)_2]^{2+}$ (b).

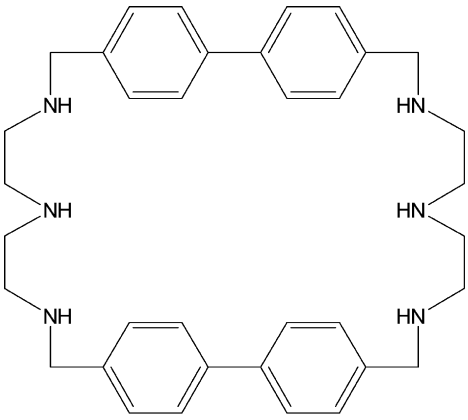

130

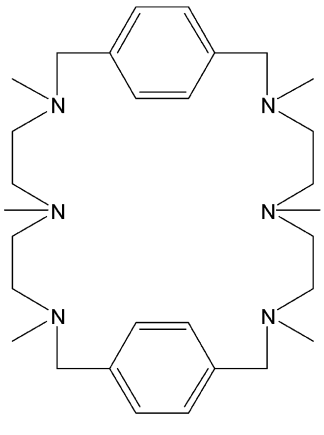

131

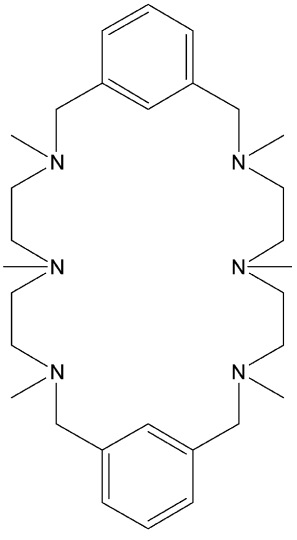

132

A weak antiferromagnetic coupling operates between the two copper(II) ions. ESR measurements indicate that from pH 4.98 to 10.74 the $\{Cu^{II}(4,4'\text{-bipy})Cu^{II}\}$ unit is stable while remarkably change was observed when the pH value decreases to 3.38, indicating a complex dissociation [135].

The four [2 + 2] macrocyclic ligands **131**···**134** allow to gain a certain control of the chemical properties of their corresponding dicopper(II) complexes. In particular, it turns out that the number of methylenic units, two or three, bonding each tertiary amine in the ligands, significantly influences the copper(I) tendency to three or four coordination and relative spatial arrangement between copper(I) metal centers (*syn* versus *anti*). Preliminary results related to the oxidative chemistry of these complexes reveal that these two parameters, carefully controlled, produce different reactivity patterns [134–140].

The reaction of **131** and **132** [136–139] with 2 equiv. of $[Cu(CH_3CN)_4](X)$ ($X^- = ClO_4^-$, $CF_3SO_3^-$, PF_6^-) in acetonitrile forms the corresponding dinuclear white, air sensitive complexes $[Cu_2(\mathbf{131})(CH_3CN)_2](X)_2$ and $[Cu_2(\mathbf{132})(CH_3CN)_2](X)_2$. The replacement of CH_3CN by *n*-PrCN in this reaction generates the corresponding complexes $[Cu_2(\mathbf{131})(n\text{-PrCN})](ClO_4)_2$, and $[Cu_2(\mathbf{132})(n\text{-PrCN})](PF_6)_2$, which are less air sensitive and thus easier to manipulate [140]. The metal ions in $[Cu_2(\mathbf{133})](ClO_4)_2$, $[Cu_2(\mathbf{133})](CF_3SO_3)_2$, $[Cu_2(\mathbf{134})](CF_3SO_3)_2$, and $[Cu_2(\mathbf{134})](PF_6)_2$, derived from the analogous ligands **133** and **134** contaning three methylenic units, are solely coordinated by the macrocyclic ligand; therefore, a three coordination is obtained [140].

The monodentate ligands present in the dinuclear complexes with **131** and **132** can easily be replaced by σ-donor/π-acceptor ligands (L = CO, *t*-BuNC, PPh_3) in CH_3CN with the consequent formation of $[Cu_2(\mathbf{131})(L)_2](X)_2$ as white solids, less air sensitive than their precursors. However, the stability of the complexes is somewhat dependent on the σ-donor/π-acceptor ligands: $[Cu_2(\mathbf{131})(CO)_2](ClO_4)_2$ and $[Cu_2(\mathbf{134})(CO)_2](CF_3SO_3)_2$ are rapidly oxidized in the solid state and in solution upon exposure to O_2, $[Cu_2(\mathbf{131})(PPh_3)_2](ClO_4)_2$ and $[Cu_2(\mathbf{132})(PPh_3)_2](ClO_4)_2$ are relatively stable in the solid state but become oxidized in O_2 exposed solutions, and acetonitrile solutions of $[Cu_2(\mathbf{131})(t\text{-BuNC})(PPh_3)_2](ClO_4)_2$ and $[Cu_2(\mathbf{132})(t\text{-BuNC})(PPh_3)_2](CF_3SO_3)_2$ can be manipulated in open atmosphere for short periods of time without apparent oxidation of the complexes [140].

The corresponding complexes $[Cu_2(\mathbf{133})(L)_2]^{2+}$ and $[Cu_2(\mathbf{134})(L)_2]^{2+}$ are also formed using acetone as the solvent, but they cannot be isolated in the solid state. In the workup process, the corresponding σ-donor/π-acceptor ligand is lost, thus generating the tricoordinated complexes. Furthermore, in the particular case of $[Cu_2(\mathbf{132})(CO)_2]^{2+}$, the established equilibrium process monitored by IR indicates the reversibility of the process in CH_3CN with the reformation of $[Cu_2(\mathbf{132})(CH_3CN)_2]^{2+}$ by simply bubbling Ar or N_2 into the solution at room temperature [140].

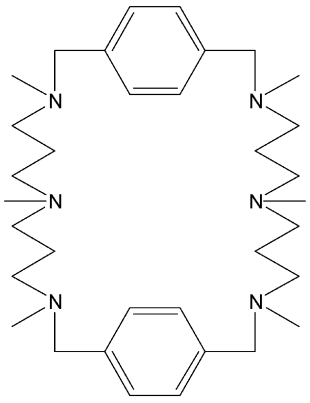

133

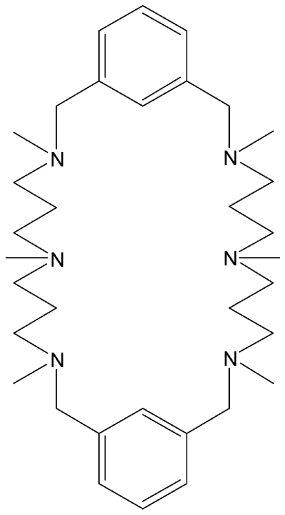

134

In $[Cu_2(\mathbf{131})(CO)_2](ClO_4)_2{\cdot}2H_2O$, the cationic part consists of the macrocyclic ligand, two copper atoms and two CO molecules acting in a terminal mode. It has a pseudo-plane of symmetry that bisects the two aromatic rings and is also perpendicular to them, thus generating two very similar halves of the cationic molecule. The copper(II) ions have a significantly distorted tetrahedral coordination. Each one is bound to three nitrogen atoms of the macrocycle while a CO molecule completes the coordination sphere. The Cu–CO vectors point in the same direction (*syn*) relative to the cavity plane of the macrocyclic ligand. The structure of $[Cu_2(\mathbf{131})(CO)_2](ClO_4)_2$ is completed by two water molecules and two perchlorate anions. One of the water molecules is bonded to one of the perchlorates via hydrogen bonding (Fig. 109a) [140].

The cationic part of $[Cu_2(\mathbf{132})(t\text{-BuNC})(PPh_3)_2](CF_3SO_3)_2$, consists also of the macrocyclic ligand binding the two metal centers and two *t*-BuNC molecules acting in a terminal fashion (Fig. 109b). The cationic moiety possesses a pseudo-C_2 axis perpendicular to the macrocyclic cavity. However, subtle differences between the structural parameters of the two copper centers are evident. The local geometry around the metal center is relatively similar to that in the case of $[Cu_2(\mathbf{131})(CO)_2](ClO_4)_2$ [140].

ADF theoretical calculations show that, in agreement with experimental findings, the *syn*-$[Cu_2(\mathbf{131})(CO)_2]^{2+}$ is more stable than the *anti* complex by 7.6 kcal mol^{-1}. In agreement with the higher stability of *syn*-$[Cu_2(\mathbf{131})(CO)_2]^{2+}$ with regard to the corresponding *anti* complex, also the CO bond dissociation energy for the latter is 8.0 kcal mol^{-1} larger than for the former since it is favoured by both terms, the deformation and the interaction energies. Similarly, *syn*-$[Cu_2(\mathbf{132})(CO)_2]^{2+}$ is more stable than *anti*-$[Cu_2(\mathbf{132})(CO)_2]^{2+}$ by 5.4 kcal mol^{-1}. The bond dissociation energy of CO in the *syn*-$[Cu_2(\mathbf{132})(CO)_2]^{2+}$, complex is lower by 3.3 kcal mol^{-1} due to a larger deformation energy (2.0 kcal mol^{-1}) and a slightly less favourable interaction ((1.3 kcal mol^{-1}). Finally, the CO dissociation energies of the *anti*-isomers in $[Cu_2(\mathbf{131})(CO)_2]^{2+}$ and $[Cu_2(\mathbf{132})(CO)_2]^{2+}$

are quite similar, the latter being larger by only 0.7 kcal mol^{-1} [140].

NMR studies, carried out on $[Cu_2(\mathbf{132})(t\text{-BuNC})](ClO_4)_2$, show the presence of different interconverting isomers [140].

Reaction of **131** and **132** with 2 equiv. of $Cu(CF_3SO_3)_2$ in CH_3CN/H_2O yields $[Cu_2(\mathbf{131})(H_2O)_2](CF_3SO_3)_4$ and $[Cu_2(\mathbf{132})(CH_3CN)_4](CF_3SO_3)_4$, respectively. In both complexes, each of the copper ions are bound to three nitrogen atoms of the macrocyclic ligand, but the coordination geometry, the nature and number of external ligands, and the intramolecular Cu···Cu distance are different. Thus, the copper ions in $[Cu_2(\mathbf{131})(H_2O)_2](CF_3SO_3)_4$ are square planar with a water molecule completing their coordination environment and the copper centers are separated by 6.9 Å. Instead $[Cu_2(\mathbf{132})(CH_3CN)_4](CF_3SO_3)_4$ is an example of a square pyramidal copper(II) complex, containing two acetonitrile ligands in *cis* orientations per metallic ion The Cu···Cu distance is 7.5 Å [140].

These complexes react with disodium terephthalate (Na_2-tereph) to form the tetranuclear complexes $[Cu_4(\mathbf{131})_2(tereph)_2](CF_3SO_3)_4$ and $[Cu_4(\mathbf{132})_2(tereph)_2](CF_3SO_3)_4$. Both the cations $[Cu_4(\mathbf{131})_2(tereph)_2]^{4+}$ and $[Cu_4(\mathbf{132})_2(tereph)_2]^{4+}$ adopt rectangular topologies resulting from a [2 + 2] self-assembly process. Interestingly, $[Cu_4(\mathbf{131})_2(tereph)_2](CF_3SO_3)_4$ crystallizes as an equimolar mixture of two isomers which differ in the relative position of the carboxylate oxygen atoms bound to the metal ion but the square planar coordination environment of the copper ions is almost superimposable in the two isomeric forms. In both isomers the carboxylate binds in a monodentate oxygen η^1 mode whereas in $[Cu_4(\mathbf{132})_2(tereph)_2]^{4+}$ it is bound in a O,O': η^1,η^1 terminal mode. The structures lead to different material parameters (Fig. 110 a and b) UV–vis and ESI-MS spectra indicate that the solid state structure of the cations is retained in solution [140].

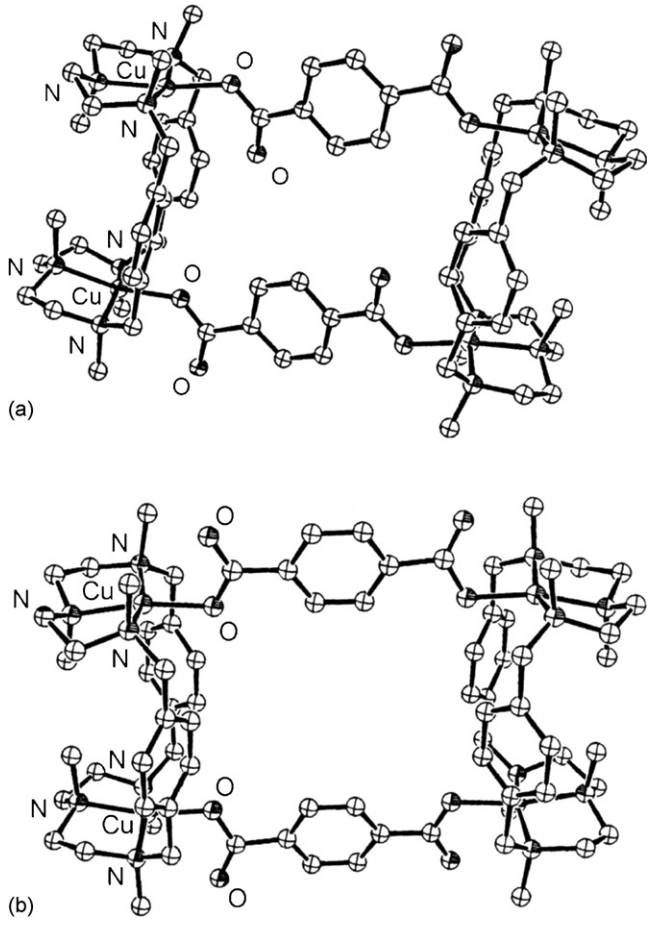

Fig. 110. Structure of $[Cu_4(\mathbf{131})_2(tereph)_2]^{4+}$ (a) and $[Cu_4(\mathbf{132})_2(tereph)_2]^{4+}$ (b).

2.6. [2 + 2] Macrocyclic ligands, derived from dialdehydes without bridging groups and functionalized triamines, and related complexes

The macrocycles H_2-**135**···**138** derive from the [2 + 2] condensation of 1,3-diformylbenzene, 1,4-diformylbenzene or 2,6-diformylpyridine with $H_2N(CH_2)_2NR(CH_2)_2NH_2$ (R = -$(CH_2)_2OH$; -$CH_2CH(CH_3)OH$; -$(CH_2)_2NHCH_2C_{10}H_6$), followed by reduction of the resulting Schiff bases with $NaBH_4$. The hydroxo groups appended at the secondary amine can serve, under particular experimental conditions, as endogenous bridges toward two metal ions.

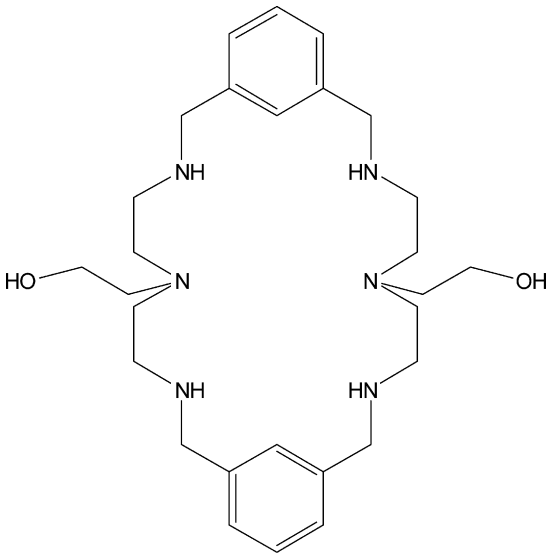

H_2-**135**

In particular the hexaaza-macrocyclic ligands H_2-**135** and H_2-**136** derive form the condensation of 2-[bis(2-aminoethyl)amino]ethanol and respectively isophthalaldehyde or terephthalaldehyde and subsequent hydrogenation of the resulting Schiff base with $NaBH_4$ [141,142].

$[Zn_2(\mathbf{135})](ClO_4)_2$ was prepared by the reaction of methanolic solutions of H_2-**135** and $Zn(ClO_4)\cdot 6H_2O$ in a 2:1 molar ratio and in the presence of $N(Et)_3$ [143]. The structure is centrosymmetric with the center point locates at the middle of the two zinc(II) ions which are pentacoordinated in a distorted trigonal bipyramidal coordination, formed by the three nitrogen atoms

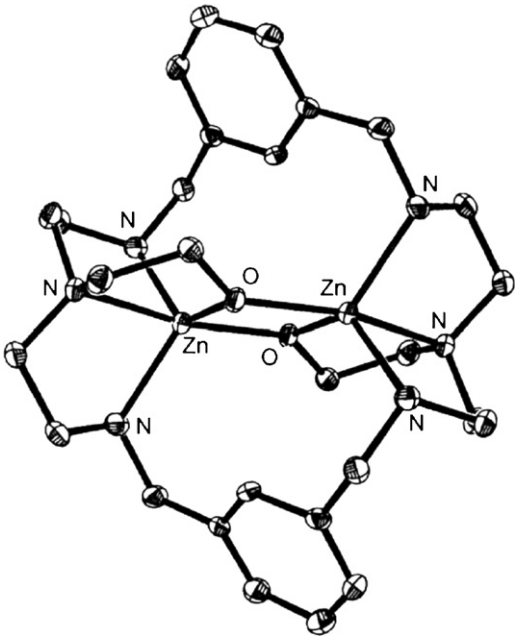

Fig. 111. Structure of $[Zn_2(\mathbf{135})]^{2+}$.

and one internal oxygen atom of the hydroxyethyl pendant, one intermolar oxygen atom from another hydroxyethyl pendant serving as bridging group [143].

The hydrolysis of 4-nitrophenyl acetate catalyzed by $[Zn_2(\mathbf{135})]^{2+}$ in 10% (v/v) CH_3CN at 25 °C, with $I = 0.10$ ($NaNO_3$) and pH 9.0, has shown a second order rate constant of $0.21\,M^{-1}\,s^{-1}$. This value is lower than that of similar mononuclear zinc(II) complexes. The stable double alkoxide-bridged structure in this complex cleavage of the bridged alkoxide followed by the binding of OH^- to form the active species containing $\{Zn^{II}(alkoxide)\}$ and $\{Zn^{II}(OH)\}$ for ester hydrolysis less easy to occur. In addition, the bridging RO^- function in the $\{Zn^{II}(OH)Zn^{II}\}$ system is less nucleophilic than single-coordinated RO^- function in the $\{Zn^{II}(OH)\}$ system. This is not surprising; the bridging coordination of alkoxide to two electrophilic metal centers may reduce the nucleophilicity of this group [143].

$[Zn_2(\mathbf{135})](Br)_2\cdot 2H_2O$, obtained by reaction of aqueous solutions, of $ZnSO_4\cdot 7H_2O$ and H_2-**135**-4HBr·$4H_2O$ in a 2:1 molar ratio, adjusted at pH 9 by adding 1 M NaOH, adopts a chair conformation. The structure is centrosymmetric with the center located in the middle of the two pentacoordinated zinc ions, which show an analogous coordination geometry close to the trigonal pyramid in a N_3O_2 coordination environment. The axial sites are coordinated by the oxygen from the pendant alcohol and one nitrogen from the diethylenetriamine moiety. A $\{Zn_2(\mu\text{-alkoxide})_2\}$ structure is located inside the macrocycle; the two zinc ions are bridged by the two deprotonated alcohol pendants located on two different sides of the plane defined by the nitrogen atoms of the macrocycle; the Zn_2O_2 core is coplanar. The Zn···Zn distance is 3.066 Å (Fig. 111) [142,143]. Compared with the structure of **135**, the whole macrocycle is distorted [144].

Potentiometric titrations of the 1:2 H_2-**135**:Zn^{II} system in water at 298.1 K show that the mononuclear complex $[Zn(H_2\text{-}\mathbf{135})]^{4+}$ appears in the pH range 5.5–7.2 (maximum at pH 6.4, 38.6%). The binuclear zinc(II) complex with two alkoxide bridges $[Zn_2(\mathbf{135})]^{2+}$ exists in the pH range 6–8 (maximum at pH 7, 51.3%). As the pH is raised $[Zn_2(\mathbf{135})(OH)]^+$ is formed with a preferred pH of 9.0, above which it is gradually converted to $[Zn_2(\mathbf{135})(OH)_2]$.

As $[Zn_2(\mathbf{135})]^{2+}$ and $[Zn_2(\mathbf{135})(OH)]^+$ are the dominant species in aqueous solution at $7 < pH < 9$, their ability to promote hydrolysis of *p*-nitrophenyl acetate at different pH (7.5, 8.5, 9.0) was tested. The highest activity, achieved when pH was raised above 8.0, parallels the increase in the concentration of $[Zn_2(\mathbf{135})(OH)]^+$ which hence shows higher catalytic activity than $[Zn_2(\mathbf{135})]^{2+}$. A remarkably higher hydrolytic activity was observed for the complex $[Zn_2(\mathbf{136})(CH_3COO)_2](ClO_4)_2\cdot 2H_2O$; this can be explained by considering the structural differences between the two compounds. The rigidity of the [26]-membered macrocycle has kept the two zinc(II) ions 8.74 Å apart and therefore cannot form the species containing the $\{Zn_2(\mu\text{-alkoxide})_2\}$ unit while the cavity size and rigidity of the [24]-membered macrocycle facilitates the formation of the inactive species containing the $\{Zn_2(\mu\text{-alkoxide})_2\}$ unit [142].

$[Cu_2(H_2\text{-}\mathbf{136})(N_3)_2](ClO_4)_2\cdot 2H_2O$ was obtained by reaction of $Cu(ClO_4)\cdot 6H_2O$ and H_2-**136** in the presence of NaN_3 and in a 2:1:2 molar ratio [141]. The presence of the crystallized water molecules and azides is confirmed by thermogravimetric measurements which show one initial endothermic peak centered at 125 °C with a weight loss corresponding to loss two crystallization water molecules; and other endothermic peak centered at 184 °C with a weight loss corresponding to further loss two azides. ESI-MS spectra show that the main species, $[Cu_2(H\text{-}\mathbf{136})(N_3)]^{2+}$ and $[Cu_2(\mathbf{136})]^{2+}$, were formed by deprotonation of the hydroxyethyl pendants and releasing azides from the copper(II) complex stepwise. The crystal structure of this dinuclear diazide copper(II) complex shows H_2-**136** binds two copper(II) ions by way of its diethylenetriamine moieties, which provide three nitrogen donors to each metal ion. The coordination set around each copper ion is further completed by the coordination of an azide and an oxygen atom of the pendant arm. Both copper(II) ions take the form of a distorted trigonal pyramid in the N_4O coordination environment. One copper(II) ion lies 0.198 Å above the trigonal equatorial N_2O plane and the two axial sites are occupied by the tertiary nitrogen atom from diethylenetriamine moiety and one nitrogen atom of azide. The other copper(II) ion lies 0.220 Å below the trigonal equatorial N_2O plane with and the two axial sites are occupied by the remaining nitrogen atom from diethylenetriamine moiety and one nitrogen from azide. The two equatorial planes are almost coplanar. The separation of the two copper(II) centers is 8.11 Å, indicating that there is no interaction between the two metal ions. The azide ions are essentially linear. The water molecules and the perchlorate group are hydrogen-bonded with different macrocyclic units (Fig. 112a) [141].

The effective magnetic moment per copper atom of $[Cu_2(H_2\text{-}\mathbf{136})(N_3)_2](ClO_4)_2\cdot 2H_2O$ remains almost unchanged over the measured 76 and 300 K temperature range ($1.64\mu_B$), indicating

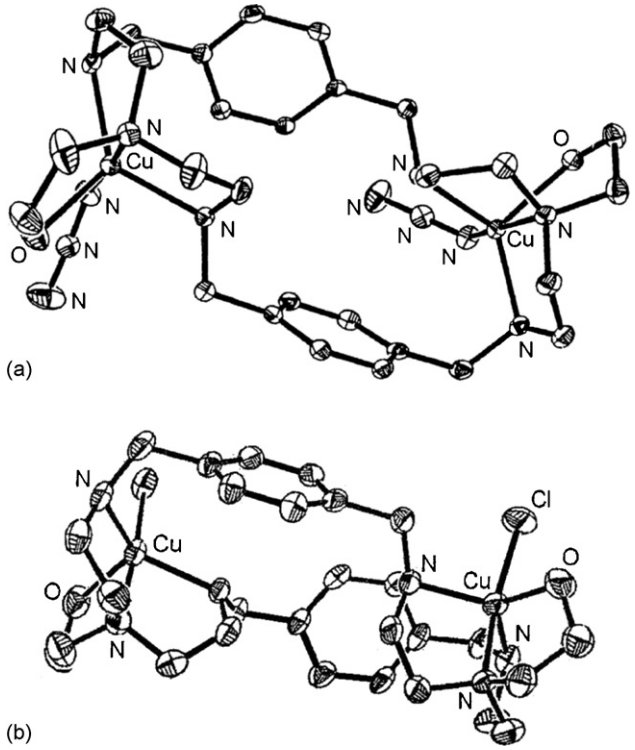

Fig. 112. Structure of $[Cu_2(H_2\text{-}\mathbf{136})(N_3)_2]^{2+}$ (a) and $[Cu_2(H_2\text{-}\mathbf{136})(Cl)_2]^{2+}$.

that there is no magnetic interaction between the neighboring copper(II) ions owing to the long intermetallic distance (8.11 Å) as revealed by X-ray structure [141].

Cyclic voltammograms for $[Cu_2(H_2\text{-}\mathbf{136})(N_3)_2](ClO_4)_2$ in dry acetonitrile shows a single quasi-reversible oxidation process centered at +1.06 V and a quasi-reversible reduction wave due to the copper(I) ions centered at −0.6 V. These results are consistent with the stabilization of the copper(II) ions in the saturated hexaamine derivatives [141].

In $[Cu_2(H_2\text{-}\mathbf{136})(Cl)_2](Cl)_2\cdot 5.5H_2O$, obtained by reaction of $CuCl_2\cdot 2H_2O$ with H_2-**136** in water, H_2-**136** binds two copper(II) ions, 8.22 Å apart, by its diethylenetriamine moieties, which provide three nitrogen donors to each copper(II) ion; a chloride anion and an oxygen atom from the hydroxyethyl pendant complete the distorted trigonal bipyramidal coordination environments about the copper(II) ions (Fig. 112b) [144].

The titration curve of H_2-**136** reveals that the two tertiary nitrogen atoms are of very low basicity and release their protons easily into aqueous solution at low pH. The buffer region occurring at higher pH corresponds to the neutralization of the remaining four ammonium groups of the ligand The complexation constants of H_2-**136** with the copper(II) ion were obtained by NaOH potentiometric titration of H_2-**136**·6HBr in the presence of copper(II) ions. In a solution containing Cu^{II} and $[H_8\text{-}\mathbf{136}](Br)_6$ in a 2:1 molar ratio the dinuclear complex $[Cu_2(H_2\text{-}\mathbf{136})]^{4+}$ is the predominant species over the pH range 5–7 while $[Cu_2(H\text{-}\mathbf{136})]^{3+}$ and $[Cu_2(\mathbf{136})]^{2+}$ are the major complexes in solution at pH > 7. The mono-deprotonated $[Cu_2(H\text{-}\mathbf{136})]^{3+}$ has a favourable pH of 7.6, above which it is gradually converted to $[Cu_2(\mathbf{136})]^{2+}$, which predominates at pH > 9.

The potentiometric investigation of equimolar aqueous solution of copper(II) ion and **136**·6HBr, also carried out by NaOH titration, reveals that the copper(II) ion readily forms a mononuclear complex with the deprotonated ligand. The species concentration distribution as a function of pH indicates that the deprotonated species $[Cu(H\text{-}\mathbf{136})]^+$ becomes predominant between pH 9 and 10.5 [144].

4-Nitrophenyl acetate (NA) hydrolysis promoted by $[Cu_2(H_2\text{-}\mathbf{136})(Cl)_2](Cl)_2$ showed a second-order rate constant of 0.41 $M^{-1}\,s^{-1}$, which is approximately 10 times greater than that of the mononuclear copper(II) complex of the related tripodal amine 1,5-diamino-3-aza(hydroxyethyl)pentane. The preference of the copper(II) alkoxide-catalyzed ester hydrolysis over copper(II) hydroxide-catalyzed hydrolysis was proved by kinetic experiments and shows evidence for the stronger nucleophilic ability of the copper(II) alkoxide than copper(II) hydroxide. In the catalytic reaction, the $\{Cu^{II}(OR)\}$ function acts as nucleophile in the first step of NA hydrolysis, giving an acyl intermediate, which is subsequently hydrolyzed via intramolecular attack of a $\{Cu^{II}(OH)\}$ function. However, intermolecular attack by external water or hydroxide should not be ruled out [144].

Trans-$[Pd_2(H_2\text{-}\mathbf{136})(Cl)_2](C1O_4)_2\cdot 2H_2O$ was obtained by reaction of H_2-**136** with two equivalents of $K_2[Pd(Cl)_4]$ in water at 60 °C and crystallized as yellow block crystals from the aqueous solution after adding $NaC1O_4$ saturated solution and stored in a refrigerator. However, reaction of H_2-**136** of *trans*-$[Pd(PhCN)_2(C1)_2]$ in methanol solution under reflux generated *cis*-$[Pd_2(H_2\text{-}\mathbf{136})(Cl)_2](Cl)_2\cdot 2H_2O$, which was recrystallized as yellow block crystals from a concentrated aqueous solution stored in a refrigerator [145].

In *trans*-$[Pd_2(H_2\text{-}\mathbf{136})(Cl)_2]^{2+}$ each palladium(II), coordinated by a diethylenetriamine moiety, adopts a distorted square planar configuration in a N_3Cl environment. The Pd···Pd distance is 7.0 Å. The two non-coordinated hydroxyethyl arms of the macrocycle ligand are located at opposite sides of the piane defined by the nitrogen atoms and the phenyl groups of the macrocyclic ligand. The cationic complex forms a chair-like conformation (Fig. 113a) [145].

In *cis*-$[Pd_2(H_2\text{-}\mathbf{136})(Cl)_2]^{2+}$ each palladium(II) ion has a distorted square configuration in a N_3C1 environment. The two palladium ions are 6.813 Å apart from each other. The two non-coordinated hydroxyethyl arms of the macrocycle ligand are located at same sides of a reference piane defined by the nitrogen atoms and the phenyl groups of the macrocyclic ligand, forming a boat-like conformation (Fig. 113b) [145].

These dinuclear palladium(II) complexes, when treated with $AgNO_3$, are converted into $[Pd_2(H_2\text{-}\mathbf{136})(NO_3)_2]^{2+}$, the interaction of which with N-acetylmethionylamine(H-AcMet-Ala), studied by ESI mass spectrum, shows both $[Pd_2(H_2\text{-}\mathbf{136})(NO_3)(AcMet\text{-}Ala)]^{2+}$ and $[Pd_2(H_2\text{-}\mathbf{136})(AcMet\text{-}Ala)_2]^{2+}$ were formed as mixed in equimolar ratio and the later species was unique one as twofold excess of the AcMet-Ala was used.

The hydrolysis of the Met-Ala bond in $[Pd_2(H_2\text{-}\mathbf{136})(NO_3)(AcMet\text{-}Ala)]^{2+}$ and $[Pd_2(H_2\text{-}\mathbf{136})(AcMet\text{-}Ala)_2]^{2+}$ was monitored by ^1H NMR via resonance of CH_3 of alamine

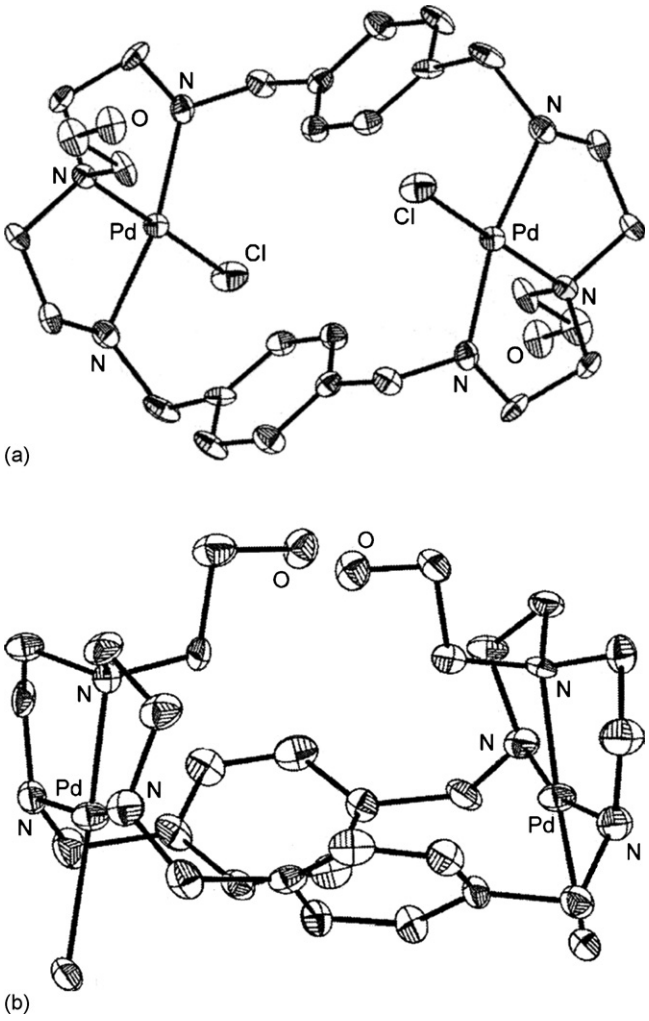

Fig. 113. Structure of *trans*-$[Pd_2(H_2\text{-}\mathbf{136})(Cl)_2]^{2+}$ (a) and *cis*-$[Pd_2(H_2\text{-}\mathbf{136})(Cl)_2]^{2+}$.

in AcMet-Ala and free alanine of hydrolytic product. In comparison with control experiment, the accelerated action of the two dinuclear palladium(II) complexes is noteworthy. The hydrolysis of Met-Ala bond in $[Pd_2(H_2\text{-}\mathbf{136})(AcMet\text{-}Ala)_2]^{2+}$ is independently carried out by each palladium(II)-coordinated diethylenetriamine moiety. The observed rate constant for hydrolysis of Met-Ala bond in $[AcMet\text{-}Ala]^-$ increases remarkably as the solution is more acidic. As $[Pd(trien)(H_2O)]^{2+}$ is unactive toward hydrolysis of methionine-containing peptides, the hydrolysis of Met-Ala bond in $[Pd_2(H_2\text{-}\mathbf{136})(AcMet\text{-}Ala)_2]^{2+}$ is promoted by the pendant hydroxyl group and probably catalyzed by general acid [145].

The macrocyclic ligand H_2-**137**, bearing 2-hydroxypropyl pendants, was synthesized as a mixture of diastereoisomers by $NaBH_4$ reduction of the corresponding Schiff base derived from the [2 + 2] condensation of 1-[bis(2-aminoethyl)amino]-2-propanol with terephthalaldehyde [146]. In $[Cu_2(\mathbf{137})(Cl)_2]\cdot 6.5H_2O$, synthesized by reaction of H_2-**137** with $CuCl_2$ in H_2O in a 1:2 molar ratio, $[\mathbf{137}]^{2-}$ binds two copper(II) ions at a distance of 8.128 Å by its diethylenetriamine moieties, which provide three nitrogen atoms to each copper(II) ion; the rest of the coordinated atoms are a chloride anion and an oxygen atom from the hydroxypropyl pendant. Each pentacoordinate copper(II) ion has a trigonal bipyramidal environment. The two hydroxypropyl arms are located on the same side of the plane defined by the nitrogen atoms and the phenyl groups of the macrocyclic ligands; thus has a boat-like conformation (Fig. 114) [146].

A study of the species distribution as a function of pH at a copper(II) concentration of 2 mM and a H_2-**137** concentration of 1 mM at 25 °C shows $[Cu(H_4\text{-}\mathbf{137})]^{4+}$, $[Cu_2(H_2\text{-}\mathbf{137})]^{4+}$, $[Cu_2(H\text{-}\mathbf{137})]^{3+}$, $[Cu_2(\mathbf{137})]^{2+}$, $[Cu_2(\mathbf{137})(OH)]^{+}$, $[Cu_2(\mathbf{137})(OH)_2]$ exist as the major copper(II) complex species under the employed experiment conditions. The dinuclear species $[Cu_2(H_2\text{-}\mathbf{137})]^{4+}$ is the predominant species over the pH range 5–6.5. The monodeprotonated $[Cu_2(H\text{-}\mathbf{137})]^{3+}$ has a favourable pH of 7.4, above which it is gradually converted into $[Cu_2(\mathbf{137})]^{2+}$, $[Cu_2(\mathbf{137})(OH)]^{+}$, $[Cu_2(\mathbf{137})(OH)_2]$; $[Cu_2(\mathbf{137})]^{2+}$ predominates at pH values of about 8.5 and this is in accordance with the X-ray crystal structure analysis.

The 4-nitrophenyl acetate hydrolysis promoted by $[Cu_2(\mathbf{137})(Cl)_2]$ shows a second-order rate constant of $0.39\ M^{-1}\ s^{-1}$, which is approximately 14 times higher than that of the dicopper macrocycle complex without hydroxy pendants, while it is comparable to that of the similar copper(II) complex with H_2-**136**, which suggests that a $\{Cu^{II}(OR)\}$ system is a better nucleophile that a $\{Cu^{II}(OH)\}$ one. In spite of the volume of RO^-, the nucleophilicity and the Lewis acidity of the metal macrocycle can also effect the carboxy ester hydrolysis [146].

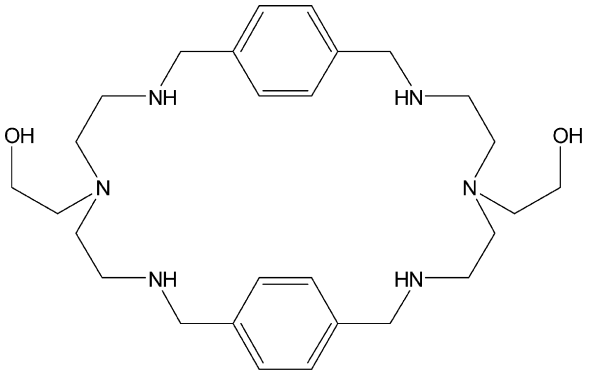

H_2-**136**

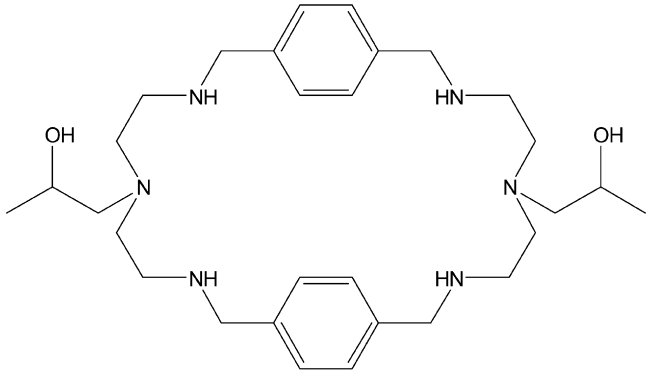

H_2-**137**

The addition of a H_2O/CH_3CN solution of H_2-**135** to an aqueous solution of $Cu(ClO_4)_2{\cdot}6H_2O$ and imidazole in a 2:1 molar ratio gives rise to a solution which, allowed to stand for 2 days, separates $[Cu_2(H_2\text{-}\mathbf{135})(\mu\text{-Im})](ClO_4)_3{\cdot}2.5H_2O{\cdot}0.5\,CH_3CN$ [147]. The cation $[Cu_2(H_2\text{-}\mathbf{135})(\mu\text{-Im})]^{3+}$ (Fig. 115a) contains two copper(II) ions bridged by an imidazolate anion with a separation distance of 5.813 Å. Each copper(II) ion is pentacoordinate with a coordination geometry between trigonal bipyramid and tetragonal pyramid. The geometry around one copper(II) ion is distorted toward the trigonal bipyramid, the apical position being occupied by the oxygen atom of one alcohol pendant. The geometry around the other copper(II) ion is distorted toward the trigonal bipyramid, the axial position being occupied by a tertiary amine nitrogen and a bridged imidazolate nitrogen. Good flexibility is manifested by the macrocycle: the distance between the two tertiary amine nitrogen atoms is 9.562 Å, which accommodates the imidazolate-bridged dicopper structure well. Each hydroxyethyl pendant affords the fifth coordination atom for each copper(II) ion at the same side of the plane defined by the four secondary amine nitrogen atoms of the macrocycle, and none of the two hydroxyethyl pendants is deprotonated. The bridged imidazolate ring is sandwiched between two phenyl rings [147].

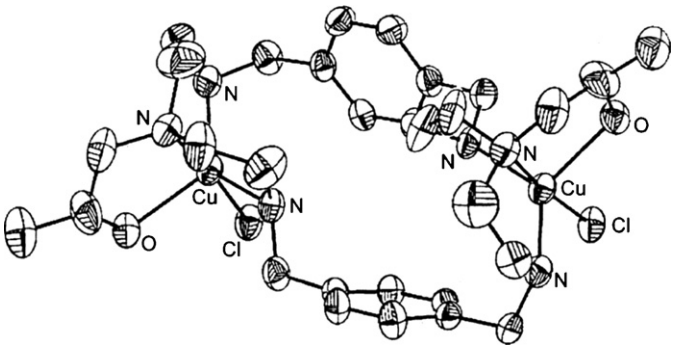

Fig. 114. Structure of $[Cu_2(\mathbf{137})(Cl)_2]$.

Magnetic measurements of $[Cu_2(H_2\text{-}\mathbf{135})(\mu\text{-Im})](ClO_4)_3{\cdot}2.5H_2O$ indicate the presence of an antiferromagnetic exchange interaction with a coupling constant of $-2J = 72.8\,cm^{-1}$. Investigations on the pH dependent ESR of the complex in frozen 50% H_2O/DMSO solution at 110 K reveal the existence of the imidazolate-bridged dicopper structure with two antiferromagnetically coupled copper(II) ions in solution mainly in the range $5.5 \leq pH \leq 12$ [147].

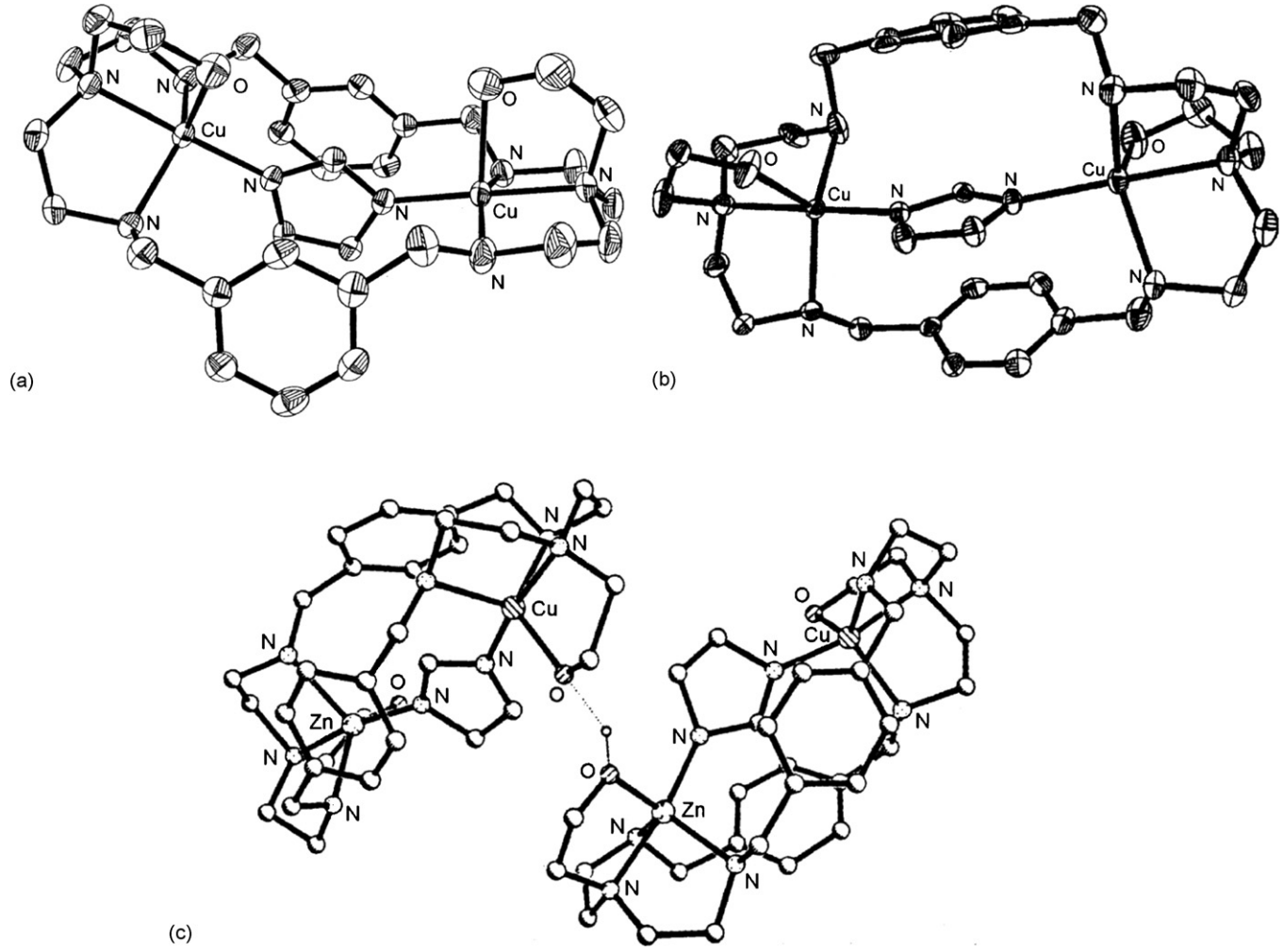

Fig. 115. Structure of $[Cu_2(H_2\text{-}\mathbf{135})(\mu\text{-Im})]^{3+}$ (a), $[Cu_2(H_2\text{-}\mathbf{136})(\mu\text{-Im})]^{3+}$ (b) and $[Cu_2Zn_2(\mathbf{136})(H\text{-}\mathbf{136})(\mu\text{-Im})_2]^{3+}$(c).

The SOD activity of the complex has been evaluated by the nitro blue tetrazolium assay and the complex catalyzed the dismutation of superoxide at pH 7.8 with an IC_{50} value of 0.36 μmol dm^{-3} [147]. The activity is in the same order of magnitude as the best SOD model complexes [148]. The result is reasonable because the macrocycle is flexible and the imidazolate-bridged dicopper center is accessible to O_2^-.

Also the imidazolated bridged homodinuclear Cu_2^{II} complex, $[Cu_2(H_2\text{-}\mathbf{136})(\mu\text{-Im})](ClO_4)_3\cdot 0.5H_2O$ and heterodinuclear $Cu^{II}Zn^{II}$ analogue, $[Cu_2Zn_2(\mathbf{136})(H\text{-}\mathbf{136})(\mu\text{-Im})_2](ClO_4)_3$ have been synthesized as possible models for copper–zinc superoxide dismutase, by reaction respectively of $Cu(ClO_4)_2\cdot 6H_2O$ with imidazole followed by the addition of the macrocycle H_2-**136** at pH ≈ 6 or of $Cu(ClO_4)_2\cdot 6H_2O$ and $Zn(ClO_4)_2\cdot 6H_2O$ with H_2-**136** and imidazole (at pH ≈ 9.5) [148,149].

The structure of $[Cu_2(H_2\text{-}\mathbf{136})(\mu\text{-Im})](ClO_4)_3\cdot 0.5H_2O$ shows that it is an imidazolate-bridged homodinuclear copper(II) complex. Each copper(II) ion is coordinated by an N_4O environment (three nitrogen and one oxygen atoms from the macrocycle, one nitrogen atom from imidazolate) with a coordination geometry between trigonal bipyramid and tetragonal pyramid. The two copper(II) ions are almost coplanar with the imidazolate ring. The bridged imidazolate ring partially sandwiches between the two phenyl rings of the macrocyclic ligand, and the imidazolate ring is approximately parallel to the two phenyl rings with a π–π stacking interaction between these rings. Additionally, the two hydroxyethyl groups are located at the different sides of the plane defined by nitrogen atoms of the macrocyclic ligand, forming a chair-like (*anti*) conformation (Fig. 115b) [148,149].

Compared to $[Cu_2(H_2\text{-}\mathbf{136})(\mu\text{-Im})](ClO_4)_3\cdot 0.5H_2O$, the structure of $[Cu_2Zn_2(\mathbf{136})(H\text{-}\mathbf{136})(\mu\text{-Im})_2](ClO_4)_3$ is different. The asymmetric unit contains two $Cu^{II}Zn^{II}$ heterodinuclear cations, $[CuZn(\mathbf{136})(\mu\text{-Im})]^+$ and $[CuZn(H\text{-}\mathbf{136})(\mu\text{-Im})]^{2+}$, joined together through hydrogen bonding as well as three perchlorate anions (Fig. 115c). The coordination geometries around the copper and zinc ions are all distorted trigonal bipyramid. Both copper(II) and zinc(II) ions are coordinated in an N_4O environment, in which three nitrogen and one oxygen atoms are from ligand $[\mathbf{136}]^{2-}$, and one nitrogen atom is from imidazolate. Discrepancies between $[Cu_2(H_2\text{-}\mathbf{136})(\mu\text{-Im})](ClO_4)_3$ and $[Cu_2Zn_2(\mathbf{136})(H\text{-}\mathbf{136})(\mu\text{-Im})_2](ClO_4)_3$ exist in the conformation of the macrocycle with two pendants, the conformation of the two phenyl spacers, and the position of the bridged imidazolate ring. Moreover, the imidazolate ring is basically carried on a boat constructed by the macrocycle with two hydroxyethyl arms, as well as the copper(II) and zinc(II) ions. It is worth noting that the two hydroxyethyl arms in the Cu_2Zn_2 complex are located on the same sides, forming a boat-like conformation, but a chair-like conformation in the Cu_2 complex. This difference in the conformation of the ligand with two arms can only be accomplished by stereochemical inversion at one (or more) of the nitrogen atoms (at least, one of the two tertiary nitrogen atoms) of the free macrocyclic ligand in the formation of the complexes [148,149].

The differences between $[Cu_2(H_2\text{-}\mathbf{136})(\mu\text{-Im})](ClO_4)_3$ and $[(Cu_2Zn_2(\mathbf{136})(H\text{-}\mathbf{136})(\mu\text{-Im})_2](ClO_4)_3$ have been assumed as substantial evidence for the formation of the heterodinuclear imidazolate-bridged $Cu^{II}Zn^{II}$ complex. The changes in the bond lengths and angles, the conformation of macrocyclic ligand and the position of imidazolate rings demonstrate that the overall ligand, especially the two flexible hydroxyethyl arms, possesses a good adjustability for the different configuration requirements for both copper(II) and zinc(II) metal ions in the course of the formation of the complexes.

The magnetic and ESR data of the dicopper(II) complex prove an antiferromagnetic interaction between the two imidazolate-bridged copper(II) ions ($-2J = 86.4\ cm^{-1}$). The X-band ESR spectra of the $Cu_2^{II}Zn^{II}$ complex are typical of the mononuclear copper(II) ion in a trigonal pyramidal environment with a d_z^2 ground state which is consistent with the X-ray result. Additionally, when the curves are magnified, a very weak signal at about 1500 G, together with a shoulder at 2800 G in the frozen-solution spectrum, assigned to a very small amount exchanged $\{Cu^{II}(Im)Cu^{II}\}$ species, can be observed; this signal is not seen in the spectrum of the solid sample even when the curve is magnified 50 times. These results show that the solid sample contains only the $\{Cu^{II}(Im)Zn^{II}\}$ species, and that this species is also the major component in aqueous solution [149].

The UV–vis spectrum of $[Cu_2(H_2\text{-}\mathbf{136})(\mu\text{-Im})](ClO_4)_3$ in water exhibits a broad d–d band centered at 720 nm with a shoulder at 610 nm. The spectrum of $[Cu_2Zn_2(\mathbf{136})(H\text{-}\mathbf{136})(\mu\text{-Im})_2](ClO_4)_3$ shows two broad bands centered at 680 nm and 820 nm for d–d transitions as expected in trigonal bipyramidal geometry for copper(II) ions [148,149].

From pH dependent ESR and electronic spectroscopic studies, the imidazolate bridges in the two complexes have been found to be stable over broad pH ranges. It was proposed that in 50% H_2O/DMSO solution $[Cu_2(H\text{-}\mathbf{136})(\mu\text{-Im})](ClO_4)_3$ evolves into $[Cu_2(\mathbf{136})(\mu\text{-Im})](ClO_4)$ at pH ≈ 8 which at pH ≈ 10 gives rise to $[Cu_2(H_2\text{-}\mathbf{136})(\mu\text{-Im})(OH)_2](ClO_4)$. These results indicate that the imidazolate-bridged dicopper(II) cation is the major component in solution in the range $5 \le pH \le 12$ and the alkoxide pendants will be reversibly substituted by OH^- anions at pH ca. 10. The imidazolate bridges have been found to be stable in the pH ranges, 6–10 for $[Cu_2Zn_2(\mathbf{136})(H\text{-}\mathbf{136})(\mu\text{-Im})_2](ClO_4)_3$.

Similar studies demonstrate that the imidazolate-bridged $\{Cu^{II}(Im)Zn^{II}\}$ moieties of complex $[Cu_2Zn_2(\mathbf{136})(H\text{-}\mathbf{136})(\mu\text{-Im})_2](ClO_4)_3$ in aqueous solution can be stable over a pH range ca. 6–10 in solution. The solution behaviour above pH 10 is more complicated than that of $[Cu_2(H_2\text{-}\mathbf{136})(\mu\text{-Im})](ClO_4)_3$.

The electrochemical properties of the two complexes have been studied by cyclic voltammetry (CV) in degassed dimethylformamide solution. The CV of $[Cu_2(H_2\text{-}\mathbf{136})(\mu\text{-Im})](ClO_4)_3$ shows two quasi-reversible redox waves at $E_{1/2} = -0.39$ V and $E_{1/2} = +0.25$ V (versus SCE), corresponding to the $Cu^{II}Cu^{I}/Cu^{I}Cu^{I}$ and $Cu^{II}Cu^{II}/Cu^{I}Cu^{I}$ redox couples, respectively. The CV of $[Cu_2Zn_2(\mathbf{136})(H\text{-}\mathbf{136})(\mu\text{-Im})_2](ClO_4)_3$ exhibits only one reversible Cu^{II}/Cu^{I} redox couple at $E_{1/2} = -0.25$ V (versus SCE), which indicates that there is only one copper ion in the complex. The difference in Cu^{II}/Cu^{I} redox potential between complexes $[Cu_2(H_2\text{-}\mathbf{136})(\mu\text{-Im})](ClO_4)_3$ and

$[Cu_2Zn_2(\mathbf{136})(H\text{-}\mathbf{136})(\mu\text{-}Im)_2](ClO_4)_3$ demonstrates that the coordination environments around the copper(II) ions of the two complexes are different and afford a substantial explanation for the difference in SOD activity of them, good for both complexes, higher in the dicopper(II) one.

The good activities of the two complexes may be attributed to the flexible macrocyclic ligand, which is able to accommodate the geometrical change from the copper(II) to the copper(I) ion, especially the two labile hydroxyethyl arms, which are proposed to be easily substituted by the substrate, O_2^-, in the catalytic process, just like the O_2^- in place of the water molecule bound to the copper site in the mechanism of dismutation of superoxide anion by native SOD. The SOD-like activity evaluation reveals that the complexes are among the list of the models with the highest activity, and the labile hydroxyethyl pendants are believed to play an importance role in the catalytic process [149].

N^1,N^1-bis(2-aminoethyl)ethane-1,2-diamine, monofunctionalized with a naphthyl group, was condensed with 2,6-pyridinecarbaldehyde in ethanol followed by in situ reduction with sodium borohydride to form the macrocycle **138**. Monofunctionalization of tris(2-aminoethyl)amine was achieved by reacting the free amine with naphthalene1-carbaldehyde in 3:1 molar ratio followed by treatment with $NaBH_4$. The excess of amine is added to ensure predominant formation of the 1:1 functionalized compound [150]

The macrocycle displays, in the pH range 2–11 and in 0.15 M NaCl aqueous solution at 298 K, six protonation steps that correspond to the protonation of the secondary amino groups. Steady state fluorescence measurements show emissions due to the monomer and to the excimer formed between the two naphthalene fragments of the macrocycle. The time-resolved fluorescence data, obtained by the time-correlated single photon counting technique, show that a significant percentage of excimer is preformed as ground-state dimers.

138 forms with the copper(II) and zinc(II) ions mono- and dinuclear complexes in 0.15 M NaCl aqueous solution at 298 K in which the nitrogen atoms in the pendant arm do not provide a strong contribution to the overall stability. NMR data of the zinc(II) complexes indicate that the arms are somewhat blocked by the presence of the metal ions suggesting the involvement of the nitrogens in the arms in the coordination. However, the large number of peaks that appear supports again the existence of different conformations for the complexes including those in which the naphthyl nitrogen would not be involved in the coordination [150].

The mononuclear complexes display $[M(H_3\text{-}\mathbf{138})]^{5+}$, $[M(H_2\text{-}\mathbf{138})]^{4+}$, $[M(H\text{-}\mathbf{138})]^{3+}$ and $[M\mathbf{138}]^{2+}$ stoichiometries. The dinuclear copper(II) complexes present $[Cu_2(H_x\text{-}\mathbf{138})]^{(4+x)+}$ stoichiometries with x values varying from 2 to −2. For 2:1 M: **138** molar ratios these species predominate throughout all the pH range studied. $[Cu_2(\mathbf{138})]^{4+}$ suffers two hydroxylation steps with the formation of $[Cu_2(\mathbf{138})(OH)]^{3+}$ and $[Cu_2(\mathbf{138})(OH)_2]^{2+}$; the hydroxo groups do not behave as bridging ligands. For the zinc(II) system, only the dinuclear species $[Zn_2\mathbf{138}]^{4+}$ and $[Zn_2(\mathbf{138})(OH)]^{3+}$ are found, this last being predominant above pH 9 [150].

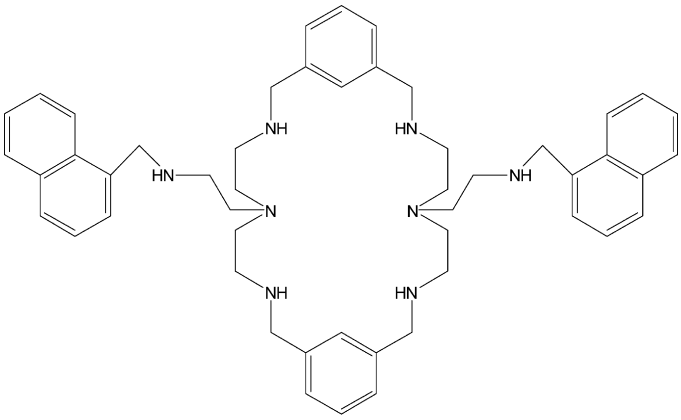

H_2-**138**

Copper(II) complexation gives rise to a chelation enhancement of the quenching effect (CHEQ) while zinc(II) complexation originates a slight chelation enhancement of the fluorescence emission effect (CHEF). The acid–base, coordination capabilities, and emissive behaviour of **138** were compared with those presented by its synthetic functionalized precursor polyamine. The differences in fluorescence properties evidenced by their zinc(II) complexes support the existence of an electron-transfer quenching mechanism form excited naphthalene to complexed pyridine [150].

3. Macrobicyclic ligands and related complexes

[1 + 1] or [3 + 2] macrobicyclic Schiff bases and related reduced polyamine analogues have been prepared according to Scheme 12. In particular the [1 + 1] cryptands have been synthesized by the condensation of equimolar amounts of methanolic solutions of the desired tripodal trialdehyde with a suitable tripodal triamine; the further reduction of the resulting Schiff base with $NaBH_4$ affords the related polyamine derivative [151]. The [3 + 2] tripodal Schiff bases have been prepared by condensation of the designed diformyl derivatives with the triamines $H_2N(CH_2)_nN[(CH_2)_nNH_2](CH_2)_nNH_2$ ($n = 2, 3$) in a 3:2 molar ratio; again, the reduction of the resulting compounds by $NaBH_4$ affords the related macropolycyclic amines.

Although the [1 + 1] and [3 + 2] Schiff bases can be obtained by self-condensation using diluted solutions and/or low reaction temperatures, the best way for their synthesis is to carry out the condensation reaction in the presence of a metal ion as templating agent [5].

The polyamine cryptands have been functionalized by the reaction of the secondary amine groups with appropriate chloro- or bromo-derivatives.

3.1. [1 + 1] Ligands and related complexes

3.1.1. Benzene-based systems

The most relevant results published in the recent past were reviewed in excellent papers [4]; the present work covers only the more recent data.

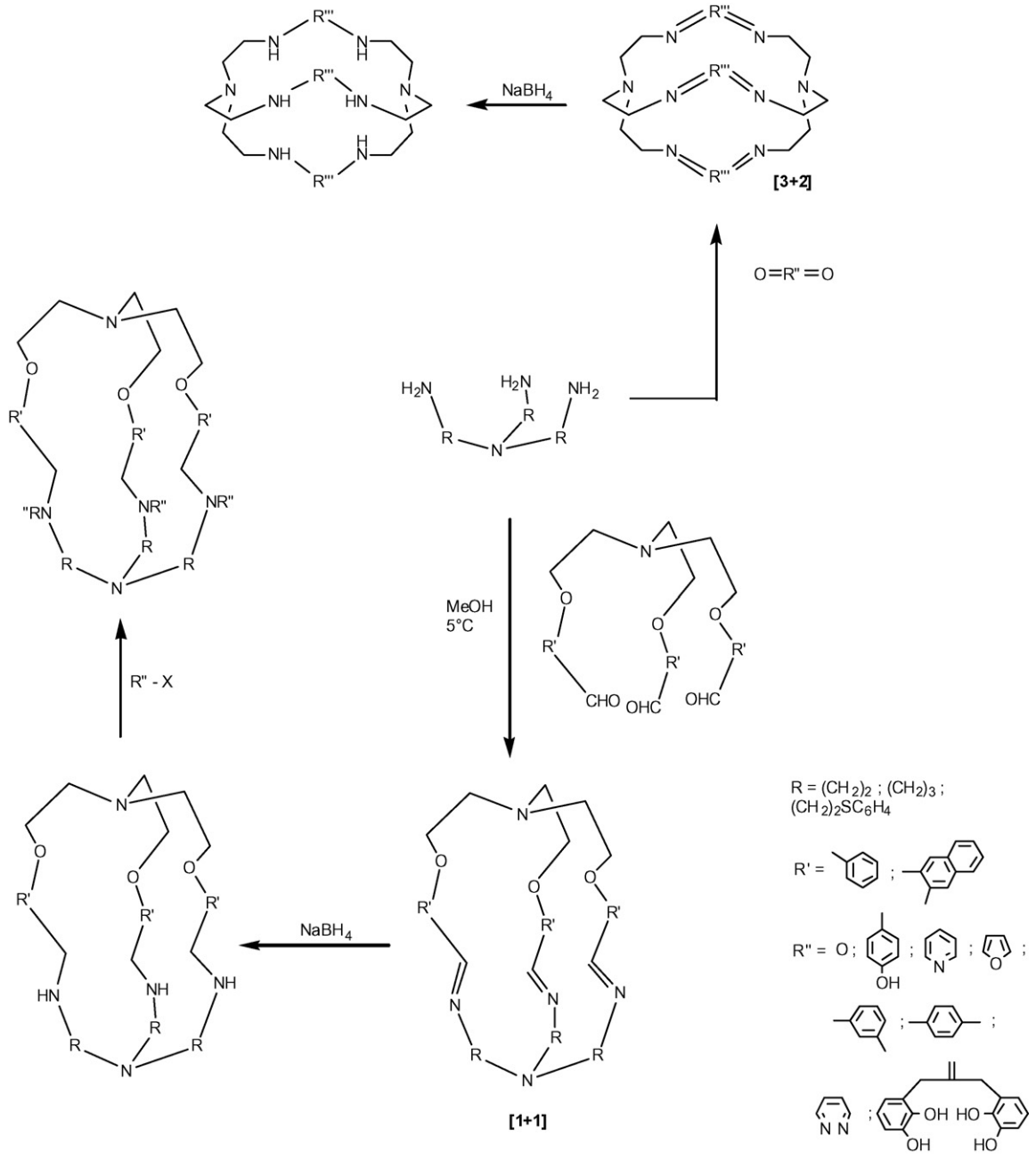

Scheme 12. [1 + 1] and [3 + 2] tripodal Schiff bases and related polyamine derivatives.

A number of cryptands has been synthesized by [1 + 1] Schiff-base condensation of the appropriate tripodal amine and tripodal trialdehyde followed by a reduction of the arising imino groups formed with $NaBH_4$. In this synthetic strategy, an alkali metal ion such as Rb^I or Cs^I is usually employed as a template and the reaction is carried out at ~40 °C. However, at low temperature (~5 °C), the reaction can proceed with comparable yields without any templating ion due to the increased conformational stability of the podand arms. This method works well if the tripodal arms contain aromatic groups which increase the rigidity of the tripods [152–156].

Non-symmetric cryptands with large cavities as **139a**···**139c** have been synthesized only in the presence of the rubinium(I) or cesium(I) ion as the template. Self-condensation reactions lead to mixtures of unidentified products. Apparently, the bigger podands cannot close-in to undergo [1 + 1] condensation in absence of a template [157].

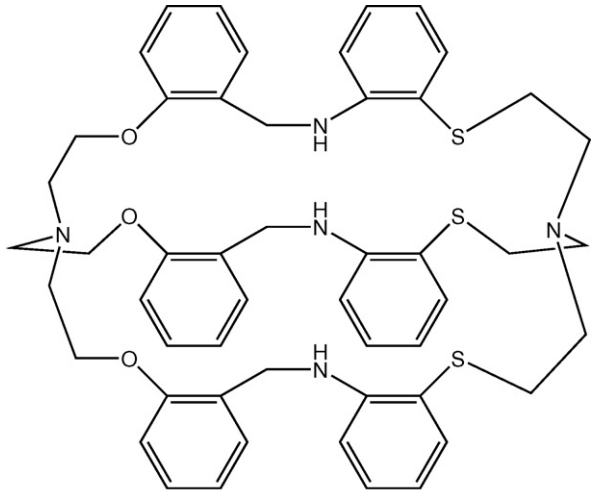

139a

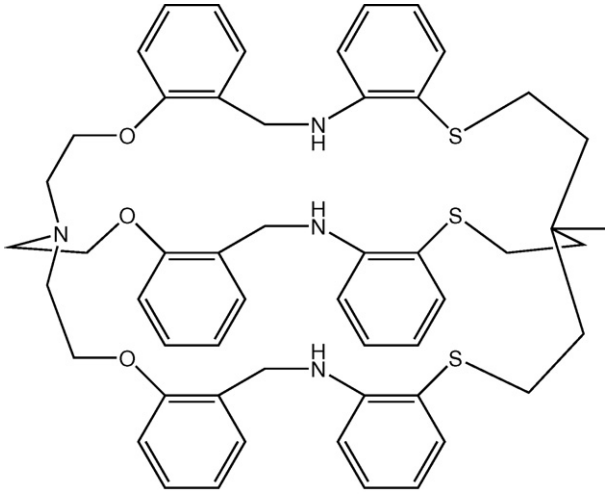

139b

139a···**139c**, containing sulphurs in addition to nitrogen and oxygen as donor, were also found to be good ligands for first-row transition metal ions although only copper(II) and nickel(II) cryptates could be isolated as pure solids [157]. The UV–vis spectroscopic data of the copper(II) and nickel(II) cryptates indicate a distorted octahedral geometry around the metal ion with coordination from three amino nitrogens and three thioether sulphurs [158,159]. The copper(II) cryptates show quasi-reversible Cu^{II}/Cu^{I} couple (ΔE_p = 140–180 mV at 100 mV s^{-1} scan rate) at $E_{1/2}$ of ca. 0.5–0.6 V versus Ag/AgCl. The low value for this couple indicates that these systems are strongly reducing. Not surprisingly, when a further equivalent of $Cu(ClO_4)_2{\cdot}6H_2O$ is added in acetonitrile, the color of the solution changes immediately to dark green and within 2 h colorless crystals of $[Cu(CH_3CN)_4](ClO_4)$ deposit. Upon addition of more copper(II) salt, more of the cuprous salt is formed. Such type of behaviour is, however, not unprecedented [160].

Each of the prepared cryptands **140**···**145** possesses a large cavity with two distinct binding sites separated by a hydrophobic spacer. The N_4 moiety derived from tris(2-aminoethyl)amine (tren) binds transition as well as heavy main-group metal ions like lead(II) and silver(I) while the ether moiety can be expected to be effective in the binding of harder cations. However, complexation studies with these cryptands show that they do not bind alkali or alkaline earth cations. The N_4 moiety, on the other hand, cannot saturate the coordination spheres of many metal ions. Therefore, the bound metal ion draws solvent molecules or counter anions from the medium to saturate its coordination requirements [154].

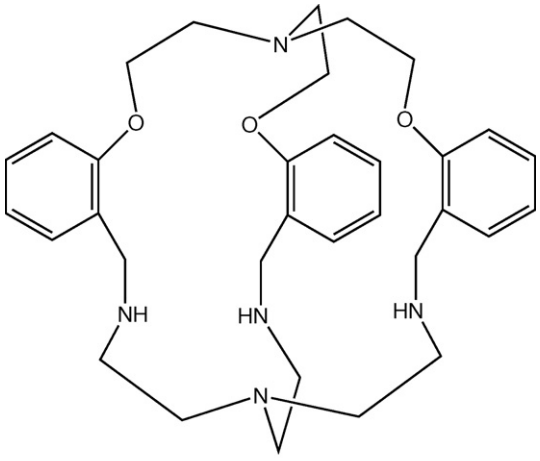

140

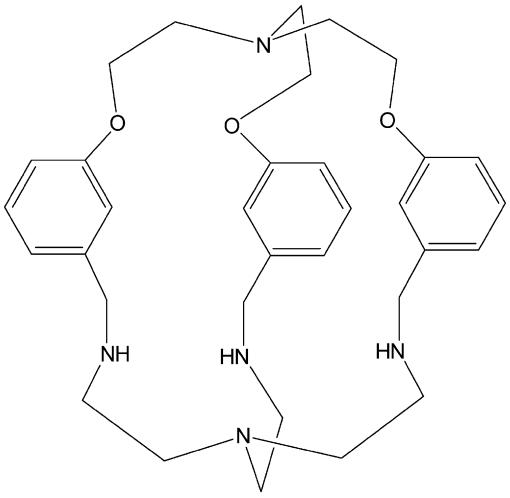

141

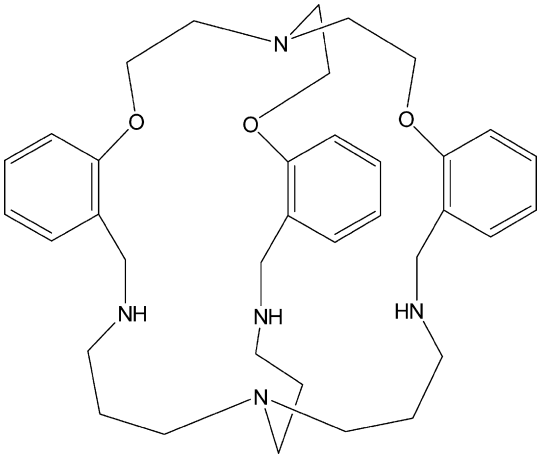

142

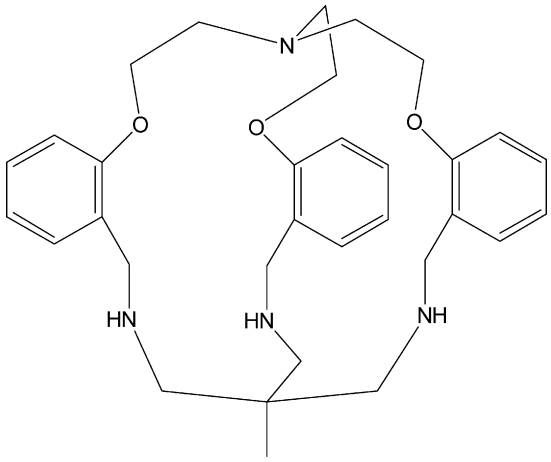

143

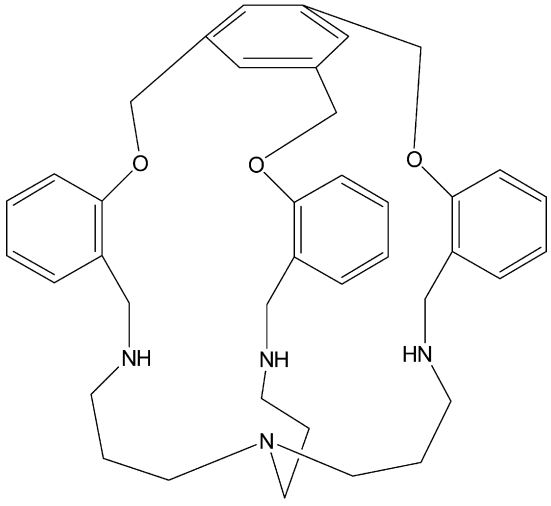

144

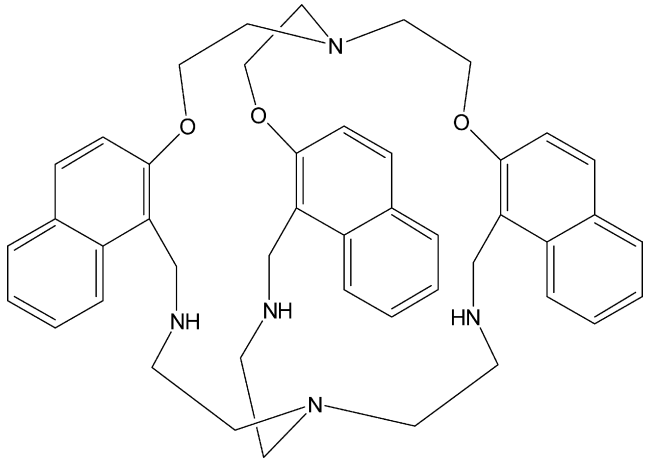

145

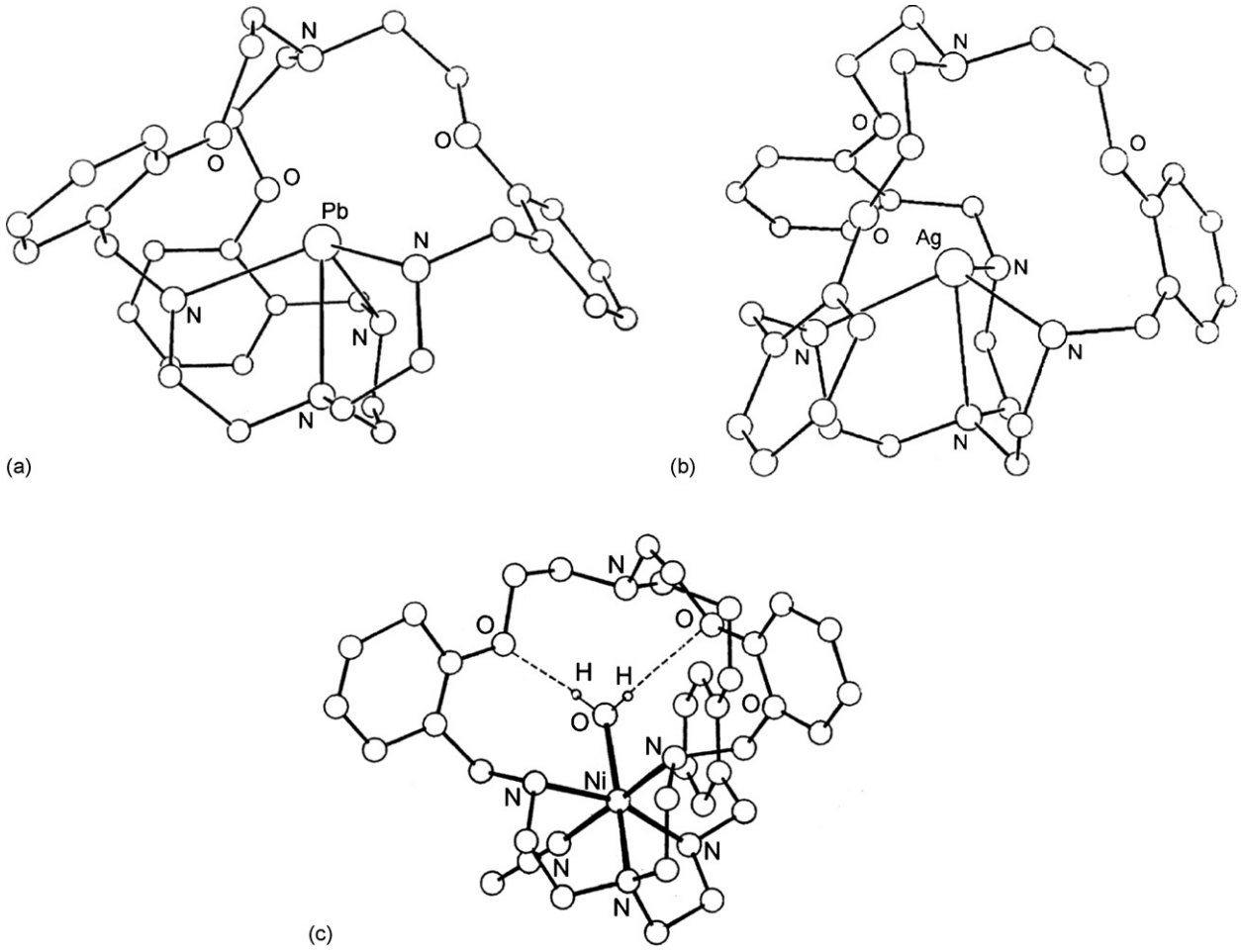

Fig. 116. Structure of $[Pb(\mathbf{140})]^{2+}$ (a), $[Ag(\mathbf{140})]^{+}$ (b), and $[Ni(\mathbf{140})]^{2+}$ (c).

The X-ray structure of the lead(II) cryptate of **140** shows (Fig. 116a) the metal ion to be pentacoordinated from N_4O donors where one of the ether oxygen atoms is also bonded to the metal ion [154].

The coordination requirements of the silver(I) ion is satisfied when it is bonded to four nitrogen atoms of **140** (Fig. 116b). The non-bonding distances between the nitrogen and the oxygen atoms of the cryptand do not change significantly upon coordination, suggesting that **140** is more suited for the silver(I) ion compared with the lead(II) ion. In fact the extraction ability of **140** toward the silver(I) ion is significantly higher than that toward the lead(II) ion [154]. Neither the lead(II) nor silver(I) ion, bonded inside **140**, shows any tendency to bind any molecule or ions to increase the coordination.

The nickel(II) ion at the N_4 end of the cavity of **140** acquires hexacoordination by binding an acetonitrile molecule from outside the cavity and a H_2O molecule inside [154] whose hydrogen atoms are bonded to the ether oxygens (Fig. 116c). This hydrogen-bonding scheme can be exploited to bind a H_2S molecule to the copper(II) ion inside the cavity. Though X-ray data were not obtained, spectroscopic investigations support this type of complexation [161].

Since **141** possesses a much larger cavity, the hydrogen atoms of the H_2O molecule bound to the copper(II) ion cannot come close to the ether oxygens [162]. Instead, the cryptate shows a π H-bonding to the aromatic groups. However, when a metal ion, anchored at the tren-end of the cavity, binds an anion such as CN^-, SCN^- or N_3^-, the top part tilts away [155] enabling the anion to avoid the hydrophobic aromatic groups. As a result, a part of the anion remains outside the cavity. In presence of the chloride anion, a different binding mode is observed. The chloride anion coordinates the nickel(II) ion and at the same time forms hydrogen-bonds with amino groups present in the bridges. Both in case of **140** and **141**, the bound metal ion is pushed out of the plane formed by the three amino groups so that it is exposed to surroundings [154].

In the pH range 2.5–10.5, **140** behaves as a tetraprotonated base $[H_4\text{-}\mathbf{140}]^{4+}$ while **141** and **142** are able to form the fully protonated species $[H_5\text{-}\mathbf{141}]^{5+}$ and $[H_5\text{-}\mathbf{142}]^{5+}$. **140** can form the fully protonated species only in very acidic solution. The first two protonation constants of **140** are considerably higher than the corresponding values for **141** and **142** while the third and fourth values are significantly lower. The higher values for the first two protonation constants of each cryptand make them topologically complementary to water molecule(s) which are tightly held inside the cavity of the protonated cryptands. **140** binds a water molecule almost at the middle of the cavity [163]. Two water molecules are bound inside the larger

cavity of **141** where each oxygen atom is almost tetrahedral [162].

142, with a tris-(3-aminopropyl)amine group instead of a tris-(2-aminoethyl)amine one and *ortho*-substituted benzene groups in the three bridges, has a collapsible cavity. Upon coordination to a zinc(II) ion, the cavity enlarges significantly and coordination geometry around the zinc(II) ion becomes near to an ideal tetrahedral. The copper(II) cryptate of this ligand can also be isolated in the solid state in pure form although no X-ray data are available [155].

The other cryptands in this series do not afford metal cryptates in the solid state in pure form, but lead to mononuclear cryptates with a distorted tetrahedral coordination geometry, as revealed by spectroscopic studies.

These cryptands, incorporating secondary amino groups in the three bridges, can easily be functionalized to give new receptors. For instance, **140** can be derivatized with three palmitoyl side groups by reaction with palmitoyl chloride in dry tetrahydrofuran in the presence of $N(Et)_3$ as base under an argon atmosphere. The isolated pale yellow cyclic compound **146**, purified by recrystallization from ethanol, forms [Cu(**146**)]$(ClO_4)_2$ when treated with $Cu(ClO_4)_2{\cdot}6H_2O$ in ethanol in a 1:1 molar ratio. The coordination of the copper(II) ion within the cryptand cavity was established by its EPR and UV–vis spectral characteristics which match closely those obtained for the well characterized underivatized cryptand complex [Cu(**140**)]$(ClO_4)_2$. Both **146** and [Cu(**146**)]$(ClO_4)_2$ act as amphiphiles and readily form unilamellar vesicles [164].

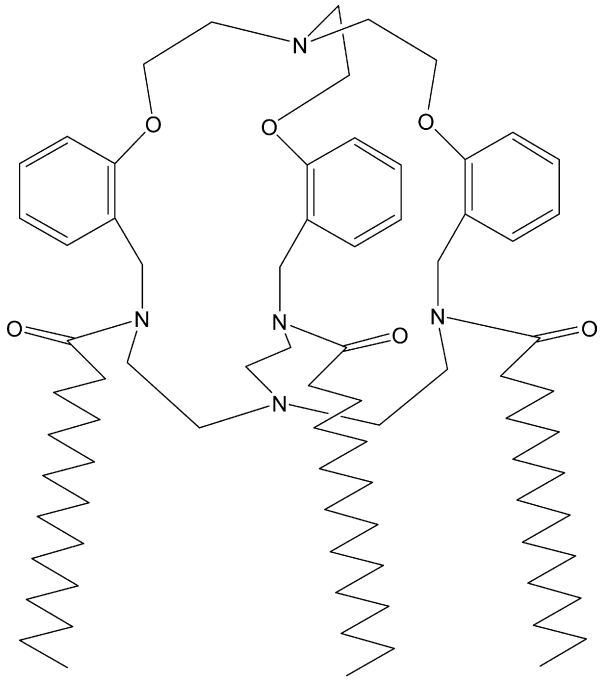

146

Furthermore, the reaction of **140** with bromoacetonitrile in anhydrous acetonitrile in the presence of anhydrous potassium carbonate affords **146a**. While **140** has an endo–exo conformation with the bridgehead nitrogen atoms at 6.272 Å distance, **146a** has an endo–endo configuration with the distance between the bridgehead nitrogen atoms of 5.939 Å [164] The metal binding properties of **146a** are drastically altered: while **146** binds the silver(I) ion at the tren end showing AgN_4 coordination, in **146a** the bridgehead nitrogen atoms are pulled inside to form a two coordinate silver(I) complex and none of the oxygen or nitrogen atoms present in the three bridges are involved in coordination. This is probably the first example where the two bridgehead atoms are pulled inside to the maximum to bind the metal ion. Likewise, the thallium(I) ion shows TlN_4 coordination with **146** while in **146a** it is loosely bound at the tren end, showing TlN_3 coordination. Upon treatment with a silver(I) salt, the thallium(I) ion can be replaced almost instantaneously. On the other hand, with copper(II) tetrafluoroborate salt in moist dimethylformamide, two of the cyanide groups in **146a** are converted to carboxylic acid groups and bind the metal ion from outside forming [Cu(H_2-**146b**)(DMF)]$(BF_4)_2{\cdot}$DMF. The copper(II) ion

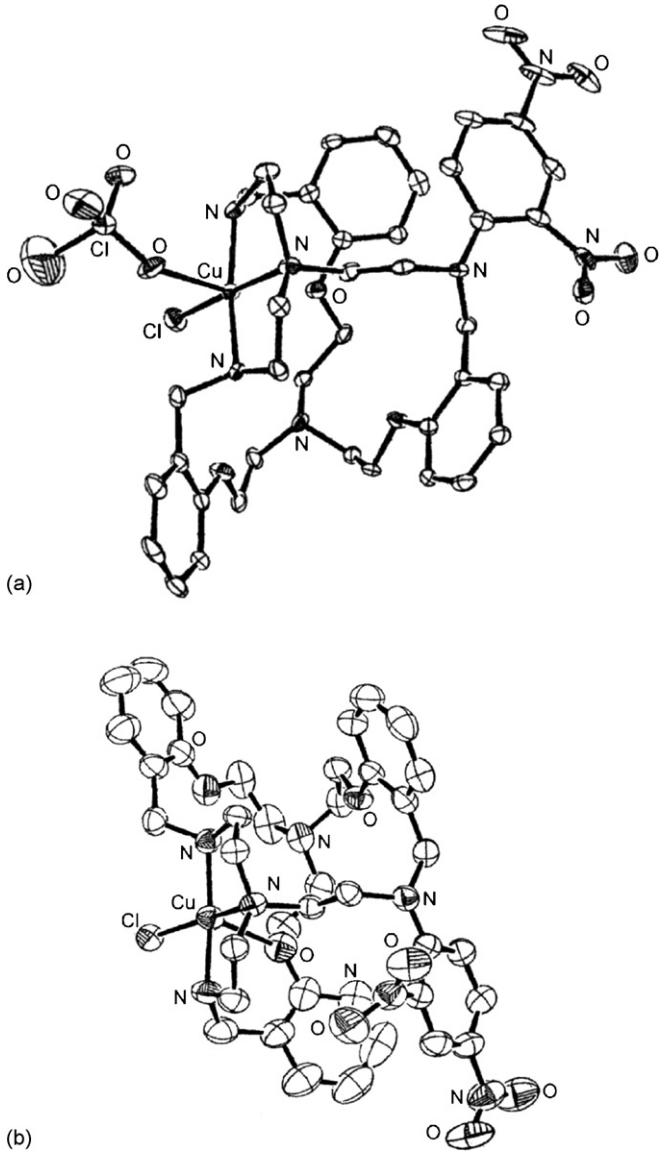

Fig. 117. Structure of [Cu(**147**)(Cl)(ClO_4)] (a) and [Cu(**147**)(Cl)]$^+$ (b).

in this complex shows distorted octahedral coordination where the two oxygen atoms from the two carboxylic acid groups and the two corresponding nitrogen atoms in the two bridges are bound equatorially. The two axial sites are occupied by the nearly bridgehead nitrogen atom and the oxygen atom of a dimethylformamide molecule [164].

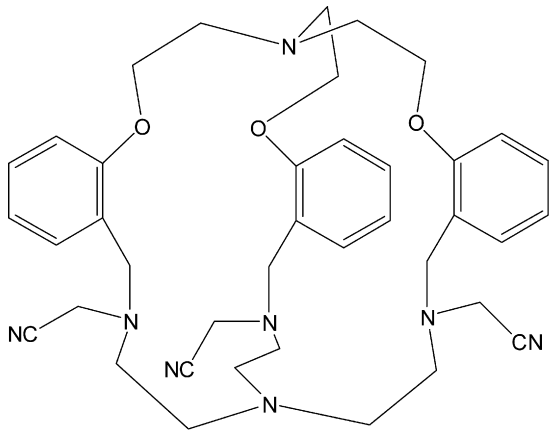

146a

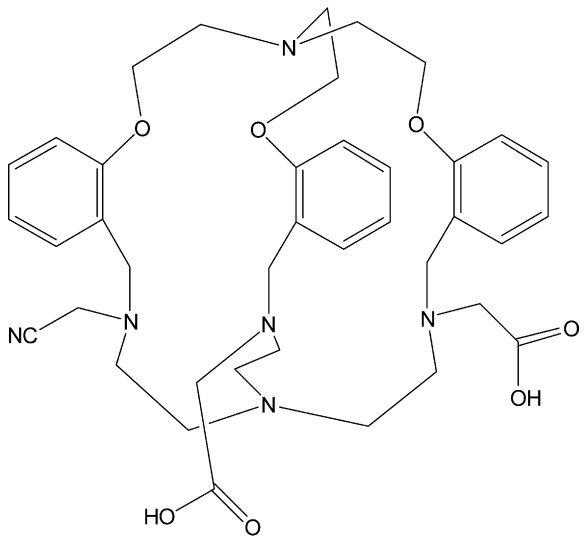

H_2-**146b**

It has been found that upon reacting 1.8 equiv. of 2,4-dinitrochlorobenzene with the unsubstituted cryptand **140**, mono-, bis-, and tris-derivatives are formed in almost equal amounts; they can be separated each other by column chromatography. The monosubstituted derivative **147**, reacts in methanol with $Cu(ClO_4)_2{\cdot}6H_2O$ or $Cu(BF_4)_2{\cdot}xH_2O$ to form $[Cu(\mathbf{147})(Cl)(ClO_4)]{\cdot}H_2O$ and $[Cu(\mathbf{147})(Cl)](BF_4)$. Furthermore, **147** reacts respectively with $Zn(ClO_4)_2{\cdot}6H_2O$ in the presence of NaN_3 and with $Cd(NO_3)_2$ in the presence of KSCN to give $[Zn(\mathbf{147})(N_3)_2]$ and $[Cd(\mathbf{147})(NCS)_2]$ [165].

In $[Cu(\mathbf{147})(Cl)(ClO_4)]{\cdot}H_2O$ the copper(II) ion is bonded to the two secondary amino nitrogen atoms and the bridgehead nitrogen atom at the tren-end, in a fashion outside the cavity. The other two coordination sites are occupied by one chloride ion and one oxygen of a perchlorate ion. The dinitrobenzene moiety remains furthest from the metal ion. As a result of this binding mode, the cryptand has undergone a significant conformational change. The two bridgehead nitrogen atoms have come much closer at 5.281 Å from the distance of 6.249 Å in **140** [165]. The metal ion has pulled the three nitrogen donors of the cryptand moiety toward itself causing these three atoms to be inverted with their lone-pairs directed at the metal ion. Thus, the cryptand has changed to an endo–exo conformation upon metal binding. The coordination geometry around the metal ion is square pyramidal where the three nitrogen and the chloride ion occupy the basal plane with the oxygen atom at the axial position. The copper(II) ion is only 0.045 Å above the mean plane described by the four basal atoms, toward the axial oxygen atom (Fig. 117a) [165].

The X-ray structure of $[Cu(\mathbf{147})(Cl)](BF_4)$ consists of discrete $[Cu(\mathbf{147})(Cl)]^+$ cations and BF_4^- anions. As in $[Cu(\mathbf{147})(Cl)(ClO_4)]{\cdot}H_2O$, the metal ion is bound to the cryptand from outside the cavity although there is a significant difference in the mode of binding in the two cases. In $[Cu(\mathbf{147})(Cl)](BF_4)$, the metal ion is again square pyramidal with two amino and one bridgehead nitrogen atoms and the chloride ion forming the basal plane, and the axial site is occupied by an ethereal oxygen atom of the cryptand moiety. The difference in the binding mode is due to the less coordinating nature of BF_4^- compared to that of the ClO_4^- anion. The coordination geometry is also more distorted from an ideal square pyramid compared to $[Cu_2(\mathbf{147})(Cl)(ClO_4)]{\cdot}H_2O$, and the metal ion is situated 0.221 Å above the mean plane described by the four atoms in the basal plane toward the axial oxygen atom (Fig. 117b) [165].

The X-ray structure of $[Zn(\mathbf{147})(N_3)_2]$ reveals that the zinc(II) ion is bonded to the cryptand through two secondary amino nitrogen atoms (the bridgehead nitrogen atom remains uncoordinated) while the other two coordination sites are occupied by two azide anions forming an almost ideal tetrahedral coordination geometry. The metal ion has pulled the two amino nitrogen atoms away from the cryptand causing severe conformational distortion, and as a result, the two bridgehead nitrogen atoms are much closer compared to $[Cu(\mathbf{147})(Cl)(ClO_4)]{\cdot}H_2O$ and $[Cu(\mathbf{147})(Cl)](BF_4)$, at 4.652 Å. The packing diagram of this complex shows that the metal-bound nitrogen atom of one of the azide groups makes a C–H···N intermolecular hydrogen bonding interaction with an aromatic proton of the neighboring cryptand forming an infinite supramolecular linear array in the crystal lattice (Fig. 118a) [160].

In $[Cd(\mathbf{147})(NCS)_2]{\cdot}1/2CH_3OH{\cdot}1/2CH_3CN{\cdot}2H_2O$, the cadmium(II) ion is bonded to the cryptand through its two secondary amines and two thiocyanate anions. The molecular structure reveals a dimeric unit, where two cadmium(II) ions are bonded to two bridging thiocyanate anions, and in addition, each metal ion is bonded to one **147** and one terminal thiocyanate anion. The crystal lattice also contains disordered solvent molecules such as methanol, acetonitrile, and water. Each cadmium(II) ion is bonded to six nitrogen atoms in a distorted octahedral environment: two secondary amino nitrogen atoms, the bridgehead nitrogen at the tren-end of the cryptand moiety, a terminal thio-

cyanate, and two bridging thiocyanates. The two bridgehead nitrogen atoms have come much closer (4.523 Å) compared to other complexes in the series. Thus, the cryptand moiety in this complex has undergone maximum distortion from its pseudo-three-fold symmetry (Fig. 118b) [165].

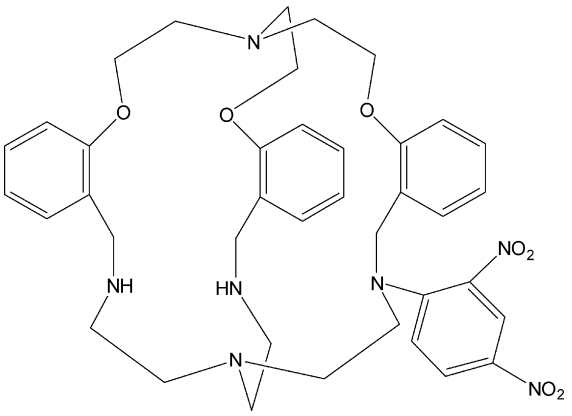

147

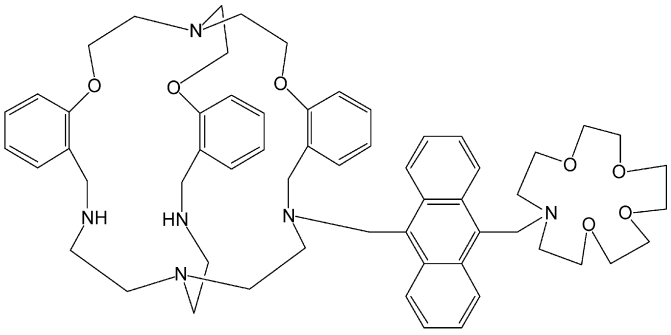

147a

Attachment of a laterally non-symmetric cryptand and a macrocycle at the 9- and 10-positions of anthracene leads to the fluorescent signaling system **147a** which gives fluorescence enhancement in the simultaneous presence of alkali and transition metal ions [166].

The synthesis of **147a** is achieved in several steps. The macrocycle 4,7,10,13-tetraoxa-l-azacyclopentadecane is derivatized with 9-bromomethylanthracene followed by bromomethylation at the 10-position of anthracene in the presence of paraformaldehyde and 30% HBr in CH_3COOH yielding 9′-methyl(4,7,10,13-tetraoxa-l-azacyclopentadecanyl)-10′-bromomethylanthracene. This compound is condensed with the di-BOC protected cryptand. Removal of the BOC groups with trifluoroacetic acid in dry tetrahydrofuran affords **147a** [166].

The fluorescence quantum yield of **147a**, slightly higher in solvents with low polarity compared to that in solvents of high polarity, in the absence of any input is extremely low, due to efficient photoinduced electron transfer (PET) operative from both donor nitrogen atom lone pairs to the excited anthracene. When sodium(I) or potassium(I) ion is added, the fluorescence quantum yield is still low because the crown-ether-receptor still remains empty keeping the PET from its side operational. In

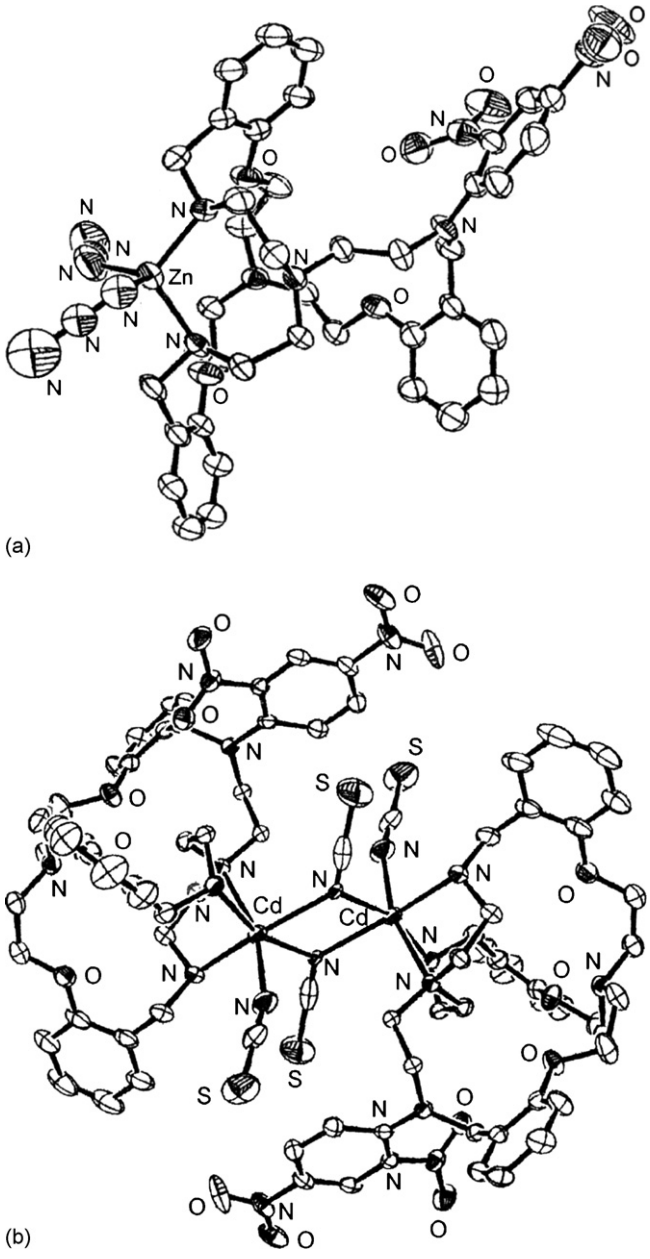

Fig. 118. Structure of $[Zn(\mathbf{147})(N_3)_2]$ (a) and $[Cd_2(\mathbf{147})_2(\mu\text{-}NCS)_2(SCN)_2]$ (b).

presence of excess of alkali metal ion, the metal may bind to the upper deck of the receptor$_2$ that does not block the PET process. In a similar fashion, with only a transition metal ion input, PET from receptor$_1$ remains operative. However, when both transition and alkali metal ions are added, the PET is blocked from both ends leading to significant recovery of fluorescence. Addition of excess of H^+ does not lead to significant recovery of fluorescence in comparison to the metal ions. The emission behaviour on titration with perchloric acid in dry THF shows that complete protonation of both the receptors yields only −20-fold enhancement of fluorescence. Also, in the situation when the sodium ion is bound to the cryptand receptor, addition of protons to the system exhibits 29-fold enhancement. Thus, the logic action in **147a** is better expressed with metal ion inputs and not with the protons.

The amount of fluorescence recovery depends upon the nature of metal ion inputs. Among all the metal ions investigated, fluorescence recovery is maximum (>100-fold enhancement) with sodium(I) and zinc(II) or iron(II) ions as inputs. The nature of the graph of a fluorescence titration of **147a** as a function of concentration of sodium(I) and zinc(II) inputs indicates a 1:1 complex formation with each of the ionic inputs. The overall fluorescence enhancement is found to be almost the same when the sodium(I) ion is added first and then the zinc(II) ion or vice versa. The complexation binding constant (K_S) determination reveals that presence or absence of zinc(II) ions do not affect the K_{Na^+} value and vice versa, which indicates a significant inter-receptor separation independent of each other. As the fluorescence is significantly recovered only in presence of both the inputs, K_S for one input could only be determined in the presence of the other, which provides a basis for formation of inclusion complexes by the receptors. A similar emission behaviour is observed in the fluorescence titration **147a** with sodium(I) or potassium(I) and iron(II) ions. This is found to be consistent for all the transition/heavy metal ions studied in combination with sodium(I) or potassium(I) ion, suggesting that alkali metal ions occupy the macrocyclic cavity while other metal ions are included in the cryptand cavity. Thus, **147a** exhibits the function of a potential and logic gate [166].

3.2. [3 + 2] Ligands bearing bridging groups and related complexes

3.2.1. Phenolate-based cryptands

The complexes $[Ln(H_3\text{-}\mathbf{148})(NO_3)](NO_3)_2{\cdot}nH_2O$ (Ln = La···Lu) have been prepared by condensation of 2,6-diformyl-4Z-phenol (Z = CH_3, Cl, $C(CH_3)_3$) with tris-(2-aminoethy)amine in the presence of the appropriate $Ln(NO_3)_3{\cdot}nH_2O$ in a 3:2:1 molar ratio [167]. All of them adopt very similar structures, with the nine coordinate metal ion bound asymmetrically to seven donor atoms in the ligand cavity and also to two oxygen atoms of a bidentate nitrate anion. The macrobicyclic cavity adapts to the lanthanide contraction, while preserving the pseudo-triple-helix conformation around the metal ion. The coordination geometry of the metal ion is a slightly distorted monocapped dodecahedron, as observed in the X-ray structure of $[Ce(H_3\text{-}\mathbf{148})(NO_3)](NO_3)_2$ (Fig. 119).

Metal template reactions between triethylammonium-(2,6-diformyl-4-methylphenolate) and tris-(2-aminoethyl)amine in the presence of the appropriate lanthanide nitrate hydrate (Ln = Gd···Lu) in a 3:2:2 molar ratio in absolute ethanol for about 12 h yield the orange solids $[Ln_2(\mathbf{148})(NO_3)_2](NO_3){\cdot}xH_2O{\cdot}yC_2H_5OH$ [168].

In the dilutetium(III) complex, which contains the cation $[Lu_2(\mathbf{148})(NO_3)_2]^+$, an independent nitrate anion and highly disordered molecules of ethanol and water, both lutetium(III) ions have crystallographically identical coordination environments: each is bound to one bridgehead nitrogen atom, three imino nitrogen atoms and three phenolate oxygen atoms. Eight coordination is completed by one oxygen of a monodentate nitrate ion and the coordination polyhedron is a distorted dodecahedron (Fig. 120) [168].

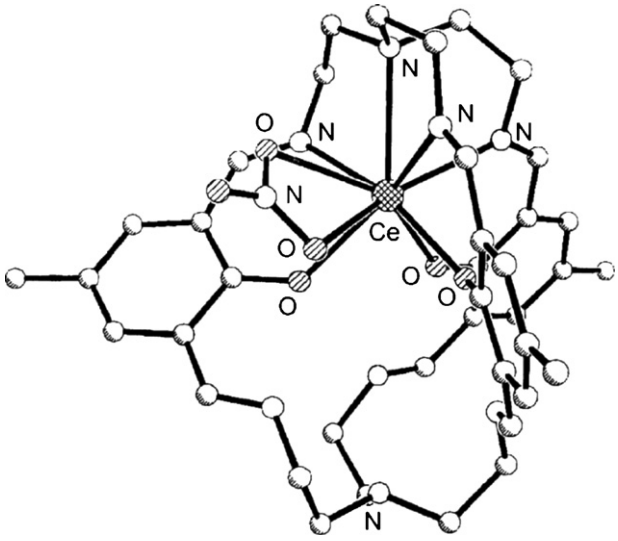

Fig. 119. Structure of $[Ce(H_3\text{-}\mathbf{148})(NO_3)]^{2+}$.

Similarly, in the gadolinium(III) and terbium(III) complexes $[Ln_2(\mathbf{148})(NO_3)_2](NO_3)$ each lanthanide(III) ion is coordinated by the three phenolate oxygen atoms, three imine nitrogen atoms and one bridgehead nitrogen atom, as well as one nitrate group on a bidentate fashion. The Gd···Gd and Tb···Tb distances are 3.500 and 3.508 Å, respectively. The coordination polyhedron around each ion is a monocapped distorted dodecahedron, where an oxygen atom of the bidentate nitrate group occupies the capping position (Fig. 121) [169].

The d,f-heterodinuclear complexes $[Ln^{III}M^{II}(\mathbf{L})(NO_3)](NO_3){\cdot}H_2O$ (Ln^{III} = La^{III}···Lu^{III}; M^{II} = Cu^{II}, Zn^{II}, Ni^{II}, Cd^{II},

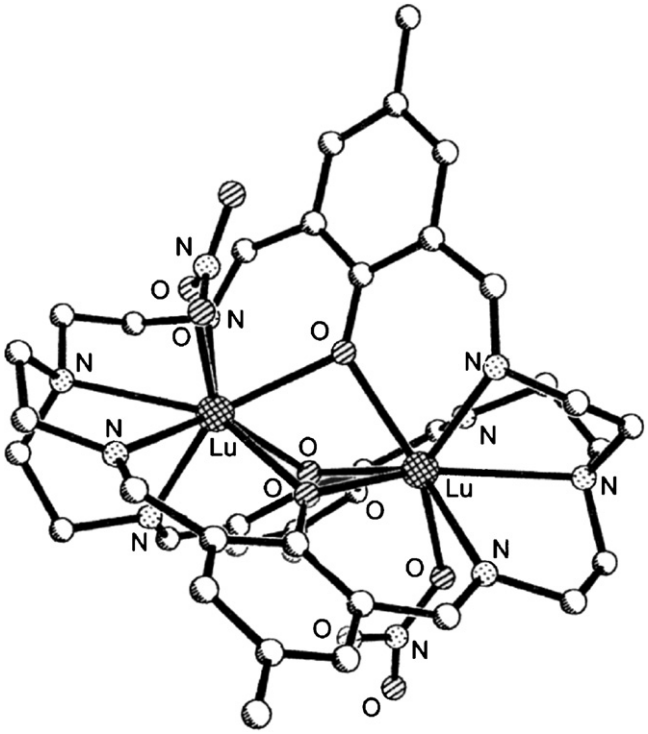

Fig. 120. Structure of $[Ln_2(\mathbf{148})(NO_3)_2]^+$.

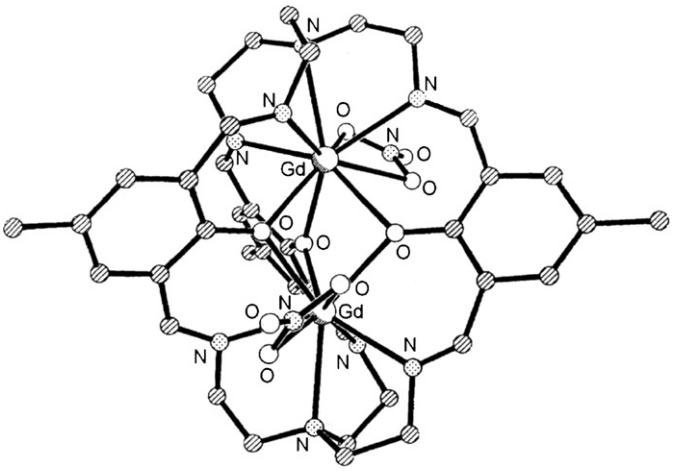

Fig. 121. Structure of $[Gd_2(\mathbf{108})(NO_3)_2]^+$.

Ca^{II}; H_3-**L** = H_3-**148**···H_3-**150**) were prepared by reaction of the desired mononuclear lanthanide(III) complex [Ln(H_3-**L**)(NO_3)]$(NO_3)_2{\cdot}nH_2O$ with the appropriate $M(NO_3)_2{\cdot}H_2O$. Because the lanthanide(III) ions in the mononuclear cryptates are kinetically inert and thermodynamically stable while the encapsulated water molecule is labile, the metal(II) ion replaces the water molecule during the reaction process. Added base removes the protons of the phenolic groups in the mononuclear lanthanide(III) precursor. Due to the flexibility of the cryptand, it is able to adjust its cavity to match the differently sized metal ions [169]. The coordination environment around the lanthanide(III) ion does not change significantly with respect to that found the homodinuclear lanthanide(III) complexes except for the fact that one nitrate anion coordinates in the heterodinuclear complexes in a monodentate fashion. The transition metal(II) ion is hexacoordinated being bound to the three μ-phenolate oxygen atoms and the other three imino nitrogen atoms. The bridgehead nitrogen atom remains uncoordinate [169]. The lanthanide(III) ion in [LnM(**148**)(NO_3)]$(NO_3){\cdot}H_2O$ ($Ln^{III}M^{II}$ = $Gd^{III}Cu^{II}$, $Lu^{III}Cu^{II}$, $Gd^{III}Zn^{II}$) is eight coordinate in a distorted dodecahedral geometry. The coordination polyhedron around the copper(II) or zinc(II) ions is a severely distorted octahedron. The Ln···M distance is 3.245 Å in the GdCu complex, 3.222 Å in the LuCu one and 3.294 Å in the GdZn one; in particular the Ln···Cu distances are similar to that reported for [DyCu(**148**)(DMF)]$(ClO_4)_2{\cdot}CH_3CN$ (3.255 Å) (Fig. 122) [169].

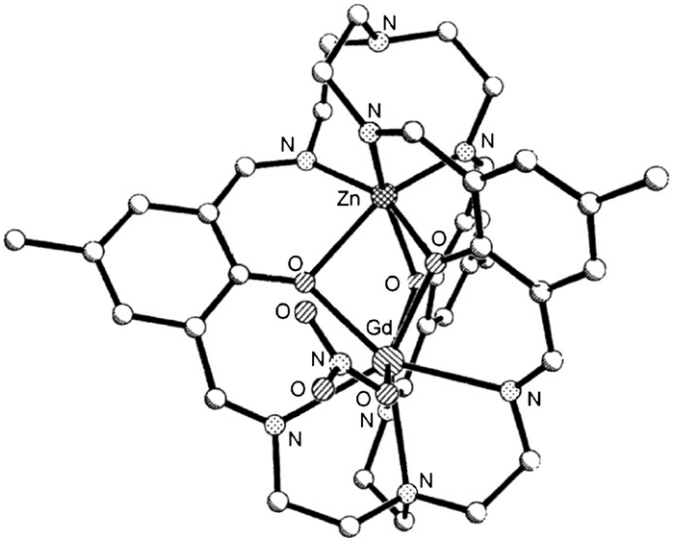

Fig. 122. Structure of $[GdZn(\mathbf{108})(NO_3)]^+$ (a).

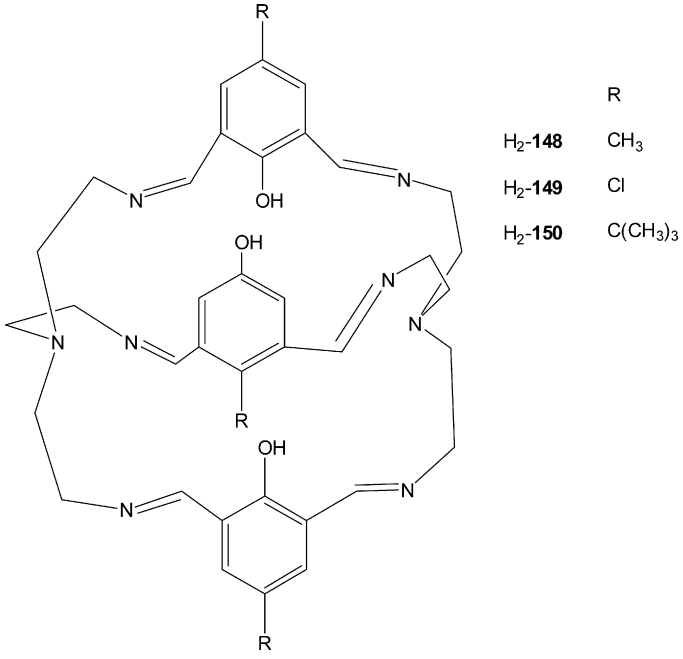

	R
H_2-**148**	CH_3
H_2-**149**	Cl
H_2-**150**	$C(CH_3)_3$

In these complexes $[\mathbf{148}]^{3-}$ adopts a sss endo–endo conformation, with the nitrogen atoms of the imine bonds pointing at the same side of the aromatic ring in the three chains and the two bridging nitrogen lone pairs directed toward the central cavity. The macrocycle $[\mathbf{148}]^{3-}$ is twisted around the bridging nitrogen axis in the five cryptates, generating triple helical structures that, in turn, induce structural chirality in this family of compounds. The cavity of the cryptand may be viewed as a trigonal antiprism defined by the six azomethine nitrogen atoms. The upper and lower triangular faces of the antiprism are connected by the three N=CH-R–CH=N (R = 1,3-(2-OH-5-CH_3-C_6H_2)) units generating two possible helical structures corresponding to two different optical isomers that can be labelled as Λ or Δ indicating either left-handed (Λ) or right-handed (Δ) structural chirality about the pseudo-three-fold symmetry axis of the complex. The X-ray crystal structures of the homodinuclear lanthanide(II) cryptates show that the ligand is helically wrapped around both metal ions, In the solid state the conformation of the cations $[Ln_2(\mathbf{148})(NO_3)_2]^+$ (Ln^{III} = Gd^{III}, Tb^{III}) is $\Lambda(\delta\delta\lambda)_5(\delta\delta\lambda)_5$ or its enantiometric from $\Delta(\lambda\lambda\delta)_5(\lambda'\lambda'\lambda')_5$. The magnetic interaction is antiferromagnetic in the case of the $Gd^{III}Gd^{III}$ cryptate ($-J = 0.194\ cm^{-1}$) but ferromagnetic for the $Gd^{III}Cu^{II}$ one ($J = 2.2\ cm^{-1}$) [169].

[LnCu(**149**)(DMF)]$(ClO_4)_2{\cdot}CH_3CN$ (Ln^{III} = Gd^{III}, Eu^{III}, Tb^{III}, Dy^{III}, Y^{III}) have been prepared by reaction of the mononuclear lanthanide(III) cryptate [Ln(H_3-**149**)(NO_3)]$(ClO_4)_2$ [170]

with $Cu(ClO_4)_2{\cdot}6H_2O$ in dimethylformamide in the presence of CoH_2. The d–d transition of the copper(II) in these cryptates is at about 850 nm, showing that the metal ion is located in an octahedral coordination environment [171].

Structural analyses confirm that the $Eu^{III}Cu^{II}$ complex is a d,f-heterodinuclear entity, isostructural with $[DyCu(\mathbf{149})(DMF)](ClO_4)_2{\cdot}CH_3CN$ [172]. In the cation $[EuCu(\mathbf{149})(DMF)]^{2+}$ the europium(III) ion is located at one end of the cavity and is eight coordinated in a distorted dodecahedron with the bridgehead nitrogen atom, three imino-nitrogen atoms, the oxygen atom of the dimethylformamide and three phenoxy atoms. The other end of cavity is occupied by the copper(II) ion, coordinated by three μ-phenolate oxygen atoms and three imino-nitrogen atoms in a distorted octahedral configuration (Fig. 123) [171].

The complexes $[Ln^{III}Cu^{II}(\mathbf{149})(DMF)](ClO_4)_2{\cdot}CH_3CN$ have similar voltammetric properties, each cryptate showing a pair of well-defined redox peaks and an irreversible cathodic peak corresponding to stepwise reduction of the copper(II) ion. The $E^1_{1/2}$ values of copper(II) ions shift negatively compared with free copper(II) ion and are influenced by the lanthanide(III) ion encapsulated in the cryptate. The sequence of influence for the Ln^{III} ions is: $Dy^{III} > Tb^{III} > Gd^{III} > Eu^{III}$. The higher the f-electron number of the lanthanide(III) ion, the more negative

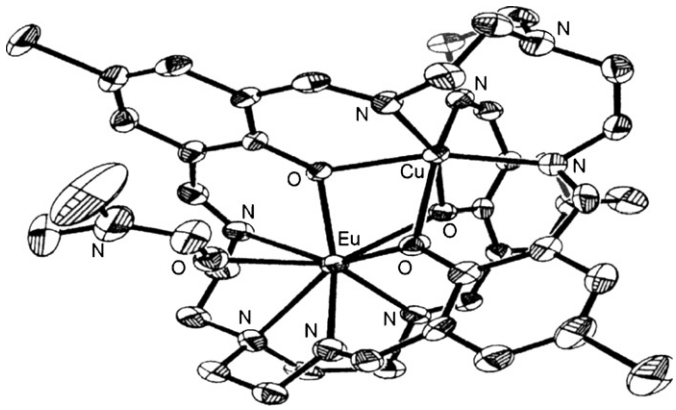

Fig. 123. Structure of $[EuCu(\mathbf{149})(DMF)]^{2+}$.

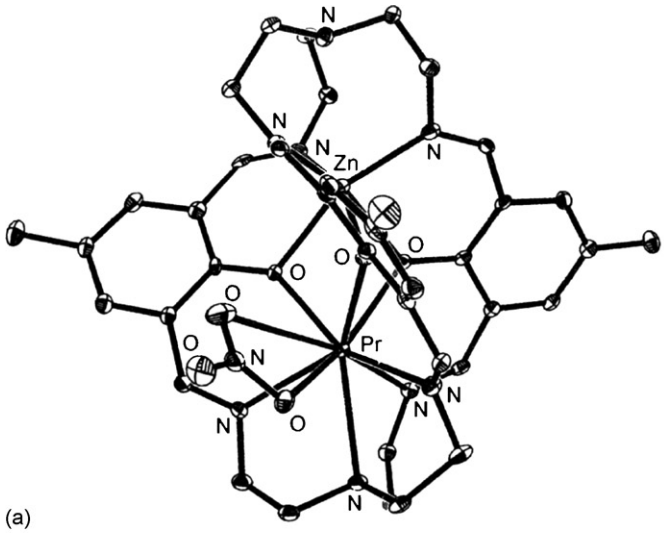

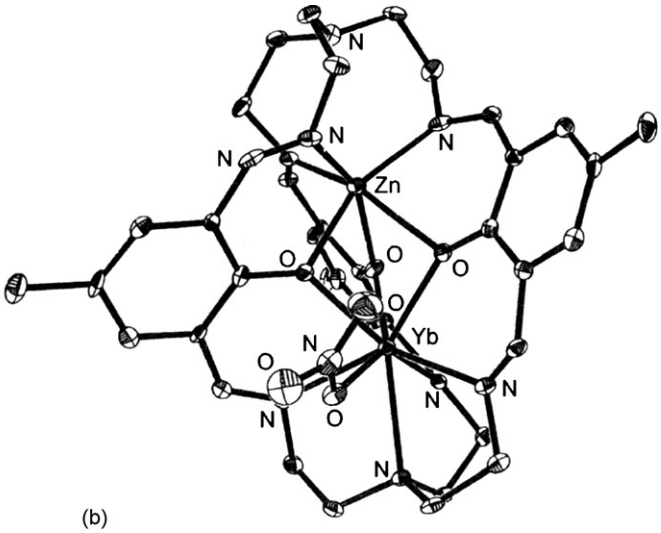

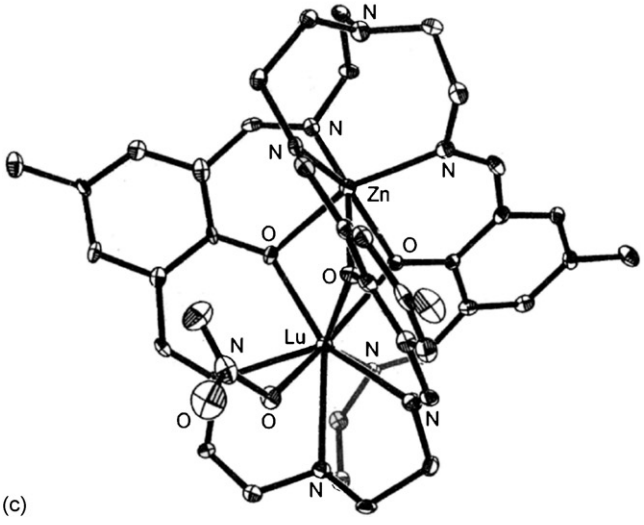

Fig. 124. Structure of $[PrZn(\mathbf{148})(NO_3)]^+$ (a), $[YbZn(\mathbf{148})(NO_3)]^+$ (b) and $[LuZn(\mathbf{148})(NO_3)]^+$ (c).

the $E_{1/2}$ values are and the more difficult it is to reduce the copper(II) ion in the cryptates [171].

Similarly, $[LnZn(\mathbf{L})(NO_3)](NO_3)\cdot xH_2O\cdot yCH_3OH$ ($Ln = Ce^{III}$ to Lu^{III} except Pm^{III}; H_3-**L** = H_3-**148**···H_3-**150**; $x = 0$–2, $y = 0$–1) were prepared by the reaction of the corresponding mononuclear cryptate $[Ln(H_3\text{-}\mathbf{L})(NO_3)](NO_3)_2\cdot xH_2O$ with CaH_2 and $Zn(NO_3)_2\cdot 6H_2O$ in a 1:1:1 molar ratio in CH_3OH/DMF [173].

In the $Pr^{III}Zn^{II}$, $Yb^{III}Zn^{II}$ and $Lu^{III}Zn^{II}$ complexes with $[\mathbf{148}]^{3-}$ the cation $[LnZn(\mathbf{148})(NO_3)]^+$ contains the lanthanide(III) and zinc(II) ions placed at opposite ends of the cryptand cavity at a distance of 3.325 Å for PrZn complex, 3.292 Å for the YbZn one and 3.269 Å for the LuZn one. These distances are about 0.15 Å shorter than the Ln···Ln distances found in the homodinuclear cryptates $[Ln_2(\mathbf{148})(NO_3)_2](NO_3)$ (Yb···Yb, 3.444 Å; Lu···Lu, 3.447 Å) [168] but slightly longer than the Dy···Cu distance reported for $[DyCu(\mathbf{149})(DMF)](ClO_4)_2\cdot CH_3CN$ (3.255 Å) [174]. In the three structures, the hexacoordinated zinc(II) ion is bound to three imino nitrogen atoms and the three μ-phenolate oxygen atoms. The bridgehead nitrogen does not participate in coordination. The lanthanide(III) ion is bound to one of the bridgehead nitrogen atoms, the other three imino nitrogen atoms, and the three μ-phenolate oxygen atoms. One or two oxygen atoms of a mono- (for the YbZn and LuZn complexes) or bidentate nitrate group (for the PrZn complex) occupy the remaining coordination positions. $[\mathbf{148}]^{3-}$ adopts an sss endo–endo conformation, with the nitrogen atoms of the imine bonds pointing at the same side of the aromatic ring in the three chains and the bridgehead nitrogen lone pairs directed toward the central cavity, similar to that found for the mono- and/or homodinuclear lanthanide(III) analogous cryptates [168,175]. The coordination polyhedron around the lanthanide(III) ion is a distorted dodecahedron. In $[PrZn(\mathbf{148})(NO_3)](NO_3)$ one oxygen atom of the coordinated nitrate is capping a triangular face of the dodecahedron. In the $Pr^{III}Zn^{II}$, $Tb^{III}Zn^{II}$ and $Lu^{III}Zn^{II}$ cryptates, the coordination polyhedron around the zinc(II) ions is a distorted octahedron that shares the triangular face defined by the three phenolate oxygen atoms with the polyhedron around the lanthanide(III) ion (Fig. 124a–c) [173].

In an attempt to prepare the zinc(II) complex with the [3 + 1] acyclic ligand H_3-**151**, $[Zn_2(\mathbf{148})](NO_3)\cdot 3H_2O$ was obtained. It is noteworthy that, although the molar ratio 1:3:1 tris-(2-aminoethyl)amine:2,6-diformyl-4-methylphenol:Zn^{II} used in the experimental procedure is unfavourable for the formation of the dinuclear cryptate, the system tends to self-organize to produce the homodinuclear zinc(II) cryptate [173]. In the dizinc(II) complex both metal(II) ions, placed into the macrobicyclic cavity, are hexacoordinate in a distorted octahedral coordination, being bound to three imino nitrogen atoms and the three μ-phenolate oxygen atoms. The bridgehead nitrogen atoms are not coordinated. The Zn···Zn distance is 3.103 Å (Fig. 125) [173]. The three five membered chelate rings of the ligand backbone coordinating the lanthanide(II) ion adopt a $(\lambda\lambda\delta)_5$ (or$(\delta\delta\lambda)_5$) conformation while the three pseudochelate rings formed by the coordination of the ligand to the zinc(II) ion adopt a $(\lambda'\lambda'\lambda')_5$ $(\delta'\delta'\delta')_5$) conformation. In the solid state

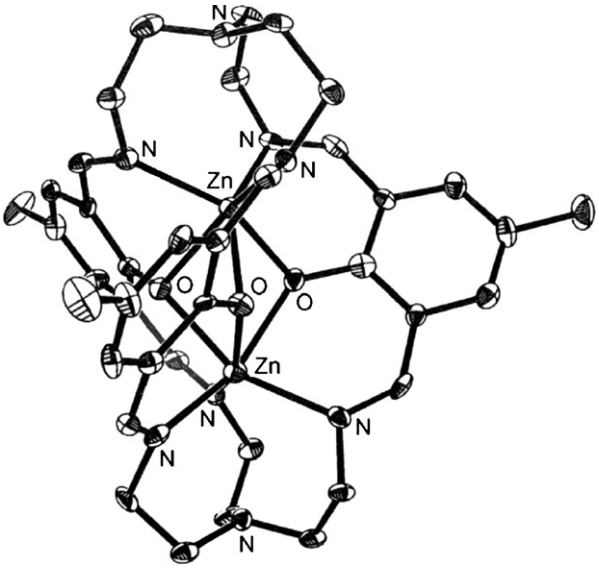

Fig. 125. Structure of $[Zn_2(\mathbf{148})]^+$.

the conformation of the three cations is $\Lambda(\delta\delta\lambda)_5(\delta'\delta'\delta')_5$ or its enantiometric form $\Delta(\lambda\lambda\delta)_5$ $(\lambda'\lambda'\lambda')_5$. A ^{1}H NMR study in CD_3CN/D_2O demonstrates that the helical structure of the LnZn complexes is essentially maintained in solution. However, while in the solid state they adopt conformations $\Lambda(\delta\delta\lambda)_5(\delta'\delta'\delta')_5$ or $\Delta(\lambda\lambda\delta)_5$ $(\lambda'\lambda'\lambda')_5$, in solution the cryptates possess C_3 symmetry $\Delta(\delta\delta\delta)_5(\delta'\delta'\delta)_5$ or $\Delta(\lambda\lambda\lambda)_5(\lambda'\lambda'\lambda')_5$ [173].

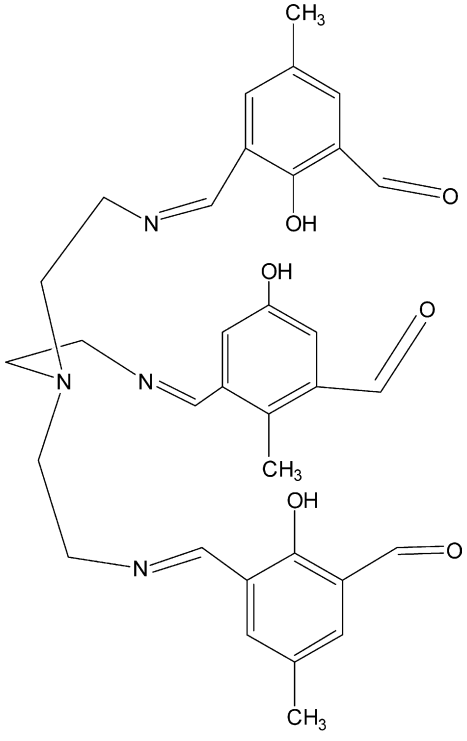

H_2-**151**

The photophysical properties of the cryptates depend on the nature of the lanthanide(III) ion: $[\mathbf{148}]^{3-}$ is a good sensi-

tizer for the europium(III) and terbium(III) at low temperatures, but the emission at room temperature is limited by the low energy of the ligand $^3\pi\pi^*$ state. While the europium(III) ion is most effectively sensitized by the ligand triplet state, the terbium(III) ion ($^5D_4$) sensitization occurs via the singlet state. The quantum yield of the metal-centered luminescence in the EuZn cryptate amounts to 1.05% upon ligand excitation. The low energy of the ligand $^3\pi\pi^*$ state allows efficient sensitization of the neodinium(III) and ytterbium(III) cryptates, which emit in the near-infrared. The ligand-to-Eu^{III} energy transfer is fairly efficient at low temperature, but back transfer is implied in the deactivation process, especially at room temperature, because the ligand triplet state lies at very low energy. Although the overall sensitization of the metal ion luminescence remains small, the corresponding monometallic europium(III) cryptate displays a much weaker emission because the oxygen atoms of the phenolic groups are protonated. The terbium(III) ion is weakly sensitized through the excited singlet state of the ligand. The low energy of the ligand triplet state allows an appreciable conversion of the visible light absorbed into infrared light emitted by neodinium(III) and ytterbium(III) ions [173].

The structure of [GdNi(**149**)(DMF)]$(ClO_4)_2$, similarly synthesized by reaction of [Gd(H_3-**149**)$(NO_3)(H_2O)$]$(ClO_4)_2$ with $Ni(ClO_4)_2{\cdot}6H_2O$ at in a 1:1 molar ratio at pH 7–8 in the presence of CaH_2, confirms that the complex is a dinuclear $Gd^{III}Ni^{II}$ entity, where the gadolinium(III) and nickel(II) ions, 3.210 Å apart, are encapsulated in the cavity of the macrocycle bridged by the oxygen atoms of three deprotonated phenyl groups. The coordination of the bridgehead nitrogen atom, three imino nitrogen atom, the dimethylformamide oxygen atom and three phenolate oxygen atoms make gadolinium(III) ion eight coordinate in a distorted dodecahedral configuration at one end of the cavity. The other end of the cavity is occupied by the nickel(II) ion which is coordinated by three phenolate oxygen atoms and three imino nitrogen atoms in a distorted octahedral configuration The distance of 9.135 Å between the two bridgehead nitrogen atoms is longer than that in mononuclear gadolinium(III) cryptate (6.963 Å) with the same ligand, implying that the macrocycle is able to be enlarged for inclusion of transition metal ions. The separations between metal ions in neighboring molecules are quite large, namely, Gd···Gd = 9.888 Å, Ni···Ni = 9.274 Å, Ni···Gd = 11.647 Å, suggesting the absence of any significant intermolecular magnetic interactions. A ferromagnetic spin coupling ($J = 0.56\ cm^{-1}$) between nickel(II) and gadolinium(III) ion occurs (Fig. 126a) [176].

Similarly, [EuCa(**149**)(DMF)]$(ClO_4)_2$ was synthesized by the reaction of [Eu(H_3-**149**)$(NO_3)(H_2O)$]$(ClO_4)_2$ with CaH_2 to neutralize the three protons of the cryptand and to replace the water molecule by the calcium ion forming [EuCa(**149**)(DMF)]$(ClO_4)_2$. The ESI-mass measurements show that the calcium(II) ion in [EuCa(**149**)(DMF)]$(ClO_4)_2$ is unstable and labile toward dissociation and replacement. Furthermore, the calcium(II) ion may be replaced by transition metals ion with the consequent formation of [EuM(**149**)(DMF)]$(ClO_4)_2$ ($M^{II} = Cd^{II}, Ni^{II}, Zn^{II}$). Thus far, the synthesis of d,f-heterodinuclear cryptates in the absence of CaH_2 failed [177].

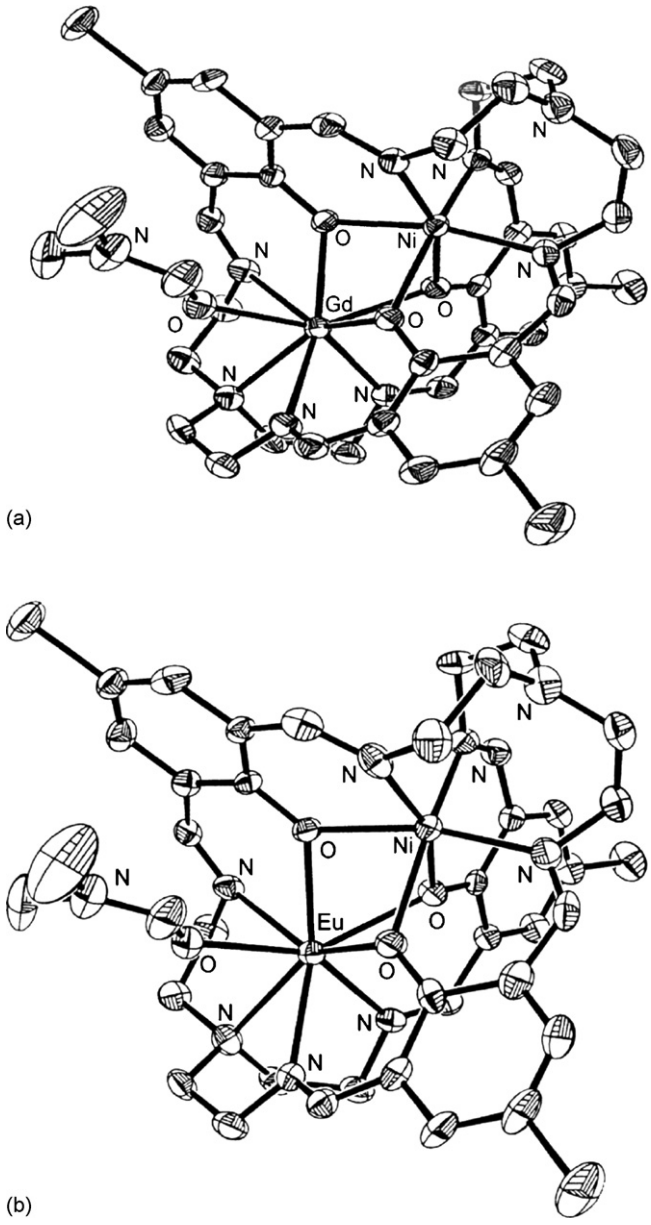

Fig. 126. Structure of [GdNi(**149**)(DMF)]$^{2+}$ (a) and [EuNi(**149**)(DMF)]$^{2+}$ (b).

The structure of [EuNi(**149**)(DMF)]$(ClO_4)_2$ confirms that the dinuclear $Eu^{III}Ni^{II}$ entity exists in the cryptate. The europium(III) center is located at one end of the cavity and is eight coordinate in a distorted dodecahedral configuration with bridgehead nitrogen atoms, three imino nitrogen atoms the oxygen atom of dimethylformamide, and three phenoxy oxygen atoms. The other end of the cavity is occupied by the nickel(II) ion which is coordinated by three μ_2-phenolate-oxygen atoms and three imino nitrogen atoms in a distorted octahedral configuration. The Eu···Ni distance is 3.220 Å (Fig. 126b) [177].

[Eu(H_3-**149**)$(NO_3)(H_2O)$]$(ClO_4)_2$ undergoes a quasi-reversible reduction process that can be ascribed to the Eu^{III}/Eu^{II} couple. The voltammograms of the $[Eu^{III}Ni^{II}(\mathbf{149})(DMF)]^{2-}$ exhibit three one-electron redox processes, assigned respectively to $Eu^{III}Ni^{II} \leftrightharpoons Eu^{II}Ni^{II}$ ($E_{1/2} = -0.990$ V), $Eu^{II}Ni^{II} \leftrightharpoons Eu^{II}Ni^{I}$ ($E_{1/2} = -1.520$ V), and $Eu^{II}Ni^{I} \leftrightharpoons Eu^{II}Ni^{\circ}$ ($E_{1/2} = -1.765$ V)

Notably, in the heteronuclear $Eu^{III}M^{II}$ cryptate the reduction potentials of Eu^{III}/Eu^{II} are a function of the divalent ions in the second site and are negatively shifted relative to the mononuclear cryptate [Eu(H$_3$-**149**)(NO$_3$)(H$_2$O)](ClO$_4$)$_2$, that is the europium(III) ion in mononuclear cryptate is reduced more easily than those in heteronuclear cryptates. The sequence of increasing difficulty of reduction in these cryptates has the order: mononuclear $Eu^{III} < Eu^{III}Ni^{II} < Eu^{III}Cd^{II} < Eu^{III}Zn^{II}$ [177].

Also luminescence spectral investigations indicate that the introduction of a second metal ion into the mononuclear europium(III) cryptate results in a negative shift of the redox potential of the europium(III) ion and a luminescence intensity change of the europium(III) ion. [EuM(**149**)(DMF)](ClO$_4$)$_2$ was shown to quench the emission of the europium(III) ion when M = Ni^{II} and to enhance the emission of the europium(III) ion when M = Ca^{II}, Cd^{II}, and Zn^{II} [177]. The introduction of a second metal ion into the mononuclear europium(III) cryptate resulted in a blue shift of the three ligand-centered bands and a small increase in the molar absorption coefficients. The introduction of the nickel(II) ion leads to quenching of the europium(III) emission by energy transfer from the excited europium(III) ion to the nickel(II) one. Conversely, introduction of zinc(II) or cadmium(III) ions into the mononuclear europium(III) cryptate leads to a three fold increase of the luminescence intensity of the europium(III) ion. However, the introduction of the calcium(II) ion leads to a clear increase of the emission of ligand-centered bands, but the emission of the europium(III) ion hardly changed because the light absorbed by the ligand was not converted efficiently into light emitted by the europium(III) ion in presence of calcium(II) ion. The order of increase in quantum yield of the europium(III) ion is: mononuclear $Eu^{III} < Eu^{III}Ca^{II} < Eu^{III}Cd^{II} < Eu^{III}Zn^{II}$ [177].

The complexes [Ln$_2$(**152**)]·nS (Ln = Gd^{III}, Tb^{III}, Dy^{III}, Er^{III}, $n = 0.5$, S = DMF; Ln = Ho^{III}, $n = 0$; Ln = Y^{III}, $n = 1$, S = DMF; Ln = Tm^{III}, $n = 2$, S = H$_2$O) have been prepared by the reaction of tris(2-aminoethyl)amine with the appropriate bis(hydroxybenzaldehyde) derivative H$_2$-**153** in the presence of Ln(CF$_3$SO$_3$)$_3$ in methanol. The complexes appear stable to hydrolysis: a dimethylformamide solution of [Ln$_2$(**152**)] remains clear upon addition of a few drops of water. In the structure of [Y$_2$(**152**)]·DMF each yttrium(III) ion is seven coordinate in a monocapped distorted octahedron, composed of three imine nitrogen atoms, one apical nitrogen atom and three oxygen atoms (Fig. 127) [178].

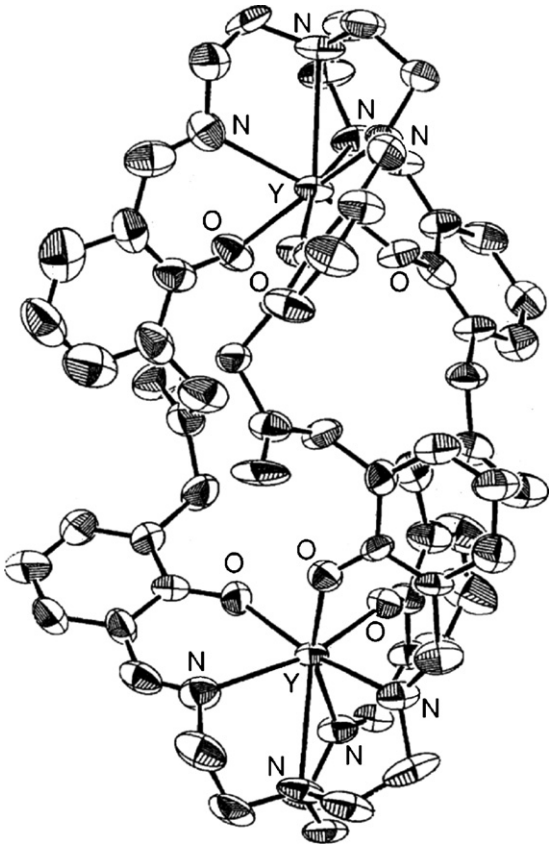

Fig. 127. Structure of [Y$_2$(**152**)].

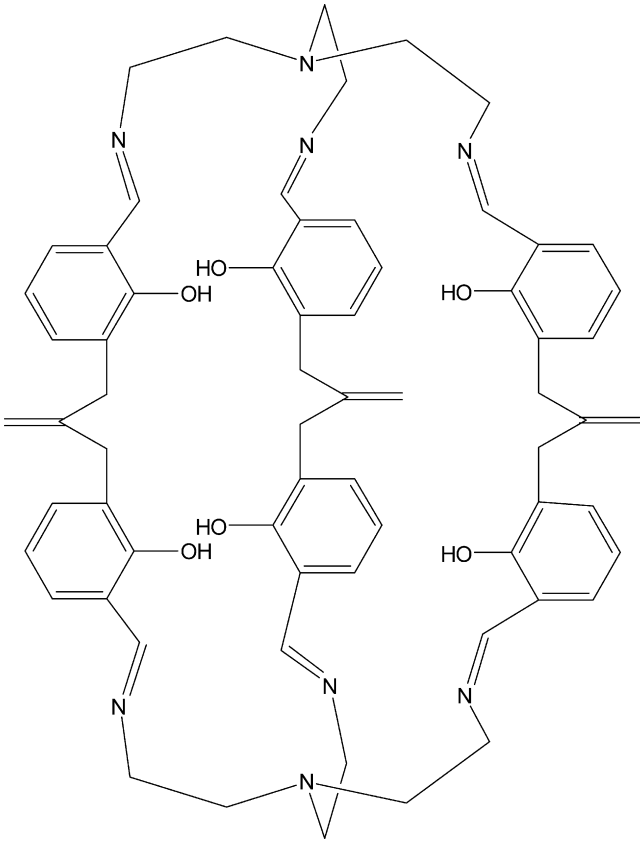

H$_6$-**152**

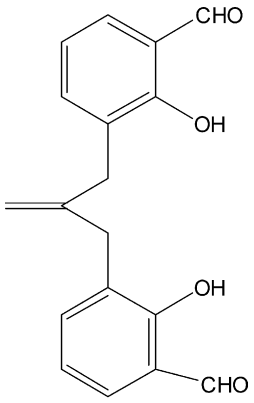

H_2-**153**

Attempts to obtain the same complexes with the lighter lanthanide(III) salts failed; this suggests that the cavity of [**152**]$^{6-}$ might be too small to include the La^{III}, Ce^{III}, Pr^{III}, Nd^{III}, Sm^{III}, Eu^{III} ions. The reaction of tris(2-aminoethyl)amine with the same bis(hydroxobenzaldehyde) precursor H_2-**153** in the presence of a mixture of $Y(CF_3SO_3)_3$ and $Ho(CF_3SO_3)_3$ in methanol gave hetero- as well as homodinuclear yttrium(III) and holmium(III) complexes as indicated by ESI-mass spectrometry. When mixtures of $Y(CF_3SO_3)_3$ and $La(CF_3SO_3)_3$ or of $La(CF_3SO_3)_3$ and $Ho(CF_3SO_3)_3$ are used, only peaks corresponding to homodinuclear yttrium or holmium complexes were observed. This result indicates that the size of lanthanum(III) ion is too large to be retained in the ligand cavity [178].

The homodinuclear lanthanide complexes [Ln_2(**152**)]·*n*S were found to be a host for Rb^I and Cs^I ions [178].

3.2.2. *Pyridazine-based cryptands*

The free cryptand **154**, readily made by reaction in alcoholic solution of 3,6-diformylpyridazine, prepared by oxidation of 3,6-bis(hydroxymethylpyrazine) with MnO_2 or by oxidation of 3,6-distyryl pyridazine with ozono [102], with tris(2-aminoethy)amine, shows a divergent conformation which allows face-to-face π–π stacking intercryptand interactions involving two of the three aromatic rings. There is no evidence of intracryptand π–π interactions, nor of any steric effect which might tend to reduce conjugation within the bisiminopyridazine moieties which remain close to planar in all three strands. **154** is solvent free and adopts a conformation where the imino-CN functions are mutually *cis*, but *trans* to the pyridazine ring CN groups (Fig. 128) [179].

154 forms the mononuclear complexes [M(**154**)](X)$_2$ (M = Co^{II}, Cu^{II}, Mn^{II}, Ni^{II}, Fe^{II}; X = BF_4^-, ClO_4^-) when reacted with the appropriate metal salt. The iron(II) complex is sensitive to air and traces of water [179–181].

A mutually *trans* disposition of the imino groups was found in [Co(**154**)](BF_4)$_2$. This conformation enables efficient coordination of the cobalt(II) ion in a six coordinate geometry intermediate between O_h and D_{3h} (Fig. 129a). Electrochemical studies establish that **154** stabilize the cobalt(II) ion [179].

In some preparations of [Cu(**154**)](BF_4)$_2$ small amounts of brown hexagon and lime green plate crystals were obtained in addition to the green rod crystals.

The crystal structure was determined for all three of the observed crystal forms. The brown hexagons were shown to be isomorphous with the green rods, whereas a different copper(II) ion geometry is observed in the lime green plates. In the green rods the copper(II) ion has a distorted trigonal bipyramidal environment as a consequence of binding to all three of the imine nitrogen atoms, the nitrogen bridgehead atom, and just one pyridazine nitrogen atom. The coordination of the copper ion has not changed the $N_{bridgehead}\cdots N_{bridgehead}$ distance of the cryptand by much [10.478 Å versus 10.443 Å in **154**] (Fig. 129b). In contrast, in the lime green plates the copper(II) ion is in a distorted octahedral environment, having bound three imine nitrogen atoms and, in this case, three pyridazine nitrogen atoms. There are two independent cryptates in the asymmetric unit, and there are some slight differences between them. The coordination of the copper(II) ion in this different binding mode has caused a slight lengthening of the $N_{bridgehead}\cdots N_{bridgehead}$ distance of the cryptand [180].

Attempts to include a second copper(II) ion did not lead to isolation of a clean product; nor did use of 2:1 stoichiometry combined with rapid isolation of the product lead to isolation of a characterizable dicopper(II) cryptate [180].

The manganese(II) ion in each of the two independent [Mn(**154**)]$^{2+}$ cryptates present in the asymmetric unit is seven

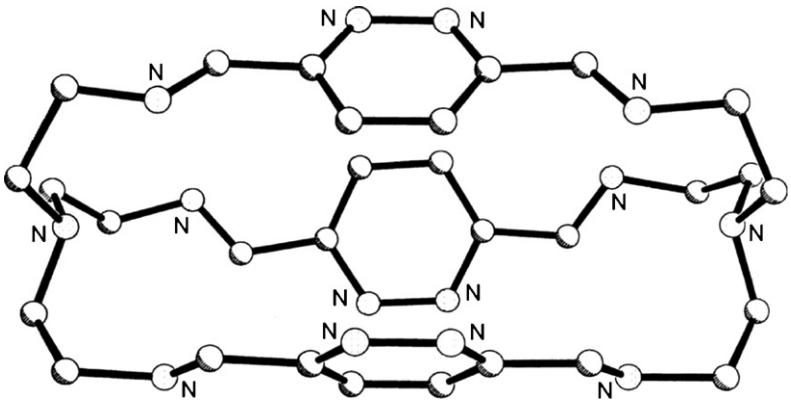

Fig. 128. Structure of **154**.

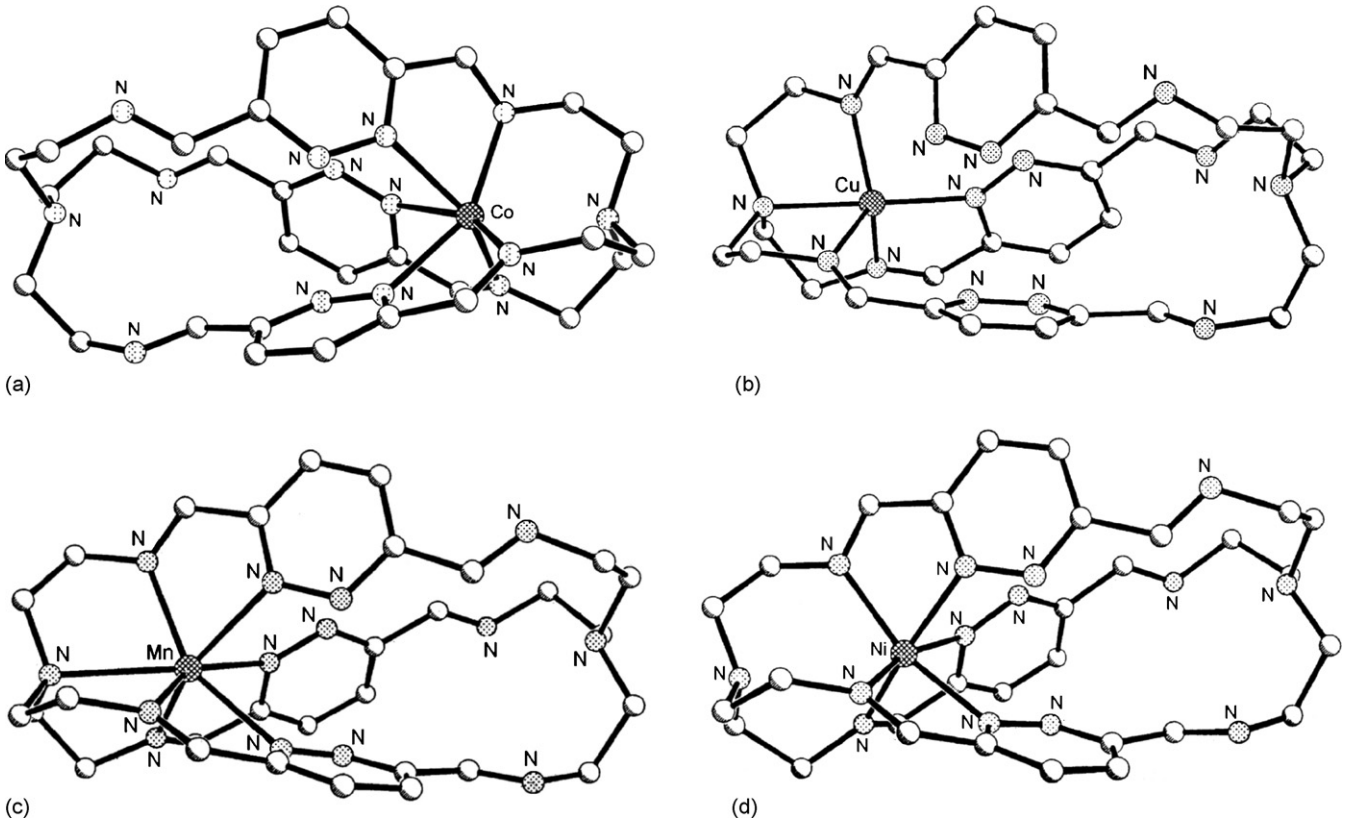

Fig. 129. Structure of $[Co(\mathbf{154})]^{2+}$ (a), $[Cu(\mathbf{154})]^{2+}$ (b), $[Mn(\mathbf{154})]^{2+}$ (c) and $[Ni(\mathbf{154})]^{2+}$ (d).

coordinate as a consequence of binding to three imine nitrogen atoms, three pyridazine nitrogen atoms and the bridgehead nitrogen atom (Fig. 129c). However, the interaction with the bridgehead nitrogen atom is comparatively weak [181].

The structure of $[Ni(\mathbf{154})](ClO_4)_2$ is very similar to that of $[Co(\mathbf{154})](BF_4)_2$. The nickel(II) ion in each of the two independent cryptates in the asymmetric unit is six coordinate as a consequence of binding to three imine nitrogen atoms and three pyridazine nitrogen atoms (Fig. 129d) [181].

The structure of $[Fe(\mathbf{154})](BF_4)_2$ is similar to that of the above mononuclear cryptate [181].

The structures of $[M(\mathbf{154})](X)_2$ ($M = Mn^{II}$, Fe^{II}, Co^{II}, Ni^{II}, Cu^{II}) indicate that **154** is able to accommodate a single, relatively stereochemically demanding, cation in geometries ranging from five to seven coordinate, although six coordination is the most common. In all of these mononuclear cryptates, all three of the strands of the organic host have all *trans* conformations. These strands would therefore have to change their conformations to all *cis* before a second metal cation could bind [179–181].

The dinuclear silver(I) complexes $[Ag_2(\mathbf{154})](X)_2$ ($X = ClO_4^-$, BF_4^-) were obtained either upon template condensation of the triamine and dialdehyde using the silver salt or, in slightly lower overall yield, by treatment of the appropriate silver(I) salt with **154**. The convergent conformation adopted in $[Ag_2(\mathbf{154})]^{2+}$ leaves the imino groups in each strand *cis* to each other and to the pyridazine nitrogen atoms. This generates an unusual, six coordinated silver(I) ion although the cation lies closer to the imino than to the pyridazine nitrogens and the Ag···Ag distance in 4.671 Å. The $N_{bridgehead}\cdots N_{bridgehead}$ distance is identical within experimental error to that in the uncoordinated cryptand **154** (Fig. 130). The ^1H NMR spectrum of $[Ag_2(\mathbf{154})]^{2+}$ demonstrates mobility of conformation down to ca. −50 °C [179].

The reaction of 2 equiv. of $[Cu(CH_3CN)_4](BF_4)$ with **154** in methanol under argon gave $[Cu_2^{I}(\mathbf{154})](BF_4)_2$ as a brown powder. When this synthesis was carried out in air, a brown powder was obtained which, by recrystallization from acetonitrile/diethylether, gave the mixed-valence complex

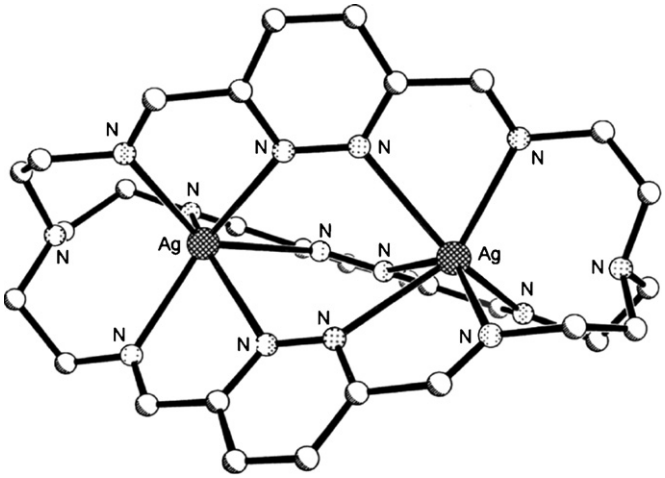

Fig. 130. Structure of $[Ag_2(\mathbf{154})]^{2+}$.

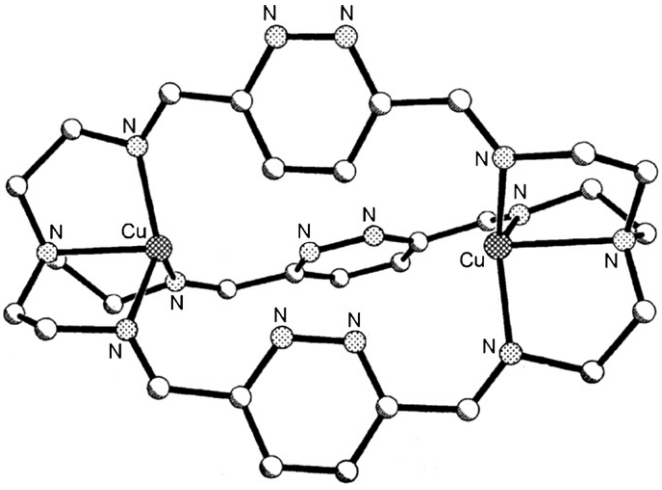

Fig. 131. Structure of $[Cu_2(\mathbf{154})]^{2+}$.

$[Cu^{I}Cu^{II}(\mathbf{154})](PF_6)_3$. The same complex was subsequently prepared in improved yield by reacting **154** with 1 equiv. of the appropriate copper(II) salt, followed by 1 equiv. of the same copper(I) salt. The mixed-valence cryptate can also be obtained by silver(I) oxidation of the dicopper(I) analogues [180].

In the crystals of $[Cu_2^{I}(\mathbf{154})](BF_4)_2$, grown by diethylether diffusion into a chloroform/acetonitrile/ethanol solution, the copper(I) ions are located within the tetraamine-derived caps, achieving their preferred distorted trigonal pyramidal geometry by coordination of the three imine nitrogen donors and the bridgehead nitrogen atom although the interactions with the imine nitrogen donors are stronger than those of the bridgehead atoms. The Cu···Cu distance is 6.478 Å (Fig. 131) [180].

The structure of $[Cu^{I}Cu^{II}(\mathbf{154})](PF_6)_3$ shows that the two copper ions have significantly different geometries: one has a distorted trigonal pyramidal geometry while the other has a distorted octahedral geometry The Cu···Cu distance is 4.960 Å (Fig. 132) [180].

Similarly, the heterodinuclear complexes $[Co^{II}Cu^{I}(\mathbf{154})](BF_4)_3$, $[Mn^{II}Cu^{I}(\mathbf{154})](ClO_4)_2(BF_4)$, $[Fe^{II}Cu^{I}(\mathbf{154})](BF_4)_3\cdot CH_3CN$ and $[Ni^{II}Cu^{I}(\mathbf{154})](BF_4)_3\cdot H_2O$ have been obtained by reaction of the appropriate mononuclear complex

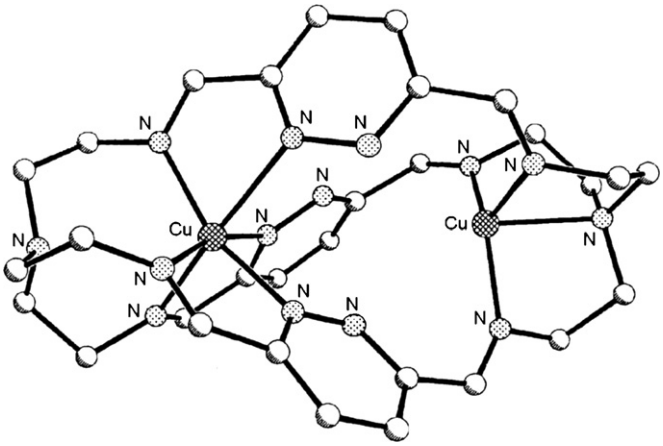

Fig. 132. Structure of $[Cu^{II}Cu^{I}(\mathbf{154})]^{3+}$.

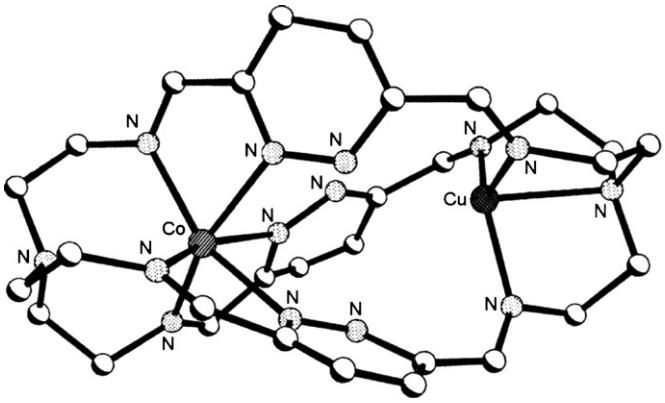

Fig. 133. Structure of $[Co^{II}Cu^{I}(\mathbf{154})]^{3+}$.

$[M^{II}(\mathbf{154})](X)_2$ ($X = ClO_4^-$, BF_4^-) with $[Cu(CH_3CN)_4](BF_4)$ in methanol or acetonitrile [181,182].

The structure of these complexes parallels each other and that of $[Cu^{II}Cu^{I}(\mathbf{154})](PF_6)_3$. In the $Co^{II}Cu^{I}$ complex the cobalt(II) ion is in a distorted octahedral environment consisting of three pyridazine and three imine nitrogen atoms (Fig. 133). This is analogous to the coordination environment of the cobalt(II) center in the structure of the monocobalt(II) complex $[Co(\mathbf{154})]^{2+}$ [179]. In contrast, the non-stereochemically demanding copper(I) ion locates in a distorted trigonal pyramidal site comprising three imine nitrogen donor atoms and the bridgehead nitrogen atom; no formal pyridazine coordination exists. In order to provide this site for the copper(I) ion, the cryptand host **154** has adopted a conformation with mutually *cis* imino functions, in contrast to the mutually *trans* conformation seen in the monocobalt(II) complex [181,182].

The structures of $[Mn^{II}Cu^{I}(\mathbf{154})]^{3+}$, $[Ni^{II}Cu^{I}(\mathbf{154})]^{3+}$ and $[Fe^{II}Cu^{I}(\mathbf{154})]^{3+}$ are similar to each other (Fig. 134a). In all cases, as observed in $[Co^{II}Cu^{I}(\mathbf{154})]^{3+}$ and $[Cu^{II}Cu^{I}(\mathbf{154})]^{3+}$, the divalent cation is six coordinate and binds to three pyridazine and three imine nitrogen atoms. Of all the $[M^{II}Cu^{I}(\mathbf{154})]^{3+}$ cryptates (M = Mn, Co, Fe, Ni, Cu), the geometry of the iron(II) ion in $[Fe^{II}Cu^{I}(\mathbf{154})]^{3+}$ is closest to a regular octahedron, indicating that iron(II) is the most stereochemically demanding cation (Fig. 134b). In the $Mn^{II}Cu^{I}$ complex the manganese(II) ion is intermediate between octahedral and trigonal prismatic while the copper(I) ion has a distorted trigonal pyramidal geometry and is coordinated by three imine nitrogen atoms and the bridgehead nitrogen atom [181].

The addition of two equivalents of zinc(II) perchlorate to **154** in acetonitrile results in the dinuclear cryptate $[Zn_2(\mathbf{154})](ClO_4)_4$. Further attempts to synthesize homodinuclear cryptates were carried out with the manganese(II) and sodium salts and resulted in $[Mn_2^{II}(\mathbf{154})(Cl)_4]\cdot H_2O$ and $[Na_2(\mathbf{154})](CF_3SO_3)_2$, respectively. The addition of two equivalents of manganese(II) perchlorate to **154** gave rise only to the mononuclear cryptate $[Mn^{II}(\mathbf{154})](ClO_4)_2$. Thus, although it appears to be possible to synthesize dinuclear complexes of **154** with non-stereochemically demanding divalent cations, the choice of counterion and/or solvent appears to be crucial [181].

The sodium borohydride reduction of the hexaimine Schiff base **154** produces the related octaamine cryptand **155**, which was recrystallized from chloroform by vapor diffusion of diethyl ether. While the pyridazine diimine units in **154** are fairly flat owing to conjugation, in **155** the amine single bonds are twisted well out of the respective pyridazine ring planes. Moreover, there are a number of intra- and intermolecular hydrogen bonds present in the structure of **155** whereas none are observed for the related Schiff base **154**. Furthermore, the pyridazine octaamine cryptand **155**, in contrast to other octaamine cryptands which have been structurally characterized, is not well preorganized for complexation on account of the transoid disposition of amine and pyridazine donors (Fig. 135) [180].

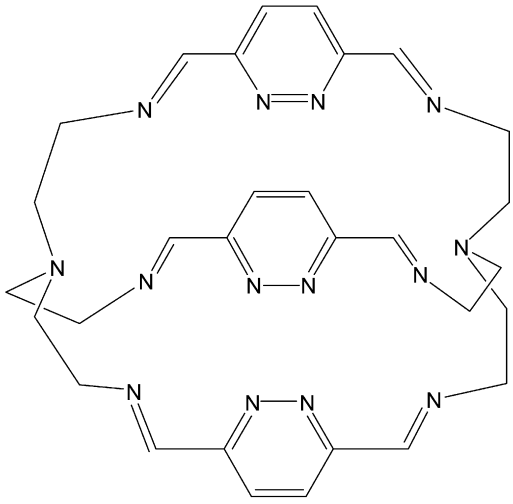

154

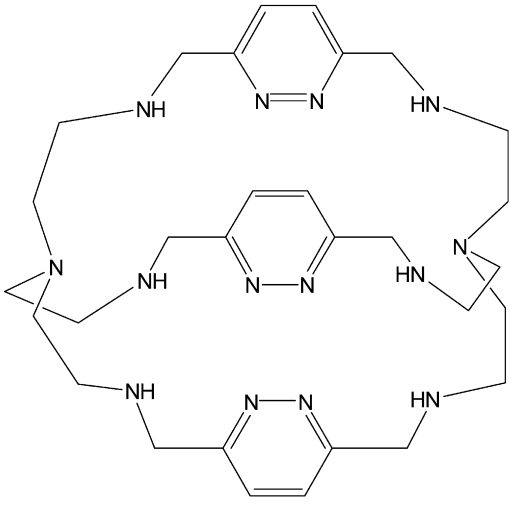

155

The reaction of **155** with 2 equiv. of copper(II) tetrafluoroborate gave $[Cu_2^{II}(\mathbf{155})](BF_4)_4$, obtained as blue crystals, by the vapor diffusion of diethyl ether into an acetonitrile solution. One drop of triethylamine was added prior to the addition of the copper(II) salt to prevent the formation of a partially protonated

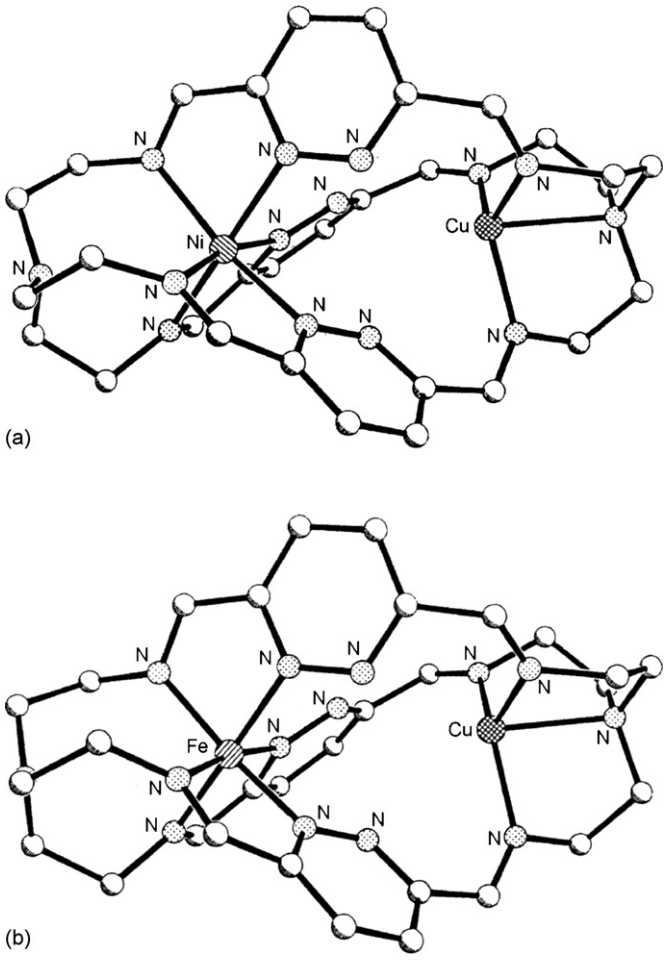

Fig. 134. Structure of $[Ni^{II}Cu^{I}(\mathbf{154})]^{3+}$ (a) and $[Fe^{II}Cu^{I}(\mathbf{154})]^{3+}$ (b).

green by-product. Attempts at forming a monocopper(II) complex of **155** were unsuccessful; both the blue powdery first crop and green powdery second crop analyzed as complex mixtures. The copper(II) ions have slightly different environments from one another: one copper(II) ion binds to one nitrogen bridgehead atom, two pyridazine nitrogen atoms, and two amine nitrogen atoms whereas the other copper(II) ion binds to one nitrogen bridgehead atom, one pyridazine nitrogen atom, and three amine nitrogen atoms. Interestingly, the copper(II) ions are not bridged by any of the three pyridazine rings as each ring coordinates via only one nitrogen atom, not both. The coordination of two copper(II) cations requires transformation of the amine and pyridazine nitrogen donors from the transoid disposition of the free ligand to cisoid in two of the three strands, while the third, very nonplanar strand is best described as *cis*, *trans*. The Cu···Cu separation is 5.874 Å (Fig. 136) [180].

The cyclic voltammogram of $[Cu_2^{I}(\mathbf{154})](BF_4)_2$ reveals two reversible one-electron waves at $E_{1/2} = -0.34$ V ($\Delta E = 0.08$ V) and $E_{1/2} = +0.33$ V (($\Delta E = 0.09$ V) assigned respectively to $Cu^{I}Cu^{I} \rightleftharpoons Cu^{I}Cu^{II}$ and $Cu^{I}Cu^{II} \rightleftharpoons Cu^{II}Cu^{II}$; the final oxidation product $[Cu_2(\mathbf{154})]^{4+}$ is stable under anaerobic conditions. $[Cu_2(\mathbf{154})](BF_4)_2$ is stable in air, however molecular oxygen is capable to oxidize this complex to $[Cu^{II}Cu^{I}(\mathbf{154})](BF_4)_3$; thus, it is possible to prepare $[Cu^{II}Cu^{I}(\mathbf{154})](PF_6)_3$ from the corre-

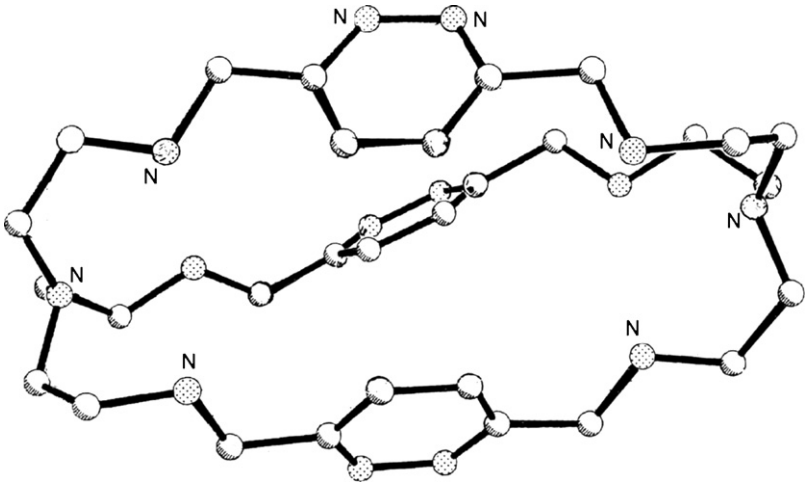

Fig. 135. Structure of **155**.

sponding dicopper(I) complex by carrying out the reaction and the subsequent recrystallization in air. Also yellow brown solutions of $[Cu^{II}Cu^{I}(\mathbf{154})]^{3+}$ are easy electrochemically oxidized to the green $[Cu_2{}^{II}(\mathbf{154})]^{4+}$ [180].

In the cyclic voltammogram of $[Cu^{II}(\mathbf{154})](BF_4)_2$ in CH_3CN, one reversible reduction wave is observed, at $E_{1/2} = -0.38$ V ($\Delta E = 0.08$ V), which is assigned to the $Cu^{II} \leftrightharpoons Cu^{I}$ redox process. The resulting dark yellow–brown reduction product is stable under argon, as shown by the unchanged cyclic voltammogram for a short period of time; however over time some precipitation of copper metal occurs.

Comparison of the K_{com} values estimated from the cyclic voltammetry results for $[Cu_2{}^{I}(\mathbf{154})]^{2+}$ and $[Cu^{I}Cu^{II}(\mathbf{154})]^{3+}$ with that obtained for $[Cu_2{}^{II}(\mathbf{108})(CH_3CN)_2](ClO_4)_4$, in which the $Cu^{II}Cu^{I}$ mixed-valence state is stabilized in acetonitrile between -0.15 and $+0.20$ V ($K_{com} = 8.3 \times 10^5$) and isolable, reveals that **154** can stabilize better the $Cu^{II}Cu^{I}$ mixed-valence species ($K_{com} = 2.1 \times 10^{11}$) [180].

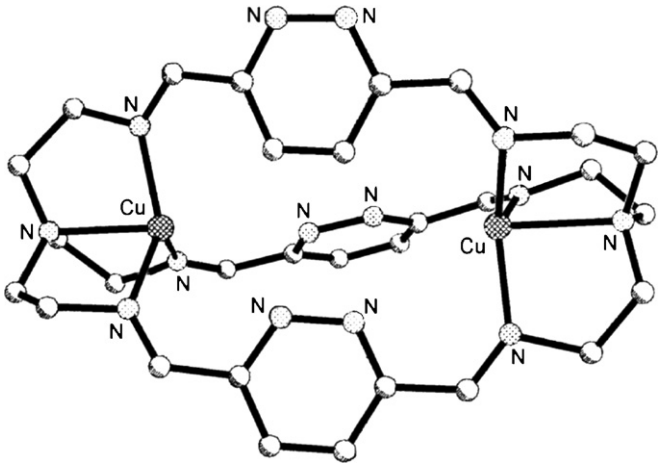

Fig. 136. Structure of $[Cu_2(\mathbf{155})]^{4+}$.

The cyclic voltammogram of $[Cu_2{}^{II}(\mathbf{155})](BF_4)_4$ shows no significant processes on scanning to positive potentials, except for an irreversible oxidation wave at about +1.20 V which is most likely to be due to ligand oxidation. The simplicity of this region, in stark contrast to complexity observed with complexes of **154**, suggests hexaimine cryptand instability when coordinated to metal(II) ions. Two probably metal-centered, one-electron quasi-reversible reduction processes are observed for $[Cu_2(\mathbf{155})](BF_4)_4$ at $E_{1/2} = -0.61$ V ($\Delta E = 0.12$ V) the metal centered: $Cu^{II}Cu^{II} \leftrightharpoons Cu^{I}Cu^{II}$ and at $E_{1/2} = -0.93$ V ($\Delta E = 0.15$ V) due to the $Cu^{I}Cu^{II} \leftrightharpoons Cu^{I}Cu^{I}$ -0.61 V one ($K_{com} = 2.6 \times 10^5$) scanning to more negative potentials, beyond -1.40 V, a stripping wave occurs at -0.55 V on the return cycle indicating that further reduction results in the deposition of copper on the electrode. These results show that **155** is more effective in stabilizing the copper(II) ion than **154**. In particular the reduced degree of stabilization of the mixed-valence form, when combined with the significantly lower redox potential, is probably sufficient to make its isolation in the solid state problematic [180].

$[Cu_2{}^{I}(\mathbf{154})](BF_4)_2$ is diamagnetic while $[Cu^{I}Cu^{II}(\mathbf{154})](BF_4)_3$ is paramagnetic $2.06\mu_B$ with the unpaired electron remaining fully localized, as proved by ESR data in dimethylformamide [183]. $[Cu^{II}(\mathbf{154})](BF_4)_2$ has a magnetic moment of $1.90\mu_B$ and an ESR spectrum typical of a mononuclear copper(II) compound [183]. $[Cu_2{}^{II}(\mathbf{155})](BF_4)_4$ has weakly antiferromagnetically interacting dicopper(II) centers ($2J = -13.2\ cm^{-1}$), as expected given the lack of bridging moieties between the copper(II) ions. This situation is similar to that applying in the dicopper(II) pyridine-spaced octaamine cryptate analog of **156** ($-2J \approx 20\ cm^{-1}$) but contrasts with the strong antiferromagnetic coupling ($-2J = 482\ cm^{-1}$), observed in $[Cu_2{}^{II}(\mathbf{108})(CH_3CN)_2](ClO_4)_4$, due to the effective overlap of the copper $d_{x^2-y^2}$ orbitals with the bridgings pyridazine orbitals in a near-coplanar conformation [180].

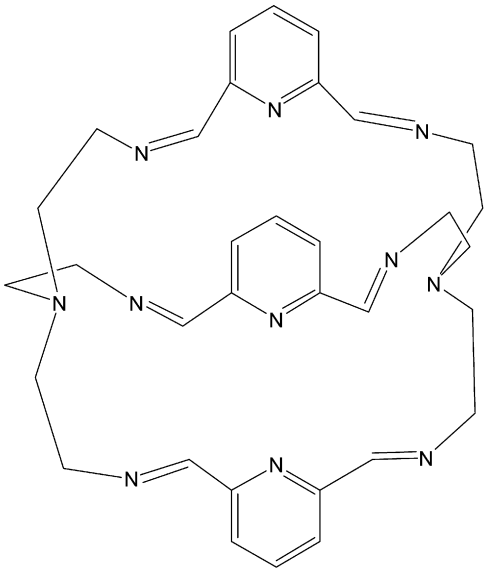

156

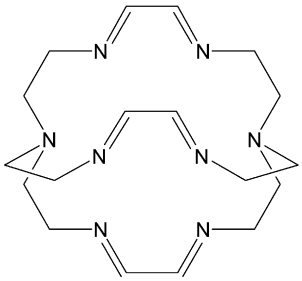

157

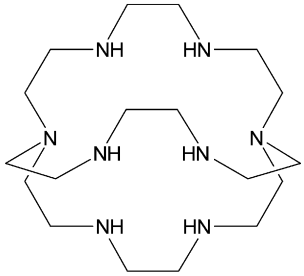

158

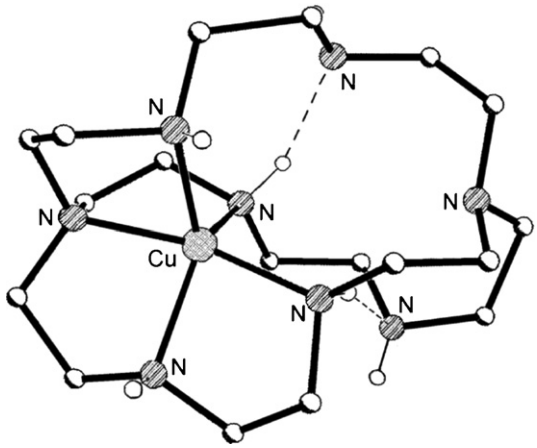

Fig. 137. Structure of $[Cu(\mathbf{158})]^{2+}$.

3.3. [3 + 2] Ligands without bridging groups and related complexes

The synthesis and properties of the Schiff base **157**, derived from the [3 + 2] condensation of glyoxal with tris-(2-aminoethyl)amine, of the related polyamine cryptand **158**, obtained by reduction of **157** with $NaBH_4$, and of the related homo- and heterodinuclear complexes have been discussed in previous reviews [5]. More recently $[Cu(\mathbf{158})](BF_4)_2{\cdot}4H_2O$ has been synthesized by reaction of 158 with $Cu(BF_4)_2{\cdot}nH_2O$ in a 1:1 molar ratio in ethanol. The similar complex $[Cu(\mathbf{158})](BPh_4)_2{\cdot}H_2O$ was obtained by the reaction of **158** with $Cu(CH_3COO)_2{\cdot}2HO$ and $NaBPh_4$ in C_2H_5OH/CH_3CN in a 1:1:2 molar ratio [183].

$[Cu(\mathbf{158})](BPh_4)_2{\cdot}H_2O$ contains two independent $[Cu(\mathbf{158})]^{2+}$ cations and four BPh_4^- anions in the asymmetric unit. The two cations are basically very similar although one of them is severely disordered. In each cation the copper(II) ion is five coordinate in an approximate trigonal bipyramidal geometry with the three amine atoms derived from one of the tren units making up the trigonal plane and the bridgehead nitrogen atom and one amine nitrogen atom derived from the second tren unit in the axial positions. The uncoordinated secondary amine groups are intramolecularly hydrogen bonded to the coordinated amine atoms across the cavity. No intermolecular hydrogen bonds occur (Fig. 137) [183].

The some cryptand **158** reacts with $Cu(CH_3COO)_2{\cdot}2H_2O$ in CH_3OH in a 1:2 molar ratio and in the presence of $NaBF_4$ to afford the mixed valence complex $[Cu^{II}Cu^{I}(\mathbf{158})](BF_4)_3{\cdot}2H_2O{\cdot}CH_3OH$. [183].

Cyclic voltammograms recorded at a glassy carbon electrode of 1 mM $[Cu^{II}Cu^{I}(\mathbf{158})](BF_4)_3$, in 0.1 M $NaNO_3$, buffered to pH 9.1 with 2-[*N*-cyclohexylamino]-ethanesulphonic acid, show only a fully reversible redox couple with $E_{1/2} = -0.40$ V versus SCE. The same results are obtained at GC electrodes in borate buffer, pH 8.7 and phosphate buffer, pH 6.8. The redox process is assigned to the one-electron reduction of $[Cu^{II}Cu^{I}(\mathbf{158})]^{3+}$ to $[Cu_2^{I}(\mathbf{158})]^{2+}$ [183].

The more complicated behaviour in CH_3CN is due to the solvent assisted dissociation equilibrium $[Cu^{II}Cu^{I}(\mathbf{158})]^{3+} \leftrightarrows [Cu^{II}(\mathbf{158})]^{2+} + [Cu(CH_3CN)_4]^{+}$. Thus, the reduction reactions $[Cu^{II}Cu^{I}(\mathbf{158})]^{3+} + e^- \leftrightarrows [Cu_2^{I}(\mathbf{158})]^{2+}$ ($E_{1/2} = -0.57$ V) and $[Cu^{II}(\mathbf{158})]^{2+} + e^- \leftrightarrows [Cu^{I}(\mathbf{158})]^{+}$ ($E_{pa} = -0.85$), and the oxidation reactions $[Cu(CH_3CN)_4]^{+} - e^- \leftrightarrows [Cu(CH_3CN)_4]^{2+}$ ($E_{1/2} = -0.55$ V), $[Cu^{II}Cu^{I}(\mathbf{158})]^{3+} - e^- \leftrightarrows [Cu_2^{II}(\mathbf{158})]^{4+}$ ($E_{pa} = 0.9$) and $[Cu^{II}(\mathbf{158})]^{2+} - e^- \leftrightarrows [Cu^{III}(\mathbf{158})]^{3+}$ ($E_{pa} = -1.15$ V) have been proposed to occur. The irreversible oxidation processes at $E_{pa} = 0.9$ V and 1.15 V, associated with oxidation of $[Cu^{II}Cu^{I}(\mathbf{158})]^{3+}$ and $[Cu^{II}(\mathbf{158})]^{2+}$, respectively, have been ascribed to ligand-centered oxidations, leading to irreversible ligand transformation, possibly of the oxidative dehydrogenation type [183].

The addition of an excess of **158** gives rise to the redox reactions $[Cu^{II}Cu^{I}(\mathbf{158})]^{3+} + \mathbf{158} \leftrightarrows 2[Cu^{II}(\mathbf{158})]^{2+}$ and/or $[Cu^{II}Cu^{I}(\mathbf{158})]^{3+} + \mathbf{158} \leftrightarrows [Cu^{II}(\mathbf{158})]^{2+} + [Cu^{I}(\mathbf{158})]^{+}$. Furthermore, the irreversibility of the reduction reaction of $[Cu^{II}(\mathbf{158})]^{2+} + e^- \leftrightarrows [Cu^{I}(\mathbf{158})]^{+}$ has been ascribed to the instability of $[Cu^{I}(\mathbf{158})]^{+}$ which evolves into $[Cu(CH_3CN)_4]^{+}$ and **158**. $[Cu(CH_3CN)_4]^{+}$, generated by this process, reacts with $[Cu^{II}(\mathbf{158})]^{2+}$ to form $[Cu^{II}Cu^{I}(\mathbf{158})]^{3+}$. Similar sequences of reactions lead to the quantitative formation of $[Cu_2^{I}(\mathbf{158})]^{2+}$. ESR spectra of $[Cu^{II}Cu^{I}(\mathbf{158})]^{3+}$ in H_2O or acetonitrile confirm

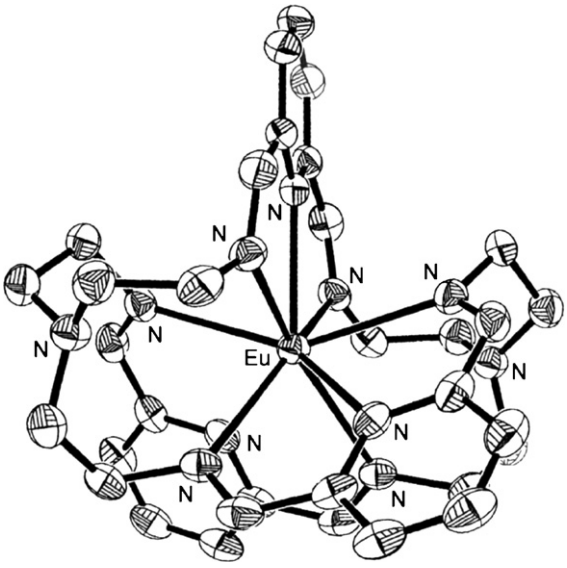

Fig. 138. Structure of $[Eu(\mathbf{156})]^{3+}$.

delocalization of the unpaired spin on the both copper nuclei [183].

The lanthanide complexes $[Ln(\mathbf{156})](NO_3)_3{\cdot}nH_2O$ ($Ln = La^{III}$, Ce^{III}, Pr^{III}, Sm^{III}, Eu^{III}, Gd^{III}, Tb^{III}) were synthesized by the reaction in CH_3CN of the appropriate lanthanide nitrate with the free Schiff base **156**, derived from the [3 + 2] condensation of 2,6-diformylpyridine with tris(2-aminoethyl)amine [185]. The conductivities of these lanthanide cryptates are typical for a 1:3 electrolyte. ESI-mass spectra of the Ce···Tb cryptates show peaks assigned to the formation of $[Ln(\mathbf{156})]^{3+}$, $[Ln(\mathbf{156})(NO_3)]^{2+}$ and $[Ln(\mathbf{156})(NO_3)_2]^{+}$. No peak of free ligand or ligand fragments is observed; the simplicity of these spectra can be attributed to the thermodynamic and kinetic stability of these cryptates. The ESI-mass spectra of $[La(\mathbf{156})](NO_3)_3{\cdot}2H_2O$ show peaks due to the species $[La(\mathbf{156})]^{3+}$ and $[La(\mathbf{156})(NO_3)]^{2+}$, together with those due to $[Na(\mathbf{156})]^{+}$ and $[Na_2(\mathbf{156})(NO_3)]^{+}$, implying that **156** can bind Na^+ (present in the system) to form an inclusion complex. The decomplexation of the lanthanum(III) ion from $[La(\mathbf{156})(NO_3)]_3$ implies that this complex is less stable than the other complexes, because of larger radius of the lanthanum(III) ion [184].

In $[Eu(\mathbf{156})](NO_3)_3$ the europium(III) ion is located in the center of the macrocycle and coordinated by three pyridyl nitrogen atoms and six imino nitrogen atoms to form a tricapped prism (Fig. 138). The complex cation has a threefold axis through the europium(III) ion and the two bridgehead nitrogen atoms. No interaction between the europium(III) ion and bridgehead nitrogens is observed. The coordination polyhedron about lanthanide(III) ion is a tricapped prism. The upper and basal planes of the prism, which are approximately parallel, are composed of the imino nitrogen atoms. The three pyridyl nitrogen atoms are located at the capping positions. The europium(III) ion is located in the symmetrical center of the prism. The tricapped prism structure is different from the unsymmetrical structure of sodium cryptate with the same ligand [184,185].

$[Ba(\mathbf{159})](ClO_4)_2{\cdot}CH_3CN$, obtained by template condensation of tris(3-aminopropyl)amine and diformylpyridine in the presence of $Ba(ClO_4)_2$ [186], when treated with an excess of $NaBH_4$ in absolute methanol gives the reduced cryptand **160**. When imidazole is added to a C_2H_5OH/CH_3CN solution of **160** and $Cu(ClO_4)_2{\cdot}6H_2O$ in a 1:1:2 molar ratio and the pH of the solution is adjusted to 9 with NaOH, $[Cu_3(\mathbf{160})(\mu\text{-}Im)(Br)_2](ClO_4)_3{\cdot}H_2O$ is obtained. In the complex cation the cryptand encapsulates three copper(II) ions which are arranged at the corners of an approximately isosceles triangle. One copper(II) ion is coordinated in a square pyramidal geometry with two imino nitrogen atoms, one pyridyl nitrogen atom pyridyl, one nitrogen of imidazole anion as a bridging ligand as well as one bromine anion. Besides the nitrogen atom of imidazolate, the second copper(II) ion [Cu(3)] ion is also coordinated to two imino nitrogen atoms and one pyridyl-nitrogen, leading to a square planar configuration. The third copper(II) ion shows a similar arrangement to the second copper(II) ion except that the imidazolate bridge is replaced by a monodentate bromine anion. The Cu···Cu separations are in the range 5.388–5.778 Å (Fig. 139) [187]. The magnetic susceptibility data show that an antiferromagnetic interaction exists between the copper(II) ions with estimated exchange integrals $J_{13} = -22.5\,cm^{-1}$ and $J_{12} = 3.13\,cm^{-1}$ [187].

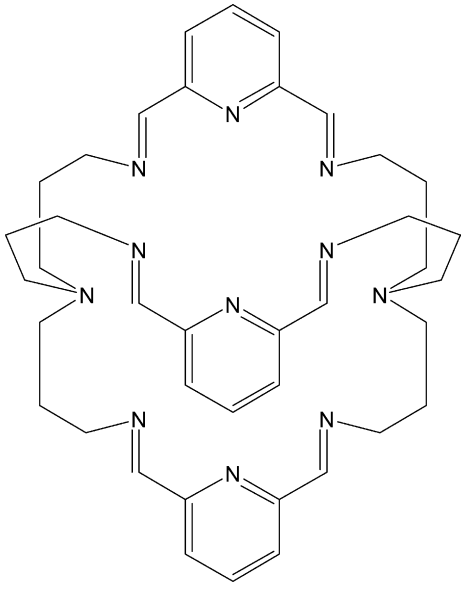

159

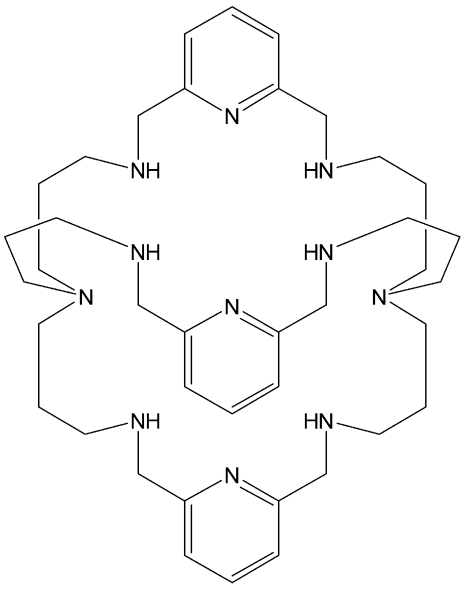

160

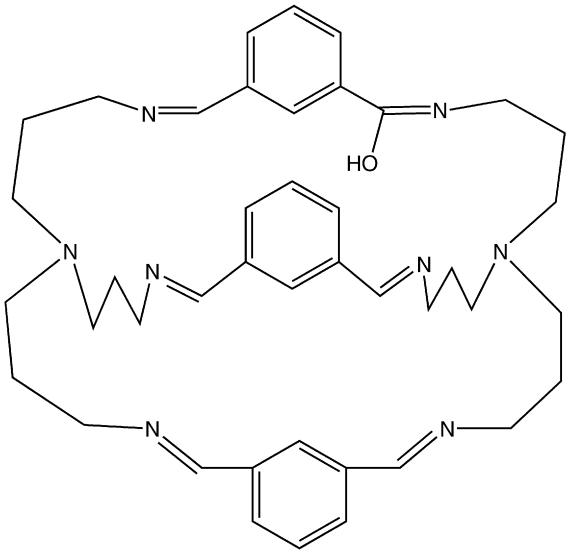

161

$[Ag_2(\mathbf{161})](ClO_4)_2{\cdot}H_2O$ and $[Ag_2(\mathbf{162})](ClO_4)_2{\cdot}1.5H_2O$ were synthesized by condensation of tris(3-aminopropyl)amine (trpn) with *m*-phthalaldehyde in the presence of silver(I) perchlorate, under aerobic and anaerobic conditions, respectively [189]. The silver(I) ions were released when the Schiff base complexes were reduced by $NaBH_4$, the final result being the [3 + 2] polyamine macrocycles **163** and **164**, respectively. Furthermore, $[Ag_2(\mathbf{162})](NO_3)_2$ crystallized from C_2H_5OH/CH_3CN after condensation of tris(3-aminopropyl)amine with *m*-phthalaldehyde in the presence of $AgNO_3$ [188].

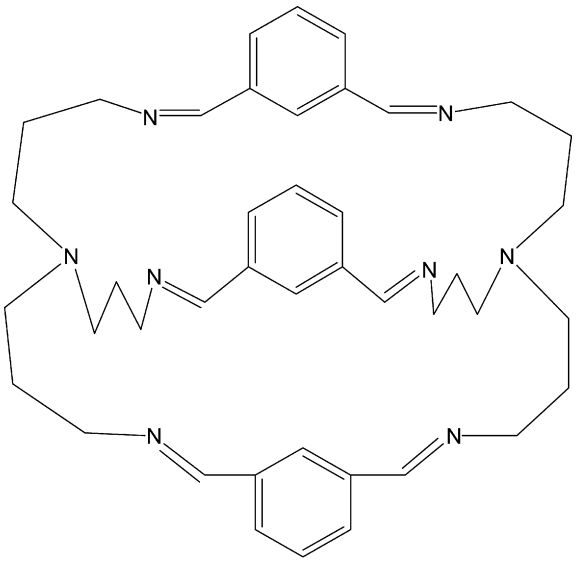

162

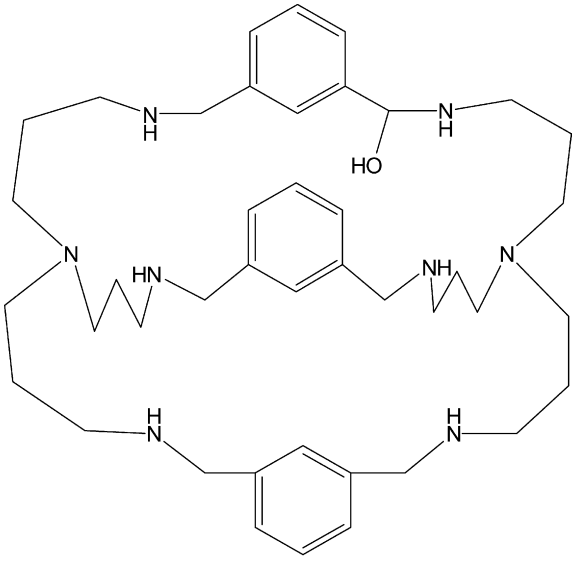

163

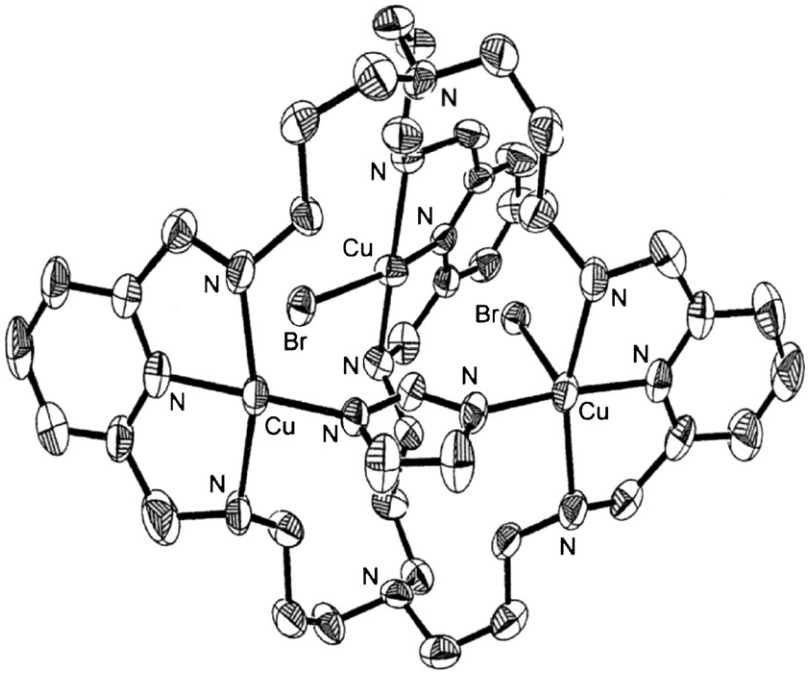

Fig. 139. Structure of $[Cu_3(\mathbf{160})(\mu\text{-Im})(Br)_2]^{3+}$.

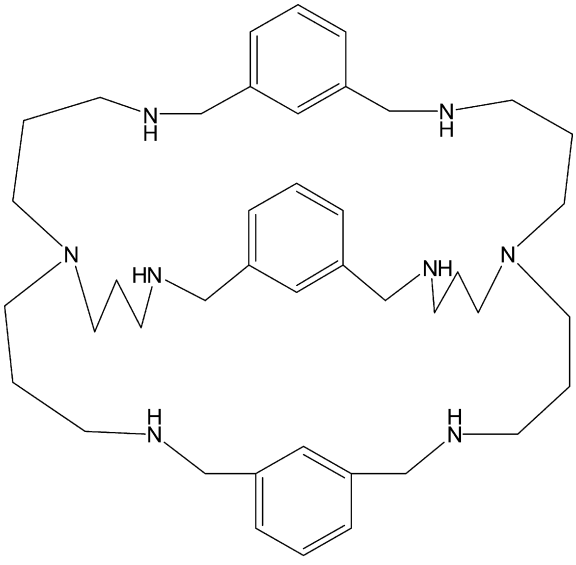

164

The ESI-mass spectrometry measurements of $[Ag_2(\mathbf{161})](ClO_4)_2$ and its hydrogenated ligand H-**163** display fragments corresponding to oxygen insertion products, while the ESI-MS spectrometry measurements of $[Ag_2(\mathbf{162})](ClO_4)_2$ and **164** do not display these peaks. Leaving **164** under atmospheric conditions does not produce an oxygen insertion product, while slowly evaporation of a methanolic solution of $[Ag_2(\mathbf{162})](ClO_4)_2$ under atmospheric conditions give rise to crystals of the oxygen insertion product $[Ag_2(\mathbf{161})](ClO_4)_2$, indicating a critical role of the silver(I) ion in such oxygen insertion reactions.

m-Formylphenylbenzoic acid and *m*-phthalaldehyde, the acid decomposed products of $[Ag_2(\mathbf{161})](ClO_4)_2{\cdot}2H_2O$ were identified by HPLC and ESI-MS. *m*-Formylphenyl formic acid was not formed from oxidation by the silver(I) ion, but from the oxygen insertion into the C=N bond of the ligand [188].

$[Ag_2(\mathbf{161})](ClO_4)_2$, $[Ag_2(\mathbf{162})](ClO_4)_2{\cdot}1.5H_2O$ and $[Ag_2(\mathbf{162})](NO_3)_2$ have a similar triple-helical structure. They retain a trigonal pyramidal N_4 cap site for silver(I) coordination, but the crystal cell parameters of $[Ag_2(\mathbf{161})](ClO_4)_2$ and $[Ag_2(\mathbf{162})](ClO_4)_2{\cdot}1.5H_2O$ are different from $[Ag_2(\mathbf{162})](NO_3)_2$. In $[Ag_2(\mathbf{161})](ClO_4)_2$, the silver(I) and silver(II) ions deviated from the plane composed of three imino nitrogen atoms while in $[Ag_2(\mathbf{162})](NO_3)_2$ the silver(I) ions lie almost coplanar with the imino nitrogen. The separation of Ag···Ag for $[Ag_2(\mathbf{161})](ClO_4)_2$ (3.974 Å) is the largest among the three analogues with the three *m*-xylyl-spaced cryptates. Also, the separations of N(bridgehead)···N(bridgehead) in $[Ag_2(\mathbf{161})](ClO_4)_2$ and $[Ag_2(\mathbf{162})](ClO_4)_2$ are larger than that of analog $[Ag_2(\mathbf{162})](NO_3)_2$. For cryptate $[Ag_2(\mathbf{161})](ClO_4)_2$, this large separation favours the attack of the dioxygen on the silver(I) and the activation of oxygen that leads to oxygen insertion into the imine group (Fig. 140a and b) [188].

Structural aspects of the binding of halides in the octaaza cryptand **165** were examined for fluoride, chloride, and bromide. $[(H_6\text{-}\mathbf{165})(F)_2(H_2O)](SiF_6)_2{\cdot}12H_2O$, $[(H_6\text{-}\mathbf{165})(Cl)(H_2O)](Cl)_5{\cdot}4H_2O{\cdot}CH_3OH$ and $[(H_6\text{-}\mathbf{165})(Br)](Br)_5{\cdot}7.23H_2O$ were all made by titration of the free base in either methanol (fluoride complex) or water (chloride and bromide complexes) with the appropriate acid. These reactions were all straightforward, resulting in readily isolable products [189].

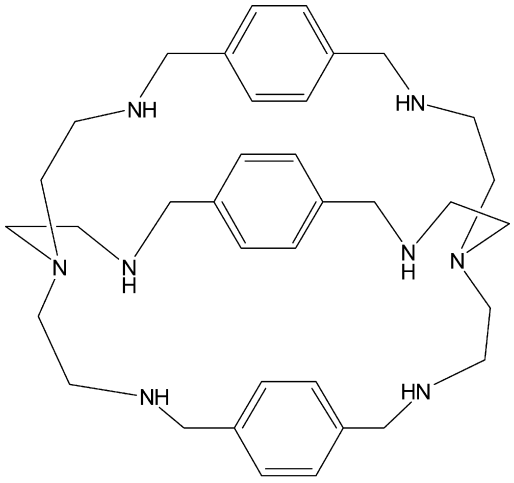

165

$[(H_6\text{-}\mathbf{165})(F)_2(H_2O)](SiF_6)_2{\cdot}12H_2O$ crystallizes in the hexaprotonated form, with the cryptand containing two internal fluoride ions (Fig. 141a). The remaining charge is satisfied by two external $[SiF_6]^{2-}$ counterions. Additionally, thirteen molecules of water complete the asymmetric unit, including one molecule of water bridging the two fluorides. Extensive hydrogen-bonding networks are observed outside of the cryptand cavity between the macrocycle, the external $[SiF_6]^{2-}$ counter anions and twelve water molecules of salvation [189].

In $[(H_6\text{-}\mathbf{165})(Cl)(H_2O)](Cl)_5{\cdot}4H_2O{\cdot}CH_3OH$ the hexaprotonated ligand contains six chlorides and five water molecules, including the internal chloride and water, as well as a molecule of methanol. As noted for $[(H_6\text{-}\mathbf{165})(F)_2(H_2O)](SiF_6)_2{\cdot}12H_2O$, a significant number of hydrogen-bonding interactions occurs between these anion receptor complexes and surrounding water molecules. The methanol molecule is just outside of the cavity between two of the cryptand arms (Fig. 141b) [189].

$[(H_6\text{-}\mathbf{165})(Br)](Br)_5{\cdot}7.23H_2O$ also crystallizes as the hexahydrobromide but contains two crystallographically independent cationic units. One units contains one bromide ion and three disordered water molecules. The second unit contains one bromide on one side of the cavity and a single water molecule centered at the other side, as observed for the chloride complex, $[(H_6\text{-}\mathbf{165})(Cl)(H_2O)](Cl)_5{\cdot}4H_2O{\cdot}CH_3OH$ (Fig. 141c) [189]. The structures of unit B and the chloride complex $[(H_6\text{-}\mathbf{165})(Cl)(H_2O)](Cl)_5{\cdot}4H_2O{\cdot}CH_3OH$ are very similar. In unit A, as noted earlier, there was disorder in the bromide position, with one bromide ion predominant. Again, there is a water molecule in the cavity. A second water molecule is also relatively close to the bromide. Two other water molecules lie between the arms of the cryptand, but they are considerably farther from the internal bromide [189].

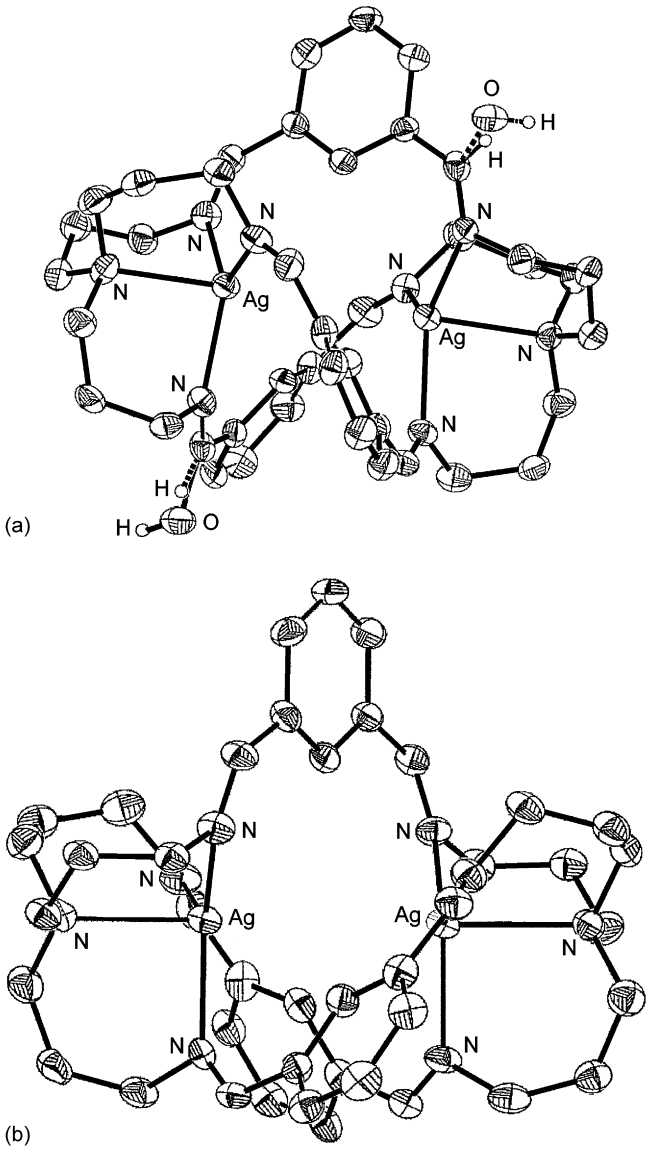

Fig. 140. Structure of $[Ag_2(\mathbf{161})]^{2+}$ (a) and $[Ag_2(\mathbf{162})]^{2+}$ (b).

Encapsulation of nitrate and perchlorate anions within the two protonated cryptate hosts $[H_6\text{-}\mathbf{166}]^{6+}$ and $[H_6\text{-}\mathbf{167}]^{6+}$, studied by potentiometric and NMR titration methods, shows dominant 1:1 complexation for both systems. Complexation constants, log K, with $[H_6\text{-}\mathbf{166}]^{6+}$ and $[H_6\text{-}\mathbf{167}]^{6+}$ are, generally, high at 3.7 and 3.4 for nitrate, and ≈3.4 and ≈2.5 for perchlorate, respectively. Good geometric complementarily was confirmed in the case of perchlorate and $[H_6\text{-}\mathbf{166}]^{6+}$ by an X-ray crystallographic structure determination of the inclusive anion cryptate For nitrate, there is evidence for 1:2 complexation in the presence of a large excess of anion, relative 1:1 and 1:2 complexation constants being in the approximate ratio 10^3:1 [190,191].

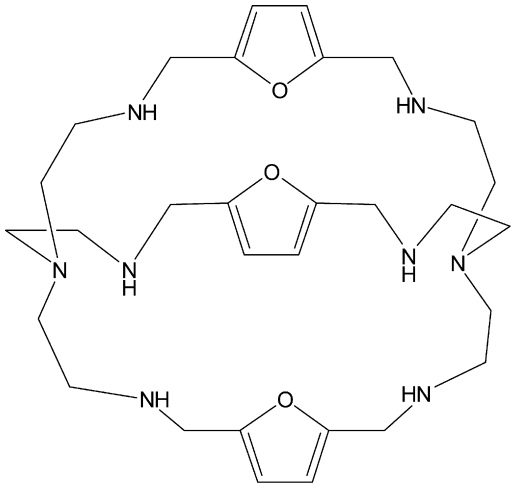

166

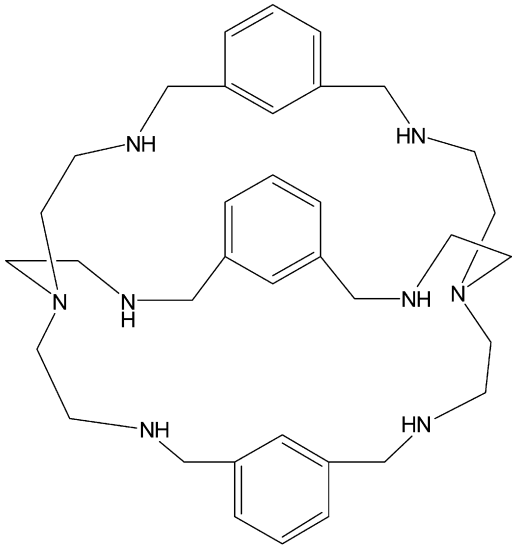

167

In $[(H_6\text{-}\mathbf{167})(ClO_4)](ClO_4)_5\cdot 3H_2O$ the protonated cryptand acts as host for one perchlorate guest which is hydrogen-bonded to three symmetry-related amines at one end of the cage and indirectly to the other set of amines via water molecules (Fig. 142a) [190,191]. The structure of $[(H_6\text{-}\mathbf{167})(NO_3)](NO_3)_4\cdot 2H_2O$, already reported in a previous review [5], reveals that two nitrate anions are encapsulate inside the hexaprotonate cryptate. This shows that in $[H_6\text{-}\mathbf{167}]^{6+}$ the nitrate recognition in the solid state differs from that normally applying in aqueous solution. The hydrogen-bonding network involved in retention of nitrate anions includes water molecules and runs through the whole structure apart from the areas occupied by aromatic rings; the shortest hydrogen-bonds operate between NH^+ and the water which tethers exclusive nitrate anions (Fig. 142b) [190,191].

Structural comparisons of anion cryptates of $[H_6\text{-}\mathbf{167}]^{6+}$ and $[H_6\text{-}\mathbf{166}]^{6+}$ emphasize the role of hydrogen bonding between protonated cryptand host and oxoanions, with or without water intermediacy, in contributing to the stabilization of the oxoanion cryptate structure. Although the co-operative effect of several weaker interactions results in stabilization of the inclusive oxoanion site, the shortest hydrogen-bond contacts in all cases are to water. In the $[H_6\text{-}\mathbf{167}]^{6+}$ perchlorate structure and its $[H_6\text{-}\mathbf{166}]^{6+}$ analogue, the shortest hydrogen-bonds are between NH– and water tethered to the inclusively bonded anion, while in the dinitrate structure of $[H_6\text{-}\mathbf{167}]^{6+}$ the externally directed $NH^+\cdots$water$\cdots$nitrate hydrogen-bonds are the shortest [190,191].

The aminocryptands **165**$\cdots$**171** have been prepared by the usual condensation of the appropriate precursors, followed by reduction of the resulting Schiff bases with $NaBH_4$ [192]. The related methylated amino-cryptands were obtained by treating the unsubstituted aminoazacryptands with formic acid/formaldehyde, followed by purification of the resulting product by chromatography. Potentiometric studies show a small increase in acidity upon nitrogen-methylation [192].

The efficiency of these amino cryptands for encapsulation and extraction of the oxoanions pertechnetate and perrhenate from aqueous was investigated and compared with that of their open-chain counterparts [192].

The aqueous formation constants for oxoanion association with these cryptands, determined by pH potentiometry and/or NMR, and single crystals X-ray analysis provide evidence for encapsulation. The extractabilities could not be explained solely on the basis of ligand lipophilicity; the level of protonation also plays an important role of the cryptand are involved in direct H-bonding to the anion. Also, as in many oxoanion structures examined, some of the shortest H-bonds involve the few molecules of hydrate water retained by the anion, which presumably have more freedom to position themselves for most efficient H-bonding. These often act as bridges between an oxoanion and a protonated amino group. The larger size and hence tighter cavity fit of the perrhenate may partly explain the higher stability of the perrhenate complexes (i.e. for $[H_6\text{-}\mathbf{167}]^{6+}$ encapsulation of $[ReO_4]^-$, $\log K = 3.71$ and of $[ClO_4]^-$, $\log K = 3.24$) and thus suggest that the oxoanion is retained in the host cavity in solution [192].

Competition between perchlorate and perrhenate for the cavity site, by altering the stoichiometric ratio used in synthesis was investigated. Single crystals isolated from solutions of 0.001 M $[H_6\text{-}\mathbf{167}](ClO_4)_6$ with ratios of added $KReO_4$ between 1:1 and 1:6 were examined by X-ray crystallography. The perrhenate ion was always found in the cavity site although varying amounts of perchlorate, in response to stoichiometry, were present in the complex. The structure of the cation thus remained unchanged as the stoichiometric ratio altered, only the distribution of the counter ions varying [192].

X-ray crystallographic structure determinations were attempted on a number of perrhenate complexes of **167** and the pyridine-spaced **171a**, hosts at the hexa-protonated level. In the presence of excess perrhenate ion crystals of $[(H_6\text{-}\mathbf{167})(ReO_4)](ReO_4)_5\cdot 5H_2O$ were isolated from ethanol (Fig. 143). The $[(H_6\text{-}\mathbf{167})(ReO_4)]^{5+}$ cation is not dramatically different from that of the perchlorate analogue, although the symmetry of the anion site is lower. The included anion is tethered by a similar mix of direct $NH^+\text{-}O^-$ and indirect (water-mediated) H-bonds. There are also H-bonds directed

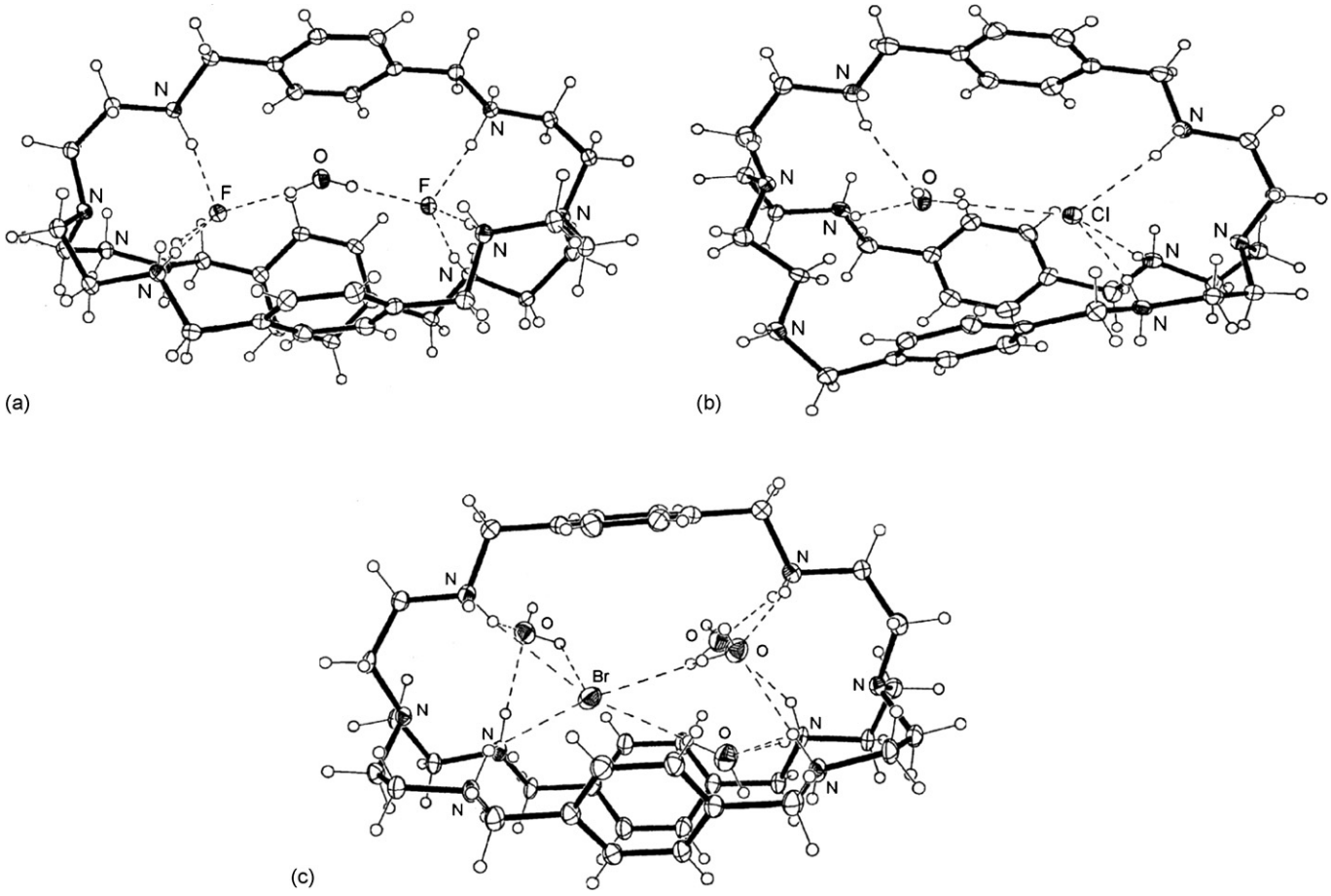

Fig. 141. Structure of $[(H_6\text{-}\mathbf{165})(F)_2(H_2O)]^{4+}$ (a), $[(H_6\text{-}\mathbf{165})(Cl)(H_2O)]^{5+}$ (b) and. $[(H_6\text{-}\mathbf{165})(Br)]^{5+}$ (c).

to anions held outside the cryptand cavity. As in the case of the perchlorate structure, one of the oxoanion atoms, pointing in the direction of the bridgehead nitrogen, is not involved in H-bonding. However, unlike the perchlorate structure, NH^+ donors from both ends of the cryptand are involved in direct H-bonding to the anion. Also, as in many oxoanion structures examined, some of the shortest H-bonds involve the few molecules of hydrate water retained by the anion, which presumably have more freedom to position themselves for most efficient H-bonding. These often act as bridges between an oxoanion and a protonated amino group. The larger size and hence tighter cavity fit of the perrhenate anion may partly explain the higher stability of the perrhenate complexes (i.e. for $[H_6\text{-}\mathbf{167}]^{6+}$ encapsulation of ReO_4^-, $\log K = 3.71$ and of ClO_4^-, $\log K = 3.24$) and thus suggest that the oxoanion is retained in the host cavity in solution (Fig. 143) [192].

In contrast in $\{(H_6\text{-}\mathbf{171a})(ReO_4)_6\cdot(H_6\text{-}\mathbf{171a})(ReO_4)_4(ClO_4)_2\cdot 3H_2O\}$ the oxoanion is not encapsulated within the cavity in the pyridine-spaced system. The host acts as a cleft rather than cavity binder, retaining three perrhenate anions in each of the clefts formed between arms of the cryptand in the relatively open host conformation adopted. This applies to both of the unique cations in the unit cell. In solution, however, no evidence for a 1:3 cryptand:ReO_4^- species was found; the 1:1 model provides a good fit to the NMR experimental data [192].

The extraction behaviour of the cryptands **166**···**171** and of the open-chain counterparts **172**···**179** toward pertechnetate and/or perrhenate was studied using the extraction system: $NaTcO_4$ or $NaReO_4$-buffer-H_2O/organic ligand-$CHCl_3$ at pH ≅ 7.4 and at a concentration of 10^{-3} M for the organic ligand and 10^{-4} M for the oxoamines, shows the more lipophilic TcO_4^- is slightly more extended then ReO_4^-.

Generally, the extractabilities for the aminocryptands are rather limited under the selected conditions, but a small increase could be found in the order **165** < **171a** < **169** ≈ < **168b** < **170** < **171b**. In all cases the methylated derivatives lead to a significantly better extraction as compared to the unsubstituted analogues. The highest extraction was observed for the pyridine spaced hexamethylated aminocage **171b**. Amazingly, within the series of tripodal tren derivatives there are pronounced differences in the extraction properties; in some cases these are enhanced, and in other cases diminished, relative to the cages. The ligands **177**, **175** and **178** give extractabilities between 16% and 26% for TcO_4^- which is comparable with the cages. In contrast, the tris-(2-naphthyl) substituted ligand **177** extracts pertechnetate with the highest efficiency of all the examinated compounds, whereas **174**, **176** and **179** show only a very weak tendency to transport this oxoanion into the organic phase.

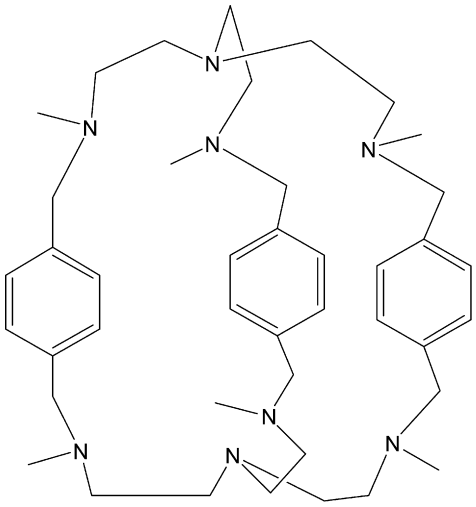

168

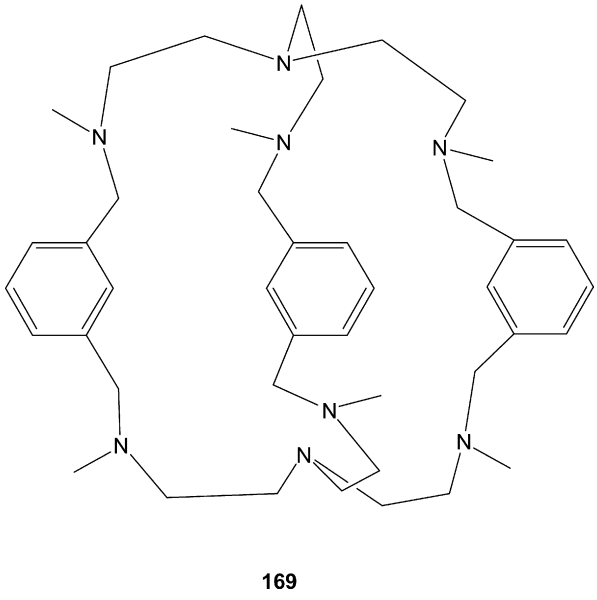

169

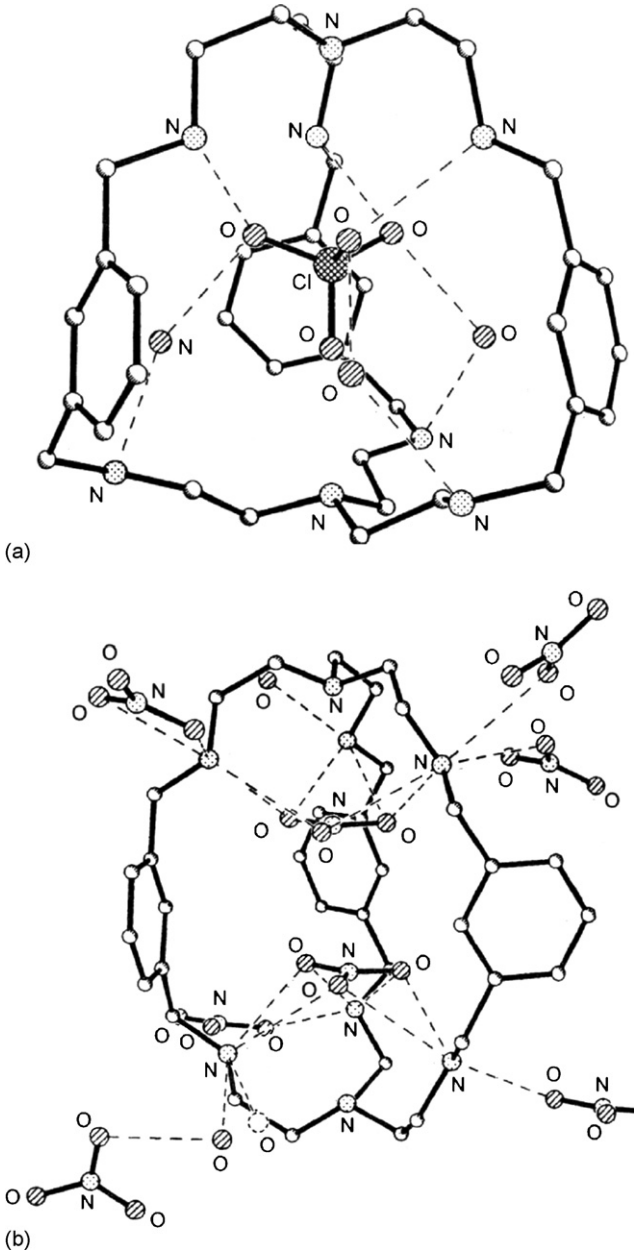

(a)

(b)

Fig. 142. Structure of $[(H_6\text{-}\mathbf{167})(ClO_4)]^{5+}$ (a) and $[(H_6\text{-}\mathbf{167})(NO_3)](NO_3)_4\cdot 2H_2O$ (b).

With increasing pH, the extractabilities of **171a**, **171b** and **175** increase. The maximum extraction is reached between pHs 7 and 8, then decreases with increasing basic conditions in solution. This trend is in agreement with the changing protonation state of the ligands. At lower pH values the ligands will be more highly protonated, and thus more hydrophilic, leading to a decrease in the extraction ability from the aqueous into the organic phase. The higher extractabilities of **171b**, as compared to **171a** at pH 7.4, are consistent with the formation of more hydrophobic species for **171b**. As expected, these results support the interpretation that the aqueous-organic phase transfer is more favoured in the case of less highly charged cryptand–anion complex species, despite their lower formation constants in aqueous solution.

Generally, the effect of pH on the perrhenate extraction by the tripodal tren derivatives is less pronounced than in the case of the cages, as illustrated by ligand **173**. The reasons for this behaviour arise from both the lower number of protonation steps, and the smaller differences in the protonation constants. Obviously, this behaviour does not strongly depend on the number and nature of the substituents.

To gain more information about the gradation of extractant lipophilicity, distribution measurements of the ligands have been performed between aqueous buffer solution (pH 7.4) and 1-octanol. The orders of increasing lipophilicity obtained for the cages are $\mathbf{171a} \approx \mathbf{171b} < \mathbf{165} < \mathbf{170} < \mathbf{169}$ and for the tripodal counterparts $\mathbf{174} < \mathbf{173} < \mathbf{172} < \mathbf{177} \approx \mathbf{178} \approx \mathbf{179}$. It is interesting to note that although the lowest lipophilicities were found for all the pyridine containing compounds, these ligands usually provide good extractabilities. In the case of the benzyl-2-naphthyl-

and biphenyl-substituted tren derivatives, although these compounds are fully located in the 1-octanol phase, they exhibit a range of extraction efficiencies. One conclusion to be drawn from these studies is that the extraction ability of the investigated ligand cannot be explained solely on the basis of lipophilicity.

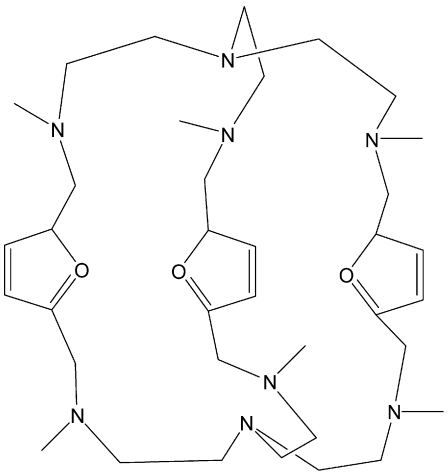

170

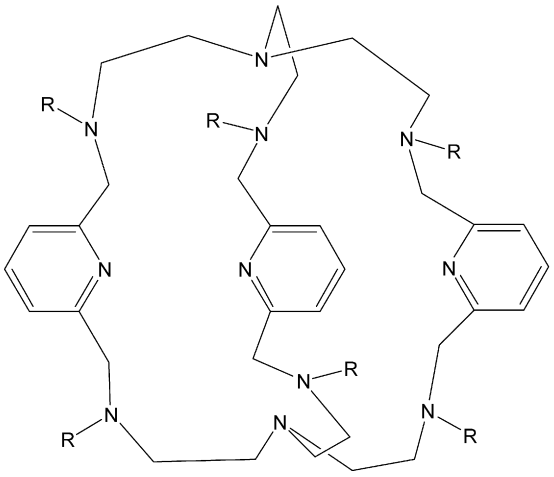

	R
171a	H
171b	CH_3

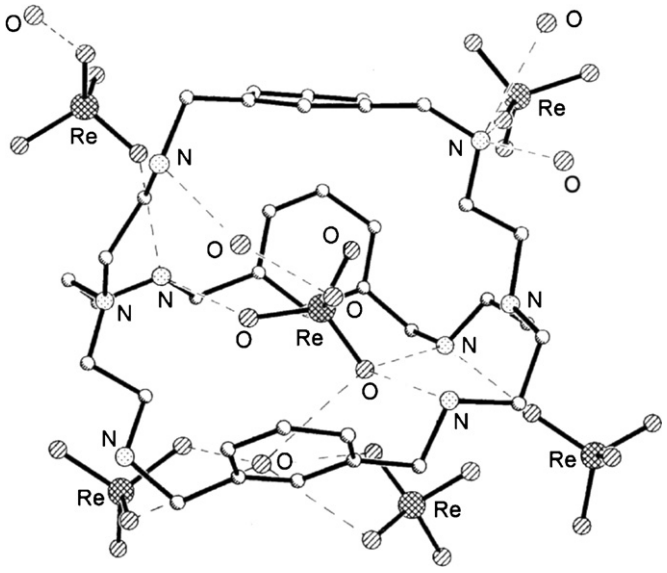

Fig. 143. Structure of $\{[(H_6\text{-}\mathbf{167})(ReO_4)](ReO_4)_5\}$.

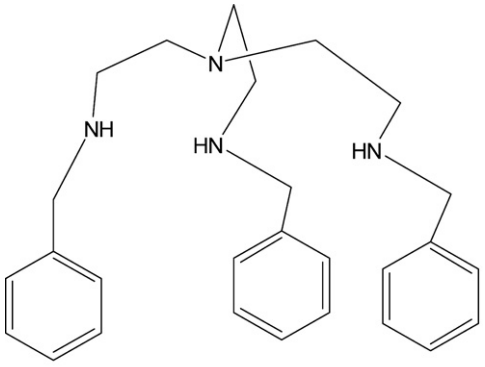

172

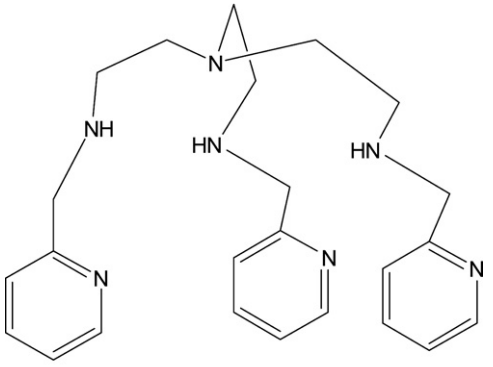

173

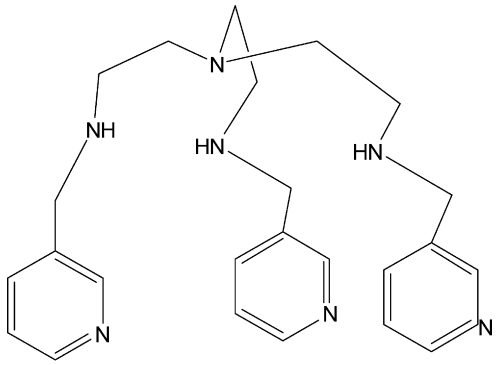

174

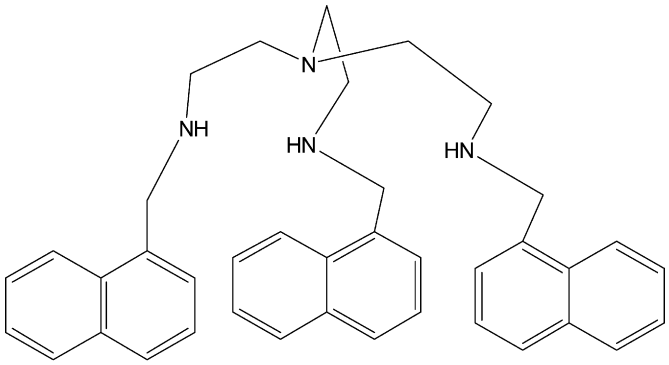

176

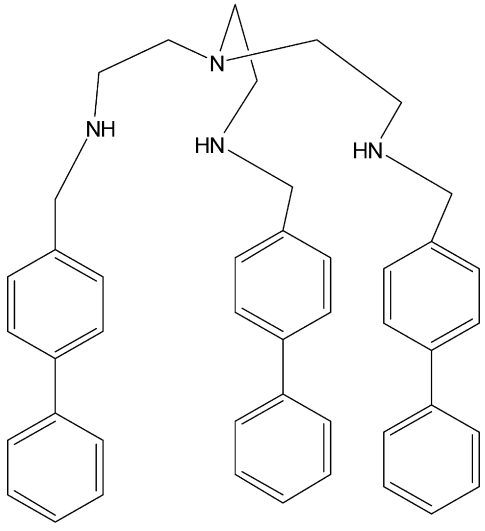

175

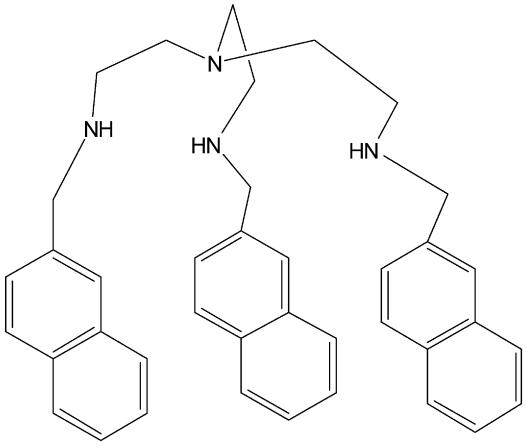

177

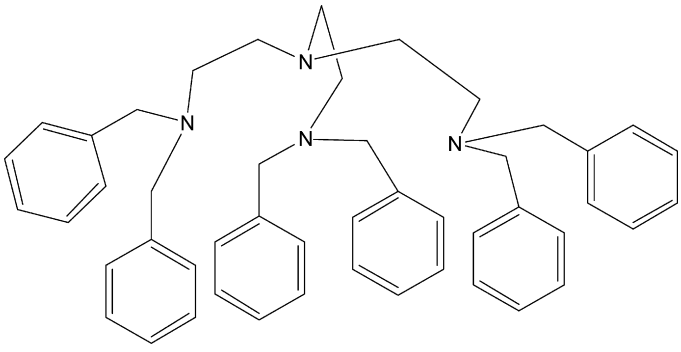

178

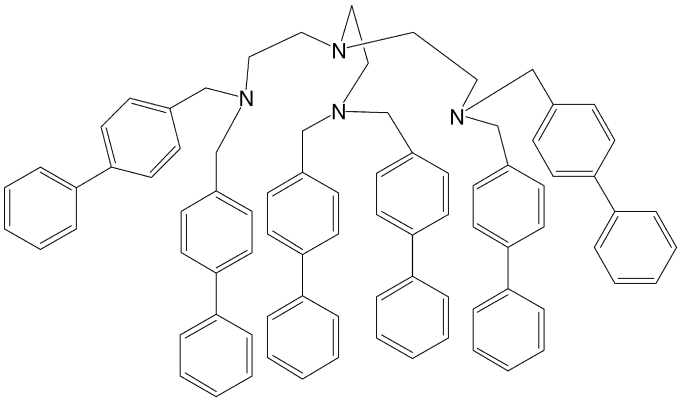

179

The results, with the open ligands, reveal an essentially linear relationship between the distribution ratio, *D*, and the ligand concentration (pH 7.4, ligand excess). The slopes of the lines in the diagram are unity, indicating a 1:1 complex composition. Similar results were obtained for the remaining' compounds. Loading experiments of the organic extracts with perrhenate for 1×10^{-3} M ligand solutions at pH 7.4 give maximum, ligand to anion ratios of up to 1:3 of the species transferred into the organic phase [192].

The cascade carbonate complexes $[M_2(\mathbf{L})(CO_3)](ClO_4)_2{\cdot}nS$ (**L** = **166**, **167**) were generated directly by treatment of the free cryptand with the appropriate cation salt and bridging anion in appropriate stoichiometry. Direct treatment of an ethanolic solution of **167** and metal salt in 1:2 stoichiometry with 1 equiv. of anion followed by recrystallization from acetonitrile led to isolation of the μ-carbonato complex, while the outcome of such treatment in a methanol solvent led instead to isolation of a η_1,η_1,μ-methylcarbonate derivative. However, with **166** the nature of the complex isolated did not depend on the solvent used: μ-carbonato cryptates were obtained with dicobalt, dinickel and dizinc systems in both ethanol and methanol solvents [193].

Structures of bridged carbonato cryptates were obtained for dicopper(II), dinickel(II), dizinc(II) and dicobalt(II) complexes, in the last case for both **166** and **167** ligands. With all four cations, the oxo-anion bridges (via at least two of the oxygen donors) the encapsulated cations which are also coordinated by the three secondary amino donors and the tertiary nitrogen bridgehead of the host. Other conditions were not identical however, as cation coordination number alters across the series together with the mode of bridging. The *anti–anti* η_1,η_1 mode B (Scheme 13) was adopted in $[Cu_2(\mathbf{167})(CO_3)](ClO_4)_2{\cdot}2H_2O$ and $[Ni_2(\mathbf{167})(CO_3)](ClO_4)_2{\cdot}2H_2O{\cdot}CH_3OH$, while the strategies used by cobalt in $[Co_2(\mathbf{167})(CO_3)](ClO_4)_2{\cdot}2H_2O$ and $[Co_2(\mathbf{167})(CO_3)](ClO_4)_2$ were more complex, also involving the third carbonate oxygen donor in coordination with utilization of modes D and E. However, it should be noted that even in $[Cu_2(\mathbf{167})(CO_3)](ClO_4)_2{\cdot}2H_2O$ and $[Ni_2(\mathbf{167})(CO_3)](ClO_4)_2{\cdot}2H_2O{\cdot}CH_3OH$ where cation coordination is restricted to two of the three carbonated oxygen donors, the third carbonate oxygen is engaged in hydrogen bonding to solvate molecules [193].

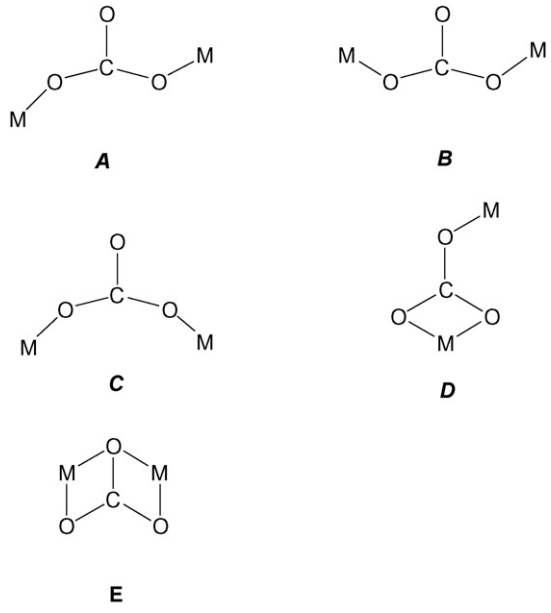

Scheme 13. Different coordination modes of the CO_3^{2-} anion.

The only case, where a *syn–anti* η_1,η_1 mode A bridged carbonate derivative is isolated, occurs in $[Zn_2(\mathbf{167})(CO_3)](ClO_4)_2$ obtainable when methanol is absent. Thus, all main modes of μ_2-carbonate bridging known to exist in isolation (i.e. excluding mode C which has so far been observed only as supporting bridge to another ligand such as μ-oxo or μ-hydroxo) are observed in this series of cryptates.

$[Cu_2(\mathbf{167})(CO_3)](ClO_4)_2{\cdot}2H_2O$, shows a trigonal bipyramidal site for both copper(II) ions, with the carbonate oxygen O-donor in the diaxial position, using the *anti–anti* bridging mode. One of the water molecules hydrogen-bonds the uncoordinated carbonate oxygens of a pair of cryptates, generating a hydrogen-bonded dimer held together by a pair of bridging water molecules. The intercryptate Cu···Cu distance is 6.785 Å compared with an intracryptate Cu···Cu separation of 5.791 Å (Fig. 144) [193].

$[Ni_2(\mathbf{167})(CO_3)(CH_3OH)_2](ClO_4)_2{\cdot}2H_2O$, exhibits the same *anti–anti* bridging mode as $[Cu_2(\mathbf{167})(CO_3)](ClO_4)_2{\cdot}2H_2O$, although each the nickel cations achieves the preferred six coordination by coordinating a methanol molecule. The uncoordinated oxygen donor of the carbonate bridge is hydrogen-bonded, to the methanol molecules. In contrast to the dicopper(II) analogue, the intramolecular nature of the hydrogen bonding leaves each nickel(II) cryptate magnetically isolated within the structure. The Ni···Ni internuclear separation (6.018 Å) is the longest in the series (Fig. 145) [193].

$[Co_2(\mathbf{167})(CO_3)](ClO_4)_2{\cdot}2H_2O$, effectively the dimer $[Co_2(\mathbf{167})(CO_3)][Co_2(\mathbf{167})(CO_3)(H_2O)_2](ClO_4)_4{\cdot}2H_2O$, crystallizes with two independent cations of different structure in the asymmetric unit. One cation exhibits the *anti–anti* μ-η_1,η_1, carbonato bridged structure seen in $[Cu_2(\mathbf{167})(CO_3)](ClO_4)_2{\cdot}2H_2O$ and $[Ni_2(\mathbf{196})(CO_3)](ClO_4)_2{\cdot}2H_2O{\cdot}CH_3OH$; as with the dinickel analogue the uncoordinated oxygen atom of the carbonate

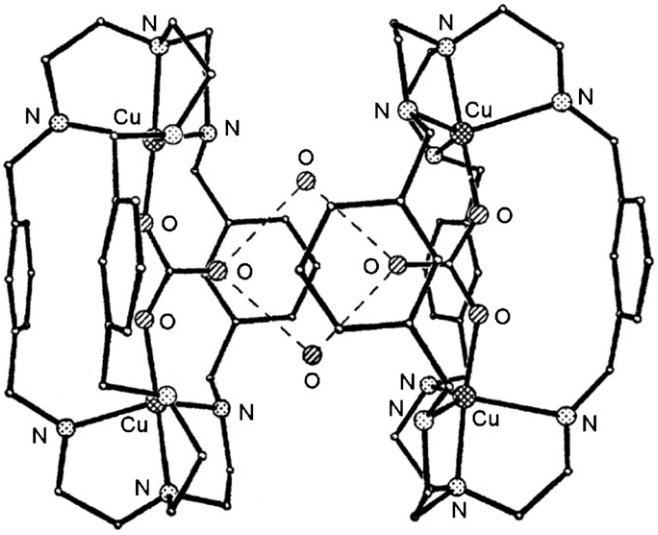

Fig. 144. Structure of $\{[Cu_2(\mathbf{167})(CO_3)]\cdot H_2O\}_2^{4+}$.

group is strongly hydrogen-bonded to two solvate molecules which are also weakly coordinated to the metal ions (Fig. 146a). The second cation shows the μ-η1,η2, variant in which all three carbonate oxygen donors are coordinated (Fig. 146b). One cobalt(II) ion is five coordinate with approximate trigonal bipyramidal geometry while cobalt(II) is six coordinate. A further consequence of the alteration in bonding mode is to bring the cobalt ions considerably closer together (Co···Co 5.939 Å, in one unit and Co···Co 5.129 Å in the other) [193].

$[Zn_2(\mathbf{167})(CO_3)](ClO_4)_2\cdot 6.5H_2O$ adopts the *syn–anti* mode, a structure intermediate between the two shown in $[Co_2(\mathbf{167})(CO_3)](ClO_4)_2\cdot 2H_2O$ (Fig. 147). This cryptate shows slightly larger M–O and M–$N_{bridgehead}$, distances than the mode B bridged carbonates, which may be due to the larger effective radius of the zinc(II) cation. The shorter internuclear M···M separation in $[Zn_2(\mathbf{167})(CO_3)](ClO_4)_2$ versus $[Co_2(\mathbf{167})(CO_3)][Co_2(\mathbf{167})(CO_3)(H_2O)_2](ClO_4)_4\cdot 2H_2O$ is a consequence of the alteration of the mode of carbonate binding [193].

$[Co_2(\mathbf{166})(CO_3)](ClO_4)_2\cdot 2H_2O$ (Fig. 148) uses a more radical approach to the challenge of utilising all three carbonate

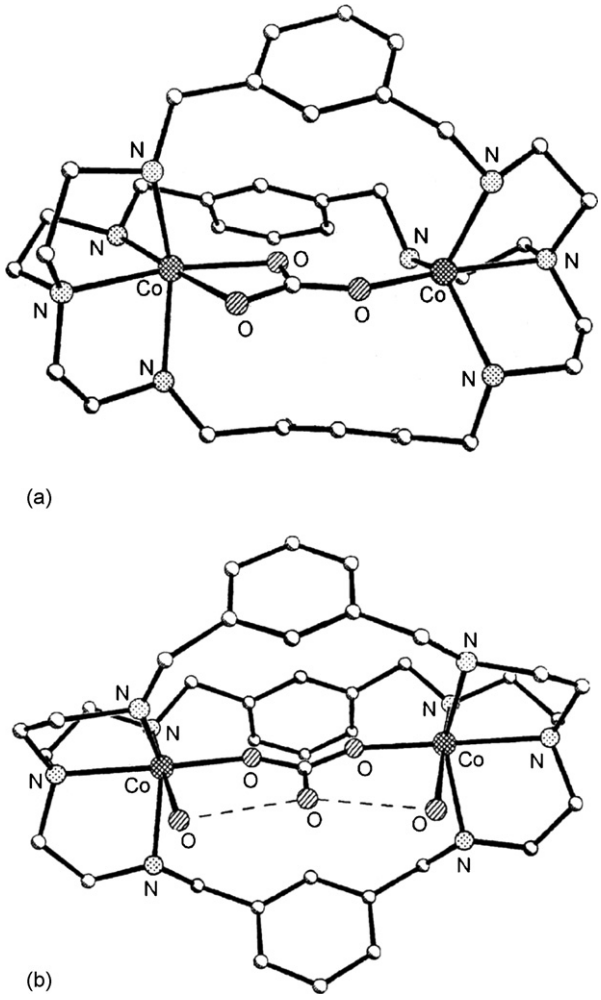

Fig. 146. Structure of the two independent cations $[Co_2(\mathbf{167})(CO_3)]^{2+}$ (a) and $[Co_2(\mathbf{167})(CO_3)(H_2O)_2]^{2+}$ (b) in $[Co_2(\mathbf{167})(CO_3)]$ $[Co_2(\mathbf{167})(CO_3)(H_2O)_2]\cdot(ClO_4)_2\cdot 2H_2O$.

oxygen donors by adopting μ-η2,η2 bridging mode. The Co···Co distance (4.292 Å) is markedly shorter than for any carbonato bridged complex of **167**. The shorter cavity in **166** encourages this more compact arrangement [193].

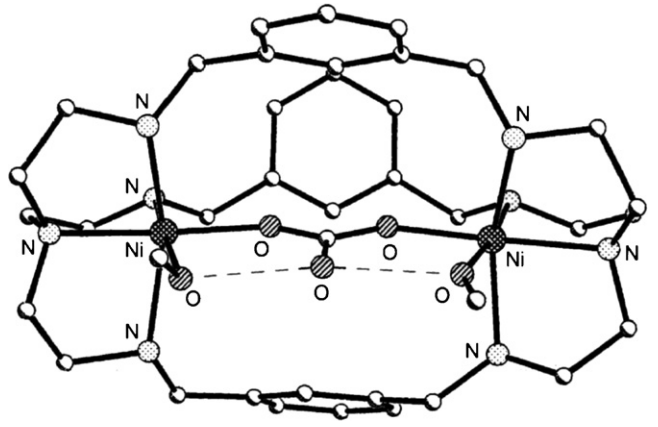

Fig. 145. Structure of $[Ni_2(\mathbf{167})(CO_3)(CH_3OH)_2]^{2+}$.

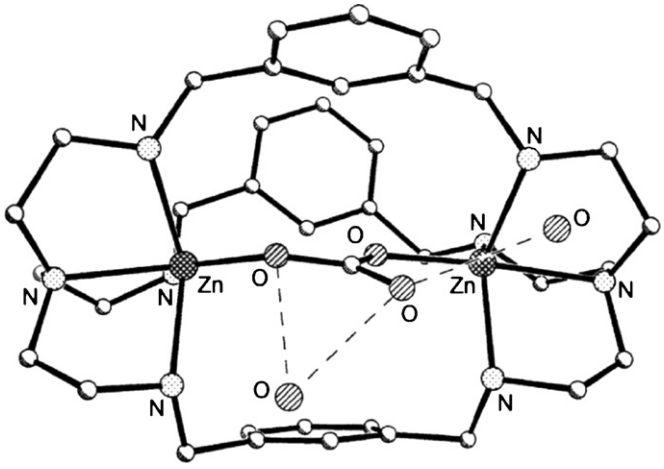

Fig. 147. Structure of $[Zn_2(\mathbf{167})(CO_3)]^{2+}$.

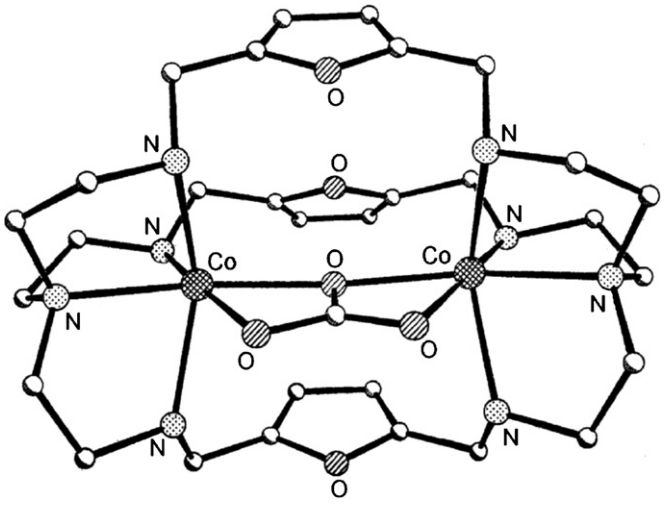

Fig. 148. Structure of $[Co_2(\mathbf{166})(CO_3)]^{2+}$.

The relatively high magnetic coupling constant observed in $[Ni_2(\mathbf{166})(CO_3)](ClO_4)_2$, which has not been structurally characterised, strongly suggests that the μ-η2,η2 bridging mode is also adopted in this cryptate. This is not surprising given the preference of the nickel(II) cation for six coordination. $[Zn_2(\mathbf{166})(CO_3)](ClO_4)_2$, also structurally uncharacterized, shows an IR spectrum similar to that of $[Ni_2(\mathbf{166})(CO_3)](ClO_4)_2$ and $[Co_2(\mathbf{167})(CO_3)](ClO_4)_2$ though with carbonate ν_3 IR absorption at somewhat lower frequencies (by 30–40 cm^{-1}), so its coordination mode is uncertain. The absence of solvation does suggest that all carbonate oxygen donors are utilized in coordination, possibly via an unsymmetric variant of mode E coordination. An attempt to generate the dicopper(II) carbonato-bridged cryptate of **166** by treatment of preformed carbonate with $[Cu_2(\mathbf{166})]^{2+}$ failed, yielding instead an impure sample of the linear μ-hydroxo bridged analogue. Overall, these results confirm the preference of **166** cryptates for monatomic or effectively monatomic bridging arrangements such as μ-η2,η2 [193].

All these structures show extensive hydrogen bonding through the lattice involving the cryptate amines, anions and solvate molecules.

The existence of B and D modes in the same crystal of $[Co_2(\mathbf{167})(CO_3)](ClO_4)_2\cdot 2H_2O$ suggests that no more than small energy differences exist between these bridging modes in the carbonate system.

The different coordination modes of the carbonate ligand, found in these dinuclear complexes (Scheme 13), show a range of ability to mediate magnetic exchange: modes A (weak antiferromagnetic to ferromagnetic), B (moderate to weak antiferromagnetic), D (weak antiferromagnetic) and E (strong antiferromagnetic).

As $[Cu_2(\mathbf{167})(CO_3)](ClO_4)_2\cdot 2H_2O$ and $[Ni_2(\mathbf{167})(CO_3)](ClO_4)_2\cdot 2H_2O\cdot CH_3OH$ and one pathway in $[Co_2(\mathbf{167})(CO_3)](ClO_4)_2\cdot 2H_2O$ utilize the *anti–anti* η1,η1, bridging mode B albeit with variation of coordination of the dinuclear carbonate moiety, this series may be compared with previous studies of this mode of bridging. Within the *anti–anti* η1,η1 bridging mode (B), magnetic exchange is observed to be weak in nickel complexes, and moderately antiferromagnetic in square-based copper complexes, where coupling constants in the range 120–140 cm^{-1} are observed. The trigonal bipyramidal coordination in $[Cu_2(\mathbf{167})(CO_3)](ClO_4)_2\cdot 2H_2O$ evidently presents a more efficient exchange pathway ($-2J \approx 200\ cm^{-1}$), resulting from favourable alignment of the magnetic d_z^2 orbital toward the a_2' carbonate molecular orbital. By contrast, the low J value of the dinickel complex $[Ni_2(\mathbf{167})(CO_3)](ClO_4)_2\cdot 2H_2O\cdot CH_3OH$ is in good agreement with previous studies of the *anti–anti* η1,η1 bridging mode ($J = -4.6\ cm^{-1}$) in nickel complexes, even though in $[Ni_2(\mathbf{167})(CO_3)](ClO_4)_2\cdot 2H_2O\cdot CH_3OH$ the intervention of hydrogen-bonded methanol may be expected to draw electron density from the carbonate bridge. It was assumed that mode B mediates the stronger of the two exchange paths in $[Co_2(\mathbf{167})(CO_3)](ClO_4)_2\cdot 2H_2O$. As expected, the J value ($-11\ cm^{-1}$) is considerably lower than that observed when a third oxygen of the carbonate provides an additional monatomic bridging pathway as in mode E, but no similar examples of mode B are known in cobalt complexes [193].

For the alternate mode D pathway of $[Co_2(\mathbf{167})(CO_3)](ClO_4)_2\cdot 2H_2O$, the interaction is as expected significantly lower, as the *syn–anti* component of the pathway is normally weak, sometimes even ferromagnetic in sense, leading to reduction or approximate cancellation of the *anti–anti* component [193].

The μ-η2,η2, mode E adopted in $[Ni_2(\mathbf{166})(CO_3)](ClO_4)_2$ and $[Co_2(\mathbf{166})(CO_3)](ClO_4)_2$ is normally associated with relatively strong interaction ($-J = 108$ and 30 cm^{-1}, respectively) [193].

Bridging methyl carbonates are generated catalytically upon exposure to atmospheric CO_2 of methanol solutions of the dinuclear transition metal cryptates with **167**, but not with **166** [193]. The two alternative procedures, used in the synthesis of these methylcarbonato derivatives, involve the treatment of a CH_3OH/CH_3CN solution of a 1:2 cryptand–cation mixture under aerobic conditions with one equivalent of preformed carbonate anion, HCO_3^- or CO_3^{2-} or the in situ reaction of the coordinated methoxo ligand with atmospheric CO_2. Identical products were obtained irrespective of whether procedure was employed [193].

Crystals of $[Cu_2(\mathbf{167})(CH_3OCOO)](ClO_4)_3\cdot 4H_2O$, $[Ni_2(\mathbf{167})(CH_3OCOO)](ClO_4)_3\cdot 4H_2O$ and $[Zn_2(\mathbf{167})(CH_3OCOO)](ClO_4)_3\cdot 2H_2O$, obtainable by both synthetic methods, show very similar structures, indicating a preference for the *syn–anti* μ-η1,η1, mode A (Fig. 149). The structure of the dicopper(II) is ordered while those of the dinickel and dizinc analogues show disorder of the methylcarbonate anion between the two equivalent *syn–anti* arrangements within the cavity. Given the similarity of the three cation structures, it is noteworthy that the metal···metal distance is significantly longer in the dizinc complex, $[Zn_2(\mathbf{167})(CH_3OCOO)](ClO_4)_3\cdot 2H_2O$ [193].

The CO_2 insertion reaction is relatively rapid for the dizinc and dicopper precursors; crystals of $[Cu_2(\mathbf{167})(CH_3OCOO)](ClO_4)_3\cdot 4H_2O$ and $[Zn_2(\mathbf{167})(CH_3OCOO)](ClO_4)_3\cdot 2H_2O$ may be isolated within hours standing in air while with the dicobalt and dinickel precursors more than 1 day is required for isolation of the

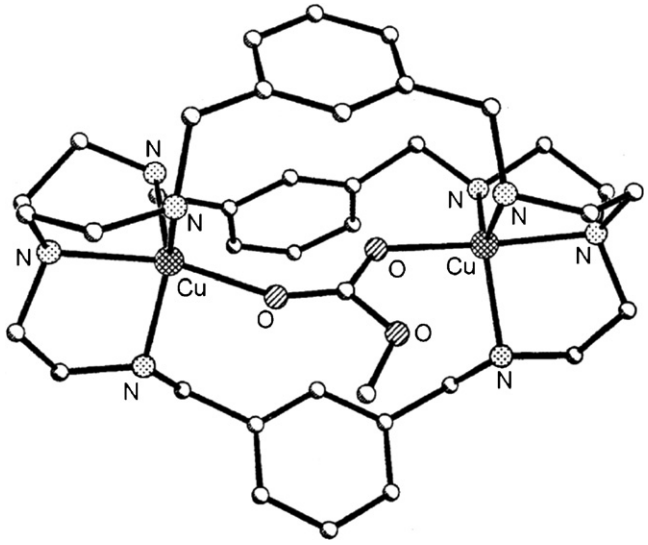

Fig. 149. Structure of $[Cu_2(\mathbf{167})(CH_3OCOO)]^{3+}$.

methylcarbonate product; in fact the mid blue crystals of $[Ni_2(\mathbf{167})(CH_3OCOO)](ClO_4)_3{\cdot}4H_2O$ are often to some extent contaminated with a paler by-product. Isolation of a CH_3OH solvate of a carbonato- rather than a methylcarbonato complex, when $[Ni_2(\mathbf{167})(CO_3)](ClO_4)_2{\cdot}2H_2O{\cdot}CH_3OH$ is recrystallized from CH_3CN/CH_3OH under aerobic conditions, indeed testifies to a relatively slow rate of CO_2 reaction with the nickel(II) complexes [193].

A mechanisms was proposed with an initial coordination of solvent methanol which deprotonates, followed by nucleophilic attack of coordinated methoxo on CO_2; effectively an insertion of CO_2 into the M–OCH_3 bond. **167** (in comparison with **166**) is particularly effective in promoting this reaction. Within the **166** system, with its shorter cavity, ready encapsulation of η_2-hydroxo was demonstrated as tightly coordinated bridge; formation of an analogous, μ_2-alkoxo complex presumably terminates the catalytic cycle by blocking the insertion reaction. Transient monodentate coordination of alkoxo within the longer **167** cavity on the other hand seems a feasible option, presenting a viable route to methyl carbonate formation. The fact that the strongest Lewis acid zinc(II) ion is much the most effective cation in the catalytic process supports the hypothesis of methanol deprotonation as the rate-determining step [193].

No evidence has been obtained for CH_3OCOO^- generation via CO_2 uptake by dinuclear assemblies held within the **166** host. When a nickel salt was allowed to stand in air over several days with the stoichiometric amount of cryptand in CH_3OH/CH_3CN solution, no crystallization of, μ-methylcarbonato or μ-carbonato cryptate was observed, but crystallization of $[Ni_2(\mathbf{166})(CO_3)](ClO_4)_2$ ensued in good yield within hours of the addition of a stoichiometric amount of preformed carbonate ion.

Although there are no previous reports of magnetic exchange in *syn–anti* μ-η_1,η_1, methyl carbonates, the intradimer interaction was prediction to be weak. Comparison may be made with the behaviour of *syn–anti* carboxylate bridged systems, which have been studied in cluster and polymeric compounds involving square pyramidal copper. These usually exhibit ferromagnetic coupling, although weak antiferromagnetic coupling has also been observed in a few instances. In the series $[Cu_2(\mathbf{167})(CH_3OCOO)](ClO_4)_3{\cdot}4H_2O$, $[Ni_2(\mathbf{167})(CH_3OCOO)](ClO_4)_3{\cdot}4H_2O$ and $[Co_2(\mathbf{167})(CH_3OCOO)](ClO_4)_3{\cdot}4H_2O$ exchange coupling is weak. It appears that small changes in geometry are crucial in determining the magnitude of the interaction in this mode of bridging. The structure of $[Co_2(\mathbf{167})(CH_3OCOO)](ClO_4)_3{\cdot}4H_2O$ was not determined, but according to its magnetic behaviour, this complex has a similar bridging geometry to $[Cu_2(\mathbf{167})(CH_3OCOO)](ClO_4)_3{\cdot}4H_2O$ [193].

The reaction of $[Cu_2(\mathbf{167})](ClO_4)_2$, prepared in situ by the preformed macrobicyclic ligand **167** and $Cu(ClO_4)_2{\cdot}6H_2O$ [194], with an excess of calcium cyanamide (CaNCN) and sodium dicyanamide ($Na[N(CN)_2]$) in CH_3CN/C_2H_5OH results in the dinuclear compounds $[Cu_2(\mathbf{167})(HNCN)](ClO_4)_3$ and $[Cu_2(\mathbf{167})\{N(CN)_2\}](ClO_4)_3{\cdot}4H_2O$. The affinity of the dicopper(II) ions for additional ligation is shown in the ready acquisition of bridging hydrogencyanamido $(HNCN)^-$ or dicyanamido $(NCNCN)^-$ ligands in a heterogeneous reaction between calcium cyanamide and a solution of the dicopper(II) cryptate $[Cu_2(\mathbf{167})]^{4+}$ [195].

The same reaction using $Cu(CF_3SO_3)_2$ instead of $Cu(ClO_4)_2{\cdot}6H_2O$ affords $[Cu_2(\mathbf{167})(NCNCONH_2)](CF_3SO_3)_3{\cdot}0.5C_2H_5OH{\cdot}0.5H_2O$. The catalytic hydration of a nitrile to an amide functional group is assumed responsible for the formation of this complex from the $\mu_{1,3}$-dicyanamido ligand. [195].

The structure of crystals $[Cu_2(\mathbf{167})](HNCN)](ClO_4)_3{\cdot}CH_3CN{\cdot}CH_3OH$, grown by vapor diffusion of CH_3OH into a solution of the perchlorate salt of the copper(II) cryptate cyanamide complex in CH_3CN, confirms that the cation contains a Cu-NCN–Cu bridge with different Cu–N–C angles. Both copper(II) ions are five coordinate, one in approximately square pyramidal geometry and the other centering a near-regular trigonal bipyramid. The bridging link is well localized, with one short and one long bond. The nitrogen atom involved in the shorter bond coordinates the copper(II) ion in the trigonal bipyramidal environment and that involved in the longer one the copper(II) ion in the irregular square pyramidal environment. The proton of the cyanamido bridge makes a weak N–H···O(ClO_3) hydrogen bond. The overall distance between the paramagnetic centers (6.024 Å) compares well with that in the azido analogue (6.027 Å) as do the relatively short Cu–N distances. The overall conformation of the cryptate, a parallel disposition of two of the xylyl rings with the third lying mutually perpendicular, is also similar to that found in the azido systems. There are some longish intermolecular π–π contacts, as found in the analogous azido-bridged cryptates. All of the cryptand amino protons are involved in weak hydrogen-bonding interactions with anions or with anions or solvate molecules (Fig. 150) [195].

In $[Cu_2(\mathbf{167})(NCNCONH_2)](CF_3SO_3)_3{\cdot}0.5C_2H_5OH{\cdot}0.5H_2O$ the structure of the cation demonstrates the consequences of bridge asymmetry, in that one copper(II) ion is near five coordinate square pyramidal, while the other approaches

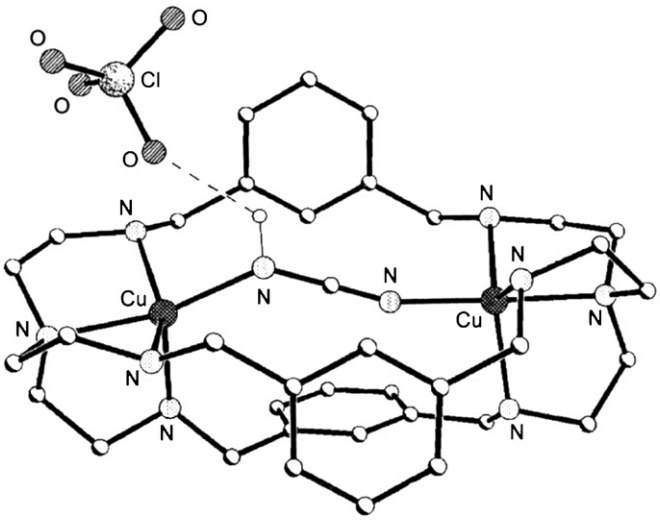

Fig. 150. Structure of $\{Cu_2(\mathbf{167})[(HNCN)](ClO_4)\}^{2+}$.

six coordinate geometry, following hemi-coordination of the amidic oxygen atom. As before the shortest Cu–N distances are those involving the 1,3-cyanamido bridge, which again shows localized bonding: one short (approximately single) bond within the 1,3-bridging entity. The irregular six coordinate site involves the effectively singly bonded C–N donor, which makes the smaller (120°) C–N–Cu bridge angle. The cyanamide link is thus less colinear with respect to the pair of copper(II) ions than the HNCN-bridge. The Cu···Cu separation is 6.133 Å. As usual in this cryptand system, there are intermolecular π–π contacts (Fig. 151) [195].

The magnetic susceptibility measurements of $[Cu_2(\mathbf{167})(HNCN)](ClO_4)_3{\cdot}CH_3CN{\cdot}CH_3OH$ in the 2–300 K show a ferromagnetic coupling ($J = 19.3\,cm^{-1}$), confirmed by the ESR spectrum of which ascertains the existence of a triplet ground state in the range 4–298 K for the polycrystalline solid [195].

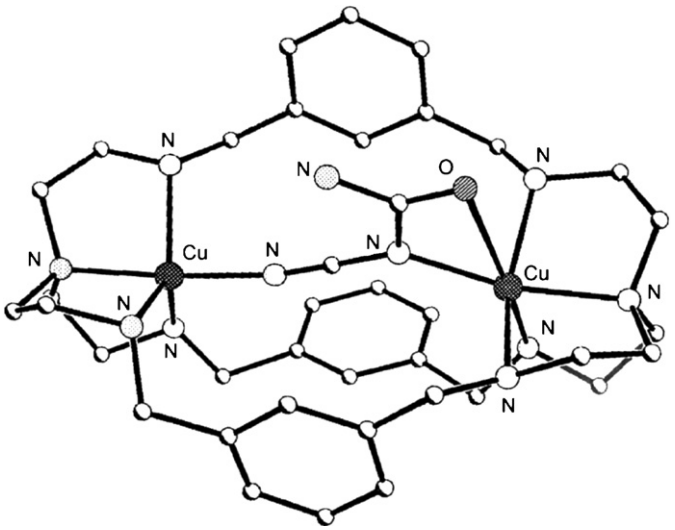

Fig. 151. Structure of $[Cu_2(\mathbf{167})(NCNCONH_2)]^{3+}$.

Also in $[Cu_2(\mathbf{167})\{N(CN)_2\})](ClO_4)_3{\cdot}4H_2O$ and $[Cu_2(\mathbf{167})(NCNCONH_2)](CF_3SO_3)_2{\cdot}0.5C_2H_5OH{\cdot}0.5H_2O$ a moderate ferromagnetic coupling occurs ($J = 9.9$ and $7.5\,cm^{-1}$, respectively) [195]. The X band ESR spectrum of $[Cu_2(\mathbf{167})(NCNCONH_2)](CF_3SO_3)_2{\cdot}0.5C_2H_5OH{\cdot}0.5H_2O$ exhibits sharper signals than that of $[Cu_2(\mathbf{167})(HNCN)](ClO_4)_3{\cdot}CH_3CN{\cdot}CH_3OH$ and provides confirmation of a triplet ground state configuration. The calculated J values, by using theoretical methods based on density functional theory are in excellent agreement with the experimental data [195].

An acetonitrile solution of $[Cu_2(\mathbf{165})](ClO_4)_4$, allowed to evaporate slowly at room temperature, was reported to form $[Cu_2(\mathbf{165})(CN)](ClO_4)_3{\cdot}2CH_3CN{\cdot}4H_2O$. An X-ray crystallographic analysis reveals that the two copper(II) ions in **165** are bridged by a cyanide anion. Each copper(II) ion is five coordinate with a slightly distorted trigonal bipyramid geometry, in which one copper ion is coordinated with four nitrogen atoms on one side of **165** and one bridged cyanide nitrogen atom, while the other copper ion is coordinated with four nitrogen atoms from the other side of **165** and one bridged cyanide carbon atom. The two bridgehead nitrogen atoms, two copper(II) ions, and cyanide anion are almost collinear [196].

The electronic spectra of $[Cu_2(\mathbf{165})](ClO_4)_4$ and $[Cu_2(\mathbf{165})(CN)](ClO_4)_3{\cdot}2CH_3CN{\cdot}4H_2O$ show bands at 699 nm in dimethylformamide and 887 nm in acetonitrile, respectively, indicating that the geometry of copper(II) is a compressed tetrahedral in $[Cu_2(\mathbf{165})](ClO_4)_4$, and a trigonal bipyramidal in the $[Cu_2(\mathbf{165})(CN)](ClO_4)_3{\cdot}2CH_3CN{\cdot}4H_2O$ [196].

When KCN solid is added to a acetonitrile solution of $[Cu_2(\mathbf{165})](ClO_4)_4$, the color of the solution changes quickly from blue to emerald green, and the maximum absorption band of the solution coincides with that for $[Cu_2(\mathbf{165})(CN)](ClO_4)_3{\cdot}2CH_3CN{\cdot}4H_2O$, indicating that the cyanide bridged dinuclear copper(II) complex forms very quickly [196].

Formation of the cyanide bridged dinuclear copper complex in acetonitrile was also confirmed by ESI-mass spectrometry. Initially, an acetonitrile solution of $[Cu_2(\mathbf{165})](ClO_4)_4$ shows three peaks due to $[Cu_2(\mathbf{165})]^{3+}$, $[Cu_2(\mathbf{165})]^{2+}$, and $[Cu_2(\mathbf{165})(ClO_4)]^{+}$. After the solution was heated at 50 °C in a sealed tube for 1 day, the above three peaks are not observed, and three new signals attributed to $[Cu_2(\mathbf{165})(CN)]^{3+}$, $[Cu_2(\mathbf{165})(CN)]^{+}$, and $[H\text{-}\mathbf{165}]^{+}$ are observed. The appearance of $[H\text{-}\mathbf{165}]^{+}$ is probably due to the reduction of copper(II) ion to copper metal during the ionization process.

The cleavage reaction involves the C–C bond activation of acetonitrile, and GC spectra in acetonitrile solution indicate that methanol is formed when an acetonitrile solution of $[Cu_2(\mathbf{165})](ClO_4)_4$ was left at room temperature in a sealed tube for 1 day. This experiment demonstrates that methanol is produced during the cleavage reaction of $[Cu_2(\mathbf{165})](ClO_4)_4$ with acetonitrile [196].

On the basis of the above experimental results, a likely cleavage mechanism was proposal where the nitrogen atom

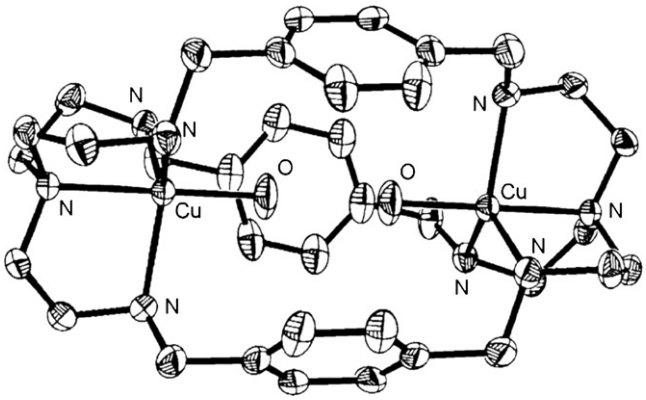

Fig. 152. Structure of $[Cu_2(\mathbf{165})(H_2O)(OH)]^{3+}$.

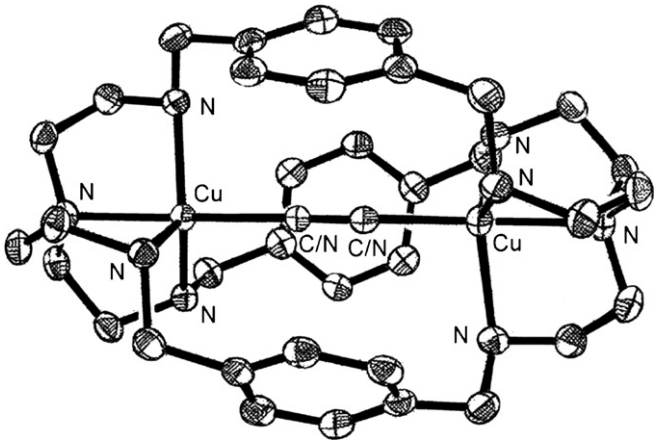

Fig. 153. Structure of $[Cu_2(\mathbf{165})(CN)]^{3+}$.

of acetonitrile binds to one copper(II) ion through its electron pair, and the other copper(II) ion interacts with the filled π orbital of the sp-hybridized acetonitrile carbon, resulting in electron flow from the π bond to the copper(II) ion, and this increases the leaving ability of cyanide and the electrophilicity of the methyl carbon, and results in cleavage by water to form methanol and cyanide bridged complex $[Cu_2(\mathbf{165})(CN)](ClO_4)_3{\cdot}2CH_3CN{\cdot}4H_2O$. The reaction rates become larger along with the increasing concentrations of water [196].

Under similar reaction conditions, there is no reaction between $[Cu(tren)](ClO_4)_2$ and acetonitrile; this is a clear demonstration that the activation of the C–C bond of acetonitrile is due to the favourable formation of a stable cyanide bridged dinuclear copper(II) cryptate. Preliminary results indicate that $[Cu_2(\mathbf{165})](ClO_4)_4$ can also cleave the C–C bond of benzonitrile at room temperature to produce phenol and the cyanide bridged complex $[Cu_2(\mathbf{165})(CN)](ClO_4)_3$. The cleavage rate for benzonitrile is much faster than that for acetonitrile as the cleavage reaction appears instantaneous upon mixing $[Cu_2(\mathbf{165})](ClO_4)_4$ and benzonitrile as assessed by ESI-mass spectra [196].

More recently it was reported that a very similar procedure, i.e. an acetonitrile solution of the tetraperchlorate salt of the *p*-xylyl-spaced dicopper(II) cryptate $[Cu_2(\mathbf{165})](ClO_4)_4{\cdot}4H_2O$ allowed to evaporate slowly in air over several days separated a green polycrystalline solid from the originally blue solution. Hexagonal plates of $[Cu_2(\mathbf{165})(H_2O)(OH)](ClO_4)_3$ were obtained by ether diffusion into an acetonitrile solution of this solid, as confirmed by an X-ray diffraction investigation which reveals the two copper(II) ions inside the macrobicycle **165** are bridged by a $H_3O_2^-$ group forming a $\{Cu^{II}(OH)\cdots(H_2O)Cu^{II}\}^{3+}$ unit. This unit includes a remarkably short O···O separation (2.325 Å) due to the colinear {Cu(O)···(O)Cu} geometry arising from the constraints of a cryptand encapsulation. It was suggested that the $\{Cu(OH)\cdots(H_2O)Cu\}^{3+}$ unit comprises two Cu(OH) groups connected by a bridging H atom with a O–H–O angle of 157° (Fig. 152). The energetic barrier for H atom transfer between the two Cu–OH groups is estimated to be less than 4 kJ mol^{-1} [197].

During the experimental procedure no formation or even a trace of $[Cu_2(\mathbf{165})(CN)]^{3+}$ was found in the absence of added cyanide reagent. Thus, it was concluded that $[Cu_2(\mathbf{165})(H_2O(OH))](ClO_4)_3$ rather than $[Cu_2(\mathbf{165})\mu\text{-}CN)](ClO_4)_3$, claimed to derive from cleavage of the C–C bond of the acetonitrile solvent, is the product of acetonitrile recrystallization of the initially formed reaction product $[Cu_2(\mathbf{165})](ClO_4)_3$ [197].

The occurence of $[Cu_2(\mathbf{L})(CN)](ClO_4)_3{\cdot}nH_2O$ ($\mathbf{L}=\mathbf{165}\cdots\mathbf{167}$, $n=1$, 2) was recently ascertained [198]. These complexes have been prepared by the reaction in CH_3OH/CH_3CN of stoichiometric amounts of $[Cu_2(\mathbf{L})(CN)](ClO_4)$, synthesized in situ by missing of the appropriate cryptand **L** with $Cu(ClO_4)_2{\cdot}6H_2O$, with KCN. Crystals, suitable for X-ray diffractometric investigations, were obtained by recrystallization of the crude products from acetonitrile by diethylether diffusion. Crystals of $[Cu_2(\mathbf{166})(CN)](CF_3SO_3)_3{\cdot}3H_2O$ were obtained in a manner analogous to the perchlorate salt, substituting copper(II) triflate for copper(II) perchlorate [198].

In the case of the **165** system, use of a slight excess of cyanide together with long residence time in solution leads also to isolation of $[Cu_2(\mathbf{165})(CN)]_2[Cu_6(CN)_{12}]{\cdot}6C_2H_5OH{\cdot}2H_2O$ which incorporates the cyano-bridged dicopper(II) cation together with cyclic hexacopper(I) dodecacyano counteranion [198].

All these complexes exhibit a single ν_{CN} infrared band in the 2100–2200 cm^{-1} region, typical of a bridging cyano group. The green color of the cryptates arises from the presence of d–d absorptions in the 600–800 nm region, deriving from the trigonal bipyramidal coordination geometry of the copper(II) cations [198].

In each of the cryptate cations, i.e. $[Cu_2(\mathbf{165})(CN)]^{3+}$, $[Cu_2(\mathbf{166})(CN)]^{3+}$, $[Cu_2(\mathbf{167})(CN)]^{3+}$, the cyano bridge is accommodated axially within the cryptand host between the pair of copper(II) cations in an essentially collinear geometry. The coordination geometry around the copper(II) ions is close to a regular trigonal bipyramid in each case (Fig. 153) [198].

These μ-cyanodicopper(II) cryptates shows moderately strong antiferromagnetic interaction in the range $-2J=150$–$200\ cm^{-1}$, at the high end of the observed range for such assemblies. The lowest magnetic exchange coupling parameter is displayed where there is slight bending of the

$\{Cu^{II}(CN)Cu^{II}\}$ assembly, enforced by the constraints of cryptate encapsulation. Thermally accessible triplet EPR spectra are observed with zero-field splittings of the order of 0.13–0.14 cm^{-1}, confirming collinear ground-state d_z^2 orbitals for copper(II) ions, consistent with their trigonal-bipyramidal coordination geometries [198].

The binding tendencies of the thiophene-containing ligand **180** toward protons and copper(II) cations (**180**:Cu^{2+} = 1:2 molar ratio) were investigated in aqueous solution by means of potentiometric titration experiments. Three dicopper(II) species are present in the 5–12 pH range, i.e. $[Cu_2(\mathbf{180})]^{4+}$, $[Cu_2(\mathbf{180})(OH)]^{3+}$ and $[Cu_2(\mathbf{180})(OH)_2]^{2+}$. The formation of $[Cu_2(\mathbf{180})(OH)]^{3+}$ takes place with a pK_a of 6.06 for the water molecule subject to deprotonation, while the second hydroxy group forms with a pK_a of 7.75, this reflecting the diminished overall positive charge of the system. Slow evaporation of a solution buffered at pH 6.9 (where $[Cu_2(\mathbf{180})(OH)]^{3+}$ is prevalent) yielded a green microcrystalline powder which analyzed as $[Cu_2(\mathbf{180})(OH)](ClO_4)_3{\cdot}3H_2O$ [199].

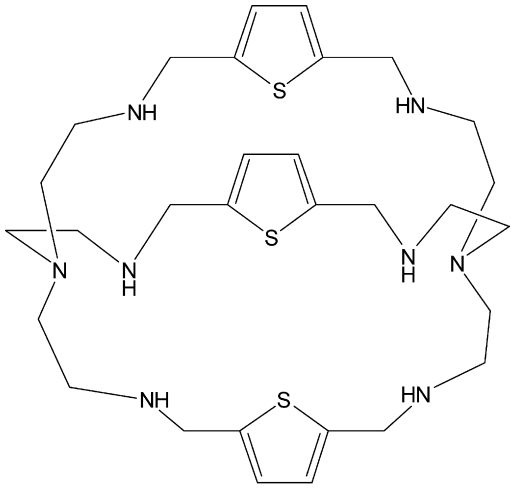

180

$[Cu_2(\mathbf{180})]^{4+}$ appears the most suitable complex to work as anion receptor as it has a void space in between the two copper ions. Unfortunately, $[Cu_2(\mathbf{180})]^{4+}$ reaches a maximum of only ~45% at pH 5.9, a pH at which large amounts of monometallic species exist ($[Cu(H\text{-}\mathbf{180})]^{3+}$, $[Cu(H_2\text{-}\mathbf{180})]^{4+}$ and $[Cu(H_3\text{-}\mathbf{180})]^{5+}$ represent the 10, 20 and 5%, respectively). Thus, to study the behaviour of the system made of **180** and the copper(II) ion in a 1:1 molar ratio, as a receptor for anions, pH 6.9 was chose: this is the lowest pH value at which no more monometallic species exist and, interestingly, it is also the value at which $[Cu_2(\mathbf{180})(OH)]^{3+}$ reaches its maximum abundance (~80%), thus representing the species prevailing by far in solution. Anions binding (A^-) has been studied on solutions of **180** + 2Cu^{2+} buffered at pH 6.9. Displacement of OH^- and binding of the chosen anion were followed by means of spectrophotometric titrations, by additions of substoichiometric quantities of A^-. The examined anions were N_3^-, NCO^-, NCS^-, Cl^-, Br^-, I^-, SO_4^{2-}, NO_3^-, HCO_3^- and CH_3COO^-. For N_3^-, NCO^- and NCS^-, the titration profile indicates

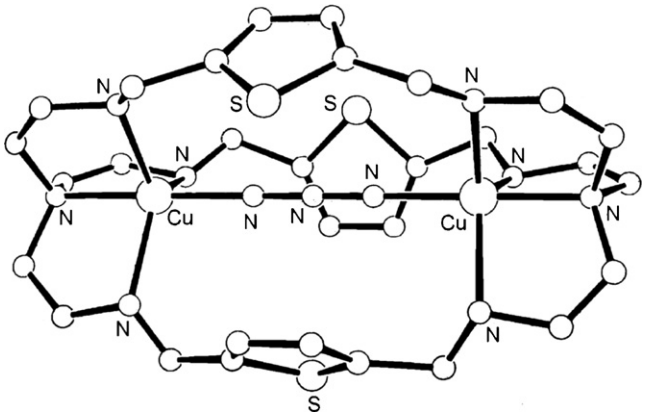

Fig. 154. Structure of $[Cu_2(\mathbf{180})(N_3)]^{3+}$.

that at $[Cu_2(\mathbf{180})(OH)]^{3+}$:anion 1:1 molar ratio the process is complete.

For these systems K_{obs} was determined, related to the constant of the displacement equilibrium by $K = K_{obs}[OH^-]$. A log K_{obs} value of 6.75 (±0.09) was determined for N_3^-, 4.79 (±0.07) for NCO^-, and 2.72 (±0.08) for NCS^-. SO_4^{2-}, NO_3^-, HCO_3^-, CH_3COO^-, Cl^-, Br^- and I^-, were instead not bound by the system or bound with log K_{obs} values $\ll 2$. This result is significantly different with what found with the analogous $\{Cu^{II}\text{-}(\mathbf{166})\text{-}Cu^{II}\}$ system [199], for which fairly high complexation constants were found also for monoatomic halide anions, which formed 1:1 complexes. To check if at any pH value halides may be bound by the dicopper complex of ligand **180**, spectra of the system $\{\mathbf{180}{:}2Cu^{2+}{:}10A^-\}$ (A^- = Cl, Br) were taken in the 2–12 pH range. However, halide binding does not take place at all [199].

The structure of crystals of $[Cu_2(\mathbf{180})(N_3)](ClO_4)_3$, obtained by slow evaporation of a solution containing **180**, copper(II) perchlorate and N_3^- in a 1:2:1 molar ratio buffered at pH 6.9 (Fig. 154), shows that the N_3^- anion is bridging the two copper(II) ions with an almost linear Cu–NNN–Cu geometry, since all the atoms lie on the threefold axis. The Cu···Cu distance is quite long (6.150 Å), if compared with 6.10 Å found for $[Cu_2(\mathbf{167})(N_3)]^{3+}$ or even better with 3.87 Å found for $[Cu_2(\mathbf{166})(Br)]^{3+}$ [199].

Possibly the dicopper(II) complexes of **180** cannot contract enough to bind monoatomic anions in an advantageous bridging mode, this suggesting an explanation for the striking difference of the $\{Cu^{II}(\mathbf{180})Cu^{II}\}$ system with respect to the $\{Cu^{II}(\mathbf{166})Cu^{II}\}$ one. Moreover, the increased length of the cage, coupled with a lack of a fixed Cu···Cu distance (as with **167**) results in the satisfactory binding of only those bidentate anions which display an intrinsically high affinity toward the copper(II) cation, coordinated by the tren unit [199–201].

4. Conclusion and future perspectives

The considerable number of papers published in the period of time considered (2002–2005) reveals the great interest toward the synthesis, characterization and possible applications of compartmental Schiff bases, their reduced homologues and the related homo- and/or heterodinuclear complexes.

In these years special effects have been devoted to the synthesis of cyclic polyamine derivatives, obtained by reduction of the related Schiff bases, by $NaBH_4$, $LiAlH_4$, etc., or by reductive demetalation of the related complexes. In these reactions the cyclic nature and coordination cavity of the Schiff bases are maintained also in the reduced polyamine derivatives. Hence, a comparison of the coordination ability of these more stable and flexible ligands with the related more rigid Schiff bases toward different metal ions (especially transition metal ions) was carried out.

The selective recognition processes at the two adjacent sites and the physico-chemical properties arising from the specific molecular aggregation deriving from these processes were investigated. In these studies a relevant role is played by the asymmetric compartmental ligands which, containing two different adjacent coordination chambers, allow different recognition processes. These different recognition processes allow the preparation of positionally pure, heterodinuclear complexes. Also symmetric compartmental macrocycles can give rise to heterodinuclear complexes, especially when the iminic nitrogens of one of the two chambers remains protonated. This protonation makes the two chambers no larger equal and favours the formation of mononuclear complexes which may be used as ligands for further heteronuclear complexation.

In the synthesis of these complexes the transmetalation reaction of suitable complex precursors has revaluated to be particularly useful, especially when the direct condensation of the appropriate formyl- and amine-precursors in the presence of the desired metal complexes failed.

Thus, some non-transition metal ions, as alkali (i.e. Na^+, K^+, Cs^+, Rb^+) or alkaline earth metal ions (i.e. Mg^{2+}, Ba^{2+}) or lead(II), reveal to be good templating agent in directing the condensation reaction toward the designed [1 + 1], [2 + 2], [3 + 3], [4 + 4], [3 + 2], etc., cyclic shape and contemporary convenient living ions, easily transmetalated by transition metal ion to give rise to the designed complexes not otherwise accessible. This synthetic pathway gives rise almost exclusively to homodinuclear complexes, although, under particular experimental conditions, mononuclear complexes have been obtained.

During these reactions, a ring contraction may occurs an ascertained for the reaction of the [4 + 4] complex $[Pb_2(\mathbf{107})](ClO_4)_2$ with transition metal ions, with the consequent formation of the smaller [2 + 2] macrocyclic complexes $[M_2(\mathbf{107})](ClO_4)_2$. Also the ring expansion form the [2 + 2] to the [4 + 4] cyclic complexes was observed for instance in the formation of the copper(II) or nickel(II) homo- and/or heteropolynuclear complexes with $[\mathbf{43}]^{4-}$, $[\mathbf{45}]^{4-}$ and $[\mathbf{105}]^{4-}$.

The asymmetric compartmental ligands, owing to the different coordinating properties of the two compartments can give rise to site migration of specific metal ions giving rise to positional isomers with different magnetic optical or electrochemical properties. These processes have been especially eluciated by X-ray diffractometry, magnetic, ESR, UV–vis and cyclic voltammetry measurements.

The formation and the stability of mixed-valent compounds was successfully studied especially by cyclic voltammetry. It was verified that, starting from appropriate homodinuclear $M^{II}{}_2$ complexes (M^{II} = Cu^{II}, Ni^{II}, Co^{II}), the mixed valent $M^{II}M^{I}$ reduced or $M^{III}M^{II}$ oxidized species can be stabilized and hence studied in a more appropriate detail.

Also the catalytic properties of homo- and heterodinuclear complexes toward oxidation of organic compounds (as substituted catechols) or hydrolysis of compounds of biological relevance was further successfully experimented.

The coordination ability of these cyclic receptions toward different metal ions and/or anion in protic or aprotic solvents was studies by potentiometric, calorimetric and spectrophotometric (UV–vis) methodologies, qualifying and quantifying the different species present at the different concentrations and pH values.

The evolution of the dinuclear systems into the polynuclear ones was pursued by different synthetic strategies. In particular appropriate precursors, capable to give rise to macrocycles larger than the [1 + 1] or the [2 + 2] ones, by multiple self-condensation quite often aided by the use of specific metal ions as templating agents, have been designed and synthesized.

Also bifunctional ligands, able to link two or more dinuclear complexes into a unique entity, have been used: in some case tetranuclear complexes, formed, in other cases ordered polymeric complexes. Furthermore, simple bridging groups (as –OH–Cl, etc.) have been employed as to link together dinuclear entities, allowing their evolution into species with higher nuclearities. The molecularity of these complexes was ascertained by X-ray structural determinations and the properties arising from these aggregations investigated especially by magnetic and ESR measurements.

Many efforts are currently in progress in order to assure the synthesis of ordered mono- or polydimensional systems, starting from the well know and fully characterized homo- and or heterodinuclear complexes. Also the use of appropriate cyclic compounds in selective activation, reactivity and catalysis and in unconventional transport and separation technology in under adequate scrutinity.

Finally, the interaction of these systems with appropriate surface, for instance the anchorage of Schiff base appropriately functionalized at the periphery of the coordination moiety by suitable group as $–Si(OR)_3$, and/or their complexes on silica or other surfaces, is an area of growing interest. The goal is to obtain modified surfaces, which maintain the preordered properties ascertained in the simpler dinuclear entities in the solid state or in solution. The rapid growing of excellent and promising results in these research fields presages quite fruitful applications in the next future.

Acknowledgments

We thank Mrs. G. Bonato and Mr. A. Aguiari, for the valuable assistance in the collecting and classifying the data and in preparing drawings and the manuscript. Also we thank Progetto FIRB RBNE019H9K, MIUR for financial support.

References

[1] V. Alexander, Chem. Rev. 95 (1995) 273.
[2] (a) D.E. Fenton, H. Okawa, Chem. Berl. 130 (1997) 433;
(b) S.R. Collinson, D.E. Fenton, Coord. Chem. Rev. 148 (1996) 19;
(c) D.E. Fenton, Pure Appl. Chem. 58 (1986) 1437.
[3] A. Martell, J. Penitka, D. Kong, Coord. Chem. Rev. 216 (2001) 55.
[4] (a) V. McKee, in: A.G. Sikes (Ed.), Advanced in Inorganic Chemistry, vol. 40, Academic Press, San Diego, USA, 1993, p. 323;
(b) J. Nelson, V. McKee, G. Morgan, in: K.D. Karlin (Ed.), Progress in Inorganic Chemistry, vol. 47, John Wiley & Sons, New York, USA, 1998, p. 167;
(c) S. Brooker, Coord. Chem. Rev. 222 (2001) 33;
(d) S. Brooker, Eur. J. Inorg. Chem. (2002) 2535.
[5] (a) P. Guerriero, P.A. Vigato, D.E. Fenton, P.C. Hallier, Acta Chem. Scand. 46 (1992) 1025;
(b) P. Zanello, S. Tamburini, P.A. Vigato, G.A. Mazzochin, Coord. Chem. Rev. 77 (1987) 165;
(c) P.A. Vigato, S. Tamburini, D.E. Fenton, Coord. Chem. Rev. 106 (1990) 25;
(d) D.E. Fenton, P.A. Vigato, Coord. Chem. Rev. 17 (1988) 89;
(e) P. Guerriero, S. Tamburini, P.A. Vigato, Coord. Chem. Rev. 134 (1995) 17;
(f) S. Tamburini, P.A. Vigato, Coord. Chem. Rev. 248 (2004) 1718.
[6] (a) D. Esteban, C. Platas-Iglesias, F. Avecilla, A. de Blas, T. Rodríguez-Blas, Polyhedron 24 (2005) 289;
(b) D. Esteban, D. Banobre, R. Bastida, A. de Blas, A. Macías, A. Rodríguez-Blas, D.E. Fenton, H. Adams, J. Mahía, Inorg. Chem. 38 (1999) 1937;
(c) C. Platas-Iglesias, D. Esteban, V. Ojea, F. Avecilla, A. de Blas, T. Rodríguez-Blas, Inorg. Chem. 42 (2003) 4299;
(d) F. Avecilla, D. Esteban, C. Platas-Iglesias, A. de Blas, T. Rodríguez-Blas, Acta Cryst. C 59 (2003) m93;
(e) D. Esteban, F. Avecilla, C. Platas-Iglesias, J. Mahía, A. de Blas, T. Rodríguez-Blas, Inorg. Chem. 41 (2002) 4337.
[7] (a) U. Casellato, S. Tamburini, P. Tomasin, P.A. Vigato, Inorg. Chim. Acta 357 (2004) 4191;
(b) D.M. Rudkevich, W.P.R.V. Stauthamer, W. Verboom, J.F.J. Engebersen, S. Harkema, D.N. Reinhouldt, J. Am. Chem. Soc. 114 (1992) 9671.
[8] P. Di Bernardo, S. Tamburini, P. Tomasin, P.A. Vigato, P. Zanonato, Dalton Trans. (2006) 4711.
[9] S. Tamburini, P. Tomasin, P.A. Vigato, S. Aime, M. Botta, M.A. Cremonini, Inorg. Chim. Acta 357 (2004) 1374.
[10] A. Caneschi, L. Sorace, U. Casellato, P. Tomasin, P.A. Vigato, Eur. J. Inorg. Chem. (2004) 3887.
[11] A. Barge, M. Botta, U. Casellato, S. Tamburini, P.A. Vigato, Eur. J. Inorg. Chem. (2005) 1492.
[12] U. Casellato, S. Tamburini, P. Tomasin, P.A. Vigato, S. Aime, A. Barge, M. Botta, Chem. Commun. (2000) 145.
[13] S. Tamburini, P.A. Vigato, M. Gatos, L. Bertolo, U. Casellato, Inorg. Chim. Acta 359 (2006) 183.
[14] M. Botta, U. Casellato, C. Scalco, S. Tamburini, P. Tomasin, P.A. Vigato, S. Aime, A. Barge, Chem. Eur. J. 8 (2002) 3917.
[15] (a) U. Casellato, S. Tamburini, P. Tomasin, P.A. Vigato, S. Aime, M. Botta, Inorg. Chem. 38 (1999) 2906;
(b) N. Brianese, U. Casellato, S. Tamburini, P. Tomasin, P.A. Vigato, Inorg. Chem. Commun. 2 (1999) 149.
[16] (a) V. van Axel Castelli, R. Cacciapaglia, G. Chiosis, F.C.J.M. van Veggel, L. Mandolini, D.N. Reinhoudt, Inorg. Chim. Acta 246 (1996) 181;
(b) H.J.J.B. Martel, S. McMahon, M. Rasmussen, Aust. J. Chem. 32 (1979) 1241;
(c) F.C.J.M. van Veggel, M. Bos, S. Harkema, H. van de Bovenkamp, W. Verboom, J. Reedijk, D.N. Reinhoudt, J. Org. Chem. 56 (1991) 225;
(d) M. Bassetti, A. Calenne, L. Mastrofrancesco, M. Salamone, G. Bocelli, A. Cantoni, A. Musatti, Eur. J. Inorg. Chem. (2006) 914.
[17] S. Tamburini, U. Casellato, L. Bertolo, P.A. Vigato, Eur. J. Inorg. Chem. (2005) 2409.
[18] Q. Zeng, M. Quiang, S. Gou, H.-K. Fun, C. Duan, X. You, Inorg. Chim. Acta 294 (1999) 1.
[19] V.B. Arion, E. Bill, M. Reetz, R. Goddard, D.S. Stöckigt, M. Maßau, V. Levitsky, Inorg. Chim. Acta 282 (1998) 61.
[20] J.P. Costes, F. Dahan, G. Novitchi, V. Arion, S. Shova, J. Lipkowski, Eur. J. Inorg. Chem. (2004) 1530.
[21] V.B. Arion, V.Ch. Kravtsov, J.I. Gradinaru, Y.A. Simonov, N.V. Gerbeleu, J. Lipkowski, J.P. Wignacourt, H. Vezin, O. Mentré, Inorg. Chim. Acta 323 (2002) 123.
[22] I. Yoon, M. Goto, T. Shimizu, S.S. Lee, M. Asakawa, Dalton Trans. (2004) 1513.
[23] P.G. Plieger, P.A. Tasker, S.G. Galbraith, Dalton Trans. (2004) 313.
[24] M. Yonumura, K. Arimura, K. Inoue, N. Usuki, M. Ohba, H. Okawa, Inorg. Chem. 41 (2002) 582.
[25] K.-J. Inoue, M. Ohba, H. Okawa, Bull. Chem. Soc. Jpn. 75 (2002) 99.
[26] M. Yonemura, H. Okawa, M. Ohba, D.E. Fenton, L.K. Thompson, Chem. Commun. (2000) 817.
[27] Y. Nakamura, M. Yonemura, K. Arimura, N. Usuki, M. Ohba, H. Okawa, Inorg. Chem. 40 (2001) 3739.
[28] A. Hori, M. Yonemura, M. Ohba, H. Okawa, Bull. Chem. Soc. Jpn. 74 (2001) 495.
[29] K. Matsumoto, K. Arimura, M. Ohba, H. Ōkawa, Bull. Chem. Soc. Jpn. 76 (2003) 1589.
[30] K. Matsumoto, N. Sekine, K. Arimura, M. Ohba, H. Sakiyama, H. Okawa, Bull. Chem. Soc. Jpn. 77 (2004) 1343.
[31] A. Hori, Y. Mitsuka, M. Ohba, H. Okawa, Inorg. Chim. Acta 337 (2002) 113.
[32] J. Manonmani, M. Kandaswamy, Polyhedron 22 (2003) 989.
[33] M. Thirumavalavan, P. Akilan, M. Kandaswamy, Inorg. Chem. Commun. 5 (2002) 422.
[34] M. Thirumavalavan, P. Akilan, M. Kandaswamy, K. Chinnakali, G. Kumar, H.K. Fun, Inorg. Chem. 42 (2003) 3308.
[35] M. Thirumavalavan, P. Akilan, P. Amudha, M. Kandaswamy, Polyhedron 23 (2004) 519.
[36] (a) S. Parimala, M. Kansaswamy, Inorg. Chem. Commun. 6 (2003) 1252;
(b) M. Thirumavalavan, P. Akilan, M. Kandaswamy, Polyhedron 24 (2005) 1781;
(c) M. Thirumavalavan, P. Akilan, M. Kandaswamy, Inorg. Chim. Acta 359 (2006) 2555.
[37] D.E. Fenton, M. Okawa, Ber/Recueil 130 (1997) 433.
[38] H. Okawa, H. Furutachi, D.E. Fenton, Coord. Chem. Rev. 174 (1998) 51.
[39] N. Brianese, U. Casellato, S. Tamburini, P. Tomasin, P.A. Vigato, Inorg. Chim. Acta 293 (1999) 178.
[40] U. Casellato, S. Tamburini, P. Tomasin, P.A. Vigato, Inorg. Chim. Acta 262 (1997) 117.
[41] M. D'Alpaos, S. Tamburini, P. Tomasin, P.A. Vigato, P. Traldi, Rapid Commun. Mass. Spectrum. 11 (1997) 178.
[42] (a) B. Dutta, P. Bag, B. Adhikary, U. Flörke, K. Nag, J. Org. Chem. 69 (2004) 5419;
(b) J.C. Byun, C.H. Han, K.J. Kim, Inorg. Chem. Commun. 9 (2006) 171;
(c) J.C. Byun, W.H. Lee, C.H. Han, Inorg. Chem. Commun. 9 (2006) 563;
(d) D. Venegas-Yazigi, S. Cortes, V. Paredes-Garcia, O. Pena, A. Ibanez, R. Baggio, E. Spodine, Polyhedron 25 (2006) 2072.
[43] D.J. White, M. Laing, H. Muller, S. Parsons, S. Coles, P.A. Tasker, Chem. Commun. (1999) 2077.
[44] D.M. Rudkevich, W.T.S. Huch, F.C.J.M. Van Veggel, D.N. Reinhoudt, in: L., Fabbrizzi, A., Poggi (Eds.), Transition Metals in Supramolecular Chemistry, NATO ASI Series, vol. 448, 1994, p. 329.
[45] W.F. Nijenhuis, A.R. van Doorn, W. Verboom, A.M. Reichwein, F. de Jong, D.N. Reinhoudt, J. Am. chem. Soc. 113 (1991) 3607.
[46] A.M. Reichwein, W. Verboom, S.H. Harkema, A.L. Spek, D.N. Reinhoudt, J. Chem. Soc., Perkin Trans. (1994) 1167.
[47] D.M. Rudkevich, W. Verboom, Z. Brzozka, M.J. Palys, W.P.R.V. Stauthamer, G.J. van Hummel, S.M. Franken, S. Harkema, J.F.J. Engbersen, D.N. Reinhoudt, J. Am. Chem. Soc. 116 (1994) 4341.
[48] D.M. Rudkevich, Z. Brzozka, M. Palys, H.C. Visser, W. Verboom, D.N. Reinhoudt, Angew. Chem. Int. Ed. Engl. 33 (1994) 467.

[49] D.M. Rudkevich, W. Verboom, D.N. Reinhoudt, J. Org. Chem. 59 (1994) 3683.
[50] D.M. Rudkevich, J.D. Mercer-Chalmers, W. Verboom, R. Ungaro, F. de Jong, D.N. Reinhoudt, J. Am. Chem. Soc. 117 (1995) 6124.
[51] K. Manseki, O. Nakamura, K. Horikawa, M. Sakamoto, H. Sakiyama, Y. Nishida, Y. Sadaoka, H. Okawa, Inorg. Chem. Commun. 5 (2002) 56.
[52] N. Takeda, M. Irisawa, M. Komiyama, J. Chem. Soc., Chem. Commun. (1994) 2773.
[53] M. Irisawa, M. Komiyama, J. Biochem. 117 (1995) 465.
[54] K. Danjobara, Y. Mitsuka, Y. Miyasato, M. Ohba, H. Okawa, Bull. Chem. Soc. Jpn. 76 (2003) 1769.
[55] H. Okawa, J. Nishio, M. Ohba, M. Tadokoro, N. Matsumoto, M. Koikawa, S. Kida, D.E. Fenton, Inorg. Chem. 32 (1993) 2949.
[56] S. Ohtsuka, M. Kodera, K. Motoda, M. Ohba, H. Okawa, J. Chem. Soc., Dalton Trans. (1995) 2599.
[57] H. Wada, T. Aono, K. Motoda, M. Ohba, N. Matsumoto, H. Okawa, Inorg. Chim. Acta 246 (1996) 13.
[58] T. Aono, H. Wada, M. Yonemura, H. Furutachi, M. Ohba, H. Okawa, J. Chem. Soc., Dalton Trans. (1997) 3029.
[59] S. Kita, H. Furutachi, H. Okawa, Inorg. Chem. 38 (1999) 4038.
[60] M. Tadokoro, H. Sakiyama, N. Matsumoto, M. Kodera, H. Okawa, S. Kida, J. Chem. Soc., Dalton Trans. (1992) 313.
[61] K. Ikeda, K. Matsufuji, M. Ohba, M. Kodera, H. Okawa, Bull. Chem. Soc. Jpn. 77 (2004) 733.
[62] (a) M. Bell, A.J. Edwards, B.F. Hoskins, E.H. Kachab, R. Robson, J. Am. Chem. Soc. 111 (1989) 3603;
(b) A.J. Edwards, B.F. Hoskins, E.H. Kechab, A. Markiewiez, K.S. Murray, R. Robson, Inorg. Chem. 31 (1992) 3585;
(c) A.J. Edwards, B.F. Hoskins, R. Robson, J.C. Wilson, B. Moubaraki, K.S. Murray, J. Chem. Soc., Dalton Trans. (1994) 1837.
[63] (a) S. Akine, T. Taniguchi, T. Nabeshima, Tetrahedron Lett. 42 (2001) 8861;
(b) A.J. Gallant, M.J. MacLachlan, Angew. Chem. Int. Ed. 42 (2003) 5307;
(c) A.J. Gallant, J.H. Chong, M.J. MacLachlan, Inorg. Chem. 45 (2006) 5248;
(d) A.J. Gallant, B.O. Patrick, M.J. MacLachlan, J. Org. Chem. 69 (2004) 8739;
(e) A.J. Gallant, J.L.-H. Hui, F.E. Zahariev, Y.A. Wang, M.J. Maclachlan, J. Org. Chem. 70 (2005) 7936;
(f) A.J. Gallant, M. Yun, M. Sauer, C.S. Yeung, M.J. MacLachlan, Org. Lett. 7 (2005) 4827.
[64] (a) B.A. Dutta, P. Bag, U. Flörke, K. Nag, J. Chem. Soc., Dalton Trans. (2002) 2760;
(b) S.S. Tandom, V. Mckee, J. Chem. 45 (2006) 4830;
(c) P. Bag, U. Flörke, K. Nag, Dalton Trans. (2006) 3236;
(d) B. Dutta, B. Adhykay, U. Flörke, K. Nag, Eur. J. Inorg. Chem. (2006) 4111.
[65] P. Biswas, M. Ghosh, S. Dutta, U. Flörke, K. Nag, Inorg. Chem. 45 (2006) 4830.
[66] (a) A.J. Atkins, D. Black, R.L. Finn, A. Marin-Becerra, A.J. Blake, L. Ruiz-Ramirez, W.-S. Li, M. Schröder, Dalton Trans. (2003) 1730;
(b) A.J. Atkins, A.K. Blake, M. Schröder, J. Chem. Soc., Chem. Commun. (1993) 353;
(c) A.J. Atkins, D. Black, A.J. Blake, A. Marin-Becerra, S. Parsons, L. Ruiz-Ramirez, M. Schröder, J. Chem. Soc., Chem. Commun. (1996) 457.
[67] B. Dutta, P. Bag, U. Flörke, K. Nag, Inorg. Chem. 44 (2005) 147.
[68] (a) J. Gao, J.H. Reibenspies, R.A. Zingaro, F.R. Woolley, A.E. Martell, A. Clearfield, Inorg. Chem. 44 (2005) 232;
(b) J. Gao, J.H. Reibenspies, A.E. Martell, Angew. Chem. Int. Ed. 42 (2003) 6008.
[69] (a) N. Kuhnert, G.M. Rossignolo, A. Lopez-Periago, Org. Biomol. Chem. 1 (2003) 1157;
(b) S.R. Korupoju, P.S. Zacharias, Chem. Commun. (1998) 1267;
(c) S.R. Korupoju, N. Mangayarkarasi, S. Ameerunisha, E.J. Valente, P.S. Zacharias, J. Chem. Soc., Dalton Trans. (2000) 2845;
(d) S.R. Korupoju, N. Mangayarkarasi, P.S. Zacharias, J. Mizuthani, H. Nishihara, Inorg. Chem. 41 (2002) 4099;
(e) M. Paluch, J. Lisowski, T. Lis, Dalton Trans. (2006) 381.
[70] Y. Miyasato, Y. Nogami, M. Ohba, H. Sakiyama, H. Okawa, Bull. Chem. Soc. Jpn. 76 (2003) 1009.
[71] D. Black, A.J. Blake, R.L. Finn, L.F. Lindoy, A. Nezhadali, G. Rougnaghi, P.A. Tasker, M. Schöder, Chem. Commun. (2002) 340.
[72] (a) W. Huang, S. Gou, D. Hu, S. Chantrapromma, H.K. Fun, Q. Meng, Inorg. Chem. 40 (2001) 1712;
(b) W. Huang, S. Gou, D. Hu, S. Chantrapromma, H.K. Fun, Q. Meng, Inorg. Chem. 41 (2002) 864.
[73] (a) M. Pascu, M. Andruh, A. Müller, M. Schmidtmann, Polyhedron 23 (2004) 673;
(b) D. Visinescu, J.-P. Sutter, C. Ruiz-Pérez, M. Andruh, Inorg. Chim. Acta 359 (2006) 433;
(c) H. Okawa, J. Nishio, M. Ohba, M. Tadakoro, N. Matsumato, M. Koikawa, S. Kida, D.E. Fenton, Inorg. Chem. 32 (1993) 2949.
[74] (a) S. Gaeta, J. Barreira Fontecha, V. McKee, Acta Cryst. Sec. C 60 (2004) o776;
(b) J. Barreira Fontecha, S. Getz, V. Mckee, Angew. Chem. Int. Ed. 41 (2002) 4553;
(c) J. Barreira Fontecha, S. Getz, V. McKee, Dalton Trans. (2005) 923;
(d) H. Shimakoshi, H. Takemoto, I. Aritome, Y. Hisaeda, Tetrahedron Lett. 43 (2002) 4809;
(e) H. Shimakoshi, T. Takemoto, I. Aritome, Y. Hisaeda, Inorg. Chem. 44 (2005) 9134;
(f) M. Hirotsu, N. Ohno, T. Nakajima, K. Ueno, Chem. Lett. 34 (2005).
[75] (a) S. Brooker, P. Caoucher, F.M. Roxburgh, J. Chem. Soc., Dalton Trans. (1996) 3031;
(b) A. Marin-Becerra, P.A. Stenson, J. Mc Master, A.J. Blake, C. Wilson, M. Schröder, Eur. J. Chem. (2003) 2389;
(c) N.D.J. Branscombe, A.J. Atkins, A. Marin-Becerra, E.J.L. McInnes, F.E. Mabbs, J. Mcmaster, M. Schröder, Chem. Commun. (2003) 1098;
(d) A. Christensen, C. Mayer, F. Jensen, A.D. Bond, C.J. McKenzie, Dalton Trans. (2006) 108.
[76] (a) L. Tei, M. Arca, M.C. Aragoni, A. Bencini, A.J. Blake, C. Caltagirone, F.A. Devillanova, P. Fornasari, A. Garau, F. Isaia, V. Lippolis, N. Schröder, S.J. Teat, B. Valtancoli, Inorg. Chem. 42 (2003) 8690;
(b) L. Tei, A.J. Blake, F.A. Devillanova, A. Garau, V. Lippolis, C. Wilson, M. Schröder, Chem. Commun. (2001) 2582.
[77] M. Formica, V. Fusi, L. Giorgi, M. Micheloni, P. Palma, R. Pontellini, Eur. J. Org. Chem. (2002) 402.
[78] T. Lu, S. Chen, Z. Mao, A.E. Martell, L. Ji, Inorg. Chem. Comm. 6 (2003) 1068;
(b) H.Y. He, A.E. Martell, R.J. Motekaitis, J.H. Reibenspies, Inorg. Chem. 39 (2000) 1586.
[79] J. Gao, J.H. Reibenspies, A.E. Martell, Inorg. Chim. Acta 346 (2003) 67.
[80] J. Gao, A.E. Martell, J. Reibenspies, Inorg. Chim. Acta 346 (2003) 32.
[81] C. Higuchi, H. Sakiyama, H. Okawa, R. Isobe, D.E. Fenton, J. Chem. Soc., Dalton Trans. (1994) 1907.
[82] C. Higuchi, H. Sakiyama, H. Ohawa, R. Jsobe, D.E. Fenton, J. Chem. Soc., Dalton Trans. (1994) 1097.
[83] D. Kong, A.E. Martell, J. Reibenspies, Inorg. Chim. Acta 333 (2002) 7.
[84] D. Kong, X. Ouyang, J. Reibenspies, A. Clearfield, A.E. Martell, Inorg. Chem. Commun. 5 (2002) 873.
[85] D. Kong, J. Mao, A.E. Martell, A. Clearfield, Inorg. Chim. Acta 338 (2002) 78.
[86] D. Kong, J.H. Reibenspies, A.E. Martell, R.J. Motekaitis, Inorg. Chim. Acta 324 (2001) 35.
[87] D. Kong, J. Reibenspies, J. Mao, A.E. Martell, A. Clearfield, Inorg. Chim. Acta 340 (2002) 178.
[88] D. Kong, J. Reibenspies, J. Mao, A. Clearfield, A.E. Martell, Inorg. Chim. Acta 342 (2003) 158.
[89] D. Kong, A.E. Martell, R.J. Motekaitis, J.H. Reibenspies, Inorg. Chim. Acta 317 (2001) 243.
[90] J.D. Wang, D. Kong, A.E. Martell, R.J. Motekaitis, J.H. Reibenspies, Inorg. Chim. Acta 324 (2001) 194.
[91] J. Wang, A.E. Martell, J.H. Reibenspies, Inorg. Chim. Acta 328 (2002) 53.

[92] (a) J.D. Wang, A.E. Martell, R.J. Motekaitis, J. Reibenspies, Inorg. Chim. Acta 322 (2001) 47;
(b) J.D. Wang, A.E. Martell, R.J. Motekaitis, J. Reibenspies, Inorg. Chim. Acta 324 (2001) 194.
[93] M. Shinoura, S. Kita, M. Ohba, H. Osaka, H. Furutachi, M. Suzuki, Inorg. Chem. 39 (2000) 4520.
[94] D. Kong, J. Mao, A.E. Martell, A. Clearfield, Inorg. Chim. Acta 342 (2003) 260.
[95] I.J. Hewitt, J.-K. Tang, N.T. Madhu, B. Pilawa, C.E. Anson, S. Brooker, A.K. Powelll, Dalton Trans. (2005) 429.
[96] (a) B. Kersting, G. Steinfeld, T. Fritz, J. Hausmann, Eur. J. Inorg. Chem. (1999) 2167;
(b) B. Kersting, G. Steinfeld, Chem. Commun. (2001) 1376;
(c) B. Kersting, Angew. Chem. Int. Ed. 40 (2001) 3987.
[97] B. Kersting, G. Steinfeld, Inorg. Chem. 41 (2002) 1140.
[98] J. Hausmann, M.H. Kingele, V. Lozan, G. Steinfield, D. Siebert, Y. Journaux, J.J. Girerd, B. Kersting, Chem. Eur. J. 10 (2004) 1716.
[99] (a) V. Lozan, B. Kersting, Eur. J. Inorg. Chem. (2005) 504;
(b) Y. Journaux, T. Glaser, G. Steinfeld, V. Lozan, B. Kersting, Dalton Trans. (2006) 1738.
[100] (a) M. Gressenbuch, V. Lozan, G. Steinfeld, B. Kersting, Eur. J. Inorg. Chem. (2005) 2223;
(b) T. Fritz, G. Steinfeld, S. Käss, B. Kersting, Dalton Trans. (2006) 3812.
[101] S. Brooker, R.J. Kelly, J. Chem. Soc., Dalton Trans. (1996) 2117.
[102] (a) U. Beckmann, S. Brooker, Coord. Chem. Rev. 245 (2003) 17;
(b) S. Brooker, D.J. de Geest, R.J. Kelly, P.G. Plieger, B. Moubaraki, K.S. Murray, G.B. Jameson, J. Chem. Soc., Dalton Trans. (2002) 2080.
[103] (a) C.D. Brandt, P.G. Plieger, R.J. Kelly, D.K. de Geest, D.K. Kennepohl, S.S. Iremonger, S. Brooker, Inorg. Chim. Acta 357 (2004) 4265;
(b) S. Brooker, R. Kelly, B. Moubarachi, K.S. Murray, Chem. Commun. (1996) 2579;
(c) S. Brooker, S.H. Hay, P.G. Plieger, Angew. Chem. Int. Ed. 39 (2000) 1968.
[104] M. Weitzer, S. Brooker, Dalton Trans. (2005) 2448.
[105] C. Ng. Yuen, R.J. Motekaitis, A. Martell, Inorg. Chem. 18 (1979) 2982.
[106] P.L. Anelli, L. Lunazzi, F. Montanari, S. Quici, J. Org. Chem. 49 (1984) 4197.
[107] C. Mirando, F. Escarti, L. Lamarque, M.J.R. Yunta, P. Navarro, E. García-Espana, M.L. Jimeno, J. Am. Chem. Soc. 126 (2004) 823.
[108] F. Escartí, C. Miranda, L. Lamarque, J. Latorre, E. García-Espana, M. Kumar, V.J. Arán, P. Navarro, Chem. Commun. (2002) 936.
[109] L. Lamarque, C. Miranda, P. Navarro, F. Escartí, J. Latorre, J.A. Ramirez, Chem. Commun. (2000) 1337.
[110] M. Kumar, V.J. Arán, P. Navarro, A. Ramos-Gallardo, A. Vegas, Tetrahedron Lett. 35 (1994) 5723.
[111] L. Lamarque, P. Navarro, C. Miranda, V.J. Arán, C. Ochoa, F. Escartí, E. García-Espana, J. Latorre, S.V. Luis, J.F. Miravet, J. Am. Chem. Soc. 123 (2001) 10570.
[112] (a) M. Kumar, V.J. Arán, P. Navarro, Tetrahedron Lett. 34 (1993) 3159;
(b) M. Kumar, V.J. Arán, P. Navarro, Tetrahedron Lett. 36 (1995) 2161.
[113] C. Mirando, F. Escartí, L. Lamarque, E. García-Espana, P. Navarro, J. Latorre, F. Lloret, H.R. Jiménez, M.J.R. Yunta, Eur. J. Inorg. Chem. (2005) 189.
[114] (a) J. de Mendoza, J.M. Ontoria, M.C. Ortega, T. Torres, Synthesis (1992) 398;
(b) J.M. Alonso, M.R. Martin, J. De Mendoza, T. Torres, Heterocycles 26 (1987) 989;
(c) J.A. Duro, J.M. Ontoria, A. Sastre, W. Schafer, T. Torres, J. Chem. Soc., Dalton Trans. (1993) 2595.
[115] (a) U. Beckmann, J.D. Ewing, S. Brooker, Chem. Commun. (2003) 1690;
(b) C.V. Depree, U. Beckmann, K. Heslop, S. Brooker, Dalton Trans. (2003) 3071;
(c) U. Beckamann, S. Brooker, C.V. Depree, J.D. Ewing, B. Moubaraki, K.S. Murray, Dalton Trans. 7 (2003) 1308.
[116] (a) S.C. Menon, H.B. Singh, R.P. Patel, S.K. Kulshreshtha, J. Chem. Soc., Dalton Trans. (1996) 1203;
(b) S.C. Menon, A. Panda, H.B. Singh, R.J. Butcher, Chem. Commun. (2000) 143;
(c) S.C. Menon, A. Panda, H.B. Singh, R.P. Patel, S.K. Kulshreshtha, W.L. Darby, R.J. Butcher, J. Org. Chem. 689 (2004) 1452;
(d) A. Panda, S.C. Menon, H.B. Singh, C.R. Bachman, T.M. Cocker, R.J. Butcher, Eur. J. Inorg. Chem. (2005) 1114;
(e) A. Panda, S.C. Menon, H.B. Singh, R.J. Butcher, J. Org. Chem. 623 (2001) 87;
(f) S. Panda, H.B. Sing, J. Butcher, Inorg. Chem. 43 (2004) 8532.
[117] (a) M.W. Alcock, P. Moore, H.A.A. Omar, J. Chem. Soc., Dalton Trans. (1987) 889;
(b) C. Cruz, S. Carvalho, R. Delgado, M.G.B. Drew, V. Félix, B.J. Goodfellow, Dalton Trans. (2003) 3172.
[118] (a) J.L. Sessler, W.B. Callaway, S.P. Dudek, R.W. Date, D.W. Bruce, Inorg. Chem. 43 (2004) 6650;
(b) N.N. Gerasimchuk, A. Gerges, T. Clifford, A. Daniby, K. Bawman-James, Inorg. Chem. 38 (1999) 5633;
(c) J.L. Sessler, W. Callaway, S.P. Dudek, R.W. Date, V. Lynch, D.W. Bruce, Chem. Commun. (2003) 2422;
(d) J.L. Sessler, T.D. Moody, V. Linch, J. Am. Chem. Soc. 115 (1993) 3346;
(e) J.L. Sessler, E. Tomat, T.D. Mody, V.M. Lynch, J.M. Veauthier, U. Mirsaidov, J.T. Markert, Inorg. Chem. 44 (2005) 2125;
(f) J.M. Veauthier, W.-S. Cho, V.M. Lynch, J.L. Sessler, Inorg. Chem. 43 (2004) 1220;
(g) J.M. Veauthier, E. Tomat, V.M. Lynch, J.L. Sessler, U. Mirsaidov, J.T. Markert, Inorg. Chem. 44 (2005) 6736.
[119] R. Li, T.A. Mulder, U. Beckmann, P.D.W. Boyd, S. Brooker, Inorg. Chim. Acta 357 (2004) 3360.
[120] (a) P.L. Arnold, A.J. Blake, C. Wilson, J.B. Love, Inorg. Chem. 43 (2004) 8206;
(b) G. Givaga, A.J. Blake, C. Wilson, M. Schröder, J.B. Love, Chem. Commun. (2003) 2508;
(c) G. Givaja, A.J. Blake, C. Wilson, M. Schröder, J.B. Love, Chem. Commun. (2005) 4423.
[121] (a) H. Ma, M. Alimendinger, U. Thewalt, A. Lents, M. Klinga, B. Rieger, Eur. J. Inorg. Chem. (2002) 2857;
(b) D. Utz, F.W. Heinemann, F. Hampel, D.T. Richens, S. Schindler, Inorg. Chem. 42 (2003) 1430.
[122] M.G. Basallote, M.J. Fernàndez-Trujillo, M.A. Mànez, J. Chem. Soc., Dalton Trans. (2002) 3691.
[123] V.V.E. Aires, C.M. Zaccaron, A. Neves, B. Szpoganicz, Inorg. Chim. Acta 353 (2003) 82.
[124] B. Graham, L. Spicca, S.R. Batten, B.W. Skelton, A.H. White, Inorg. Chim. Acta 358 (2005) 3983.
[125] (a) R. Menif, A.E. Martell, J. Chem. Soc., Chem. Commun. (1989) 1523;
(b) J. Gao, J.H. Reibenspies, A.E. Martell, Inorg. Chim. Acta 338 (2002) 157.
[126] J. Gao, J. Reibenspies, A.E. Martell, S. Yizhen, D. Chen, Inorg. Chem. Commun. 5 (2002) 1095.
[127] (a) W. He, F. Liu, C. Duan, Z. Guo, S. Zhou, Y. Liu, L. Zhu, Inorg. Chem. 40 (2001) 7065;
(b) C. Chen, A.E. Martell, Tetrahedron 47 (1991) 6895;
(c) W. He, Z. Ye, Y. Xu, Z. Guo, L. Zhu, Acta Crystallogr. Sect. C 56 (2000) 1019.
[128] C. Anda, A. Llobet, A.E. Martell, J. Reibenspies, E. Berni, X. Solans, Inorg. Chem. 43 (2004) 2793.
[129] (a) Q. Lu, R.J. Motekaitis, J.J. Reibenspies, A.E. Martell, Inorg. Chem. 34 (1995) 4958;
(b) M.W. Hosseini, J.M. Lehn, J. Am. Chem. Soc. (104) (1982) 3525;
(c) M.W. Hosseini, J.M. Lehn, Helv. Chim. Acta 69 (1986) 587;
(d) J.M. Lehn, R. Merie, J.P. Vigneron, I. Waksman-Bkouche, C.J.J. Pascard, Chem. Soc., Chem. Commun. (1991) 62;
(d) B. Dietrich, M.W. Hosseini, J.M. Lehn, R.B. Sessions, J Am. Chem. Soc. 103 (1981) 1282;
(e) E. Kimura, A. Sakonaka, T. Yatsunami, M. Kodama, J. Am. Chem. Soc. 103 (1981) 3041;
(f) A. Bencini, A. Bianchi, M.I. Burguete, E. García-Espana, S.V. Luis, J.A. Ramirez, J. Am. Chem. Soc. 114 (1992) 1919;

(g) Q. Iu, R.J. Motekaitis, J. Reibenspies, A.E. Martell, Inorg. Chem. 34 (1995) 4959;
(h) R.J. Motekaitis, A.E. Martell, Inorg. Chem. 35 (1996) 4597.
[130] (a) C. Anda, A. Llobet, V. Salvadó, J. Reibenspies, A.E. Martell, R.J. Motekaitis, Inorg. Chem. 39 (2000) 2986;
(b) C. Anda, A. Llobet, V. Salvadó, A.E. Martell, R.J. Motekaitis, Inorg. Chem. 39 (2000) 3000.
[131] C. Anda, A. Llobet, A.E. Martell, B. Donnadieu, T. Parella, Inorg. Chem. 42 (2003) 8545.
[132] S. Carvalho, C. Cruz, R. Delgado, M.G.B. Drew, V. Félix, Dalton Trans. (2003) 4261.
[133] D.A. Rockcliffe, A.E. Martell, J.H. Rebenspies, J. Chem. Soc., Dalton Trans. (1996) 167.
[134] M.G.B. Drew, J. Nelson, S.M. Nelson, J. Chem. Soc., Dalton Trans. (1981) 1678.
[135] A.-R. Song, Y. Song, X.-M. Ouyang, Y.-Z. Li, W.-Y. Sun, Inorg. Chem. Commun. 8 (2005) 186.
[136] R. Menif, A.E. Martell, P.J. Squattrin, A. Clearfield, Inorg. Chem. 29 (1990) 4723.
[137] M. Pietraszkiewicz, R. Gasiorowski, Chem. Ber. 123 (1990) 405.
[138] A. Llobet, J. Reibenspies, A.E. Martell, Inorg. Chem. 33 (1994) 5946.
[139] T. Clifford, A.M. Danby, P. Lightfoot, D.T. Richens, R.W. Hay, J. Chem. Soc., Dalton Trans. (2001) 240.
[140] M. Costa, R. Xifra, A. Llobet, M. Solà, J. Robles, T. Parella, H. Stoeckli-Evans, M. Neuburger, Inorg. Chem. 42 (2003) 4456.
[141] (a) D.-X. Yang, S.-A. Li, D.-F. Li, J. Xia, K.-B. Yu, W.-X. Tang, J. Chem. Soc., Dalton Trans. (2002) 4042;
(b) A. Company, L. Gómez, J. Maria López Valbuena, R. Mas-Ballesté, J. Benet-Buchhholz, A. Llobet, M. Costas, Inorg. Chem. 45 (2006) 2501.
[142] (a) S.-A. Li, D.-F. Li, C.-Y. Duan, J. Xia, D.-X. Yang, W.-X. Tang, Inorg. Chem. Commun. 4 (2001) 651;
(b) S.-A. Li, D.-F. Li, D.-X. Yang, J. Huang, Y. Xu, W.-X. Tang, Inorg. Chem. Commun. 6 (2003) 221.
[143] D.-X. Yang, S.-A. Li, W.-X. Tang, Acta Crystallogr. Sect. C 58 (2002) o11.
[144] S.-A. Li, J. Xia, D.-X. Yang, Y. Xu, M.-F. Wu, W.-X. Tang, Inorg. Chem. 41 (2002) 1807.
[145] G. Yang, H. Tang, Y. Li, J. Hong, Z. Guo, L. Zhu, Inorg. Chem. Commun. 8 (2005) 862.
[146] J. Huang, S.-A. Li, D.-F. Li, D.-X. Yang, W.-Y. Sun, W.-X. Tang, Eur. J. Inorg. Chem. (2004) 1894.
[147] D.-X. Yang, S.-A. Li, D.-F. Li, M. Chen, J. Huang, W.-X. Tang, Polyhedron 22 (2003) 925.
[148] H. Ohtsu, Y. Shimazaki, A. Odani, O. Yamauchi, W. Mori, S. Itoh, S. Fukuzumi, J. Am. Chem. Soc. 122 (2000) 5733.
[149] (a) S.-A. Li, D.F. Li, D.-X. Yang, Y.-Z. Li, J. Huang, K.-B. Yu, W.-X. Tang, Chem. Commun. (2003) 880;
(b) D. Li, S. Li, D. Yang, J. Yu, J.H. Huang, Y. Li, W. Tang, Inorg. Chem. 42 (2003) 6071.
[150] M.P. Clares, J. Agiular, R. Acucejo, C. Lodeiro, M.T. Albeida, F. Pina, J.C. Lima, A.J. Parola, J. Pina, J. Seixas de Melo, C. Soriano, E. García-España, Inorg. Chem. 43 (2004) 6114.
[151] B. Sarkar, P. Mukhopadhay, P.K. Bharadwaj, Coord. Chem. Rev. 236 (2003) 1.
[152] K.G. Ragunathan, P.K. Bharadwaj, Tetrahedron Lett. 33 (1992) 7581.
[153] P. Ghosh, S. Sengupta, P.K. Bharadwaj, J. Chem. Soc., Dalton Trans. (1997) 935.
[154] P. Ghosh, P.K. Bharadwaj, J. Chem. Soc., Dalton Trans. (1997) 1467.
[155] D.K. Chand, P.K. Bharadwaj, Inorg. Chem. 35 (1996) 3580.
[156] D.K. Chand, P.K. Bharadwaj, Tetrahedron 53 (1997) 10517.
[157] P. Ghosh, R. Shukla, D.K. Chand, P.K. Bharadwaj, Tetrahedron 51 (1995) 3265.
[158] B.P. Kennedy, A.B.P. Lever, J. Am. Chem. Soc. 95 (1973) 6907.
[159] K.G. Ragunathan, P.K. Bharadwaj, J. Chem. Soc., Dalton Trans. (1992) 2417.
[160] C.F. Martens, A.P.H.J. Schenning, R.J.M.K. Gebbink, M.C. Feiters, J.G.M. Linden, J. van der Heck, R.J.M. Nolte, J. Chem. Soc., Chem. Commun. (1993) 88.
[161] K.G. Ragunathan, P.K. Bharadwaj, Proc. Ind. Acad. Sci. 107 (1995) 519.
[162] D.K. Chand, P.K. Bharadwaj, Inorg. Chem. 37 (1998) 5050.
[163] (a) A. Bencini, A. Bianchi, E. Garcia-Espana, M. Micheloni, J.A. Ramirez, Coord. Chem. Rev. 188 (1999) 97;
(b) M. Ciampolini, N. Nardi, B. Valtancoli, M. Micheloni, Coord. Chem. Rev. 120 (1992) 223.
[164] (a) P. Ghosh, K. Tapan, P.K. Bharadwaj, Chem. Commun. (1996) 189;
(b) D. Ray, P.K. Bharadwaj, Eur. J. Inorg. Chem. (2006) 1771.
[165] P. Mukhopadhyay, B. Sarkar, P.K. Bharadwaj, K. Nattinen, K. Rissanen, Inorg. Chem. 42 (2003) 4955.
[166] B. Bag, P.K. Bharadway, Chem. Commun. (2005) 513.
[167] C. Platas, F. Avecilla, A. De Blas, C.F.G.C. Geraldes, T. Rodríguez-Blas, H. Adams, J. Mahía, Inorg. Chem. 38 (1999) 3190.
[168] F. Avecilla, A. De Blas, R. Bastida, D.E. Fenton, J. Mahía, A. Macías, C. Platas, A. Rodríguez, T. Rodríguez-Blas, Chem. Commun. (1999) 125.
[169] F. Avecilla, C. Platas-Igelsias, R. Rodríguez-Cortiñas, G. Guillemont, J.C.G. Bünzli, C.D. Brondino, C.F.G.C. Geraldes, A. De Blas, T. Rodríguez-Blas, J. Chem. Soc., Dalton Trans. (2002) 4658.
[170] (a) C.-J. Feng, Q.-H. Luo, C.-Y. Duan, M.-C. Shen, Y.-J. Liu, J. Chem. Soc., Dalton Trans. (1998) 1377;
(b) Q.-Y. Chen, Q.-H. Luo, Y.-J. Liu, C.-Y. Duan, J. Chem. Crystallogr. 30 (2000) 177;
(c) C.-J. Feng, Q.-H. Luo, Y.-Z. Xu, Synth. React. Inorg. Met. Org. Chem. 30 (2000) 1449.
[171] Q.Y. Chen, Q.-H. Luo, D.-G. Fu, J.-T. Chen, J. Chem. Soc., Dalton Trans. (2002) 2873.
[172] Q.-Y. Chen, Q.-H. Luo, L.-M. Zheng, Z.-I. Wang, J.-T. Chen, Inorg. Chem. 41 (2002) 605.
[173] R. Rodríguez-Cortinas, F. Avecilla, C. Platas-Iglesias, D. Imbert, J.C.G. Bunzli, A. de Blas, T. Rodríguez-Blas, Inorg. Chem. 41 (2002) 5336.
[174] Q.-Y. Chen, Q.-H. Luo, Z.-L. Wang, J.-T. Chen, J. Chem. Commun. (2000) 1033.
[175] C. Platas, F. Avecilla, A. De Blas, T. Rodríguez-Blas, C.F.G.C. Geraldes, E. Tóth, A.E. Mebach, J.-C.G. Bünzli, J. Chem. Soc., Dalton Trans. (2000) 611.
[176] Q.-Y. Chen, Q.-H. Luo, L.-M. Zheng, Z.-L. Wang, J.T. Chen, Inorg. Chem. 41 (2002) 605.
[177] Q.-Y. Chen, Q.-H. Luo, X.-L. Hu, M.-C. Shen, J.T. Chen, Chem. Eur. J. 8 (2002) 3984.
[178] M. Kanesato, H. Houjou, Y. Nagawa, K. Hiratani, Inorg. Chem. Commun. 5 (2002) 984.
[179] S. Brooker, J.D. Ewing, J. Nelson, Inorg. Chim. Acta 317 (2001) 53.
[180] S. Brooker, J.D. Ewing, T.K. Ronson, C.J. Harding, J. Nelson, D.J. Speed, Inorg. Chem. 42 (2003) 2764.
[181] T.K. Ronson, J. Nelson, G.B. Jameson, J.C. Jeffery, S. Brooker, Eur. J. Inorg. Chem. (2004) 2570.
[182] S. Brooker, J.D. Ewing, J. Nelson, J.C. Jeffery, Inorg. Chim. Acta 337 (2002) 463.
[183] J. Coyle, A.J. Downard, J. Nelson, V. McKee, C.J. Harding, R. Herbst-Irmer, Dalton Trans. (2004) 2357.
[184] X.-L. Hu, Y.-Z. Li, Q.-H. Luo, Polyhedron 23 (2004) 49.
[185] V. McKee, M.R.J. Dorrity, J.F. Malone, D. Marrs, J. Nelson, J. Chem. Soc., Chem. Commun. (1992) 383.
[186] Z.-Q. Pan, R.-S. Luo, R.-H. Luo, C.-Y. Duan, M.-C. Shen, N.-X. Zhang, Y.-J. Liu, X.-A. Mao, Polyhedron 18 (1999) 2185.
[187] Q.-Y. Chen, Z.-Q. Pan, Q.-H. Luo, L.-M. Zhen, X.-L. Hu, Z.-L. Wang, Z.-Y. Zhou, C.-H. Yeung, J. Chem. Soc., Dalton Trans. (2002) 1315.
[188] Z.-L. Wang, Q.-H. Luo, C.-Y. Duan, C.-Y. Shen, Y.-Z. Li, Dalton Trans. (2004) 1104.
[189] M.A. Hossain, P. Morehouse, D. Powell, K. Bowman-James, Inorg. Chem. 44 (2005) 2143.
[190] M.J. Hynes, B. Maubert, V. McKee, R.M. Town, J. Nelson, J. Chem. Soc., Dalton Trans. (2000) 2853.
[191] S. Mason, T. Clifford, L. Seib, K. Kuczera, K. Bowman-James, J. Am. Chem. Soc. 120 (1998) 8899.
[192] D. Farrell, K. Gloe, K. Gloe, G. Goretzki, V. McKee, J. Nelson, M. Nieuwenhuyzen, I. Pál, H. Stephan, R.M. Town, K. Wichmann, Dalton Trans. (2003) 1961.

[193] Y. Dussart, C. Harding, P. Dalgaard, C. McKenzie, R. Kadirvelraj, V. McKee, J. Nelson, J. Chem. Soc., Dalton Trans. (2002) 1704.
[194] C.J. Harding, Q. Lu, J.F. Malone, D.J. Marss, N. Martin, U. McKee, J. Nelson, J. Chem. Soc., Dalton Trans. (1995) 1739.
[195] A. Escuer, V. McKee, J. Nelson, E. Ruiz, N. Sanz, R. Vicente, Chem. Eur. J. 11 (2005) 398.
[196] T. Lu, X. Zhuang, Y. Li, S. Chen, J. Am. Chem. Soc. 126 (2004) 4760.
[197] A.D. Bond, S. Derossi, F. Jensen, F.B. Larsen, C.J. McKenzie, J. Nelsen, Inorg. Chem. 44 (2005) 5987.
[198] A.D. Bond, S. Derossi, C.J. Harding, E.J.L. McInnes, V. McKee, C.J. McKenzie, J. Neslon, J. Wolowske, Dalton Trans. (2005) 2403.
[199] V. Amendola, L. Fabbrizzi, C. Mangano, P. Pallavicini, M. Zema, Inorg. Chim. Acta 337 (2002) 70.
[200] V. Amendola, E. Bastianello, L. Fabbrizzi, C. Mangano, P. Pallavicini, A. Perotti, A. Manotti-Lamfredi, F. Uguzzoli, Angew. Chem. Int. Ed. Engl. 39 (2000) 2917.
[201] L. Fabbrizzi, P. Pallavicini, L. Parodi, A. Taglietti, Inorg. Chim. Acta 238 (1995) 5.